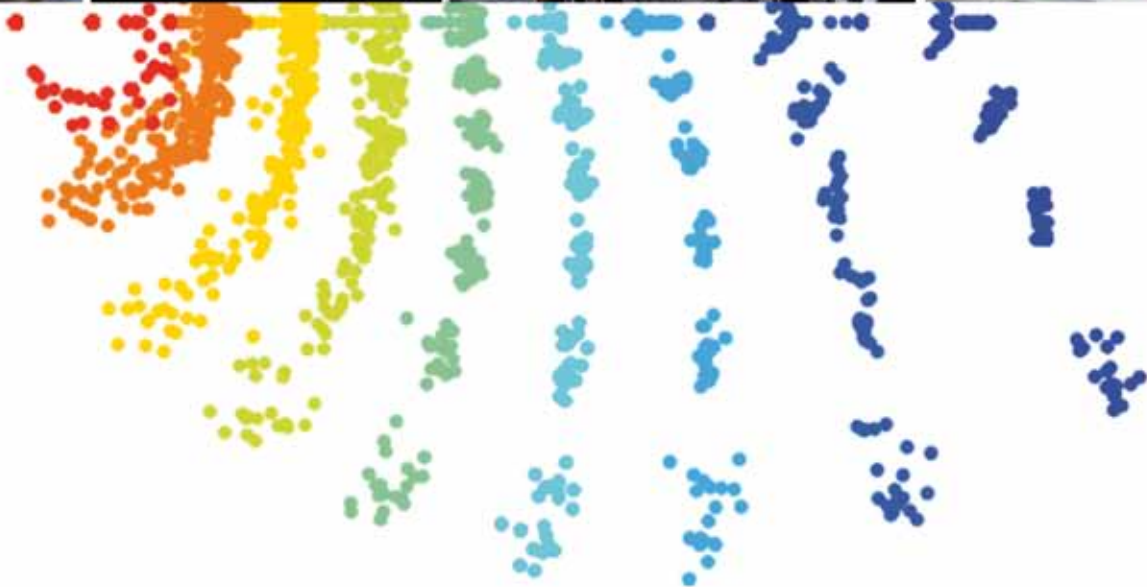




Max Planck Institute
for Dynamics
and Self-Organization

Research Report 2011



IMPRINT
Max Planck Institute for Dynamics and Self-Organization
Am Faßberg 17
37077 Göttingen (Germany)
www.ds.mpg.de

COVER
yef design, Hamburg

PRINTED BY
PR Druckerei, Göttingen

© Juni 2011

TABLE OF CONTENTS

INTRODUCTION: MISSION AND VISION

6

Departments

8

Department of Nonlinear Dynamics

8

Research Group: Theoretical Neurophysics

12

Department of Dynamics of Complex Fluids

15

Department of Fluid Dynamics, Pattern Formation and Nanobiocomplexity

18

Research Groups

24

Droplets, Membranes and Interfaces

24

Network Dynamics

26

Biophysics and Evolutionary Dynamics

28

Onset of Turbulence and Complexity

30

Biomedical Physics

32

Max Planck Fellow Group Polymers, Complex Fluids and Disordered Systems

34

Emeritus Group Molecular Interactions

36

RESEARCH

38

I: Frontiers far from Equilibrium

38

II: Transport in Complex Media

73

III: Disorder in Space and Time, Stochasticity

110

IV: Control

133

V: Patterns and Instabilities

158

VI: Networks

217

PUBLICATIONS

242

SERVICES

264

DIRECTORS

Prof. Dr. Stephan Herminghaus (Managing Director)

Prof. Dr. Eberhard Bodenschatz

Prof. Dr. Theo Geisel

SCIENTIFIC ADVISORY BOARD

Prof. Dr. Pierre C. Hohenberg, New York University (USA)

Prof. Dr. Uzy Smilansky, Weizmann Institute of Science (Israel)

Prof. Dr. David Campbell, Boston University (USA)

Prof. Dr. Jerry P. Gollub, Haverford College (USA)

Prof. Dr. Andreas Herz, LMU Munich (Germany)

Prof. Dr. Alain Karma, Northeastern University Boston (USA)

Prof. Dr. Alexei R. Khokhlov, Moscow State University (Russia)

Prof. Dr. David Quéré, ESPCI Paris (France)

Prof. Dr. Cynthia Volkert, Georg August University Göttingen (Germany)





Max Planck Institute for Dynamics and Self-Organization

INTRODUCTION: MISSION AND VISION	6
Departments	8
Department of Nonlinear Dynamics	8
Research Group: Theoretical Neurophysics	12
Department of Dynamics of Complex Fluids	15
Department of Fluid Dynamics, Pattern Formation and Nanobiocomplexity	18
Research Group	24
Droplets, Membranes and Interfaces	24
Network Dynamics	26
Biophysics and Evolutionary Dynamics	28
Onset of Turbulence and Complexity	30
Biomedical Physics	32
Max Planck Fellow Group Polymers, Complex Fluids and Disordered Systems	34
Emeritus Group Molecular Interactions	36
RESEARCH	38
I: Frontiers far from Equilibrium – Statistical Physics of Strongly Driven Systems	38
I-1 Interactions between Large and Small Scales in Turbulence	38
I-2 Lagrangian Tetrad Dynamics in Fluid Turbulence	40
I-3 Dissipative Scales in Turbulence	42
I-4 Classical Experiments in Turbulence	44
I-5 Göttingen Turbulence Facility	46
I-6 Rayleigh-Bénard Turbulence	49
I-7 Turbulence in Atmospheric Flows	51
I-8 Rain in a Test Tube	53
I-9 Phase Transitions in driven Granular Systems	55
I-10 Ergodic Theory of Granular Fluids	57
I-11 Packing Non-Spherical Objects	60
I-12 Noisy Traveling Waves	62
I-13 Building Blocks of Turbulence	66
I-14 The Origin of Species from the Primordial Soup	69
I-15 Photodissociation and Recombination of Molecules with Atmospheric Relevance	71
II: Transport in Complex Media	73
II-1 Turbulence in Complex Fluids	73
II-2 Particles in Turbulence	75
II-3 Warm Clouds and Turbulence	79
II-4 Non equilibrium Molecular Transport in Spiny Neuronal Dendrites	81
II-5 Anomalous Kinetics in Physical and Biological Systems	83
II-6 Theory of Parity-Time-Symmetric Photonics	86
II-7 Waveguides in the Retina and Light Scattering in the Eye	89
II-8 Liquid Fronts in Porous Media	91
II-9 Fluidization of Granular media	94
II-10 Microfluidics of Nematic Liquid Crystals and Nematic Colloids	97
II-11 Surfactant Advection to Interfaces	99
II-12 Micellar Transport in Emulsions	101
II-13 Wetting of Elastic Substrates	103
II-14 Dynamics of Moving Contact Lines on Heterogeneous Surfaces	105
II-15 Integrable Systems and Related Mathematical Structures	107
III: Disorder in Space and Time, Stochasticity	110
III-1 Statistics of Eukaryotic Chemotaxis	110
III-2 Transport in Correlated Weakly Disordered Systems – Stochastic Theory of Random Caustics	113
III-3 The Nature of Fluctuations in Human Musical Rhythms and the Measurement of Long Range Correlations	115
III-4 Statistical Mechanics of Static Granular Media	118
III-5 Evolutionary Impact of Range Expansions	121
III-6 Graph Theory and Statistical Physics of Complex Disordered Systems	124
III-7 Statistical Physics of Neuronal Action Potentials	126

133	IV: Control
133	IV-1 Cognitive Self-Organization of Movement Coordination and Planning in Robots
135	IV-2 Theory and Dynamics of Human Pointing Movements
137	IV-3 Impact of Microscopic Motility on the Swimming Behavior of Trypanosomes
139	IV-4 Self-Assembled Granular Walkers
142	IV-5 Collective Behavior of Artificial Squirmer
145	IV-6 Multiphase Flow in Electric Field
147	IV-7 Elimination of Turbulence
149	IV-8 Control of Spatio-Temporal Chaos in the Heart
154	IV-9 Natural Computation and Autonomous Robot Control
158	V: Patterns and Instabilities
158	V-1 Pattern Formation and Spatial Forcing in Thermal Convection
160	V-2 Spiral Waves, Cell-Cell Signaling and Cell Aggregation
163	V-3 Pattern Formation and instabilities in the Actin Cortex of Motile Cells
168	V-4 Coupling Chemical Oscillators through Bilayer Membranes
171	V-5 Patterns, Structures, and Surface Ordering in Complex Fluids
174	V-6 Dynamics of Droplets in Microchannels
176	V-7 Magneto-microfluidics and Phyllotaxis
179	V-8 Biophysical Aspects of Biofilm Formation
184	V-9 Evolutionary Dynamics: The Speed of Adaptation
188	V-10 Transition to Turbulence in Shear Flows
191	V-11 Data Driven Modeling of Cardiac Dynamics and Model Evaluation
196	V-12 Time Series Analysis of Cardiovascular Biodata
201	V-13 Electro-mechanical Waves and Instabilities in Cardiac Tissue
205	V-14 Non-Additive Dendritic Coupling in Neural Circuits
207	V-15 Timing-Based Information Processing in Biological Systems
211	V-16 Self-Organization in the Evolution of Neural Circuits
217	VI: Networks
217	VI-1 Self-Organized Criticality and Avalanches in Neural Networks
220	VI-2 Interplay of Self-Organization and Molecular Guidance Clues in the Formation of Neural Circuits
222	VI-3 Dynamic Interactions between Neuronal Circuits
225	VI-4 Flux Cycles as Fundamental Building Blocks of Non-Equilibrium Steady States
227	VI-5 Network Dynamics as an Inverse Problem
230	VI-6 Renewable Energy Sources in Future Power Grids
232	VI-7 Impact of Single Links in Growing Networks
234	VI-8 Chaotic Dynamics and Information Decay in Spiking Neural Networks
240	VI-9 Freely Switchable Networks of Biological Neurons
242	PUBLICATIONS
242	Department of Nonlinear Dynamics
246	Research Group Theoretical Neurophysics
247	Department of Dynamics of Complex Fluids
251	Department of Fluid Dynamics, Pattern Formation and Nanobiocomplexity
254	Max Planck Research Group Droplets, Membranes and Interfaces
255	Max Planck Research Group Network Dynamics
257	Max Planck Research Group Biological Physics and Evolutionary Dynamics
258	Max Planck Research Group Onset of Turbulence and Complexity
259	Max Planck Research Group Biomedical Physics
260	Max Planck Fellow Group Polymers, Complex Fluids and Disordered System
261	Emeritus Group Molecular Interactions
264	SERVICES

Introduction: Mission and Vision



Max Planck Institute for Dynamics and Self-Organization

MAX-PLANCK-GESELLSCHAFT

THE PROPENSITY OF open systems to break symmetries and generate patterns, structures, and functions – in other words: to self-organize – is one of the most fascinating and at the same time ubiquitous conditions in nature. It is visible on large scales in the emergence of stars, galaxies, and galaxy clusters, on intermediate scales in cloud formation, turbulence, and swarming phenomena, and on smaller scales in neural networks like the human brain, or even the nano-scale functions of life on the cellular and sub-cellular level. An essential property of these systems is that they dwell far from thermal equilibrium, in marked contrast to the systems treated in current textbooks, which are at – or at least close to – equilibrium throughout. The listing above underpins the importance to venture out of this limitation, and to subject collective behavior far from equilibrium to a dedicated investigative effort. This should span the wide arc from the quest for possible general principles underlying self-organization phenomena to in-depth investigations focused on particularly relevant systems. This endeavour is the mission of the Max Planck Institute for Dynamics and Self-Organization.

Only the deep understanding of well-chosen paradigm systems will lead to a clearer general picture of self-organization phenomena. The research at this institute therefore focuses on certain classes of systems which are of particular scientific, applicational, and social rele-

vance. The research units are the three departments, plus a varying number of independent research groups, most of which are on temporary assignments. The theory department (headed by Theo Geisel) focuses on theoretical and computational neuroscience, nonlinear dynamics, and transport phenomena in complex systems. The experimental department of Eberhard Bodenschatz investigates turbulence and other pattern formation phenomena in fluids, the physics of clouds, and self-organization in biological systems. In the experimental department of Stephan Herminghaus, dry and wet granular systems are studied as paradigm systems far from thermal equilibrium, furthermore self-organization in emulsions, soft autonomous micro-systems, and geophysical systems. The research program of the three departments is complemented by the independent groups, with research on dynamical networks (Marc Timme), turbulence in shear flows (Björn Hof), evolution on the cellular scale (Oscar Hallatschek), transport phenomena in emulsion systems (Jean-Christophe Baret), self-organized collective behavior of heart muscle cells (Stefan Luther), theoretical neurophysics (Fred Wolf), as well as polymers, complex fluids and disordered systems (Annette Zippelius).

Göttingen, April 2011
Stephan Herminghaus, Eberhard Bodenschatz, Theo Geisel
(from right to left)



Department of Nonlinear Dynamics

Theo Geisel

Research in the Theory Department of the Institute is motivated by such questions as: How do the neurons in our brain cooperate when we perceive an object or perform a task? How does the dynamics of such networks depend on their topology? What are the general principles governing the formation of patterns and neuronal representations in the cortex? What are the dynamical properties of mesoscopic systems and how can they be described semiclassicaly? Are there statistical principles underlying human travel and can they be used to forecast the geographical spread of epidemics?

These questions typically address the complex dynamics of spatially extended or multicomponent nonlinear systems which still reserve many surprises. As an example, we found unstable attractors in networks of spiking neurons, a phenomenon which would neither have been guessed nor understood without mathematical modelling and which many physicists consider an oxymoron. They have a full basin of attraction, but due to their unstable character they allow the network to switch easily and rapidly between different attractors under external stimulation. They may play a functional role in the central nervous system by providing it with a high degree of flexibility to respond to frequently changing tasks.

The example illustrates the need and the role of mathematical analysis for the understanding of complex systems in nature. The concepts and methods developed previously in nonlinear dynamics and chaotic systems can now help us clarify the dynamics and function of spatially extended and multicomponent natural systems. On the other hand rigorous mathematical analysis of the dynamics of such systems often cannot rely on mainstream recipes but poses new and substantial challenges. In particular, neural systems exhibit several features that make them elude standard mathematical treatment: The units of the

network e.g. communicate or interact at discrete times only and not continuously as in many-body theory in physics. There are significant interaction delays, which make the systems formally infinite-dimensional. Complex connectivities give rise to novel multi-operator problems, for which we have devised new methods based on graph theory to obtain rigorous analytic results.

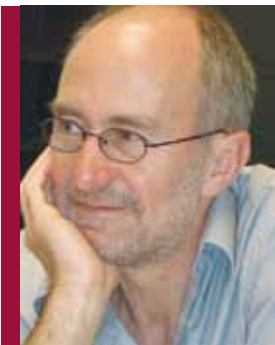
We have previously applied graph theory also in our work on quantum chaos. Similarly we used random matrix theory not only in quantum mechanical systems, but also for the stability matrices of synchronized firing patterns in disordered neural networks. Neuronal spike trains may be considered as stochastic point processes and so may energy levels of quantum chaotic systems. This list demonstrates to which extent cross-fertilization among our various areas of research is possible; in fact it has often been substantial for our progress. The scientists of this department feel that the breadth of existing research activities and the opportunity of intense scientific exchange are key prerequisites for the success of our work. These features are also important for establishing and sustaining a culture of analytic rigor in theoretical studies which attempt to work in proximity to biological experiments.

Theoretical studies of complex systems are scientifically most fruitful when analytical approaches to mathematically tractable and often abstract models are pursued in close conjunction with comprehensive computational modeling and advanced quantitative analyses of experimental data. The department thus naturally has a strong background in computational physics and operates considerable computer resources. Research for which this is essential besides the network-dynamics mentioned above includes e.g. studies of pattern formation in the developing brain, the dynamics of spreading epidemics, and transport in mesoscopic systems. The De-

partment of Nonlinear Dynamics was created by the Max Planck Society in 1996, when the focus of the institute was on mesoscopic systems. Meanwhile our group has shifted its accents and tackled new subjects in the interest of a coherent research program. Besides, this department has initiated and hosts the federally (BMBF) funded Bernstein Center for Computational Neuroscience Göttingen, in which it cooperates with advanced experimental neuroscience labs in Göttingen. With the help of this funding the department has created the positions of Bernstein Fellows, independent junior fellows who can define their own research program and profit from varying collaborations. Our group is closely connected with the Faculty of Physics, it is financed to a large part by the Max Planck Society and to a smaller part by the University of Göttingen through its Institute for Nonlinear Dynamics. It thus has a bridging role between the Faculty of Physics and the MPIDS.

Our recent research achievements demonstrate that abstraction and mathematical rigor do not obstruct but in fact deepen our understanding of complex systems, whether we are studying applications for the development of new photonic technologies, the self-organization of complex neuronal circuits, or the collective dynamics of complex neuronal

activity patterns. In physical systems, key examples are provided by our recent theoretical work on light propagation in a new class of artificial photonic materials with unique optical properties that obey combined parity-and-time-reversal symmetry [e.g. Bendix et al., Phys. Rev. Lett. 2009, and West et al., Phys. Rev. Lett. 2010] or our novel results on random caustics in Hamiltonian flows with weak disorder potentials [Metzger et al., Phys. Rev. Lett. 2010], from which extreme events in physical systems ranging from semiconductor electronics to tsunamis can originate. In neuronal systems, recent highlights are our studies revealing the impact of single neurons and single synapses on the critical collective behavior of large neuronal networks [Kirst, Geisel, Timme, Phys. Rev. Lett. 2009, Levina, Herrmann, Geisel, Phys. Rev. Lett. 2008, Nagler, Levina, Timme, Nature Physics 2010], the laws that govern the dynamical spread of correlations in networks of cortical neurons [Tchumatchenko et al., Phys. Rev. Lett. 2010], and the self-organization of biological neural networks [Keil et al., PNAS 2010, Kaschube et al., Science 2010]. These results substantiate the intriguing fact that nature has chosen the language of mathematics not only to write the book of physics, but also to write chapters in the book of biology.



Prof. Dr. Theo Geisel

studied Physics at the Universities of Frankfurt and Regensburg, where he received his doctorate in 1975. After postdoctoral research at the MPI for Solid State Research in Stuttgart and at the Xerox Palo Alto Research Center he became Heisenberg Fellow in 1983. He had appointments as Professor of Theoretical Physics at the Universities of Würzburg (1988-1989) and Frankfurt (1989-1996), where he also acted as a chairperson of the Sonderforschungsbereich Nichtlineare Dynamik before becoming director at the MPI for Fluid Dynamics (now MPI for Dynamics and Self-Organization) in 1996. He also teaches as a full professor in the Faculty of Physics of the University of Göttingen; he initiated and heads the Bernstein Center for Computational Neuroscience Göttingen.



Dr. Demian Battaglia

studied physics at the University of Turin and received his PhD in 2005 at the International School for Advanced Studies (SISSA, Trieste), doing research at the interface between statistical mechanics and theoretical computer science. From 2006 to 2008 he was Postdoc at the Laboratory of Neurophysics and Physiology (University Paris Descartes). In 2009 he joined the group of Theo Geisel for another Postdoc at the MPI for Dynamics and Self-organization. Since May 2010, he is principal investigator of the Bernstein Center for Computational Neuroscience Göttingen.



Dr. Stephan Eule

studied physics at the Westfaelische-Wilhelms University in Muenster where he received his doctorate in theoretical physics in 2008. In 2009 he joined the Department of Nonlinear Dynamics at the Max Planck Institute for Dynamics and Self-Organization where he works on problems related to fluctuating physical and biological systems and the description of anomalous transport processes.



Dr. Ragnar Fleischmann

studied physics at the Johann-Wolfgang-Goethe University in Frankfurt am Main and received his PhD in 1997. The thesis was awarded the Otto-Hahn-Medal of the Max-Planck-Society. From 1997 to 1999 he was Postdoc in the group of Theo Geisel at the Max-Planck-Institut für Strömungsforschung and from 1999 to 2000 in the group of Eric Heller at Harvard University. Since 2000 he works as a scientific staff member in the Department for Nonlinear Dynamics.



Dr. Denny Fliegner

studied physics at the University of Heidelberg and received his doctoral degree in theoretical particle physics in 1997. From 1997 to 2000 he was a Postdoc at Karlsruhe University working on parallel computer algebra and symbolic manipulation in high energy physics. He joined the group of Theo Geisel at the Max Planck Institut for Dynamics and Self-Organization as an IT coordinator in 2000.



Dr. Anna Levina

studied mathematics at the St. Petersburg State University, Russia and received her doctorate in mathematics from the University of Göttingen in 2008. Her thesis was carried out in the group of Theo Geisel at the Max Planck Institute for Dynamics and Self-Organization and was awarded the Otto Hahn medal of the Max Planck Society. In 2011 she started working part-time again on self-organized criticality in neuronal networks as a postdoctoral fellow in the MPIDS and the Bernstein Center Göttingen.



Dr. Jan Nagler

studied physics at the Christian-Albrechts-University Kiel and received his doctorate in theoretical physics from Bremen University in 2003. Jan worked as a postdoctoral researcher at Bremen University and Boston University (USA). He has recently joined the Department of Nonlinear Dynamics of the MPIDS as a senior postdoctoral researcher in the SPICE group. His research comprises nonlinear dynamics, statistical physics and stochastic processes with applications in biology, ecology, epidemiology and social sciences.



Prof. Dr. Fred Wolf

studied physics and neuroscience at the University in Frankfurt, where he received his doctorate in theoretical physics in 1999. After postdoctoral research at the Interdisciplinary Center for Neural Computation of the Hebrew University of Jerusalem (Israel), he became a research associate at the MPI für Strömungsforschung in 2001. Since 2001 he spent various periods as a visiting scientist and program director at the KITP (Santa Barbara, USA). In 2004 he became head of the research group Theoretical Neurophysics at the MPIDS. He is a founding member of the Bernstein Center for Computational Neuroscience Göttingen and faculty member of several Physics and Neuroscience PhD programs at the University of Göttingen. Since 2011 he is Section Coordinator for Computational Neuroscience of the German Neuroscience Society.



Dr. Annette Witt

studied mathematics at the Humboldt-University Berlin and received her doctorate in theoretical physics from the University of Potsdam in 1996. Her thesis was awarded the Otto-Hahn-Medal of the Max Planck Society. Annette worked as a postdoctoral researcher at the University of Potsdam, the Istituto Nazionale di Ottica Applicata (Florence, Italy), the GeoResearch Center Potsdam, the Environmental Change Research Centre (London, U.K.) and King's College London. She has recently joined the Department of Nonlinear Dynamics of the MPIDS where she develops statistical tools for time series analysis with applications to neuroscience.

Bernstein Fellows



Dr. Armin Biess

studied physics at the Universities of Ulm and Heidelberg with major interest in theoretical physics. He received a doctorate in Applied Mathematics in 2004 from the Weizmann Institute of Science, Israel, and conducted postdoctoral research in the Mathematics Department of this institute. In January 2008 he joined the Max Planck Institute for Dynamics and Self-Organization and Bernstein Center for Computational Neuroscience Göttingen as a Bernstein Fellow.



Dr. Dmitry Tsigankov

studied theoretical physics at the St. Petersburg State Technical University in St. Petersburg, Russia. He received a PhD degree in physics from University of Utah, UT, USA in 2004. From 2004 to 2008 he has been a postdoctoral researcher at the Cold Spring Harbor Laboratory, NY, USA in the department of theoretical neuroscience. He became a Bernstein Fellow in the Max Planck Institute for Dynamics and Self-Organization in January 2009.

Research Group Theoretical Neurophysics

Fred Wolf

The brains of humans and animals arguably are among the most complex systems in nature. Their operation crucially depends on principles and processes of dynamics and self-organization in spatially distributed multi-component systems: Even during the neuronal processing of the most elementary sensory stimulus large ensembles of interacting nerve cells distributed throughout the brain are activated and the processing power of biological neuronal circuits results from the collective dynamics of these ensembles of cells. On a structural level, the amount of information in a mammalian genome is insufficient to specify the detailed wiring of biological neuronal networks. Complex nervous systems therefore utilize processes of dynamical self-organization to generate functionally useful processing architectures. Finally, even individual nerve cells are complex spatially extended dynamical systems and many single neuron computations critically depend on the dynamical interaction of a multitude of sub-cellular components such as ion channels and interacting sub-compartments of the cell. Neuronal processing has thus for a long time provided a rich source of challenging research questions for the theoretical and computational physics of complex systems. Over the past decade, however, experimental methods have matured that enable precise quantitative measurements on all phenomena mentioned above in living neural systems. The convergence of these theoretical and experimental developments is currently driving the emergence of a genuine physics of cooperative neuronal processes (see Wolf & Geisel, *Nature Phys.* 2008).

The Research Group Theoretical Neurophysics focuses on selected problems in neurobiology

and biophysics that provide challenging problems for the development of mathematical theory and computational methods in neuroscience and biology and are mature enough to enable precise quantitative experiments. Our work extends from the formulation and development of novel mathematical approaches tailored to the specifics of neuronal systems dynamics, over the development of analysis methods for turning biological experimental observations into theoretically informative quantitative data, to the development of experimental paradigms specifically designed to provide insight into cooperative and dynamical aspects of nervous system function. To enable a direct interaction of theory and experiment, many projects are pursued in close collaboration with experimental biological research groups around the world.

Currently three problems are at the core of our research agenda: (1) The self-organization of neuronal circuits in the visual cortex. In this system our analyses demonstrate that biological neural networks follow apparently universal quantitative laws which require the development of adequate mathematical theories of neuronal self-organization. Several lines of evidence indicate that non-local interactions characteristic of neuronal circuits lead to qualitatively novel types of dynamics in such systems (e.g. Kaschube et al. *PNAS* 2009, Keil et al. *PNAS* 2010, Kaschube et al. *Science* 2010, *Science* 2011). (2) The dynamics of large networks of pulse-coupled neurons and its impact on the representation of sensory information. Here the ergodic theory of network dynamical systems provides a natural language that links details of the network dynamics to information rep-

resentation and decay (e.g. Monteforte & Wolf PRL 2010, Junek et al. Neuron 2010). (3) The biophysical nature and dynamics of high-bandwidth action potential encoding mechanisms in biological neurons. This problem requires the integration of concepts from non-equilibrium statistical physics with the biophysics of membranes and ion channels. Its solution is essential for the construction of a next generation of dynamically realistic network models (e.g. Naundorf et al. Nature 2006, Tchumatchenko et al. PRL 2010, Wei & Wolf PRL 2011). The Research Group Theoretical Neurophysics was established in 2004 by the appointment of Fred Wolf on the associate professor level (W2) by the President of the Max Planck Soci-

ety. Wolf's Group is part of the Department of Nonlinear Dynamics. It comprises researchers with backgrounds mostly in theoretical physics but also in biophysics and cellular neurobiology. It closely collaborates with experimental neuroscience laboratories at the Max-Planck Institutes for Experimental Medicine (Göttingen), for Biophysics (Frankfurt) and for Biological Cybernetics (Tübingen), at Duke and Carnegie Mellon University (USA), the Hebrew University, the Weizmann Institute of Science and the Technion (Israel), and at the Universities of Göttingen and Jena. It is supported by the DFG, the Human Frontier Science Program, the German Israeli Research Foundation, the Volkswagen Foundation and the BMBF.



Prof. Dr. Fred Wolf

studied physics and neuroscience at the University in Frankfurt, where he received his doctorate in theoretical physics in 1999. After postdoctoral research at the Interdisciplinary Center for Neural Computation of the Hebrew University of Jerusalem (Israel), he became a research associate at the MPI für Strömungsforschung in 2001. Since 2001 he spent various periods as a visiting scientist and program director at the KITP (Santa Barbara, USA). In 2004 he became head of the research group Theoretical Neurophysics at the MPIDS. He is a founding member of the Bernstein Center for Computational Neuroscience Göttingen and faculty member of several Physics and Neuroscience PhD programs at the University of Göttingen. Since 2011 he is Section Coordinator for Computational Neuroscience of the German Neuroscience Society.



Dr. Andreas Neef

received his Diploma in physics in 2000 from the University of Jena, Germany. He joined the MRC Laboratory of Molecular Biology, Cambridge (UK) as a visiting scientist to work on retinal neurons and then went on to do his PhD at the Research Centre Jülich, Germany, where he received his doctorate from Cologne University in 2004. After being a postdoctoral researcher at the Institute for Biological Information Processing I in Jülich (2004) and at the Bernstein Center for Computational Neuroscience, Göttingen he became a Bernstein Fellow associated with the Department of Fluid Dynamics, Pattern Formation, and Nanobiocomplexity in 2006.



Dr. Tatjana Tchumatchenko

Studied physics at the Technical University of Darmstadt where she graduated in 2006 with a Thesis in astrophysics. She then joined the RG Theoretical Neurophysics at MPIDS. In 2010 she obtained a PhD in Theoretical Physics for her thesis research on correlations and synchrony in cortical neurons. Tatjana Tchumatchenko received a fellowship of the German National Merit Foundation 2004-2006 and a postdoctoral research fellowship of the Volkswagen Foundation in 2011.



Dr. Dmitry Tsigankov

studied theoretical physics at the St.Petersburg State Technical University in St.Petersburg, Russia. He received a PhD degree in physics from University of Utah, UT, USA in 2004. From 2004 to 2008 he has been a postdoctoral researcher at the Cold Spring Harbor Laboratory, NY, USA in the department of theoretical neuroscience. He became a Bernstein Fellow in the Max Planck Institute for Dynamics and Self-Organization in January 2009.

Department of Dynamics of Complex Fluids

Stephan Herminghaus

We investigate mechanisms of self-organization and self-assembly by studying selected complex fluid model systems. Our interest ranges from fundamental aspects of dissipative collective behavior to the physics of prototype bio-systems. Consequently, a wide scope of methods is employed, including analytical statistical theory, advanced simulation tools, and cutting edge experimental techniques. What is most intriguing to us is the question whether there are general common 'principles' behind the various instances of structure formation and emergence in open systems.

On the fundamental side, wet granular materials have proved to be versatile model systems for studying collective behavior in systems violating detailed balance on the microscopic level. Their particular charm is their being right at the border of complex interfaces, soft matter, and systems far from thermal equilibrium, thereby rejoining fields of expertise of different subgroups of the department. On the complex side, biological matter and bio-systems are the most intricate systems we are studying, but we try to concentrate on those which are still simple enough to be described by physical and physicochemical principles.

Our strength in investigating the dynamics of soft matter interfaces has recently won us a grant

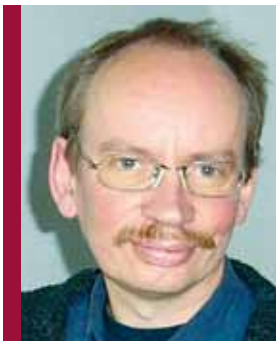
from BP international, by which we were able to significantly augment our research on liquid interfaces in complex environment. The grant provides a total of eleven full time equivalents plus consumables for five years (with an option for another five years), for basic research related to the pore scale physics in oil reservoirs. Other projects are spanning the range from complex soft interfaces to the generation of artificial micro- and nano-devices, which play important roles as building blocks of soft functional systems altogether. These projects, which involve the development of unconventional concepts in microfluidic systems, are strongly fertilized by the insight we gain in non-equilibrium systems, and pushed by the need for soft manipulation techniques for our bio-related projects.

Recently, there have been substantial fluctuations in our personnel. Ralf Seemann has moved to a chair in experimental physics at the Saarland University. Some resources have been given to Jean-Christophe Baret, who joined the institute as an independent Max-Planck Research group leader. Furthermore, Matthias Schröter and Lucas Goehring have joined the group and widen our scope towards dry granular systems, packing problems, and pattern formation in geosystems, respectively.



Prof. Dr. Stephan Herminghaus

received a PhD in Physics from the University of Mainz in 1989. Postdoctoral stay at the IBM Research Center in San Jose, California (USA), in 1990. Habilitation at the University of Konstanz in 1994. Head of an independent research group at the MPI for Colloids and Interfaces, Berlin, from 1996 until 1999. Full professor at the University of Ulm from 1999 until 2003. Since 2003 Director at the MPI for Dynamics and Self-Organization, Göttingen. Since 2005, additional appointment as an adjunct professor at the University of Göttingen. Appointed as Professeur Invité at Université Paris VI for the winter term 2006/7.



Dr. Christian Bahr

studied Chemistry at the Technical University Berlin and received his PhD in 1988. Research stays and postdoctoral work took place at the Raman Research Institute (Bangalore, India) and the Laboratoire de Physique des Solides of the Université Paris-Sud (Orsay, France). After his Habilitation for Physical Chemistry at the Technical University Berlin in 1992, he moved 1996 to the Physical Chemistry Institute of the University Marburg as a holder of a Heisenberg-Fellowship. 2001-2004 he worked as a software developer in industrial projects. In 2004 he joined the group of Stephan Herminghaus at the MPI for Dynamics and Self-Organization. Research topics comprise experimental studies of soft matter, especially thermotropic liquid crystals, phase transitions, structures of smectic phases, thin films, interfaces and wetting.



Dr. Martin Brinkmann

studied Physics and Mathematics at the Free University of Berlin between 1990 and 1998 where he received his Diploma in Physics. After an internship at the Dornier Labs (Immenstaad, Lake Constance) in 1999 he joined the theory group of Prof. Reinhard Lipowsky at the MPI of Colloids and Interfaces (Potsdam, Germany) to work on wetting of chemically patterned substrates. In 2003 he received his doctorate from the University of Potsdam. During a postdoctoral stay in the Biological Nanosystems Group at the Interdisciplinary Research Institute in Lille (France) he explored wetting of topographic substrates as a possible way to manipulate small liquid droplets. Since the beginning of 2005 he investigates wetting of regular and random geometries in the department Dynamics of Complex Fluids at the MPI for Dynamics and Self-Organization.



Dr. Manfred Faubel

Physics studies at the University of Mainz (diploma 1969), and in Göttingen (PhD in 1976). Postdoctoral stays at the Lawrence Berkeley Laboratory, 1977, and in Okasaki at the Institute for Molecular Sciences in Japan, 1981. Employed by the MPI für Strömungsforschung since 1973. Molecular beams studies of rotational state resolved scattering cross sections for simple benchmark collision systems, such as $\text{Li}^+\text{-H}_2$, He-N_2 and for reactive F-H_2 scattering. Since 1986 exploration of the free vacuum surface of liquid water microjets. Photoelectron spectroscopy of aqueous solutions with synchrotron radiation at BESSY/Berlin (1999 to present), and, by laser desorption mass spectrometry of very large ions of biomolecules from liquid jets in vacuum (in a collaboration with MPI-BPC).



Dr. Kristian Hantke

started his Physics study at the Philipps-University Marburg in 1996 and received the Bachelor of Science in Physics at the UMIST, Manchester in 2000 after an Erasmus internship. In 2001 he joined the semiconductor-physics group of Prof. W. Rühle in Marburg, where he worked on the optical properties of dilute III-V nitrides. He received his Diploma in 2002 and his PhD in Physics in 2005. After studying the optical injection of spin currents during a post-doctoral stay at the Philipps-University in Marburg he joined the group of Prof. S. Herminghaus at the MPI for Dynamics and Self-Organization in 2007. As technical laboratory assistant he is responsible for the operation of a new CARS setup in combination with a confocal microscope.



Dr. Thomas Pfohl

studied Chemistry at the Johannes-Gutenberg University, Mainz, and received his doctorate in Physical Chemistry from the University of Potsdam in 1998. After his postdoctoral research at the Materials Research Laboratory, University of California, Santa Barbara, from 1998 to 2000, he became a research assistant at the Department of Applied Physics at the University of Ulm from 2000 until 2004. In 2001 he received a research funding to lead his "Independent Emmy Noether Junior Research Group" by the DFG. Since 2004 he is project leader "Biological Matter in Microfluidic Environment" at the Department "Dynamics of Complex Fluids" at the Max-Planck-Institute of Dynamics and Self-Organization.



Dr. Matthias Schröter

studied philosophy and physics at the Universities of Frankfurt and Kassel. He obtained his PhD in 2003 from the University of Magdeburg; working in the group of Ingo Rehberg on pattern formation in electrodeposition. During his Postdoc with Harry Swinney at the Center for Nonlinear Dynamics at the University of Austin he studied the statics and dynamics of granular media. Since May 2008 he is a senior research fellow in the Department of complex fluids. Main research topics are the statistical mechanics of static granular media and driven suspensions as a model system of glassy behavior.



Prof. Dr. Ralf Seemann

studied physics at the University of Konstanz where he received his diploma in 1997. The diploma work was carried out at the MPI of Colloids and Interfaces in Berlin-Adlershof. He received his doctorate in 2001 from the University of Ulm where he experimentally studied wetting and rheological properties of complex fluids. In 2003 he received the science award of Ulm. During a stay as postdoctoral researcher at the University of California at Santa Barbara, he explored techniques to structure polymeric materials on the micro- and nano-scale. Since 2003 he is a group leader at the MPI for Dynamics and Self-Organization, Göttingen. Ralf Seemann was appointed as professor at the Saarland University in 2007. Among others he is concerned with wetting of topographic substrates, wet granular media, and discrete microfluidics.



apl. Prof. Dr. Jürgen Vollmer

studied physics at the University of Utrecht (NL). In 1990 he joined Prof. Harri Thomas group at the Universität Basel (CH), where he worked on applications of transient chaos, and became interested in the phase behavior and kinetic properties of microemulsions. He pursued postdoctoral studies on the foundations of statistical transport theory and on the kinetics of complex fluids in Essen, Brussels and Mainz, where he was a Schloessmann research fellow of the MPG from 2001-2002. In 2003 he joined the AG Komplexe Systeme at the Philipps Universität Marburg, and since April 2007 he is a member of the department Dynamics of Complex Fluids at the MPIDS. In 2001 Jürgen Vollmer obtained his habilitation in Theoretical Physics from the University of Essen, and he was head of the AG Komplexe Systeme in Marburg in the academic year 2004/05.

Associated Scientist



apl. Prof. Dr. Folkert Müller-Hoissen

received his doctorate in theoretical physics from the University of Göttingen in 1983. After postdoc positions at the MPI for Physics in Munich and the Yale University in New Haven, USA, he returned to the University of Göttingen as an assistant professor (Hochschulassistent), obtained the Habilitation in 1993 and became a Privatdozent. Since 1996 he carries on his research in mathematical physics at the MPI for Fluid Dynamics, which meanwhile evolved into the MPI for Dynamics and Self-Organization. Since 2000 he is adjunct professor at the University of Göttingen. His present research focus is the theory of integrable partial differential and difference equations, applications in theoretical physics and related mathematical structures.

Department of Fluid Dynamics, Pattern Formation and Nanobiocomplexity

Eberhard Bodenschatz

COMPLEX SYSTEMS impact all levels of our everyday lives. The complexity of these systems should not be mistaken for the meaning of the word complicated, but rather reflects the robust properties of a system that emanate from its highly nonlinear properties. The dynamics of complex systems is prescribed by a set of external parameters, their geometrical arrangement and structure, and by the fact that they need energy to function. The behavior of complex systems can range from being well structured to highly disordered. Due to the nonlinearities, small changes in parameters can lead to a complete change in structure and dynamics. Although different in detail, the fundamental physical mechanisms of complex systems can be described by unifying principles. Searching for and understanding those principles is the focus of the Laboratory of Fluid Dynamics, Pattern Formation and Nanobiocomplexity (LFPN).

We are focusing on well-defined problems in the physics of fluid dynamics, pattern formation, cellular biology and biomedicine. In our approach we are relying heavily on methods from the fields of nonlinear dynamics, pattern formation, and non-equilibrium statistical mechanics. Currently we are investigating pattern formation, spatiotemporal chaos and turbulence in thermal convection; particle transport in fully developed turbulence of simple and complex fluids with implications to fundamental theories, but also to practical issues like turbulent mixing, particle aggregation, and cloud micro-physics; the spatio-temporal dynamics of the electric signals in the heart; and the intra-cellular, self-organizing processes leading to eukaryotic cell motility and chemotaxis.

Prof. Eberhard Bodenschatz directs LFPN in collaboration with the Max Planck Research Group Leader Prof. Stefan Luther, who heads the Biomedical Physics Group. LFPN has an excellently

equipped microscopy facility, a cell biology laboratory, and shares with the other groups a class 1000 clean room for micro-fabrication. It established the Göttingen Turbulence Facility, which provides a set of experimental systems and a compressed gas facility to achieve ultra-high turbulence levels with well-controlled measurable scales. LFPN is well known for its advanced imaging systems for three-dimensional particle tracking. For investigations of cloud micro-physics LFPN has a laboratory at the Environmental Research Station Schneeferner House on the Zugspitze, Germany's highest mountain.

Our research has been and will continue to be truly interdisciplinary from engineering, material science, geophysics, and applied mathematics, to chemistry, biology, and medicine. The research of LFPN is connecting seamlessly to the other departments, the Research Groups, and of the Max-Planck-Fellow. We are a member of the International Collaboration for Turbulence Research, the Göttingen Heart Research Center, and are collaborating with groups at the Max Planck Institute for Biophysical Chemistry, the Physics department and the Medical Center at the University of Göttingen. Further national and international collaborations exist with groups at U. Braunschweig, Cornell U., ENS Lyon, U. Ilmenau, National Central University Taiwan, Leibniz Inst. f. Trop. Res. Leipzig, U. Lille, U. Nancy, Max Dellbrück C. Berlin, Michigan Tech., Observatoire de Nice, Politecnico di Milano, Polytecnico di Torino, Princeton U., Rockefeller U., UC Santa Barbara, UC San Diego, and Wesleyan U.



Prof. Dr. Eberhard Bodenschatz

received his PhD. in theoretical physics from Bayreuth U. in 1989. From 1989 to 1992 he was a post-doctoral associate in experimental physics at UC Santa Barbara. From 1992 until 2005 he was Professor of Physics at Cornell U. In 2003 he became Associate Director and in 2005 Director at the Max Planck Institute. Since 2005 he is Adjunct Professor of Physics and of M&AE at Cornell U. In 2007 he was appointed Professor of Physics at Göttingen U. His scientific work is in the physics of complex systems with emphasis on fluid dynamics and biophysics. He is Alfred P. Sloan Research Fellow, Cottrell Scholar and Fellow of the American Physical Society. He is editor in chief of *New J. Phys.*, on the editorial board of *Ann. Rev. Cond. Mat. Phys.*, the chair of the Advisory Boards of the Kavli Institute for Theoretical Physics (UCSB), a member of the advisory board of arXiv, a Director of the Materials Research Society and a founding member of the Heart Research Center Göttingen (HRCG).



Prof. Dr. Carsten Beta

studied Chemistry at the Universities of Tübingen and Karlsruhe and at the Ecole Normale Supérieure in Paris (France). In 2001, he joined the Department of Gerhard Ertl at the Fritz Haber Institute of the Max Planck Society in Berlin and in 2004 received his doctorate in Physical Chemistry from the Free University Berlin. He then moved to the US as a postdoctoral research fellow in the group of Eberhard Bodenschatz at Cornell University and as a visiting scientist at the University of California at San Diego. Since 2005 he is a group leader at the Max Planck Institute for Dynamics and Self-Organization in Göttingen. In 2007, he was appointed as a Juniorprofessor at the University of Potsdam and was promoted to an associate professorship (W2) in 2009.



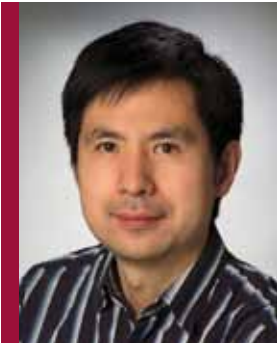
Dr. Azam Gholami

received her BSc from Sharif University in Tehran and her MSc from Institute for advanced studies in Basic Sciences (IASBS), in Zanjan, Iran. In 2003, she started her graduate work in Physics at Hahn-Meitner Institute (Berlin) working with Prof. E. Frey studying polymer physics and modeling cell motility, receiving her degree in 2007 from Ludwig-Maximilian-University of Munich. In January 2008, she joined the Bodenschatz group in Max-Planck Institute for Dynamics and Self-organization as a post-doctoral research associate to work on actin-based motility.



Dr. Mathieu Gibert

received his M.D. (2004) and PhD (2007) in Physics from the Ecole Normale Supérieure in Lyon (France). During his PhD he introduced a new and promising experimental configuration of Turbulent Thermal Convection in a vertical channel and was involved in the first Lagrangian measurements of temperature, velocity and local heat flux in the classical Rayleigh-Bénard turbulent flow ("smart particle" project). In October 2007 he joined the Bodenschatz group in the MPI-DS. He obtained a Marie Curie Fellowship to conduct his research on Turbulence and particle interaction with turbulent flows. As an example, he recently developed the first measurement technique able to acquire the full 3D-motion of finite-size particles (translation/rotation) together with the fluid velocity field around it.



Dr. Xiaozhou He

received his PhD from NANO Science and Technology Institute, Hong Kong University of Science and Technology (HKUST) in 2009. His PhD research is on the experimental study of the thermal dissipation rate and temperature fluctuation statistics in turbulent Rayleigh-Bénard convection. From January to October in 2010, he worked as a post-doctoral research associate in the physics department of HKUST. In November 2010, he joined Professor Bodenschatz' group in the Max Planck Institute for Dynamics and Self-Organization as a post-doctoral research associate and worked on turbulent Rayleigh-Bénard gas convection under high pressure.



Prof. Dr. Valentin Krinsky

studied physics at the Institute of Physics and Technology, Moscow, where he also received his PhD in 1964. After 8 years at the Institute of Biological Physics in Puschino, he was habilitated in 1972. He was appointed Head of the Autowave Laboratory in 1976, and full Professor of Biological Physics at the Institute of Physics and Technology, Moscow in 1980. He was a visiting Professor at the Univ. de Santiago, Santiago de Compostela, Spain (1992), Directeur de Recherche, Centre National de la Recherche Scientifique, INLN, Nice, France, (1993-2004), visiting Professor at Washington University, St. Louis, (2003-2005) and Kyoto University (2006-2007). His research interests include highly nonlinear waves in biological excitable tissues and novel approaches for the termination of life-threatening chaos in the heart. In 2007 he joined the MPI DS to work with Prof. Luther and Prof. Bodenschatz on cardiac dynamics.



Prof. Dr. Stefan Luther

received his doctorate in physics from the Georg-August-Universität Göttingen in 2000. From 2001-2004 he was postdoctoral researcher at the University of Enschede. From 2004-2007 he was visiting scientist at the Laboratory of Atomic and Solid State Physics, Cornell University, and research group leader at the Max Planck Institute for Dynamics and Self-Organization. Since 2007 he is head of the Max Planck Research Group Biomedical Physics. He was appointed adjunct Professor (Honorarprofessor) at the Georg-August-Universität Göttingen in 2008 and adjunct Associate Professor at the Department of Biomedical Sciences, Cornell University in 2009. In 2008, he received the Medical Technology Innovation Award from the German Ministry for Education and Research (BMBF). He is a faculty member of the Georg August University School of Science (GAUSS) and founding member of the Heart Research Center Göttingen (HRCG).



Gisa Luther

studied physics at the University of Hannover and of Oldenburg and graduated in 1996. From 1997-2001, she worked for Bull GmbH (Langen) as an assistant project manager in software engineering and system integration. In 2002, she joined WestLB Systems GmbH (Muenster) as project manager in software engineering. From 2004-2007 she was a visiting scientist at the Laboratory of Atomic and Solid State Physics, Cornell University, Ithaca NY. Since 2004 she is senior researcher at the Max Planck Institute for Dynamics and Self-Organization. Her research interests include numerical modeling of complex hydrodynamic systems and cardiac dynamics.



Dr. habil Holger Nobach

received his doctorate in electrical engineering from the University of Rostock in 1997. During his post-doctoral research, between 1998 and 2000 on an industrial research program with Dantec Dynamics in Copenhagen and between 2000 and 2005 at the Technical University of Darmstadt, he developed measurement techniques for flow investigations. Since 2005 he is a senior scientist at the Max Planck Institute for Dynamics and Self-Organization with a research visit at Cornell University, NY, USA between 2005 and 2006. In 2007 he has got the habilitation in mechanical engineering from the Technical University of Darmstadt. He works on experimental investigation of turbulent flows and thermal convection with improved and extended optical measurement systems and advanced signal and image processing. He is editor for ISRN Signal Processing.



Dr. Noriko Oikawa

studied physics at Nihon University in Tokyo, Japan, and received her bachelor's degree in 2000. In 2005 she received her PhD from Kyushu University, Japan, under the supervision of Prof. S. Kai. Her dissertation theme was pattern formation and controlling spatiotemporal chaos in electroconvection of liquid crystals. From 2005-2008 she was postdoctoral researcher in the Kyushu University working with Prof. K. Fukuda. She joined the Bodenschatz group in the MPI for Dynamics and Self-Organization as a postdoctoral research associate in 2008. She is currently working on synchronization in signaling waves of *Dictyostelium discoideum* cells.



Prof. Dr. Ulrich Parlitz

studied physics at the Georg-August-Universität Göttingen, where he also received his PhD in 1987. After five years at the Institute for Applied Physics of the Technische Universität Darmstadt he returned to Göttingen in 1994 where he was habilitated in 1997 and was appointed apl. Professor of Physics in 2001. He was a visiting scientist at the Santa Fe Institute (1992), the UC Berkeley (1992), and the UC San Diego (2002, 2003). His research interests include nonlinear dynamics, data analysis, complex systems, and cardiac dynamics. In September 2010 he joined the MPRG Biomedical Physics headed by Prof. S. Luther at the Max Planck Institute for Dynamics and Self-Organization. He is faculty member at the Georg August University School of Science (GAUSS) and a member and principal investigator at the Bernstein Center for Computational Neuroscience (BCCN) Göttingen.



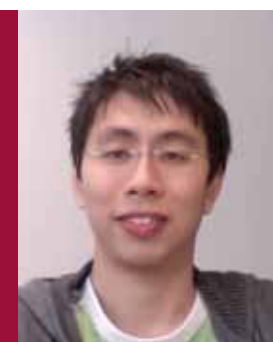
Dr. Claudia Richter

studied biology at the University of Rostock, with a focus on animal physiology and forensic biology. After receiving her Diploma in 2005 she worked for one year at the department of forensic genetics at the Institute of Legal Medicine in Rostock. She received her PhD in February 2011 and since March 2011 works as a postdoctoral associate in the MPRG Biomedical Physics headed by Prof. S. Luther at the Max Planck Institute for Dynamics and Self-Organization in Göttingen. Her research interests include biophysical, molecular and genetic research, biomaterials, tissue engineering and cardiac dynamics.



Dr. Ganapati Sahoo

studied Physics at Utkal University, Bhubaneswar, India where he received his BSc and MSc degrees. He received his doctorate in theoretical physics from Indian Institute of Science, Bangalore, India in 2010. During his PhD he carried out various Direct Numerical Simulations of magnetohydrodynamic turbulence. He then joined as an assistant professor in KIIT University, India. Since March 2011, he is a member of Prof. Bodenschatz's group at MPIDS, Göttingen and is working on direct numerical simulations of fluid flows.



Dr. Ewe Wei Saw

received his M.D. PhD (2008) in Physics from Michigan Tech. University (U.S.A.). His dissertation work dealt with preferential clustering of heavy particles in turbulence. Since May 2009 he joined the turbulence group of professor Bodenschatz as a postdoc researcher. His mainly focus on experiments pertaining to studies of interaction between turbulence and heavy particle, with specialization on relative velocity statistics of heavy particle and study turbulence induced particle collisions. He also works on development and application of experimental techniques for Lagrangian Particle Tracking inside the pressurized environment of the Göttingen Turbulence Facility.



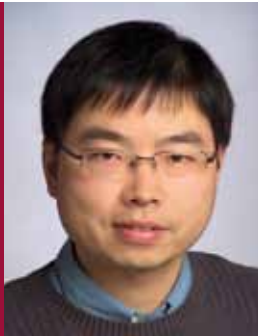
Dr. Amgad Squires

Amgad Squires studied physics at Mount Allison University, Canada, where he presented an honours thesis on Renormalization Group Improvement in Perturbative Quantum Chromodynamics. He received his PhD from Cornell University in 2011 where he presented a thesis on “Wave Emission from Heterogeneities for Low-Energy Termination of Cardiac Arrhythmias” under the supervision of Dr. Eberhard Bodenschatz and Dr. Robert Gilmour. During this time he worked for two years as a Teaching Assistant at Cornell University and five years as a Graduate Research Assistant. He is now a postdoctoral associate in the MPRG Biomedical Physics headed by Prof. S. Luther at the Max Planck Institute for Dynamics and Self-Organization in Göttingen. His research interest include understanding, treating and preventing cardiac arrhythmias, optical mapping techniques, data analysis and simulation, and he has a growing interest in dynamics on and of complex networks.



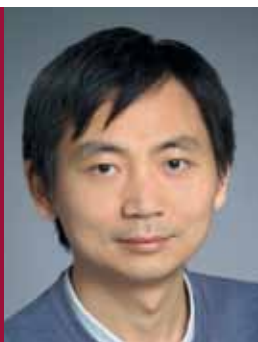
Dr. Marco Tarantola

studied biology at the Julius Maximilians University of Würzburg and graduated in 2005 at the Institute of biotechnology. In 2006, he started his graduate work in biophysical chemistry with Professor A. Janshoff studying dynamics of epithelial monolayers by acoustic and impedimetric whole cell biosensors. He received his PhD in January of 2010 from the Institute of Physical Chemistry at the Johannes Gutenberg University of Mainz. During 2010, he accomplished coordination of the CRC-proposal “SFB 937 Collective behavior of soft and biological matter” (accepted end of 2010) in the group of Professor Annette Zippelius, Theoretical Physics, at the Georg August University of Göttingen. By the end of 2010, he joined the Max-Planck Institute for Dynamics and Self-organization as a postdoctoral researcher in the Bodenschatz department to work on Dictyostelium discoideum chemotaxis with a focus on oscillations, leading edge instabilities and adhesion of migrating Dictyostelium cells.



Dr. Heng-Dong Xi

received his M. Phil (2003) and PhD (2007) in Physics from The Chinese University of Hong Kong. During his dissertation work on the dynamics of the large-scale circulation (LSC) in Rayleigh-Bénard convection (RBC), he discovered the periodic sloshing motion of LSC, observed the flow mode transition and for the first time provided direct experimental evidences that linked the heat transfer and the flow structure, the two important aspects in turbulent RBC. In January 2009, he joined MPIDS as a postdoctoral fellow. He was awarded an Alexander von Humboldt postdoctoral fellowship from April 2010 to March 2012. His current research is on the experimental investigation of turbulence-polymer interaction and the role of turbulence in cloud dynamics.



Dr. Haitao Xu

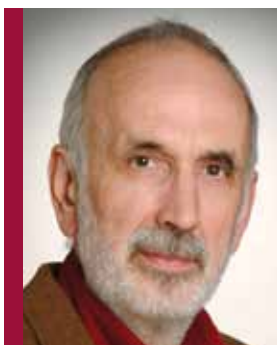
received his PhD in Mechanical Engineering from Cornell University in 2003 for his work on collisional granular flows. From 2003 to 2006, he was a post-doctoral researcher at the Laboratory of Atomic and Solid State Physics, Cornell University, where he, together with other colleagues, developed the Lagrangian particle tracking technique for high Reynolds number turbulence measurements. In August 2006, he joined MPIDS, where he is now a senior scientist. Currently, his main research interest is to reveal, through particle tracking measurements and novel statistical analysis, the Lagrangian properties of fluid turbulence and the interactions between turbulence and additives, such as particles or flexible long-chain polymers.



Dr. Vladimir S. Zykov

studied physics at the Institute of Physics and Technology, Moscow and graduated in 1973. He received his PhD in 1979 from the Institute of Biological Physics in Puschino. After 10 years at the Institute of Control Sciences, Moscow he was habilitated in 1990 and occupied the position of leading scientific researcher. In 1992 he was invited to join the group of Prof. S.C. Mueller at the Max Planck Institute of Molecular Physiology, Dortmund, where he was working till 1996. He was a research scientist at the Otto-von-Geuricke-University, Magdeburg (1996-2001) and at the Technical University, Berlin (2001-2010). In July 2010 he joined the department of Prof. E. Bodenschatz at the Max-Planck Institute for Dynamics and Self-Organization. His research interests include pattern formation processes in nonlinear media, in particular, with permanently changing parameters and external conditions, and control methods of self-organization processes.

Associated Scientist



Dr. Reinhard Schinke

received his diploma in Physics from the University of Goettingen in 1974 and his PhD in Physics from the University of Kaiserslautern in 1976. Following a postdoctoral year at the IBM research laboratory in San Jose (California) he joined the MPI for Fluid Dynamics in Goettingen in 1980. In 1988 he obtained the habilitation in Theoretical Chemistry from the TU Munich. His research centers around the dynamics of molecular interactions in the gas phase (chemical reactions, photodissociation, energy transfer). He is author of the monograph "Photodissociation Dynamics" (Cambridge University Press, 1993) and he received several awards: Dozentenstipendium of the Fonds of the Chemical Industry (1991), Max-Planck-Research award (1994) and Gay-Lussac/Humboldt award of the French Ministry of Sciences (2002).

Research Group Droplets, Membranes and Interfaces

Jean-Christophe Baret

STUDYING THE PHYSICS and physical chemistry of interfaces in multiphase flows has a practical relevance to understand the behavior of foams (used for example in food technology...), emulsions (cosmetics, medicine, biotechnology,...) or membranes (material sciences, cell biology...). The focus of our group is the fundamental study of interfaces in liquid systems through the dynamics of droplets, bubbles and emulsions. Using microfluidic tools, we produce controlled liquid structures and investigate the transient states in droplet formation, emulsification or coalescence and the influence of external fields on the dynamics of droplet interfaces. We use soft-lithography techniques to produce microfluidic modules tailored for droplet manipulation at high-throughput (up to about 10 000 droplets per second). These modules enable the production and reinjection of droplets, as well as droplet pairs or multiple emulsion. One of the most important property of these microfluidic modules is the accurate control on droplet volumes, the droplet-to-droplet size variation being of the order of a few percent. Microfluidics also enables the shapes and geometry of interfaces to be controlled which provides means to extract quantitative informations on interfaces, in static and dynamic configurations. We are, for example, interested in the transient states of emulsion stabilization by surfactants and their link to surface tensions and we develop new tools to measure surface tensions at the millisecond time-scale based on microfluidic liquid manipulation. Our approach should bring a better understanding of the short-time dynamics of surfactant adsorption to interfaces for which only a few experimental tools are available. The use of microfabrication techniques also enables droplets and interfaces to be positioned in external fields, for example electric

or magnetic fields. These fields are then tools for droplet actuation. The electric field is, for example, used to induce controlled fusion of droplet pairs or in other geometries is a versatile tool to sort droplets. Combining optical readout of the droplet content (for example fluorescence) and the ability to actuate droplets in electric fields, we designed and used a microfluidic cell sorter: a cell is sorted as a function of its enzymatic activity revealed by a fluorogenic assay performed in the droplets. The sorting occurs at rates up to 2000 droplets per second. This example shows how droplets in emulsion can be used as independent micro-reactors for the miniaturization of biochemical assays at high-throughput. In collaboration with biologists and biochemists, we use these droplets to screen cells, genes and chemical compounds in droplets at a high-throughput in biological applications such as directed evolution, drug screening or diagnostics. Besides the microfluidic developments required for these applications, the fundamental understanding and the subsequent control of surfactants and emulsion physical-chemistry is crucial in this technology. We believe that the tools we are setting up will provide new insights into emulsion science for biochemical applications. But more generally, we also believe that they will prove relevant tools for a better understanding of the physics and physical chemistry of interfaces in dynamic regimes. The group has been started by Dr. Jean-Christophe Baret in August 2010 after a 3 month 'setting up phase'. It is an international group of 6 members with backgrounds in Physics, Physical-chemistry and Engineering.



Dr. Jean-Christophe Baret

studied physics and chemistry at the Ecole Supérieure de Physique et de Chimie Industrielle de la Ville de Paris (ESPCI, Paris, F) and at the Université Pierre et Marie Curie (Paris, F). He performed his PhD project on electrowetting and electrocapillarity at Philips Research Laboratories Eindhoven (NL) and received his PhD degree from the University of Twente (NL) in 2005. From 2005 to 2009, he was a post-doctoral researcher and EMBO fellow at ISIS (Institut de Sciences et d'Ingénierie Supramoléculaire, Strasbourg, F) where he used microfluidic tools for the miniaturization of biochemical assays. Since 2010, he is an independent Research Group Leader at the Max-Planck Institute for Dynamics and Self-Organization in Göttingen.



Dr. Benoît Semin

Benoît Semin received his PhD in fluid Mechanics from Ecole polytechnique, Palaiseau, France, under the supervision of Dr. Harold Auradou and Dr. Marc François. He obtained his bachelor's and master's degrees in 2004 and 2007 from Ecole Normale Supérieure, Paris. In October 2010, he joined the group of Dr. Jean-Christophe Baret in a collaboration with Dr. Matthias Schröter as a post-doctoral researcher at the Max-Planck-Institute for Dynamics and Self-Organization, Göttingen.



Dr. Xiaopeng Qu

Xiaopeng Qu received his Ph.D. degree from the Mechanical Engineering Department of Hong Kong University of Science and Technology, Hong Kong, China, under the supervision of Prof. Huihe Qiu. He obtained his bachelor's degree in 2002 from Shandong University, China and master's degree in 2005 from Chinese Academy of Sciences, China. In October 2010, he joined the group of Dr. Jean-Christophe Baret as a post-doctoral researcher at the Max-Planck-Institute for Dynamics and Self-Organization, Göttingen.

Research Group Network Dynamics

Marc Timme

Many complex multi-dimensional systems consist of a large number of units that co-act via non-trivial interaction networks. The resulting dynamics are typically genuinely emergent, i.e., they cannot be explained by considering the intrinsic dynamics of the individual units alone. Examples come from a wide range of spatial and temporal scales and include non-local communication and transportation networks, complex disordered systems in physics, the activity of neuronal circuits in the brain, as well as autonomous “intelligent” systems of modern robotics. All of these multi-dimensional systems immediately impact our everyday lives, yet their cooperative dynamics and the mathematical foundations underlying them are still poorly understood.

In the Network Dynamics Group, we are trying to understand the structure and dynamics of complex networks in physics, biology and engineering with a focus on the theory and analysis of spiking neuronal networks and on natural computations by dynamical systems. For instance, spatio-temporal patterns of neural spiking activity are key ingredients of information processing in the brain; we investigate the theoretical fundamentals underlying the mechanisms for generating such patterns in complex neural networks. More recently, we branched out to also work on foundations and applications in the areas of computer science, statistical physics of disordered systems, artificial computation and robotics, and, most recently, gene evolution as well as modern power grids operating with increasing fractions of renewable energies.

As one recent example, we invented an adaptive neuron-like chaos control method for implementing self-organized behavioral control to yield autonomous robots with behavioral gate patterns of unprecedented complexity. We are

also developing new mathematical and computational tools required for understanding these highly complex systems.

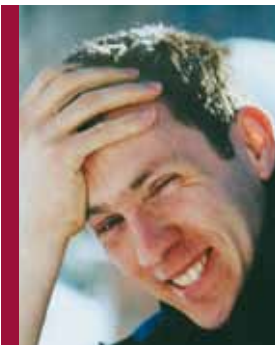
The Network Dynamics Group was established in December 2006. Marc Timme is a founding member of the Bernstein Center for Computational Neuroscience (BCCN) Göttingen; we are actively participating in frontiers research, in part also via direct collaborations with researchers at the Faculties of Physics and Biology at the University of Göttingen. The group further collaborates with researchers at Harvard University (USA), the Radboud University Nijmegen (The Netherlands), the University of Exeter (UK), Cornell University (USA) and the Warwick Mathematics Institute (UK). It is supported by a major grant from the Max Planck Society, by the Göttingen Graduate School for Neuroscience and Molecular Bioscience (GGNB), the International Max Planck Research School (IMPRS) for the Physics of Biological and Complex Systems, a visitor's grant from the German Academic Exchange Service (DAAD), and by the Federal Ministry for Education and Science (BMBF) Germany. Finally, in collaboration with the Faculty of Physics and the Faculty of Computer Science, we recently won a grant from the NVIDIA Corporation, USA, for establishing a CUDA Teaching Center Göttingen.

Research in our team falls into three broad areas of science: Theory and analysis of complex neural systems; Natural computation and autonomous control for intelligent systems and Network evolution, robustness and statistical physics. Many of the scientific projects in these three areas require an exact analysis or the development of new mathematical tools; we thus also intensely work on the mathematical foundation underlying the dynamics of systems in nature and technology. Among the individual project topics there are three theoretical directions focus-

ing on the relation between interaction topologies of a network and their consequences for spatio-temporal dynamics and function as well as one time series analysis project aiming at accessing timing-based, stimulus-induced information, foremost in biological neural circuits. In two key projects we address how artificial neuron-like systems may perform real-world tasks such as memorizing, computing and controlling autonomous robots. Here we focus on further developing modern nonlinear dynamics and apply principles of self-organization to artificial and autonomous technical systems such that they compute or behave in a bio-inspired, “intelligent” way.

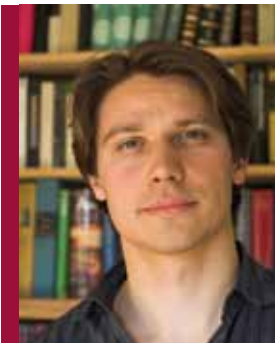
Two further projects address the stochastic nature of the dynamics of early evolution, aiming at explaining fundamental processes underlying self-organization and in particular speciation in the presence of horizontal gene transfer and the dynamical influence of introducing distributed renewable power sources on the stability and robustness of electric power grids of the future.

Finally, the statistical physics of complex disordered systems provides not only challenges about the structure of extended systems interacting on lattices or more complicated graphs but also about their computational tractability.



Prof. Dr. Marc Timme

studied physics at the University of Würzburg, Germany, at the State University of New York at Stony Brook, USA, and at the University of Göttingen, Germany. He received an MA in physics in 1998 (Stony Brook) and a doctorate in theoretical physics in 2002 (Göttingen). After working as a postdoctoral researcher at the Max Planck Institute for Dynamics and Self-Organization, Göttingen, from 2003, he was a research scholar at the Center of Applied Mathematics, Cornell University, USA, from 2005 to 2006. In October 2006 he became the head of the research group Network Dynamics of the Max Planck Society. He is a faculty member at the Georg August University School of Science (GAUSS) and a founding member of and a principal investigator at the Bernstein Center for Computational Neuroscience (BCCN) Göttingen.



Dr. Christoph Kolodziejcki

studied physics at the University of Würzburg and the University of Göttingen; he received his Diploma in Physics in 2005 (Würzburg) and his doctorate in Theoretical Physics in 2009 (Göttingen) with a thesis on the dynamics of synaptic connections following Hebbian plasticity and its relation to reinforcement learning. He was rewarded with the Dr. Berliner – Dr. Ungewitter prize his outstanding graduation. After visiting the Gatsby Computational Neuroscience Unit at the University College London for half a year, he joined the Network Dynamics Group in January 2010. In 2011 he was a guest lecturer at the Kigali Institute of Science and Technology in Rwanda for one semester. In the Network Dynamics group he has continued working on synaptic dynamics co-acting with the dynamics of spatio-temporal patterns as well as on chaos control for autonomous systems.



Dr. Fabio Schittler Neves

studied physics at the Federal University of Rio Grande do Sul, Brazil, where he obtained his B.Sc. in 2003 and his M.Sc. in theoretical physics in 2006 with a thesis on the effects of non-monotonicity in artificial neural networks. He has continued his studies in that field in the Network Dynamics Group and received his doctorate from the University of Göttingen in 2010 with a thesis on the computational properties of neural networks exhibiting heteroclinic cycles. He continuously studying this novel paradigm of computing by heteroclinic switching and its real-world applications in autonomous agent control and general-purpose computation.

Research Group Biophysics and Evolutionary Dynamics

Oskar Hallatschek

EVOLUTIONARY DYNAMICS is a great example of the fact that chance can produce powerful results, since random mutations are the fuel for biological evolution. Predicting the evolutionary consequences of stochastic processes is at the heart of our theoretical research efforts. Our projects extend from fundamental studies on stochastic reaction diffusion systems to explicit models of adaptive evolution. We are driven by basic evolutionary puzzles such as “How fast is evolution?” (see project V-9), or “Under which circumstances, is evolution driven by survival of the luckiest rather than the fittest?” (project III-5). Answering these questions involves the analysis of complex stochastic systems, which sometimes requires the invention of novel statistical physics methods. For instance, we have recently developed an exact method to predict the accumulation of random mutations in finite populations, which was an open problem for half a century (project I-12).

In order to test our models in the lab, we use microbes grown in liquid media, on agar plates and in micro-fluidic devices. Amongst others, the combination of theory and experiment has revealed novel patterns of chance and adaptation, that have also been found in natural populations of multicellular species. Our microbiological experiments also lead to unique biophysical research questions, such as “What forces can be generated by microbial populations when they grow in confined geometries?” (see project V-8). More generally, we are interested in the role of viscoelasticity and hydrodynamics in the formation of organized microbial colonies. Ultimately, our interdisciplinary approach involving collaborations with numerous physicists and biologists, might help to control the formation and

adaptation of biofilms, which are microbial communities involved in numerous infectious disease and responsible for large industrial costs. The Research Group was founded in 2009 and presently employs 3 postdocs, 6 PhD students, 4 diploma and master students and one technician.



Dr. Oskar Hallatschek

studied physics at the University of Heidelberg and ETH Zürich, and obtained his doctoral degree in theoretical biophysics in 2004 from the Freie Universität Berlin. In 2005, he received fellowships from the German Research Society and the German Academic Exchange Service to pursue postdoctoral research at Harvard University, where he worked with Prof. David Nelson and Sharad Ramanathan on experimental and theoretical evolution. He moved back to Germany in 2009 to start an independent Max Planck Research Group on “Biophysics and Evolutionary Dynamics” at the Max-Planck-Institut for Dynamics and Self-Organization in Göttingen.



Dr. Erik Andreas Martens

received his M.Sc. in physics at ETH Zürich in 2004, and wrote his Master’s thesis in fluid dynamics with Tomas Bohr at the Technical University of Denmark and Niels Bohr Institute. He received his Ph.D. at Cornell University in 2009 with a thesis on “Cooperative Behavior in Networks of Coupled Oscillators” under the supervision of Steven Strogatz. In 2009 he joined the Research Group for Biophysics and Evolutionary Dynamics.

Research Group Onset of Turbulence and Complexity

Björn Hof

THE DYNAMICS ENCOUNTERED in nonlinear systems are often extremely complex and disordered. One of the most familiar and at the same time most relevant examples is the turbulent motion of fluids. Turbulent flows arise on many different scales ranging from the formation of stars and planets to flows in the atmosphere, rivers and blood vessels. The classical way to approach turbulent flows is to decompose averaged and fluctuating quantities. Theoretical progress has been limited to asymptotically large Reynolds numbers (Re) and even here many fundamental questions have been left unanswered.

In contrast our work is concerned with turbulence when it first arises and the dynamics are the least complex. As our recent studies show, here tools from nonlinear dynamics and critical phenomena can be applied. In doing so substantial progress can be made towards achieving a conceptual understanding of the origin as well as the nature of fluid turbulence. Our main focus is on linearly stable shear flows which we study in pipes, channels as well as in Couette and Taylor Couette geometries. Despite their central role in fluid dynamics and unlike in situations where the base flow is linearly unstable a physical understanding of the transition to turbulence has been lacking. By combining detailed experiments with highly resolved simulations and the simultaneous study of different flows we could for the first time describe the transition process and uncover the phase transition at which turbulence becomes sustained. These insights now provide a unique opportunity to study the increasing complexity of turbulence encountered at higher Reynolds numbers. At the same time we can exploit our knowledge of the sustaining mechanisms to control turbu-

lent flows. In first control experiments we demonstrated that it is even possible to fully relaminarize turbulent structures in the transitional regime. We have meanwhile developed new methods that also allow us to relaminarize pipe flows in experiments at higher Reynolds numbers where the entire domain is turbulent. More detailed studies are presently carried out.

More recently we have extended our interests to situations where complexity arises through interaction of shear flows and other self organizing processes. These Projects take up more than one third of the group's activities and include the formation of biofilms and the swimming of plankton larvae in shear flows, the influence of polymers on the phase transition in pipe flow as well as the impact of shear on droplet formation during phase separations.

The group has been started by Dr. Björn Hof in March 2008 and presently has 15 members including 4 postdocs, 6 PhD students 2 technicians, 3 master students. An important feature of our group is the multidisciplinary background of the group members, comprising physicists, mathematicians and engineers. The group is collaborating with Prof. D. Barkley, University of Warwick (applied maths), Prof. B. Eckhardt, University of Marburg (theoretical physics), Dr. G. Jekely, MPI for developmental biology Tübingen (biology), Prof. P. Cvitanovic, Georgia Tech (theoretical physics), Dr. Fernando Mellibovsky, UPC Barcelona (aerospace engineering) and Dr. Ashley Willis, University of Sheffield (applied maths).



Dr. Björn Hof

studied physics at the Universities of Marburg and Manchester. He received his PhD in physics from the University of Manchester (UK) in 2001. From 2001 to 2003 he was a research associate at the University of Manchester where he studied transition to turbulence in pipe flow. From 2003 to 2005 he continued his investigation of pipe flow as a research associate at the Delft University of Technology. In 2005 he took up an appointment as RCUK fellow at the School of Physics, University of Manchester. Since 2007 he is the leader of an independent junior research group at the Max Planck Institute for Dynamic and Self-Organization.



Dr Alberto de Lozar

studied physics at the Universidad de Sevilla (Spain) finishing in 2001. During the last year of his studies he joined a research group at this University where he investigated numerically a model for catalyzed chemical reactions dynamics. In 2001 he got a PhD scholarship from the Graduiertenkolleg "Non Equilibrium Phenomena and Phase Transitions in Complex Systems". He received his PhD in physics from the Universitaet Bayreuth in 2005. The title of his thesis was "Liquid crystal dynamics: defects, walls and gels". In 2006 he started his research in Fluid Mechanics as a Research Associate at the University of Manchester (UK). His investigations include carefully performed experiments combined with computer simulations. From 2008 he will start as a Research associate at the Max Planck Institute for Dynamic and Self-Organization.



Dr. Markus Holzner

studied engineering at Trento University (Italy) finishing in 2003. During the last year of his studies he joined a research group at Glasgow University (UK) where he investigated experimentally turbulent flows over permeable beds in open channels. In 2004 he started his PhD focusing on turbulent mixing and entrainment using experimental and numerical techniques. He received his PhD in natural sciences from ETH Zurich in 2007. The title of his thesis was "Experimental and numerical study on the small scale features of turbulent entrainment". Dr. Holzner continued to work on the dynamics of small scale turbulence as a Postdoc at ETH Zurich until he joined the junior research group of Dr. Hof at the Max Planck Institute for Dynamics and Self-Organization in Göttingen. Here he carries out experimental research on the topic of transition to turbulence in pipe flow.



Dr. Marc Avila

studied Mathematics at the Universitat Autònoma de Barcelona, where he graduated in 2004. In 2008 he received his PhD in Applied Physics from the Universitat Politècnica de Catalunya. He was a Research Scholar at Arizona State University from 2006 to 2008, when he joined the Max Planck Institute for Dynamics and Self-Organization in Göttingen as a postdoctoral researcher.

Research Group Biomedical Physics

Stefan Luther

SELF-ORGANIZED COMPLEX spatial-temporal dynamics underlies dynamic physiological and pathological states in excitable biological systems including the heart and brain. Nonlinear dynamics and statistical physics provide novel analytical concepts to enhance the understanding of these complex spatial-temporal systems. Based on these concepts, the Max Planck Research Group Biomedical Physics (MPRG BMP) aims to develop highly innovative experimental and theoretical approaches towards modeling, analysis and control of electrical-mechanical forms of heart disease. We are driven by the vision that the systematic integration and evaluation of dynamics on all levels from sub-cellular, cellular, tissue, and organ to the in vivo organism is key to the understanding of complex biological systems and will open – on a long-term perspective – new paths for translating fundamental scientific discoveries into practical applications that may improve human health. In this endeavor, the theory of dynamical systems plays a central role in integrating biological experiments with mathematical developments. We are applying this translational approach to cardiac arrhythmias, a highly significant cause of mortality and morbidity worldwide. The term dynamical disease was coined for cardiac arrhythmias, suggesting that they can be best understood from the dynamical system's perspective, integrating multidisciplinary research on all relevant spatial and temporal scales. The MPRG BMP focuses on the following objectives: physiological modeling of cardiac dynamics and electro-

mechanical instabilities, multivariate analysis, classification and prediction of biosignals, and control of arrhythmias by novel approaches. These aims will be achieved by a data driven, integrative strategy that combines high-resolution imaging techniques with state of the art numerical modeling through innovative state and parameter estimation and model evaluation methods. Based on this approach, we have successfully developed a novel method for low-energy termination of electrical turbulence in the heart. In collaboration with our research partners, we demonstrated sustained energy reduction of 90% in in vitro and in vivo experiments, compared to conventional, state of the art defibrillation methods. For this achievement, we received the Innovationspreis Medizintechnik 2008 (Medical Technology Innovation Award 2008) from the German Ministry for Education and Research (BMBF). Our group continues to strive for excellence in the development of innovative diagnostic and therapeutic approaches. We greatly benefit from the outstanding interdisciplinary research environment and infrastructure within the Max Planck Institute for Dynamics and Self-Organization. The MPRG BMP has been founding member of the Göttingen Heart Research Center (HRCG), which aims at fostering cross-disciplinary collaborative cardiovascular research within the Göttingen Research Campus. Our research receives funding from the BMBF and the European Community's Seventh Framework Programme FP7/20072013 under grant agreement 17 No. HEALTH-F2-2009-241526, EUTrigTreat.



Prof. Dr. Stefan Luther

received his doctorate in physics from the Georg-August-Universität Göttingen in 2000. From 2001-2004 he was postdoctoral researcher at the University of Enschede. From 2004-2007 he was visiting scientist at the Laboratory of Atomic and Solid State Physics, Cornell University, and research group leader at the Max Planck Institute for Dynamics and Self-Organization. Since 2007 he is head of the Max Planck Research Group Biomedical Physics. He was appointed adjunct Professor (Honorarprofessor) at the Georg-August-Universität Göttingen in 2008 and adjunct Associate Professor at the Department of Biomedical Sciences, Cornell University in 2009. In 2008, he received the Medical Technology Innovation Award from the German Ministry for Education and Research (BMBF). He is a faculty member of the Georg August University School of Science (GAUSS) and founding member of the Heart Research Center Göttingen (HRCG).



Prof. Dr. Ulrich Parlitz

studied physics at the Georg-August-Universität Göttingen, where he also received his PhD in 1987. After five years at the Institute for Applied Physics of the Technische Universität Darmstadt he returned to Göttingen in 1994 where he was habilitated in 1997 and was appointed apl. Professor of Physics in 2001. He was a visiting scientist at the Santa Fe Institute (1992), the UC Berkeley (1992), and the UC San Diego (2002, 2003). His research interests include nonlinear dynamics, data analysis, complex systems, and cardiac dynamics. In September 2010 he joined the MPRG Biomedical Physics headed by Prof. S. Luther at the Max Planck Institute for Dynamics and Self-Organization. He is faculty member at the Georg August University School of Science (GAUSS) and a member and principal investigator at the Bernstein Center for Computational Neuroscience (BCCN) Göttingen.



Prof. Dr. Valentin Krinsky

studied physics at the Institute of Physics and Technology, Moscow, where he also received his PhD in 1964. After 8 years at the Institute of Biological Physics in Puschino, he was habilitated in 1972. He was appointed Head of the Autowave Laboratory in 1976, and full Professor of Biological Physics at the Institute of Physics and Technology, Moscow in 1980. He was a visiting Professor at the Univ. de Santiago, Santiago de Compostela, Spain (1992), Directeur de Recherche, Centre National de la Recherche Scientifique, INLN, Nice, France, (1993-2004), visiting Professor at Washington University, St. Louis, (2003-2005) and Kyoto University (2006–2007). His research interests include highly nonlinear waves in biological excitable tissues and novel approaches for the termination of life-threatening chaos in the heart. In 2007 he joined the MPI DS to work with Prof. Luther and Prof. Bodenschatz on cardiac dynamics.



Gisa Luther

studied physics at the University of Hannover and of Oldenburg and graduated in 1996. From 1997-2001, she worked for Bull GmbH (Langen) as an assistant project manager in software engineering and system integration. In 2002, she joined WestLB Systems GmbH (Muenster) as project manager in software engineering. From 2004-2007 she was a visiting scientist at the Laboratory of Atomic and Solid State Physics, Cornell University, Ithaca NY. Since 2004 she is senior researcher at the Max Planck Institute for Dynamics and Self-Organization. Her research interests include numerical modeling of complex hydrodynamic systems and cardiac dynamics.



Dr. Claudia Richter

studied biology at the University of Rostock, with a focus on animal physiology and forensic biology. After receiving her Diploma in 2005 she worked for one year at the department of forensic genetics at the Institute of Legal Medicine in Rostock. She received her PhD in February 2011 and since March 2011 works as a postdoctoral associate in the MPRG Biomedical Physics headed by Prof. S. Luther at the Max Planck Institute for Dynamics and Self-Organization in Göttingen. Her research interests include biophysical, molecular and genetic research, biomaterials, tissue engineering and cardiac dynamics.



Dr. Amgad Squires

Amgad Squires studied physics at Mount Allison University, Canada, where he presented an honours thesis on Renormalization Group Improvement in Perturbative Quantum Chromodynamics. He received his PhD from Cornell University in 2011 where he presented a thesis on "Wave Emission from Heterogeneities for Low-Energy Termination of Cardiac Arrhythmias" under the supervision of Dr. Eberhard Bodenschatz and Dr. Robert Gilmour. During this time he worked for two years as a Teaching Assistant at Cornell University and five years as a Graduate Research Assistant. He is now a postdoctoral associate in the MPRG Biomedical Physics headed by Prof. S. Luther at the Max Planck Institute for Dynamics and Self-Organization in Göttingen. His research interest include understanding, treating and preventing cardiac arrhythmias, optical mapping techniques, data analysis and simulation, and he has a growing interest in dynamics on and of complex networks.

Max Planck Fellow Group Polymers, Complex Fluids and Disordered Systems

Annette Zippelius

Very complex behavior of physical systems can originate from very simple ingredients. In our research group we try to understand how macroscopic complexity appears in the collective behavior of strongly interacting many particle systems. Polymers, for instance, can be idealized as hard spheres (monomers) linked together randomly in a network. Even though this is an extremely idealized point of view, many macroscopic properties of polymer melts, solutions or gels can be understood from this model, for example the random localization of particles in the gel as well as rheological properties.

The behavior of a simple system can become very complex as soon as it is pushed out of equilibrium. A granular fluid is a prototype of such a system which is relatively simple in the equilibrium limit and extremely complex as soon as dissipation is switched on, showing for instance clustering instabilities, correlations between translation and rotation or highly non-Gaussian energy distributions. At sufficiently high densities granular fluids can undergo a jamming transition into an amorphous solid state. The emergent solid turns out to be highly fragile and susceptible to even minute changes in the external control parameters. It is this interplay and coexistence of flowing and solid states that poses challenging new questions, like for the origins of flow localization or shear thickening.

Complexity can also be induced by disorder. Disorder is present in most, if not all, systems encountered in reality and its influence is often such that it cannot be neglected. To the contrary, even infinitesimal disorder can lead to effects which are absent in an idealized ordered state. A particular challenge is disorder in low dimensions, a typical example being the spin glass. Here, the nature of the low temperature

phase is far from being understood. Recent development of new methods and tools has made significant progress possible in this area.

Our research group consists of the head of the group, two postdoctoral researchers and three PhD students in physics. Additionally, we have several diploma students who work on related projects.



Prof. Dr. Annette Zippelius

studied physics in Munich and Boulder (Colorado) and received her PhD in 1977 in Munich. She was a postdoc in Harvard and Cornell. In 1983 she became a scientific staff member at the Forschungszentrum Jülich. Since 1988 she is a full professor in the Faculty of Physics at the University of Göttingen. She was awarded the Leibniz-prize of the DFG in 1998, is a member of the Wissenschaftsrat since 2005 and became a Max Planck research fellow in 2006.



PD Dr. Timo Aspelmeier

studied Physics in Göttingen and Edinburgh and received his PhD in 2000 in Göttingen. He was a Postdoc at Virginia Tech from 2000 to 2001 in the group of Beate Schmittmann and Royce Zia and from 2002 to 2004 in the group of Alan Bray and Michael Moore in Manchester. He returned to Göttingen in 2004 where he obtained his Habilitation in 2006 and became a member of the Max Planck Fellow group in 2007. He currently works on equilibrium and nonequilibrium statistical physics of complex liquids and disordered systems.



Dr. Claus Heussinger

Dr. Claus Heussinger studied physics in Bayreuth and Würzburg and received his PhD in 2007 in Munich. Before joining the Max Planck Fellow group in 2010 he was a postdoc in the group of Jean-Louis Barrat in Lyon, France. He works in the field of elasticity and rheology of soft amorphous materials.

Emeritus Group Molecular Interactions

Jan Peter Toennies

TOGETHER WITH the late Hans Pauly (1928 – 2004) we came to Göttingen in 1969 from the University of Bonn to establish the new research direction of molecular beam investigations of chemical elementary collision processes. In the following years the Institute became one of the leading international centers for experimental and theoretical research in determining with unprecedented precision the van der Waals forces between atoms and molecules. These forces are of fundamental importance for understanding both the static and dynamic properties of gases, liquids and solids and their phase transitions. Our research led to the development of a new model for the van der Waals interaction, the Tang-Toennies potential, which is widely used for accurate simulations in place of the well known Lennard-Jones potential

In the course of these studies our group observed in the late 1970's that helium free jet gas expansions behaved in a remarkable way. Instead of the usual velocity distributions with $\Delta v/v \approx 10\%$, the helium atom beams had very sharp velocity distributions and were nearly monoenergetic with $\Delta v/v \leq 1\%$. This unexpected observation was found to be related to the extremely weak interatomic forces between He atoms, with the consequence that their collision cross section, at the ultra-low ambient temperatures ($\approx 10^{-3}$ K) in the expanding gas, rises to 259.000 \AA^2 , more than 4 orders of magnitude larger than the cross section at room temperature.

These nearly monoenergetic helium atom beams have found widespread applications. In expansions with small concentrations of molecules the excess of helium atoms serves to cool the molecules down to temperatures of several degrees K. This became a great boon for mo-

lecular spectroscopy since at these temperatures the hot bands that otherwise obscure the molecular spectra are eliminated. Our group exploited the helium atom beams for exploring the structures and vibrations at the surfaces of solid crystals. In complete analogy to neutrons which are routinely used to study the structures and phonon dispersion curves inside solids, helium atoms are the ideal scattering probe method for investigating the structures and dispersion curves of phonons at solid surfaces, which are not accessible with neutrons. The study of over 200 different surfaces by helium atom scattering (HAS) and the complimentary method of inelastic electron scattering (EELS) have led to a profound knowledge of interatomic forces at surfaces and how atoms and molecules interact with metal surfaces, which is of basic importance for understanding catalysis.

In the following years we became even more fascinated by this unusual element helium, which is the only substance which exhibits superfluidity, a collective quantum phenomena similar to superconductivity. In its superfluid state below 2.2 K liquid helium flows without friction, just as the electrons in a superconductor flow without resistance. Thus it was natural to ask if small clusters and droplets of helium might also exhibit superfluidity. Our finding that atoms and molecules were trapped in the droplet's interior opened up the possibility to employ their spectroscopy to interrogate the physical properties of helium droplets. Surprisingly the sharp spectral features of the embedded molecules indicated that the molecules rotate freely as if they were in a vacuum and not at all strongly hindered as expected for an ordinary liquid. Subsequent experiments revealed that this remarkable behavior was related to the superfluidity

of these droplets and has since been accepted by the science community as a new microscopic manifestation of superfluidity. Helium nanodroplets are now being used in more than 25 laboratories worldwide as a uniquely cold (0.15–0.37 K) and gentle matrix for high resolution molecular spectroscopic investigations of atoms, molecules, and “taylor made” clusters, their chemical reactions, and their response to photoexcitation. Our group used this technique to provide the first evidence that para-hydrogen molecules which, like He atoms are spinless bosons, can also exhibit microscopic superfluidity. Our most recent experiments were directed at exploring the nature of small pure clusters ($N \leq 100$) of helium and hydrogen molecules. To this end we developed an apparatus to study the matter-wave diffraction of cluster beams from nanostructured transmission gratings. These experiments led to the first evidence for the existence of the dimer and the precise measurement of its size and of the van der Waals interactions of a number of atoms and molecules with solid surfaces. Unexpected magic numbers were found in larger clusters ($N \leq 50$), which have led to the first insight into the elementary excitations of these nano-sized superfluids. At the present time we are collaborating with several groups in the U.S., Spain and Italy in three main areas of research: (1) The surprising finding that inelastic HAS detects all the phonon modes of thin (3–8 monolayers) films of lead (a superconductor) has been clarified in recent Density Functional Perturbation Theory calculations. These reveal a new interaction mech-

anism in which the He atoms interact largely with the electrons at the surface and thereby indirectly excite the vibrations of the positive ion core lattice. Surprisingly the inelastic HAS mode intensities are found to be proportional to the electron-phonon coupling constants for each selected wavevector. Thus the HAS technique is the first to be able to provide such detailed information on the electron phonon coupling constant of a superconducting metal film. (2) In our laboratory we discovered that solid helium flows into vacuum in an unexpected manner which we called the “geyser” effect. We are presently analyzing data for the flow of the solid through a 100 micron capillary which also exhibits the same effect. These results are of current interest in connection with the controversial reports of supersolidity. (3) In collaboration with theoreticians in Spain and the USA we are extending our Quantum Theorem of Corresponding States studies of the effect of quantum delocalization on the properties, including superfluidity, of small quantum fluid clusters including para- H_2 clusters. One of the most fascinating results coming from these investigations is the discovery that para- H_2 clusters consisting of 18 and 33 particles undergo a new type of superfluid induced structural transition.



Prof. Dr. Dr. h.c. mult. J. Peter Toennies

Studied physics and chemistry at Brown University, Providence, USA where he received his Ph.D. in 1957. He came to Germany in 1957 where he was a postdoc and “Assistent” 1957–1965 in Wolfgang Paul’s Physics Institute in Bonn. After his habilitation (1965) he was a Dozent until becoming director at the MPI Strömungsforschung in Göttingen (1969–2002). Since 1971 he is Associate Professor at the University of Göttingen and Adjunct Professor at the University of Bonn.

I: Frontiers far from Equilibrium – Statistical Physics of Strongly Driven Systems

I-1 Interactions between Large and Small Scales in Turbulence

G. Bewley, M. Gibert, H. Xu, E. Bodenschatz
K. Chang, F. Di Lorenzo, G. Voth (Wesleyan, USA)

TURBULENCE IS OFTEN viewed as consisting of eddies of different sizes. Consequently, measures of turbulence are loosely categorized into large and small-scale quantities. It is generally believed that the large, energy-containing scales are flow-dependent, while the smaller scales are universal and independent of the large scales. This scale separation has been the cornerstone of our understanding of turbulence and finds supports in various observations [1]. There is some evidence, however, that the large scales interact with the small scales [2-4]. Here we report two experiments in which we studied quantitatively the interactions between large and small scales. In the first experiment, we measure small-scale quantities conditioned on large-scale velocities in two flows possessing different degrees of large-scale anisotropy. The conditional statistics show a strong dependence on the large scales in both cases. In the second experiment, we systematically varied the large-scale anisotropy of the turbulence in a single apparatus. We found a relationship between a scaling exponent of the large scale and one of the structure functions at smaller scales. Following [4, 5], we measured the second order longitudinal velocity structure function, $D_{LL} = \langle [u(x) - u(x+r)]^2 \rangle$ conditioned on the average velocity, $u_c = [u(x) + u(x+r)]/2$, which represents the instantaneous large-scale velocity. For r in the inertial and in the dissipative range, the conditional statistics, D_{LL} , should be independent of u_c if the large scale do not influence the small scales directly. The measurements were carried out in two flows: the von Kármán swirling flow, in which the fluctuations in the radial direction are 1.5 times those in the axial direction [6, 7], and the

LEM flow, which is close to homogeneous and isotropic [8]. For both flows, the conditional D_{LL} depends strongly on u_c (figure 1), which shows a dependence of the small scales on the large scales. In a collaborative work with other groups, we observed a similar dependence in other laboratory flows and in numerical simulations [9]. The exact reason for such dependence is under investigation, but we noticed that such dependence is weaker if the ratio of the apparatus size to the forcing scale of the flow is larger [9].

In the second experiment, we tuned the large-scale anisotropy in a novel apparatus, the “soccer ball”, which consisted of 32 loudspeaker-driven air jets pointed toward the center of a nearly spherical chamber. The degree of anisotropy was controlled exactly by varying the strength of individual jets. By mapping the strengths of the jets according to their distances from an axis, we generated homogeneous and *axisymmetric* turbulence in the center of the chamber [10]. We measured velocities at two points in the homogeneous region simultaneously using Laser Doppler Velocimetry (LDV). By varying both the distance and the orientation between the two points, we measured the Eulerian transverse velocity correlation functions $g(x)$ in both axial and radial directions at various degrees of anisotropy.

We used two measures of the large scales, the root mean square (RMS) of the velocity fluctuations, u , and the integral scale of the velocity correlation function, L . In isotropic turbulence, both of these measures have a single value. In anisotropic turbulence, the measures depend on the direction in which they are calculated. This is because the characteristic lengths depended

strongly on the anisotropy in the velocity fluctuations. As shown in figure 2, the relationship is a power law with an exponent of about -3. We show below that this scaling exponent between large-scale quantities is prescribed by the small-scale dynamics of turbulence.

We consider correlation functions, $g(x)$, that can be in either radial ($x=r$) or axial ($x=z$) directions. We conjecture that (i) the viscosity is so small that the dissipative scales are of negligible size; (ii) the correlation functions are self-similar, i.e., $g(x)$ is universal through a rescaling of the separation, x ; (iii) the second order structure functions, D , are isotropic at small scales, which constrains the correlation functions through the linear relation between D and g : $D=u^2(1-g)$; (iv) the correlation functions approach a power law with exponent n for small inertial range separations, i.e., $g(x)=1-bx^n$ for $x \rightarrow 0$. We checked all

these assumptions and verified that they are satisfied in our flow. It then follows that the ratio of the integrals, L , of the two correlation functions is a power law of the ratio of the corresponding RMS velocities for the two correlation functions, i.e., $L_z/L_r=(u_z/u_r)^{-2/n}$. Note that n should be $2/3$ according to Kolmogorov's theory. Thus we would expect a power of -3, which is consistent with figure 2. This shows that the integral length scales are a robust measure of anisotropy. New apparatuses with tunable degrees of large-scale anisotropy, namely the LEM and the soccer-ball, make studies of anisotropy at small scales possible [11]. The response of small scales to sudden perturbations at large scales is also an interesting problem [12]. The investigation of this transient process is facilitated by the real-time optical data downloading interfaces developed in our group.

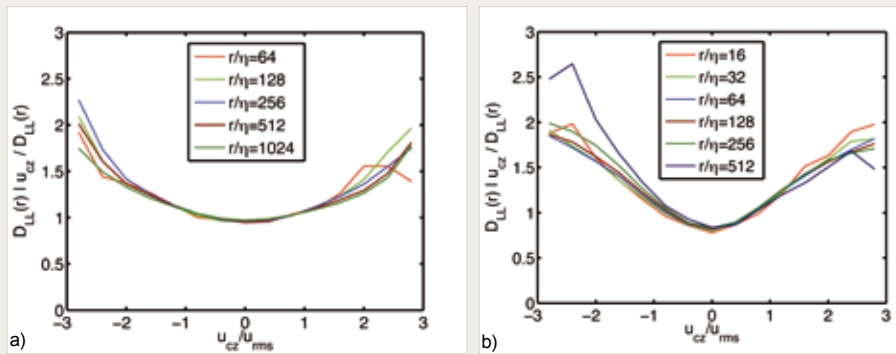


Figure 1

The ratio of the conditional and unconditional Eulerian velocity structure functions at different scales r/η , plotted against the average velocity u_c . These ratios should be of constant value 1 if the velocity increments are independent of the average velocity u_c (a) Data from the von Kármán flow [7]; (b) Data from the LEM flow [8].

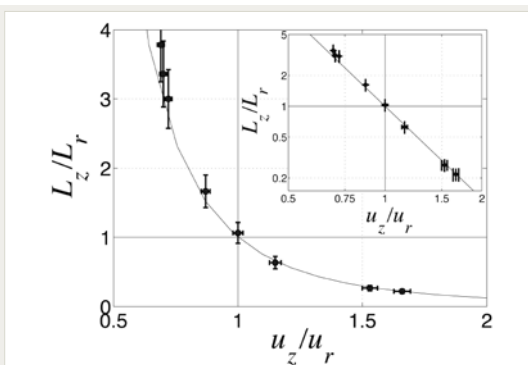


Figure 2

The ratio between the integral scales of transverse correlation functions with separations stretching in two different directions. This quantity is shown as it varies with the ratio of velocity fluctuations in the two directions, u_z/u_r . The direction of L_z and u_z was close to z -axis of the turbulence, while for L_r and u_r it was close to the r -axis. The inset shows the same data with logarithmic scales on both axes of the plot. The data follow approximately a power law of the velocity fluctuation ratio with exponent -3.0 ± 0.2 . The dashed line is a power law with exponent -3.0.

[1] U. Frisch, *Turbulence: the legacy of A.N. Kolmogorov*, Cambridge University Press (1995)
 [2] K. R. Sreenivasan, R. A. Antonia, *Annu. Rev. Fluid Mech.* **29**, 435 (1997)
 [3] X. Shen, Z. Warhaft, *Phys. Fluids* **12**, 2976 (2000)
 [4] K. R. Sreenivasan, B. Dhruva, *Prog. Theor. Phys. Supp.* **130**, 103 (1998)
 [5] D. Blum et al., *Phys. Fluids* **22**, 015107 (2010)
 [6] G. Voth et al. *J. Fluid Mech.* **469**, 121 (2002)
 [7] N. T. Ouellette et al., *New J. Phys.* **8**, 109 (2006)
 [8] R. Zimmermann et al., *Rev. Sci. Instrum.* **81**, 055112 (2010)
 [9] D. Blum et al. *in preparation*
 [10] K. Chang, G. P. Bewley, E. Bodenschatz, *submitted*
 [11] L. Biferale, I. Procaccia, *Physics Reports* **414**, 43 (2005)
 [12] Y. Zhou, P. K. Yeung, J. G. Brasseur, *Phys. Rev. E* **53**, 1261 (1996)

I-2 Lagrangian Tetrad Dynamics in Fluid Turbulence

H. Xu, E. Bodenschatz

A. Pumir (ENS-Lyon, France), E. Siggia (The Rockefeller University, USA)

TURBULENCE DYNAMICS beyond the pictorial description of Kolmogorov (K41) is extremely complicated. In the dissipative range, where the flow field is differentiable, the dynamics is best studied through the velocity gradient. A natural question is how to extend the concept of velocity gradient into the inertial range, where the velocity field is not smooth. As such an attempt, we study the tetrad-based velocity gradient, i.e., a coarse-grained velocity gradient sampled by only four points in space, as first proposed in [1]. By varying the distance between the four-points forming the tetrads, we can also probe the scale dependence of the inertial range dynamics.

For any set of four points \mathbf{r}^a , ($a=1, \dots, 4$), in three dimensional turbulence, a velocity gradient \mathbf{M} can be defined such that $\mathbf{u}^a = \mathbf{M} \cdot (\mathbf{r}^a - \mathbf{r}_c^a)$, where \mathbf{r}_c^a is the “center-of-mass” of the four points and \mathbf{u}^a is the fluctuating velocity relative to the center-of-mass. Obviously this tetrad-based velocity gradient \mathbf{M} differs from the more familiar filtered/coarse-grained velocity gradient $\overline{\mathbf{M}}' = \int \mathbf{m}(\mathbf{x}) d\mathbf{x}$ where \mathbf{m} is the “true” velocity gradient and l is the length scale of interest. The latter may be approximated by averaging over many points in a volume with size l , as studied in [2]. On the other hand, the two gradients \mathbf{M} and $\overline{\mathbf{M}}'$ bear many similarities [3]. The tetrad-based velocity gradient \mathbf{M} is much easier to access experimentally. Moreover, following the tetrad in turbulence not only provides the Lagrangian dynamics of \mathbf{M} , but also reveals the important information about shape deformation.

We study the tetrad-based velocity gradient \mathbf{M} in both experiments and numerical simulations. Experimentally we tracked hundreds of tracer particles in a high Reynolds number von Kármán water flow up to $R_\lambda = 815$. The reconstructed three-dimensional particle trajectories were then differentiated to obtain particle velocities

and accelerations. Tetrad statistics were gathered by selecting four points that form a nearly isotropic tetrahedron with edge length r_0 [4]. The experiments are complemented with direct numerical simulations (DNS), which cover a range of smaller Reynolds numbers $R_\lambda \leq 170$, but resolve all the scales of the flow, especially the dissipation range [5].

Figure 1 shows the joint probability density functions (PDFs) of the two invariants of \mathbf{M} : $Q = -\text{tr}(\mathbf{M}^2)/2$ and $R = -\text{tr}(\mathbf{M}^3)/3$, measured experimentally at $R_\lambda = 690$ for tetrads with two different sizes in the inertial range. If the velocity field were Gaussian, then the PDFs would be symmetric about $R=0$. The measured PDFs, on the other hand, clearly skewed towards the $R>0$ side, more specifically, along the branch of the discriminant. The velocity gradients in that region correspond to two stretching directions and one compressive direction, which tend to flatten the initially isotropic tetrads into sheet-like objects. This feature has been observed for the “true” velocity gradient \mathbf{m} [6] and the filtered velocity gradient $\overline{\mathbf{M}}'$ [2]. It is also noticeable from figure 1 that as the scale r_0 increases, the PDF becomes more symmetrical, consistent with the expectation that the velocity field is uncorrelated at large scales. The same features are also observed in DNS.

Aside from the PDFs, more interesting dynamics can be revealed by studying the evolution of R and Q following the tetrads, as done previously in the dissipative range for the true velocity gradient \mathbf{m} [7, 8]. For initially isotropic tetrads in the inertial range, the tetrad model [1] predicts the follow equations for ensemble-averaged R and Q

$$\frac{dR}{dt} = \frac{2}{3}(1 - \alpha)Q^2 + 3\zeta R$$

and

$$\frac{dQ}{dt} = -3(1 - \alpha)R + 2\zeta Q$$

where α and ζ are two unknown constants that can be determined by fitting the equations to experimental data. As shown in figure 2, the model prediction agrees well with experiments. Similar agreement was also observed for DNS.

In summary, by combining state-of-the-art experiments, numerical simulations, and theoretical analysis, we established a powerful machinery to probe turbulence dynamics in the inertial

range through Lagrangian tetrads. The shape deformation of the tetrads is tightly coupled to the tetrad-based velocity gradient \mathbf{M} [9] and is the focus of our current study. Based on this approach we hope to develop a simplified, effective field theory for the inertial range dynamics of turbulent flows, guided by theoretical considerations and constrained by the available experimental and numerical data.

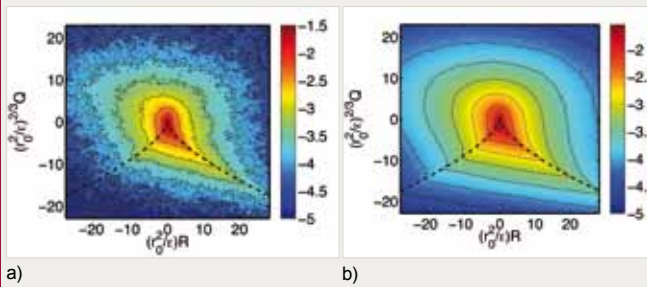


Figure 1

Experimentally measured joint PDFs of R and Q , the invariants of the tetrad-based velocity gradient \mathbf{M} , in a von Kármán flow $R_\lambda=690$. The color is mapped using the logarithmic of the probability, as shown in the colorbars. The dashed lines mark the discriminant $4Q^3+27R^2=0$. Plots (a) and (b) are for nearly isotropic tetrads with edge lengths of $r_0/\eta=400$ ($r_0/L=1/6$) and $r_0/\eta=830$ ($r_0/L=1/3$), respectively, where η is the Kolmogorov scale and L is the integral scale. At both r_0 , the PDFs are skewed toward the positive R branch of the discriminant, which corresponds to flattening of the isotropic tetrads to sheet-like objects.

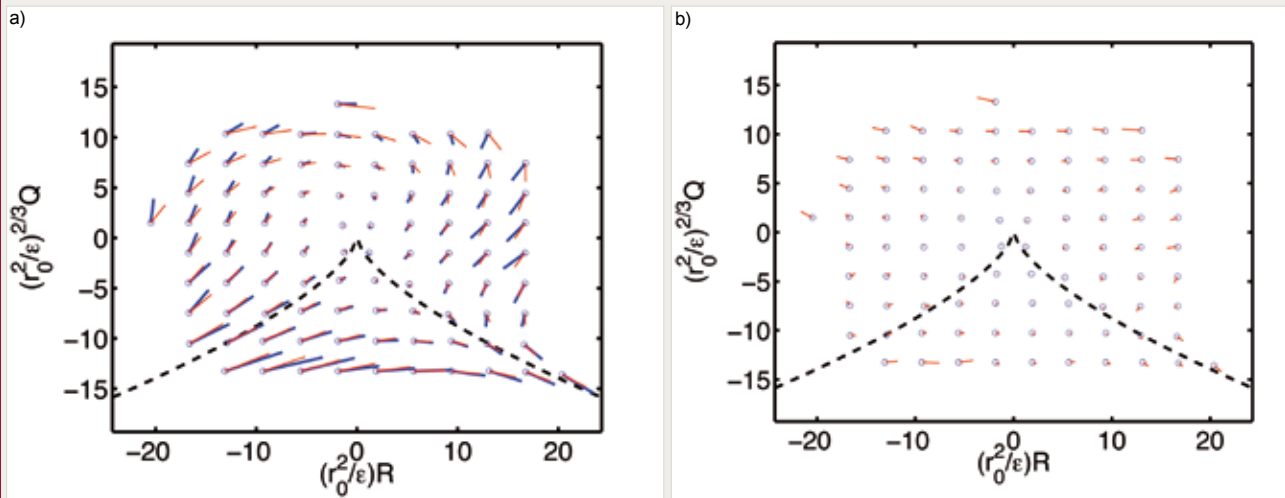


Figure 2

Comparison of the tetrad model prediction on the dynamics of the tetrad-based velocity gradients with experiments at $R_\lambda=690$, $r_0/\eta=830$, i.e., same conditions as shown in figure 1(b). (a) The vectors $(dR/dt, dQ/dt)$ on the (R, Q) map. The thick blue lines are the measurements while the thin red lines are the model prediction. (b) The difference between the measurements and the model prediction. In both plots, the dashed lines mark the discriminant $4Q^3+27R^2=0$.

- [1] M. Chertkov, A. Pumir, B. I. Shraiman, *Phys. Fluids* **11**, 2394 (1999)
- [2] B. Lüthi et al, *J. Turbul.* **8**, 45 (2007)
- [3] C. Meneveau, *Annu. Rev. Fluid Mech.* **43**, 219 (2011)
- [4] H. Xu, N. T. Ouellette, E. Bodenschatz, *New J. Phys.* **10**, 013012 (2008)
- [5] A. Pumir, B. I. Shraiman, M. Chertkov, *Phys. Rev. Lett.* **85**, 5324 (2000)
- [6] J. M. Wallace, *Phys. Fluids* **21**, 021301 (2009)
- [7] P. Vieillefosse, *Physica A* **125**, 150 (1984)
- [8] B. J. Cantwell, *Phys. Fluids A* **4**, 782 (1992)
- [9] H. Xu, A. Pumir, E. Bodenschatz, *Nat. Phys.* doi: 10.1038/nphys 2030 (2011)

I-3 Dissipative Scales in Turbulence

W. Pauls
J. Zudrop

IN MATHEMATICAL SENSE, scale separation means that the description of a system simplifies when the control parameters tend to certain limiting values. One example of such a reduction is the homogeneous isotropic fluid turbulence at infinite Reynolds numbers. In turbulence the smallest, dissipation range represents another range of scales where the features are expected to be independent of the way the flow is driven. Therefore, we seek to reduce the system while keeping the essential features of turbulence at dissipative scales. A straightforward approach would be to consider turbulent flows in the limit of very small Reynolds numbers. In such a limit, one could completely neglect the non-linear term in the Navier-Stokes equation (NSE), which may yield solutions with analytic properties entirely different from the original NSE.

To analyze the properties of the solutions of the NSE at small scales, we consider decaying solutions in the simplest domains possible, e.g., the whole space or a periodic box. Under these conditions, we show that in the limit of vanishing Reynolds numbers, real-valued solutions of the NSE can be represented by superpositions of complex-valued solutions of the same NSE with simpler complex-valued initial conditions. In principle, these solutions are unphysical, but have the major advantage of being easier to analyze. In other words, they represent the reduced system we are looking for.

When complex-valued solutions are considered in the whole space R^d (d is the number of dimensions), and initial conditions are chosen so as to reduce the interaction of modes, some analytical results can be obtained by the Renormalization Group method. A special type of solutions (Li-Sinai type solutions, LSt) of the Burgers equation and NSE has been constructed [1-3] for which the Fourier transform of the velocity field is close to a Gaussian distribution. In this

case, the analytical properties of LSt-solutions can be derived from their Fourier space representation by a simple argument [4]. For example, for the LSt solution of the two-dimensional NSE, we obtain for the velocity field complex singularities $|z - z^*|^{-3/2}$ and $|z - z^*|^{-2}$. Following this work we have given an elementary construction of LSt-solutions for the inviscid Burgers equation, explicitly relating them to stable distributions. We further generalized the LSt-construction in the case of the viscous Burgers equation showing that there also exist solutions whose Fourier transforms are close to non-Gaussian stable distributions [4].

The second approach is to consider the corresponding equations in a periodic box, e.g. $[0, 2\pi]^d$. It turns out that for suitably chosen initial conditions the Fourier coefficients of the solution can be calculated recursively by repeated integration without any truncation or time stepping errors [5]. In addition, this method allows us to consider rather arbitrary dissipation terms, e.g., the exponentially growing dissipation term studied in [5]. For solutions at large times, the complexities associated with the calculation of the Fourier coefficients for arbitrary dissipation can be further reduced. In this case the Fourier coefficients are related by algebraic recursions, resembling the inviscid case [6]. We used this approach for solutions of the one-dimensional Burgers equation and determined accurately the asymptotic structure of their Fourier coefficients [7].

For two-dimensional NSE, it is hard to handle analytically the recursion relations. Our approach is to solve these equations numerically using high-precision arithmetic and algorithms for fast polynomial multiplication [8], implemented in the package MATHEMAGIX [9]. The analytic properties of the solutions can then be deduced from the asymptotics of the Fourier co-

efficient for $|k| \rightarrow \infty$ as discussed in [10]. In real flows with finite Reynolds numbers, the inertial range and the dissipation range are connected to each other. One manifestation of such mutual influence is the bottleneck effect, a pile-up of energy at the upper end of the inertial range due to the suppression of transfer to the dissipation scales. If the standard viscous term $\nu \Delta$ is replaced by a hyper-dissipative one $-\nu^{2\alpha-1}(-\Delta)^{2\alpha}$, the

bump in the spectrum grows with increasing α . The hyper-viscosity also leads to oscillations in the solutions that are related to the bottleneck, as shown recently [11]. Using asymptotic solutions of the one-dimensional boundary layer Burgers equation, we evaluated the importance of the oscillations for the bottleneck [7]. The asymptotic solutions approximate well the solutions of the Burgers equation near the bottleneck (figure 1).

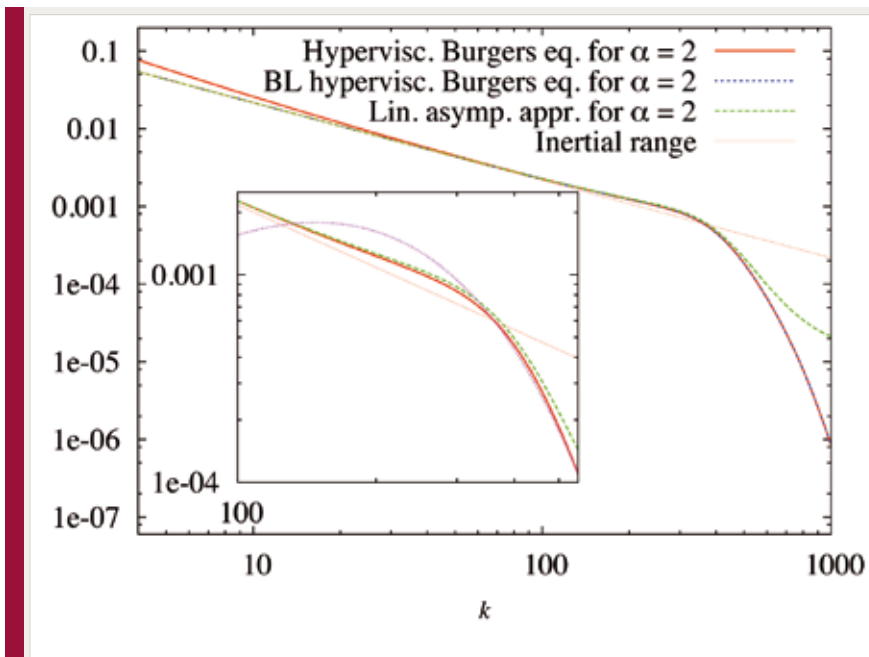


Figure 1

Log-log scale representation of the Fourier coefficients of a solution of the one-dimensional Burgers equation with hyper-dissipation $-\nu^{2\alpha-1}\partial_x^{2\alpha}$. We compare this solution with the appropriately rescaled solution of the boundary layer Burgers equation, the rescaled linearized asymptotic solution and the inertial range scaling $\propto k^{-1}$. In the inset the numerical solution of hyperviscous Burgers equation (red solid line) is compared with the functional form $k^2 e^{-\delta k}$ (magenta dotted line) in the dissipation range, the rescaled linearized asymptotic solution (green dashed line) and the inertial range scaling (thin red solid line).

- [1] D. Li and Ya. G. Sinai, *J. Eur. Math. Soc.* **10**, 267 (2008)
- [2] D. Li and Ya. G. Sinai, *Current Develop. Math.* **2006**, 181 (2008)
- [3] D. Li and Ya. G. Sinai, *J. Math. Phys.* **51**, 015205 (2010)
- [4] W. Pauls, *submitted*.
- [5] C. Bardos et al., *Commun. Math. Phys.* **293**, 519543 (2010).
- [6] W. Pauls et al., *Physica D* **219**, 40 (2006)
- [7] W. Pauls and J. Zudrop, in preparation
- [8] J. van der Hoeven, *J. Symbolic Comput.* **34**, 479542 (2002)
- [9] <http://www.mathemagix.org/>
- [10] W. Pauls, *Singularities of Incompressible Inviscid Flows*, PhD thesis, (2007)
- [11] S. S. Ray et al., *submitted*

I-4 Classical Experiments in Turbulence

G. Bewley, H. Nobach, H. Xu, E. Bodenschatz
Z. Warhaft (Cornell, USA), L. Smits (Princeton, USA)

RICHARDSON, KOLMOGOROV, and others envisioned in turbulence a cascade of kinetic energy from large-scale energetic fluid motions to small-scale dissipative fluid motions. The theory founded on this picture depends on a separation in the size of the energetic and dissipative motions, a separation that tends to arise with increasing Reynolds number [1]. High Reynolds numbers were also thought to produce in the small scales the necessary statistical isotropy and homogeneity, though this now appears not to be the case [2]. These conditions limit not only the reach of the theory in a practical sense, but also our ability to test the theory [3]. There is one flow that is known to satisfy closely the conditions of statistical isotropy and homogeneity, the flow generated by a grid of crossed bars in a wind tunnel [4, 5]. However, previous experiments have not reached high Reynolds numbers. The aim of this project is to test theories at high Reynolds numbers, and in situations that were previously well characterized at lower Reynolds number.

In the variable density wind tunnel, described in the section on the Göttingen Turbulence Facility, we generated grid turbulence at Taylor Reynolds numbers, $R_\lambda = u\lambda/\nu$, between 150 and 1700. Previous studies reached Reynolds numbers no higher than about 500 [6, 7] for passive grids. Only with active grids were higher Reynolds numbers possible [8]. Our data provide the first possibility to compare active and passive grid data at these Reynolds numbers. As shown in Table 1, the Reynolds number could be varied by using two gases, air and sulfur hexafluoride, and by changing the pressure of the gases. The mean speed of the flow was kept constant at about 5 m/s. A biplanar grid of crossed square bars, of classical construction [4], generated the turbulence. The solidity of the grid was 35% and the spacing of the bars was 107 mm. Metal wire screens sta-

tioned upstream of the grid settled the flow incident on the grid. We measured the flow velocities with hot-wire anemometers stationed sufficiently far downstream that the flow was fully developed (67 times the grid spacing, or 7.1 m, downstream of the grid).

The energetic scales of turbulent motion originate at the grid. When the viscosity is small, the grid geometry and flow speed dominate their generation. However, we also observed a small but systematic influence of the viscosity on two measures of the large scale, the integral scale and the turbulence intensity. A decrease of the kinematic viscosity by a factor of 100 caused a decrease in the integral scale by about 15% and an increase in the turbulence intensity by about 20%. The turbulence intensity and the integral length were 2.5% and 8.5 cm, respectively, at the highest Reynolds numbers.

The most pronounced effect of a decrease in viscosity is an increased spectral separation between the energetic scales of motion and the dissipative scales of motion. This effect can be seen in figure 1(a) as a shift of the dissipative cutoff to higher wave numbers as the viscosity is decreased. Here, we normalized the spectra by Kolmogorov's length scales. Also noticeable in figure 1 is the premature cutoff of the spectra acquired at the highest Reynolds numbers. This was caused by the probes, which were much larger than the Kolmogorov scale at these Reynolds numbers. Motions at scales far from the dissipative ones were conjectured by Kolmogorov to be unaffected by viscosity. Under this assumption, he predicted power law scaling for the spectrum. As can be seen in figure 1(b), the prediction does not hold for our data. At the lowest Reynolds numbers the data may follow a power law, but with a shallower exponent than the prediction [8]. The shape of the 1D-spectra evolved as the viscosity decreased, and a bump emerged close to the small-scale cut-

off, a feature known as the bottleneck [9]. At the highest Reynolds numbers, the bottleneck may have disappeared. It is difficult at any Reynolds number to assign unambiguously a power law for the intermediate range of scales.

The data allow us for the first time to investigate turbulence in a symmetric flow at higher Reynolds numbers than previously observed. As expected, we found the dissipative scales of motion to be strongly affected by viscosity. Surprisingly, the energetic scales also changed. The behavior of the inertial range of scales eludes clear power-law description and war-

rants further investigation. In a next step, we are installing further screens to reduce shear present in the flow. In collaboration with Prof. Lex Smits from Princeton University, we will use micro-machined hot-wires that should resolve the smallest scales. These measurements will be combined with particle tracking measurements of acceleration. We will also install the active grid, which will likely provide Taylor Reynolds numbers up to 8000, also resolved by the Princeton micro hot-wires. The Reynolds number space reached with the passive and active grids will overlap.

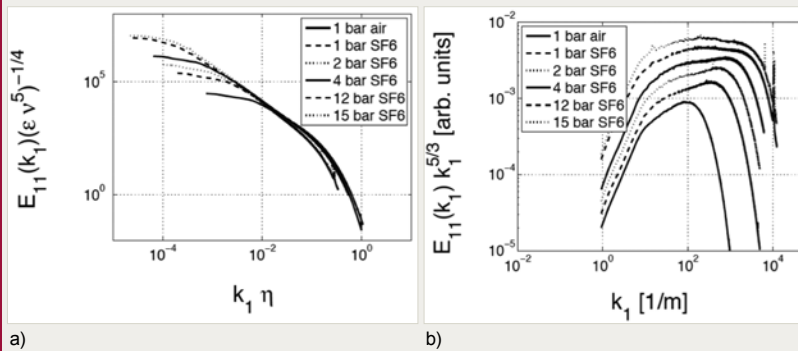


Figure 1 Power spectra of the streamwise velocity fluctuations. In (a), the 1D-spectra are normalized by the Kolmogorov scale η . This should cause the dissipative scales of the spectra to collapse, which they do, except for the spectra corresponding to the two largest Reynolds number experiments. In those two cases, the Kolmogorov scale was much smaller than the probe size. In this figure, the higher Reynolds number data extend further to the left. In (b), the spectra are compensated by Kolmogorov's scaling prediction. In these units, the probe size corresponds to a value of about 10^4 . For clarity, the spectra are shifted vertically by a multiplicative factor. The Reynolds numbers are larger for curves that are higher in the figure.

Working fluid	Pressure [Bar]	ρ [kg/m ³]	ν [10 ⁻⁶ m ² /s]	U [m/s]	u' [m/s]	ϵ [m ² /s ³]	R_λ	η [μm]	τ_η [ms]
Air	1	1.29	14.0	5.1	0.12	0.0080	148	806	43
SF ₆	1	5.96	2.56	5.0	0.10	0.0089	294	215	18
SF ₆	2	12.1	1.27	5.2	0.12	0.014	441	111	9.7
SF ₆	4	24.7	0.620	5.1	0.11	0.0098	624	70	8.0
SF ₆	12	82.9	0.190	5.2	0.13	0.013	1285	27	3.9
SF ₆	15	108	0.149	5.2	0.13	0.0099	1706	24	3.9

Table 1

A list of the conditions under which experiments were performed. ρ is the mass density of the fluid, ν is the kinematic viscosity, U is the speed of the mean flow, u' is the fluctuation in the direction of the mean flow, ϵ is the energy dissipation rate per unit mass, and $\eta=(\nu^3/\epsilon)^{1/4}$ and $\tau_\eta=(\nu/\epsilon)^{1/2}$ are the Kolmogorov length and time that characterize the dissipative scales. In the calculation of $R_\lambda=u'\lambda/\nu$, we determined the dissipation rates, ϵ , through Kolmogorov's 4/5ths law and the Taylor scale through the isotropic relation $\lambda_g=(15\nu u'^2/\epsilon)^{1/2}$ [1]. The normalized dissipation rate, $\epsilon L/u^3$, is approximately equal to $1/2$ for all of the data.

[1] Frisch, U., "Turbulence: the legacy of A.N. Kolmogorov", Cambridge University Press, Cambridge (1995)
 [2] X. Shen, Z. Warhaft, *Phys. Fluids* **12**, 2976 (2000)
 [3] K. R. Sreenivasan, B. Dhruva, *Prog. Theor. Phys. Supp.* **130**, 103 (1998)
 [4] G. Comte-Bellot, S. Corrsin, *J. Fluid Mech.* **25**, 657 (1996)
 [5] T. D. Dickey and G. L. Mellor, *J. Fluid Mech.* **99**, 13 (1980)
 [6] C. M. White, A. Karpets, K. R. Sreenivasan, *J. Fluid Mech.* **452**, 189 (2002)
 [7] A. L. Kistler and T. Vrebalovich, *J. Fluid Mech.* **26**, 37 (1966)
 [8] L. Mydlarski, Z. Warhaft, *J. Fluid Mech.* **358**, 135 (1998)
 [9] D. A. Donzis, K. R. Sreenivasan, *J. Fluid Mech.* **657**, 171 (2010)

I-5 Göttingen Turbulence Facility

G. Ahlers, G. Bewley, E. Bodenschatz, F. Di Lorenzo, M. Gibert, S. Lambertz, H. Nobach, E.-W. Saw, H.-D. Xi, H. Xu
 D. Funfschilling (ENSIC Nancy, France), Z. Warhaft (Cornell University, USA), A. Tsinober (Imperial College, GB),
 Researchers from ICTR: International Collaboration for Turbulence Research – www.ictr.eu

INVESTIGATIONS OF the fundamental properties of turbulence require flows with high Reynolds numbers under well-controlled conditions. The flow properties need to be resolvable by modern measurement technology from the largest to the smallest spatial and temporal scales. On Earth the highest turbulence levels (Reynolds numbers $\sim 10^7$) are found in the atmospheric boundary layer. Even the most violent flows on Earth, such as plinian volcanic eruptions, have similar turbulence levels. The observations of natural flows are difficult, as the conditions are rarely stationary and the scales of the flow are very large, which makes detailed measurements utmost difficult. For example, when considering the turbulent motion of clouds in the atmospheric boundary layer, the largest scales of the flow are typically 100 m, while the smallest scales are fractions of millimeters. Another complication is that clouds are carried by a mean wind. With current measurement technology it is very difficult, if not impossible, to resolve all scales of the dynamics of turbulent clouds. Finally, the turbulence generation mechanisms in nature are multifold and it is difficult to investigate how the turbulence depends on its generation mechanisms. In the foreseeable future computational fluid dynamics can substitute experiments only for moderate Reynolds numbers at idealized flow conditions. Therefore, experimental facilities that generate turbulent flows at high Reynolds numbers are essential for the research.

High Reynolds numbers at manageable temporal and spatial scales can be realized by employing the principle of physical self-similarity. The turbulence Reynolds number is $Re = \rho v L / \eta$, where ρ is the density of the fluid, v is the fluctuating velocity, L is the energy injection scale and η is the molecular dynamical viscosity. One

way to achieve high Reynolds numbers is to use cryogenic helium gas. In this case very high Reynolds numbers can be achieved, but with very small spatial and temporal scales that currently cannot be fully resolved by measurement technology. In addition, many methods well tested at room temperature are difficult to use at cryogenic temperatures. An alternative to cryogenic helium is to increase the density of room temperature gas by pressurizing it. This increases the Reynolds number, as the molecular dynamical viscosity is approximately independent of pressure. In addition, by using a heavy gas, like sulfur hexafluoride (SF_6) it is possible to reach high Reynolds numbers already at moderate pressures of only 10-20 bar. In Göttingen we have decided to follow this path. The institute installed a gas handling and liquefaction system that handles and stores 13 tons of SF_6 and supports three facilities that use pressurized SF_6 gas at up to 19 bar. In addition to serving the in-house experimentalists, the GTF provides visitors with the opportunity to study phenomena in turbulent flows under well-controlled conditions at high Reynolds and Rayleigh numbers.

The properties of turbulence can either be measured from the spatial (Eulerian) perspective, or from the perspective of particles carried by the flow, the so-called Lagrangian perspective. While Eulerian measurements have traditionally been conducted in wind tunnels with hot-wire anemometry, only recently it has become possible to conduct Lagrangian measurements with high accuracy at high Reynolds numbers thanks to advances in imaging technology. For Lagrangian Particle Tracking, neutrally buoyant particles are tracked in three dimensions with three to four high-speed cameras by stereoscopic imaging of



Figure 1

The Building: The facilities are housed in a newly constructed building that has been optimized for vibration isolation and high temperature stability. It has been equipped with control systems that make possible the safe use of the pressurized gases and of lasers. High bandwidth fiber optics link the facilities to an 80 processor data analysis cluster. A 36m² class 1000 clean room is available for micro fabrication of sensors, like the hot-wire probes needed for the Eulerian measurements in the Variable Density Turbulence Tunnel.

a laser-illuminated measurement volume. In the wind tunnel, the system will be mounted on a sled, moving with the mean velocity of the wind tunnel flow (up to 5m/s), driven by a linear motor from Bosch Rexroth. At a frame rate of tens of kHz, the data acquisition is limited by the camera on-board memory to one or two seconds observation time followed by

a data transfer of 15 min to a computer cluster through a Gigabit Ethernet for post processing. To overcome these limitations we are developing a real-time processing system based on an optical Real-Time Output (RTO) of the cameras from Vision Research's Phantom V-Series. The system allows a higher transfer rate (2.125 GB/s for Phantom V640) and features a customer-modified receiver system for the RTO based on the X5-TX from Innovative Integration (PCIe-D/A card with an Virtex 5 SX95T FPGA from Xilinx), which we re-programmed to perform data compression of about 90%. This system will allow us to investigate, for example, the slowly varying large scale dynamics or transient states of a turbulent flow recovering from anisotropic perturbation real-time and non-stop.

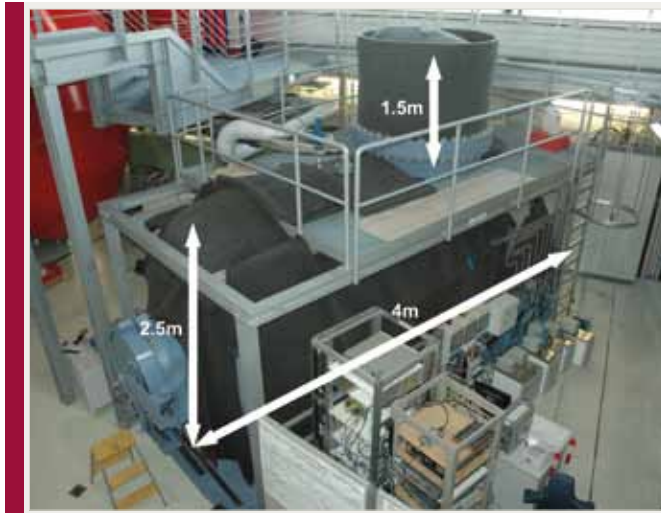
A test system of high-speed cameras and a communication system have been installed in the Pressure Cylinder (figure 4) as preparation for future experiments. A particle (droplet) generation device using the principle of controlled condensation, and a "proof of concept" experiment involving Lagrangian particle tracking within high pressure SF₆ is in preparation.



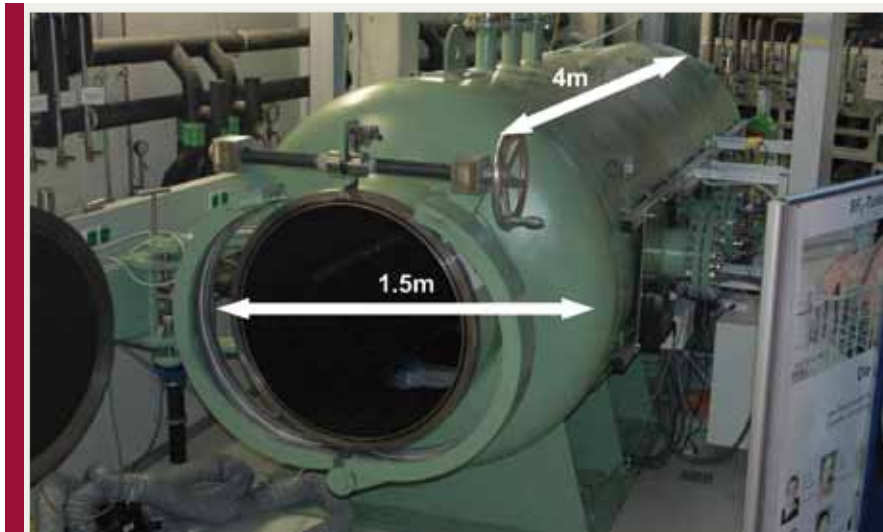
Figure 2

The Variable Density Turbulence Tunnel is an upright recirculation wind tunnel with two long measurement sections (7 and 9 m long with a cross-sectional area of 1.9 m²) that make possible particle tracking in the decaying turbulence behind passive or active grids, mounted at the entrance of each measurement section. Our active grid is unique in that each of 129 position-controlled paddles can be moved independently. This may allow us to vary the mean velocity, the amplitude of the fluctuations, or the correlation lengths over the cross section of the tunnel. We can then study turbulence under various conditions of the large scale, such as homogeneous shear or mixing across a turbulence-intensity interface, as well as transitions between different large scale conditions. Reynolds numbers of up to Re~10⁷ are possible when filled with SF₆ at 15 bar. Two sleds, driven by linear motors can be installed that allow measurement devices (e.g. cameras and optics) to be moved with the mean velocity of up to 5 m/s of the circulating gas. The tunnel is pressure and temperature controlled, and has optical and electrical access. The circulating gas can be filtered to <1 μm in order to provide a clean gas. Equipment can be installed either on the sleds

or all along the measurement sections. Measurement equipments to be used in the tunnel are hot wires, high-speed cameras and LDV/PDA system. Specifications: length 18 m, height 6 m, inner diameter 1.8 m, pressure 1 mbar-15 bar, temperature 20-35°C, mech. power 210 kW, cooling power 280 kW, kin. visc. SF₆ (15 bar) 1.5×10⁷ m²/s, $\langle u \rangle_{\max} = 5$ m/s, $u_{\text{rms,max}} = 1$ m/s, $L_{\text{max}} = 0.45$ m, $R_{\lambda,\text{max}} \sim 10^4$, $\epsilon_{\text{max}} = 1.4$ W/kg, $\eta > 8$ μm, $\tau_{\eta} > 0.4$ msec.

**Figure 3**

The High Pressure Convection Facility (U-Boot) is a general-purpose pressure vessel. Similarly to the turbulence tunnel, all equipment can be used inside the vessel for measurements from heat transport and PIV to 3D-Lagrangian Particle Tracking (LPT). It has been designed to house different experiments e.g. for the investigations in Lagrangian mixers and of turbulent thermal convection. It houses a turbulent cylindrical Rayleigh-Benard experiment of 1.1m diameter and 2.2m height that reaches Rayleigh numbers as large as $Ra \sim 10^{15}$. Specifications: length 5.3m, max. height 4.0m, outer diameter 2.5m, straight cylinder length 4m, dome 1.5m high and 1.2m in diameter, pressure 1mbar-20bar, temperature: 20-35°C, cooling power <math> < 50\text{kW}</math>, $Ra_{\text{max}} = 7 \times 10^{14}$ at high Ra only weakly non Boussinesq.

**Figure 4**

The Pressure Cylinder (Cigar) is a general-purpose pressure vessel. Similarly to the turbulence tunnel, all equipment can be used inside the vessel for measurements from heat transport and PIV to 3D-Lagrangian Particle Tracking (LPT). Specifications: inner diameter 1.5m, length 4.0m, two accesses.

**Figure 5**

Gas Handling System consisting of 4 tanks, 2.8m³ each, height 4m, diameter 1m, oper. pressure 1mbar-15bar, evacuation of tunnel air (1bar→1mbar) 2.5h, pressurizing SF₆ (1mbar→20bar) 8h, depressurizing SF₆ (15bar→1mbar) 22h, filling with air (1mbar→15bar) 1h.

I-6 Rayleigh-Bénard Turbulence

G. Ahlers (UCSB, USA), E. Bodenschatz, D. Funfschilling (Nancy, Fr), X. He, H. Nobach, F. Winkel

TURBULENT CONVECTION in a fluid heated from below and cooled from above (Rayleigh-Bénard convection, RBC) has been at the center of scientific inquiry for a long time [1]. The reasons are twofold – on the one hand, RBC serves as a model system for buoyancy driven convection as found in numerous astrophysical, geophysical, atmospheric, and industrial processes – on the other hand, it is a model for a system, where the large-scale turbulent properties are dominated by the dynamics of thin boundary layers. One important question of interest is the dependence of the heat transport, *i.e.*, the Nusselt number Nu , on the dimensionless temperature difference, the Rayleigh number Ra , in the limit of large Ra . It is expected theoretically that this dependence may change from an effective power law with exponent $Y_{\text{eff}} \cong 0.31$ to one with $Y_{\text{eff}} \cong 0.39$; this change is predicted to be associated with a transition of the viscous boundary layers at the plates from laminar to turbulent [1]. This is of importance as an extrapolation of laboratory measurements to astrophysically and geophysically relevant ranges requires an understanding of $Nu(Ra)$ well above this transition. Such extrapolations at present are uncertain by orders of magnitude as nominally equivalent laboratory experiments using helium gas at temperatures near 5 K and in the range $Ra \leq 10^{15}$ [2] or $Ra \leq 10^{17}$ [3] disagree on whether there is a transition [2] or not [3]. The uncertain situation described above motivated us to construct a very large convection sample cell, located in an even larger pressure vessel known as the Uboot [4]. This experiment has a cylindrical shape with 1.12m diameter and 2.24m height. The top and bottom plates are made of oxygen-free copper, and the sidewall is made of Plexiglas. The Uboot, and with it the sample cell, can be filled with a suitable gas, usually sulfur hexafluoride, at pressures up to 19 bars; this gas served as the convection

fluid. We investigated two situations, one, the *open sample*, where the Plexiglas sidewall had a 1mm gap at the bottom and top plate, thus permitting a high impedance in/out flow; two, the *closed sample*, where the bottom and top were hermetically sealed. Measurements with the open sample, which had been reported in [4, 5], are shown in figure 1a. The Nusselt number itself varied by over an order of magnitude over our Ra range and is difficult to display with adequate resolution. Thus we show the reduced Nusselt number $Nu/Ra^{0.3}$. The various symbols and colors correspond to various sample pressures and operating conditions. The lower (upper) branch was attained when the mean sample temperature T_m was higher (lower) than the Uboot temperature T_U . Values of Nu between the two extremes could be attained as well by changing $T_m - T_U$, but the data shown correspond reasonably well to the largest and smallest values that could be reached. It was tentatively concluded that this bistability, or stability range, might be due to a “chimney effect” [5]. It is unclear why such a small perturbation should cause such dramatic changes of the heat transport, by a factor of 1.7 or so at the largest Ra . Apparently the system becomes extremely sensitive to external perturbations at these large values of Ra . We therefore investigated a *closed sample*, where the “chimney effect” was excluded. The data obtained are shown in figure 1b as colored symbols. Also shown there, for comparison, are the data from figure 1a, but these data are now given as black symbols. We see that the upper branch is similar to that found for the *open sample*; but the lower branch now is much higher; *i.e.*, the dependence of Nu upon $T_m - T_U$ is much smaller. However, a difference between the upper and lower branches prevails. Further experiments suggest that the behavior may be similar to a phase transition in the presence of an external field. The upper branch,

both for the open and the closed sample, shows $Nu \sim Ra^{0.36}$, which is significantly larger than the value near 0.31 obtained from numerous measurements at lower Ra , but a bit smaller than the value 0.38 associated with the high- Ra regime predicted by Kraichnan [1]. The lower branch, on the other hand, is fit well by an effective power law with $Y_{\text{eff}} = 0.318$, which is quite consistent with effective exponents obtained in numerous smaller- Ra measurements. We note with interest that a possible theoretical explanation for the existence of different branches of $Nu(Ra)$, with values for Y_{eff} in the range from about 0.14 to about 0.38, has been given in a recent paper by Grossmann and Lohse [6]. We are currently constructing an experiment with equal diameter and height to test the dependence on aspect ratio. This experiment will be mounted inside the

Uboot on a rotating table. Thus it will also allow the investigation of the influence of rotation on the turbulent heat transport.

One aim of our investigations is to extend our work to the study of moist turbulent convection. Currently we are exploring turbulent moist convection at moderate Rayleigh numbers in an aspect ratio width/height = 3 convection cell. As working fluid we employ a binary gas mixture of SF_6 and He near the critical pressure and temperature of SF_6 . We conjecture that SF_6 droplets form by homogeneous nucleation below the upper cold plate and that above a He rich layer accumulates that prevents the condensation of SF_6 on the cold plate. This effect will, however, compete with the enrichment of the heavier SF_6 at the cold top plate due to thermo diffusion and only the experiments can test the conjecture.

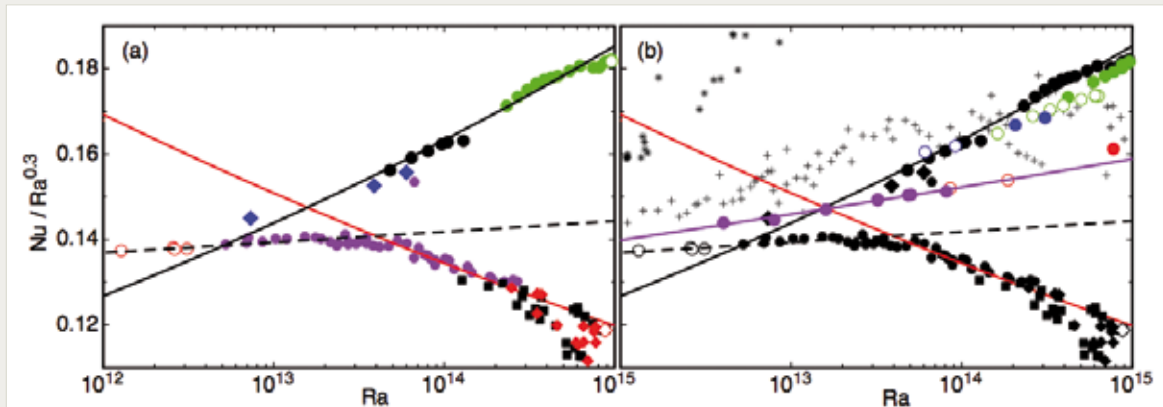


Figure 1

The reduced Nusselt number $Nu/Ra^{0.3}$ as a function of the Rayleigh number Ra on a logarithmic scale. The dashed, solid red, and solid black lines correspond to $Y_{\text{eff}}=0.308$, 0.250, and 0.355. The purple solid line corresponds to $Y_{\text{eff}}=0.318$. (a): Data from the open sample. The various symbols and colors are for data taken at various pressures and operating conditions. The data on the upper (lower) branch were obtained at a mean temperature T_m of about 21°C (25°C). (b): The data from the *open sample* are shown again as black symbols. The blue, green, purple, and red symbols are from the *closed sample*. The green and blue data are for $T_m \cong 21^\circ\text{C}$ and are close to the upper branch of the open sample; the purple and red data are for $T_m \cong 31^\circ\text{C}$. They are much higher than the lower branch of the “open” sample but still below the upper branch. The black pluses are data from Ref. [3]. The black stars are from [2] as tabulated in [7]. For this data $T_U \cong 24^\circ\text{C}$.

- [1] G. Ahlers, S. Grossmann, and D. Lohse, *Rev. Mod. Phys.* **81**, 503 (2009)
- [2] X. Chavanne et al., *Phys. Rev. Lett.* **79**, 3648 (1997)
- [3] J. Niemela et al, *Nature* **404**, 837 (2000)
- [4] G. Ahlers, D. Funfschilling, and E. Bodenschatz, *New J. Phys.* **11**, 123001 (2009)
- [5] G. Ahlers, D. Funfschilling, and E. Bodenschatz, *New J. Phys.* **13**, 049401 (2011)
- [6] S. Grossmann and D. Lohse, *Phys. Fluids* **23**, 045108 (2011)
- [7] X. Chavanne et al., *Phys. Fluids* **13**, 1300 (2001)

I-7 Turbulence in Atmospheric Flows

H. Xu, E. Bodenschatz
S. Risius, A. Pumir (ENS-Lyon, France)

A CENTRAL ASSUMPTION in the classical Kolmogorov 1941 (K41) theory is the decoupling between the large, forcing scales, which are flow dependent, and the small, universal scales present at “sufficiently large” Reynolds numbers. Most laboratory flows are limited to moderate Taylor micro-scale Reynolds number $R_\lambda \leq 10^3$ and by carefully designing the turbulence generation mechanisms they try to minimize the effect of the large-scale flow on the small-scales. Atmospheric flows provide a high Reynolds number alternative for the study of the K41 hypothesis, however, with the caveat that, at the forcing scales, they depend strongly on the environment. Here we report examples from our year-long measurement campaign of the turbulent boundary layer at the Environmental Research Station Schneefernerhaus (UFS) at an elevation of 2700 m.

As shown in figure 1, our experimental setup consists of five ultrasonic anemometers that are arranged to form two nearly regular tetrahedra, on the roof of the Environmental Research Station Schneefernerhaus (UFS) near the top of Zugspitze, the highest mountain in Germany. For over a year, sampling synchronously at 10 Hz these sensors have been measuring the three components of the wind velocities and the (virtual) temperature. The distances between the sensors are approximately 2 m, well with-

in the inertial range of the turbulent flow at UFS. We first examined the turbulence measured from the top sensor only, which is located approximately 6 m above the roof of UFS. As shown exemplarily in figure 2, the Eulerian velocity structure functions, measured with Taylor’s frozen turbulence hypothesis, demonstrate a well-developed inertial range. Note that the dissipative scales are not resolved due to the size of the sensors. We determine the energy dissipation rate ϵ by fitting the structure functions to the inertial range $r^{2/3}$ scaling. The dissipation rate normalized by the integral scale L and the fluctuating velocity u , $C_\epsilon = \epsilon L/u^3$, is believed to be a constant and has been studied in various flows [1-3]. We found that for $1500 \leq R_\lambda \leq 3500$, C_ϵ remained constant at approximately 0.5 (see figure 3a). The value of $C_\epsilon \approx 0.5$ agrees well with recent results from laboratory flows at $R_\lambda \leq 1200$ [3]. In figure 3, we distinguished winds coming from the east to those from the west, which are the two dominant wind directions at UFS. The difference in topography between the two directions results in different values of C_ϵ . As a measure of large-scale anisotropy, we plot in figure 3b the invariants of the Reynolds stress tensor on the so-called “Lumley-triangle” [4]. The flow is clearly anisotropic as expected for a boundary layer flow. It is interesting to note that in general the flow coming from the east is more iso-



Figure 1

The ultrasonic anemometers located at UFS, Zugspitze, Germany. The measurement station is approximately 2700 m above sea level.

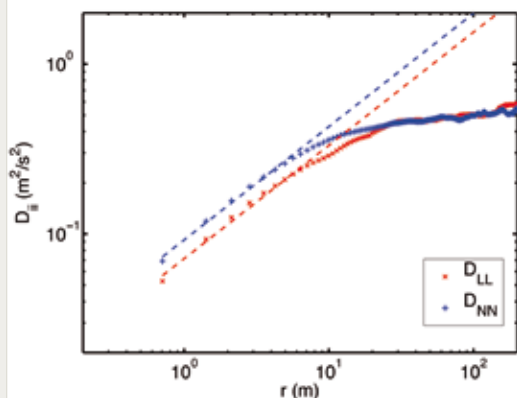


Figure 2

An example of Eulerian velocity structure functions measured by the top sensor, using Taylor's frozen flow hypothesis. The measurements consisted of 11 quasi-steady flow events between September and December 2010, which were coming from the west ± 30 degrees, had a mean speed of 7 ± 0.1 m/s and had been steady for at least 2 minutes (equivalent to 56 large-eddy sweeping times). The dashed lines are the fitted $r^{2/3}$ laws, from which the energy dissipation rate was determined to be $6.1 \times 10^{-3} \text{ m}^2/\text{s}^3$. The Reynolds number of the flow, defined as $R_\lambda \equiv (15uL/\nu)^{1/2}$, was 2420.

tropic than that from the west. Moreover, when R_λ increases, the flow from the east shows a tendency to become more isotropic, while the flow from the west deviates more from isotropy. This is most likely due to the influence of the building structure and the closer vicinity of the mountain on the west side of the measurement site. It is worth to point out, however, that the degree of large-scale isotropy of the atmospheric flow at UFS is comparable to, and often better than, that of the often-used von Kármán swirling laboratory flow (not shown).

We are now studying the influence of the larger-scale flows on the inertial ranges by investigating multi-point Eulerian statistics. This includes the statistics of passive scalar fluctuations, which are related to the spatial structure of the flow [5, 6], and the velocity dynamics using the tetrad model proposed by Chertkov et al. [7]. This way we hope to gain further insights into the generic features of real world turbulence and to better understand how theoretical models, simulations and findings from laboratory experiments can be applied to flows found in the "real" world.

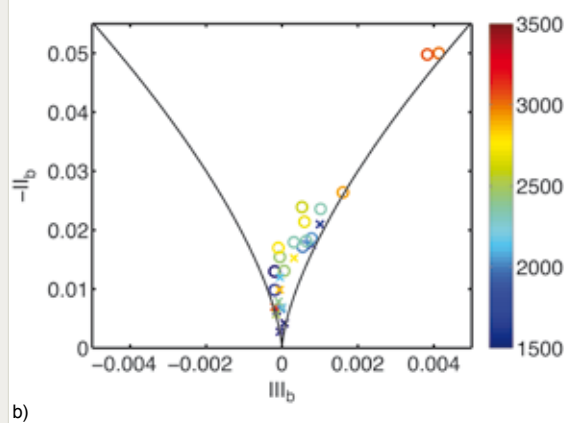
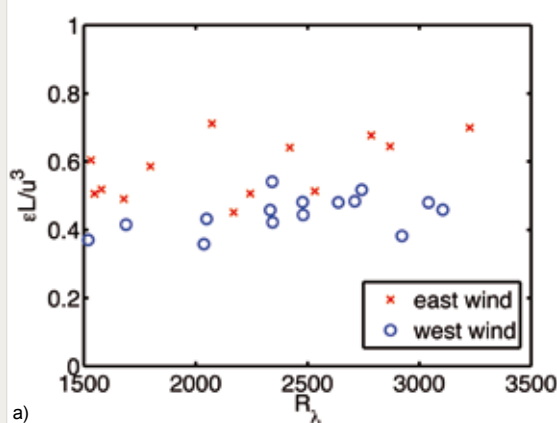


Figure 3

(a) Normalized energy dissipation rate C_ϵ as a function of R_λ . The circles are for winds coming from the west and the crosses are for winds coming from the east. (b) The invariants of the Reynolds stress tensors shown on the "Lumley triangle". Points closer to the origin represent flows more isotropic. As in (a), circles and crosses stand for flows from the west and the east, respectively. The symbols are color coded with the Reynolds number R_λ , as shown by the colorbar on the side.

- [1] K. R. Sreenivasan, *Phys. Fluids* **10**, 528 (1998)
- [2] B. R. Pearson, P.-Å. Krogstad, and W. van de Water, *Phys. Fluids* **14**, 1288 (2002)
- [3] P. Burattini, P. Lavoie, and R. A. Antonia, *Phys. Fluids* **17**, 098103 (2005)
- [4] J. L. Lumley and G. R. Newman, *J. Fluid Mech.* **82**, 161 (1977)
- [5] L. Mydlarski, et al., *Phys. Rev. Lett.* **81**, 4373 (1998)
- [6] Z. Warhaft, *Annu. Rev. Fluid Mech.* **32**, 203 (2000)
- [7] M. Chertkov, A. Pumir, and B.I. Shraiman, *Phys. Fluids* **11**, 2394 (1999)

I-8 Rain in a Test Tube

J. Vollmer, B. Hof

I. Benczik, T. Lapp, M. Wilkinson (Open University, UK)

IN NATURE and technology one commonly encounters situations where a mixture is subjected to a slow temperature change, which drives it deeper into the phase-coexistence region. The (equilibrium) thermodynamic response to such a driving is a mass exchange between the phases. For a binary mixture the hydrodynamic transport equations describing such a flow [1] have been formulated in terms of the ratio $\varphi(\mathbf{x},t) = \phi(\mathbf{x},t) / \phi_0(T(t))$ of the local concentration $\phi(\mathbf{x},t)$ and its expected equilibrium value $\phi_0(T(t))$ for the temperature $T(t)$. The normalized density evolves according to the well-established advection diffusion equation, except that this equation is augmented now by a source term which takes the form of an exponential decay of the normalized density away from its equilibrium values ± 1 . The decay rate ξ is a function of the peculiarities of the temperature protocol the system is subjected to. In tailored laboratory experiments care may be taken however to fix ξ to an almost constant value [2, 3].

For $\xi \leq (\sqrt{3}-1)^2 D/\Lambda^2$ a system with equilibrium diffusion coefficient D and relevant spatial scale Λ for diffusive transport can follow a spatially uniform change of temperature by setting up a steady-state diffusion current. For laboratory systems there only is some little convection as long as the inequality holds even when Λ amounts to the system size. For larger values

of ξ the system becomes unstable with respect to the nucleation of new droplets [4].

For mixtures of methanol and hexane filled into a test tube the critical heating rate turns out to be about one Kelvin per hour [4]. Experimental systems heated with slightly larger heating rates go through repeated cycles of droplet nucleation, coarsening and precipitation, with typical periods of the order of an hour [3]. This finding might be of considerable relevance for the microphysics of clouds since the values of ξ encountered in thunderstorm clouds appear to be very similar to the ones used in the laboratory experiments, and since the time scales for the growth of small (cloud) droplets to large (rain) droplets appear to be very similar to typical oscillation periods in the laboratory experiments, too.

A key observation to strengthen this relation is that the time scales are hardly affected by the flow [3]. To clarify the role of the convection strength on the demixing dynamics, we adopted a reactive flow approach [5]. To this end we follow (numerically and based on working our rate equations) the evolution of the composition field in the framework of an advection-reaction-diffusion model with superimposed nucleation and coagulation of droplets. In agreement with the experimental findings, the model shows an oscil-

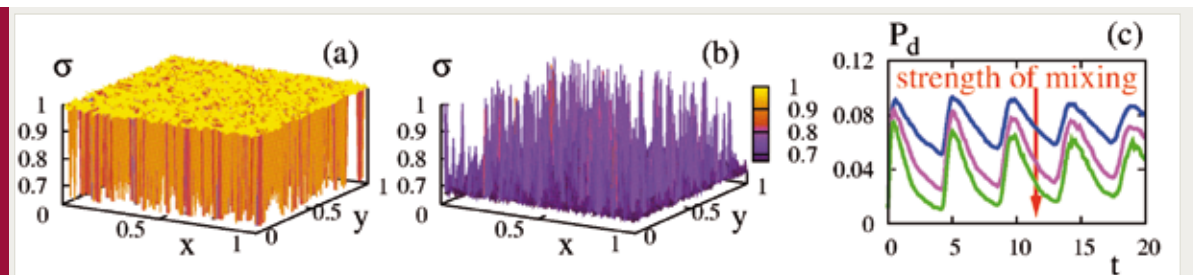


Figure 1

(a) Snapshots of the composition field at $t=2$ (a) and $t=40$ (b) for $\xi = 0.01$ and $A = 0.8$. The simulation has been started with no droplets and a supersaturation close to the spinodal composition. (c) Oscillations of the droplet density for $\xi = 0.01$ and different flow rates: $A=0.8$ (blue line), $A=2.4$ (red line), and $A=6.4$ (green line).

latory variation of the composition field (figure 1a and b) in which no spatial structures are found. Moreover, the model also shows that the features of the macroscopic flow do not have significant effects on the frequency of the oscillations (figure 1c), excluding hydrodynamic instabilities as the possible origin of the oscillations. Currently we use this framework to explore the influence of the concentration diffusivity on shape and ξ dependence of the oscillations. Further processes will be added one at a time. To gain insight into the dominant processes in the experiments we follow the demixing of iso-butoxyethanol and water with high-resolution

imaging [6] that admits to resolve the motion of individual droplets (figure 2a). This mixture is amenable to high precision experiments since it has a lower miscibility gap with a critical temperature slightly above room temperature, and since droplets can be marked by fluorescent dye. We observe a very broad size distribution of droplets (figure 2b) where the smallest droplets can be regarded as tracer particles for the flow and the largest show a constant Stokes sedimentation velocity according to their respective size. Particle tracking based on a tailor made code, allows us to simultaneously resolve droplet size as well as droplet and flow velocities.

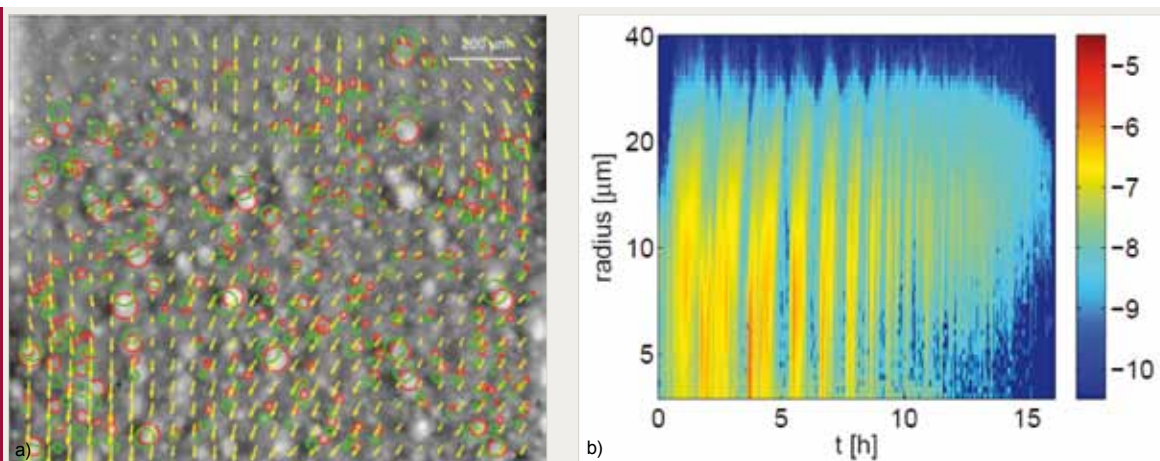


Figure 2

(a) Snapshot of a picture with iso-butoxyethanol droplets in a mixture of iso-butoxyethanol and water. The arrows correspond to the flow field, the red circles mark the droplets found in the image and the green circles their position and radius in the next image. (b) Size distribution of the droplets for a mixture subjected to a temperature ramp with $\xi = 1.05 \times 10^{-5} \text{s}^{-1}$. The droplet number density per radius, in units μm^{-4} , is color coded on a decadic logarithmic scale as indicated to the right of the figure.

- [1] M.E. Cates, J. Vollmer, A. Wagner, D. Vollmer, *Phil. Trans. Roy. Soc. (Lond.) Ser. A* **361**, 793-807 (2003)
- [2] G.K. Auernhammer, D. Vollmer, J. Vollmer, *J. Chem. Phys.* **123**, 134511 ()
- [3] J. Vollmer, G.K. Auernhammer, D. Vollmer, *Phys. Rev. Lett.* **98**, 115701 (2007)
- [4] J. Vollmer, *J. Chem. Phys.* **129**, 164502 (2008)
- [5] I.J. Benczik, J. Vollmer, *EPL* **91**, 36003 (2010)
- [6] M. Rohloff, T. Lapp, J. Vollmer, B. Hof: "Particle tracking for polydisperse sedimenting droplets" (in preparation)

I-9 Phase Transitions in driven Granular Systems

S. Herminghaus, M. Brinkmann, J. Vollmer

K. Huang, Z. Khan, A. Fingerle, K. Roeller, M. Scheel, H. Ebrahimnezhad Rahbari

COLLECTIVE PHENOMENA in systems consisting of a large number of coupled similar sub-systems are at the same time ubiquitous and of great fundamental interest. In the realm of thermal equilibrium, these phenomena are comprehensively described by the theory of phase transitions and critical phenomena. Of particular importance, however, are systems far from thermal equilibrium, such as social systems, biological tissue, or large computer networks, which are not covered by these concepts. Granular matter, which breaks detailed balance at the microscopic scale, provides a well accessible model system to study collective phenomena in strongly driven systems. External driving is necessary to balance the energy which is lost into the atomic degrees of freedom. The fact that phenomena very similar to equilibrium phase transitions (such as melting or liquid-gas coexistence, cf. figure 1) are observed in driven granular systems suggests to systematically compare these effects to their equilibrium counterparts, in order to obtain deeper insight into possible common aspects of systems far from thermal equilibrium. We investigate phase transitions and critical phenomena in dry and wet granular matter by means of experiments, simulations, and by analytic theory.

We concentrate on simplified granulates which consist of spherical grains of approximately

equal size. In experiments, we use sub-millimetric glass spheres, while in simulations the grains are assumed to be perfect spheres, with rotational degrees of freedom neglected. It turned out that these simple model systems account very well for the complex behavior of dry and even wet granular matter [1-3]. For the wet case, we use a simple capillary force model, the main feature of which is the hysteretic nature of the force. This results in the loss of a well defined amount of energy at each impact, as opposed to dry granulates, where each impact is associated with the loss of a certain percentage of it. We could show that this simple capillary model, which assumes a two-body force only, correctly describes the physics even at a liquid content where most of the capillary bridges have already merged to form larger or liquid clusters. This amazing result can be understood by some simple geometric arguments, and turns out to be applicable even to non-spherical grains [4, 5]. Furthermore, we found that the particular form of the two-body force is of minor relevance. For the location of the liquid-gas phase boundaries, for instance, only the amount of energy lost at each impact and the finite rupture distance of the capillary bridges is relevant [6-8]. In particular, we can use a hysteretic interaction 'potential' of triangular shape (corresponding to a piecewise constant force) as well as of rectangular shape (figure 2). The latter corresponds to

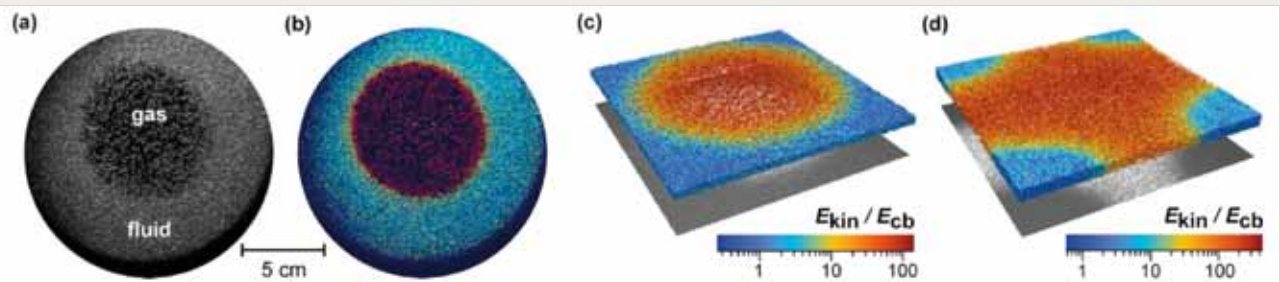


Figure 1

(a) Top view of a closed Petri dish containing glass beads (bright dots) wetted by water, under vertical agitation. (b) Same as (a), but colored according to the granular temperature as determined by optical time correlation. (c) Event-driven simulation of the experiment with a minimal capillary model. (d) Same as (c), after the 'bubble' has reached the boundary, and rearranged to minimize the fluid/gas interface.

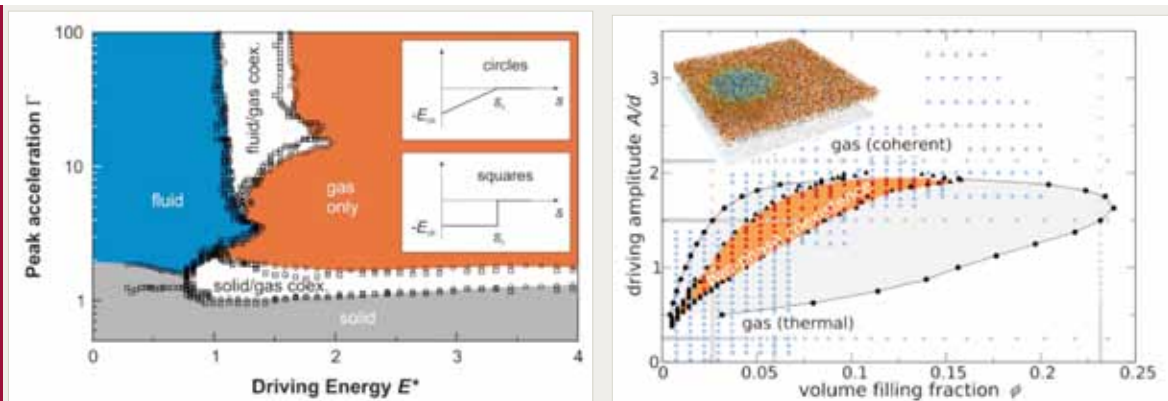


Figure 2

Left panel: the phase diagram for wet granular matter under vertical excitation, as revealed by dynamical simulations with two strongly different hysteretic interaction potentials (insets). Clearly, the shape of the potential is almost irrelevant for the location of the phase boundaries. Right panel: the phase diagram for fluid-gas coexistence in a dry granulate under vertical agitation. A spinodal and a binodal line, as well as a critical point are clearly observed.

forces occurring only on a set of zero measure on the time axis. It thereby enables event-driven simulation, which speeds up computation enormously. We successfully applied this model to several settings, including the yielding of wet granular piles under shear [9-11].

The wide range of validity of the two-body force model and thus its adequacy to describe experimental results suggests to use these systems to investigate the impact of microscopic non-equilibrium on phase transitions in general. As a paradigm, we consider liquid-gas coexistence, which we found in both wet and dry granular matter, and which is known as well from usual van der Waals

gases. Our general method is now to use simulations for investigating quantitatively several physical aspects of phase transitions in cohesive and dissipative systems. These simulations are validated wherever possible by experiments. We thereby interpolate smoothly between systems far from equilibrium and systems arbitrarily close to equilibrium. We investigate the change of critical exponents, entropy production, interfacial tension etc. as we traverse the plane spanned by cohesiveness and dissipation (figure 3). The goal is to pin down which concepts from equilibrium statistical physics carry over to systems far from equilibrium, and which do not.

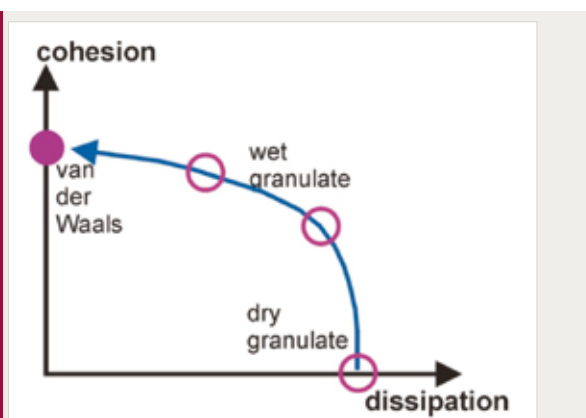


Figure 3

The various systems under study may be depicted in a plane spanned by the cohesiveness and the dissipation of the particle interactions. A van der Waals gas is cohesive, but conservative, while a dry granulate has dissipation, (restitution coefficient less than unity) but no cohesion. Wet granulates, which dwell in the plane, can serve to interpolate between both extremes and to pin down peculiarities of non-equilibrium systems.

- [1] A. Fingerle, S. Herminghaus, "Equation of State of Wet Granular Matter", *Phys. Rev. E* **77**, 011306 (2008)
- [2] S. Ulrich et al., "Cooling and Aggregation in Wet Granulates", *Phys. Rev. Lett.* **102**, 148002 (2009)
- [3] S. Ulrich et al., "Dilute wet granular particles: non-equilibrium dynamics and structure formation", *Phys. Rev. E* **80**, 031306 (2009)
- [4] M. Scheel et al., "Morphological Clues to Wet Granular Pile Stability", *Nature Mater.* **7**, 189 (2008)
- [5] M. Scheel et al., "Liquid distribution and cohesion in wet granular assemblies beyond the capillary bridge regime", *J. Phys.: Condens. Matter* **20**, 494236 (2008)
- [6] A. Fingerle, K. Roeller, K. Huang, S. Herminghaus, "Phase Transitions Far from Equilibrium in Wet Granular Matter", *New J. Phys.* **10**, 053020 (2008)
- [7] K. Huang, M. Sohaili, M. Schröter, S. Herminghaus, "Fluidization of granular matter wetted by liquid 4He", *Phys. Rev. E* **79**, 010301(R) (2009).
- [8] K. Huang, K. Roeller, S. Herminghaus, "Universal and non-universal aspects of wet granular matter under vertical vibrations", *Eur. Phys. J.* **179**, 25 (2009)
- [9] S. H. Ebrahimpzad Rahbari, J. Vollmer, S. Herminghaus, M. Brinkmann, "A response function perspective on yielding of wet granular matter", *Europhys. Lett.* **87**, 14002 (2009)
- [10] K. Roeller, J. Vollmer, S. Herminghaus, "Unstable Kolmogorov Flow in Granular Matter", *Chaos* **19**, 041106 (2009)
- [11] S. H. Ebrahimpzad Rahbari, J. Vollmer, S. Herminghaus, M. Brinkmann, "Fluidization of wet granulates under shear", *Phys. Rev. E* **82**, 061305 (2010)

I-10 Ergodic Theory of Granular Fluids

J. Vollmer

K. Röller, J. Blaschke, F. Glassmeier, I. Fouxon (Tel Aviv University, Israel)

THE DYNAMICS of granular materials is out of equilibrium on a very fundamental level because the interaction between granular particles is governed by dissipative contact forces. As a consequence closed systems undergo free cooling [1]. Only open systems, where energy is injected, e.g. by tapping or shearing, can approach non-trivial steady states (e.g. [2]) where dissipation and energy input balance. In these out-of-equilibrium systems the inelastic and hysteretic particle interactions break time-reversal symmetry, and resulting correlations between velocities of near-by particles break the molecular chaos assumption. Consequently, the established theoretical framework to derive ensembles, thermodynamic relations, kinetic theory and hydrodynamic transport equations do not apply.

In spite of these fundamental differences to equilibrium systems, there are granular steady states closely reminiscent to solid, liquid and gas phases, and there even is phase coexistence with a well-defined surface tension. On the other hand, there is no equipartition. Consequently the rules to determine coexisting phases strongly differ from equilibrium systems. To explore the similarities and differences we study a hierarchy of model systems with increasing complexity which set the ground for an ergodic theory of granular matter.

The hysteretic interaction of the thin-thread model combines features of Hamiltonian and dissipative systems. Since the same amount of energy is lost in each collision, an ensemble of particles started with the same energy will remain an iso-energy ensemble when time is measured in terms of the number of collisions. To explore details of the resulting phase space structure we focus on two grains in a box with periodic boundary conditions [3].

We find that the phase-space volume shrinks due to folds emerging in regions where one can-

not decide whether a trajectory scarcely misses a disk or preforms a collision followed by a deflection due to breaking a capillary bridge formed after the collision (figure 1a). The folding gives rise to a filigrane fractal structure in the phase-space distribution. From the point of view of working averages for observables (which vary smoothly over phase space), it is sufficient to consider the coarse grained steady state density. As an example we predict the free cooling of this gas – cf figure 1b.

It is not at all obvious whether clustering still occurs when energy is injected into the granular gas represented by the Sinai billiard. In particular for sheared systems there are always regions in phase space where energy dissipation by far exceeds the energy injection such that the clustered state can be reached in a finite time. From this perspective clustering in the sheared granular gas amounts to an interesting example of transient chaos where the system is expected to settle into the absorbing state. Lees-Edwards boundary conditions provide a conceptually simple means to provide an energy flux mimicking shear flow. They provided us with a setting to explore under what conditions non-trivial, fluid-like steady states occur.

In numerical simulations we observe asymptotic states where the average energy grows linearly in time (figure 2a), and the energy distributions take a close to exponential form (figure 2b). For such a distribution the standard deviation agrees with the mean, such that there always is a finite flux into the clustered state. The clustering rate can be calculated based on a stochastic representation of the dynamics (figure 2c). We find that it decays only algebraically in time, and that for sufficiently high driving there can be a finite probability that the gas does not cluster at all. Present work focuses on generalizing this result to systems with inelas-

tic collisions and to explore the role of ring collisions in dense systems.

In order to pin down the consequences of the loss of equipartition in granular gases we consider the motion of a wedge-shaped Brownian particle.

When such a particle is immersed at rest into a gas, it will move with a preferred direction until equipartition is reached. At that point the ensemble average over the realizations of the Brownian motion will result in a finite displacement R from the starting point. In the subsequent equilibrium steady state, the ensemble average of the position remains at the constant position R while the variance of the distribution grows linearly in time [4]. When immersed into a granular gas where the collisions between the wedge and the gas particles are inelastic the situation is dramatically different [5]. Rather than approaching to a state with a zero drift velocity, the systems approaches a steady state with a finite average drift.

We generalized the analysis of [5] to cases where the velocity distribution of the granular

particles is no longer Maxwellian, i.e. beyond the dilute gas limit, and to situations where the isotropy of the velocity distribution is broken. The latter is expected to arise in granular gases subjected to gravity that are kept in the fluid state by shaking the bottom plate of the container.

As a minimal model, we have considered a squeezed-Gaussian velocity distribution in two dimensions. The squeezing factor, α , represents the factor with which the x coordinate of the Gaussian is squeezed compared to the y coordinate.

In contrast the effect of varying the restitution coefficient r , even a slight variation of the anisotropy α results in dramatically larger changes of the drift velocity (figure 3a). Moreover, non-trivial α result in much larger drift velocities; even a reversal of the movement is possible for $\alpha < \alpha_c < 1$. Consequently, for granular Brownian motors, the effect of anisotropy is far more pronounced than those caused by inelastic collisions between wedge and particles.

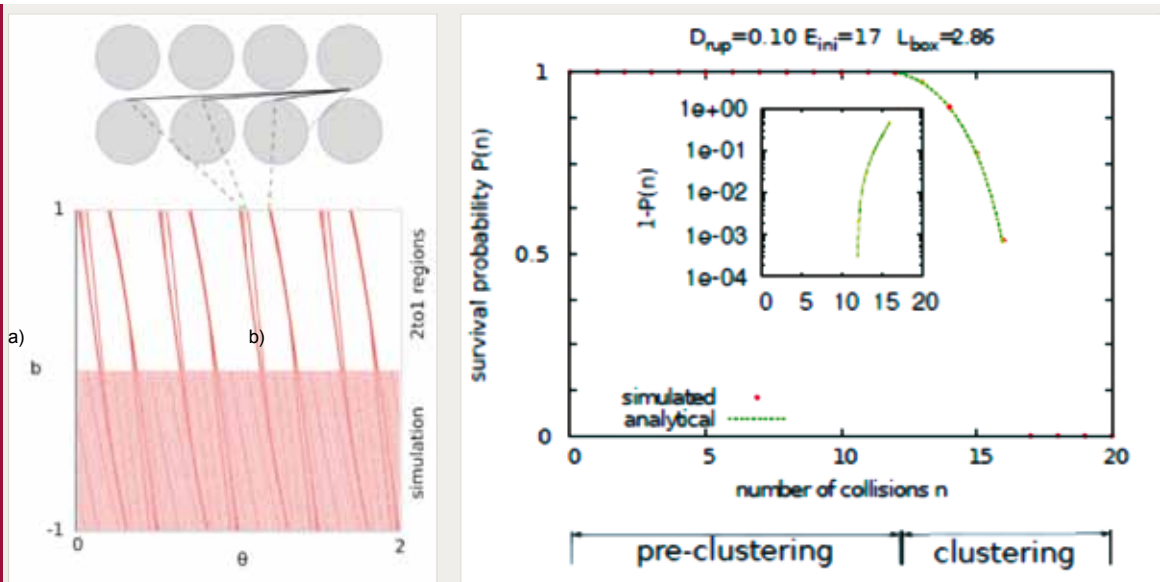
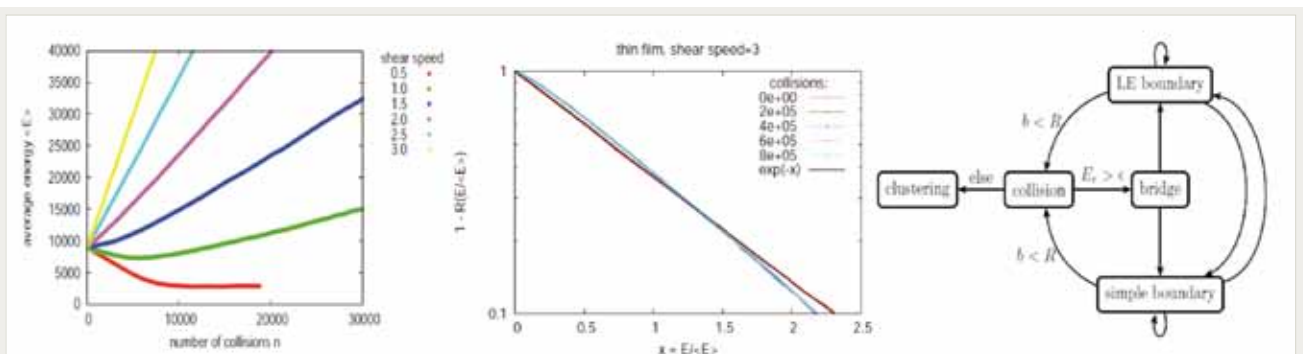
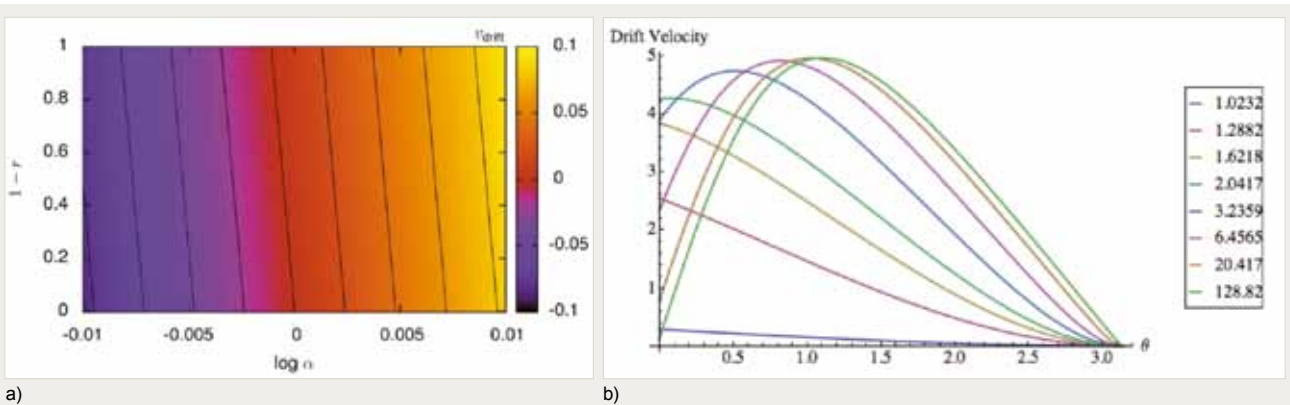


Figure 1

(a) The pre-collision density (“simulation”) and the expected 2 to 1-regions (“theory”) match perfectly. Depending on the angle the stripe pattern can be assigned to the geometrical structure. To additionally check whether the origin of the first order stripe pattern lies in the geometric arrangement of scatters the radius was chosen large enough to block the diagonal channels (red dotted line). (b) The probability $P(E)$ that a system started with an initial energy 17 times larger than the energy required and other arbitrary initial condition has not clustered after performing n collisions. Simulation data and analytical prediction fit perfectly. As shown in the inset, clustering is expected to first arise after 12 collisions.


Figure 2

(a) The ensemble average of the system energy $\langle E \rangle$ does not relax to a steady-state value. Two regimes in which $\langle E \rangle$ is a linear function of the number of collisions n are identified. Initially it is $\langle E \rangle \sim s^2/2 - 1$, i.e. there is critical shear speed s_0^c so that $\langle E \rangle$ decreases for $s < s_0^c$ and increases for $s > s_0^c$. For larger n , $\langle E \rangle$ grows even for $s < s_0^c$. The results are independent of the initial energy. (b) For large times the rescaled energy $x := E/\langle E \rangle$ follows an exponential distribution up to small deviations for small x . (c) Implementation of the sheared billiard in terms of a flow diagram, where “LE boundary” denotes crossing of a Lees-Edwards boundary, and “simple boundary” a crossing of the remaining two simple periodic boundaries. Crossing of boundaries can be followed by another crossing of a boundary or a collisions. The latter either leads to the clustered state, or a capillary bridge is ruptured, and subsequently a boundary must be crossed.


Figure 3

(a) Drift velocity of Brownian motor against different anisotropy factors α and restitution coefficients r . α was varied between 0.977 and 1.023, whereas r was varied between 0 and 1. The effect of anisotropy α clearly dominates the one of inelastic collisions. (b) Drift velocity of Brownian motor against different wedge angles for a range of anisotropies, $1.01 < \alpha < 128.83$. This optimal wedge angle approaches 0.356π for large anisotropies.

Furthermore, we have found that wedges with wedge angle approximately 0.356π move fastest for highly anisotropic gas velocities (figure 3b). Hence, determining the α -dependence of the drift velocity constitutes a relatively easy means to probe the anisotropy of a granular gas. The experiments to probe this prediction are under way.

- [1] S. Ulrich, T. Aspelmeier, K. Röller, A. Fingerle, S. Herminghaus, A. Zippelius, *Phys. Rev. Lett.* **102**, 148002 (2009)
- [2] K. Roeller, J. Vollmer, S. Herminghaus, *Chaos* **19**, 041106 (2009)
- [3] Franziska Glasmeier, Diploma Thesis, Göttingen 2010. (Franziska was awarded the Dr. Berliner – Dr. Ungewitter – price for excellent performance in her studies.)
- [4] S. Sporer, C. Goll, K. Mecke, *Physical Review E* **78**, 011917 (2008)
- [5] B. Cleuren, C. van den Broeck, *EPL* **77**, 50003 (2007)

I-11 Packing Non-Spherical Objects

M. Schröter, S. Herminghaus

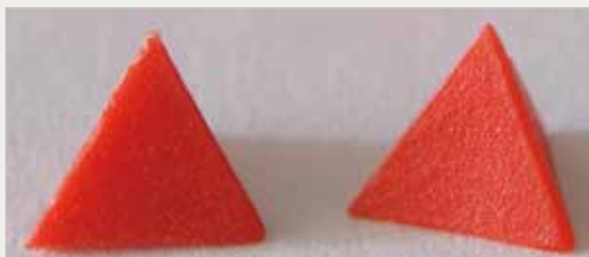
M. Neudecker, S. Ulrich (University Göttingen)

THE JOKE OF physicist treating any object in a first approximation as a sphere has even found its way into popular culture as evidenced by the spherical chicken joke in the American TV series *The Big Bang Theory* [1]. This approach is also tremendously popular in the field of granular physics, but most granular materials like sand, snow, salt or sugar are not comprised of spherical particles. Only recently, researchers have started to look into packings made from ellipsoids or tetrahedra and how their physics differs from sphere packings. One particular question, which has attracted quite some attention [2], was the quest for the densest possible packing of tetrahedra. In the last five years several numerically working groups have increased this upper bound from 72 to 85.6 percent volume fraction, discovering interesting structures like quasi crystals [3] on their way.

Our approach is more based on statistical mechanics: what is the probability of obtaining a certain volume fraction? Using the poly-propylene particles shown in figure 1 a) we find that typical experimental protocols like pouring and

tapping will reproducibly result in packings with volume fractions between 44 and 64 percent. This doesn't contradict the significantly denser numerical results found above; it just shows that those configurations found after millions of Monte-Carlo moves under high pressure have almost zero configurational entropy.

To get deeper insight in the way tetrahedra pack, we look inside the packing using our inhouse X-ray tomography. A typical scan is shown in figure 1 b). The subsequent image processing is considerably more complicated than for sphere packings: every tetrahedron has not only its center of mass coordinates but also an angular orientation. Additionally, face to face contacts complicate the separation of the raw data into individual particles. These problems have now been solved by developing new algorithms for pattern matching; the code has been written in a way to make it easy to adapt it to other platonic shapes. Figure 2 a) shows as an example of our first results the radial distribution functions which exhibits only weak signs of long range order.



a)

Figure 1

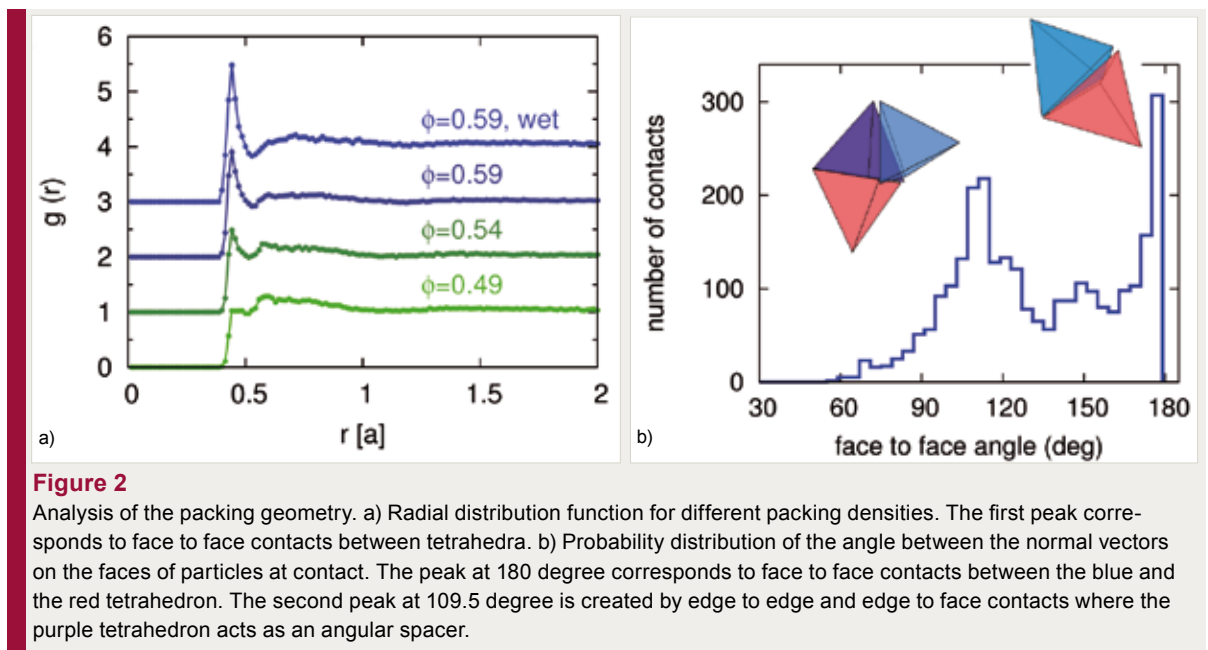
Packing of frictional tetrahedra. a) The tetrahedra are produced by injection molding of poly-propylene and have an edge length of 7 mm. b) X-ray tomography is used to determine the position and orientation of each tetrahedron in a packing of approximately 10000 tetrahedra.



b)

The first scientific question we have started addressing is the nature of the finite pressure, zero shear jamming transition. In previous experimental work on tetrahedral dice [4] a single packing fraction was studied and found to be isostatic (the number of mechanical constraints given by the contacts matches the numbers of degrees of freedom of the particles); provided the particles were considered to be frictionless.

We are still in the process of analyzing our data, but the first results clearly disagree with [4]: both number and type (see figure 2 b) of contacts depend strongly on the packing fraction and taking into account the frictional nature of the particles the packing seem to be hyperstatic. It remains to be seen if for tetrahedra the onset of mechanical rigidity is indeed linked to the contact number as predicted by the Jamming paradigm.



- [1] <http://en.wikipedia.org/wiki/Sphericalcow>
- [2] Kenneth Chang, The New York Times, 4. January 2010, <http://www.nytimes.com/2010/01/05/science/05tetr.html>
- [3] Haji-Akbari et al., *Nature* **462**, 773 (2009)
- [4] Jaoshvili et al., *Phys. Rev. Lett.* **104**, 185501 (2010)

I-12 Noisy Traveling Waves

O. Hallatschek, K. Korolev (Massachusetts Institute of Technology)

THE WAVE-LIKE spread of discrete entities pervades our everyday life. For example, the spread of ions, pathogens and beneficial mutations control the human heart beat, the yearly threat of influenza and evolutionary progress [1]. A thorough understanding of how these waves form and spread has numerous applications ranging from the control of chemical reactions [2, 3] to the prediction of epidemic outbreaks [4, 5]. Great research effort has therefore been made on the question of how traveling waves emerge in complex systems from the multiplicity of relatively simple interactions, in particular the random dispersal of particles and reactions between particles. To simplify the analysis, most theoretical studies have been neglecting number fluctuations, which are inevitable in systems of discrete particles. However, when stochastic simulations became feasible, it was found that those previously ignored fluctuations can have a strong impact on the dynamics of waves [6, 7]. Simple models of biological evolution and of population expansions featured as the prime example for this drastic sensitivity on noise because they are dominated by the few most fit individuals in a population. As a consequence, number fluctuations represent a singular perturbation of the deterministic problem. With the added difficulty of particle discreteness, the analysis of traveling waves became one of the important challenges of statistical physics and mathematical biology that mostly defied systematic analytical techniques.

Earlier studies on stochastic reaction diffusion systems have mainly focussed on the singular limit of small stochastic fluctuations. In the first project below, we investigate traveling waves in the opposite limit when number fluctuations dominate. In a second project, we show that number fluctuations can also drive traveling waves, which is in contrast to the current paradigm of noise acting as an effective “drag” force.

In the third and most important project, we show that there is an exact way to introduce finite particle numbers in reaction diffusion systems, in which the only non-linearity is due to the conservation of population size. This approach, which allows quite generally to analyze number fluctuations in reaction diffusion systems, is illustrated using the example of simple models of asexual adaptation. The relevance of our work is underscored by a commentary article written by D. S. Fisher that accompanied our paper in the PNAS [8, 9].

Fisher waves in the strong noise limit

Our current understanding of traveling waves in reaction diffusion systems is shaped by studies of traveling waves when fluctuations are absent or weak. The opposite limit of strong fluctuations or noise is relatively unexplored, yet arguably of equal importance. Not only does it occur naturally, when the driving forces of traveling waves are weak; it also unravels fundamentally different and often counterintuitive aspects of traveling waves. Our recent study [10] of the strong noise limit focused on two intimately related questions of how fast traveling waves move and what their shape is. Our findings are in stark contrast to the commonly used deterministic and weak-noise approximations. The velocity of a broad class of traveling waves (Fisher-Kolmogorov waves [1]) in one and two spatial dimensions was shown to exhibit a linear and a square-root dependence of the speed on the particle density. Furthermore, instead of smooth sigmoidal wave profiles, we observe fronts composed of a few rugged kinks that diffuse, annihilate, and rarely branch; this dynamics is shown to lead to power-law tails in the distribution of the front sizes [10].

Noise driven evolutionary waves

Mutations that increase an organism’s fitness are the fuel for biological evolution. When such

beneficial mutations enter a spatially extended population, they spread through the population in a “wave of advance”, first described by R. Fisher and A. Kolmogorov [1]. The force driving these traveling waves is Darwinian selection, which favors individuals with higher fitness. In Ref. [11], we have described a new type of traveling mutant wave that is driven by non-selective forces instead – namely by random genetic drift, which refers to the randomness in the reproduction process, see figure 1. These noise-driven waves promote the economical use of a limited resource because they occur whenever a mutation increases the growth yield, which refers to the biomass produced per unit of resource. Since a change in growth yield and growth rate often occur together and with opposite signs, we argue that both types of mechanisms will jointly decide over the fate of a novel mutation. We predict that the population evolves towards an evolutionary optimal carrying capacity, at which selective and non-selective forces just balance. The simplicity of our model, which lacks any complex interactions between individuals, suggests that noise-induced pattern formation may arise in many complex biological systems including evolution.

The noisy edge of traveling waves

Simple models of evolution [6, 12] provide spectacular examples of noisy traveling waves because of their drastic sensitivity to rare fluctuations in the wave tip. As illustrated in figure 2 (left), these waves describe the continual increase of growth rate, also called fitness, due to spontaneous mutations in a finite population. The wave speed, which is a measure for how quickly populations adapt, increases without bound if number fluctuations are neglected [6]. To reproduce a **steady** state with constant wave speed observed in stochastic simulations, any analysis has to incorporate number fluctuations, at least heuristically by introducing an ad hoc “cutoff” in the noisy tip of the wave [6]. The relationship between traveling speed and population size has been investigated extensively in

the recent literature [13], with some controversy regarding the universal behavior, in order to interpret growth rate measurements in microbial evolution experiments.

A closer look at the models underlying these fitness waves reveals their characteristic structure: reproduction of individuals is implemented by a standard branching process. That is individuals replicate according to their current growth rate, see figure 2. The growth rate, on the other hand, is subject to small variations due to random mutations, which are modeled through a random walk, for instance by standard diffusion [6]. In addition, all evolution models contain a nonlinearity that limits the total population size. This accounts for the fact that natural populations must stay finite due to resource limitations.

Our recent study [8, 9] published in PNAS establishes a natural generalization of the above models. Instead of enforcing a fixed population size, we allow for a whole class of constraints. Analyzing the behavior of evolution models (in fact any kind of branching random walk) under the set of all possible constraints, we find that a unique constraint exists for which evolution models are exactly solvable. It turns out that these solvable models allow for accurate predictions of how quickly populations adapt as a function of population size and mutation rates, see figure 2 (right). Our study thus provides the first rigorous approach to noisy traveling waves. More generally, our method is shown to apply to a broad class of models, in which number fluctuations are generated by branching processes. Due to this versatility, the method of model tuning may serve as a promising route towards unraveling emergent properties of complex discrete particle systems.

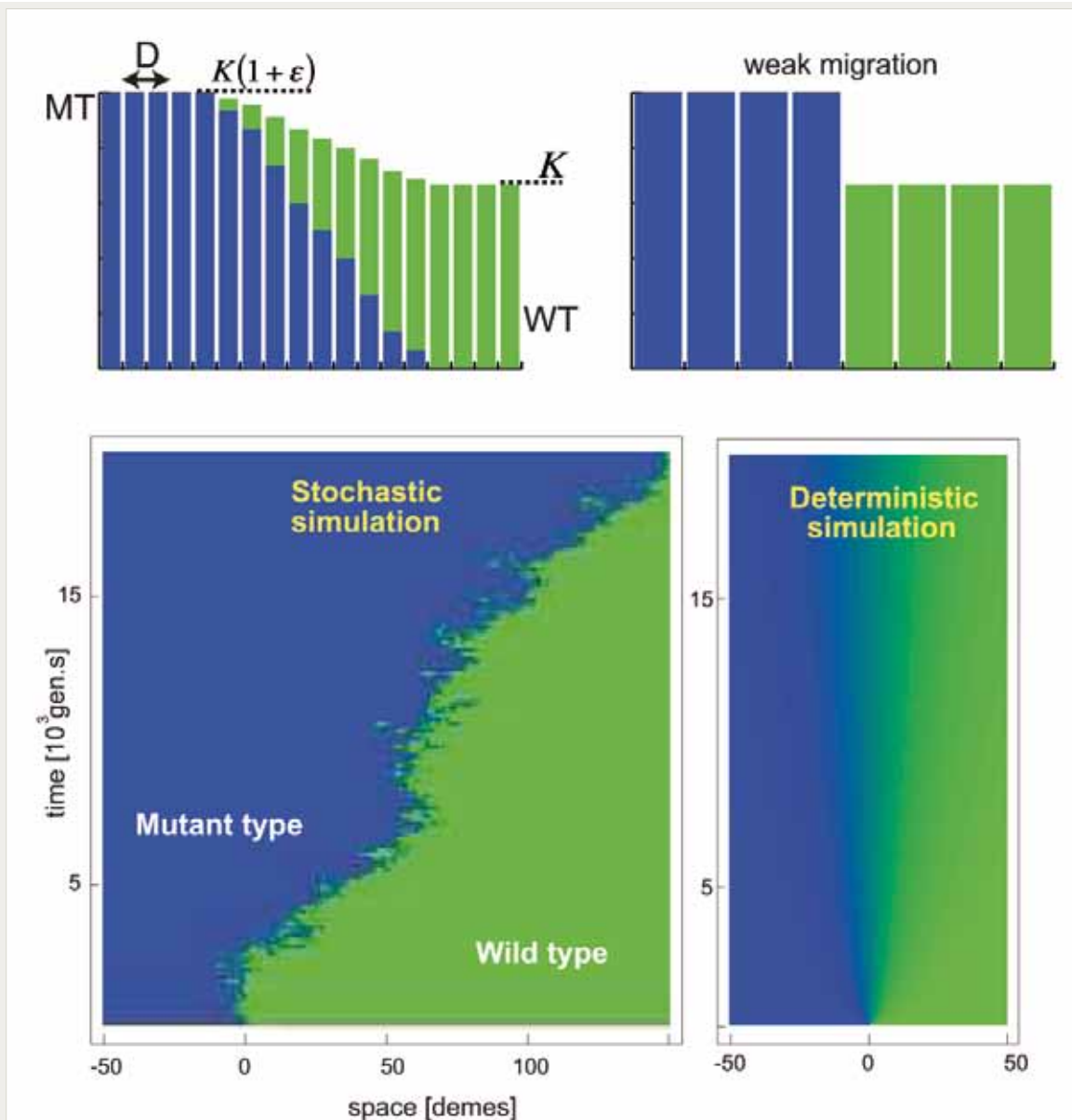


Figure 1

Noise can drive traveling waves. A computer model is used to simulate the competition for a common resource between two species, mutants (blue) and wild type (green). Mutants are assumed to use resources more economically than the wild-type. As a consequence, higher population densities can be sustained in the mutant regions. Yet, mutants are unable to invade the wild-type population unless the randomness in the reproduction process (genetic drift) is implemented in the computer model. a) The spatially extended population is represented by a linear array of local populations, called demes. Individuals migrate between neighboring demes at a rate D per generation. The population size of the demes ranges from K for demes that are occupied by wild-type only to $K(1 + \epsilon)$ for mutant only demes. Due to the diffusive mixing of both types, the transition from MT to WT occurs in general over more than one deme. b) For very low migration rates, demes are either fixed for the wild-type (WT) or the mutant type (MT), and the transition between both regions is step-like. c) Representative results of stochastic (left) and deterministic (right) simulations with parameters $K = 30$, $D = 0.05$ and $\epsilon = 0.1$. Horizontal and vertical axes represent space and time, respectively. The color shading intermediate between blue (100% mutants) and green (100% wild-type) indicates the mixture between both types at a given deme. Note that i) mutants invade the wild-type population only in the stochastic simulations, ii) the transition region between mutants and wild type remains stable in the stochastic case but gradually blurs in the deterministic simulations.

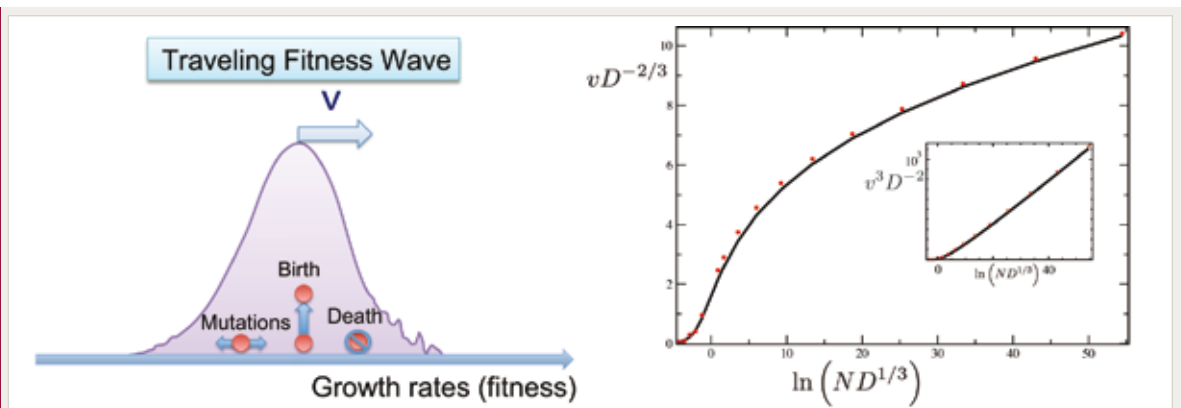


Figure 2

Left: A paradigmatic example for noisy traveling waves are “fitness” waves arising in simple models of evolution. The colored particles represent individuals with characteristic growth rates, or fitnesses (horizontal axis). Individuals can mutate, replicate (“birth”) and be eliminated from the gene pool (“death”), as illustrated. These simple dynamical rules give rise to a distribution of growth rates resembling a bell-like curve at steady state, which propagates towards higher growth rates like a solitary wave. The random fluctuations in the tails of the wave have precluded any rigorous analysis in the past. Right: The relation between the scaled speed, $vD^{-2/3}$, and the scaled population size $ND^{1/3}$ as obtained numerically for an exactly solvable “tuned” model (black line) and from stochastic simulations of a corresponding evolution model with a rigid population size constraint [6] (red points). Here, D is a measure of mutation rates and N represents the total population size. The speed of adaptation v is the average increase of growth rate per generation. Notice that both curves approach each other in the limit of large and small N . The data are consistent with the asymptotic scaling $v \sim \ln^{1/3} N$ (see inset) and $v \sim N$ for large and small population sizes, respectively.

- [1] J. D. Murray, *Mathematical Biology I*, Springer (2004)
- [2] A.T. Winfree, *Science* **175** (4022), 634–636 (1972)
- [3] Y. Kuramoto, *Dover Pubns.* (2003)
- [4] B.T. Grenfell, O.N. Bjornstad, and J. Kappey, *Nature* **414** (6865), 716–723 (2001)
- [5] D. Brockmann, L. Hufnagel, and T. Geisel, *Nature* **439** (7075), 462–465 (2006)
- [6] L. Tsimring, H. Levine, and D. Kessler, *Phys. Rev. Lett.* **76** (23), 4440–4443 (1996)
- [7] E. Brunet and B. Derrida, *Phys. Rev. E* **56** (3), 2597–2604 (1997)
- [8] O. Hallatschek, The noisy edge of traveling waves, *Proceedings of the National Academy of Sciences* **108** (5), 1783 (2011)
- [9] D.S. Fisher, Leading the dog of selection by its mutational nose, *Proceedings of the National Academy of Sciences* **108** (7), 2633 (2011)
- [10] O. Hallatschek and KS Korolev, Fisher waves in the strong noise limit, *Phys. Rev. Lett.* **103** (10), 108103 (2009)
- [11] O. Hallatschek, Noise Driven Evolutionary Waves, *PLoS Comput. Biol.* **7** (3), e1002005 (2011)
- [12] M. M. Desai and D. S. Fisher, Beneficial mutation selection balance and the effect of linkage on positive selection, *Genetics* **176** (3), 1759 (2007)
- [13] S.C. Park, D. Simon, and J. Krug, *Journal of Statistical Physics* **138** (1), 381–410 (2010)

I-13 Building Blocks of Turbulence

B. Hof, A. deLozar, M. Holzner, M. Avila

F. Mellibovsky (UPC Barcelona), A. Willis (University of Sheffield), P. Cvitanovic (Georgia Tech)

ALTHOUGH TURBULENCE is relevant to a multitude of processes throughout nature our conceptual understanding of this phenomenon is very limited. The equations describing fluid motion, the Navier Stokes equations, have been known for a long time. However, for the vast majority of situations we are unable to solve these equations analytically. The problem stems from the nonlinear nature of these partial differential equations and as common for nonlinear systems, at large amplitudes the dynamics are extremely complex and chaotic. Most studies of turbulence attempt a statistical description of the dynamics at very large Reynolds numbers (Re). Our approach is different: we attempt to obtain a more fundamental understanding of the structures underlying turbulence in parameter regimes where turbulence first occurs. Our expectation is that here the dynamics are less complex and possibly sufficiently low dimensional to be able to identify the structures (unstable solutions) underpinning the turbulent dynamics. The main focus here is on elucidating the temporal complexity of turbulence in pipe flow at low Re.

In recent years based on ideas from nonlinear dynamics theory some new concepts have been suggested which could provide guidance [1]. Here it has been proposed that the turbulent state evolves around unstable solutions of the governing equations which arise already at fairly low Reynolds numbers. Due to their instability, individual solutions can not persist in practical flows and if at all can only be expected to show up transiently. In analogy to other chaotic systems such unstable states can form a complex entity [1] (i.e., a turbulent repeller) through further bifurcations and entanglement, which gives rise to chaotic motion. Indeed such unstable solutions have been found numerically for a variety of flows including that of a fluid down a

straight pipe [1] (see figure 1 bottom row). Our earlier experiments [2] (figure 1 top row) have given a first indication that these unstable states can be observed transiently in a turbulent flow and therefore they are indeed relevant to fluid turbulence. The formation of a chaotic repeller is also supported by our observation that the decay of spots of turbulence is a memoryless process [3, 4]. Such behavior is well known from lower dimensional systems where chaotic dynamics are observed for very long times until the system suddenly escapes to a local attractor in a different part of the phase space (here the laminar flow).

Edge states in decaying turbulence

In this project we focus on decaying turbulence testing if in fading turbulence clearer visits to unstable solutions occur. The investigation is limited to low Reynolds numbers (here Re=1900). Indeed we observe that approximately 20 diameters downstream from where the decay sets in, flow fields frequently show a simple one fold symmetry (see figure 2 top row) with two high speed streaks close to the wall separated by one low speed region and corresponding streamwise vortices inbetween. This structure is reminiscent of a particular state that has been identified recently in numerical simulations of pipe flow, the so called 'edge state' [5]. The important feature of this state is that it separates initial conditions that become turbulent from those which go directly to the laminar state. As it marks the border between the laminar and turbulent flows it is plausible that it may play an important role during the transition to and from turbulence. The 'edge state' itself is chaotic and it has been shown that imbedded in it is an unstable travelling wave solution which has the same symmetry features (i.e. asymmetric with two high and one low speed streaks).

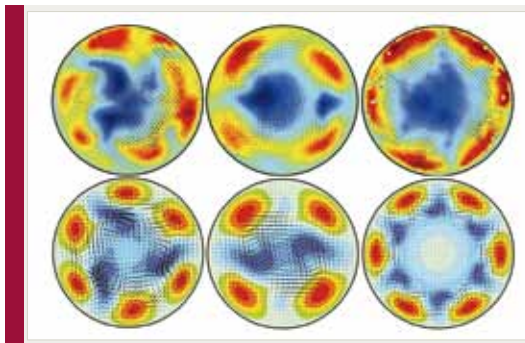


Figure 1

Cross sectional view of velocity fields in a pipe. High/low streamwise velocities are shown in red/blue (the laminar parabolic velocity field has been subtracted). Top row: Experimental observations of travelling wave transients in a turbulent flow. Bottom row: Numerical calculations of exact unstable travelling wave solutions (from [2]).

In figure 2 we show that the symmetry as well as the dynamics observed in experiments (top row) closely match those of the edge state observed in numerical simulations computed at the same Re (lower row figure 2). In order to probe if the experimental observations indeed correspond to the edge state the experimental velocity field was used as the initial condition for a Newton-Raphson algorithm. Applying this method the velocity field was found to directly converge to the asymmetric travelling wave imbedded in the edge state confirming, that the experimental flow was indeed in the close vicinity of the edge [6]. As a final test we simultaneously measured velocity fields at two downstream locations which enabled us to determine the advection speed of the experimental structures. The velocity of the asymmetric state in the experiment (i.e. figure 2 top row) was found to be identical to that of the numerical edge state ($U=1.46$ in both cases) and also very close to the phase velocity of the asymmetric travelling wave of the same wavelength ($U=1.53$). Hence we could for the first time quantitatively link structures observed in (decaying) turbu-

lence in an experiment to an exact (numerical) solution of the Navier Stokes equation. Also this is the first observation of the edge state in an experiment, providing evidence for its relevance to the transition process.

Quest for unstable periodic orbits

While in pipe flow so far a large number of unstable travelling waves solutions (i.e. equilibria) have been identified, only very few periodic orbits have been found. Unstable periodic orbits are however of particular importance in chaotic systems as they provide the skeleton underpinning the chaotic/turbulent dynamics [7]. A particular difficulty in pipe flow (in contrast to plane Couette flow) is the non-zero mean velocity which results in a downstream propagation of the exact coherent states. In a frame of reference moving at the correct phase velocity a travelling wave reduces to an equilibrium solution. As all travelling waves (and all relative periodic orbits) travel at different phase speeds there is no simple choice for a reference frame. This problem can be resolved by applying a so called 'slicing technique' [8] that

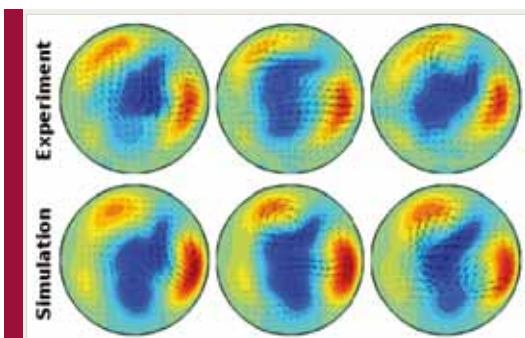


Figure 2

Comparison between decaying turbulence in the experiment (top row) and a direct numerical simulation of the edge state (bottom row), both at $Re=1900$. Each row displays three instances of a quasiperiodic cycle (spaced by $\pi/3 D$ in both cases). Colour levels show the out of plane velocity field relative to the Hagen Poiseuille profile. Identical colour levels are chosen for experiments and simulations (dark blue corresponding to $-0.7 U_{\text{mean}}$ and dark red to $0.7 U_{\text{mean}}$). In plane velocities are indicated by arrows.

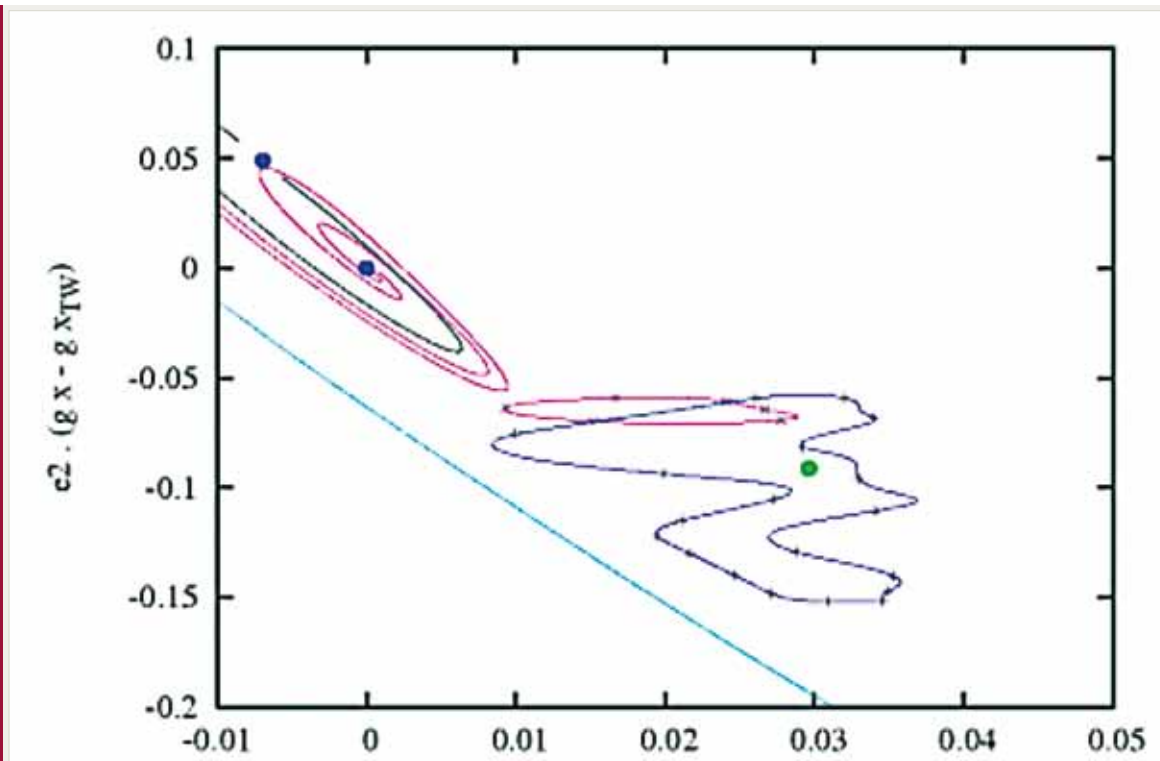


Figure 3

Phase space projection local to a Travelling Wave (TW) at $(0,0)$, the two projection axes correspond to the eigenvectors associated to the leading eigenvalues of the TW. The projection is generated after applying the slicing algorithm so that Travelling waves appear as fixed points (solid circles). Lines correspond to trajectories starting at different travelling waves, whereas the lines with crosses correspond to relative periodic orbits found with Netwon-Krylov methods. (Courtesy of Dr A.P. Willis).

maps all the structures to a common reference frame and allows to reconstruct a phase space where travelling waves occur as equilibria and relative periodic orbits as cycles. Starting from known travelling wave solutions as initial conditions such a reconstruction allows educated guesses for potential locations of periodic orbits. Applying these methods has recently lead to the discovery of several orbits (see figure 3) which are embedded in the vicinity of the turbulent dynamics.

- [1] B. Eckhardt, et al. *Annu. Rev. Fluid Mech.*, **39**, 447-468 (2007)
- [2] B. Hof, et al. *Science*, **305**, pp 1594-1598 (2004)
- [3] B. Hof, et al. *Nature*, **443**, 05089, pp 59-62 (2006)
- [4] B. Hof et al. *Phys. Rev. Lett.*, **101**, 214501 (2008)
- [5] T.M. Schneider, B. Eckhardt and J.A. Yorke, *Phys. Rev. Lett.*, **99**, 034502 (2007)
- [6] A. de Lozar, F. Mellibovsky, M. Avila and B. Hof in preparation (2011)
- [7] P. Cvitanovic, ChaosBook.org
- [8] Froehlich and P. Cvitanovic, arxiv.org/abs/1101.3037 (2011)

I-14 The Origin of Species from the Primordial Soup

H. Kielblock, O. Hallatschek, M. Timme

S. Eule, S. Grosskinsky (University of Warwick, United Kingdom)

What is the impact of horizontal gene transfer?

Since Darwin's seminal work *On the Origin of Species* [1] in 1859 it is commonly believed that the evolution of species may be represented by a 'tree of life': in this picture, all of today's species are connected by lineage splittings that occurred at past times, until, at the beginning of evolution, all branches converge to one least common ancestor. However, this view is now strongly debated [2] since the importance of horizontal gene transfer (HGT) in microbial mutations has been realized. Horizontal gene transfer is a process by which genes might be virally transferred between single cell organisms that coexist in time. A dominance of HGT in microbial evolution implies that most individuals share parts of their gene sequences with other individuals. Thus, no distinct species – with the individuals having distinct features – are formed, but rather most individuals share many features simultaneously. Such a state where no distinct species exist is sometimes called "reactive soup" (cf. figure 1). It is not clear yet how evolution in such a scenario proceeds [3]. Even more, it is largely unknown, how speciation may take place under such circumstances and thus how today's structure of species distribution – the coarse structure of all current life – could have emerged.

Mathematically tractable models and general theoretical statements are considered inevitable for answering these questions [3], but very few analytical studies on early evolution, in particular in the presence of HGT, exist so far. Actually, existing stochastic models to study evolution such as e.g. Moran processes [4] completely focus on the classical processes of selection and mutation. We use such stochastic models and extend them to incorporate the process of HGT, so that we may study the influence of HGT on the overall evolutionary dynamics. Thus, we now aim at clarifying and classifying relevant speciation options and identifying how finite population sizes and related stochastic fluctuations may influence early evolutionary processes.

Spontaneous switching in finite systems

In the model class we are developing and analyzing, a finite number of individuals (genotypes) coexists in time and evolves by producing offspring, mutating and dying randomly. In mathematical terms, these models constitute modifications of well-known stochastic Moran processes [4]. One main new contribution is an underlying network structure that characterizes which genotypes may mutate into which other genotypes. The general properties of Moran processes effectively make them a random walk on a high-dimensional Markov chain.

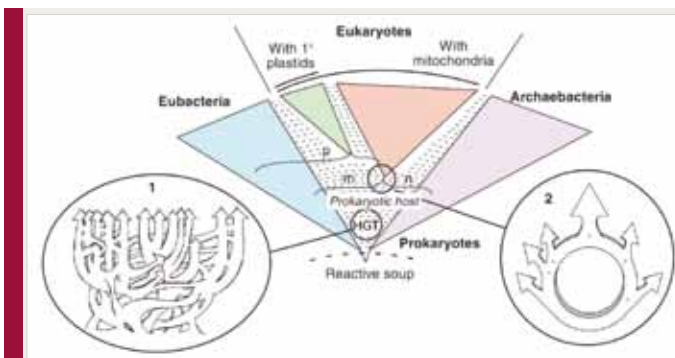


Figure 1

A current view of microbial evolution from a "reactive soup". The main figure shows the proposed evolution of the three main domains of life (Eubacteria, Archaeobacteria and Eukaryotes) from the reactive soup including horizontal gene transfer between the different domains. Inset 1 shows horizontal gene transfer leading to a strongly interconnected 'tree' of life. Inset 2 shows the proposed evolution of Eukaryotes from Eubacteria and Prokaryotes, which leads to a ring-like structure rather than a tree. Figure taken from [3].

Already the simplest non-trivial model network, consisting of only two populations of genotypes that may mutate into each other (without HGT), yields results that were not expected from mean field theory (i.e. do not occur for infinite populations). We uncovered a switching phenomenon, where most of the time almost all of the individuals are of one but not of the other genotype; some characteristic timespan later, a switching occurs and most individuals mutated to the other genotype.

We derived the Focker-Planck-equation describing the dynamics of the system and analytically derived its stationary solution. With this solution we were able to find the parameter regime, in which switching occurs. It is the parameter regime in which genetic drift dominates over the dynamic force caused by mutations. Using Markov chain theory, in the parameter regime where switching occurs we derived a closed analytical formula for the switching time in dependence of the number of individuals and the mutation probability.

Switching times through fitness valleys

Using the results derived above we were able to analytically derive a formula for the switching times in fitness valley systems, where a population evolves from one genotype of high fitness to another one through some genotypes of lower fitness [5]. These results can be used to estimate speciation times in evolutionary dynamics without HGT and may thus be useful to quantify the influence of HGT on the speed of evolution.

Horizontal gene transfer induces hypergraph structure.

In our model standard point mutations define a lattice-like network topology, while HGT introduces shortcuts that may accelerate evolutionary processes. Even more, point mutations are represented by relatively simple two-node processes, i.e. the mutation from one node to another one. On the other hand, HGT has to be represented by a three-node process: An individual of one genotype interacts with an individual of some other genotype receiving ge-

netic material so that it mutates to a third genotype. Therefore, the probability of HGT events to occur depends nonlinearly on the distribution of individuals on different genotypes and HGT induces a hypergraph structure into the network model.

In the last decade the importance of HGT on early evolution has been realized. However, no way to incorporate HGT into existing theories and models has been achieved so far. Now we extended the existing models to incorporate the complex three-node processes induced by HGT. The resulting new types of models open up the possibility to also conceptually analyze qualitative as well as quantitative (e.g. time scale and populations size) key aspects about the impact of HGT.

HGT and the primordial soup

Our current focus lies on the investigation of the dynamics in the primordial reactive soup in the evolution model described above. Under which circumstances do the evolutionary dynamics lead to a reactive soup where no distinct species exist? Is massively occurring HGT a prerequisite for such a state? What are the minimal requirements such that speciation actually occurs? We are currently trying to identify the relevant features for selection, interaction, mutation and the likelihoods for the occurrence of HGT. Finally, we will address the problem how the process of speciation leading to today's Darwinian evolution may emerge from the reactive soup. We hope that these findings will help to gain a better understanding of the processes that underly evolution in its early stages.

Part of the material presented here has been taken, sometimes in modified form, from the Research Report 2011 of the Network Dynamics Group (c) Marc Timme, et al., MPIDS.

- [1] C. Darwin, *On the Origin of Species*, John Murray, London (1859)
- [2] C. R. Woese, *Proc. Natl. Acad. Sci. USA* **99**, 8742 (2002)
- [3] T. Dagan and W. Martin, *Genome Biol.* **7**, 118 (2006)
- [4] P. Moran, *The statistical processes of evolutionary theory*, Oxford University Press, Oxford (1962)
- [5] H. Kielblock, M. Timme and S. Grosskinsky, *How to cross a fitness valley – A network approach* (Talk), DPG Spring Meeting, Dresden, Germany (2011)

I-15 Photodissociation and Recombination of Molecules with Atmospheric Relevance

R. Schinke

The investigation of elementary reactions in the gas phase (exchange reactions, photodissociation, unimolecular dissociation etc.) is important for understanding the complicated chemistry in combustion and in atmospheric processes. Our theoretical studies aim at reproducing detailed experimental data by ab initio methods, explaining measured data on the basis of fundamental equations and making predictions for experiments, which are difficult to perform in the laboratory. The tools are global potential energy surfaces (PESs), calculated in the Born-Oppenheimer approximation by solving the electronic Schrödinger equation, and the solution of the nuclear Schrödinger equation for the intramolecular dynamics of the atoms on these PESs [1, 2]. In recent years we concentrated our activities on ozone (O_3), nitrogen dioxide (NO_2), and nitrous oxide (N_2O). These three molecules are under intense experimental investigations in many laboratories.

The studies of the photodissociation of O_3 ,
 $O_3 + h\nu \rightarrow O + O_2$
 are more or less completed and the results have been summarized in Ref. 3. The photo absorption cross section of ozone in the wavelength region from the near IR to the near UV shows four different bands: Wulf, Chappuis, Huggins and Hartley. Each band corresponds to one (or several) particular electronic states which are excited by the photon. Calculations have been performed for all bands. The quantitative description of process (1) requires the calculation of PESs of all electronic states involved, each being a function of the three internal coordinates of O_3 . In addition, the non-Born Oppenheimer coupling elements are required if more than one state is involved – and that is indeed the case in all bands. Global PESs have been determined for a total of ten states. Quantum mechanical dynamics calculations, i.e., the

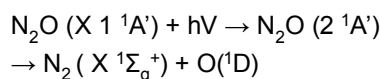
solutions of either the time-independent or the time-dependent Schrödinger equation, yield the absorption spectrum and the final rotational-vibrational product state distributions. In addition they reveal, in combination with classical mechanics calculations, the dissociation mechanisms and explanations for certain prominent features like diffuse vibrational structures and predissociation lifetimes. The comparison of the theoretical results with detailed experimental data is generally very good [3]. The calculations performed in Göttingen over the past five years yielded – for the first time – a quite complete dynamical picture of reaction (1) up to photon energies of ~ 9 eV.

The photodissociation of NO_2 ,



is equally important and challenging. First calculations [4] have significantly added to the understanding of this process, but also raised further questions concerning the interpretation of some experimental results.

N_2O is a long-lived atmospheric trace gas with significant impact on global warming and the depletion of ozone. It is mainly removed by photolysis in the stratospheric UV window ($\sim 47,500$ to $55,000$ cm^{-1}). This absorption band, which is due to the



electronic transition, is currently studied by us in significant detail [5, 6]. We have calculated accurate PESs for the ground and the excited state as well as the transition dipole moment functions. The calculated absorption cross section agrees well with the measured one (see figure 1). One of the goals was to unravel the vibrational dynamics causing the weak structures superimposed to the broad Gaussian-type background. Our calculations unambiguously showed that they are caused by periodic orbits in the upper electronic state performing

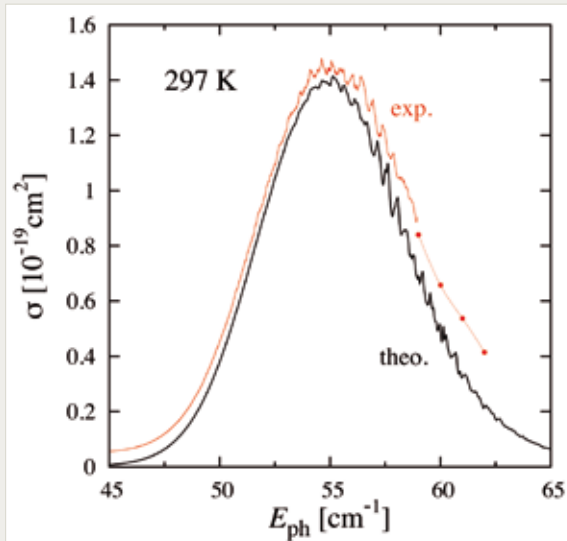


Figure 1

Comparison of calculated and experimental room temperature absorption cross section. For clarity, the experimental cross section is slightly shifted upward.

large amplitude bending and NN stretch motion. We have also studied the temperature dependence of the cross section [7] and have calculated the partitioning of the excess energy among the product degrees of freedom [8]. In collaboration with a Danish group we currently investigate the isotope dependence of the absorption cross section from which insight of the introduction of N_2O in the atmosphere and its removal are expected [9].

In addition to the photodissociation of ozone we have also studied its recombination,



in collisions of O atoms and O_2 ; here, the atom (or molecule) M is necessary to carry away the excess energy. The recombination rate coefficient shows a strong isotope dependence [10]. However, despite many experimental and theoretical studies over several decades it is not yet really understood [11]. Even the most advanced quantum mechanical study left important questions unresolved [12]. For example, the recombination rate for symmetric ozone molecules like 16-18-16 appears to be smaller than for non-symmetric molecules like 16-16-18. In

recent studies we attempted to find an answer for this intriguing result in the stabilization step and investigated the energy transfer in Ar- O_3 collisions [13, 14]. However, the necessary approximations did not allow to arrive at convincing conclusions. The recombination of ozone and its dependence on the oxygen isotopes is still an open problem.

- [1] R. Schinke. Photodissociation Dynamics. Cambridge University Press, Cambridge (1993)
- [2] S.Yu. Grebenshchikov, R. Schinke and W. L. Hase. In Unimolecular Kinetics, edited by N. Green. (Elsevier, Amsterdam, 2003)
- [3] S. Yu. Grebenshchikov, Z.-W. Qu, H. Zhu and R. Schinke, *Phys. Chem. Chem. Phys.* **9**, 2044 (2007)
- [4] R. Schinke, S. Yu. Grebenshchikov and H. Zhu, *Chem. Phys.* **346**, 99 (2008)
- [5] R. Schinke, J. Suarez and S. C. Farantos, *J. Chem. Phys.* **133**, 091103 (2010)
- [6] R. Schinke, *J. Chem. Phys.* **134**, 064313 (2011)
- [7] R. Schinke, *Chem. Phys.*, submitted
- [8] J. A. Schmidt, M. S. Johnson, U. Lorenz, G. C. McBane and R. Schinke, *J. Chem. Phys.*, submitted (2011)
- [9] J. A. Schmidt, M. S. Johnson and R. Schinke, in preparation
- [10] K. Mauersberger, D. Krankowsky, C. Janssen and R. Schinke, *Adv. At. Mol. Opt. Physics* **50**, 1 (2005)
- [11] R. Schinke, S. Yu. Grebenshchikov, M. V. Ivanov and P. Fleurat-Lessard, *Annu. Rev. Phys. Chem.* **57**, 625 (2006)
- [12] S. Yu. Grebenshchikov and R. Schinke, *J. Chem. Phys.* **131**, 181103 (2009)
- [13] M. V. Ivanov, S. Yu. Grebenshchikov and R. Schinke, *J. Chem. Phys.* **130**, 174311 (2009)
- [14] M. V. Ivanov and R. Schinke, *Mol. Phys.* **108**, 259 (2010)

II Transport in Complex Media

II-1 Turbulence in Complex Fluids

H.-D. Xi, H. Xu, E. Bodenschatz

FOR TURBULENCE in Newtonian fluids, kinetic energy is injected into the flow at the large scales, transferred through inertial scales, and finally dissipated to heat by viscosity at Kolmogorov scale η . This picture of the energy cascade is altered in a turbulent flow with a small amount of polymer additives. Polymers can extract/feedback energy from/to the flow when they are stretched or coil back, thus interrupt the cascade at certain scales. An important dimensionless parameter to characterize the flow of polymer solution is the Weissenberg number $Wi \equiv \tau_p / \tau_\eta$, where τ_η is the Kolmogorov time and τ_p is the polymer relaxation time. When $Wi \approx 1$ or larger, the polymers are stretched by the flow and start to affect the flow [1]. In addition, the Taylor microscale Reynolds number R_λ and the polymer concentration ϕ also play important roles. Our previous measurements were conducted with a certain molecular weight polymer at different R_λ and ϕ [2-4], or for fixed ϕ as a function of R_λ [5]. The Weissenberg number Wi was not varied independently. In the experiments reported here we kept both R_λ and ϕ unchanged while varying Wi .

We studied turbulence in the central region of a von Kármán Swirling Flow, where the turbulence is nearly homogeneous. We used polyacrylamide (PAM, molecular weight 18×10^6 and 6×10^6) at fixed concentration of 5 ppm. By changing the solvent viscosity ν and the energy injection rate ε according to $\varepsilon \propto \nu^3$, we could keep R_λ (and also η) unchanged, which we verified from the measurements of the Eulerian second order velocity structure functions. We varied Wi from 0 to 3 according to $Wi \propto \nu^2$. We observed a sharp transition in the RMS acceleration around $Wi \approx 1$ (figure 1), but no appreciable change in the RMS velocity.

This is consistent with previous observations that polymers suppresses small-scale quantities, such as fluid acceleration, but has little effect on large-scale properties, such as velocity fluctuations [2-4]. Moreover, figure 1 shows that the suppression of the small scales occurs rapidly, corresponding to the coil-stretch transition.

To probe the polymer effects on the energy cascade, we measured the Eulerian transverse velocity structure function $D_{NN}(r)$. When $Wi > 1$, D_{NN} was modified over a wide range of scales and this range broadened with increasing Wi (figure 2). This could be explained by Lumley's "time criterion" [6], which suggests that polymers affect turbulence at scales whose turbulence dynamic times are smaller than τ_p . This criterion thus gives a length scale $r^* \propto (\varepsilon \tau_p^3)^{1/2}$ below which polymer effects may be observed. When the Kolmogorov length η was fixed, such as in our experiments here, the Lumley scale would grow with Wi as $r^*/\eta \propto Wi^{3/2}$. However, a simple rescaling using r/r^* could not collapse $D_{NN}(r)$ with different Wi , as we also observed previously, where Wi was changed by varying R_λ [4]. In fact, de Gennes [7] argued that r^* is the upper bound of the scales at which *the polymers may be stretched by the flow*, but the scale r^{**} at which *the polymer effect on turbulence becomes appreciable* is given by a balance between turbulent kinetic energy and the elastic energy stored in polymer chains. Using K41 energy spectrum, de Gennes further proposed that $r^{**} \propto Wi^\alpha \Phi^\beta N^Y \eta$, where N is the number of monomers per polymer chain, and the scaling exponents α , β and Y are known algebraic functions of a parameter n that relates the polymer elongation with spatial scale r [7]. To identify n , we fitted the measured $D_{NN}(r)$ at small r for different Wi ,

together with those from previous experiments [4]. Figure 3 shows the collapse with r^{**} calculated from the fitted n . For all these data, the fitted n lies in the range of 0.27 ± 0.09 . In [4], it was proposed to use $r/(vT_p)^{1/2}Wi^X$, with $X = -0.58 \pm 0.09$ to collapse the data with varying Wi (while not keeping R_λ constant). For $n = 0.27 \pm 0.09$, the corresponding scaling exponent X is $X = -0.49 \pm 0.22$, in agreement with the values reported in [4]. In de Gennes' argument, the parameter n reflects the flow topology and is a measure of the strength of stretching by the flow. For laminar flows into a point sink, $n = 1$ in 2D and $n = 2$ in 3D. In a turbulent flow field, only some regions are dominated by strain and these regions are changing dynam-

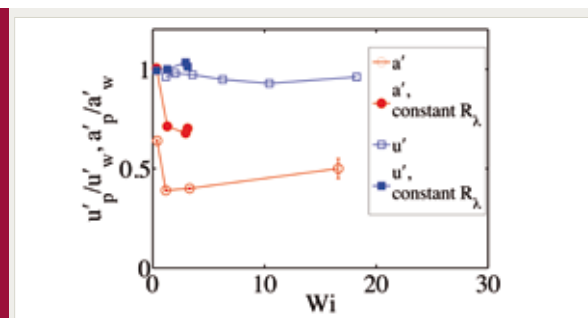


Figure 1

The RMS velocity u' and RMS acceleration a' as functions of Wi . Both u' and a' are normalized by the corresponding values with pure solvents (the subscripts "p" and "w" stand for polymer solutions and the pure solvents, respectively). The polymer concentrations were fixed at 5 ppm. Open symbols: data from [3, 4] with R_λ varying with Wi . Solid symbols: present study, with R_λ kept at 210, except the highest Wi case, which was at $R_\lambda = 160$.

ically [8, 9]. Therefore, n should be regarded as a parameterization of the averaged effect and may be smaller than 1. In summary, we studied experimentally the effect of Wi on turbulence-polymer interaction. We show that the polymer effect on turbulence is consistent with the elastic theory by de Gennes [7]. Currently we are investigating the effect around the onset of coil-stretch transition at $Wi \approx 1$. In addition, we are attempting to calculate directly the parameter n from velocity gradient measurements in Newtonian flow turbulence.

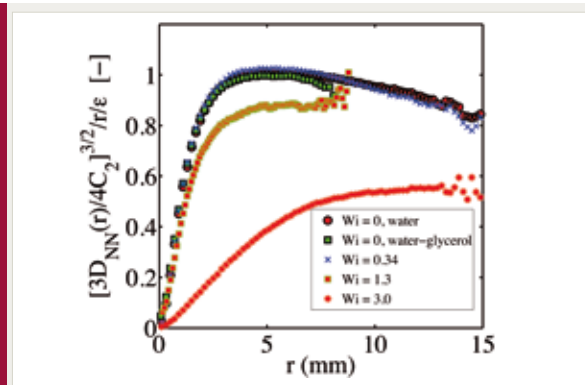


Figure 2

The second order Eulerian transverse velocity structure functions compensated by the inertial range scaling for the Newtonian flow of pure solvents. In this plot, the Newtonian flow data display plateaus of value 1 in the inertial range. All the data shown in the figure are at $R_\lambda = 210$.

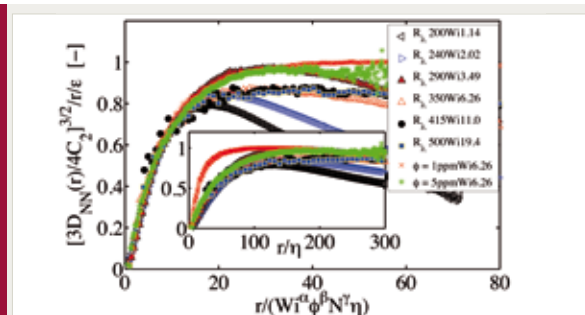


Figure 3

Collapsing of the compensated Eulerian velocity structure functions with varying Wi , R_λ , and ϕ , when r normalized by the length scales r^{**} . Data from [4] are also included. The $Wi = 1.3$ and $Wi = 3.0$ data from current measurements are not shown here because they are above the critical concentration observed in [4]. In the inset, the same data are plotted with r normalized by the Kolmogorov scale.

- [1] S. Berti et al., *Europhys. Lett.* **76**, 63 (2006)
- [2] A. Crawford et al., *Advances in Turbulence IX*, 307 (2002)
- [3] A. M. Crawford et al., *New J. Phys.* **10**, 123015 (2008)
- [4] N. T. Ouellette, H. Xu, and E. Bodenschatz, *J. Fluid Mech.* **629**, 375 (2009)
- [5] A. Liberzon, et al., *Phys. Fluids* **21**, 035107 (2009)
- [6] J. L. Lumley, *J. Polymer Sci.* **7**, 263 (1973)
- [7] P. G. de Gennes, *Physica A* **140**, 9 (1986)
- [8] J. Schumacher, K. R. Sreenivasan, V. Yakhot, *New J. Phys.* **9**, 89 (2007)
- [9] D. A. Donzis, P.-K. Yeung, K. R. Sreenivasan, *Phys. Fluids* **20**, 045108 (2008)

II-2 Particles in Turbulence

G. Bewley, M. Gibert, E.W. Saw, H. Xu, E. Bodenschatz

S. Klein, S. Lambertz, J. Bec (CNRS-Nice, France), L. Collins (Cornell, USA), A. Pumir (CNRS-Lyon, France), F. Schmitt (CNRS-Wimereux, France), R. Shaw (Michigan Tech. Univ., USA), Z. Warhaft (Cornell, USA)

THE INTERACTION between particles and turbulent flow occurs in many natural and industrial processes. Examples can be found in systems as different as the evolution of atmospheric clouds [1], the deposition of particles in human respiratory system [2], and the early stage of star or planet formation [3]. When a particle is smaller than the smallest scales of turbulence (Kolmogorov length scale η) and has the same density as the surrounding fluid, it follows the flow faithfully and its back-reaction to the flow is negligible. These passive particles have been used extensively as tracers in flow measurements [4]. An interesting problem is when the particles' inertia becomes important. This occurs when either the densities differ from that of the fluid or/and if their sizes are larger than the Kolmogorov scale η . We have been studying these effects in two different experiments. Let us first consider particles smaller than η , but with densities larger than the fluid density. For these "heavy-but-small" particles, the problem of interest is the relative velocity and acceleration between them, at both inertial and dissipative scales of the turbulence. The first set of measurements was carried out in a horizontal von Kármán water flow. We compared the dynamics of 3 types of particles with different relative densities ($\rho_p/\rho_f \approx 1, 4$ and 8) but the same size ($d_p \approx \eta$). The Stokes numbers (defined as the ratio of the particle response time to the Kolmogorov time) were in the range $0.1 \leq St \leq 0.5$. We observed an increase of relative velocity with St for particle separations in the inertial range [5], which could be qualitatively explained by a simple model based on the widely used equation of motion for point-mass particles [6, 7]. The model, however, failed to account for the scale-dependence of the increase of relative velocity. We attribute this to the preferential dis-

tribution of inertial particles in strain-dominated regions, which are not captured by the model. We showed later that this preferential sampling could be probed from the alignment angles between relative velocity and relative acceleration (figure 1), as co-linear alignments appear more frequently in strain-dominated fields [8]. This dynamical interpretation opens a new way to study the preferential concentration effect of inertial particles through two-points statistics. For problems such as collision and coalescence of droplets in clouds, the relative velocity between particles at scales below the Kolmogorov scale is of interest, which we investigate in a new turbulence chamber named the "Soccer Ball/R2D2". The device utilizes 32 loudspeaker driven air jets to create homogeneous and isotropic turbulence with negligible mean flow in the center of the chamber. Particles with significant inertial effects ($St \approx 1$) can be reached with small liquid droplets ($d_p \ll \eta$) due to the large density ratio, which is hard to achieve in the von Kármán water flow. In figure 2, we show the measured relative velocity variances as a function of separation distances, for droplets with two different sizes. Clearly, the relative velocities increase with particle size (or Stokes number), similar to what we observed in the von Kármán water flow experiments for particle separations in the inertial range. Moreover, for both particles, the relative velocities remain constant even for the smallest distances between particles measured, which implies significant enhancement to collision frequency due to particle inertia. Our next step is to study quantitatively the relative velocity and preferential concentration [9] of inertial particle, and their effects on particle collisions.

In the second set of experiments, we study the interaction between turbulent flows and neutral-

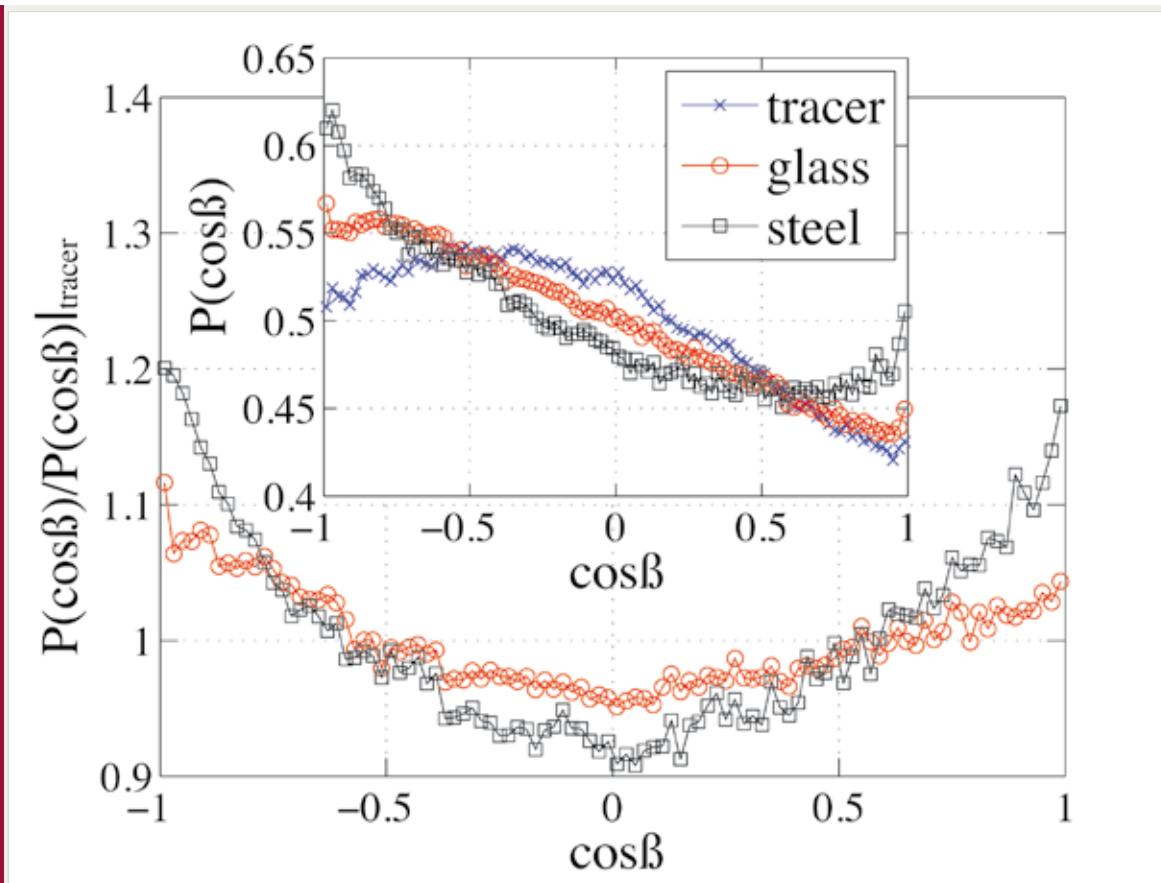


Figure 1

Probability density function (PDF) of the cosine of the angle β between the relative velocities and the relative accelerations for the three types of particles at separation $r/\eta = 28 \pm 7$. The main plot shows the PDFs for glass and steel particles, normalized by that measured for tracer particles. The inset shows the un-normalized PDFs. The enhancement of co-linear alignments is clearly visible for particles with appreciable inertia.

ly buoyant particles with size larger than the Kolmogorov scale. This problem not only is of theoretical importance, but also finds applications in, e.g., plankton dynamics [10]. At present, fully resolved simulations of turbulent flows coupled with finite-sized particles are demanding and are limited to very low Reynolds numbers. Significant advances in the field require measurements of the particle motion (both translation and rotation) together with the surrounding fluid velocity field at high Reynolds numbers. For such a measurement, we used water-soaked superabsorbent polymer particles, which have the same density and index of refraction as water and are made visible by the injection of a few fluorescent markers on their surfaces. The same fluorescent

particles, of diameter $100 \mu\text{m}$, were seeded into the flow as tracers for the measurement of fluid velocity field. After obtaining the trajectories of all the fluorescent particles using our particle tracking technique, we used an efficient algorithm to identify the group of particles whose mutual distances remained constant along their trajectories, which corresponded to the markers on the surfaces of the large particles and were used for further calculation of the translation and rotation of the large particles. Figure 3 shows an example of the trajectories of these markers, together with the trajectories of the fluid tracers, from a measurement in the von Kármán water flow. Using this technique, we studied the distribution of longitudinal velocity differences between the

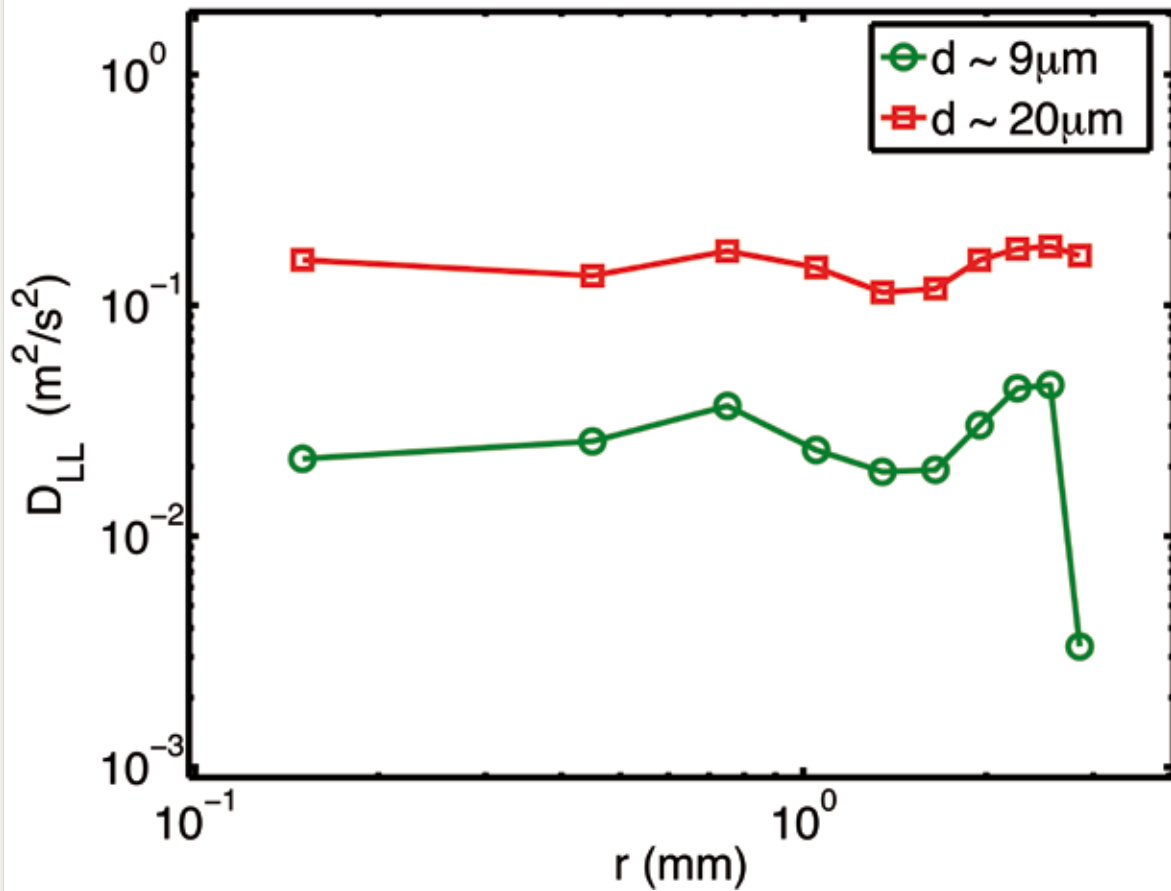


Figure 2

Variance of the velocity differences between particle pairs, as a function of their separation within the dissipative scale ($< 20 \eta$, in this case $\eta \sim 200 \mu m$). All particles here are smaller than η . It can be seen that the larger, heavier particles with $d_p \sim 20 \mu m$ ($St \sim 0.4$) have larger velocity differences relative to the smaller particles ($St \sim 0.08$). This suggests that heavier particles will sustain non-zero relative velocity even at zero separation distance.

larger particles and the surrounding fluid (figure 4). A boundary layer of size about one particle radius is clearly visible, where the fluid velocity was affected by the presence of the large particle and hence relative velocity deviated significantly from the expected scaling for fluid turbulence without particles. These results are also observed in a very recent low-Reynolds-number numerical simulation that resolved the boundary layers around solid particles [11]. A quantitative comparison of these results is underway. Our results also enlighten the presence of a recirculation zone and the wake behind the large particles (not shown here).

In summary, stepping from our Lagrangian particle tracking technique developed for turbulence measurement, we are venturing into a less studied and even more interesting field of particles in turbulence. In addition to the cases of “heavy-but-small” and “large, neutrally buoyant” particles described above, we are extending the study to the dynamics of copepods and the formation of planet from protoplanetary disks.

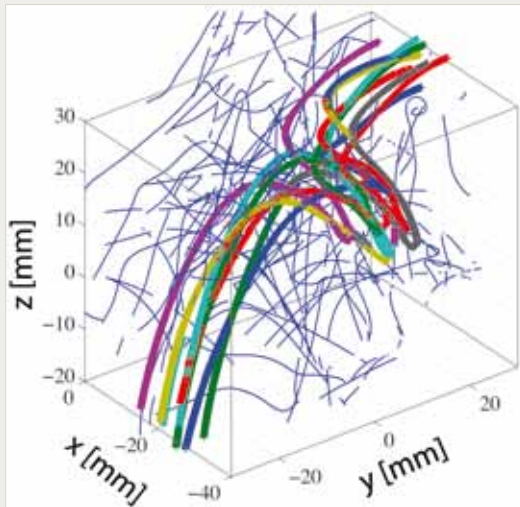


Figure 3

Examples of measured particle trajectories in the von Kármán water flow. The duration of the measurement was 0.3 second and the frame rates of the cameras were 3000 frames per second. The thick colored curves represent the trajectories of the markers on the surface of a large, neutrally buoyant particle. The thin blue ones were the trajectories of tracers particles seeded in the flow.

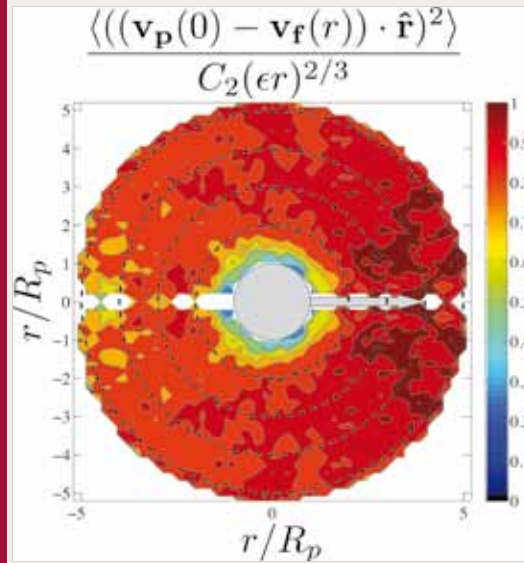


Figure 4

Cylindrical symmetry average around the velocity direction of the big particle (represented by the grey circle in the center). Second order moment of the distribution of longitudinal velocity differences (along the separation vector \mathbf{r}) normalized by the expected value for a fluid particle (K41). Far from the particle, the flow field is undisturbed (ratio is 1); but close to the particle, one can see a zone where the correlation between the particle velocity and the flow velocity is very high.

- [1] R. A. Shaw, *Annu. Rev. Fluid Mech.* **35**, 183 (2002)
- [2] A. Guha, *Annu. Rev. Fluid Mech.* **40**, 311 (2008)
- [3] A. Johansen et al., *Nature* **448**, 1022 (2007)
- [4] N. T. Ouellette, H. Xu, E. Bodenschatz, *Exp. Fluids* **40**, 301 (2006)
- [5] M. Gibert, H. Xu, E. Bodenschatz, *Europhys. Lett.* **90**, 64005 (2010)
- [6] R. Gatignol, *J. Mech. Theor. Appl.* **2**, 143 (1983)
- [7] M. Maxey, J. Riley, *Phys. Fluids* **26**, 883 (1983)
- [8] M. Gibert, H. Xu, E. Bodenschatz, *arXiv:1002.3755* (2010)
- [9] E-W. Saw et al., *Phys. Rev. Lett.* **100**, 214501 (2008)
- [10] J. Mann et al., *J. Plankton Res.* **28**, 509 (2006)
- [11] H. Homann, J. Bec, *J. Fluid Mech.* **651**, 81 (2010)

II-3 Warm Clouds and Turbulence

G. Bewley, E.-W. Saw, H. Xi, H. Xu, E. Bodenschatz

S. Risius, S. Raasch (Univ. Hannover, Germany), J. Schumacher (TU Ilmenau, Germany), R. Shaw (Michigan Tech. Univ., USA), H. Siebert (IfT, Germany)

CLOUDS ARE dispersions of water droplets and ice particles embedded in and interacting with a complex and turbulent flow. Like other phenomena in the atmosphere, clouds are highly non-stationary, inhomogeneous, and intermittent. They embody an enormous range of spatial and temporal scales. Strong coupling across those scales between turbulent fluid dynamics and microphysical-chemical processes, e.g., evaporation and condensation, freezing and melting, deposition and sublimation are inherent to cloud evolution [1] (see figure 1). As discussed in [1], the effect of turbulence on clouds is largely unknown. A noticeable example is the rain formation in warm clouds. Cloud droplets are initiated by water vapor condensation on aerosol particles (cloud condensation nuclei, CCN). The growth of cloud droplets by condensation slows down with the increase of droplet size. It is believed that collision-coalescence dominates for droplets of size 10-20 μm and larger. When analyzing the growth rate by coalescence, the difference in gravitational settling velocities due to droplet size difference had long been regarded as the leading mechanism for raindrop initiation. However, this approach overestimates the time to rain formation by up to a factor of 10. Recent studies suggest that the collision rate among droplets could be greatly enhanced due to hydrodynamic interactions between droplets and turbulence [2, 3]. In addition, turbulence governs entrainment and mixing of dry, moist, and droplet-laden air. To a large extent, the difficulty in this problem lies in the fact that cloud turbulence spans a huge range of spatial and temporal scales. At present, it remains extremely difficult to mimic cloud conditions in laboratory experiments or numerical simulations. Field observations using state-of-the-art measurement techniques constitute one of the promising options.

We have been carrying out measurements of cloud-turbulence interactions at Umwelt Forschungsstation Schneefernerhaus (UFS) on the top of Zugspitze (2700 m above sea level). The wind at UFS is preferentially in the east-west direction, which helps reduce the complexity in the design of the measurement apparatus. Moreover, there is a relatively high probability to have clouds covering the observation site at UFS in the summer. Since August 2009, we have conducted 3 field campaigns at UFS. We have successfully set up ultrasonic sensor arrays to monitor the atmospheric turbulence and have conducted pilot Lagrangian particle tracking measurements of cloud droplets using a prototype device consisting of three high speed cameras installed in a stationary, water-proof box (figure 2). These measurements are complemented by simultaneous cloud microphysics measurements, including temperature, liquid water content, droplet number density, droplet size, and Eulerian air velocity measurements, carried out by our collaborators H. Siebert from Leipzig and R. Shaw from Michigan Tech. Analysis of these data is on the way. Currently, we are constructing an apparatus that will use a "sled" to drive our droplet-tracking system at the mean wind speed, by which we can follow cloud droplets for longer times. The droplet-tracking system, similar to the one tested in the prototype, will be driven by a linear motor with a speed up to 7.5 m/s along a 6.6 m long rail (see figures 2 & 3). In each run of the sled, the high-speed cameras can record up to 1 second of the motion of cloud droplets, which is equivalent to approximately 30 Kolmogorov times, more than enough to resolve droplet dynamics relevant to collision and coalescence.

In addition to field observations, we also conduct well-controlled laboratory experiments in

our pressurized wind tunnel and in small-scale turbulence generators (e.g. the “soccer-balls” [4]), in which the turbulence properties can be fine tuned. By compressing gases, e.g., air, nitrogen, or SF₆ (an inert, heavy gas), to high pressure, we can reduce gas kinematic viscosities and the flow in the wind tunnel can reach a condition very close to that in natural clouds – much closer than those achieved in previous lab experiments. In these experiments, we can study not only the hydrodynamic interaction between droplets and turbulence; we can also change the microphysical properties of the flow, such as supersaturation and temperature. Moreover, we are working together with two numerical simulation groups to study the mixing and entrainment in cumulous clouds. S. Raasch from Hannover is modeling the dynamics of a complete cumulous cloud throughout its life-

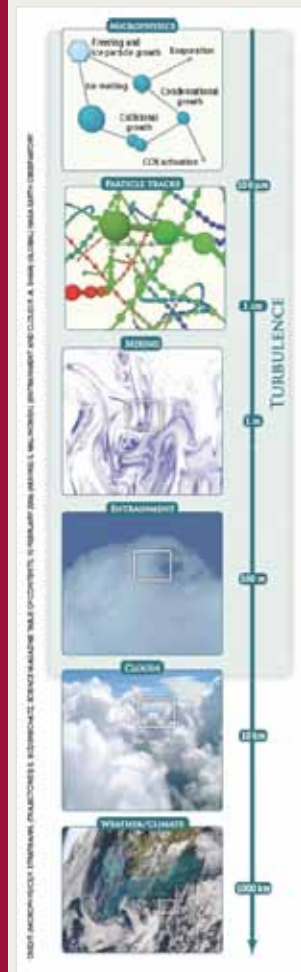


Figure 1 (From Ref. [1]) The range of scales covered by clouds and the dominating phenomena/problems at different scales.



Figure 2 The topography of the UFS at Zugspitze, showing with the prototype of droplet-tracking device, the sonic sensors, and the future installation of the “sled”.

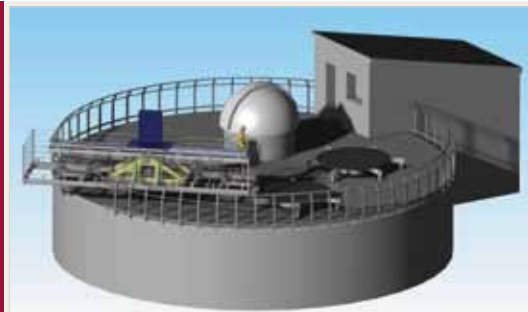


Figure 3 Computer generated image of the “sled”. The total length of the apparatus is 8 m long, with a 6.6 m long rail. A linear motor drives the droplet-tracking device at a speed of up to 7.5 m/s along the rail. The inclination of the sled can be adjusted within ±14° relative to the horizontal plane, according to the instantaneous mean wind direction measured by the sonic sensors.

time using LES together with Lagrangian droplets. J. Schumacher from Illmenau is modeling the detailed interaction between turbulence (resolved by DNS) and cloud droplets (treated as Lagrangian particles) at the interface between the cloud and clear air, including condensation and evaporation. The combined data, spanning a wide range of scales, from field observations, lab experiments, and numerical simulations would possibly elucidate the role of turbulence in clouds.

[1] E. Bodenschatz, et al, *Science* **327**, 971 (2010)
 [2] R. A. Shaw, *Annu. Rev. Fluid Mech.* **35**, 183 (2002)
 [3] G. Falkovich, A. Fouxon, M. G. Stepanoc, *Nature* **419**, 151 (2002)
 [4] C. Chang, G. Bewley, E. Bodenschatz, *under review*

II-4 Non-equilibrium Molecular Transport in Spiny Neuronal Dendrites

D. Tsiganov, S. Eule

RECENT ADVANCES in imaging techniques allowed a direct observation of molecular diffusion inside neural cells in vivo [1]. Neurons have highly elaborated dendritic arbors of complex geometries. Most of the synaptic contacts with other neurons are formed on dendritic spines, which are small membrane protrusions of various sizes and shapes along the dendritic shaft. With the use of local photolysis of caged compounds the fluorescence of molecules that were initially located in a single spine [1] or a part of a dendrite [2] can be imaged over time. It was found that diffusion of various molecules is strongly influenced by the presence of dendritic spines as it was recognized that spines act as transient traps for diffusing molecules.

In this project we investigate a model of stochastic molecular transport in the spiny dendrites of neurons. We show that if the molecules interact with each other inside the spines then the trapping times depend on the occupancy of the traps. In addition we consider the biologically relevant case when the pool of molecules is being constantly replenished. This is of importance since the molecules in the neurons eventually dissociate and thus have a finite lifetime. Due to the on-site interactions between the random walkers, the trapping times can become significantly larger than the typical timescale of diffusion between the spines. Therefore we can neglect the diffusion between the sites and consider in-

stantaneous jumps on an array of discrete sites (see figure 1). Thus in this model the molecules perform a random walk between the spines that trap the walkers with the trapping time in each spine being dependent on the number of molecules in the respective trap. Then the system can be described by the following non-linear master equation

$$\begin{aligned} \frac{dP_n(j,t)}{dt} = & \sum_i W_{ij} \left(\frac{n+1}{\tau(n+1)} P_{n+1}(j,t) - \frac{n}{\tau(n)} P_n(j,t) \right) + \\ & + \sum_i W_{ji} \sum_m \frac{m}{\tau(m)} P_m(i,t) (P_{n-1}(j,t) - P_n(j,t)) + \\ & + \frac{1}{\tau_{\text{life}}} (n_0 P_{n-1}(j,t) - n_0 P_n(j,t) + (n+1) P_{n+1}(j,t) - n P_n(j,t)) \end{aligned}$$

This system of nonlinear differential equations describes the dynamics of the probability $P_n(j,t)$ that site j has exactly n walkers at time t , given that the connectivity between the sites is described by the matrix W . These equations describe the non-equilibrium dynamics of a driven diffusive system which evolves towards a steady state which is far from equilibrium and falls into class of zero-range processes [3].

We obtain steady state distributions for the occupancies when the connectivity matrix is translational invariant, as is the case for nearest neighbor connectivity on a 1D ring, which is a representation of the dendritic branch topology. In the biologically important case when the trapping times are given by $\tau(n) = \tau_0 n^\alpha$ the steady state distribution is given by:

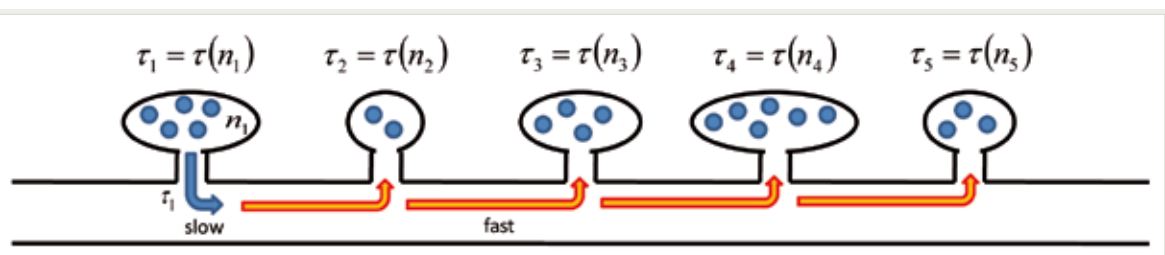


Figure 1

Schematic representation of the model. The molecules diffuse along the dendritic shaft while being captured inside the spines. The trapping times inside the spine are typically much longer than the diffusion times and depend on the occupancy of each individual spine.

$$P(n) = P_0 \frac{\left(M_{1-\alpha} + n_0 \frac{\tau_0}{\tau_{life}} \right)^n}{\prod_{m=1}^n \left(m^{1-\alpha} + m \frac{\tau_0}{\tau_{life}} \right)}$$

Here

$$M_{1-\alpha} = \sum_{m=1}^{\infty} m^{1-\alpha} P_m$$

is $(1-\alpha)$ th moment of the distribution, that gives

the average rate of jumps in the system. The steady state distributions for various lifetimes and types of on-site interactions are shown on figure 2. Hence we show for a system of molecules in neuronal spiny dendrites which is in a state far from equilibrium that inter-spine molecular transport results in non-trivial distributions of accumulated molecules due to self-organization phenomena.

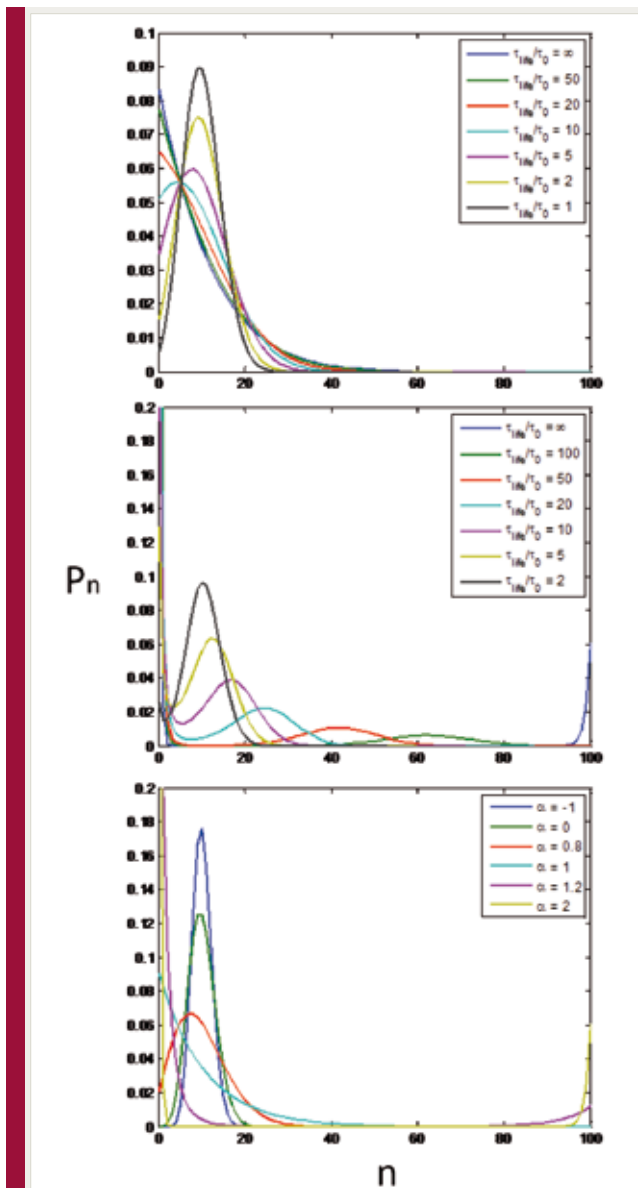


Figure 2

Stationary distributions of trap occupancies. Top panel: the distributions of trap occupancies for different lifetimes are shown for the case $\alpha=1$. Middle panel: the same for $\alpha=2$, note that for this case in the equilibrium every molecule resides in one trap (winner-take-all regime). Bottom panel: the stationary distributions for different on-site interaction types (different values of α) when molecule lifetimes are infinite.

- [1] Gray NW, Weimer RM, Bureau I, Svoboda K. *PLoS Biol.* 4 (11), e370 (2006)
- [2] Santamaria F, Wils S, De Schutter E, Augustine GJ. *Neuron* Nov 22 52 (4), 635-48 (2006)
- [3] Evans MR and Hanney T, *J. Phys. A: Math. Gen.* 39, R195-R240 (2005)

II-5 Anomalous Kinetics in Physical and Biological Systems

S. Eule, T. Geisel

V. Belik, D. Lammouroux, M. Lukovic, J. Nagler, R. Friedrich (WWU Münster)

MANY COMPLEX systems in nature are exposed to a constant flux of energy and thus are in a state far from equilibrium. A common feature of such systems is the occurrence of intricate fluctuations which can either be induced by a complex environment or stem from internal processes. It has become common practice that whenever the kinetics resulting from these fluctuations deviate from the standard patterns of Gaussian or Poissonian statistics, one speaks of anomalous kinetics. In order to describe the increasing number of physical and biological systems exhibiting such an anomalous behavior quantitatively, new stochastic mathematical models need to be developed.

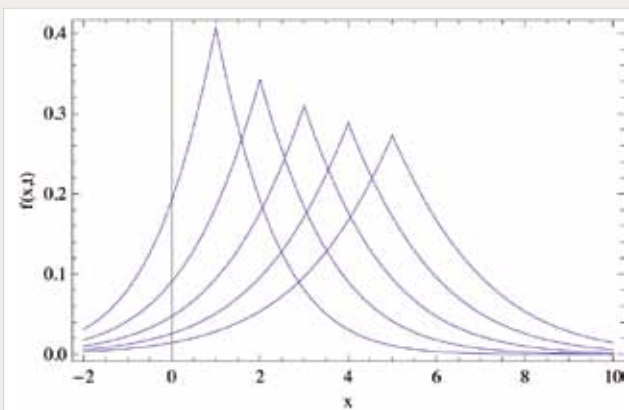
Our research group focuses on the description of stochastic processes which are governed by long, scale-free waiting time distributions. Well-known examples belonging to this class are the Continuous Time Random Walk and the Lévy Walk [1, 2]. We are interested in the mathematical formulation of stochastic processes whose dynamics are governed by anomalously long waiting times and additionally are subjected to the impact of a deterministic internal dynamics. For this class of processes we are able to formulate a generalized Fokker-Planck equation of the form

$$[\partial_t - \mathcal{L}]f(x, t) = \int_0^t dt' \phi(t - t') \mathcal{L}_{FP} e^{(t-t')\mathcal{L}} f(x, t')$$

where the Liouville operator L describes the deterministic internal dynamics, \mathcal{L}_{FP} is the Fokker-Planck operator and the integral kernel $\phi(\tau)$ is related to the waiting time statistics of the anomalous dynamics [3]. Applying this equation we can formulate a subdiffusive reaction-diffusion equation also for nonlinear reaction kinetics which is of relevance for pattern formation in biological systems and in complex media. The simplest case of the generalized Fokker-Planck equation leads to an anomalous advec-

tion-diffusion equation in which the advection is regular but the diffusion is governed by anomalous dynamics, which is interesting in the context of diffusion of contaminants in porous media. The time-evolution of the probability density distribution of such a process is plotted in figure 1. Based on this simple example, we discuss the non-trivial role of external forces in systems exhibiting anomalous diffusion. Similar to the effect of external potentials in Lévy Flight processes [4, 5], we show that the inclusion of external forces depends on the physical context and introduce the concept of decoupled and biasing forces [6]. This concept clarifies the fact that external forces can affect the dynamics of a Continuous Time Random Walk in two different ways. On the one hand external forces can influence the motion of a particle during the long waiting periods and are therefore decoupled from the diffusion process, see figure 1. On the other hand one can also think of an external force which affects the diffusion process only at the transitions and thus is biasing the transition, see figure 2. To gain a better understanding of these processes, we also have formulated the corresponding Langevin description, based on the mathematical concept of subordination [7]. This description allows for a thorough analysis of the sample paths of such processes [6].

In a related project we consider the motion of particles in a field of randomly distributed scatterers. Mapping this problem onto a master equation describing the anomalous diffusion of inertial weakly damped particles [8] we have derived the governing master equation for this problem [9]. This work is motivated by numerical simulations of particle motion in magnetohydrodynamic turbulence [10]. In another important application of the stochastic process developed in [8], we model the motility of run and tumble bacteria with non-exponentially distributed run-times. Such a non-Poissonian

**Figure 1**

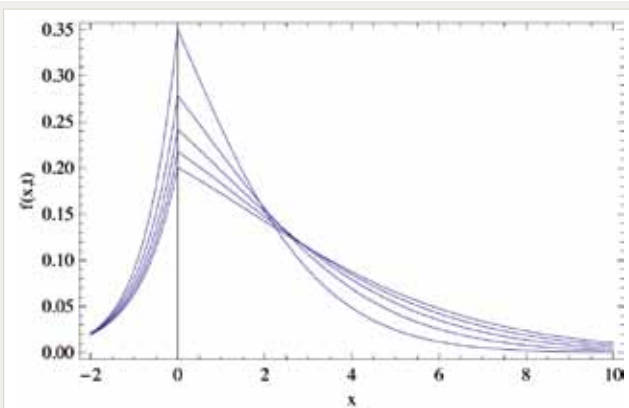
Evolution of the probability distribution function for a subdiffusive process in presence of a constant decoupled external force for the consecutive times $t=1-5$ with the initial condition $f(x,0)=\delta(x)$. This case generalizes the regular advection-diffusion equation to advected subdiffusive processes governed by Continuous Time Random Walk dynamics.

switching behavior between the run and the tumble state of the flagella motor has been measured in experiments with wild-type E.Coli bacteria described in [11]. Shifting the focus from bacteria to general biological movement models [12], we can also formulate a non-Markovian velocity jump model. This model generalizes the standard formulation of correlated random walk models in ecology to also account for scale-free, Lévy Walk like movement patterns which have been observed for an increasing number of foraging animals, see e.g. [13].

In recent years empirical studies have generated a controversy if animals forage according to Lévy Walk patterns or if the indications for a Lévy foraging behavior are only due to a poor accuracy of the employed statistical methods. In this context we examine the convex hull enclosing the trajectory of a Lévy Walk, see figure 3. The convex hull is the minimal polygon enclosing a particular trajectory and serves as

a model for the home range of a foraging animal [14]. With the help of numerical simulations, we find that the convex hull is a statistically robust quantity to discriminate between the origin of different stochastic sample paths even in the absence of the complete trajectory. Thus the analysis of convex hulls of movement patterns of foraging animals in principle allows for a quantification of how Lévy-Walk-like or how anomalous this movement pattern is.

Another important problem in the theory of ecological systems is their viability, for which biodiversity plays an essential role. Motivated by a model of mobile, cyclically competing species proposed by Reichenbach et al. [15], we investigate the impact of the carrying capacity on the biodiversity in such model systems where species compete for limited resources. The incorporation of a carrying capacity facilitates the investigation of the role of the population size on the mean extinction times of the species. Thus

**Figure 2**

Effect of a biasing external force on the time-evolution of the probability distribution of a Continuous Time Random Walk process with the same parameters as in figure 1. The probability distributions are again plotted for the consecutive times $t=1-5$. In contrast to the decoupled case, the shape of the probability distribution gets more asymmetric with time, reflecting the effect of the bias. Note the persistence of the maximum at the origin, indicating that there is no internal dynamics during the waiting times.

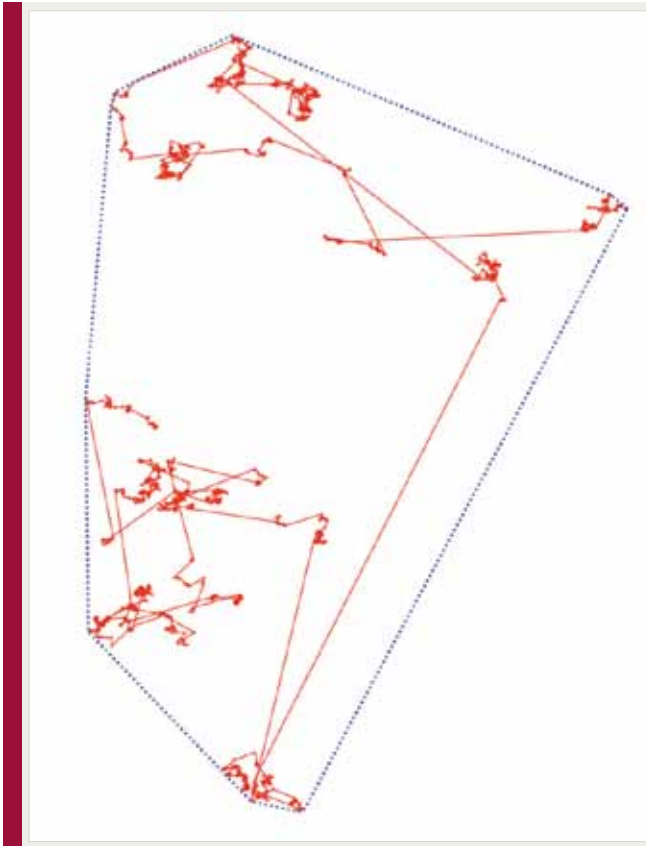


Figure 3

Picture of a Lévy Walk trajectory (red). The blue dotted polygon depicts the convex hull of the Lévy Walk trajectory.

our model is able to distinguish between system size and population size effects on the species diversity in the considered class of ecosystems with cyclic, non-hierarchical interactions among the competing species.

In contrast to the rather erratic motion of animals, human mobility patterns are more regular, as human individuals typically only visit a limited number of locations frequently. Consequently individuals display spatially constrained movement patterns, despite their potentially high mobility rate.

We scrutinize the impact of these mobility patterns on the geographic spread of emergent infectious diseases such as H1N1 or SARS.

Contrary to the standard reaction-diffusion description of spatial disease dispersion our model exhibits dynamical features such as the existence of a bounded front velocity and a novel invasion threshold [16].

- [1] T. Geisel, J. Nierwetberg and A. Zacherl, *Phys. Rev. Lett* **54**, 616 (1985)
- [2] R. Metzler and J. Klafter, *Phys. Rep.* **339**, 1 (2000)
- [3] S. Eule, R. Friedrich, F. Jenko and I.M. Sokolov, *Phys. Rev. E* **78**, 060102(R) (2008)
- [4] D. Brockmann and T. Geisel, *Phys. Rev. Lett.* **90**, 170601 (2003)
- [5] D. Brockmann and T. Geisel, *Phys. Rev. Lett.* **91**, 048303 (2003)
- [6] S. Eule and R. Friedrich, *EPL* **86**, 30008 (2009)
- [7] M. Magdziarz, A. Weron and J. Klafter, *Phys. Rev. Lett.* **101**, 210601 (2008)
- [8] R. Friedrich, F. Jenko, A. Baule and S. Eule, *Phys. Rev. Lett.* **96**, 230601 (2006)
- [9] H. Affan, R. Friedrich and S. Eule, *Phys. Rev. E* **80**, 011137 (2009)
- [10] H. Homann, R. Grauer, A. Busse and W.C. Müller, *J. Plasma Phys.* **73**, 821 (2007)
- [11] E. Korobkova, T. Emonet, J.M.G. Villar, T.S. Shimizu and P. Cluzel, *Nature* **428**, 6982 (2004)
- [12] E.A. Codling, M.J. Plank and S. Benhamou, *J. Roy. Soc. Interf.* **5**, 813 (2008)
- [13] N.E. Humphries et al., *Nature* **465**, 1066 (2010)
- [14] J. Random-Furling, S.N. Majumdar and A. Comtet, *Phys. Rev. Lett.* **103**, 14062 (2009)
- [15] T. Reichenbach, M. Mobilia and E. Frey, *Nature* **448**, 1046 (2007)
- [16] V. Belik, T. Geisel and D. Brockmann, *Phys. Rev. X* (2011), in press.

II-6 Theory of Parity-Time-Symmetric Photonics

T. Kottos, R. Fleischmann, O. Bendix

M. C. Zheng, C. T. West, H. Ramezani, H. Cao (Yale, USA), D. Christodoulides (UCF, USA), T. Prosen (Ljubljana, Slovenia), B. Shapiro (Technion, Israel).

IN THE LAST few years considerable research effort has been invested in developing artificial materials appropriately engineered to display properties not found in nature. In the electromagnetic domain, such metamaterials make use of their structural composition, which in turn allows them to have complete access of all four quadrants of the real ϵ - μ plane. Several exotic effects ranging from negative refraction to superlensing and from negative Doppler shift to reverse Cherenkov radiation can be envisioned in such systems. Quite recently, the possibility of synthesizing a new family of artificial optical materials that instead rely on balanced gain/loss regions has been suggested. This class of optical structures deliberately exploits notions of parity (P) and time (T) symmetry [1] as a means to attain altogether new functionalities and optical characteristics. Under PT-symmetry, the creation and absorption of photons occurs in a controlled manner, so that the net loss or gain is zero. In optics, PT symmetry demands that the complex refractive index obeys the condition $n(r)=n^*(-r)$, in other words the real part of the refractive index should be an even function of position, whereas the imaginary part must be odd. PT-synthetic materials can exhibit several intriguing features. These include among others, power oscillations, absorption enhanced transmission, double refraction and non-reciprocity of light propagation. Other exciting theoretical results within the framework of PT-optics include the study of Bloch oscillations, and the realization of coherent perfect laser absorbers. Recently the first experimental realizations of PT symmetric systems have been reported [2-4].

To date, most of the studies on optical realizations of PT synthetic media have relied on the paraxial approximation which maps the sca-

lar wave equation to the Schrödinger equation, with the axial wavevector playing the role of energy. This formal analogy, allows one to investigate experimentally fundamental PT-concepts that may impact several other areas, ranging from quantum field theory and mathematical physics, to solid state and atomic physics. Among the various themes that have fascinated researchers, is the existence of spontaneous PT-symmetry breaking points (exceptional points) where the eigenvalues of the effective non-Hermitian Hamiltonian describing the dynamics of these systems abruptly turn from real to complex.

In Ref. [5] we show that nonlinear optical couplers involving a balanced gain-loss profile can act as unidirectional optical valves. This is made possible by exploiting the interplay of nonreciprocal dynamics arising from PT symmetry, and self-trapping phenomena associated with Kerr nonlinearities, which mold the flow of light in a surprising way (see figure 1). Such directed dynamics can be exploited in the realization of a new generation of optical isolators or diodes. Currently, such unidirectional elements rely mainly on the Faraday effect, where external magnetic fields are used to break the space-time symmetry. This in general requires materials with appreciable Verdet constants – typically noncompatible with light-emitting wafers. Thus, our proposal [5] for optical diodes can find direct applications to on-chip optical circuitry.

In Refs. [6, 7] we investigated the PT-symmetric scenario for more complicated coupled waveguide structures, where imperfections are taken into consideration. It was pointed out that the exact PT phase (real eigenvalue regime) is extremely fragile to impurities or boundary effects that lead to the creation of localized modes. Thus, there are many systems which, in spite

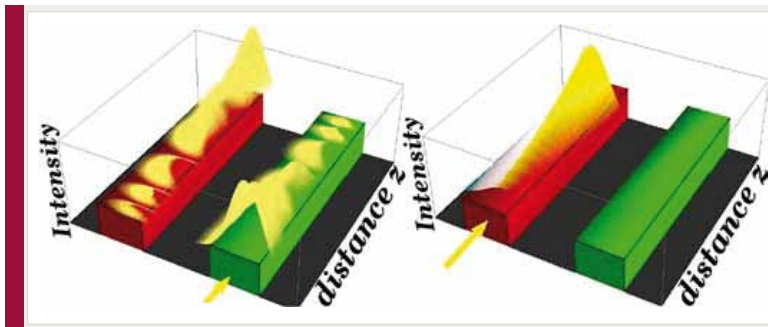


Figure 1
The unidirectional beam propagation in two nonlinear coupled PT symmetric waveguides allows the realization of unidirectional optical devices.

of being PT-symmetric, never exhibit in practice an entirely real spectrum (the breaking of PT -symmetry does not necessarily affect transport because it might take a very long distance – proportional to the inverse imaginary eigenvalue – before a propagating beam will ‘discover’ the existence of localized modes). A renormalization theory that describes the flow of the critical gain/loss parameter (that dictates the PT-exceptional point) as a function of impurities strength (disorder) was suggested in Ref. [7]. Furthermore, in Ref. [8] we proposed structures which avoid this problem altogether. This is done by giving up global PT symmetry and resorting to *local* PT symmetry that fulfills the criteria of a generalized PT symmetry [9]. A pos-

sible realization of such a locally PT symmetric system is depicted in figure 2.

In Ref. [10] we investigated beam dynamics in PT-synthetic optical media. We found that the beam power evolution is insensitive to microscopic details of the system and that it follows three distinct universal laws which depend only on the magnitude of the gain or loss parameter. Our theoretical calculations were confirmed numerically for the experimentally realizable case of a lattice consisting of horizontally coupled PT-symmetric dimers.

Finally in Ref. [11] we explored the possibility of synthesizing PT-symmetric objects which can become unidirectionally invisible at the exceptional points. In recent years the subject of

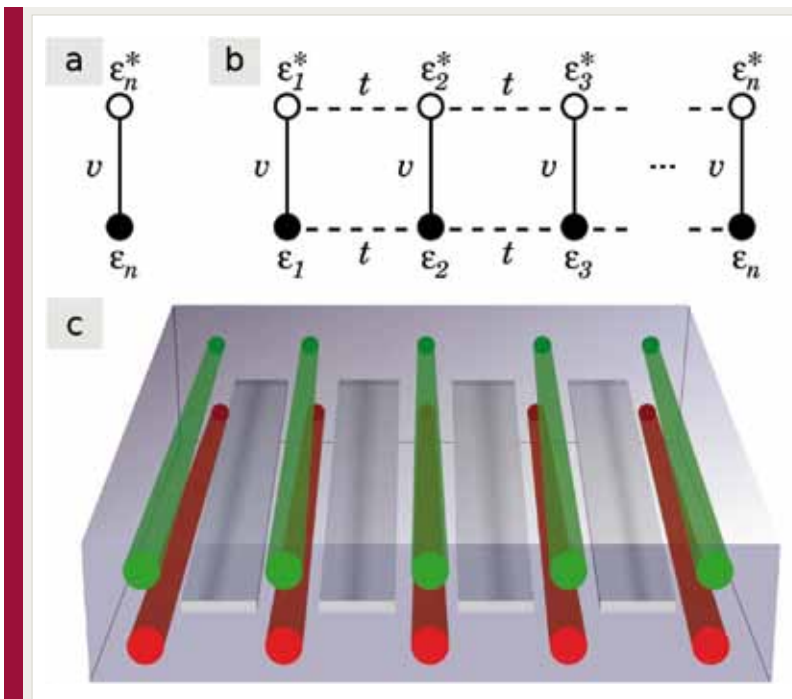


Figure 2
Local PT symmetry. (a) Individual dimers with strong coupling v are (b) coupled together with coupling parameter $t < v$ leading to robust pseudo hermitian behavior. (c) A possible realization with optical waveguides.

cloaking physics has attracted considerable interest, specifically in connection to transformation optics. In Ref. [11], our notion of invisibility stems from a fundamentally different process. As opposed to surrounding a scatterer with a cloak medium, in our case the invisibility arises because of spontaneous PT-symmetry breaking. This is accomplished via a judicious design that involves a combination of optical gain and loss regions and the process of index modulation. Specifically, we consider scattering from PT-synthetic Bragg structures and investigate the consequences of PT symmetry in the scattering process. It is well known that passive gratings (involving no gain or loss) can act as high efficiency reflectors around the Bragg wavelength. Instead, we find that at the PT sym-

metric breaking point (exceptional point), the system is reflectionless over a broad frequency band around the Bragg resonance when light is incident from one side of the structure while from the other side its reflectivity is enhanced. Furthermore, we show that in this same regime the transmission phase vanishes – a necessary condition for evading detectability.

In conclusion, we have made considerable progress in the fundamental understanding of PT symmetry in complex optical systems [6-8, 10] and have made first steps towards designing actual and useful PT symmetric photonic metamaterials and devices [5, 11]. Currently we are expanding some of the unique properties of PT-dynamics in the frame of thermal transport and electronics LRC transmission lines.

- [1] An introduction to PT Symmetry can e.g. be found in C. Bender, *Contemporary Phys.* **46**, 277-292 (2005)
- [2] A. Guo, G. J. Salamo, D. Duchesne, R. Morandotti, M. Volatier-Ravat, V. Aimez, G. A. Siviloglou, and D. N. Christodoulides, *Phys. Rev. Lett.* **103**, 093902 (2009); C.E. Rüter, K. G. Makris, R. El-Ganainy, D. N. Christodoulides, M. Segev, and D. Kip, *Nat. Phys.* **6**, 192-195 (2010)
- [3] K. G. Makris, R. El-Ganainy, D. N. Christodoulides and Z.H. Musslimani, *Phys. Rev. Lett.* **100**, 103904 (2008)
- [4] Tsampikos Kottos, *Nature Physics* **6**, 166 (2010)
- [5] H. Ramezani, T. Kottos, R. El-Ganainy, D. N. Christodoulides, *Phys. Rev. A* **82**, 043803 (2010)
- [6] O. Bendix, R. Fleischmann, T. Kottos, and B. Shapiro, *Phys. Rev. Lett.* **103**, 030402 (2009)
- [7] C. T. West, T. Kottos, T. Prosen, *Phys. Rev. Lett.* **104**, 054102 (2010)
- [8] O. Bendix, R. Fleischmann, T. Kottos, and B. Shapiro, *J. Phys. A: Math. Theor.* **43**, 265305 (2010).
- [9] Ali Mostafazadeh, *J. Math. Phys.* **43**, 205 (2002); C.M. Bender, M.V. Berry, A. Mandilara, *J. Phys. A: Math. Gen.* **35**, L467–L471(2002)
- [10] Mei Zheng, Demetrios Christodoulides, Ragnar Fleischmann, und Tsampikos Kottos, *Phys. Rev. A* **82**, 010103(R) (2010)
- [11] H. Ramezani, Z. Lin, T. Eichelkraut, T. Kottos, H. Cao, D. N. Christodoulides, under review (2011)

II-7 Waveguides in the Retina and Light Scattering in the Eye

O. Bendix, R. Fleischmann, T. Geisel

IT HAS BEEN very convincingly shown in recent experiments that certain glial cells in the retina of vertebrates, called Müller cells, are capable of channeling light [1]. This finding might help to unravel a well known puzzle connected to the vertebrate eye: the inverse construction of the retina. Light that is projected from the lens of the eye onto the retina has to pass several layers of neural tissue before it reaches the light receptors that are located in the outermost layer of the retina. Though not strongly absorbing, these layers of neural tissue present fluctuations in the refractive index and thus scatter light and let this structure of the retina appear rather inefficient.

The inner layers of the retina are radially penetrated by the very long Müller cells with their funnel shaped end foot on the inner edge of the retina. The stalk of their main cell body is rod-like with a very high aspect ratio: less than $3\ \mu\text{m}$ wide and up to more than 0.1mm long. They have been attributed a number of functions, from stabilizing the retina to playing a crucial role in healing processes. For these functions they sprout various protrusions of their cell body.

In the experiments of Ref. [1] single Müller cells extracted from the retina were placed between

two optical fibers in a homogeneous medium with a similar index of refraction as the average index of refraction of the tissue surrounding the Müller cells in the retina. The stalks of the Müller cells have only an approximately 2% increased index of refraction and the cells were shown to guide the light from one fiber to the other even if slightly bend.

Embedded in the retina, however, the Müller cells will be surrounded by a fluctuating index of refraction. How can light be guided by a channel that is only defined by a slight change in the index of refraction, when the index of refraction of its surrounding medium fluctuates on the same scales? We studied this question by calculating scattering wave functions in a Gaussian correlated Gaussian random field penetrated by a flat channel, as shown in figure 1a. Due to the great length of the Müller cells of up to several hundred wavelengths of the light, we reduced the numerical cost by using a two dimensional wave model, corresponding to a vertical cut through the Retina. As illustrated in figure 1a we found that the light can be well guided by the channel even under these circumstances and found intensities comparable to those measured in the experiment. We examined different kinds of shape distortions (a few examples are

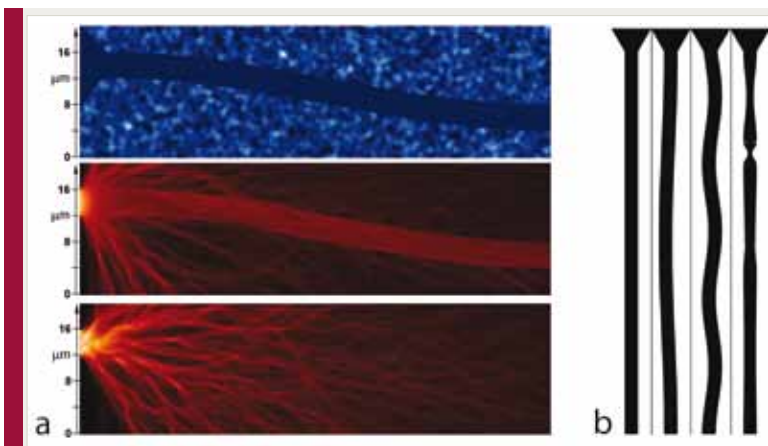


Figure 1

Light propagation through a simple retina model. (a) The disordered field modeling the index of refraction fluctuations penetrated by a flat channel of slightly elevated index of refraction (of approx 2%; upper panel). A narrow beam of light incident to a narrow region in the presence of a model Müller cell is guided along the channel (middle panel) and scattered in the absence of a Müller cell (lower panel). (b) A few examples of shape variations in the Müller cell model studied numerically.

II-8 Liquid Fronts in Porous Media

M. Brinkmann, R. Seemann, S. Herminghaus
K. Singh, M. Jung, H. Scholl (Saarland University)

THE PROCESS OF (forced) imbibition of a liquid into a random porous medium plays a key role in many problems of general interest, such as oil recovery, irrigation in agriculture, or wetting of raw material powders in industrial chemistry. Inspired by this tremendous practical importance, many experiments have already been carried out in search of a thorough physical understanding of the basic mechanisms involved. However, a satisfactory agreement with theory has not yet been achieved. This is in part due to difficulties inherent to the experiments performed so far.

Many imbibition experiments, e.g. employing paper as the random medium [1], suffer from problems related to the swelling of fibers, a poorly defined roughness of the fiber network, and evaporation of the wetting phase [2]. Other more conceptual reasons for theories to fail are entrainments of air in advancing fronts in realistic scenarios. This is captured neither by percolation models nor by theories on interface roughness statistics like the KPZ equation, but may be accounted for by more recently developed phase field models [3]. We could show *in-situ* that interface roughness theory works well for a simple 2D model system [4]. However, results on more realistic 3D systems, like columns of glass beads [5] which allow for a microscopic analysis of the advancing front, exist to date only for *ex-situ* studies [6]. High resolution real-time mapping of the advancing front in a realistic setting has never been done up to now, but is indispensable for the development of theoretical models of the temporal evolution of the front topology.

Based on our experience with fast x-ray tomography at ID15A (ESRF, Grenoble) which helped us to unravel a liquid exchange process and to clarify the static distribution of liquid within granular piles and thus to understand their complex mechanical behavior [7-11] we further adapted

and optimized the usage of ultrafast x-ray tomography to image multiphase flow in porous media in real time. Using the tomography setup at ID 15A acquisition times for a full tomography of about one second at a pixel resolution of $5.5 \mu\text{m}$ at 1500^3 voxels are possible for our systems which allows mimicking typical reservoir flow conditions in model systems. We aim at understanding the flow behavior on a pore size level depending on parameters like front velocity, matrix wettability, and liquid viscosity.

The liquid fronts in the glass and basalt bead packs are different in their shape: the front in the water wet glass system has more fingers whereas the liquid front in the oil wet basalt pile is more compact. Differences in the front morphology are very hard to visualize and to quantify both in cross sections and in 3D renderings. It will be one of the main goals for the future to develop means to quantitatively describe the front shape and its evolution in time. This will be done in close collaboration with theoretical and numerical considerations. In a first approach we analyzed the experimentally determined front length and the oil saturation as function of time. The temporal evolution of the residual oil saturation is shown in figure 3 for random packings of either glass beads or basalt beads, as also shown in figures 1 and 2, respectively. The results are reproducible and the different cases can be distinguished from each other. Recent test measurements seem to indicate that the different behavior for the water and oil wet matrix is enhanced for increased front velocity.

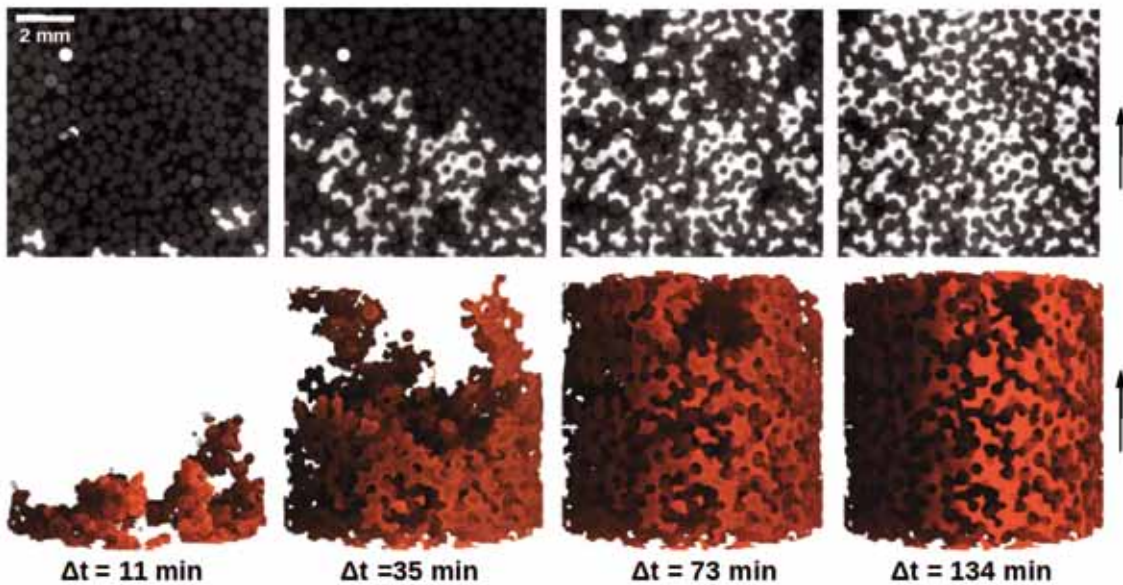


Figure 1

A time-series of water imbibition in a glass-bead matrix initially filled with oil; the average front velocity is about $1 \mu\text{m/s}$. The upper row shows the 2D slices of grey scale image at different time steps during aqueous phase (white) imbibition in oil (black) filled glass beads (grey). The lower row shows the same time steps rendered only for water in three dimensions.

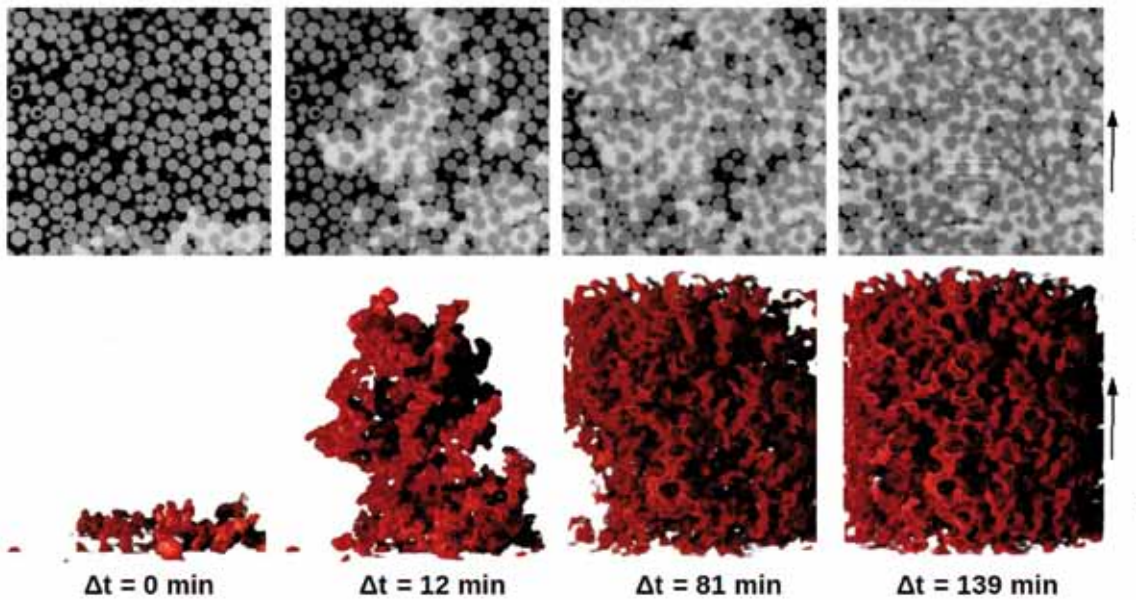


Figure 2

A time-series of water imbibition in a basalt-bead matrix initially filled with oil; the average front velocity is about $1 \mu\text{m/s}$. The upper row shows the 2D slices of gray scale image at different time steps during aqueous phase (white) imbibition in oil (black) filled basalt beads (grey). The lower row shows the same time steps rendered only for water in three dimensions.

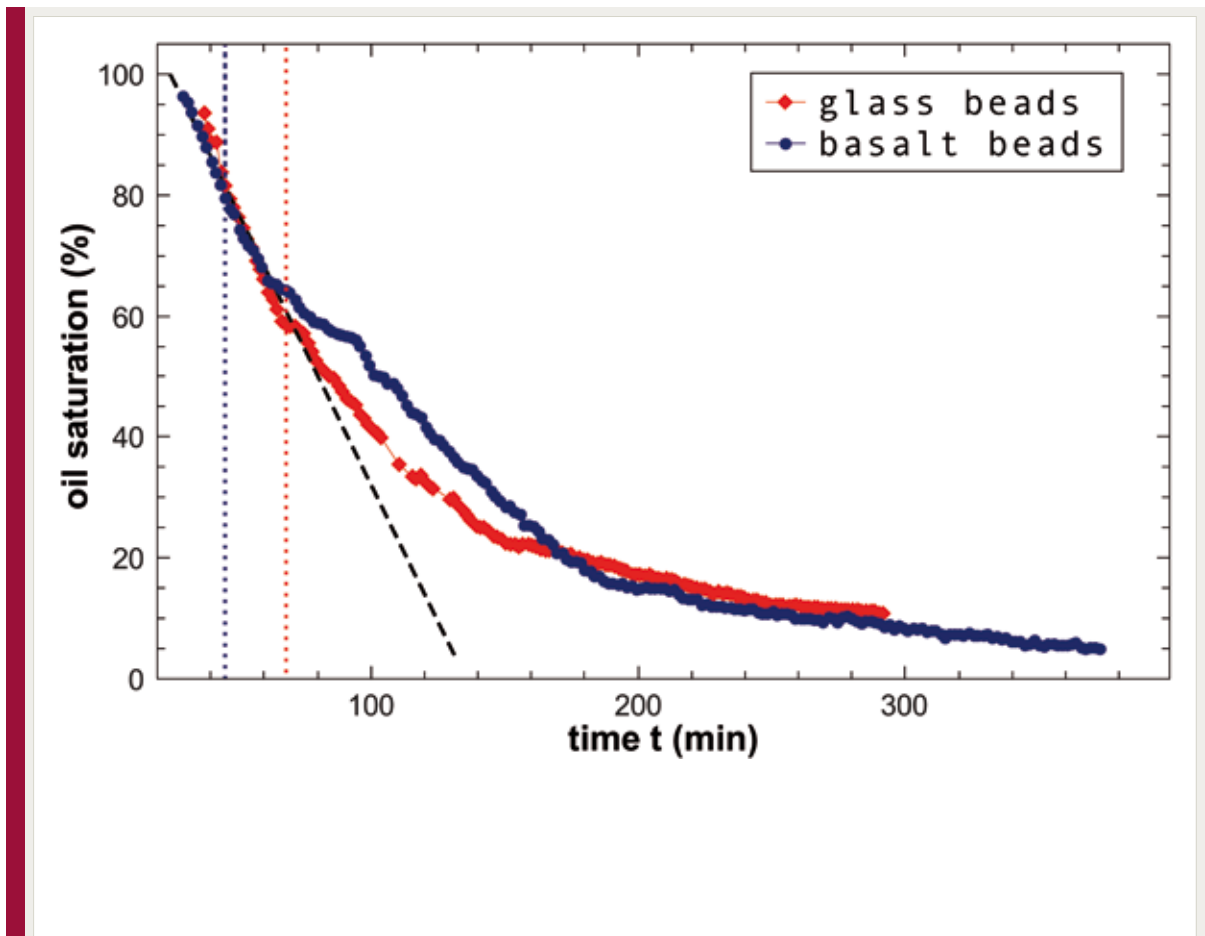


Figure 3

Residual oil saturation as function of time. The dashed line indicates the expectation from volume conservation which is valid as long as the water/oil front remains within the imaging area (indicated with open stars), up to this points all the data should be identical. For larger times we find in fact a different oil displacement behavior for the water wet glass matrix (black and red data) and the oil wet basalt matrix (blue data) at an average front velocity of $1 \mu\text{m/s}$. The grey data show the front behavior in an oil wet basalt matrix at a front velocity of $10 \mu\text{m/s}$. To allow for comparison the time scale of this run was scaled.

- [1] V. K. Horváth, F. Family, and T. Vicsek, *Phys. Rev. Lett.* **67**, 3207 (1991); S. V. Buldyrev, et al., *Phys. Rev. A* **45**, R8313 (1992); V. K. Horváth and H. E. Stanley, *Phys. Rev. E* **52**, 5166 (1995)
- [2] M. Dubé, M. Rost, and M. Alava, *Eur. Phys. J. B* **15**, 691 (2000)
- [3] M. Dubé et al., *Phys. Rev. Lett.* **83**, 1628 (1999)
- [4] D. Geromichalos, F. Mugele, and S. Herminghaus, *Phys. Rev. Lett.* **89**, 104503 (2002)
- [5] T. Delker, D. B. Pengra, and P.-Z. Wong, *Phys. Rev. Lett.* **76**, 2902 (1996)
- [6] D. Geromichalos, M. M. Kohonen, F. Mugele, and S. Herminghaus, in: *Contact Angle, Wettability & Adhesion (Zeist, Netherlands)* **3**, 385 (2003)
- [7] M. Scheel, D. Geromichalos, and S. Herminghaus, *S. J. Phys.: Condens. Matter* **16**, S4213 (2004)
- [8] M. Scheel, et al. *Nature Mater.* **7**, 189 (2008)
- [9] M. Scheel, et al. *J. Phys.: Condens. Matter* **20**, 494236 (2008)
- [10] M. M. Kohonen, D. Geromichalos, M. Scheel, C. Schier, and S. Herminghaus, *Physica A* **339**, 7 (2004)
- [11] Z. Fournier, et al. *J. Phys.: Condens. Matter* **17**, 477 (2005)

II-9 Fluidization of Granular media

J. Vollmer, M. Brinkmann, M. Schröter

I. Battiato, C. Gögelein, S. Herminghaus, S. H. Rahbari, J. Blaschke,
D. Kadau (ETH Zürich, Switzerland), H. Herrmann (ETH Zürich, Switzerland)

Arguably, the conceptually simplest setting to study fluidization of a granular packing are tilt experiments. They show a remarkable difference of wet and dry granulates: Dry granular particles tend to start flowing at the surface. In contrast, when capillary bridges induce attractive interactions between the grains, fluidization is rather triggered close to the bottom of the system. To sort out the origin of this difference we consider a regular two-dimensional packing of monodisperse particles with random masses [1].

The static contact network is described by unit vectors \mathbf{e}_{ij} for neighboring particles i and j . To emphasize their orientation relative to the inclination on the plane they are denoted as \mathbf{e}^{up} and \mathbf{e}^{down} in figure 1a, and stability is formulated as a constraint on the forces f^{up} and f^{down} acting along the respective bonds. For a dry packing all forces f must be compressive, $f < 0$, while a wet packing can support also tensile forces smaller than the capillary bridge force f_b i.e., $f < f_b$ with $f_b > 0$. For the considered packings this leads to an explicit prediction of the critical tilt angle as a function of the stacking angle β and the largest mass M encountered in an uphill column of the pile (figure 1b). Generalization of the result to predict the packing threshold of disordered and of three-dimensional packings are in progress.

Rather than by gravitational forces and tilting, a pile can also be fluidized by hydrodynamic shear forces. They arise for instance from creeping motion of a fluid flowing in the pore-space between grains. Attractive forces can arise from capillary bridges formed by another liquid wetting the grains. In [2] we propose a minimal multi-scale model for the effect of hydrodynamic shear on the fluidization threshold in this situation.

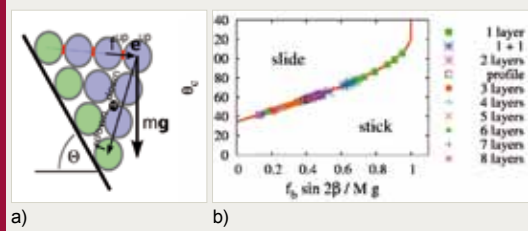


Figure 1

(a) Regular packing of grains with a non-trivial height profile. The grains in the lower-most row (shaded in green) are fixed, they form a wall supporting the pile. The others move when θ is increased beyond the critical slope θ_c . There are tensile forces acting at the indicated capillary bridges along the uphill direction of the pile. The force balance for the grain at the top of the tree amounts to $f^{\text{up}} \mathbf{e}^{\text{up}} + f^{\text{down}} \mathbf{e}^{\text{down}} = m\mathbf{g}$, where m is the mass of the considered particle and g the gravitational acceleration. (b) Parameter dependence of the yield angle θ_c for packings with different height profiles, as specified to the right of panel (b): “1+1” denotes one layer plus an additional grain in the 2nd layer, and “profile” denotes a height profile with voids in the 2nd and few particles in the 3rd row. For $\theta < \theta_c$ the grains stick together. For larger θ the pile topples. All data lie on the master curve indicated by the solid red line. See Ref. [1] for details.

Our model combines a continuum-scale approach for the computation of the average drag force exerted on the grains and a pore-scale description for determining the force propagation in the pile. We consider expanded random close packed (crystalline) structures which generalize the packing shown in figure 1a from two-dimensional to three-dimensional arrangements. In this setting we analytically determined the fluidization threshold, and identified critical parameters for the onset of instability. The control parameters include i) the capillary number Ca^* which represents the ratio between de-stabilizing hydrodynamic viscous forces and stabilizing capillary forces, and ii) geometric properties of the pile. While the capillary number allows us to

identify the order of magnitude of the fluidization threshold, structural properties of the pile other than porosity, have a minor (but still quantifiable) effect on the pile stability. Specifically we show that the orientation of the crystalline structure relative to the average drag force exerted by the fluid, impacts the onset of instability by a factor of 2 (see figure 2).

As a next step we will explore how closely this prediction matches the stability threshold for disordered packings. First applications will target the breakup of weak colloidal gels in shear cells, and the fluidization of liquid beds.

A setup ideally suited for the latter purpose is a liquid bed of monodisperse glass beads (diameter $3\mu\text{m}$) placed in a mixture of water and lutidine [3]. This mixture has a lower critical point slightly above room temperature and, thus, demixes upon increasing the temperature (see, figure 3a). If we add glass spheres to this mixture, the formation of capillary bridges takes place due to the preferential wetting of the hydrophilic spheres by the water-rich phase of the phase-separated water-lutidine mixture. Figure 3b shows a series of confocal images of a monolayer of glass beads. The great advantage of the water-lutidine system is that the bridge formation can be precisely tuned by increasing

the temperature. Moreover, the bridges disappear within seconds when the temperature is decreased below the demixing point due to intermolecular diffusion.

The cluster formation in three dimensional packings has been previously studied in our group using x-ray micro tomography [4]. Recently, we have also designed a temperature-controlled fluidized bed setup involving the water-lutidine mixture. This setup is currently used to study the effect of capillary bridges on the fluidization process and the compactification of loose packings.

In addition, the experimental system is ideally suited to study the interplay between transport through wetting layers on the glass beads, and the cohesion of the wet granular assembly. A numerical implementation of such a model, employing the contact dynamics simulation method, is currently being developed in cooperation D. Kadau and H. Hermann at the ETH Zürich.

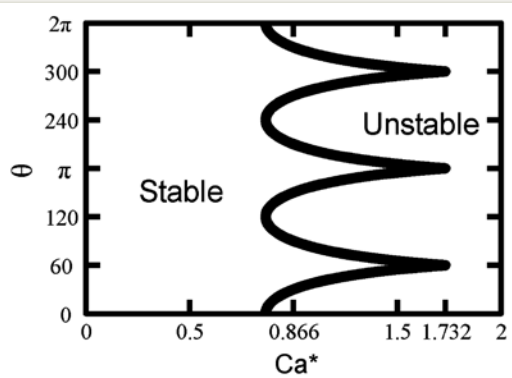


Figure 2

Stability diagram of a granular pile with an extended hexagonal structure as a function of the capillary number Ca^* and the orientation θ of the pile with respect to the flow direction. The porosity of the sample enters the definition of the capillary number.

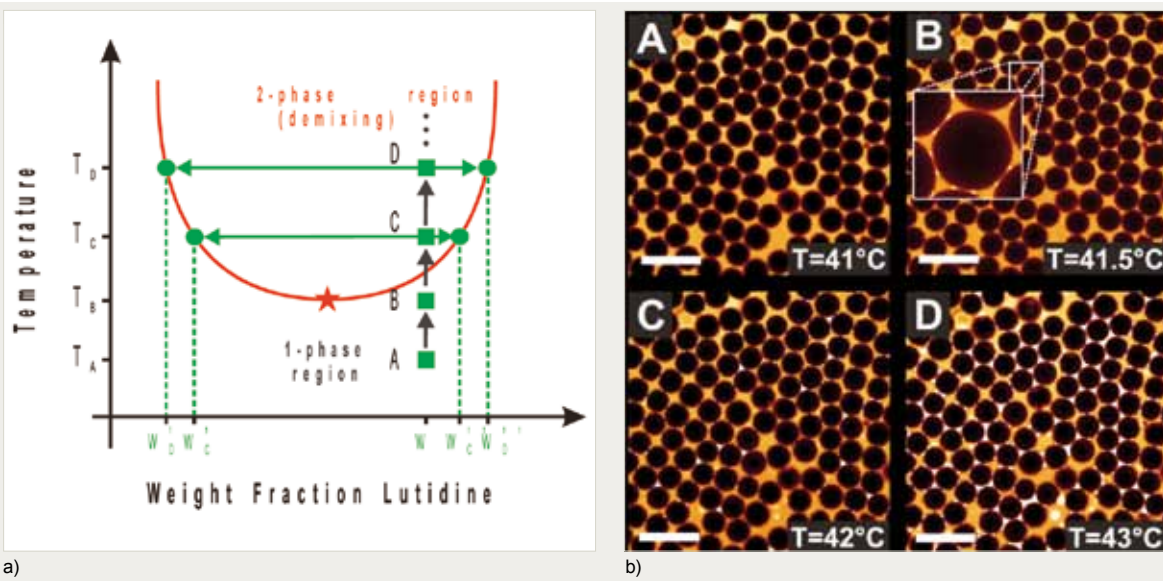


Figure 3

(a) Schematic phase diagram of the water-lutidine mixture, and (b) a series of confocal images taken at increasing temperature. Notice that the images in figure 3b correspond to the points depicted in the phase diagram of figure 3a. The temperature in panel A lies below the binodal line and, thus, no bridges are observed. In panel B, we increased the temperature to reach the two-phase region of the phase diagram, and the formation of bridges is observed. Panels C and D show the increase of the bridge volume and the formation of larger clusters at higher temperatures. The length of a scalebar is 150 μm .

- [1] S.H. Ebrahimpour Rahbari, J. Vollmer, S. Herminghaus, M. Brinkmann, *EPL* **87**, 14002 (2009)
- [2] I. Battiato, J. Vollmer: "Fluidization of Wet Granular Matter under Hydrodynamic Shear", arXiv: 1105.2594.
- [3] C. Gögelein, M. Brinkmann, M. Schröter, S. Herminghaus, *Langmuir* **26**, 17184 (2010)
- [4] M. Scheel, R. Seemann, M. Brinkmann, M. Di Michiel, A. Sheppard, B. Breidenbach, S. Herminghaus, *Nature Materials* **7**, 189 (2008)

II-10 Microfluidics of Nematic Liquid Crystals and Nematic Colloids

C. Bahr, S. Herminghaus
A. Sengupta, U. Tkalec

NOVEL COLLOIDAL systems consisting of micrometer-sized particles dispersed in nematic liquid crystals have recently attracted large interest [1]. In these systems, the colloidal pair interaction is not of the van der Waals or electrostatic type, but stems from the elasticity of the director field of the nematic host. A direct manipulation of these systems can be achieved by means of optical tweezers. A different manipulation approach could be the use of forces which are present when the system flows through an appropriate microfluidic device. Although the influence of flow on the nematic volume phase has been studied theoretically and experimentally since the early 1970s, the study of nematic liquid crystals in the field of microfluidics is still at an early stage and a systematic study of the influence of the channel dimensions and geometry, the anchoring conditions on the channel walls, the magnitude of the flow rate, or other parameters does not exist.

We thus started with the study of a pure (without colloidal particles) nematic phase flowing through simple straight microchannels. The channels, prepared by bonding a PDMS relief on a glass substrate, had a rectangular cross section (width 50 – 100 micrometer, depth 5 – 30 micrometer). The plasma treatment, which is needed to bond the glass substrate to the PDMS relief, causes degenerate planar anchoring conditions on both the glass and the PDMS surface and for our initial studies we did not modify these conditions. Thus, near all four channel walls, the liquid crystal molecules prefer to align parallel to a wall but there is no preferred alignment direction within the plane of the wall. The nematic phase flowing through the microchannel is studied by polarizing optical microscopy and fluorescence confocal optical microscopy. By varying the flow rate and/or the vertical dimension of the channel, different forms of flow-

and confinement-induced textures and topological defect structures evolve [2]. For small channel depths of 5 – 10 micrometer, we observe with increasing flow rate the following sequence of structures: (i.) disclination lines connecting the top and bottom walls of the channel (and thus being oriented perpendicular to flow) moving in the direction of flow leaving a set of parallel π -walls behind, (ii.) disclination lines aligned parallel to the flow direction and pinned with both ends on a channel wall, (iii.) disclination lines, aligned parallel to the flow direction, with one end pinned on a channel wall and one freely floating end, and (iv.) a chaotic-like regime in which disclination lines and loops are freely floating, intertwining, annihilating and crossing each other. The same sequence of structures is observed when the depth of the channel is increased at constant flow rate. Figure 1 shows the stability regimes of the different structures in the channel depth vs. flow rate parameter plane. The different flow-induced structures are currently studied in detail and we started with structure (i.), i.e., the evolution and morphology of the π -walls.

A π -wall separates regions which differ by the orientation of the nematic director by an angle of π . It is not a real “wall” since the director orientation changes continuously when going from one region to another. In the microchannel, the π -walls are created by the impact of flow on disclination lines of strength ± 1 or $\pm 1/2$. The disclination lines, which extend from the top to the bottom of the channel, are moved downstream by the flow and leave a set of parallel π -walls behind which extend up to several hundred micrometers in length. They appear as alternating dark and bright stripes between crossed polarizers (figure 2). The detailed structure of the π -walls can be manipulated to some extent by varying flow rate and direction [3].

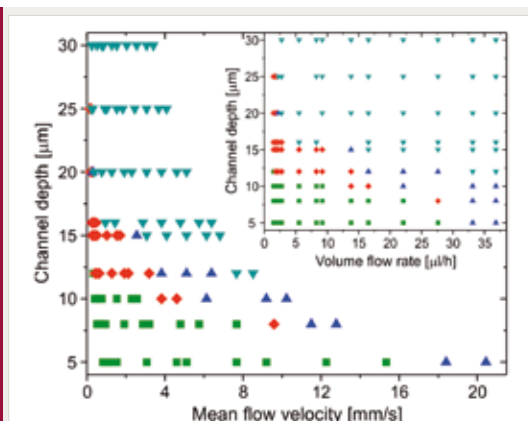


Figure 1

Flow-induced structure regimes in a nematic liquid crystal as a function of the mean flow velocity and channel depth. Green squares: π -wall generation by moving disclinations; red diamonds: generation of disclinations pinned with both ends on the channel wall; blue triangles: generation of disclinations with one freely floating end; turquoise triangles: “chaotic” regime. Inset shows the dependence of the regimes on volume flow rate and channel depth.

Preliminary studies of nematic liquid crystals containing colloidal particles have shown that the flow-induced structures like π -walls and disclination lines can be used to guide the transport of the particles through the microchannels (figure 3). A key point for the continuation of these studies will be the use of channels possessing other anchoring conditions (unidirectional planar, homeotropic, tilted) on the channels walls, since the anchoring of the nematic director will essentially determine the details of the flow-induced structures.

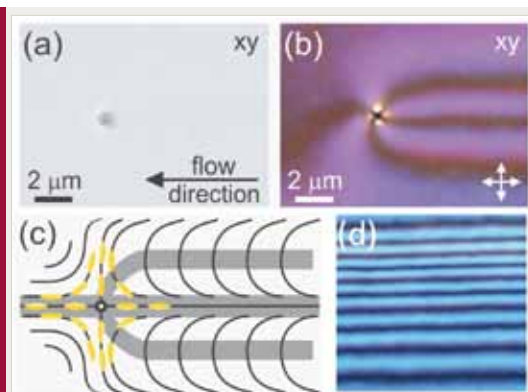


Figure 2

Creation of π -walls by a disclination line of strength -1 moving along the flow of the nematic liquid crystal. The disclination line is parallel to the z -coordinate, i.e., it connects the bottom and the top wall of the shallow microchannel. The following images show the xy -plane. (a) Unpolarized micrograph: the dark point indicates the scattering of light by the disclination line (perpendicular the image plane) at the leading end of the forming π -wall structure. (b) Micrograph between crossed polarizers: the alternate dark and bright regions are caused by the continuous change of the director orientation. (c) Schematic representation of director field in the xy -plane. (d) After the passing of several disclinations, the microchannel is filled with several parallel π -wall sets.

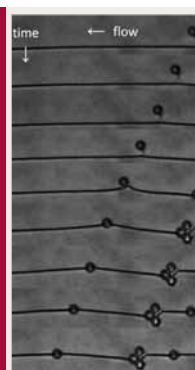


Figure 3

Capture of a colloidal particle (diameter 5 micrometer) by a disclination line which is aligned parallel to the flow direction of the nematic liquid crystal; once the particle is trapped, it follows the course of the disclination. The time difference between the micrographs is 0.1 seconds.

- [1] I. Musevic, M. Skarabot, U. Tkalec, M. Ravnik, S. Zumer, *Science* **313**, 954 (2006)
- [2] A. Sengupta, S. Herminghaus, Ch. Bahr, *Mol. Cryst. Liq. Cryst.*, *accepted*.
- [3] A. Sengupta, U. Tkalec, Ch. Bahr, *Soft Matter*, *accepted*.

II-11 Surfactant Advection to Interfaces

J.-C. Baret, M. Brinkmann
Q. Brosseau, B. Semin, E. Kadivar

DROPLET-BASED microfluidics is proven a very effective tool for the miniaturization and automation of biological assays, for example, for single cell analysis, DNA screening or drug screening [1-4]. In order to reliably function as microreactors, the droplets have to fulfill three major constraints: they must be stable against coalescence (they should not fuse), biocompatible (they should not influence the biochemical reaction), and their components must remain encapsulated over time (they must be tight). These three properties are controlled by the surfactant molecules which (i) stabilize the droplets against coalescence [5-6], (ii) influence cell viability in droplets [7] and (iii) modify the transport properties of molecules as demonstrated in the case of model drugs in water-in-oil microemulsions [8].

The fine control of the droplet size distribution, of droplet actuation and the accessibility of short timescales (~ 1 ms) in microfluidic emulsification – hardly achieved in bulk-emulsification – makes it appealing as a new tool to study quantitatively the physics and physical chemistry of interfaces and emulsions (figure 1).

We first studied the influence of surfactant dynamics on emulsion stabilization against coalescence. In classical emulsification processes, surfactants play two roles: first, they reduce the interfacial tension, facilitating droplet defor-

mation and rupture and second, they reduce droplet coalescence. Here we use a microfluidic emulsification system to completely uncouple these two processes, allowing stabilization against coalescence to be studied quantitatively, and independently of droplet formation. We have demonstrated that, in addition to the classical effect of stabilization by an increase of surfactant concentration, the dynamics of adsorption of surfactant at the water-oil interface is a key element for droplet stabilization. Microfluidic emulsification devices can therefore be tailored to improve emulsification while decreasing the concentration of surfactant by increasing the time before the droplets first come into contact (figure 2).

The dynamics of surfactant adsorption was here indirectly measured through coalescence probabilities. We are now developing a direct measurement of the surfactant adsorption using a microfluidic chip for surface tension measurement. It has proven very difficult to study the short-time dynamics of surfactant adsorption at the water-oil interface at the millisecond time-scale using conventional techniques. For example, in the standard pendant drop technique used to measure surface tension, a few seconds are required to obtain the mechanical equilibrium of the droplet. The early time kinetics is therefore hidden. Microfluidic devices allow the preparation of highly con-

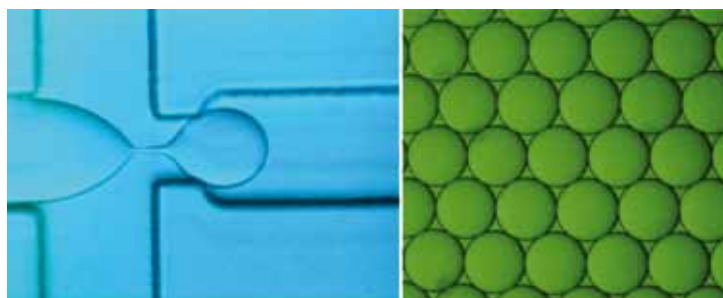


Figure 1

Example of the production of a water in oil emulsion in microfluidics by flow-focussing (left), and picture of the emulsion plated on a glass slide. The droplet produced in microfluidics are monodisperse and stabilised by a surfactant to prevent coalescence. Here the droplet diameter is about 100 microns. The control of volumes and interfaces makes it appealing for the study of interfacial phenomena.

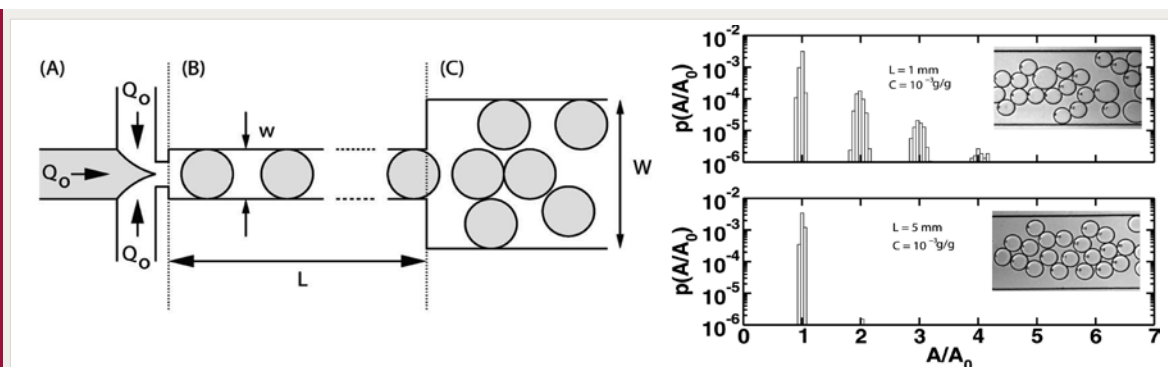


Figure 2

Microfluidics for the study of coalescence. Sketch of the device and measurements of droplet stability as a function of incubation length L for a fixed concentration of surfactant ($C = 10^{-3}$ g/g). (a) $L = 1$ mm (incubation time of 7 ms); the emulsion is unstable as measured by the area distribution of the droplets showing peaks corresponding to fusion of 2, 3,... droplets ($A_0 = 1914 \mu\text{m}^2$ is the area of the non fused droplets). (b) $L = 5$ mm (incubation of 36 ms); the proportion of fused droplets is less than 10^{-3} ($A_0 = 2028 \mu\text{m}^2$). Increasing the length of the channel after production helps stabilize emulsions [9].

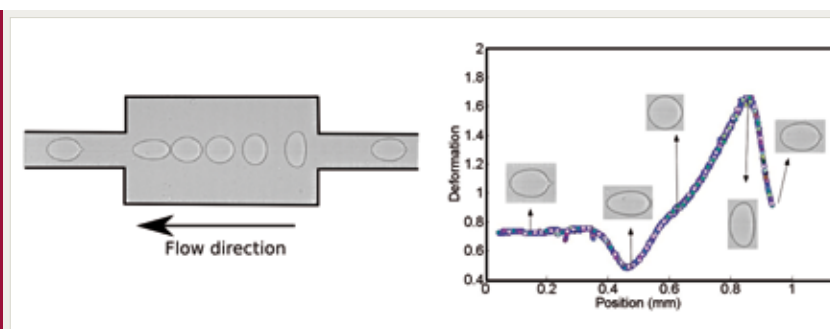


Figure 3

Microfluidics for surface tension measurements. Measuring the deformation of droplet in a flow field will provide means to measure surface tensions at the millisecond timescale (droplet size is 100 microns). We are using this system to measure the dynamics of surfactant adsorption to interfaces.

trolled monodisperse droplets, at frequencies of kHz or higher. We are now developing microfluidic devices to measure surface tensions on chip at time scales of the order of 1 ms. Taking advantage of the high throughput of the microfluidic devices, we have access to large number of measurements in one single run which increases the accuracy of our measurement by providing statistically relevant data. We have designed here a microfluidic chip with a series of consecutive expansion chambers where hydrodynamic stress forces the droplet to deform (figure 3). By measuring the response of the droplet to the forcing we have access to surface tension measurement at the millisecond timescale. Finally, we combine these measurements with numerical simulation of droplet deformation in microchannels for a better understanding of the interactions between the hydrodynamic stress and the resulting deformation of the droplet (see section V.7).

- [1] A. Huebner, et al., *Lab Chip* **8** (8), 1244-1254 (2008)
- [2] J.-C. Baret, et al., *Lab Chip* **9** (13), 1850-1858 (2009)
- [3] L. Mazutis, et al., *Anal. Chem.* **81** (12), 4813-4821 (2009)
- [4] J.-C. Baret et al., *Chem. Biol.* **17**, 528-536 (2010)
- [5] J. Bibette, F. Leal-Calderon and P. Poulin, *Rep. Prog. Phys.* **62**, 696-1033 (1999)
- [6] N. Bremond, A. R. Thiam and J. Bibette, *Phys. Rev. Lett.* **1** (2), 024501 (2008)
- [7] J. Clausell-Tormos, et al., *Chem. Biol.* **15** (5), 427-437 (2008)
- [8] N. Chidambaram and D. J. Burgess, *AAPS Pharm. Sci.* **1**(3), *E 11* (1999)
- [9] J.-C. Baret, et al., *Langmuir* **25** (11), 6088-6093 (2009)

II-12 Micellar Transport in Emulsions

J.-C. Baret, S. Herminghaus
B. Semin, X. Qu, S. Thutupalli

IN SECTION II-11, we focused on the adsorption of surfactants towards interfaces which is a key to understand the stabilization of emulsions at short time scales [1]. Once the emulsion is formed, it is a system out of equilibrium since the energy of the system is larger than the energy of a system where the two immiscible phases are separated [2]. Surfactant stabilize the system by providing an energy barrier to be overcome to destabilize this metastable system. Therefore the long term destabilization of the emulsion is a dynamic problem and here once again the surfactant plays a key role in this process.

One way to destabilize emulsion at large time-scale is through the exchange of molecules between droplets and we address here the question of transport of molecules in an emulsion. Two types of molecules can be exchanged between the droplets of the dispersed phase; the molecules of the solvent of the dispersed phase itself (Ostwald ripening) or molecules solubilised in the dispersed phase. Using a fluorinated oil as the continuous phase of the emulsion, the solubility of molecules in the oil phase is limited. We can then focus of the influence of surfactant molecules on the transport dynam-

ics. Understanding the transport of molecules in emulsions is not only beneficial for the optimization of microreactors for biochemical applications, but is of relevance for phase separation applications [3] or (bio-)chemical synthesis in emulsions [4] where the exchange rate of reagents controls the reaction. The ability of droplets to exchange material is also a key to understand collective behavior in droplets assemblies, as observed with Belousov-Zhabotinski reaction in droplets [5, 6].

The study of solubilisate exchange has already been performed in bulk systems [7], but these studies do not capture the microscopic details of the exchange at the single droplet or interface level. Recently, microfluidic systems have been developed for the measurement of the transport of molecules between two droplets demonstrating the capabilities of microfluidics for quantitative analysis of the exchange process [8]. Here, we address the dynamics of molecular exchange between droplets in emulsions. We measure experimentally the relaxation to equilibrium of an emulsion (produced in microfluidics) containing droplets with different concentration of a fluorescent probe (figure 1). The packing geometry, the dimension of the system and the number of

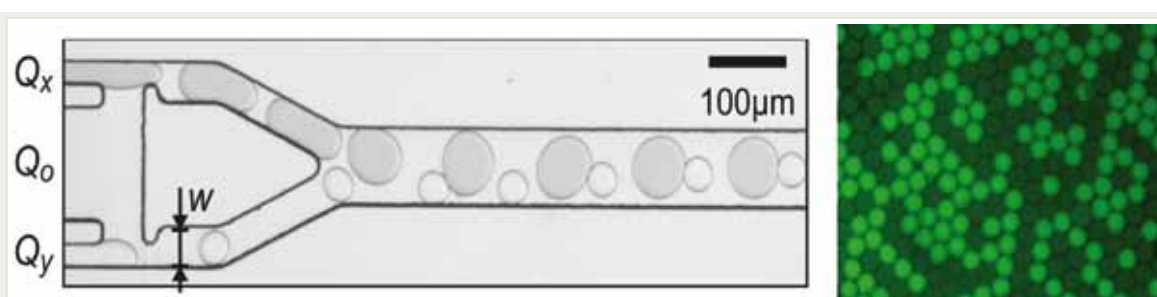


Figure 1

Using microfluidic systems we can control the emulsion composition in a very well defined manner: size, composition, different, ratio of the different populations... These emulsions constitute model tools for the study of transport in complex fluids. Left: two droplet populations are produced with different sizes using hydrodynamic coupling of two nozzles [10]. Right: Emulsion produced in microfluidics (droplet diameter is about 40 microns) with two different concentrations of fluorescein (epifluorescence microscopy).

closest neighbors are ingredients to take into account, besides the effect of the surfactant concentration or of the chemistry of the molecule to be exchanged. Using microfluidic systems, we can control the arrangement of droplets, their packing [9] and the initial condition on the concentration of the molecules in the droplets: we can tune on-demand the local distribution of molecules in 1-dimension, 2-dimensions or 3-dimensions and measure the equilibration of the system (see for example figure 1). We observed that the local variations in concentrations are damped with a short time scale while the long-range variations are damped much slower. Hence, a single exchange rate parameter defined at the droplet level (microscopic rate) is not sufficient to describe the kinetics at the emulsion scale (macroscopic rate). The emulsion in its whole has to be considered. We combine our experiments with extremal model for the exchange. Although the exchange problem is in fact diffusion-like, we can make use of emulsions to study these diffusion processes under conditions that have not been studied yet. Indeed we can prepare a system with large local variations in concentration (droplet to droplet variation) and measure the relaxation of the concentration from the scale of droplet pairs to the scale of the whole emulsion (up to several millions of droplets). Such an experiment is hardly possible in bulk and besides its interest for emulsion sciences would also be of interest as a new model system to probe diffusion processes at short length and time-scale. The knowledge gained from this type of studies will be beneficial for the design and understanding of soft autonomous microsystems – for example microrobots – where the motion of such element can be controlled by local gradients in concentrations of a ‘fuel’ chemical compound [6]. This project has an extension in the proposal for the Second Funding Period of the SFB-755 which has been positively evaluated in January 2011. In this SFB project, we want to use fluorescence tools and X-Ray visualisation techniques to look at the details of membranes and surfactant structures through which transport occurs.

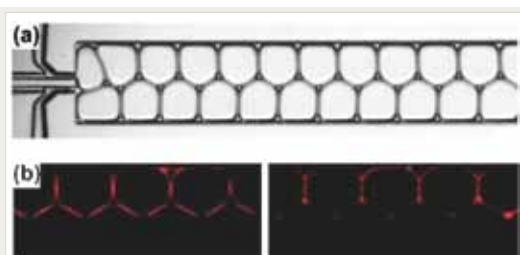


Figure 2

Transport of dye molecules and formation of lipid bilayers. Microfluidics provide tools to study the formation of bilayer. (a) Gel emulsion in a channel (500 μm wide) at very low volume fraction of the continuous oil phase (below 10%). (b) Micrograph of an emulsion like the one shown in (a), taken at the fluorescence wavelength of the dye (di-4-anepps) which was fed into the upper row of droplets. Illumination is by UV light. Left: as prepared. Right: a few seconds later, when membranes have formed. Reprinted from [6]. The formation of such layers has potentially a large influence on the dynamics of transport between the droplets.

- [1] J.-C. Baret, et al., *Langmuir* **25** (11), 6088-6093 (2009)
- [2] J. Bibette, F. Leal-Calderon and P. Poulin, *Rep. Prog. Phys.* **62**, 696-1033 (1999)
- [3] P. Mary, V. Studer and P. Tabeling, *Anal. Chem.* **80** (8), 2680-2687 (2008)
- [4] H. Matsumiya, Y. Yatsuya and M. Hiraide, *Anal. Bioanal. Chem.* **385** (5), 944-947 (2006)
- [5] M. Toiya, V. K. Vanag and I. R. Epstein, *Angewandte Chemie, Int. ed.* **47**, 7753-7755 (2008)
- [6] S. Thutupalli, S. Herminghaus and R. Seemann, *Soft Matter* **7**, 1312-1320 (2011)
- [7] P. D. I. Fletcher, A. H. Howe and B. H. Robinson, *J. Chem. Soc. Faraday Trans.* **1**, 83, 985-1006 (1987)
- [8] Y. Bai, et al., *Lab. Chip* **10** (10), 1281-1285 (2010)
- [9] E. Surenjav et al. *Appl. Phys. Lett.* **95** (15), 154104 (2009)
- [10] L. Frenz et al., *Langmuir* **24** (20), 12073-12076 (2008)

II-13 Wetting of elastic Substrates

M. Brinkmann, R. Seemann

O. Claussen, D. Michler, C. Herrmann (Saarland University)

THE INTERPLAY between the elasticity of a porous matrix, its geometry and wettability properties can give rise to a wide variety of interesting phenomena ranging from spontaneous symmetry breaking and pattern formation to anomalous imbibition dynamics [1]. Examples for elastic materials which change their mechanical properties drastically between the wet and the dry state are biological materials like leather, wool, or sponges, as well as industrial products such as solidified foams made of soft polymeric materials or disordered assemblies of fibres used in aerosol filters, just to name a few. Wetting of macroscopic fibre networks is relevant to many industrial production processes and applications, in particular, to textile industry. The impact of wettability on the shape of a liquid droplet resting on one or two cylindrical fibers has been recently demonstrated both in numerical calculations and in electrowetting experiments [2].

To study the mechanical properties of wet fibrous materials we developed a discrete element model that accounts for the aligning torques generated by elongated capillary bridges as proposed by Virozub [3]. Using this model we started our investigations with effectively two-dimensional networks similar to the Poissonian (“Mikado”) model proposed to study active networks [2]. In our model, a capillary bridge is formed instantaneously once a crossing of two fibers is formed. This process corresponds to a capillary condensation at fixed undersaturated vapor of the wetting liquid. In contrast to most other models of fiber networks, the capillary bridges represent mobile bonds as their position on the fibers is not fixed. The aligning torques are counterbalanced by elastic forces that build up in the network in response to the deformations. At a certain threshold strength of the capillary bridges, the fibers start to bundle which leads to heterogeneous distribution of the

wetting liquid. This heterogeneity in terms of the density of fibers and capillary bridges can be seen in the snapshots shown in figure 1.

The interplay between elastic deformations and capillary forces can be observed in wetting experiments on topographically structured substrates made of elastic silicone rubber (PDMS) [4]. Thus one observes ordered breath figures during condensation of water droplets on a hydrophobic PDMS substrate equipped with an array of parallel lamellae, cf. the series of micrographs shown in figure 2a. In this case the aspect ratio of the lamellae, i.e. the ratio of lamella height to lamella width is higher than 3.5. The time sequence in figure 2 demonstrates that the order of the droplets strongly increases as the condensation proceeds. A lateral ordering effect is absent on hydrophilized PDMS samples. Instead, neighboring lamellae collapse in a zipper-like motion (figure 2b). Only a

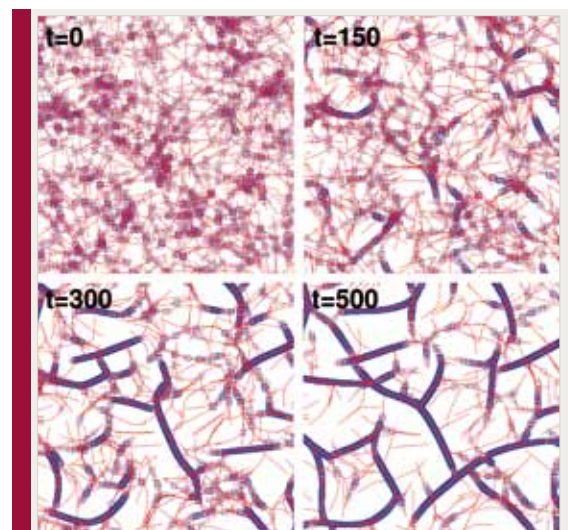


Figure 1

Sequence of snapshots of a wet elastic fiber network simulation. Crossing fibers (red lines) deform under the action of capillary bridges (blue squares) and form bundles. The fiber network is mechanically relaxed in the presence of a viscous fluid.

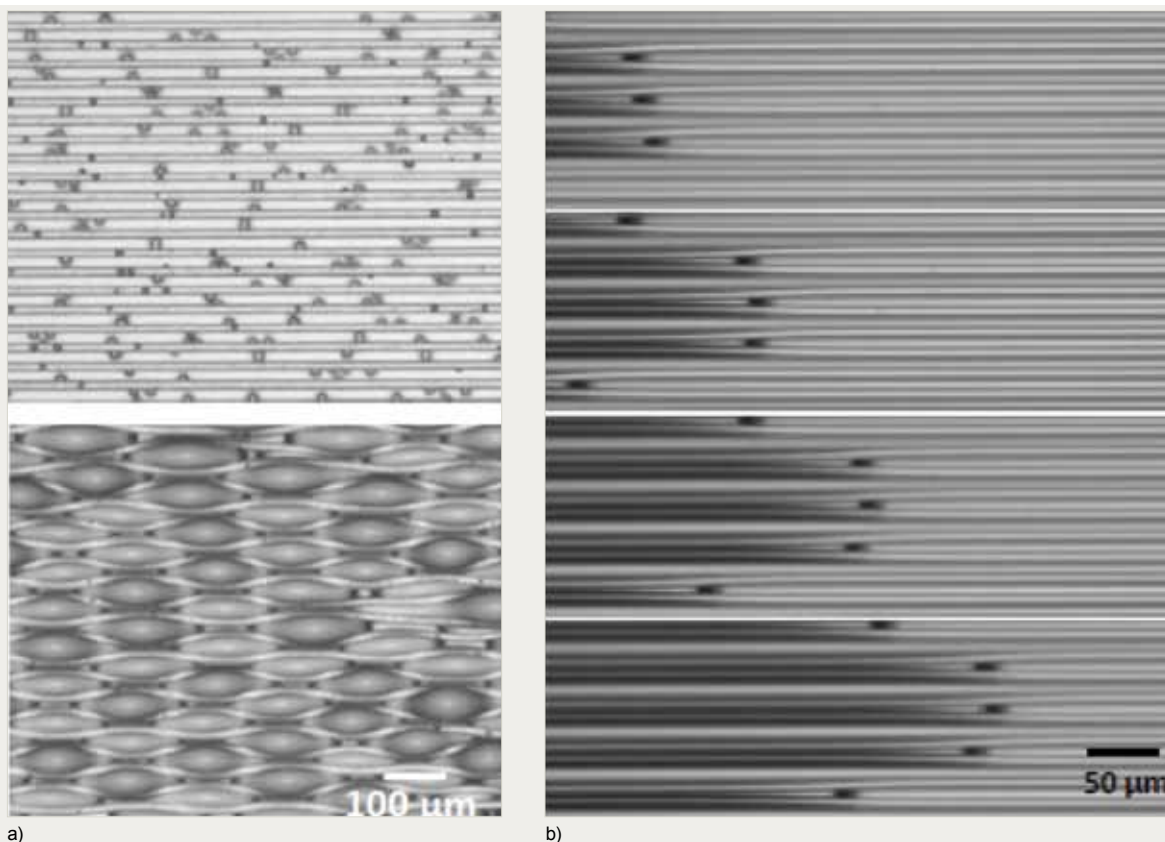


Figure 2

a) Breath figures of water droplets condensing on a native hydrophobic PDMS substrate with linear surface grooves at time $t=0$ and at $t=18\text{min}$. b) Zipper motion of collapsing lamellae on a hydrophilic PDMS surfaces. The aspect ratio of the grooves and ridges is 3 and 5.9, respectively.

small number of defects per row are observed in the final configuration which indicates that the pairing process is initialized in few sites and quickly spreads over the whole sample.

To understand the experimental findings we started to investigate the equilibrium profiles of the lamella in a simplified model that allows to solve the shape equation analytically. In this model the lamellae is treated as a thin elastic plate which is deformed under the action of interfacial forces and the Laplace pressure of the liquid. To further reduce the complexity of the problem we considered first solutions being translationally invariance along the direction of the lamellae, i.e. an effectively two-dimensional system. Despite these simplifications one observes a rich spectrum of possible states which is due to multiple solutions for given control pa-

rameter liquid volume, elasticity, and aspect ratio of the distance between neighboring lamellae.

- [1] Anderson D M, Imbibition of a liquid droplet on a deformable porous substrate. *Physics of Fluids* 17, 087104 (2005)
- [2] H. B. Eral et al., *Drops on functional fibers: from barrels to clamshells and back*, *Soft Matter*, DOI: 10. 1039/CDSM01403F, (2011); C. Heussinger and E. Frey, *Stiff Polymers, Foams, and Fiber Networks*, *Phys. Rev. Lett.* 96, 017802 (2006)
- [3] Virozub A, Haimovich N, and Brandon S, Three-Dimensional Simulations of Liquid Bridges between Two Cylinders: Forces, Energies, and Torques, *Langmuir* 25, 12837-12842 (2009)
- [4] Bico J, Capillarity induced folding of elastic sheets, *Eur. Phys. J. Special Topics* 166, 67 (2009).

II-14 Dynamics of moving Contact Lines on heterogeneous Surfaces

M. Brinkmann

M. Sanchez de la Lama, C. Semprebon, D. Herde

THREE PHASE contact lines between two fluid phases moving on a heterogeneous and rough substrates are encountered in many everyday phenomena such as rain droplets running down the leaves of a tree or a dirty window pane. A thorough understanding of the contact line dynamics on chemically heterogeneous and rough surfaces is relevant to a large number of industrial processes and applications such as coating of surfaces by liquid films or immiscible two phase flow in porous media, to name a few. Since the discovery that the problem of a moving contact line on a rigid substrate for a no-slip boundary condition may become ill-defined in a continuum picture, [1] a large number of models have been proposed to circumvent these problems. However, only recently the effect of heterogeneity and roughness on the dynamics of a liquid front has been included into a description of the contact line dynamics [2].

One of the starting points of this project is the depinning of contact lines from surface topographies such as regular patterns of posts with circular or square cross section. Employing numerical minimizations of the interfacial energy we were able to predict the static advancing and receding contact angle of a droplet resting on various geometrically structured surface [3]. A closer inspection of the depinning transition from square posts revealed that more than one mode of advancement of the contact line is encountered in certain regions of the control parameter aspect ratio of the posts and material contact angle of the substrate. At material contact angles slightly above 45° , one observes a qualitatively different behavior of the advancing contact angle as function of the post spacing which is due to coalescence events of the wetting liquid ahead of the front. In other words, the liquid flows around a post rather than detaching from it. Currently, the impact of post ge-

ometry on the appearance of different advancing modes is investigated comparing posts of square and circular cross section to square arrays of spherical caps.

The dynamics of a contact line moving on a plane but chemically heterogeneous substrate is investigated using two substantially different approaches. In the first approach, we solve the standard continuum problem taking into account the position dependent wettability of the substrate as shown in figure 1a. The second method is a particle based mesoscale simulation technique belonging to the class of Multi-particle Collision Dynamics (MPC) which allows for the transport of momentum and mass and, at the same time, for a phase separation of particles with different color, see also figure 2.

In the first approach the steady Stokes equation is solved for incompressible fluids using boundary element methods, as we assume the Reynolds numbers of the immiscible two phase flow to be small. To relief the stress singularity we impose a partial slip boundary condition on the substrate and resolve the contact line region on the scale of the slip length in order to avoid a “numerical slip”. A position dependent microscopic contact angle at the two contact points can be prescribed by means of the interpolation scheme of the liquid-fluid interface. To keep the level of complexity low, we started our investigations with the apparently simple problem of the droplet mobility on plane substrates with a sinusoidally varying wettability. Inspection of figure 1 shows that the terminal droplet velocity for different amplitudes of the wettability shows a discontinuous behavior. Such a discontinuous behavior has already been found describing the droplets by a thin film equation, i.e. in the long wavelength limit [4].

In order to extend our understanding of contact line dynamics to smaller length scales we em-

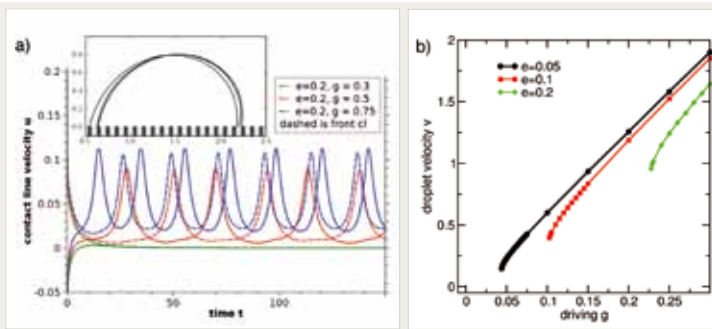


Figure 1

a) Boundary element simulation of a droplet in two dimensions moving on sinusoidally varying wettability with amplitude e for zero average wettability (contact angle 90°) and driven by gravity g acting horizontally. Shown are the velocities of the front and back contact line as function of time for a series of wettability amplitudes. b) Terminal average droplet velocity as function of driving g for different wettability amplitudes.

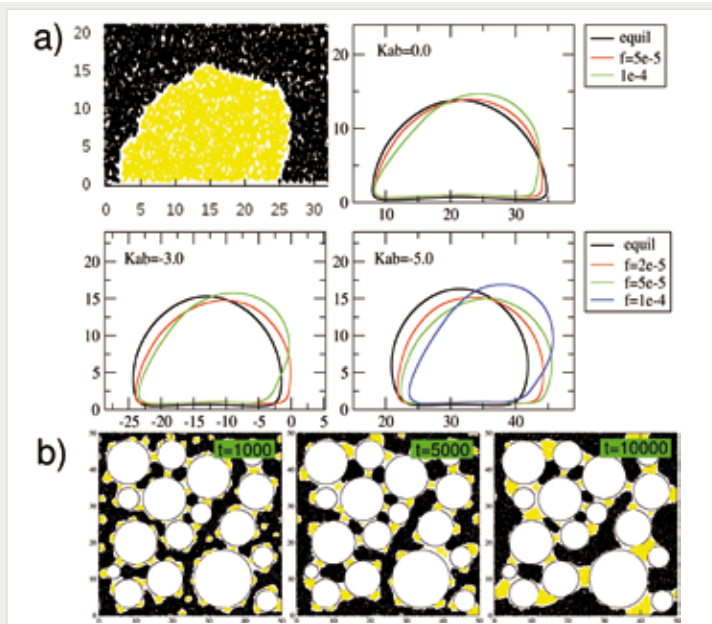


Figure 2

a) Top left: Snapshot of the particle configuration of a 2D wetting droplet in a simulation using the modified multicolor model. Top right and lower row: Average droplet shapes for different interaction with the walls as given by the parameter K_{ab} , and driving strength f . b) Coarsening of a phase separating two component fluid mixture in a porous medium for a high wettability of the yellow phase and a poor wettability of the black phase on the substrate.

ploy a mesoscale model of the immiscible two phase flow that captures the relevant physics and coarse-grains the irrelevant atomistic details [5]. The multicolor model of Inoue employs successive free-streaming and local multi-particle collision steps [6]. In each of these effective collision steps the total color flux is aligned with the color gradient. In this way a separation of particles with different colors is induced. Different wettabilities are introduced by placing virtual particles of certain color into the walls. Figure 2 shows a series of droplets for different wettability. Besides the interaction of the fluids with the wall these virtual particles are necessary to obtain the correct fluid dynamic boundary condition at the walls.

- [1] C. Huch and L. E. Scriven, *Hydrodynamic model of steady movement of a solid/liquid/fluid contact line*, *J. Coll. Int. Sc.*: **35**, 85 (1971)
- [2] N. Savva, S. Kalliadas, G. Pavliotis, Two-Dimensional Droplet Spreading over Random Topographical Substrates, *Physical Review Letters* **104**, 084501 (2010)
- [3] P.S.H. Forsberg, C. Priest, M. Brinkmann, R. Sedev, J. Ralston, Contact Line Pinning on Microstructured Surfaces for Liquids in the Wenzel State, *Langmuir* **26**, 860–865 (2009)
- [4] U Thiele, E. Knobloch, On the depinning of a driven drop on a heterogeneous substrate, *New Journal of Physics* **8**, 313 (2006)
- [5] G. Gompper et al., *Adv. Polym. Sci.* **221**, 1 (2009)
- [6] Y. Inoue et al., *J. Comp. Phys.* **201**, 191 (2004)

II-15 Integrable Systems and Related Mathematical Structures

F. Müller-Hoissen
A. Dimakis (Chios, Greece)

INTEGRABLE SYSTEMS frequently appear as approximations or special cases of physical models, ranging from fluid dynamics to string theory. Classical integrable systems with an infinite number of degrees of freedom are given by nonlinear partial differential or difference equations (PDDEs) for which there are – not necessarily easy to apply – methods to solve them in an *exact* way. Corresponding solutions often exhibit unexpected features, like solitons or soliton-like structures. A famous example in two spatial dimensions is the Kadomtsev-Petviashvili (KP) equation, which in particular describes shallow water surface waves that form network-like patterns (see [1] for a recent review).

Combinatorics of KP-II line solitons

Although the line soliton solutions of the KP-II equation have already been known since more than thirty years, their combinatorial structure has been investigated only quite recently (see [1] and references therein). In [2] we addressed the problem of characterizing the full evolution in a “tropical” approximation. Complete results were obtained for the subclass of tree-shaped line soliton patterns given by

$$u = \frac{\partial^2}{\partial x^2} \log \tau \quad \text{with} \quad \tau = \sum_{k=1}^{M+1} e^{\theta_k}, \quad \theta_k = p_k x + p_k^2 y + p_k^3 t + c_k,$$

where $p_k, c_k, k = 1, \dots, M + 1$, are real constants. Using a tropical approximation (“Maslov dequantization”), we have $\log \tau \cong \max \{\theta_1, \theta_2, \dots, \theta_{M+1}\}$. In a plot of $\log \tau$, KP line solitons then correspond to the boundary lines between planes associated to regions where one of the phases θ_k dominates. It turns out that the above solutions describe rooted planar trees that are binary except at certain transition events (coincidences of more than three phases). The essential information about the evolution resides in the coordinates of the latter events, which depend on the constants p_k, c_k . They can indeed be ex-

plicitly determined for any $M > 1$. In the tropical approximation, a soliton solution in the above family thus corresponds to a *chain of rooted planar binary trees*. Moreover, a transition from one tree to the next is given by a *right rotation* [3, 4], see figure 1 and figure 2. Depending on the values of the parameters p_k, c_k , there are different chains. It turns out that each soliton solution from the above family determines a maximal chain in a *Tamari lattice*, see figure 3.

Originally, Tamari lattices appeared as partially ordered sets (posets) where the elements are given by proper parenthesizations of a sequence of $M + 1$ letters and the ordering given by rightward (or alternatively leftward) application of the associativity rule: $(ab)c \rightarrow a(bc)$. For a word with four letters ($M = 3$), there are two possible chains, namely

$$\begin{aligned} ((ab)c)d &\rightarrow (a(bc))d \rightarrow a((bc)d) \rightarrow a(b(cd)), \\ ((ab)c)d &\rightarrow (ab)(cd) \rightarrow a(b(cd)). \end{aligned}$$

These two chains form a pentagon, which is the Tamari lattice T_3 . The associativity lattices first appeared in Dov Tamari’s doctoral thesis in 1951, written at the Sorbonne in Paris (see also [5] and figures 4 and 5). In a quite obvious way, parenthesizations of words are in bijection with rooted planar binary trees, and the rightward associativity rule translates into the right rotation in a tree. Tamari lattices can be viewed as poset structures on a special class of convex polytopes, called associahedra. They appeared in Jim Stasheff’s thesis in 1961 (see also [6]).

There are more general KP-II line soliton solutions that are no longer trees. In good approximation they can be understood as superimpositions of solutions from the above tree class [2], though this picture does not yield a simple understanding of solutions obtained via certain coincidence limits of involved parameters. Apart from this and to the extent to which the KP-II equation describes *shallow water waves* (cf. [1]),

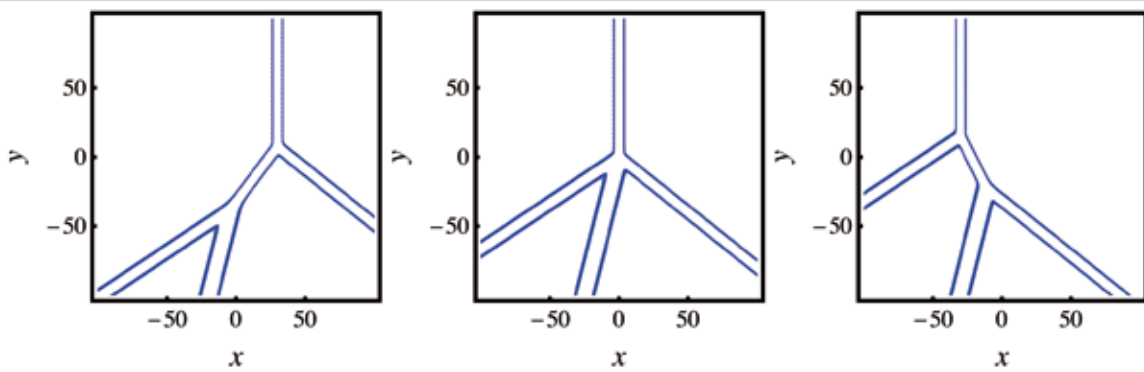


Figure 1

Contour plots at $t = -30, 0, 30$ of the exact KP-II line soliton solution with $M = 3$, $p_1 = -1, p_2 = -1/2, p_3 = 1/4, p_4 = 1$ and $c_k = 0$. The evolution corresponds to a right rotation, see also figure 2.

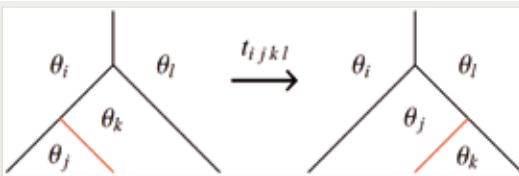


Figure 2

Right rotation in a tree. Such a transition may take place somewhere in a bigger tree. t_{ijkl} is the time at which the four phases $\theta_i, \theta_j, \theta_k, \theta_l$ coincide. The graphs only depict the *qualitative* tree structure of a solution. As seen in figure 1, the branch that “rotates” inside the tree does not change orientation, it is rather parallel-transported along the bounding branches.

we conclude that underlying their evolution is a very simple rule: right rotation in a tree.

Bidifferential calculus approach to integrable PDEs

This framework [7] may be regarded as an abstraction of the essential structure underlying the self-dual Yang-Mills (sdYM) equation, which is well-known for generating many integrable PDEs by symmetry reductions. Two familiar potential forms of the sdYM equation generalize to $\bar{d}d\phi = d\phi d\phi$ and $d(\bar{d}g g^{-1}) = 0$, where \bar{d} and d are antiderivations of degree 1 acting on a graded algebra, such that $d^2 = \bar{d}^2 = d\bar{d} + \bar{d}d = 0$. With suitable choices of d, \bar{d} , and suitable reductions, the equation for ϕ respectively g generates various integrable equations. The bidifferential calculus framework treats continuous and discrete equations (and whole hierarchies) on an equal footing. In [8] a unified derivation of soliton solutions of matrix nonlinear Schrödinger-

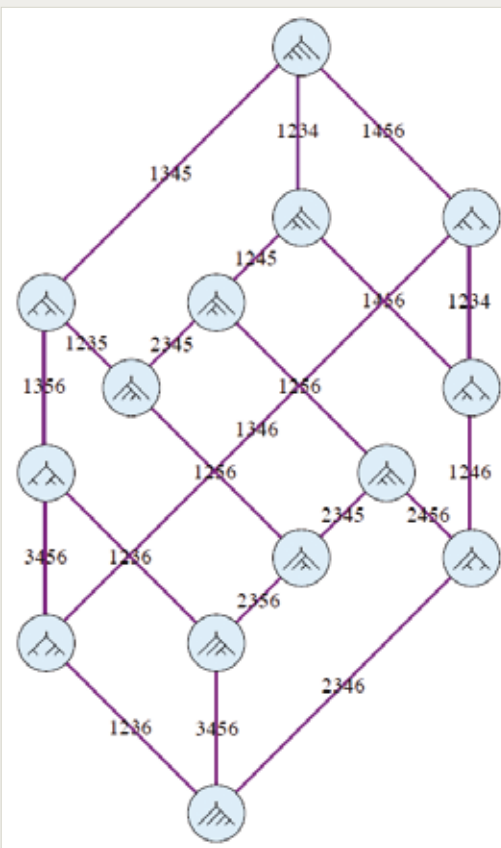
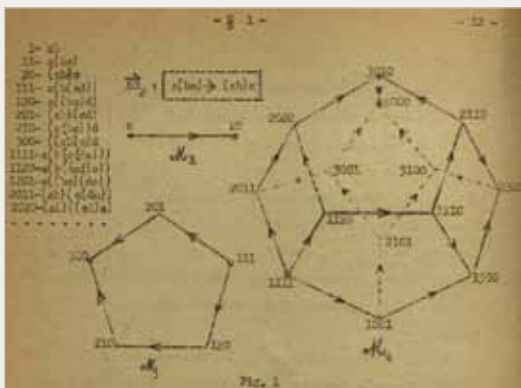


Figure 3

The Tamari lattice T_4 in terms of rooted planar binary trees. The partial order is downwards (by right rotation). The numbers assigned to the edges refer to transition times. For example, 1345 stands for t_{1345} , the time at which the four phases $\theta_1, \theta_3, \theta_4, \theta_5$ coincide. The highest node is the asymptotic soliton tree pattern as $t \rightarrow -\infty$. The possible evolutions are given by the downward chains ending in the lowest node, which is the asymptotic soliton tree pattern as $t \rightarrow +\infty$. Which chain is realized depends on which of the available transition times in the next step comes first, and this in turn depends on the parameters in the solution formula.


Figure 4

Dov Tamari (1911-2006), born as Bernhard Teitler in Germany, emigrated to Palestine in 1933, became a professor of mathematics at the Technion in Haifa and later professor of SUNY at Buffalo, USA. This year (2011) would have been Tamari's hundredth birthday.


Figure 5

Excerpt from Tamari's thesis (Paris, 1951), representing the lattice in figure 3 as a poset structure on the associahedron.

er (NLS) systems and their discretizations has been presented. A corresponding treatment of matrix AKNS hierarchies appeared in [9], also featuring a new integrable vector version of the short pulse equation.

Further recent work related to integrable PDDEs

A study of noncommutative (e.g. matrix) versions of the BKP and CKP equations and hierarchies appeared in [10]. A nonassociative structure that emerged from an exploration of the (noncommutative, e.g. matrix) KP hierarchy [11] led to powerful methods in the theory of quasi-symmetric functions [12].

- [1] Y. Kodama, *J. Phys. A: Math. Theor.* **43**, 434004 (2010)
- [2] A. Dimakis and F. Müller-Hoissen, *J. Phys. A: Math. Theor.* **44**, 025203 (2011)
- [3] D. Knuth, *The Art of Computer Programming, Vol. 3*, Addison-Wesley, Reading, MA, USA (1973)
- [4] J. Pallo, *The Computer Journal* **29**, 171 (1986)
- [5] S. Huang and D. Tamari, *J. Comb. Theory (A)* **13**, 7 (1972)
- [6] J. Stasheff, *Transactions Am. Math. Soc.* **108**, 275 (1963)
- [7] A. Dimakis and F. Müller-Hoissen, *Discr. Cont. Dyn. Syst. Suppl.* **2009** 208 (2009)
- [8] A. Dimakis and F. Müller-Hoissen, *Inverse Problems* **26**, 095007 (2010)
- [9] A. Dimakis and F. Müller-Hoissen, *SIGMA* **6**, 055 (2010)
- [10] A. Dimakis and F. Müller-Hoissen, *Inverse Problems* **25**, 045001 (2009)
- [11] A. Dimakis and F. Müller-Hoissen, *Glasgow Math. J.* **51A**, 49 (2009)
- [12] A. Dimakis and F. Müller-Hoissen, *J. Pure Appl. Algebra* **214**, 449 (2010)

III Disorder in Space and Time, Stochasticity

III-1 Statistics of Eukaryotic Chemotaxis

G. Amselem, M. Theves, A. Bae, C. Beta, E. Bodenschatz
H. Bödecker, T. Frank

CHEMOTAXIS, the directed motion of cells in a chemical gradient, plays a central role in the life of both prokaryotes and eukaryotes. It is essential for various processes like wound healing, cancer metastasis, or embryogenesis. One of the most widely studied model organisms for eukaryotic chemotaxis is the social amoeba *Dictyostelium discoideum*, which shares many of its biochemical pathways with mammalian cells. After six hours of starvation, *Dictyostelium* becomes chemotactic to cAMP, and shows directional motion in gradient profiles whose magnitudes range over four decades [1]. Quantitative studies of *Dictyostelium* chemotaxis have started more than 30 years ago, reporting the evolution of the chemotactic index (CI) – the ratio between the length of a cell track in the gra-

dient direction and the total length of the track – as a function of the gradient of cAMP [1-4]. However, a comprehensive interpretation of the data was hindered by the fact that *Dictyostelium* cells are not only sensitive to the gradient of cAMP, but also to the average concentration of cAMP that surrounds them [4]. For this reason, no unambiguous relationship between the CI and the gradient is found, when different data sets from the literature are compared (see figure 1a). The aim of our work was two-fold. First, we derived a universal scaling that allowed collapsing the data sets from figure 1a on a single curve (figure 1b). Second, we implemented a stochastic description of chemotactic cell motion in terms of a Langevin-type equation. This description goes beyond the traditional measure of the CI in that it takes fluc-

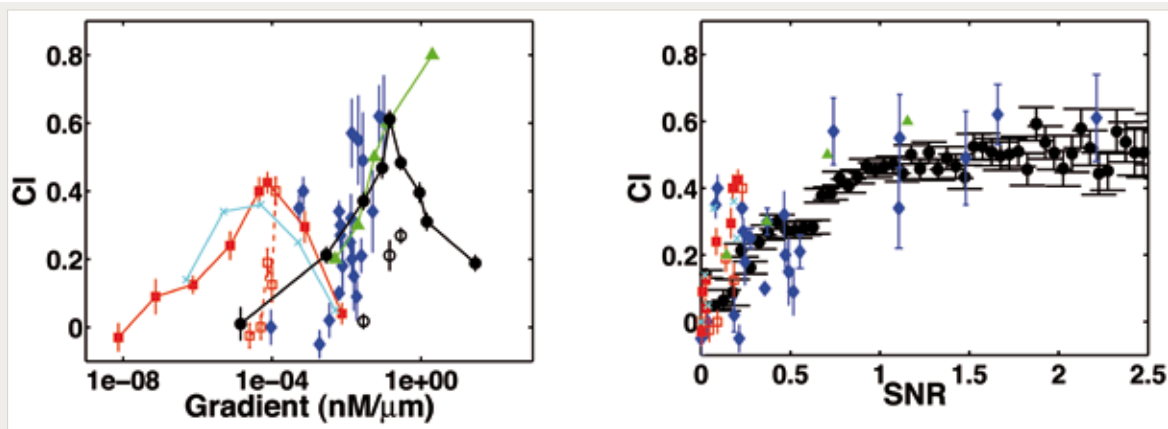


Figure 1

(a) Chemotactic index as a function of the gradient of cAMP. Filled black circles: our data for linear concentration profiles running from 0 to a concentration c_{\max} . Empty black circles: our data for linear concentration profiles running from $c_{\min} \neq 0$ to c_{\max} . Blue diamonds: data from Fuller et al. [4]. Cyan crosses: data from Varnum and Soll [2]. Red squares: data from Fisher et al. [3] (full squares: figure 5, empty squares: figure 6 in [3]). Green triangles: data from Bosgraaf et al. [5]. (b) Chemotactic index as a function of the signal to noise ratio at the level of the second messenger. All data collapse onto one universal curve.

tuations into account and provides a model in the form of a stochastic differential equation.

Let us first turn to the question of a unifying scaling for the data sets displayed in figure 1. The first step of the chemotactic process is the binding of cAMP to the Dictyostelium cAR1 receptor at the cell membrane. In our previous work, we showed that Dictyostelium is able to sense extremely shallow gradients [1]. A difference in the receptor occupancy between cell front and back of only 10 to 100 molecules is required to induce a directional response. From this observation we can conclude that a full understanding of the evolution of the CI with the cAMP profile has to take into account that binding and unbinding of cAMP to the receptor is a stochastic process. Thus, at a given gradient value, fluctuations in the difference of the receptor occupancy increase with the average concentration of cAMP. These fluctuations are transmitted in the intracellular chemotactic signaling network. An estimate of the fluctuations at the second messenger level inside the cell is provided in [8], where a signal to noise ratio (SNR) is defined, comparing the fluctuations in the intracellular second messenger gradient to its average value. For a thorough test of the definition of the SNR given in Ref. [8], we used microfluidic devices to produce linear gradients of cAMP with systematically varying cAMP gradient and average concentration. Cells were automatically tracked over 40 minutes with a time-lapse of 40 seconds [7]. For more than 700 cell tracks the CI as well as the SNR were estimated at each point in using the values of the gradient and of the local background concentration [6]. The resulting data, binned according to the value of the SNR, shows that the CI continuously grows until the SNR reaches unity [6]. Note that cells in the same bin experience the same SNR but in general different gradients and different average cAMP concentrations. Moreover, all data sets from the literature match this curve. We thus conclude that the SNR at the level of the second messenger, in our case the G protein, is the key quantity that controls the chemotactic behavior of Dictyostelium.

In future work, we will test the role of the SNR, using Dictyostelium mutant cells that underex-

press or overexpress the cAR1 receptor or the G protein. We will furthermore extend the SNR analysis to neutrophil chemotaxis, and compare the chemotactic efficiency of neutrophils with the performance of Dictyostelium cells at a given SNR. Finally, we will design a microfluidic channel in which the concentration profile of cAMP is such that the SNR is constant throughout the channel. This will give us optimal conditions to study the characteristics of cell motion such as directionality and persistence length under what the cell perceives as a constant stimulus.

For a more thorough understanding of chemotactic cell motion that goes beyond population-averaged quantities like the CI, we developed a description in terms of a Langevin-type stochastic differential equation. It is derived directly from experimental data using a technique pioneered in Ref. [9]. This method is based on a separation of the deterministic and stochastic parts of cell motion using conditional averages. Prior to the analysis of chemotactic cell motion, we applied this approach to random movement of Dictyostelium cells [11]. The separation into deterministic and stochastic parts of the movement shows that the cells undergo a damped motion with multiplicative noise. Both contributions to the dynamics display a distinct response to external physiological stimuli. In particular, we found that the deterministic component depends on the developmental state and ambient levels of signaling substances, while the stochastic part does not. Moreover, an analytic expression for the velocity distribution function was derived from this model. In the case of chemotactic data, angle resolved conditional averages were applied to obtain the deterministic and stochastic contributions to directional cell motion. In agreement with our results on random (non-chemotactic) cells, we found linear deterministic damping and multiplicative noise [6, 12]. In the presence of an external gradient, however, the deterministic part shows a clear angular dependence that takes the form of an additional force pointing in gradi-

ent direction. The stochastic part, on the other hand, does not depend on the orientation of the external cue. With increasing gradient steepness, both speed and directionality of the chemotactic motion go through a maximum that coincides with a maximum in the CI. Numerical simulations of our probabilistic model yield quantitative agreement with the experimental distribution functions of velocity and prop-

agation angle. In summary, the separation of cell motion into a deterministic and a stochastic part can be related to physiologically distinct processes. The Langevin equation is therefore a tool that (i) allows us to describe the full temporal evolution of cell motion, leading, e.g., to the histograms of cellular velocity and (ii) provides us a better insight into the different parts and mechanisms of cell motion.

- [1] L. Song, S.M. Nadkarni, H. U. Bodeker, C. Beta, A. Bae, C. Franck, W.-J. Rappel, W. F. Loomis, and E. Bodenschatz, *Eur. J. Cell. Biol.* **85**, 981 (2006)
- [2] B. Varnum and D. R. Soll, *J. Cell Biol.* **99**, 1151 (1984)
- [3] P. R. Fisher et al., *J. Cell Biol.* **108**, 973 (1989)
- [4] D. Fuller et al., *Proc. Nat. Acad. Sci.* **107**, 9656 (2010)
- [5] L. Bosgraaf et al., *J. Cell Sci.* **121**, 3589 (2008)
- [6] G. Amselem, Ph.D. Thesis, Göttingen (2010)
- [7] M. Theves, Diplomarbeit, Göttingen (2009)
- [8] M. Ueda and T. Shibata, *Biophys. J.* **93**, 11 (2007)
- [9] S. Siegert et al., *Phys. Lett. A* **243**, 275 (1998)
- [10] S. L. Blagg et al., *Curr. Biol.* **13**, 1480 (2003)
- [11] H. U. Bodeker et al., *Europhys. Lett.* **90**, 28005 (2010)
- [12] G. Amselem, M. Theves, A. Bae, E. Bodenschatz, C. Beta, submitted.

III-2 Transport in Correlated Weakly Disordered Systems – Stochastic Theory of Random Caustics

J. Metzger, R. Fleischmann, T. Geisel

EVEN THE smallest fluctuations of a medium can have dramatic influence on the properties of wave or particle flows penetrating it. This is most strikingly observable by the appearance of large density fluctuations in the flow caused by weak, correlated random disorder potentials varying only on energy scales of a few percent of the kinetic energy. These density fluctuations appear in typical branch-like structures as illustrated in figure 1. Such *branched flows* have been observed on a wide range of spatial scales, from the branching of electron flows in semiconductor microdevices [1] to the branching of sound waves in the oceans on scales of thousands of kilometers [2]. It is also believed to be a mechanism underlying the formation of freak ocean waves and tsunamis [3], and is closely related to the theory of rain shower activation in turbulent clouds [4].

Our research is aimed at understanding the mechanisms behind the branching of flows and at quantifying the frequency and intensity with

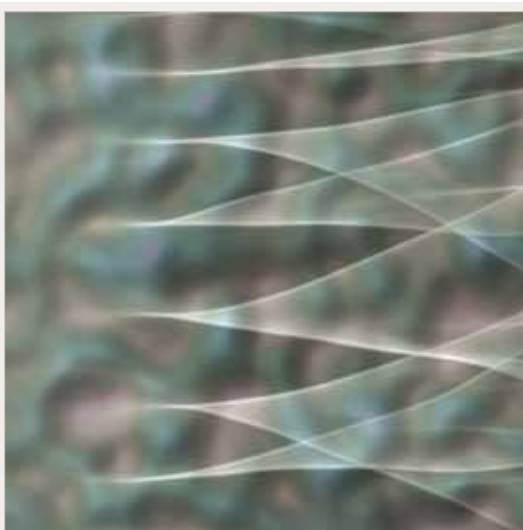


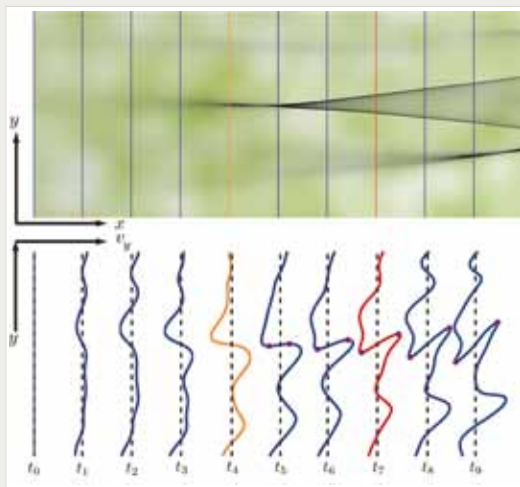
Figure 1

While the individual paths of the rays or particles only deviate ever so slightly from straight lines the flow exhibits branches of very high density.

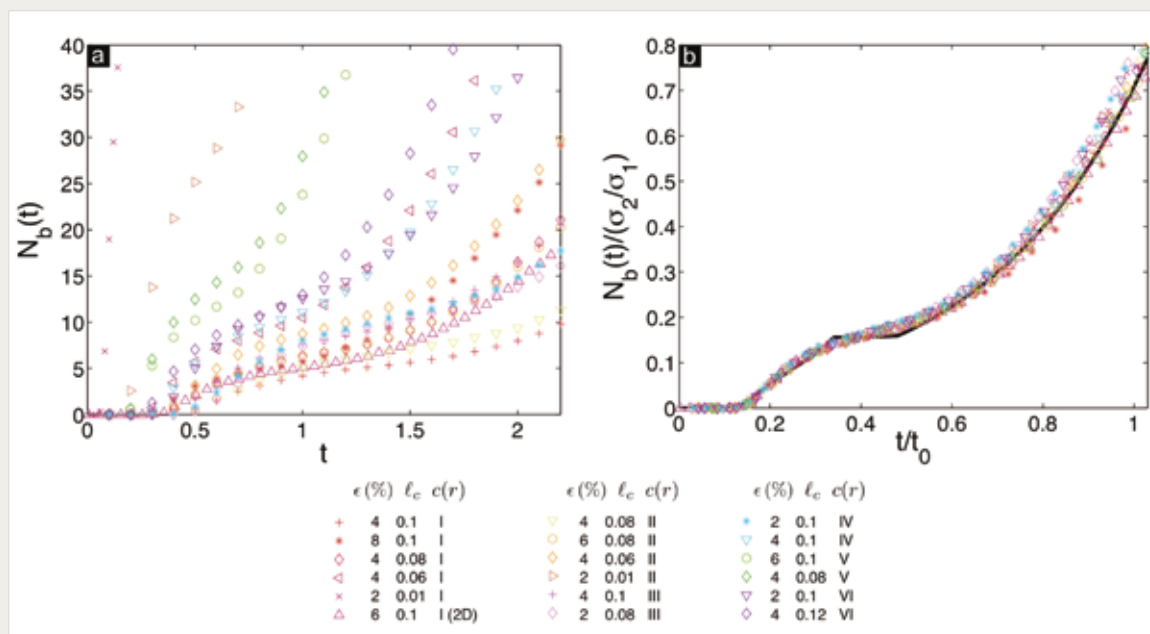
which branches occur, depending on the properties of the disorder potential underlying the flow. The analytical and numerical research is performed in the context of two-dimensional Hamiltonian systems, using spatially varying Gaussian random fields as our model disorder potentials.

Branching is caused by the formation of random *caustics*, i.e. regions where the particle or wave flow is randomly focused by the consecutive action of the random forces of the disorder potential, and thus the study of branching is also a study of the *singularities* of the flow, where the classical ray density diverges and the corresponding wave intensity is very high. The birth of a branch is illustrated in figure 2, where the classical analogues of a wavefront propagating through time (the equitemporal lines of the flow) are shown in position and phase space. Once the cumulative effect of the random potential is such that the wavefront develops turning points in phase space, its projection onto position space is singular and a caustic is formed. Since the equations describing the locations of the caustics are nonlinear and stochastic with correlated noise, the analysis of the branch statistics is challenging and only results for the far field had been known until recently [5]. We have now been able to derive an expression for the number of branches for all distances from a source [6]. By deriving a scaling relation, we were moreover able to show that this quantity follows a *universal law*, valid for a wide range of different parameters and correlation functions describing the disorder (cf. figure 3).

As an application of our theoretical study we have recently shown branching to have a dramatic effect on the direct current response properties of semiconductor microdevices in collaboration with experimentalists from the Max Planck Institute for Solid State Research [7].

**Figure 2**

The top panel shows a flow emerging from a plane source from the left, forming a branch. Here the flow density (encoded in gray) is very high. The weak random potential causing the appearance of the branch is colored in white and green (high and low potential). In the lower panel, the wave fronts corresponding to the straight lines in the top panels are shown in a part of the phase space $y-v_y$. At the turning points (purple) which are the caustics, the flow density diverges, and upon projection of the caustics onto position space these can be seen to constitute the boundaries of the branch.

**Figure 3**

Number of branches N_b in a flow as a function of distance or time t from the source, for different parameters and types of disorder potentials. When scaled appropriately, all these curves collapse onto our theoretical prediction [6], shown as the solid black line in panel b.

- [1] e.g. M. A. Topinka et al., *Nature* **410**, 183 (2001), M. P. Jura et al., *Nature Physics* **3**, 841 (2007)
- [2] M. Wolfson, S. J. Tomsovic, *Acous. Soc. Am.* **109**, 2693 (2001)
- [3] M. V. Berry, *New J. Phys.* **7**, 129 (2005); M. V. Berry, *Proc. R. Soc. A* **463**, 3055 (2007); E. J. Heller, L. Kaplan and A. Dahlen, *J. Geophys. Res.* **113**, C09023 (2008)
- [4] M. Wilkinson, B. Mehlig, and V. Bezuglyy, *Phys. Rev. Lett.* **97**, 048501 (2006)
- [5] L. Kaplan, *Phys. Rev. Lett.* **89**, 184103 (2002)
- [6] J. J. Metzger, R. Fleischmann and T. Geisel, *Phys. Rev. Lett.* **105**, 020601 (2010)
- [7] D. Maryenko, J. J. Metzger, F. Ospald, R. Fleischmann, T. Geisel, V. Umansky, K. v. Klitzing and J. H. Smet, (2011) *under review*

III-3 The Nature of Fluctuations in Human Musical Rhythms and the Measurement of Long Range Correlations

H. Hennig, A. Witt, R. Fleischmann, J. Nagler, F.J. Theis, T. Geisel

A. Fredebohm, Y. Hagmayer (Department of Psychology, Göttingen University), B.D. Malamud (Department of Geography, King's College London, U.K.)

HAVE YOU ever wondered why music generated by computers and rhythm machines sometimes sounds unnatural? One reason for this is the absence of small inaccuracies that are part of every human activity. Professional audio software therefore offers a so-called *humanizing technique*, by which the regularity of musical rhythms can be randomized to some extent. But what exactly is the nature of the inaccuracy in human musical rhythms? Studying this question for the first time, we found that the temporal rhythmic fluctuations exhibit scale-free long-range correlations (LRC), i.e. a small rhythmic fluctuation at some point in time does not only influence fluctuations shortly thereafter, but even after tens of seconds [1]. On the one hand this characterization of the rhythmic time series is relevant in the study of neurophysiological mechanisms of timing and on the other hand it also led to a patent for humanizing musical sequences [2]. We found that listeners showed a high preference for long-range correlated humanized music over conventionally (uncorrelated) humanized music.

The generation of musical rhythm is a form of human dynamics, a field which is presently the focus of numerous investigations. Many human actions are neither periodic in time, nor fully random, but exhibit scaling laws. Examples include human coordination [3, 4] and the scaling laws of human travel [5]. The neuronal mechanisms of timing in the millisecond range are still largely unknown and subject to empirical research [6, 7].

The preference for a piece of music is influenced by many aspects such as cultural background and taste. Nevertheless, there are universal statistical properties of music. Early numerical studies indicated $1/f$ -noise in musical

pitch and loudness fluctuations [8]. In reverse, $1/f$ -noise was used to create stochastic musi-

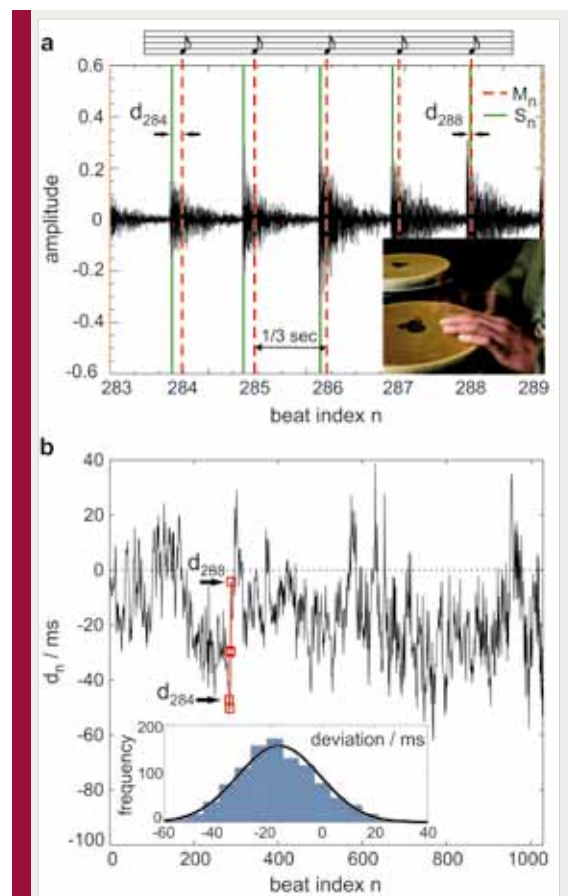


Figure 1

Presence of temporal inaccuracies in a simple drum recording. A professional drummer (inset) was recorded tapping with one hand on a drum trying to synchronize with a metronome at 180 beats per minute (a) An excerpt of the recorded audio signal is shown. The beats detected at times S_n (green lines) are compared to the metronome beats (red dashed lines). (b) The deviations $d_n = S_n - M_n$ fluctuate around a mean of -16.4 ms, i.e. on average the subject slightly anticipates the ensuing metronome clicks. Inset: The probability density function of the time series is well approximated by a Gaussian distribution (standard deviation 15.6 ms). A detrended fluctuation analysis of d_n is shown in figure 2c (middle curve).

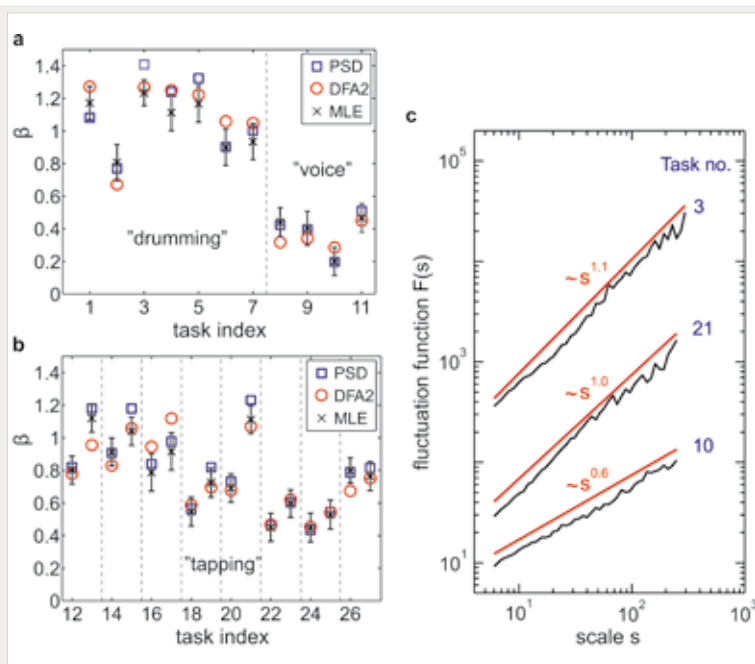


Figure 2

Evidence for long-range correlations in time series of deviations for drumming, vocal and tapping tasks. The tasks correspond to complex drum sequences and rhythmic vocal sounds (a) and are compared to hand tapping on the drumhead of a drum (b). The time series analysis reveals LRC for the entire data set. The exponents β obtained by different methods (maximum likelihood estimation, DFA and PSD) show overall good agreement. (c) A DFA for three representative time series is shown, corresponding to drumming a complex pattern with hands and feet simultaneously involved (top), tapping (middle) and vocal rhythms (bottom curve). DFA involves calculation of the fluctuation function $F(s)$ measuring the average variance of a time series segment of length s [5]. The power law scaling indicates LRC.

cal compositions. Most listeners judged these compositions to be more pleasing than those obtained using uncorrelated noise.

Here, we investigate the statistical nature of fluctuations in complex rhythmical tasks and their influence on the perception of musical performances. We examine the correlation properties of deviations from the exact beats for various combinations of hand, feet, and vocal performances, by both amateur and professional musicians.

A simple example of a recording is shown in figure 1: A test person followed metronome clicks beating with one hand on a drum. In all recordings the subjects were given metronome clicks over headphones, a typical procedure in professional drum recordings. We used the metronome grid to compute the inaccuracies of beats of complex drum sequences (tasks “drumming”). Furthermore we analyzed recordings of vocal performances (tasks “voice”), consisting of short rhythmic sounds according to a metronome. For comparison with less complex sensorimotor coordination tasks [4] we also included tapping recordings (tasks “tapping”).

A signal is called long-range correlated if its power spectral density (PSD) asymptotical-

ly scales in a power law, $S(f) \sim (1/f)^\beta$ for small frequencies and $0 < \beta < 2$. Negative deviations from $\beta=1$ involve fluctuations with weaker persistence than flicker noise which is superpersistent. Thus, the scaling exponent β is important for characterizing the universality class of a long-ranged correlated system. The accurate extraction of these exponents from short time series requires very careful data analysis. We applied several methods that measure the strength of long-range correlations in short time series, namely detrended fluctuations analysis (DFA) [4], zero padding PSD, and maximum likelihood estimation (MLE), while our choice of algorithms was corroborated by ref. [9, 10] (see also “How to measure LRC in short time series” below).

We found LRC for all tasks and subjects that were able to follow the rhythm for a sufficiently long time, as shown in figure 2a-b. Surprisingly, for over 40% of the recordings the LRC differ distinctively from the $1/f$ -type (flicker noise). Moreover, in an interdisciplinary collaboration with the Psychology Department of Göttingen University, we tested the preference for music a) with uncorrelated temporal fluctuations and b) by introducing LRC. The test subjects showed

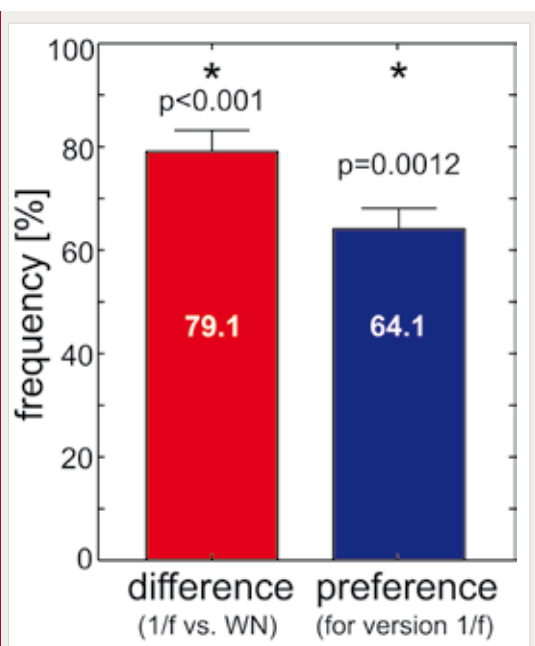


Figure 3

Perception analysis showing that 1/f humanized music is preferred over white noise humanizing. The versions 1/f and WN (white noise) were compared by 39 listeners. Two samples were played in random order to test subjects, all singers from Göttingen choirs, who were asked either one of two questions: (1) “Which sample sounds more precise?” (red bar) or (2) “Which sample do you prefer?” (blue bar) The answers to the first question provide clear evidence that listeners were able to perceive a difference between the two versions (t-test, $p < 0.001$). Furthermore, the 1/f humanized version was significantly preferred to the WN version (t-test, $p = 0.0012$).

a strong preference for long-range correlated over uncorrelated humanized music, see figure 3.

This study provides strong evidence for LRC in a broad variety of rhythmic tasks such as hand, feet, but also vocal performances. Therefore these fluctuations are unlikely to be evoked merely e.g. by the motor control and mechanics of a limb movement. Another observation rather points to mechanisms of rhythmic timing that involve memory processes: We found that LRC were entirely absent in individuals who frequently lose rhythm and reenter following the metronome. This may originate from a resetting of memory in the neurophysical mechanisms

controlling rhythmic timing (e.g. neuronal ‘population clocks’ [7]). In the other cases, the existence of strong LRC shows that these clocks have a long persistence even in the presence of a metronome. Also human EEG data [11] as well as interspike-interval sequences of human single neuron firing activity [12] showed LRC. Such processes might be neuronal correlates of the LRC observed here in rhythmic tasks.

In conclusion, the statistical nature of temporal fluctuations in complex human musical rhythms was studied. We established that the favorable fluctuation type for humanizing interbeat intervals coincides with the one generically inherent in human musical performances.

How to measure LRC in short time series

The reliable measurement of long range correlations is not only required for recording of human dynamics, as this type of correlations has been identified as a common property of time series from many scientific disciplines. For instance, LRC have been found in environmental processes, for trajectories of tracer particles in hydrodynamic flows, in granular materials and condensed matter physics, neurosciences and econophysics.

For modelling purposes and classification tasks it is important to determine the strength of LRC as accurately as possible and to quantify the uncertainty of this estimate. We have compared four common analysis techniques for quantifying long-range correlations: (a) Power-spectral analysis, (b) Detrended Fluctuation analysis, (c) Semivariogram analysis, and (d) Rescaled-Range (R/S) analysis. To evaluate these methods, we have constructed large ensembles of synthetic time series which differ in (i) lengths (ii) correlation strengths and (iii) one point probability distribution (Gaussian, log-normal or Levy). We have evaluated the four techniques by statistically comparing their performance. Our analysis reveals that the performance of spectral techniques is in general very good, with the maximum-likelihood estimator performing best, but also the rather simple log-periodo-

gram estimator is not biased and giving confidence intervals of 'acceptable' size for most practical applications. Detrended fluctuation analysis is appropriate for fractional noises with positive persistence and with non-heavy-tailed and rather symmetric one-point probability distributions. We do not recommend to use semi-variogram and Hurst's rescaled range analysis.

- [1] H. Hennig, R. Fleischmann, A. Fredebohm, Y. Hagmayer, J. Nagler, A. Witt, F. J. Theis, T. Geisel, submitted (2011)
- [2] H. Hennig, R. Fleischmann, F. J. Theis, T. Geisel, EU patent No. 07117541.8 (patent pending). US patent No. 7,777,123 (2010)
- [3] D. L. Gilden, T. Thornton, M. W. Mallon, *Science* **267**, 1837–1839 (1995)
- [4] A. L. Goldberger et al., *Proc. Natl. Acad. Sci. USA* **99**, 2466–2472 (2002)
- [5] D. Brockmann, L. Hufnagel, T. Geisel, *Nature* **439**, 462–465 (2006)
- [6] R. M. Memmesheimer, M. Timme, In: *Handbook on biological networks*. World Scientific, Singapore (2009)
- [7] C.V. Buhusi, W.H. Meck, *Nature Rev. Neurosci.* **6**, 755–765 (2005)
- [8] R. Voss, J. Clarke, *Nature* **258**, 317–318 (1975)
- [9] B. Pilgram et al. *Physica D* **114**, 108 (1998)
- [10] A. Witt, B. D. Malamud, submitted (2011)
- [11] K. Linkenkaer-Hansen, V. V. Nikouline, J. M. Palva, R. J. Ilmoniemi, *J. Neurosci.* **21**, 1370-1377 (2001)
- [12] J. Bhattacharya, J. Edwards, A. N. Mamelak, E. M. Schuman, *Neuroscience* **131**, 547–555 (2005)

III-4 Statistical Mechanics of Static Granular Media

M. Schröter

J.-F. Métayer, T. Aste (University of Kent), C. Radin (UT Austin), G. Schröder-Turk (University Erlangen), H. Swinney (UT Austin)

STATISTICAL MECHANICS has proven to be an invaluable tool for understanding systems in and close to thermal equilibrium. However, granular media are composed of macroscopic particles with dissipative collisions and frictional contacts; these systems are intrinsically far away from thermal equilibrium. Still the last two decades saw the development of an appropriately extended kinetic theory which provides a good description for dilute, granular gases where the only interactions are binary collisions [1].

For static granular matter, where enduring, frictional contacts prevail, the situation is less clear. More than 20 years ago Sam Edwards and coworkers proposed a statistical mechanics approach for these systems based on three postulates [2, 3]:

1) The microstates of the system are the mechanical stable configurations at a given densi-

ty. The logarithm of the number of these states provides a configurational entropy.

2) Static packings are athermal and at rest, kinetic energy can therefore be neglected. Consequently, volume instead of energy is the relevant extensive variable. The Hamiltonian has to be replaced by a function W which gives the volume of the system as a function of the coordinates (and orientations) of the particles.

3) The derivative of volume with respect to configurational entropy is a configurational temperature which is called compactivity.

In recent years there has been increased activity in testing if these postulates can be extended to a fully-fledged, predictive theory of granular solids. A good overview can be found in the presentations given at the 2009 workshop at the Lorentz-center in Leiden [4].

Recent experimental progress in our group is here reported along the lines of Edward's initial postulates given above:

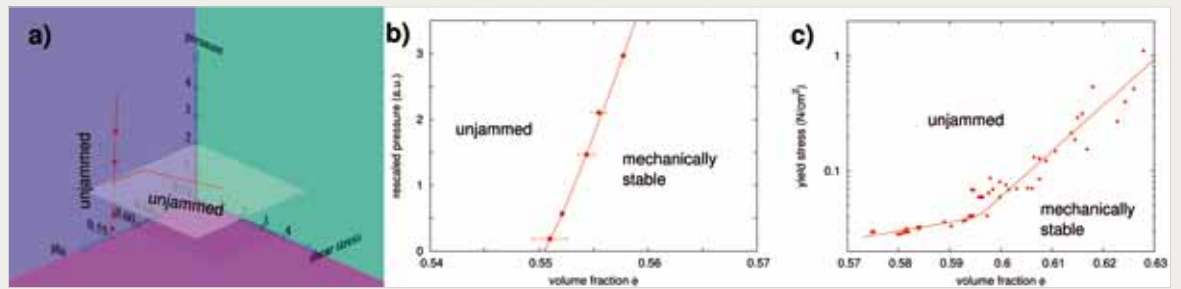


Figure 1

Phase diagram of frictional sphere packings. a) Schematic sketch. All sphere packings are mechanically stable at high enough volume fraction and zero pressure and shear stress, corresponding to the origin of the diagram. Moving away from the origin the packings will unjam at a certain point in the phase space. b) At zero shear stress (the purple plane in panel a) the transition between solid-like and fluid like behavior is often referred to as Random Loose Packing. The experimental data points are from [8]. c) Packings can also be unjammed by shearing. The experimental data from [6] correspond to the translucent plane parallel to the pink base in panel a).

1) The Edward's approach is only applicable for mechanically stable configurations, yet a full phase diagram delineating granular solids and liquids is still work in progress. Figure 1 outlines the boundaries in the volume fraction versus pressure respective shear stress planes of the phase diagram. While these results are related to the Jamming phase diagram (for a recent review see [5]). The frictional nature of granular contacts does result in a number of qualitative differences [6, 8].

2) The volume function W requires to tessellate the space between grains. This is often done using Voronoi cells. Figure 2 demonstrates that the Voronoi volumes of sphere packings have interesting scaling properties which are independent of the actual experimental or numerical protocol used to create the packing. This is an encouraging sign for the universality of such a volume based approach.

3) Using a fluctuation-dissipation relation, the

configurational temperature of a sample can be determined from its volume fluctuations when in contact with a "granular heat bath". Realizing such a heat bath with flow pulses in a water-fluidized bed, we have for the first time measured the compactivity of a granular sample (figure 3, taken from [7]).

There remain a number of open questions which need to be answered before the viability of the Edward's approach can be assumed to be proven. How ergodic are the different ways of external driving of the (dissipative) granular samples? What is the role of correlations between the individual Voronoi volumes? In what cases do we need a second, tensorial temperature to account for the hyperstatic nature of frictional particle packings? But it is already now apparent, that Leo Kadanoff was right when he stated: "One might even say that the study of granular materials gives one a chance to reinvent statistical mechanics in a new context." [11]

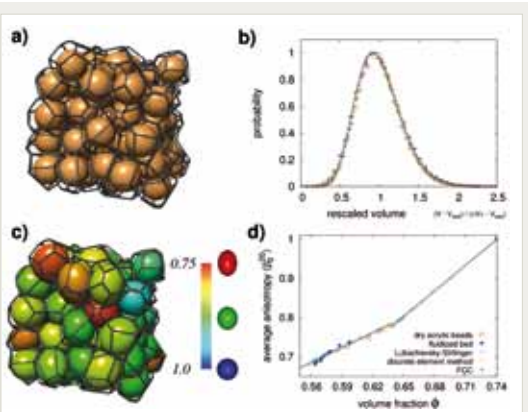


Figure 2

Voronoi volumes of sphere packings exhibit characteristic scaling properties. a) Rendering of a subset of a packing of acrylic spheres; the volume fraction is 0.586. The black wire frame delineates the Voronoi cells. b) Distribution of Voronoi volumes versus rescaled volume; V_{\min} is the volume of a regular Delaunay tetrahedron for four spheres in contact, $\langle V \rangle$ is the average volume per elementary cell. The different symbols correspond to 18 different experimental datasets with volume fractions between 0.56 and 0.64. The black line is a Gamma distribution with a shape factor of 12 [9]. c) The same subset of particles as in panel a with the beads replaced by ellipsoids that match the anisotropy and orientation of the Voronoi cells. The anisotropy is quantified by the eigenvalue ratio β of a Minkowski Tensor representation of the Voronoi cells. Isotropic cells have $\beta = 1$. d) Average anisotropy of the Voronoi cells as a function of the volume fraction. The different symbols correspond to experimental and numerical datasets obtained with different preparation protocols with and without friction and gravity. The kink in the slope corresponds to Random Close Packing. For more information see [10].

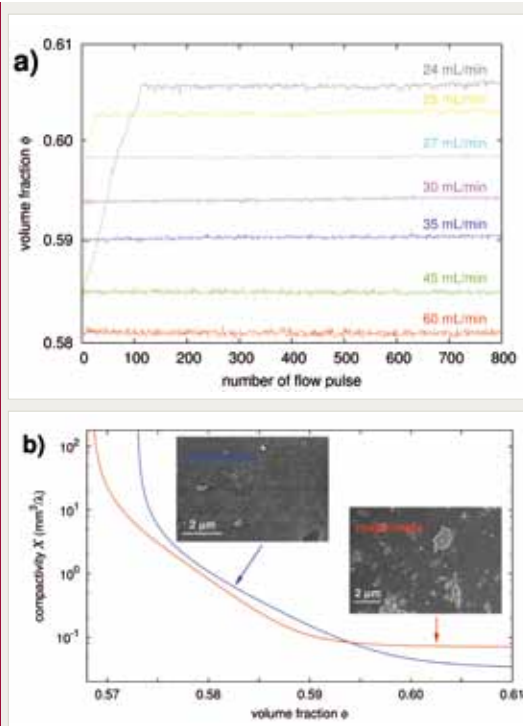


Figure 3

Measuring the configurational temperature of static granular media. a) Stationary state volume fluctuations of sphere packings. To drive the system from one mechanically stable state to another, the packing is repeatedly “tapped” by flow pulses in a water-fluidized bed. Different flow rates during the pulses result in different average volume fractions, the volume fluctuations are Gaussian distributed. b) Based on the standard deviation of the fluctuations in panel a, the configurational temperature, also called compactivity, of the beads can be computed as a function of their volume fraction. The compactivity depends on the surface roughness and therefore friction of the glass beads as the two SEM close up of the 250 μm diameter spheres show. Data are from [7].

- [1] Brilliantov and Pöschel, *Kinetic Theory of Granular Gases*, Oxford University Press (2004)
- [2] Edwards and Oakeshott, *Physica A* **157**, 1080 (1989)
- [3] Mehta and Edwards, *Physica A* **157**, 1091 (1989)
- [4] <http://www.lorentzcenter.nl/lc/web/2009/340/info.php3?wsid=340>
- [5] van Hecke, *J. Phys.: Cond. Mat.* **21**, 033101 (2010)
- [6] Métayer, Suntrup III, Radin, Swinney, and Schröter, *Europhys. Lett.* **93**, 64003 (2011)
- [7] Schröter, Goldman, and Swinney, *Phys. Rev. E* **66**, 030301(R) (2005)
- [8] Jerkins, Schröter, Swinney, Senden, Saadatfar, and Aste, *Phys. Rev. Lett.* **101**, 018301 (2008)
- [9] Aste, Di Matteo, Saadatfar, Senden, Schröter, and Swinney, *Europhys. Lett.* **79**, 24003 (2007)
- [10] Schröder-Turk, Mickel, Schröter, Delaney, Saadatfar, Senden, Mecke, and Aste, *Europhys. Lett.* **90**, 34001 (2010)
- [11] Kadanoff, *Rev. Mod. Phys.* **71**, 435 (1999)

III-5 Evolutionary Impact of Range Expansions

O. Hallatschek

J. Nullmeier, S. Boekhoff

POPULATION EXPANSIONS in space are common events in the evolutionary history of many species [1] and have a profound effect on their genealogy. It is widely appreciated that any range expansion leads to a reduction of genetic diversity because the gene pool for the new habitat is provided only by a small number of individuals, which happen to arrive in the unexplored territory first. In many species, the genetic footprints of these “pioneers” are still recognizable today and provide information about the migrational history of the species. For instance, a frequently observed south-north gradient in genetic diversity (“southern richness to northern purity” [2]) on the northern hemisphere is thought to reflect the range expansions induced by the glacial cycles. In the case of humans, the genetic diversity decreases essentially linearly with increasing geographic distance from Africa [4], which is indicative of the human migration out of Africa. It is hoped, that the observed patterns of neutral genetic diversity can be used to infer details of the corresponding colonization pathways.

Such an inference requires an understanding of how a colonization process generates a gradient in genetic diversity, and which parameters chiefly control the magnitude of this gradient. Traditional models of population genetics, which mainly focus on populations of constant size and distribution, apply to periods before and after a range expansion has occurred, when the population is at demographic equilibrium. However, the spatio-temporal dynamics in the transition period, is less amenable to the standard analytical tools of population genetics, and has therefore been only poorly studied. Yet, it is clear that these transition periods have a strong impact on evolution, through the mechanism of “gene surfing” [3]: As compared to individuals in the wake, the pioneers at the colonization front are much more successful in passing their genes on to future generations, not only

because their reproduction is unhampered by limited resources but also because their progeny start out from a good position to keep up with the wave front (by means of mere diffusion). The offspring of pioneers thus have a tendency to become pioneers of the next generation, such that they, too, enjoy abundant resources, just like their ancestors. Therefore, pioneer genes have a good chance to be carried along with the wave front and attain high frequencies, as if they “surf” on the wave.

The projects presented below address the phenomenon of gene surfing from two complementary perspectives. First, we analyze forward in time the effect of gene surfing on newly arising mutations and pre-existing genetic variation in the population. Second, we analyze backward in time the starlike genealogies that are created by range expansions.

The effect of gene surfing on standing genetic variation

To investigate the effect of gene surfing on genetic variation, previous research focussed mainly on single mutations arising at the front of expanding populations (figure 1a). However, since mutations happen at a regular basis, we expect some variation to be prevalent in natural populations before the expansion starts – this pre-existing variation is also called “standing genetic variation” (figure 1b). In a simulational study, we included for the first time both standing variation and recurrent mutations, to see whether the effect of a range expansion on standing variation is different from its effect on recurrent mutations and whether the surfing of standing variation might dominate the patterns of genetic diversity in human populations. In order to quantify the effect of gene surfing, we mimic the dispersal of humans out of Africa by the combination of diffusion and local logistic

growth. We start our simulations with an ancestral population located in the Middle East containing a homogeneous mixture of two variants of a gene (alleles). These variants are assumed to confer no significant increase in growth rate (“neutrality” assumption). We simulate the combined genetic dynamics (mutation events) and population dynamics (propagation and migration) as a function of the initial ratio between both variants. Simulations are run one million times using the same initial condition. The simulation results are used to estimate the probability distribution of the allele frequency after the range expansion for a range of initial allele frequencies. We find that range expansions can push even initially rare alleles to occupy a macroscopic fraction of the final population. The probability distribution of the allele frequency after range expansions is governed by a power law (see figure 1 right). By comparing human genome data from the 1000 genomes project [4] to our simulation results, we hope to reconstruct demographic parameters for human paleolithic and neolithic population expansions.

The coalescent in expanding populations

The continual turnover of a population naturally leads to a description of gene dynamics in terms of branching processes: The lineage of a gene

branches if it occurs in more than one offspring of an individual that carries the gene. Backward in time, however, lineages do not branch (assuming no recombination within the gene). Instead, if one follows two lineages backward in time they will coalesce in their most recent common ancestor. The associated time T_{MRCA} to the most recent common ancestor quantifies the degree of divergence between two descendants. Since this time is observable through the number of acquired (neutral) genetic differences, there is tremendous interest in understanding the statistics of coalescence processes.

The standard model of coalescence due to Kingman is widely used to interpret genetic diversity data obtained from samples within a population. The Kingman coalescent, however, is only applicable to well-mixed populations. It can be extended to spatially extended populations (the structured coalescent), but there is almost no theoretical work on populations that vary in space and time [5]. Here, we summarize our preliminary results on the coalescence properties backward in time to be able to predict the genetic diversity within an expanding population. In our coalescent study, we focus on range expansions triggered by the slow motion of an external boundary, for instance as a consequence of a climate change. A specific example is provided by the population of the com-

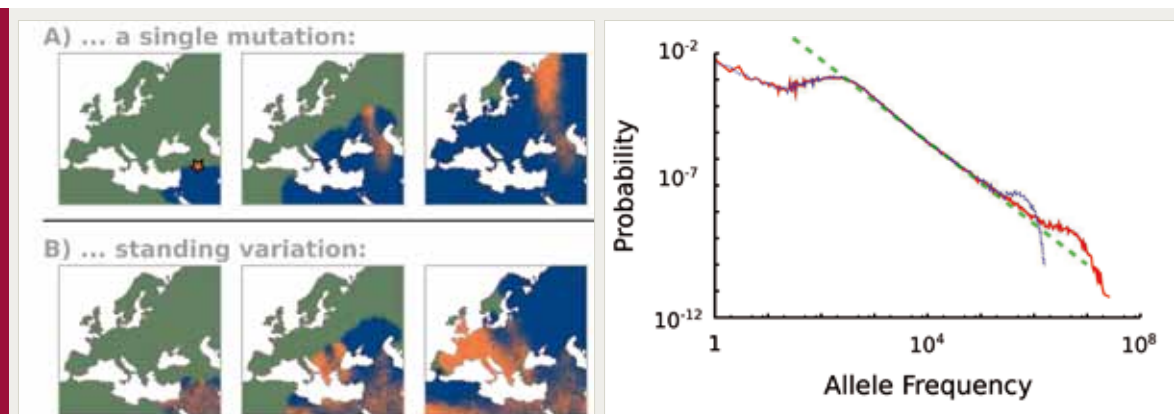


Figure 1

Simulations of gene surfing. Left: Range expansions of humans starting in the Middle East are simulated for two different scenarios: (a) a single neutral mutation arises at the expanding front (star). (b) the initial population carries the mutation with a probability of 50% (standing genetic variation). Right: The probability distribution function of the allele frequency after the range expansion reveals a power law for several orders of magnitude. This indicates a strong influence of range expansions on the genetic composition of populations and predicates that even initially rare alleles can reach very high frequencies.

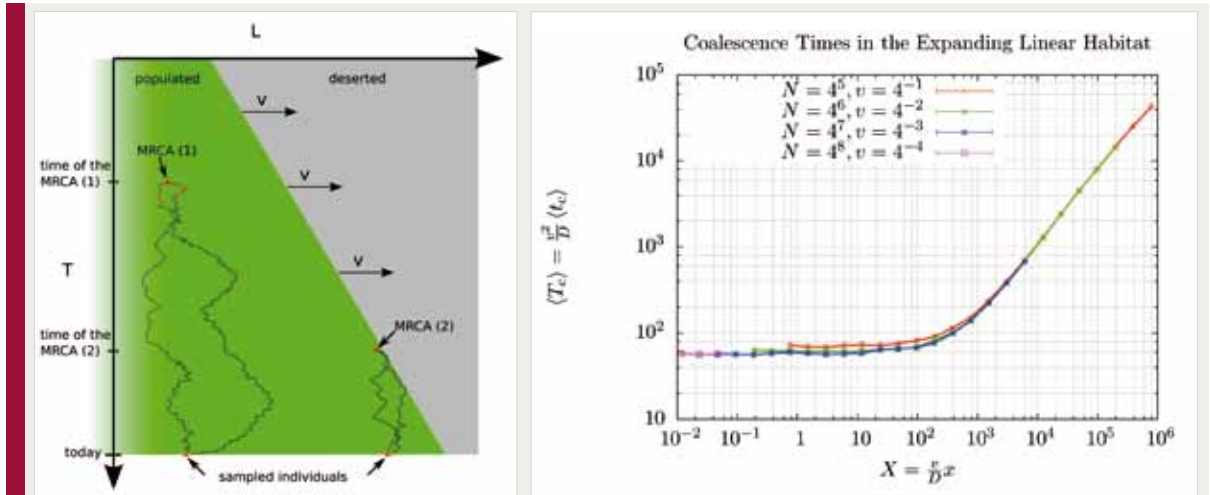


Figure 2

The coalescent process in expanding populations. Left: A one-dimensional model of an expanding population. The green and grey areas correspond to the populated and empty regions, respectively. The coalescence process starts at time 0 (bottom line) and runs backward in time. The coalescence processes of two lineages sampled from the same place is illustrated for two paradigmatic cases: Coalescence either occurs without the influence of the front (1), or is triggered by the moving boundary (2). Right: Mean coalescence times $\langle T_c \rangle$ of two lineages sampled from the same location X . Lengths and times are given in characteristic scales. Data is shown for four different values of both the deme size and expansion velocity (see legend). Notice the collapse of all data sets, the plateau close to the front and the power law for large X .

mon vole (*Microtus arvalis*) living in an alpine glacier valley [6]. The ongoing melting of the glacier triggers the range expansion of the vole population. Range expansions caused by the externally imposed motion of a habitat boundary have to be distinguished from the invasive range expansions described in the first part of this report. We model the expanding population by a linear chain of well-mixed subpopulations (called demes) with nearest neighbor migration. New demes are removed at a constant rate on one side of the linear habitat to describe the constant motion of the species range margins backward in time.

We find that the coalescence process within our model exhibits two qualitatively different dynamics, as illustrated in figure 2 (left). If two lineages are sampled sufficiently far from the boundary, the coalescence process is identical to a population with stable demography until a crucial cutoff time, when the moving boundary has reached the sampling location. On the other hand, if two lineages are sampled close to the front, the coalescence will occur shortly after the wall has arrived, because the reflecting boundary pushes the two lineages against one another thereby strongly increasing the frequency of their encounters and hence their coalescence rates. As a consequence, the mean coales-

cence time becomes independent of starting position. Both regimes can be discerned in a plot of the mean coalescence time versus sampling position as a power law for large distances and a plateau for short sampling distances, see figure 2 (right). The plateau value increases with increasing boundary motion and decreasing diffusion constant. The above scaling arguments can be extended to predict the full distribution of coalescence times in an expanding population as a function of the speed of the boundary, the population density, the diffusion constant and the sampling locations in one and two dimensions. These results can be used to infer past range expansions from the observed patterns of genetic diversity.

- [1] L. L. Cavalli-Sforza, P. Menozzi, and A. Piazza, *Science* **259** (5095), 639 (1993)
- [2] G. M. Hewitt, *Biological Journal of the Linnean Society* **58** (3), 247–276 (1996)
- [3] O. Hallatschek and D.R. Nelson, *Gene surfing in expanding populations*, *Theoretical population biology* **73** (1), 158–170 (2008)
- [4] R. M. Durbin, D. L. Altshuler, G. R. Abecasis, D. R. Bentley, A. Chakravarti, A. G. Clark, F. S. Collins, F. M. De La Vega, P. Donnelly, M. Egholm, et al. *Nature* **467** (7319), 1061–1073 (2010)
- [5] M. DeGiorgio, M. Jakobsson, and N. A. Rosenberg. *Proceedings of the National Academy of Sciences*, **106** (38), 16057 (2009)
- [6] G. Heckel, R. Burri, S. Fink, J. F. Desmet, and L. Excoffier. *Evolution*, **59** (10), 2231–2242 (2005)

III-6 Graph Theory and Statistical Physics of Complex Disordered Systems

F. van Bussel, D. Fliegner, M. Timme
C. Ehrlich (TU Dresden), S. Stolzenberg (Cornell, USA)

Efficient computation of graph invariants

In how many ways can you color the vertices of a graph such that no two adjacent vertices have the same color? Given a set of q different colors, the answer to this question is provided by the chromatic polynomial $P(q)$ of a graph, an important graph invariant. A network or graph is defined as a set of vertices and a set of edges connecting these vertices. Characterizing the relevant global properties of most larger-scale graphs generally is a huge computational challenge – the computational effort typically increases exponentially with the size of the network.

Recently, we have invented a novel class of computational methods to solve this (and several related enumeration problems) on classes of graphs that are of immediate interest in applications. This allows solutions to a number of problems which were previously computationally inaccessible.

Symbolic pattern matching using a partition function representation

The starting point of the new method [1, 2] is a remarkable connection between graph theory and statistical physics. In particular, the chromatic polynomial is equivalent to the zero-temperature partition function of the anti-ferromagnetic Potts model. Here one considers a set of q -level spin systems on a lattice, where adjacent spins interact repulsively if they are in the same state. The partition function then counts the number of degenerate ground states. In particular, the Potts antiferromagnet describes the phenomenon of ground state entropy without frustration, an exception to the third law of thermodynamics.

In general, the calculation of this function is computationally hard. But using the physics representation of a partition function, an efficient solution is possible for many classes of graphs, in particular sparsely connected systems, which

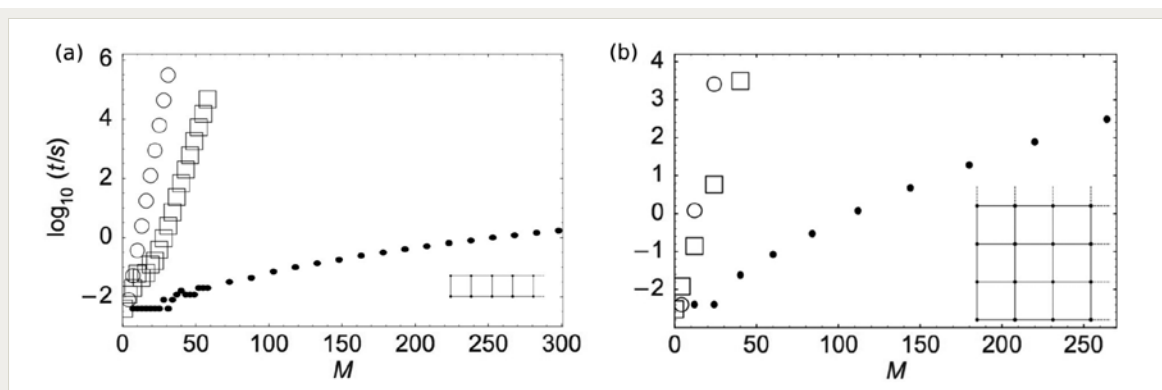


Figure 1

Computation time t (in s) for square lattice samples of sizes $2 \times n$ (a) and $n \times n$ (b) increases with the number of edges M of the graph. The new method (\bullet) drastically outperforms standard methods used in Mathematica (\circ) and Maple (\square), both with respect to the scaling of the algorithm (quantified by the local slope) and the absolute effectiveness (quantified by the absolute times needed), even for moderately sized graphs.

are important in practical applications. In the new algorithm, the summations needed for the calculation of the partition function are interpreted as symbolic operators, and the expressions occurring during the evaluation are implemented as elements of an abstract ring satisfying certain identification rules [1]. It is then possible to carry out the summations symbolically and sequentially. The final algorithm first analyzes and exploits the specific structure of the graph in order to represent it in a close to optimal way before performing the actual calculations.

Accessing higher dimensions for the first time

The novel method dramatically outperforms existing ones on most graphs, including many of practical interest (cf. figure 1). For instance, studies of antiferromagnetic Potts partition functions were so far restricted to small two-dimensional systems and solutions to real-world, three-dimensional systems could not be ac-

cessed, neither analytically nor numerically, despite the Potts model being accepted as a paradigmatic standard model for many decades. Using the new method, we now computed Potts partition functions of two- and three-dimensional lattices of significant size (cf. figure 1 b). We are currently developing modified algebraic methods to further access samples of representatives of all Bravais lattices. These results yield insights about possible phase transitions in antiferromagnetic systems that exhibit positive ground state entropy.

Furthermore, we successfully completed the first attempt to access chromatic polynomials of random graphs [3] (cf. figure 2), a key ensemble in graph theory and its applications. We are currently working towards a generalization of our new method to further graph structural properties of physical interest, e.g. the graph reliability polynomial $R(p)$ which tells us the probability of a graph being connected given that each edge disappears with probability p .

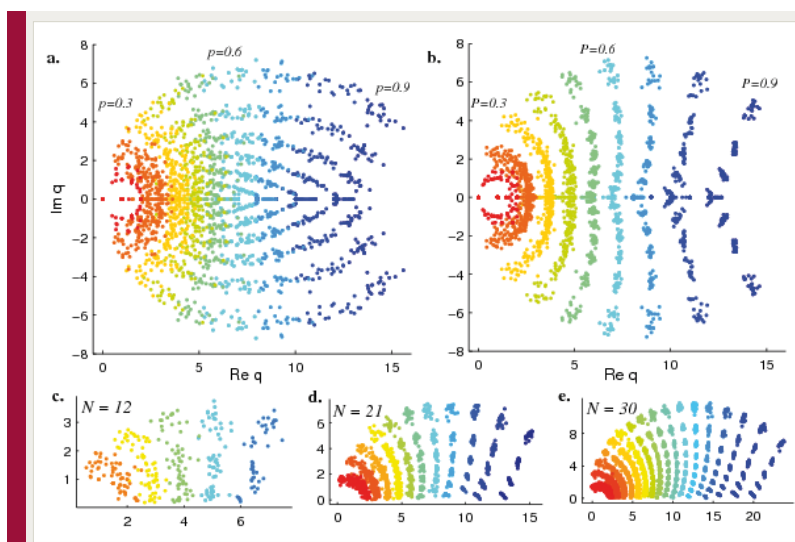


Figure 2

Complex zeros of chromatic polynomials of random graphs. (a) Zeros for graphs on $N=20$ vertices with selection probability $p \in \{0.1, 0.2, \dots, 0.9\}$; (b) Zeros for graphs with the number M of edges determined by fixed edge density $P = [2M/(N-1)] \in \{0.1, 0.2, \dots, 0.9\}$; (c), (d) and (e) Zeros with positive real part for $G(N, M)$ graphs for selected N and $M = [KN/2]$ determined by a fixed average degree $K \in \{3, 4, 5, 6, \dots\}$. In all figures, chromatic zeros for 20 sample graphs per parameter set are plotted together. The edge density P is indicated by color, running from red (low density) to blue (high density).

- [1] D. Kozen and M. Timme, *Indefinite Summation and the Kronecker Delta*, Technical Report, Cornell University **1813**, 8352 (2008), <http://hdl.handle.net/1813/8352>.
- [2] M. Timme, F. van Bussel, D. Fliegner, and S. Stolzenberg, *New J. Phys.* **11**, 023001 (2009).
- [3] F. van Bussel, C. Ehrlich, D. Fliegner, S. Stolzenberg, and M. Timme, *J. Phys. A: Math. Theor.* **43**, 175002 (2010).

III-7 Statistical Physics of Neuronal Action Potentials

A. Neef, F. Wolf

T. Tchumatchenko, W. Wei, A. El Hady, E. Lazarov, K. Bröking, N. Chapochnikov, R. Fleischmann, P. Öz, H. Schrobsdorf, T. Geisel, E. Bamberg (MPIBP Frankfurt), I. Fleidervish (Ben Gurion University, IL), M. Gutnick (Hebrew University, IL), F. Kirchhoff (U Saarland), S. Löwel (U Göttingen), W. Stühmer (MPIEM Göttingen), M. Volgushev (U Connecticut, USA)

IN ALL neurons of the cerebral cortex, the results of single neuron computations are encoded into action-potential sequences. The dynamics of cortical action potential generators thus determines how much and which information is transmitted to other cells in the brain and conversely which aspects of intracellular activity are not communicated to the receiving neurons. The reduction of information by action potential encoding in neocortical neurons is in fact tremendous. It has been estimated that of the 1000 bits per second that are contained in the ongoing membrane potential fluctuations of a typical cortical neuron only roughly 30 bits are encoded into its output sequence of action potentials [1].

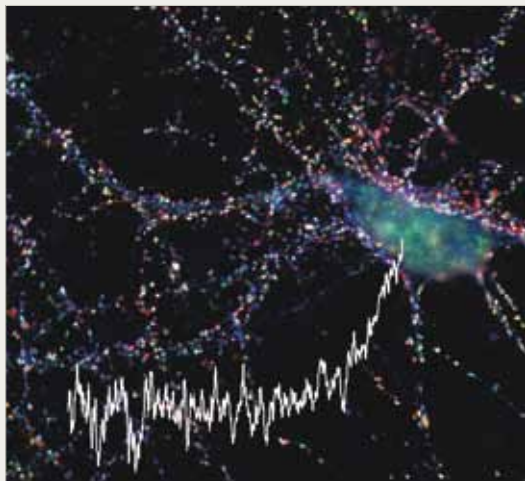


Figure 1

Neurons in operating cortical circuits receive strongly fluctuating synaptic input currents. The irregular temporal fluctuations of these currents result from the huge number of independent synaptic inputs. A typical neocortical neuron receives on the order of 10000 individual synapses. In the micrograph, individual synapses onto a single neuron are fluorescently labelled (bright dots). White line: example of a numerically synthesized model input current (micrograph c/o T.Dresbach).

Under physiological conditions cortical neurons are operating in a so called fluctuation driven regime (figure 1), in which the mean synaptic input current into a typical neuron would be – by itself – insufficient to drive AP firing. Action potentials are instead driven by depolarizing current fluctuations of the irregular, time dependent total synaptic current. *In vivo*, these strongly fluctuating currents result from high frequency barrages of synaptic inputs to which the cells are continuously exposed. Such barrages are an unavoidable consequence of the high degree of connectivity characteristic of cortical networks: A typical cortical neuron receives on the order of 10000 synaptic inputs. Assuming the presynaptic cell's firing rates on the order of 1 Hz one predicts that many thousand discrete synaptic inputs impinge in every second on a typical cortical neuron. Understanding and mathematically modelling the dynamical encoding properties of cortical neurons under such naturalistic conditions constitutes a key step in building adequate and powerful models of cortical network dynamics and brain function. In our research on action potential encoding in cortical neurons, we are using an approach integrating (1) biophysical modelling, (2) stochastic dynamical systems theory and – in collaboration with experimental groups – (3) *in vivo* recording of the behavior of action potential initiation in the intact brain, and (4) biophysical and optogenetic *in vitro* experiments to unravel the computational rules and biophysical mechanisms of this key step of neuronal computation [2-11].

Our previous analyses highlighted the very rapid onset of action potentials in cortical neurons [3] and predicted that this type of AP initiation dynamics should strongly enhance the ability of cortical neurons to lock the firing times of

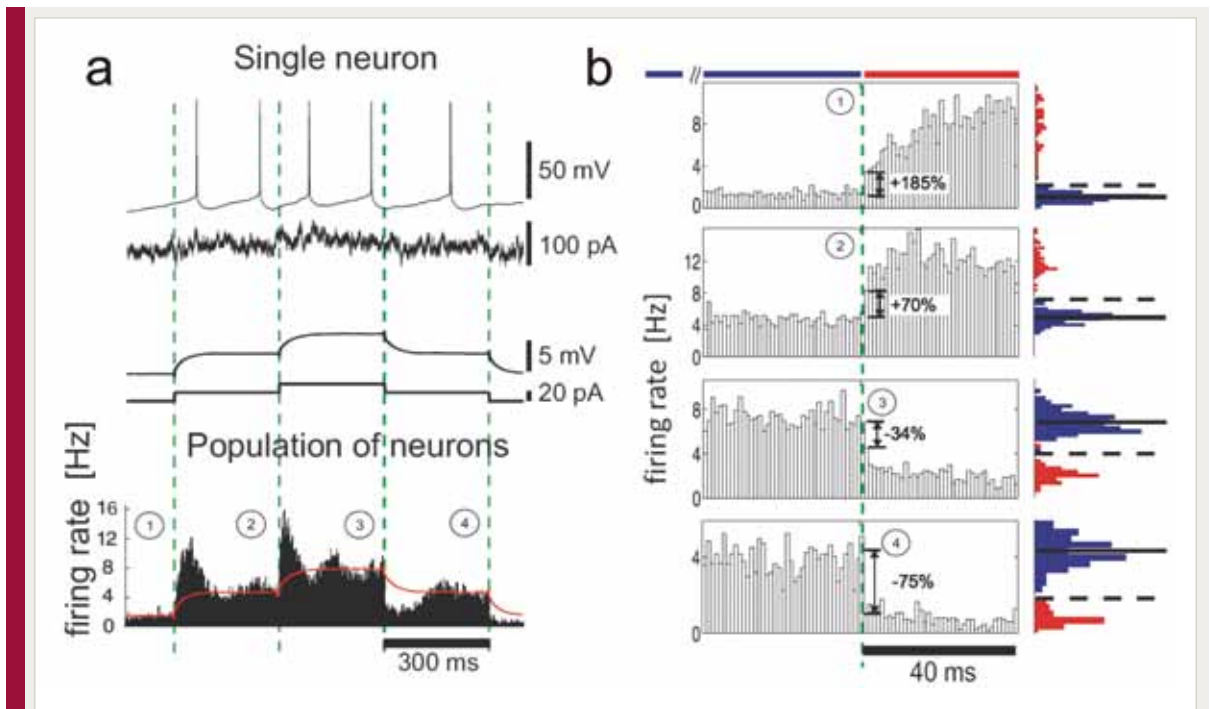


Figure 2

Populations of neocortical neurons respond to changing statistics of their input currents on the millisecond scale. (a) From top to bottom: membrane potential of a representative neuron in response to a fluctuating current with immersed steps of mean current (shown below), mean membrane potential response to steps in mean current without the fluctuations (shown below), population firing rate in response to different realizations of the pseudorandom current, bin size 1ms. The population firing rate is constructed over repetitions pooled from 15 cells totalling 175 min of recording and 52000 spikes. Red line: mean membrane potential. (b) Zoom-in on responses in (a). Blue and red histograms denote distributions of spike counts in 1ms-bins 120 ms before (blue bar) and 40 ms after each step (red bar). In the distributions before the step solid horizontal lines denote the mean and dashed lines 3 s.d. Dashed green lines in b indicate the onset of steps.

their action potentials to high frequency components of their synaptic inputs [2-4]. Over the past years a series of experimental studies has clearly verified this prediction [12-14]. In a seminal paper Köndgen et al. showed that the transmission function of layer 5 pyramidal neurons for a noisy sinusoidal signal does not decay until about 200 Hz [12]. Later experiments confirmed such high cut-off frequencies for signals coded by both the mean current and noise strength and in other types of cortical neurons [13, 14]. This high bandwidth of neuronal AP encoding presumably is instrumental for cognitive tasks that require interactions between multiple brain regions in short time intervals. To support such operations neuronal ensembles must be able to rapidly detect and transmit input changes. In order to directly reveal the speed of such neuronal population responses we examined pop-

ulations of neocortical pyramidal neurons subjected to artificial fluctuating current injection (figure 2). We found that populations of neocortical neurons can in fact alter their firing rate within 1 millisecond in response to somatically delivered weak current signals presented on a fluctuating background. Signals with the amplitudes of miniature postsynaptic currents can be robustly and rapidly detected in the population firing rate. Moreover, the population firing rate of neocortical neurons can reliably follow weak signals varying at frequencies up to 50 times faster than the firing rate of individual neurons. Notably, we also found that this response is limited to mean encoding. Signals encoded in the fluctuation variance require extraordinary large signal amplitudes to be detected rapidly – a fact that was not reported in the single previous study examining on such responses [15].

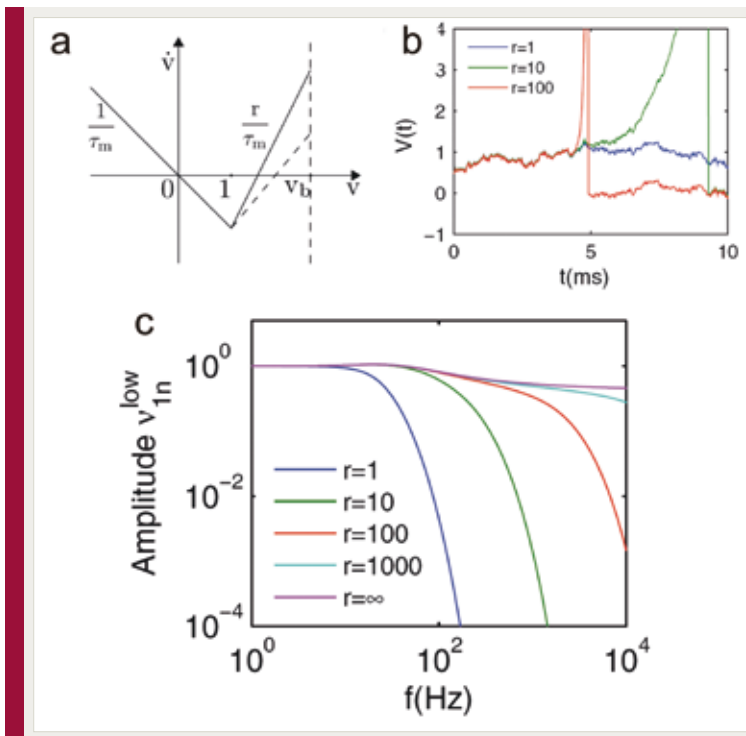


Figure 3

An analytically solvable model for dynamic population coding reveals that the population cut-off frequency is set by the time scale of action potential initiation. Rapid action potential generators can faithfully follow input modulations that are orders of magnitude faster than the population mean firing rate. (a) scheme of the model dynamics, (b) examples of voltage trajectories for different choices of action potential onset rapidness, r , (c) amplitude of predicted dynamic response as a function of stimulus frequency. Bandwidth strongly increases with action potential onset rapidness, r (modified from Wei & Wolf, PRL 2011).

Previous theoretical studies of biophysical neuron models predicted cut-off frequencies of the order of the average firing rate or the inverse membrane time constant (below 20 Hz), much lower than the experimentally observed values (e.g. [16]). The origin of the high cut-off frequencies found in cortical neurons is thus enigmatic and currently not well understood. Sodium channel activation properties, however, appear crucial for this phenomenon. Numerical investigations of neuron models with dynamical AP generation, like the exponential integrate-and-fire (EIF) model or the generalized theta neuron, suggest that details of sodium channel activation can strongly influence the dynamical response of neuronal populations, e.g. [16, 2]. What was missing, however, was a transparent understanding of how and when the cut-off frequency of a population can dissociate from the basic single neuron time scale set by the mean firing rate and the time constant of membrane potential relaxation.

In a recent study we were able to close this gap by introducing an analytically solvable model which explicitly describes the dynamical AP initiation process [11]. A neuron initiates an AP

when the membrane potential passes an unstable fixed point, the voltage threshold. In the leaky integrate-and-fire (LIF) model, for which the linear response was known analytically, this unstable fixed point is located at an absorbing boundary and a spike is triggered immediately when the membrane potential reaches this threshold. As a consequence, boundary induced artifacts dominate the response for high signal frequencies in the LIF model. One important advantage of our new model is that such boundary induced artifacts can be separated out mathematically, isolating the physically meaningful part of the response function. We first solved the linear response for different encoding paradigms for white noise input currents. We found that for a wide range of parameter settings the cut-off frequency is directly proportional to the AP onset rapidness for a noise coded signal (figure 2). It therefore dissociates from the membrane time constant and can become arbitrarily large (figure 3). For mean current coded signals, however, the cut-off frequency was confined by the membrane time constant. In further studies, we showed that also this confinement can be broken when a finite correlation

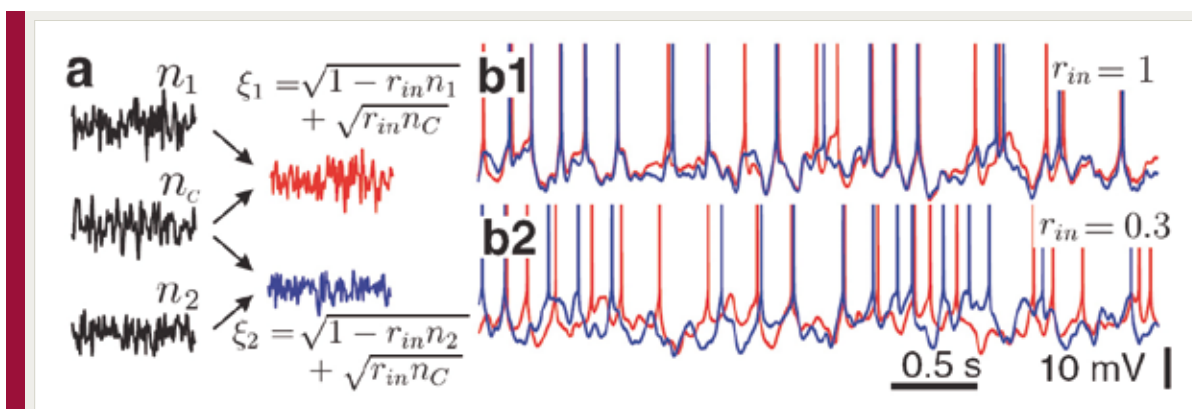


Figure 4

Increasing input current correlation induces more pronounced synchronization of neuronal spiking in cortical neurons. The theory developed in (Tchumatchenko et al., PRL 2010) quantitatively predicts how this synchronization depends on baseline firing rates and the temporal correlations of the input currents. (a) Generation of two fluctuating currents mimicking correlated synaptic inputs with a correlation coefficient r injected into neurons to emulate neuronal cross correlations *in vitro*. (b) Voltage traces of two neurons (superimposed red and blue) subject to currents with $r=1$ (b1) and $r=0.3$ (b2).

time in the synaptic noise is taken into account and high cut-off frequencies can be obtained for a large AP onset rapidness. These novel analytical results further corroborate our previous prediction that the high AP onset rapidness of cortical neurons is the origin of the occurrence of high cut-off frequencies [2, 3]. Our results provide an explicit relationship between the spike onset dynamics and the population cut-off frequency that is currently tested in physiological experiments [11].

The very high onset rapidness of APs in cortical neurons suggests that the extreme limit of a threshold neuron may capture essential aspects of cortical neuron AP generation. Using a highly tractable simple threshold neuron model independently solved by our group and by Sompolinsky and coworkers [18, 8] we found that this is indeed the case for interneuronal spike correlations resulting from correlated input currents into pairs of neurons [8] (figures 4, 5a). In the past, interneuronal spike correlations were often studied theoretically using the Fokker-Planck formalism. However, this approach is technically very demanding and allowed for explicit expressions in special limits only. We found that our alternative modeling framework, based on the threshold crossings of smooth

random functions [3, 18, 8], can provide a mathematically transparent and highly tractable description of spike correlations driven by inputs of arbitrary temporal structure and correlation strength. Using this approach, we calculated quantities which previously had escaped a theoretical description including, (1) peak spike correlations for arbitrary input correlation strength, (2) rate independent peak shape in the high correlation regime (figure 5b), (3) complete spike correlation functions for weak correlations, and (4) asymmetric spike correlation functions in neuron pairs with different firing rates (figure 6). *In vitro* experiments strongly suggest that this model is capable of describing spike correlations in cortical neurons with good accuracy [8]. In a related study we used this novel formalism to re-examine the power of count correlations for characterizing the degree of interneuronal input and spike correlations [7]. In many studies, correlation coefficients and count correlations are used to measure correlations between neurons, to design synthetic spike trains and to build population models. We thus investigated under which conditions such count correlation coefficients reflect the degree of input synchrony and when they can be used to build population models. We found that correlation

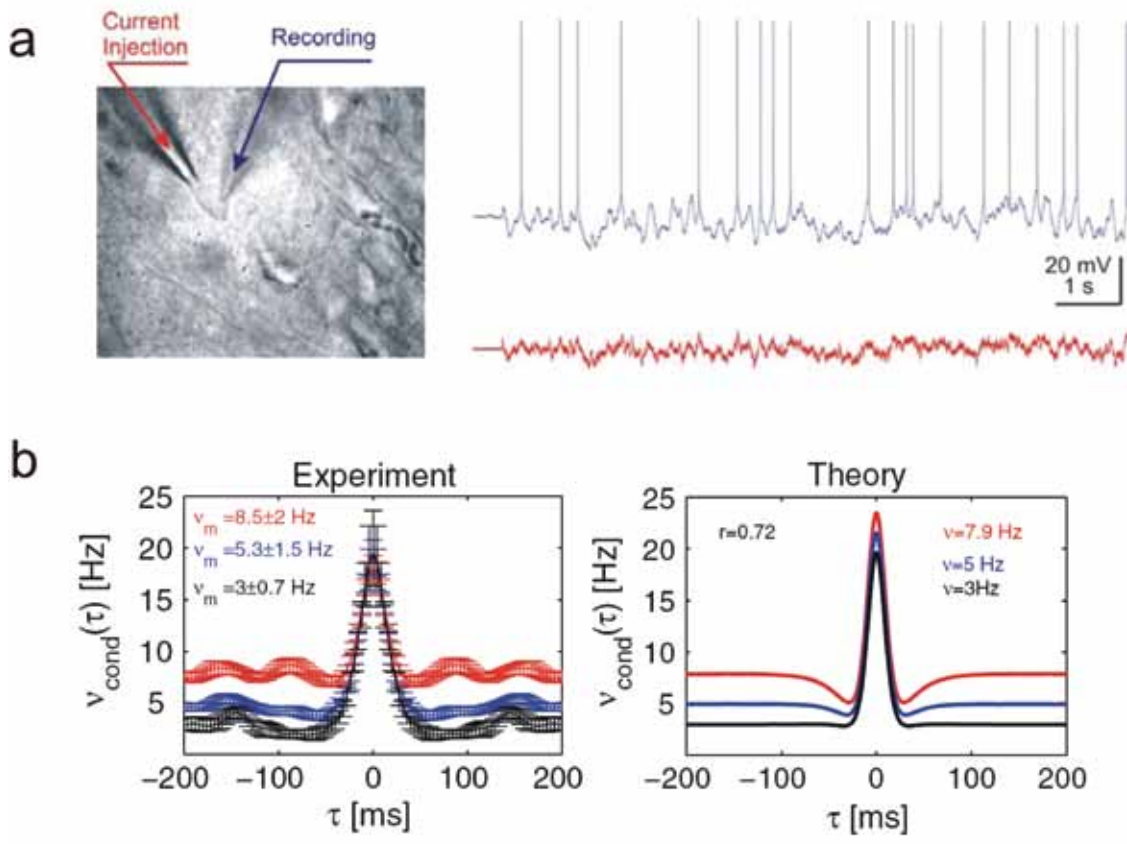


Figure 5

Interneuron correlations are well predicted by a simple and mathematically highly tractable threshold neuron model. (a) Scheme of the experimental approach. (b) Comparison of measured and predicted spike correlation functions (modified from Tchumatchenko et al. PRL 2010).

coefficients can be a poor indicator of input synchrony for some cases of input correlations. In particular, count correlations computed for large time bins were found to vanish despite the presence of input correlations. These findings suggest that network models or potential coding schemes of neural population activity need to incorporate temporal properties of correlated inputs and take into consideration the regimes of firing rates and correlation strengths to ensure that their building blocks are an unambiguous measure of synchrony.

While these results show that the theoretical characterization of dynamical response properties currently is rapidly progressing, experimental studies aimed at these features are still subject to substantial limitations. The perhaps

most important limitation results from the invasive nature of the whole cell recording configuration used for dynamic current injection. A central shortcoming of this technique results from the dialysis of the cell that limits the recording duration that can be achieved to at most one hour. Longer recording durations would be needed to characterize individual neurons under varying stimulus conditions and to open the way for mechanistic studies.

Optogenetic stimulation approaches (figure 7a) hold the promise to overcome this limitation by providing remote optical stimulation of neurons without disruption of their physiological state and high spatial and temporal resolution allowing targeted interrogation of individual neurons. When combined with non-invasive recording of

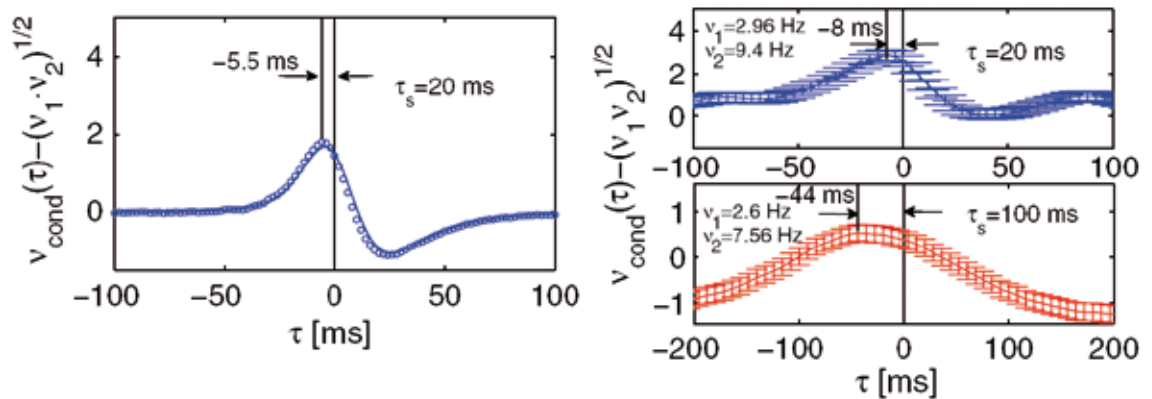


Figure 6

Asymmetric spike correlations between neurons of different firing rates. (Left) Analytical solution in the weak correlation limit (solid line) and numerical simulations (circles). Arrows denote the peak position. (Right) experimentally measured spike correlation functions for different correlation times. As theoretically predicted the induced delay increases linearly with the correlation time (modified from Tchumatchenko et al. PRL 2010).

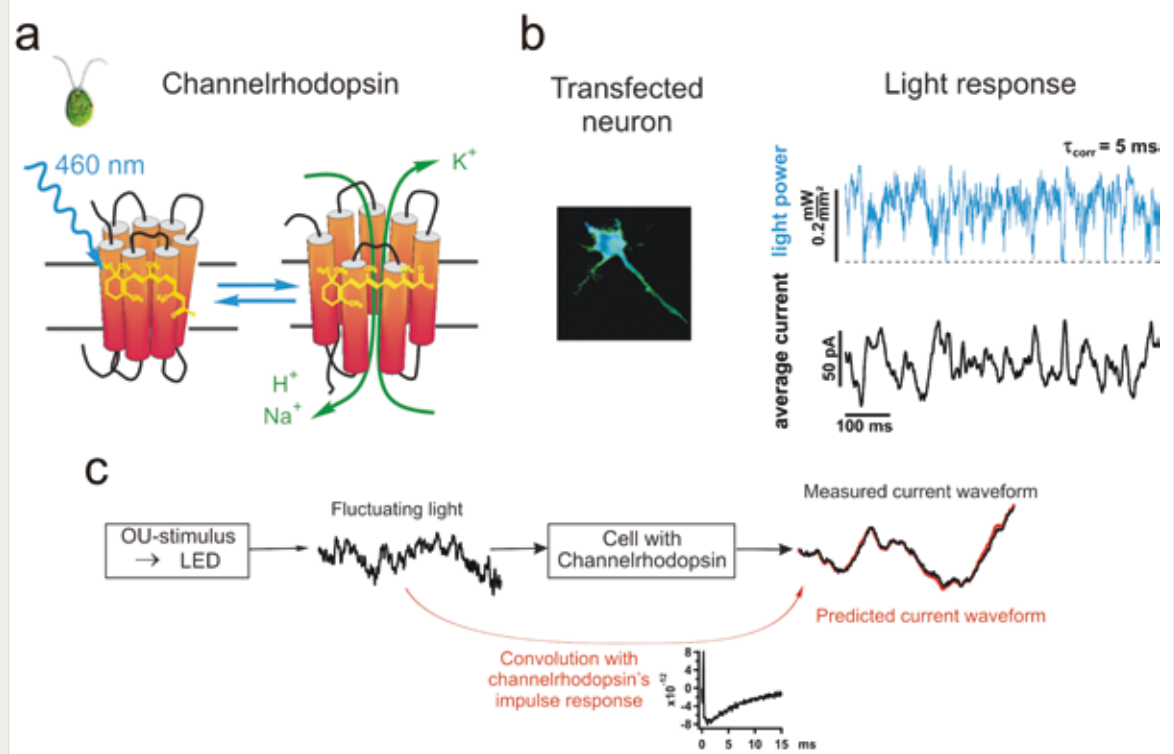


Figure 7

Optogenetic approach for non-invasive continuous fluctuating stimulation. **a** Schematic of the light-gated ion channel channelrhodopsin II from the single celled green algae *Chlamydomonas reinhardtii* (inset). Blue light illumination directly induces the opening of a channel pore selectively permeable to cations. **b** Example of continuous fluctuating light stimulation of cells expressing the engineered channelrhodopsin ChIEF. Upper graph: example trace of an Ornstein-Uhlenbeck pseudo-stochastic light waveform. Lower graph: fluctuating photo current induced by the light waveform shown above. **c** ChIEF-mediated currents can be accurately predicted by linear response theory from the measured impulse response of the channel.

action potential timing, such experiments could extend the feasible duration of experiments and the number of neurons studied by orders of magnitude. To enable the experimental determination of dynamic response properties, optogenetic tools have to satisfy a set of requirements: First, the light gated channels must be able to produce large photocurrents for prolonged times. Second they must be able to follow a pre-designed fluctuating light pulses precisely and reproducibly. Finally, the photocurrent should be precisely and quantitatively predictable, because it is not directly measured in a non-invasive experiment. To examine whether currently available optogenetic tools can meet these requirements, we performed *in vitro* experiments to determine the mapping of fluctuating light waveforms to induced photocurrents in a non-spiking cellular model (figures 7b, c). We char-

acterized the reproducibility of the light induced fluctuating currents and tested whether the fluctuating photocurrent can be predicted by linear systems theory. We found good evidence that ChIEF [18] and, to a lesser degree, ChR2 [19] are suited to induce a well defined, temporally fluctuating current upon stimulation with light pulses designed as an Ornstein Uhlenbeck process. Both channels respond to a light stimulus similar to a low-pass filter with a time constant of 8 ms, in the range of typical synaptic time constants. The currents were highly reproducible and could be predicted with high accuracy by a simple convolution procedure (figure 7c). In ongoing work we are examining whether such a non-invasive approach can be used to establish a high-throughput method for characterizing the encoding dynamics in cortical neurons cultured on multi-electrode arrays.

- [1] G. de Polavieja, et al. *J Neurosci* **25**, 5657 (2005)
- [2] B. Naundorf, T. Geisel, F. Wolf, *J Comput. Neurosci.* **18**, 297 (2005)
- [3] B. Naundorf, F. Wolf, M. Volgushev, *Nature* **440**, 1060 (2006)
- [4] B. Naundorf, F. Wolf, M. Volgushev, *Nature* **445**, E2 (2007)
- [5] M. Volgushev, A. Malyshev, P. Balaban P, M. Chistiakova, S. Volgushev, F. Wolf, *PLoS One* **3**, e1962 (2008)
- [6] G. Baranauskas, A. Mukovskiy, F. Wolf, and M. Volgushev *Neuroscience*. **167**, 1070 (2010)
- [7] T. Tchumatchenko, T. Geisel, M. Volgushev, F. Wolf, *Front. Comput. Neurosci.* **4**, 1 (2010)
- [8] T. Tchumatchenko, A. Malyshev, T. Geisel, M. Volgushev, F. Wolf, *Phys. Rev. Lett.* **104**, 058102 (2010)
- [9] A. El Hady, A. Neef, J. Nagpal, E. Bamberg, T. Geisel, W. Stühmer, F. Wolf, *Stochastic optical stimulation, Janelia farm conference Genetic manipulation of neuronal activity II* (2010)
- [10] A. Neef, M. Gutnick, F. Wolf, I. Fleidervish *Am. Soc. Biophys. Meeting* (2011)
- [11] W. Wei, F. Wolf, *Phys. Rev. Lett.* **106**, 088102 (2011)
- [12] H. Köndgen et al., *Cereb. Cortex* **18**, 2086 (2008)
- [13] C. Boucsein et al., *J. Neurosci.* **29**, 1006 (2009)
- [14] M. Higgs and W. Spain., *J. Neurosci.* **29**, 1285 (2009)
- [15] G. Silberberg et al., *J. Neurophysiol.* **91**, 704 (2004)
- [16] N. Fourcaud-Trocmé, D. Hansel, C. van Vreeswijk, N. Brunel, *J Neurosci.* **23**, 11628 (2003)
- [17] Y. Burak, S. Lewallen, H. Sompolinsky, *Neural Comput.* **21**, 2269 (2009)
- [18] J. Y. Lin et al. *Biophys J.* **96**, 1803 (2009)
- [19] G. Nagel et al., *Proc Natl Acad Sci USA.* **100**, 13940 (2003)

IV Control

IV-1 Cognitive Self-Organization of Movement Coordination and Planning in Robots

F. M. Hesse, G. Martius, T. Geisel, J. M. Herrmann

AN APPROPRIATE motor response requires information about the current state of the control system, the context and the intentions of an agent. In this sense, the information about the current sensory input is not sufficient for action selection unless the agents can use a sufficiently flexible input-output map which can account for a multitude of situations. We are interested in mechanisms that enable a robotic or living agent to achieve this flexibility and to use it in the purposeful interaction with the environment. We emphasize the role of self-organization for the formation and maintenance of this ability during development and live-long learning. As a result, the agent will have at its disposal a repertoire of many behavioral options that can be used as building blocks for goal-oriented behavior, as fall-back behaviors and for the exploration of new behaviors. We are in particular interested in the developmental aspects of motor behavior in animals which we study by means of simulated biomorphic robotic models. In simplified examples, it can be shown explicitly that flexible behavior can be achieved by following an objective function that describes both the sensitivity of the behavior with respect to sensory inputs and the predictability of the sensory effect caused by performing an action. In physically realistic simulations of autonomous robots with various sensory configurations and body shapes, we obtain a continuous flow of behaviors that explores the variety of interactions of the robot with its environment. There remains, however, a restriction to self-organized solutions of relatively simple control problems such as the coordination of limb movements.

In order to achieve complex and goal-directed behaviors, we consider an architecture where the low-level criticalization is complemented by additional learning mechanisms which evaluate the learning progress of the low-level adaptation in various environmental situations [1] or which use external reward signals to select behaviors which are generated by the self-organizing controller [2].

While the self-organising control algorithm suggest a number of parallels in animal development and learning, we want to mention here a new development which aims at a reconciliation of free exploration and goal-directed behavior. Because the objective of a behavior is often not described explicitly, the self-organising aspect remains essential, but it is now focussed towards desired behavior. We have studied a number of ways to introduce the information about the goal into the system in dependence on what type of information is available. We can use information about symmetries of the task, about special solutions, reward signals, correlation among sensor data or task-dependent cost functions. In all these cases, however, the effect of the additional information is weak such that the intrinsic generation of behavior is merely biased rather than controlled. These studies contribute to the emerging field of guided self-organisation which is relevant also for biological evolution and development, socioeconomic theory and computational neuroscience.

As a further application, the project group has worked on a control paradigm for myoelectric prosthesis [5, 6] that is based on the mentioned principle for self-organization of movement. It

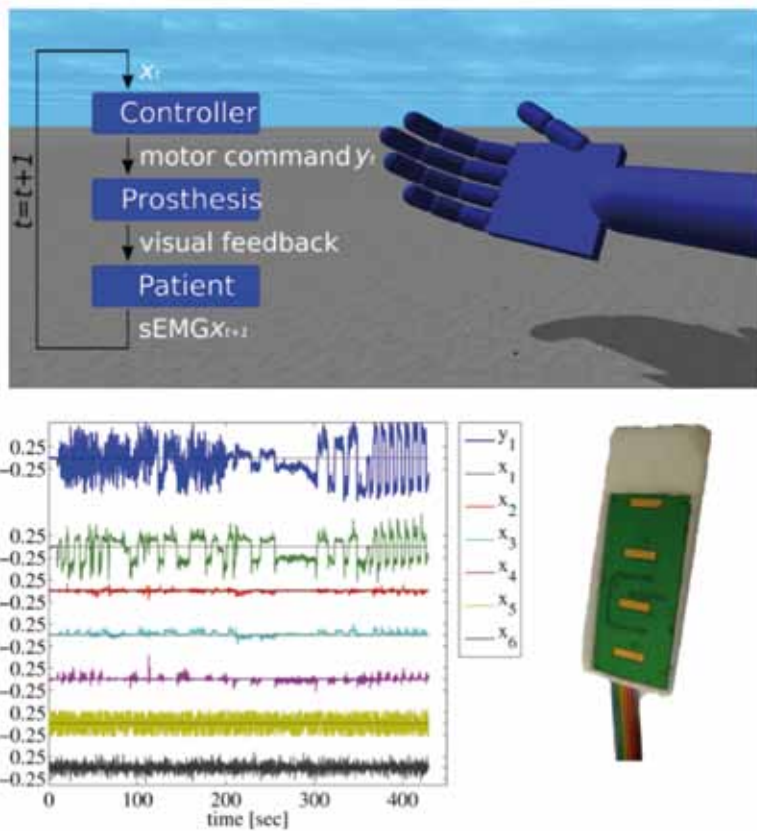


Figure 1

Emergence of intuitive prosthetic control. A participant interacts via myoelectric sensors (bottom right) with a simulated hand prosthesis according to the closed loop paradigm (top). The algorithm simultaneously selects control actions (y) and sensory features (x) by a dynamical interaction between man and machine (bottom left). This leads to a formation of a repertoire of controllable movements by self-organization which can later be used for voluntary control of the degrees of freedom of the hand.

allows for an automatic selection of input signals that are relevant for certain movements. The explorative character of the algorithm leads to the production of predominantly those movements for which the human subject produces control signals most reliably. At the same time the human participant tries to exert control such that a number of movements are realized. These movement options can later be reactivated by the user in order to control the prosthesis purposefully and in a forward fashion. This approach of learning by self-organization can be contrasted to the pattern recognition approach where predefined prosthesis control commands are used, whereas here the movements of the prosthesis and the corresponding myoelectric signals are negotiated by an on-line adaptation scheme that is used during a relatively short training phase. The control commands are adapted for individual subjects such that an intuitive, discrete or proportional control can be easily acquired.

- [1] F. Hesse, R. Der, J. M. Herrmann, in: L. Berthouze et al. (eds), *EpiRob, Cognitive Studies* **134**, 37-44 (2007)
- [2] G. Martius, J. M. Herrmann, R. Der in F. Almeida e Costa (ed.), *ECAL 2007, LNCS 4648, Springer*, 766-775 (2007)
- [3] F. Hesse, G. Martius, R. Der, and J. M. Herrmann, A Sensor-Based Learning Algorithm for the Self-Organization of Robot Behavior Algorithms **2** (1), 398-409 (2009)
- [4] G. Martius and J. M. Herrmann, Taming the beast: guided self-organization of behavior in autonomous robots, *Proceeding SAB'10 Proceedings of the 11th international conference on Simulation of adaptive behavior: From animals to animats Springer-Verlag Berlin, Heidelberg* (2010)
- [5] F. Hesse & J. M. Herrmann, Homeokinetic Prosthetic Control: Collaborative selection of myosignal Features, *19th IEEE International Symposium on Robot and Human Interactive Communication*, pp. 437-442, Viareggio, Italy (2010)
- [6] F. Hesse & J. M. Herrmann, Homeokinetic Proportional Control of Myoelectric Prostheses. *IEEE/RSJ International Conference on Intelligent Robots and Systems (IROS)*, pp. 1786-1791, Taipei, Taiwan (2010)

IV-2 Theory and Dynamics of Human Pointing Movements

A. Biess

D. G. Liebermann (Tel Aviv University, Israel), T. Flash (Weizmann Institute of Science, Israel)

IN THIS project we investigate the computational principles that underlie the generation of voluntary human arm movements through modeling, experiments and simulations. When reaching for an object, visual information about the object's (spatial) coordinates in task space is projected onto the retina. This information is further transformed into neural commands that result in appropriate muscle activation patterns to move the arm towards the object. Continuous feedback, visual and proprioceptive, is provided to the CNS and used for movement control. The mechanisms involved in this sensorimotor transformation process are still largely unknown. One attempt to unravel the computational strategies of the motor system is made by collecting behavioral data using motion capture systems. By studying the kinematics and dynamics of movements for different motor tasks and different subject groups (healthy subjects versus patients with motor disorders), possible strategies of the motor system may be inferred. One prominent modeling approach towards an understanding of the motor system is based on

the assumption that human arm movements are planned and optimized by the CNS prior to movement execution. Accordingly, it has been suggested that movement strategies can be derived from integral principles, similar to action principles in physics. Two classical, but fundamentally different cost functionals have been proposed in this context, namely, the minimum-jerk model (MJ) [1] and the minimum torque-change (MTC) model [2]. Although both models lead to similar predictions, their underlying assumptions regarding movement optimization and control are fundamentally different. In this project we have put these models into a wider context by showing their equivalence in the Riemannian arm configuration space that is equipped with a metric derived from the inertial properties of the arm (kinetic energy metric). For this purpose, we have extended the one-parameter class of mean-squared derivative (MSD) cost functionals, for which the original MJ model is a particular member, to Riemannian space. Interestingly, the solution to the corresponding variational problems is given by

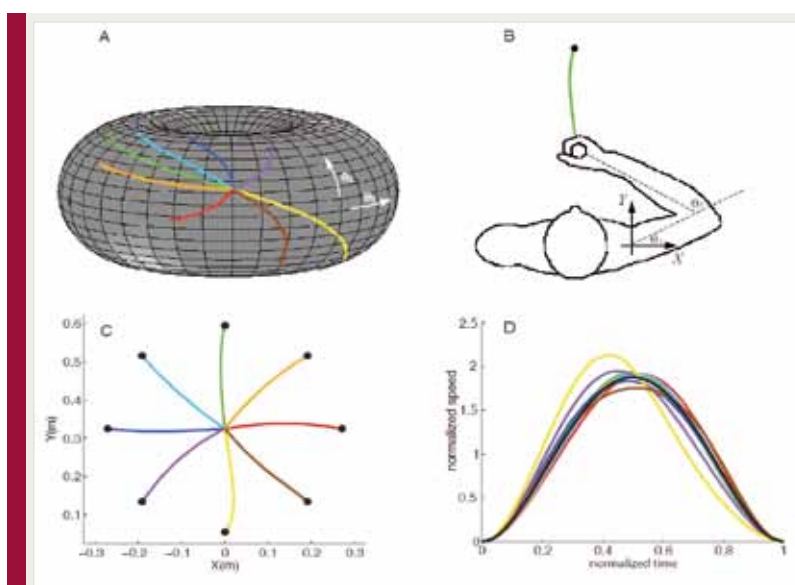


Figure 1

(A): Configuration manifold for arm movements where only two degrees of freedom are involved and geodesic paths as they follow from the geodesic model. (B): Definition of the motor task and arm configuration coordinates. (C): Geodesics hand paths as predicted by the geodesic model for arm movements in the XY-plane from a central initial target to circularly arranged final targets (radius: 27cm). (D): Normalized hand speed profiles along the geodesic paths of C as they result from the geodesic model (color code as in C). The black line shows the speed profile of the original MJ model.

re-parametrized geometric paths, which are the shortest and straightest paths in the arm configuration manifold. The configuration manifold for arm movements with only two degrees of freedom is depicted in figure 1A, whereas the motor task and the definitions of the arm coordinates are shown in figure 1B. We could further show that geodesic paths in the arm configuration manifold correspond to least-effort movements, where effort is defined as the amount of muscular torques that act on the arm during movement execution. Thus, it is argued that geodesic paths are an emergent property of the motor system to minimize muscular effort. Examples of geodesic paths, hand paths and speed predictions for arm movements from a central initial target to circularly arranged final targets are shown in figure 1 A, C and D, respectively [3]. In addition, the geodesic model is inherently independent of the choice of coordinates that are used to describe arm configura-

tions. We could further derive movement invariants from symmetries of the underlying manifold (Killing vector fields), which are important signatures for model evaluation. One striking prediction of the geodesic model is the decoupling of spatial and temporal movement features, which is in agreement with experimental findings, showing that spatial features of unconstrained arm movements (e.g., the arm postures) are not affected by moderate scaling of temporal features (e.g., the hand speed) [4]. Thus, we have hypothesized that spatial aspects of the movement are encoded separately from temporal ones, and are integrated in the motor system at a later processing stage into a complete spatiotemporal pattern. This assumption will also form the basis for intended future studies in patients with visuo-spatial neglects, who, according to our hypothesis, fail to integrate spatial and temporal movement patterns into coherent motor responses.

- [1] T. Flash and N. Hogan. *J. Neurosci.* **5**, 1688 (1985)
- [2] Y. Uno and M. Kawato and R. Suzuki. *Biol. Cybern.* **61**, 89 (1989)
- [3] A. Biess, T. Flash and D.G. Liebermann. *Phys Rev E.* **83**, 031927 (2011)
- [4] K.C. Nishikawa and S.T. Murray and M. Flanders. *J. Neurophys.* **81**, 2582 (1999)

IV-3 Impact of Microscopic Motility on the Swimming Behavior of Trypanosomes

S. Uppaluri, J. Nagler, E. Stellamanns, N. Heddergott (Bio Center, University Würzburg), S. Herminghaus, M. Engstler (Bio Center, University Würzburg), T. Pfohl

WE SEEK to further our understanding of the swimming mechanism of trypanosomes – parasites responsible for deadly disease in humans and cattle. We found that differences in cell shape, possibly resulting from varying body stiffness, correlate to directionality in cell movement. In addition, using high speed microscopy we uncovered extremely fast dynamics of the flagellum tip, up to 50 times faster than the whole cell swimming speed. Together our results imply that physical parameters such as cell stiffness may influence a trypanosome's ability to invade tissue.

Single cell motility is essential for many physiological functions. Microorganisms, particularly parasites, have developed sophisticated swimming mechanisms to cope with a varied range of environments. African Trypanosomes, causative agents of fatal illness in humans and animals, use an insect vector (the Tsetse fly) to infect mammals, involving many developmental changes in which cell motility is of prime importance. While there have been many efforts to uncover the molecular biology of motility in trypanosomes (see figure 1a for cell schematic) and other microorganisms, a quantitative understanding of parasite motility is still lacking.

Our studies reveal that differences in cell body shape contribute to the directional motion of the cell and are thus correlated with a specific *motility mode*. Straighter cells swim more directionally while cells that exhibit little net displacement appear to be more bent [1]. As seen in the example trajectories in figure 1b, trypanosomes from the same population which are exposed to identical environmental conditions exhibit dramatically different behaviors which we classify as motility modes. Trypanosome self propagation has been shown to be essential for host antibody removal [2] and one of these motility modes may increase local hydrodynamic drag on surface proteins.

While some trypanosomes ‘tumble’ with no persistence in direction (tumbling walkers), a second group of cells are highly directional (persistent walkers) and the remaining population is comprised of cells that swim directionally with constant cell orientation but occasionally stop, tumble and reorient themselves and then move directionally again (intermediate walkers). Typical displacements calculated between every 100 frames of recordings for each motility mode are shown in figure 1c. Tumbling walkers and persistent walkers maintain low and high displacement values

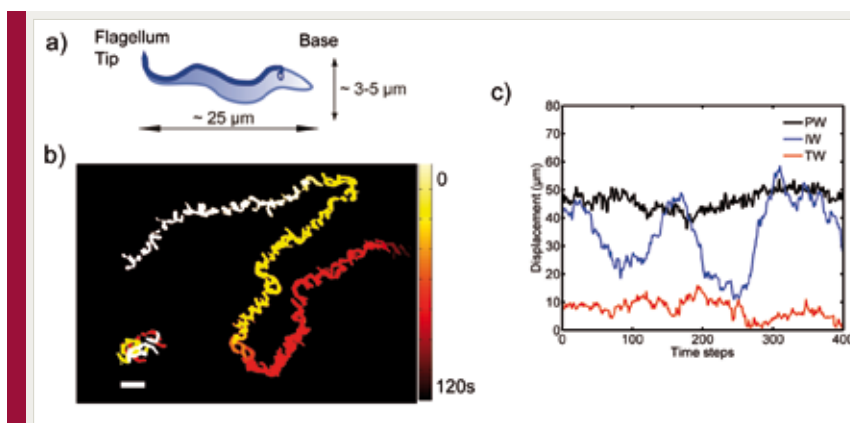


Figure 1

a) Trypanosome schematic. b) Cells exhibit diverse trajectories. c) While tumbling walkers (TW) and persistent walkers (PW) maintain low and high displacement values respectively, intermediate walkers (IW) alternate between these two modes.

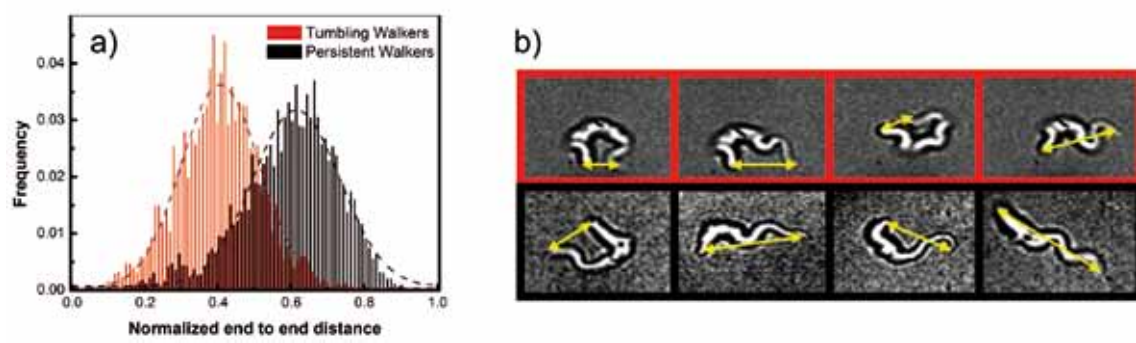


Figure 2

a) Histograms of end to end distances for motility modes. b) Snapshots of tumbling walkers (red), and persistent walkers (black).

respectively, whereas intermediate walkers seem to alternate between these two modes during the observation interval.

In order to investigate the physical mechanism responsible for the observed motility behaviors, we examine trypanosomes at higher magnifications and at a high temporal resolution (1000 Hz). We chose a straightforward approach and examined the variations in the distance between the two ends of the cell (normalized by the length of the cell) over time. Histograms of the end-to-end distances (figure 2a) clearly show that persistent cells are associated with an elongated cell shape while tumbling walkers are more bent. Snapshots of the high speed movies of individuals (figure 2b) demonstrate, as shown in the same figure, that cells swimming with directional persistence (black boxes) appear to take a more stretched body shape. Ascribing the shape of the trypanosome to a worm-like chain [3, 4] and assuming equal energy utilization for self propelling motion in both motility modes, we find that persistent cells have three times more flexural rigidity than tumbling walker cells. The directional cells may be stiffer due to reorganization of motor proteins and crosslinking within the microtubules found both in the cell body and the flagellum. The assumption of equal energy utilization for motility from one cell to another is supported by the fact that the velocity distribution for all motility modes is the same. It is not unlikely that these observations are due to an interplay of differences in flexural rigidity and also energy utiliza-

tion for cell motion and remains to be confirmed through direct measurements. Nevertheless, these results are in qualitative agreement with theoretical work by Wada and Netz [5] on motility of the bacterium *Spiroplasma* in which softer cells were shown to flex more significantly due to random thermal fluctuations and thus were less efficient in directional motion.

Notably, the high temporal resolution allows us to examine the extremely fast cell body dynamics; the flagellum tip of the persistent walker moves over 40 times faster than the average reported whole cell swimming speed of 20 $\mu\text{m/s}$. Our results indicate that macroscopic motility modes could be correlated to varying cell stiffness. The analysis of cell end-to-end distance provides a rapid screen for identification of differences in microscopic properties of cells. Different motility modes, possibly resulting from varying body stiffness, could be of consequence on host invasion during different infective stages.

- [1] Uppaluri S, Nagler J, Stellamanns E, Heddergott N, Herminghaus S, Engstler M, Pfohl T. Impact of microscopic motility on the swimming behavior of parasites: straighter trypanosomes are more directional. PLoS Computational Biology, accepted
- [2] Engstler M, Pfohl T, Herminghaus S, Boshart M, Wiegertjes G, Heddergott N, Overath P. Hydrodynamic Flow-Mediated Protein Sorting on the Cell Surface of Trypanosomes. *Cell* **131** (3), 505-515 (2007)
- [3] Köster S, Pfohl T. An *in vitro* model system for cytoskeletal confinement. *Cell Motility and the Cytoskeleton* **66** (10), 771-776 (2009)
- [4] Rubinstein M, Colby RH. *Polymer Physics*. Oxford University Press, USA (2003)
- [5] Wada H, Netz RR. Hydrodynamics of helical-shaped bacterial motility. *Phys. Rev. E* **80** (2), 021921 (2009)

IV-4 Self-Assembled Granular Walkers

S. Herminghaus, M. Brinkmann, R. Seemann
Z. Khan, M. Scheel, A. Steinberger

MECHANISMS OF locomotion in microscopic systems are of great interest not only for technological applications, but also for the sake of understanding, and potentially harnessing, processes far from thermal equilibrium. Down-scaling is a particular challenge, and has led to a number of interesting concepts including thermal ratchet systems and asymmetric swimmers. We investigate a granular ratchet system employing a particularly robust mechanism which can be implemented in various settings. The system consists of wetted spheres of different sizes which adhere to each other, and are subject to a symmetric oscillating, zero average external force field. An inherent asymmetry in the mutual force network leads to force rectification and hence to locomotion.

When a bi-disperse mixture of glass beads is moistened by a fluid and shaken vertically and sinusoidally, small clusters of beads occasionally take off from the surface of the pile and rapidly climb up the container walls against gravity. Figure 1 (left panel) demonstrates this effect: a cluster of beads spontaneously formed and climbed out of a pile of glass spheres wetted by 1 % (of total volume) with a glycerol-water mixture. The upper surface of the granular pile can be seen as the dark region at the bottom of the images. These ‘climbers’ are held together and against the wall by capillary bridges; they are led by one large bead with one or more small beads trailing below. This effect is very robust, as we have observed it using numerous different wetting liquids (silicone oil, glycerol-water mixtures, ethylene glycol).

Figure 2 shows experimental measurements of the walkers’ velocity for vibration frequencies ranging from 60 to 90 Hz (symbols) against the peak acceleration of the horizontal (harmonic) vibration, for a walker with bead radii of 0.3 mm and 0.2 mm, respectively. We see that the fre-

quency does not seem to play a key role, but the peak acceleration does. The solid grey curve represents the prediction of a simple force balance model (see below), while the dashed line takes into account a more sophisticated friction model [1].

In order to understand this effect, it is important to consider the tangential and normal forces at the three points of contact involved in this system. Although the relation between the external acceleration and the forces is non-linear due to the geometry-mediated back-action of the tangential forces onto the normal forces, it can be expressed in a rather simple matrix formalism which treats the three normal forces as a three-vector. Quite remarkably, it turns out that even when the dependence of the friction forces on the velocity and on the normal force was completely linear, a net locomotion velocity would be predicted. This is a valuable hint at explaining the robustness of the locomotion effect. Differences in the force law result in differences in the quantitative prediction, as reflected by the grey (linear force law) and dashed (more elaborate friction law) curves in figure 2 [1].

As the degree of asymmetry must be a relevant control parameter (a symmetric walker would not know in which direction to move), we expect that the asymmetry of the walker would have an effect on the locomotion velocity. We thus characterize the asymmetry by the angle formed between the centers of the spheres and the horizontal, as shown schematically in the inset of figure 3. The velocity vanishes for symmetric walkers composed of spheres with identical radii on a well-levelled substrate, and increases with the degree of asymmetry. The solid curve again represents the prediction of the simple theory, displaying satisfactory agreement.

Another striking feature of the experimental system is that the walkers self-align with the direction

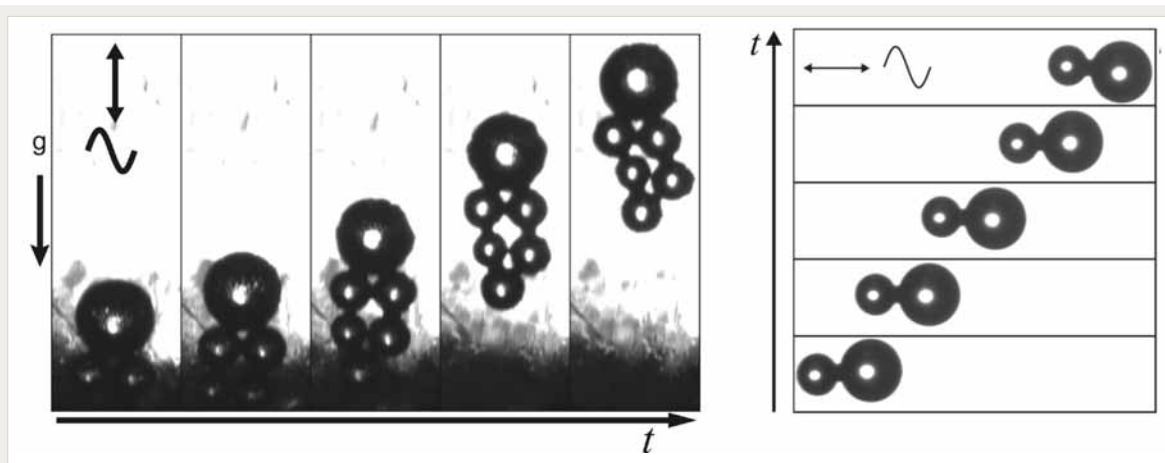


Figure 1

Left: A wet granular ‘climber’. As the glass container is vertically agitated at about 70 Hz, with a peak acceleration well above the acceleration of gravity, clusters of differently sized glass beads spontaneously leave the wet pile (slightly below the lower rim of the photograph) and climb up the container wall. The large bead has a diameter of about one millimeter. Right: top view of a ‘walker’ consisting of just two beads set upon a horizontal glass plate, which is shaken sinusoidally in horizontal direction. The velocity of the walker is several millimeters per second, the diameter of the large bead is 0,6 mm.

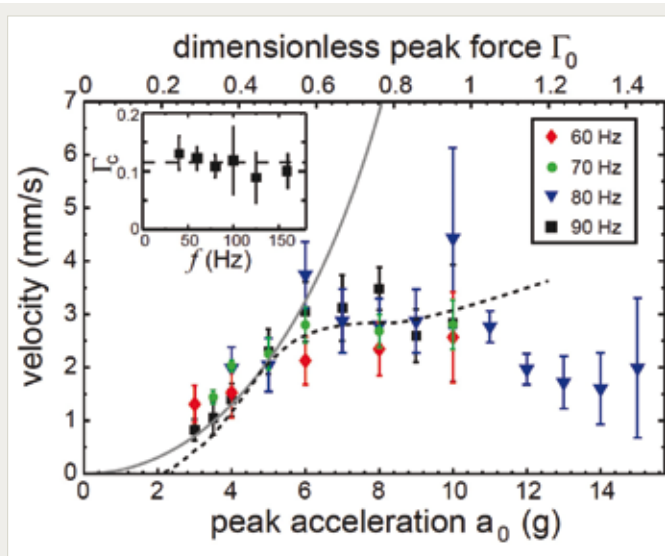


Figure 2

The (horizontal) walker velocity as a function of the applied horizontal (peak) acceleration for different frequencies of the vibration. The latter is obviously not a relevant parameter. The grey curve represents the prediction from a simple ‘linear’ friction law, the dashed curve corresponds to a more sophisticated model. Obviously, the effect does not depend strongly upon these details in a wide range of parameters. Inset: the critical peak acceleration at which motion sets in, as a function of frequency. Clearly, neither here the frequency is relevant.

of the excitation while migrating across the substrate. In order to understand the stability of the walker's direction of locomotion, we consider the sideways motion of the walker in the plane of the substrate, when it is not perfectly aligned with the shaking direction. At any finite horizontal acceleration, the equation of motion of rolling sideways is a pendulum equation, with the acceleration as the coefficient determining the free oscillation frequency. This is, however, itself a harmonically periodic function of time, by virtue of the external excitation. Sideways rolling is thus described by a differential equation of Mathieu type (which is well known from the theory of quadruple traps). It is well known that its solutions represent damped oscillations for a wide range of parameters if the average acceleration is zero, as in our case. This means that the walker will tend to align with the direction of excitation, thereby extracting the maximum energy from the applied acceleration field.

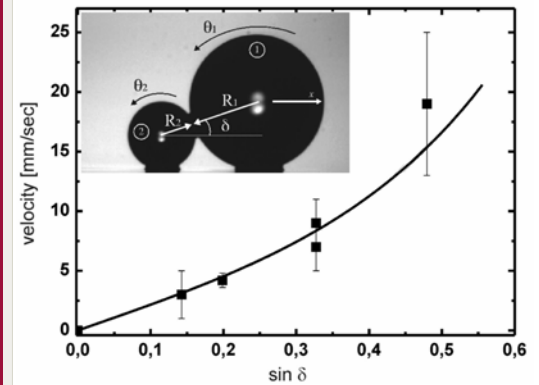


Figure 3

The locomotion velocity as a function of the asymmetry of the bead pair. Clearly, the velocity vanishes in the symmetric case, as it should. The solid curve represents the prediction from the simple pseudo-linear friction model and agrees satisfactorily with the data.

[1] Z. Khan, A. Steinberger, R. Seemann, S. Herminghaus, „Wet Granular Walkers and Climbers”, *New J. Phys.* **13** (2011) (in press)

IV-5 Collective Behavior of Artificial Squirmers

S. Herminghaus, R. Seemann
S. Thutupalli

EMULSIONS WITH sufficiently complex contents are quite promising for the realization of self-assembled soft functional devices with functions down to the nanoscale [1]. Of particular interest are the surfactant layers forming at the droplet surfaces, which under certain circumstances may form membranes of molecular thickness and serve as platforms for nanoscale building blocks [1, 2]. Suitable interaction of droplet contents with the surfactant layers may lead to further functions, such as locomotion, as we could show. For droplets laden with the reactands for the Belousov-Zhabotinski-reaction, for instance, bromine is released with a rate varying periodically in time. When the surfactant is abundantly present in the oil phase and contains a C-C double bond, such as mono-olein, the latter is spontaneously saturated as the bromine reaches the surfactant layer. As a consequence, the quality of the surfactant is changed and thus the surface corresponding tension.

When the droplet undergoes some motion, e.g., by thermal fluctuation, the bromination density in the surfactant layer, and thus the surface tension, acquires a spatial variation along the droplet surface (cf. figure 1). When the sign of the change in surface tension is right, as it is with mono-olein, the concomitant Marangoni stress serves to support this motion. It is readily shown [3] that above a certain bromination rate in the droplet, the Marangoni stress leads to a self-sustained locomotion of the droplet, accompanied with a dipolar flow field around the droplet (cf. figure 1, bottom). Since the particles are neither purely pulling nor pushing themselves through the surrounding medium, they are called squirmers. Because of the abundance of pristine surfactant in the oil phase (concentration well above the critical micelle concentration), the latter does not change its properties noticeably, such that the droplet performs a persistent random walk, not hesitating to cross its

own path [3]. Its velocity changes periodically in pace with the Belousov-Zhabotinski-oscillation in its interior (figure 2b). If the concentration of the reactands is properly adjusted, a temporally constant bromine release can as well be established, leading to a constant (and tunable) velocity (figure 2a).

These observations strongly suggest to use this kind of active droplets for investigating collective phenomena with artificial squirmers. Organisms

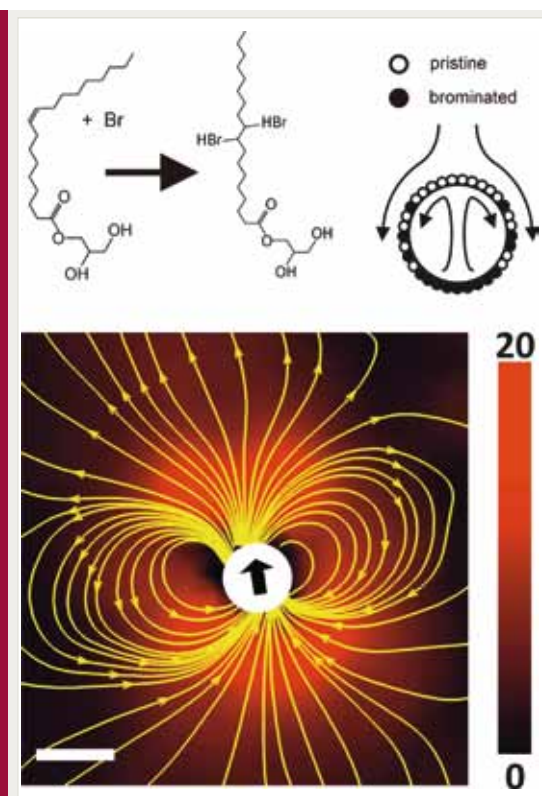


Figure 1

Top: Principle of operation of a simple model squirmer. The surfactant, which is abundantly present in the oil phase, is spontaneously saturated by the bromine released from inside the droplet. When the droplet moves, the spatial variation of bromination density which thus emerges leads to a Marangoni stress which sustains this motion. Bottom: Velocity field around an artificial squirmer as measured by particle image velocimetry. We observe a roughly dipolar flow field. Scale bar: 100 microns.

such as cyanobacteria, Paramecium, and Volvox belong to the class of swimmers referred to as squirmers, and are driven by tangential and/or radial deformations of the cell surface. Squirming motion is very appealing for elucidating the hydrodynamics of microscale swimming, since the velocities in the near and far field around such a swimming organism are well described analytically. This makes such swimmers ideally suited for the quantitative study of many open questions regarding hydrodynamic effects on their interaction with surfaces and with each other, their behavior in external flow, and the origins of coupled and collective behavior. However, in contrast to natural organisms, a significant appeal of model systems is the ability to provide quantitative control and minimize the individual variations pertinent to biological systems.

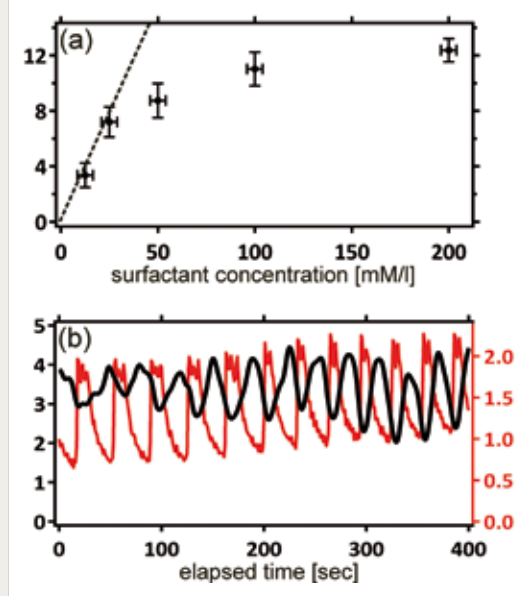


Figure 2

Top: The squirmer velocity (in microns per second) at constant bromine release rate, as a function of the surfactant density in the oil phase. The critical micelle concentration is about 1.5 mM/l. Bottom: The squirmer velocity (in microns per second, black curve) as a function of time, when the Belouzhov-Zhabotinski-oscillation takes place within the droplet. The red curve indicates the optical transmission of the droplet, thereby visualizing the chemical oscillation.

We therefore have investigated the collective motion of many droplets as described above in a closed container, with variable total number density (figure 3). First of all, it could be observed that neighboring droplets showed a strong tendency to attract each other and continue moving in parallel. This behavior is well known from simulations of hydrodynamic interactions between squirmers with dipolar flow fields [4]. Furthermore, we could clearly observe that the spatial correlation between the squirmers changed in response to the variation of their number density. Figure 4 shows the combined angular and spatial correlation for two different densities. Although there is clearly some long-range correlation already at the lower density (red curve), several clearly distinct peaks arise as the density is further increased (black curve). This points to the presence of long range order in a direction perpendicular to the direction of motion, and may directly be traced to the effective attraction between neighboring droplets due to hydrodynamic interaction.

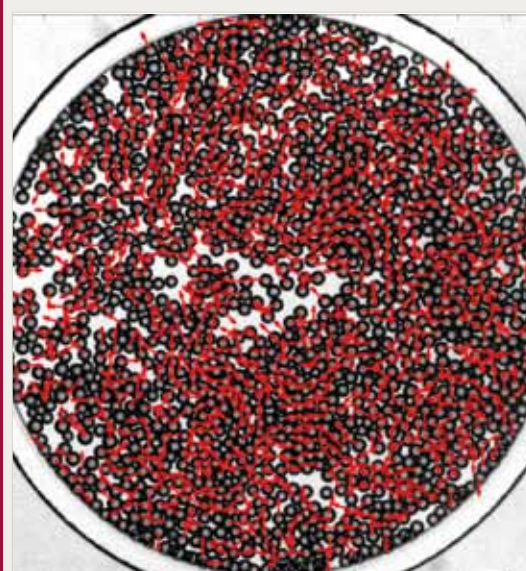


Figure 3

Artificial squirmers in a flat container, the droplet diameter is about 100 microns. The average areal density is 0.78 (densest packing would be 0.91). The red arrows indicate the direction of motion. Both great fluctuations in density and a propensity of aligning velocities in parallel are clearly visible.

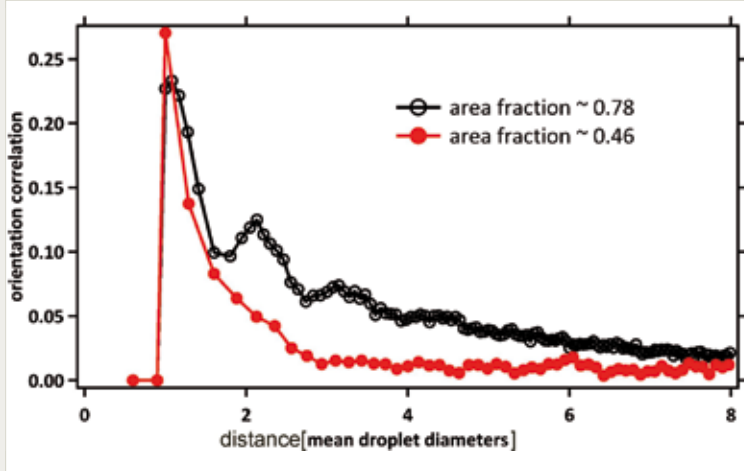


Figure 4

The orientation correlation as a function of the distance of the centers of droplets. For an areal density of 0.46, there is already a clear tendency towards clustering, as it is visible from the strong increase of the red curve towards direct droplet contact. However, only when the density is further increased the correlation shows more structure. The black curve, which corresponds to an area density of 0.78 (cf. figure 3), clearly exhibits three (perhaps four) distinct peaks, indicating the emergence of long-range orientational correlation.

- [1] Y. Iwashita, S. Herminghaus, R. Seemann, C. Bahr, „Smectic membranes in aqueous environment“, *Phys. Rev. E* **81**, 051709 (2010)
- [2] S. Thutupalli, S. Herminghaus, R. Seemann, „Bilayer membranes in micro-fluidics: from gel-emulsions to soft functional devices“, *Soft Matter* **7**, 1312 (2011)
- [3] S. Thutupalli, R. Seemann, S. Herminghaus, „Simple model squirmers with tunable velocity“, *submitted to N.J.P* (2011)
- [4] T. Ishikawa, M. P. Simmonds, T. J. Pedley, “Hydrodynamic interaction of two swimming model micro-organisms”, *Journal of Fluid Mechanics* **568**, 119 (2006)

IV-6 Multiphase Flow in Electric Field

J.-C. Baret, M. Schroeter
S. H. Tan, B. Semin

MICROFLUIDIC DEVICES allow the preparation of highly controlled emulsions, monodisperse [1], bidisperse [2] as well as multiple emulsions [3] or foams [4]. Because droplet-based microfluidic systems also enable a variety of other operations, all at frequencies of kHz or higher, splitting [5], fusion [6], and sorting [7, 8] they have broadened the range of applications of emulsions into areas such as cell-based assays [8] or the synthesis of new materials [9]. The use of electric fields is one of the most versatile actuation mechanism for droplets. It is fast, mainly because it does not contain mechanical parts and can easily be integrated on chip (figure 1). We are using several microfabrication techniques to manufacture electrodes on chip. We can use these electrodes to fuse droplets by electrocoalescence or to sort droplets. Both mechanisms have a great potential for applications in biotechnology, for example as a high-throughput cell sorting system [7, 8].

The microfluidic cell sorter that we have developed is based on dielectrophoretic actuation. The contrast of dielectric constant between water and oil provides means to actuate droplets in a gradient of electric field (analogous to magnetic actuation). By coupling hydrodynamics and dielectrophoretic actuation with a decision to trigger the field based on a fluorescence readout, we have been able to sort droplets at rates up to 2000 droplets per second. When the droplets contain cells, different cell populations can then be separated [7, 8]. We are now interested in the use of electric field to increase the control of passive modules for droplet manipulation; we want to understand better the limits of dielectrophoretic actuation. It has been demonstrated recently that dielectrophoretic actuation can be used to control the release of a chemical in droplets [10]. We want to demonstrate that combining electric field to the classical droplet

actuation modules we can gain an active control on fluid flow.

Besides biotechnological applications, the interactions of electric field on liquid structure has a great potential for many industrial applications such as tunable lenses or displays [11]. Interestingly, it is also of relevance in oil industry, for example, as a potential tool to improve oil extraction from rocks and soils. It has been experimentally demonstrated that, applying an electric field between the inlet and the outlet of a porous medium filled with oil, while liquid is pumped through the medium, enhances the quantity of oil that can be extracted [12, 13] but the exact underlying mechanism is still unclear. Electric field can modify the behavior of fluid according to several mechanisms (electrowetting, electrophoresis, dielectrophoresis, electroosmosis) and we are now developing microfluidic tools to study this process and determine the mechanism involved. We believe that a combination of high speed microscopy observation and microfluidic control of the fluids will provide a quantitative insight. We have started to integrate electrodes with model porous media and to use them for the analysis of oil recovery (figure 2). In the long run, our aim is to manufacture porous media as artificial rock and study the effect of the electric field on porous media with a complexity close to real soil samples (wettability, pore dimensions...). This project is a part of the project Geomorph funded by BP.

Finally, the effect of electric field on multiphase fluid structures is a part of our more general study of the influence of external fields on multiphase flow. We consider experimentally alternative actuation mechanisms such as thermal gradients and concentration gradients for surface tension driven actuation. We have also recently started experiments using magnetic actuation of ferrofluid droplets flowing in microfluidic



Figure 1

Microfluidic chip for the study of droplets in electric fields. The chips produced by soft-lithography can be easily manufactured with electrodes for a local control of electric fields (left). We can use for example these electrodes for dielectrophoretic sorting of droplets (right): droplet flow in the upper channel when the electric field is applied while by default (no field applied) the droplets flow in the lower channel of the sorter. In practice the decision to sort (i.e. to apply the field) is taken within a few microseconds after a fluorescence readout of the droplet.

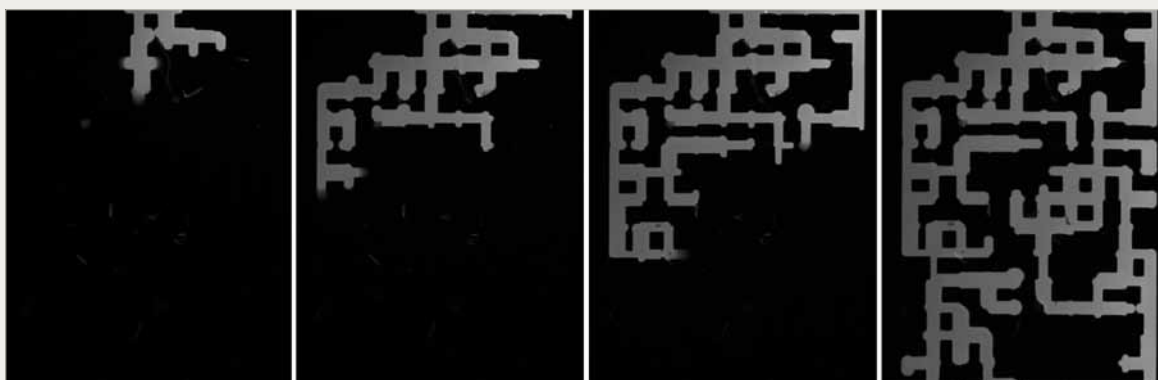


Figure 2

Water imbibition in a model porous medium. At the time of the percolation, there is a significant volume of oil trapped in the structure. Using our microfluidic tools, we study the influence of electric fields and currents in the remaining oil volume in the pore [12,13].

channels. Using such system we want to compare the magnetic actuation with the dielectrophoretic actuation. Other applications of magnetic-microfluidic are presented in the section V.8.

- [1] C. Priest, S. Herminghaus, and R. Seemann, *Appl. Phys. Lett.* **88** (2), 024106 (2006)
- [2] L. Frenz et al., *Langmuir* **24** (20), 12073-12076 (2008)
- [3] L.-Y. Chu, et al., *Angewandte Chemie Int Ed*, **46** (47), 8970–8974 (2007)
- [4] D. Weaire and W. Drenckhan. *Adv Colloid Interface Sci.* **137** (1), 20–26 (2008)
- [5] D.A. Link et al., *Phys. Rev. Lett.* **92** (5), 054503 (2004)
- [6] K. Ahn, et al., *Appl. Phys. Lett.* **88** (26), 264105 (2006)
- [7] J.-C. Baret, et al., *Lab Chip* **9** (13), 1850-1858 (2009)
- [8] J.J. Agresti et al., *PNAS* **107** (14), 6550-6550 (2010)
- [9] L Frenz, et al. *Angewandte Chemie Int Ed.* **47**, 6817–6820 (2008)
- [10] A.R. Abate et al., *PNAS* **107** (45), 19163-19166 (2010)
- [11] F. Mugele and J.-C Baret, *J. Phys. Cond. Matt.* **17** (28), R705-R774 (2005)
- [12] M.A. Aggour et al., *J. Pet. Sci. Eng.* **11**, 91-102 (1994)
- [13] K. Wittle and C.W. Bell, *US Patent 7,325,604* (2008)

IV-7 Elimination of Turbulence

B. Hof, M. Avila, D. Samanta, B. Song and M. Holzner

THE ENERGY costs for fluid transport in pipes and channels are largely caused by turbulent drag. At Reynolds numbers (Re) common in oil pipelines the drag of the fully turbulent flow can be as much as 100 times larger than that of the equivalent laminar flow. On the other hand pipe and duct flows are linearly stable so that in principle they could be held laminar. Turbulence is triggered by finite amplitude perturbations and with increasing Reynolds number the amplitude required to trigger turbulence decreases [1]. Consequently it becomes more and more difficult to keep the flow laminar as the Reynolds number increases. In practical situations perturbations at the inlet are usually sufficient to trigger turbulence once $Re > 2000$. Unlike in most control projects where the aim is to reduce the turbulent drag by a certain percentage the goal of this project is to develop methods to fully relaminarize an already turbulent flow. Apart from the fact that relaminarization provides the maximum feasible drag reduction, a further big advantage over ordinary control schemes is that once the flow is relaminarized at a certain location in a pipe or duct, downstream of this point it will remain in that state given the conduit is reasonably straight and smooth (i.e. perturbation levels are subcritical). Consequently the drag is not only reduced in the control region (as in common control schemes) but in the en-

tire downstream region which substantially increases the potential for energy savings.

In a first test case we were able to relaminarize intermittently turbulent pipe duct and channel flows [2]. Here we exploited the circumstance that in this Reynolds number regime turbulence only occurs in localized spots and these spots extract kinetic energy from the laminar flow just upstream. By inducing a second spot in this upstream region the original spot loses its energy source and decays. Hence at these Reynolds numbers the mean shear can only support turbulence locally but not in extended regions and turbulent spots are characterized by a distinct interaction distance [3]. Making use of this observation we applied a continuous local disturbance to an intermittently turbulent flow. As the turbulent fluid moves downstream from the perturbation point there is no laminar fluid in its vicinity upstream and consequently it decays at a certain distance (~ 20 diameters) downstream. In numerical simulations we were able to show that this decay is linked to the shape of the velocity profile and that turbulent spots require a parabolic profile upstream of their trailing edge. In simulations of a turbulent spot we locally added a volume forcing just upstream of the turbulent region which reduces the speed close to the centreline and increases close to the walls leaving the mean speed unchanged.

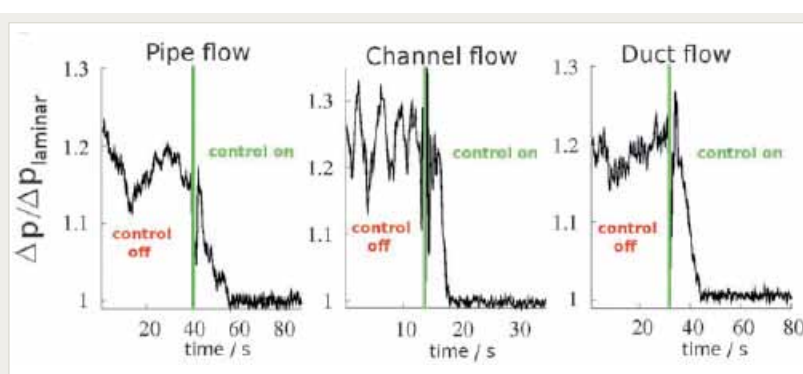


Figure 1

Drag reduction resulting from relaminarization of intermittently turbulent flows in pipe ($Re=2030$), channel ($Re=1400$) and duct ($Re=1740$) (from [2]).

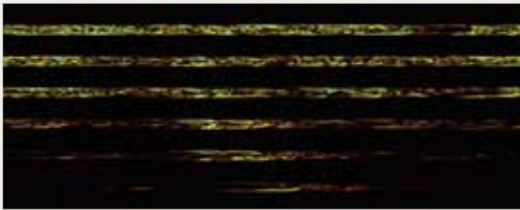


Figure 2

Control of a turbulent flow at $Re=2500$. After the volume force is applied the flow returns to laminar (colours correspond to iso-surfaces of streamwise vorticity).

Just as in the experiments here also the turbulent spot decays. While in experiments the annihilation of one turbulent spot by another one upstream only works at low Reynolds numbers ($Re \leq 2000$), in the simulations the forcing when applied globally works in fully turbulent flows (see figure 2). Although a volume forcing of this kind is not available in experiments this example nevertheless shows that in principle it is possible to relaminarize flows by relatively simple passive methods (i.e. without knowledge of the detailed turbulent flow structure). We have devised other methods that can be applied in experiments and are applicable at higher Reynolds numbers. Figure 3 shows an example of a blowing and suction method applied to a fully turbulent flow at $Re=4000$. The flow is initially turbulent but relaminarizes downstream of the control point once activated. Following the actuation the viscous drag decreases by more than a factor of two in this case. While this blowing and suction scheme is difficult to apply in practice we are developing two other methods (patent application PCT/EP2010/067959) which potentially could be of practical interest.

The relaminarization schemes also raise fundamentally interesting questions. In case of the volume forcing (figure 2) we are trying to understand how the decay of turbulence is connected to the changed flow structure. The forcing amplitude can be seen as an additional parameter which may help us to understand under what conditions turbulence is sustained. Insights into this problem could help to understand why tur-

bulence first arises in pipes at $Re \sim 2000$ whereas in channels it occurs at ~ 1000 and in Couette flow at approximately ~ 300 .

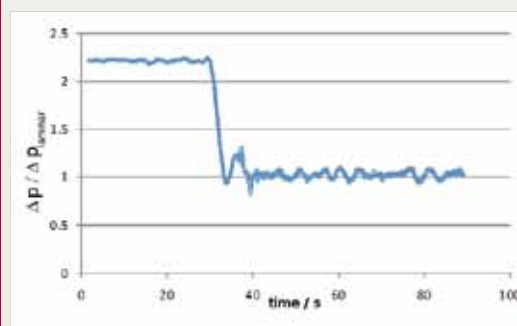


Figure 3

Control of turbulent flow at $Re=4000$. After applying a blowing and suction control method at one location of the experiment the flow downstream returns from the turbulent drag (Blasius scaling) to the laminar drag.

- [1] B. Hof, A. Juel and T. Mullin, *Phys. Rev. Lett.* **91**, 244502 (2003)
- [2] B. Hof et al., *Science* **327**, 1491 (2010)
- [3] D. Samanta, A. de Lozar and B. Hof, *J. Fluid Mech.* accepted (2011)

IV-8 Control of Spatio-temporal Chaos in the Heart

S. Luther

A. Squires, P. Bittihn, D. Hornung, R. Richter, A. Behrend, J. Schroeder-Schetelig, U. Parlitz, V. Krinsky, E. Bodenschatz, A. Pumir (Lyon), M. Zabel (Univ. Medicine Göttingen), S. Lehnart (Univ. Medicine Göttingen), G. Hasenfuss (Univ. Medicine Göttingen), F.H. Fenton (Cornell), E.M. Cherry (Cornell/RIT), R.F. Gilmour (Cornell)

SPATIOTEMPORALLY CHAOTIC wave dynamics underlie a variety of debilitating crises in extended excitable systems including the heart. Current strategies for controlling these dynamics employ global, large-amplitude perturbations acting indiscriminately on the system as a whole. For example, the automated external defibrillator commonly found in airports gives via two electrodes a high-energy (1000 V, 30 A, 12 ms) electric shock to terminate the chaotic and ultimately lethal wave dynamics underlying ventricular fibrillation. The adverse effects of such large shocks have motivated a search for less harmful strategies. It is well known that control of spatiotemporal chaos requires multiple control sites. Creating such sites in living tissue, however, is a long-standing problem. We have shown that natural anatomical heterogeneities within cardiac tissue can provide a large and adjustable number of control sites for low-energy termination of malignant wave dynamics. This allows us to terminate ventricular fibrillation in canine cardiac tissue using small amplitude pulsed electric fields with up to two orders of magnitude lower energies than those used for defibrillating shocks. We quantify the physical mechanism underlying the creation of control sites using fully time resolved high-spatial resolution imaging of wave emission and high-resolution magnetic resonance imaging of cardiac structure. Our method avoids the invasive implantation of multiple electrodes and, more importantly, has the potential to control the tissue where the chaotic state is most susceptible, *i.e.*, at rotating wave cores. This approach promises to significantly enhance current technologies for the termination of life-threatening cardiac arrhythmias, a leading cause of mortality and morbidity in the industrialized world. For this innovation, we have received the In-

novationspreis Medizintechnik 2008 (Medical Technology Innovation Award 2008) from the German Ministry for Education and Research (BMBF).

Low-energy Control of Atrial Fibrillation

Atrial fibrillation (AF) is the most common sustained cardiac arrhythmia worldwide affecting an estimated 5.5 million people worldwide. Complications associated with chronic AF include increased risk of both thromboembolism and stroke. Left untreated, paroxysmal AF often progresses to permanent AF, which is resistant to therapy. Although underlying anatomic or pathophysiological factors may fuel its progression, AF itself may lead to its own perpetuation through electric, structural, and metabolic remodeling of atrial tissue. The realization that AF begets AF has led to management strategies that are designed to avoid the progression of AF by reducing the frequency and duration of AF episodes. One such strategy, cardioversion, attempts to reset all electrical activity in the atria and requires the use of large (>5 V/cm) electric field gradients. These high energies cause pain and trauma to the patient, damage the myocardium, and reduce battery life in implanted devices. Another strategy, antitachycardia pacing (ATP), seeks to avoid the development of permanent AF by suppressing paroxysmal AF. ATP consists of a train of 8 to 10 low-energy stimuli delivered as a pacing ramp or burst at 50 Hz via a single pacing electrode. ATP is effective in treating spontaneous atrial tachyarrhythmias, especially slower tachycardias, but it is not very effective for converting AF. To overcome the limitations of ATP and cardioversion, we proposed a new technique that employs a series of low-amplitude pulsed electric fields to overdrive AF and thereby terminate

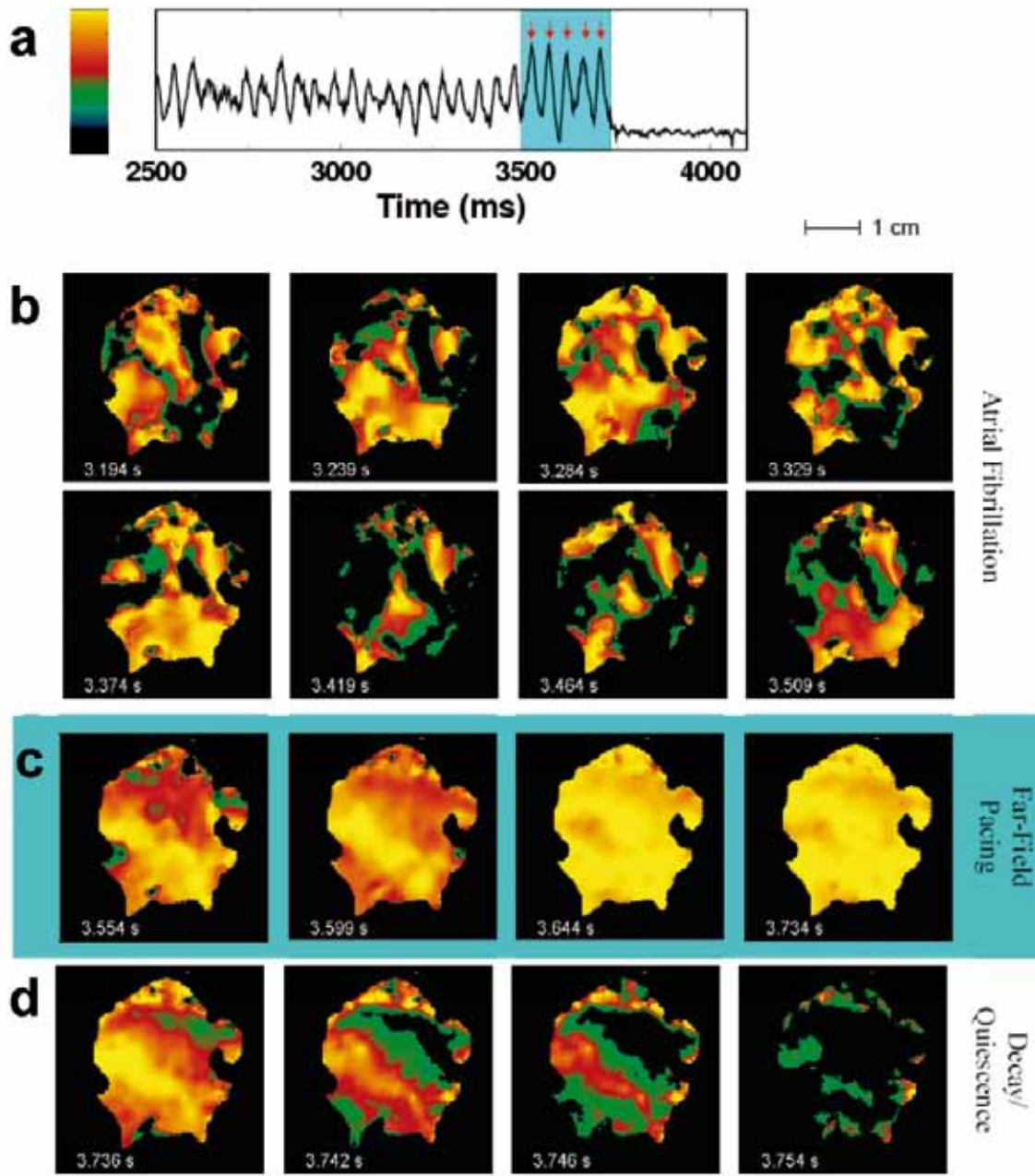


Figure 1

Successful termination of AF. (A) Optical signal from 1 pixel during AF showing successful defibrillation after delivery of 5 far-field pulses of 1.4 V/cm at a cycle length of 45 ms (red arrows). (B) Optical signal during fibrillation; color represents voltage (see color bar in (A)). Frames are 45 ms apart in time and show the complex wave patterns during fibrillation. (C) Effects of shocks 1, 2, 3, and 5 (left to right), with the first 2 panels showing partial capture and the last 2 showing global capture. (D) Evolution to full repolarization and quiescence after shock 5. Throughout, light blue shading indicates time during applied shocks (from [2]).

it, a strategy suggested by previous experimental studies with the use of physically implanted electrodes. The technique, which we call low-energy anti-fibrillation pacing (LEAP), takes ad-

vantage of the fact that after an electric field pulse, virtual electrodes may arise at interfaces separating regions with different conductivities [1]. These sites may be macroscopic, such as

blood vessels or ischemic regions, or smaller-scale discontinuities, including areas of fibrosis or abrupt changes in fiber direction. Virtual electrodes may become a secondary source (*i.e.*, a site of wave emission), depending on the extent of the conductivity discontinuity and the electric field strength.

Using optical mapping in isolated perfused canine atrial preparations (figure 1), we have shown that a series of pulses at low field strength (0.9 to 1.4 V/cm) is sufficient to entrain and subsequently extinguish AF with a success rate of 93% (69 of 74 trials in 8 preparations) [2]. We further demonstrated that the mechanism behind LEAP success is the generation of wave emission sites within the tissue by the applied electric field, which entrains the tissue as the field is pulsed (figure 2).

In conclusion, we found that AF in our *in vitro* experiment can be terminated by LEAP with only 13% of the energy required for cardioversion. These results for AF have been confirmed in *in vivo* experiments. Furthermore, LEAP has been successfully applied for the low-energy termination of ventricular fibrillation *in vitro* and *in vivo* [3].

Cell Culture Experiments

The mechanism underlying the recruitment of wave emission from heterogeneities in electrical conductance is shown in figure 2A. In the presence of an electric field, the membrane potential in the vicinity of a heterogeneity is decreased and increased, *i.e.* depolarized and hyperpolarized. If the membrane potential is increased above excitation threshold in a region sufficiently large, an excitation wave is created. This mechanism can be studied experimentally in cardiac cell cultures, as shown in figure 2B, which permit a direct comparison with theory. Using artificial heterogeneities of well-defined size, we measured the characteristic dependence of the electric field strength required to initiate an excitation wave from the radius of the heterogeneity and find good agreement with theory. In cardiac cell cultures, well-de-

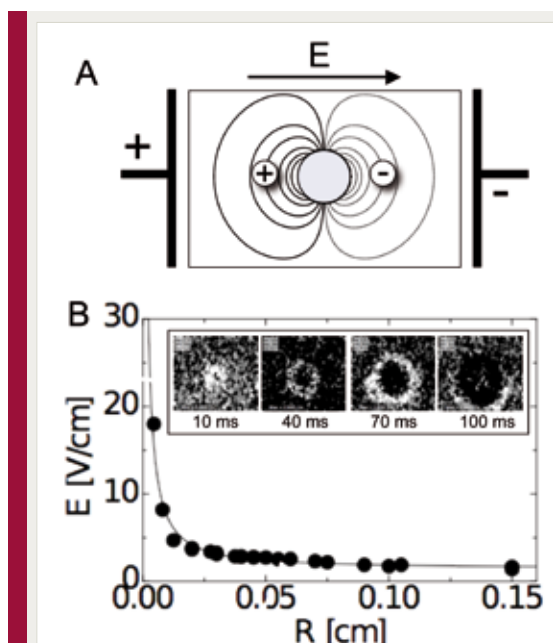


Figure 2

(A) Schematic of the mechanism underlying wave emission from heterogeneities in electrical conductance. In the presence of an electric field, the membrane potential in the vicinity of a heterogeneity (gray circle) will be decreased (hyperpolarized, gray lines) or increased (depolarized, black lines), with respect to the resting membrane potential. If tissue depolarization exceeds the excitation threshold in a sufficiently large region, an excitation wave will be emitted (panel B, inset). (B) Dependence of electric field strength required to induce the emission of an excitation wave from a heterogeneity of radius R . Black circles indicate data from cell culture experiments. Inset shows an example of a wave emitted from an artificial heterogeneity due to a single electric field pulse (field of view $2 \times 2 \text{ cm}^2$). Times are given with respect to the onset of the pulse.

finer heterogeneities were created using photolithography. Experiments in cardiac cell cultures are underway to identify and characterize LEAP mechanisms in a simplified but well-controlled setting.

Unpinning Spiral Waves

While LEAP provides remarkable energy reduction compared to conventional therapeutic approaches, the underlying mechanisms remain largely elusive. Further optimization of LEAP requires identifying the mechanisms underlying the interaction of spiral waves and pacing-

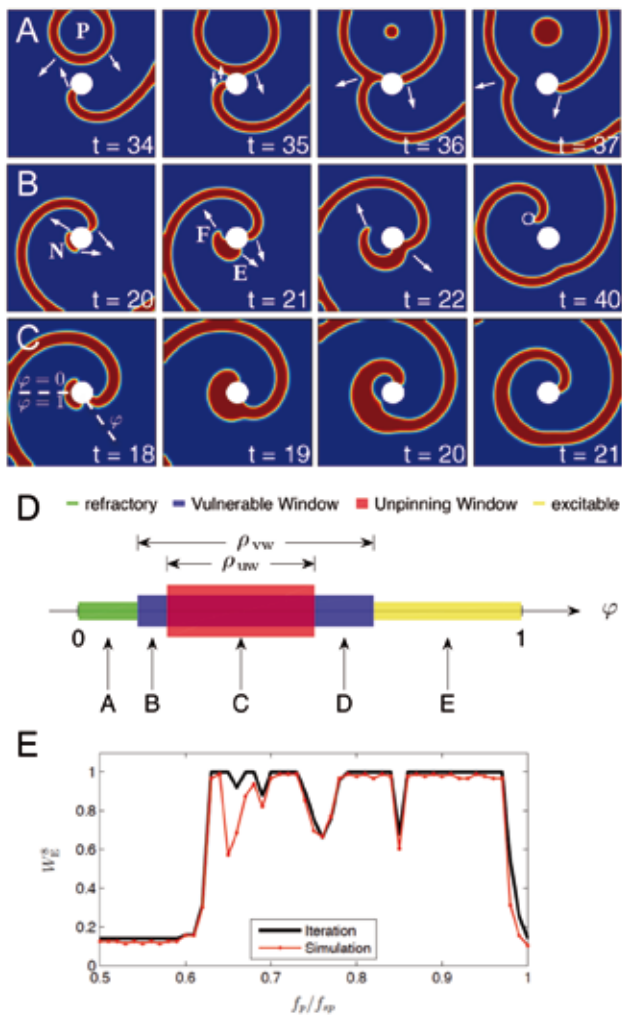


Figure 3

(A) Unsuccessful unpinning of spiral wave pinned to circular heterogeneity by nearby periodic pacing site (P). (B) Successful unpinning by LEAP. The nucleation of a new wave N by LEAP in the refractory tail of the original spiral leads to the formation of a free end F, which forms an unpinned spiral (new spiral core indicated by a circular white line), while the pinned end E of the pacing wave collides with the original spiral (from [4]). (C) The net effect of an unsuccessful LEAP pulse is a phase shift, which depends on the phase φ of the spiral before the pulse. Thus, the reaction of the spiral to an unsuccessful pulse can be fully described by a so-called phase response curve. (D) Schematic view of the spiral's response to an LEAP pulse. A–E denote different LEAP regimes in phase space. A leads to no phase resetting, whereas B, D and E cause the phase to reset. C corresponds to successful unpinning (from [5]). (E) Unpinning success rate W_E^8 for 8 LEAP pulses as a function of the pacing frequency f_p normalized by the spiral's rotation frequency f_{sp} . Black line: Prediction from the single pulse phase response map measured as described in panel C. Fixed points and periodic orbits of the iterative map lead to $W_E^8 < 1$. Red line: Real success rate from direct numerical simulation.

induced perturbations. One of the constituents of these complex dynamics is the interaction of pinned spirals – spiral waves that are anchored at anatomical obstacles such as fatty tissue, scars or blood vessels – with pulses of an electric field. The importance of pinned spirals lies in the fact that this kind of wave is resistant to other strategies of low-energy control such as antitachycardia pacing (ATP, see figure 3A). In a generic model of excitable media, we demonstrated that this significant limitation of ATP for unpinning spiral waves from obstacles could be overcome by LEAP [4,5,6]. The basic mechanism by which unpinning is achieved through LEAP is shown in figure 3B. A spiral wave anchored to a circular obstacle can be considered

as a nonlinear phase oscillator with the phase (determined by the position of the spiral on the circle, see figure 3C) evolving uniformly in the unperturbed case. In this setting, we identified phase regimes of the rotating wave that result in different responses to a single electric field stimulus (see figure 3D) and investigated their dependence on the electric field strength and obstacle size [5]. In particular, we found that the response of the spiral wave to an LEAP perturbation can be characterized by a phase response map. Using this approach, mechanisms such as phase resetting can be observed, which are also known from other nonlinear oscillatory systems. These properties were used to predict the response of a pinned spiral wave to period-

ic pulse trains [7,8], a process that is probably taking place during the application of LEAP. Using an iterative map constructed from the phase response map, we were able to accurately predict unpinning success rates as a function of the pacing frequency and specifically to understand the occurrence of low success rates for certain frequency regimes (see figure 3E). These low success rates were due to a frequency locking mechanism between the spiral and the pacing, which is directly connected to periodic orbits of the iterated map.

Outlook

Physiological numerical models (see Sec. V-11) will be used to further optimize LEAP parameters (frequency, electric field strength, number of pulses, etc.) for atrial and ventricular arrhythmias. Signal analysis will play an important role in adaptive parameter selection depending on the characteristic spatial-temporal dynamics (see Sec. V-12). In collaboration with our clinical partners, we will design further studies to determine whether this marked reduction in energy can increase the effectiveness and safety of terminating tachyarrhythmias clinically.

- [1] A. Pumir et al., *Phys. Rev. Lett.* **99**, 208101 (2007).
- [2] F.H. Fenton et al., *Circulation* **120**, 467-476 (2009).
- [3] S. Luther et al. *Nature* (accepted for publication)
- [4] P. Bittihn et al., *New J. Phys.* **10**, 103012 (2008).
- [5] P. Bittihn et al., *Phil. Trans. R. Soc. A* **368**, 2221-2236 (2010).
- [6] A. Pumir et al., *Phys. Rev. E* **81**, 010901(R) (2010).
- [7] A. Behrend, P. Bittihn, S. Luther, *Computing in Cardiology* **37**, 345-348 (2010).
- [8] A. Behrend, P. Bittihn, S. Luther, *Biomed Tech* 2010; **55** (Suppl. 1), DOI 10.1515/BMT.2010.339.

IV-9 Natural Computation and Autonomous Robot Control

F. Schittler Neves, C. Bick, C. Kolodziejski, M. Timme
F. Fix, G. Weber, F. Wörgötter (U Göttingen)

NEURONAL NETWORKS are functionally flexible to a high degree. They integrate sensory information across multiple modalities (such as olfaction, vision, and touch) in real time, process them given previously formed memories, and finally initiate goal-oriented behaviorally relevant output patterns [7]. Interestingly, even small biological neural systems turn out to be remarkably versatile; networks of just a few neurons may generate a variety of output patterns which, for example, result in different locomotive gait patterns. The network in which computation is taking place is also re-adjusting continuously to learn new, previously unknown patterns, thus adapting to a changing environment [8]. We are currently studying two approaches to both understand these forms of complex, adaptive dynamics and exploit them in real world applications.

Systems that support heteroclinic cycles have been of particular interest in recent years, in particular because of their computational capabilities [3]. In certain systems of neuronal units, states can be encoded in form of saddle sets and connecting heteroclinic orbits [9, 2, 1] implying spatio-temporal activity patterns on a macroscopic scale. Due to the instability of the saddles, there is no “trapped state” as in typical attractor dynamics but the dynamics are rather governed by finite-time transient phenomena. These dynamics yield a highly sensitive (to inputs) but at the same time noise-robust environment-dependent integration of information. Similarly, chaotic dynamical systems exhibit a large variety of possible output activities that might be exploited systematically using control schemes. Chaotic attractors typically contain many unstable periodic orbits such that controlling chaos may stabilize the system to many different periodic outputs. We recently extend-

ed standard delayed-feedback control of chaos to make it both adaptive and neuronal, thus suitable for implementation in neuron-like devices. Using one chaotic central pattern generator, we gained access to a variety of distinct periodic motions that can then be mapped onto different (behavioral) patterns [4]. Classical pattern generators relied on having a specific controller for each pattern; this becomes obsolete in our approach. The applications of this idea are numerous, ranging from gait control of robotic walkers to vehicle motion control; we implemented this idea to control locomotion of a hexapod robot, achieving a behavioral versatility of unprecedented complexity.

Universal Computation by Heteroclinic Switching

Generic features of systems exhibiting heteroclinic switching may be exploited for new kinds of universal computation, e.g. using natural representations in terms of high-dimensional trajectories in network dynamical systems. Networks of pulse-coupled units such as spiking neural circuits exhibit non-trivial invariant sets in the form of attracting yet unstable saddle periodic orbits where units are synchronized into groups. Connections between unstable and stable manifolds from different saddles often support switching processes in those networks [9] and may enable novel kinds of neural computations. Whereas encoding capacities and simple computations have been investigated theoretically [2] the practical use of switching dynamics for processing information is far from understood.

In our recent studies, we showed that certain persistent switching processes naturally emerge in the presence of system inhomogeneities and are fully controllable by small external

signals. We exploited this feature for inventing a new kind of computation. As an example, we provide general transition rules for the switching process in a small network of pulse-coupled oscillators [3], thereby providing a theoretical basis for computation by persistent switching processes. Furthermore, we designed an artificial neural system that serves as a universal computer. We show that systems with small asymmetries may perform basic bitwise operations by mapping given inhomogeneous inputs into specific state sequences (figure 1). Our results explicitly show the capability of simple pulse-coupled systems to perform generic logic computation via a persistent switching process. We are currently strengthening this new area of research by studying the interaction of systems presenting such switching dynamics and by extending our work towards agent-based autonomous systems and their hardware implemen-

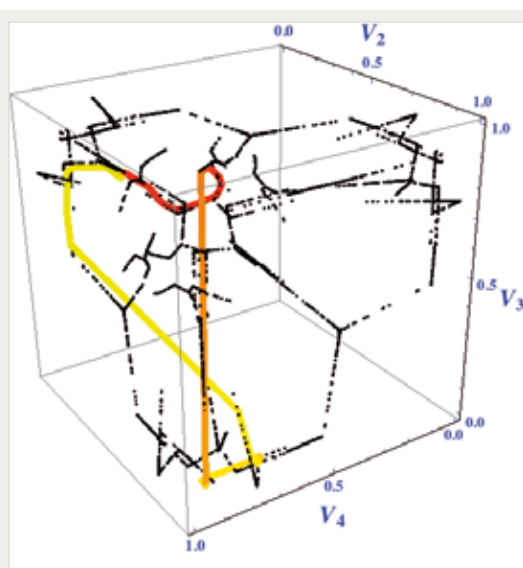


Figure 1

Switching paths in a state space hyperplane for a network of five neural oscillators. Black dots represent noise-induced paths covering all possible switchings; the colored line represents a specific limit cycle generated by asymmetric current. Each time oscillator number one is reset, the potential of oscillators two to four are plotted as a three dimensional line and, for the colored line, the potential of oscillator number five is given by a color gradient from zero (yellow) to one (red).

tations. Our recent results show that neuronal computation by switching dynamics provides a natural way to represent changing input signals due to the saddle properties and at the same time reliably encode information due to the heteroclinic properties, both interesting features for autonomous navigation.

In summary, network dynamical systems exhibiting complex switching processes provide an interesting new view about how nonlinear systems may compute in a natural way.

Nonlinear Dynamics for Autonomous Systems

We employ methods from chaos control and generalize them for a neural implementation that is both adaptive and resembles the modular architecture of biological neural systems. To this end we study a simple example of a single control circuit that acts as one stimulus-controlled central pattern generator (CPG) for a variety of gait patterns. The generic dynamics of our CPG is chaotic and thus contains a large number of unstable periodic orbits (UPOs). A neurally implemented, stimulus-dependent chaos control method will stabilize a UPO and thus determines an appropriate periodic motor pattern. Using this approach to join standard nonlinear dynamics with neural network and learning theory, the robot implemented (figure 2) is capable of simultaneously coordinating inputs from 20 sensors to generate 11 different behaviors (for example, orienting, taxis, and various gaits). It successfully transverse an obstacle course with slopes, rough terrain, and holes in the ground. Our control mechanism drastically simplifies the sensor-motor coordination problem, thus enabling us to set up a versatile autonomous system. Furthermore, the control becomes more flexible and it is easy to add new behaviors by mapping a new period not used so far onto a new motor pattern. Using a single CPG also simplifies learning by associating sensory inputs with appropriate motor output. Due to the modular nature of the CPG controller its applicability is not limited to various robots,

but could equally well be integrated into other types of autonomous systems such as cars, and possibly even prostheses and orthoses. Finally, chaos itself is even exploited constructively in our hexapod robot providing a way of self-untangling.

The chaos control method is an essential part of the approach. How can we ensure that this new adaptive control is fast and reliable? In order to get optimal performance, one needs an

More generally, we are currently working towards further joining the theory of nonlinear dynamical systems with neural approaches to guide future developments for autonomous systems. A specific next step is to implement motor memory exploiting the single-CPG architecture by using synchronization between two similar (or identical) CPG-circuits. One circuit receives its control both directly from the sensory system and from a second circuit that acts as a memory

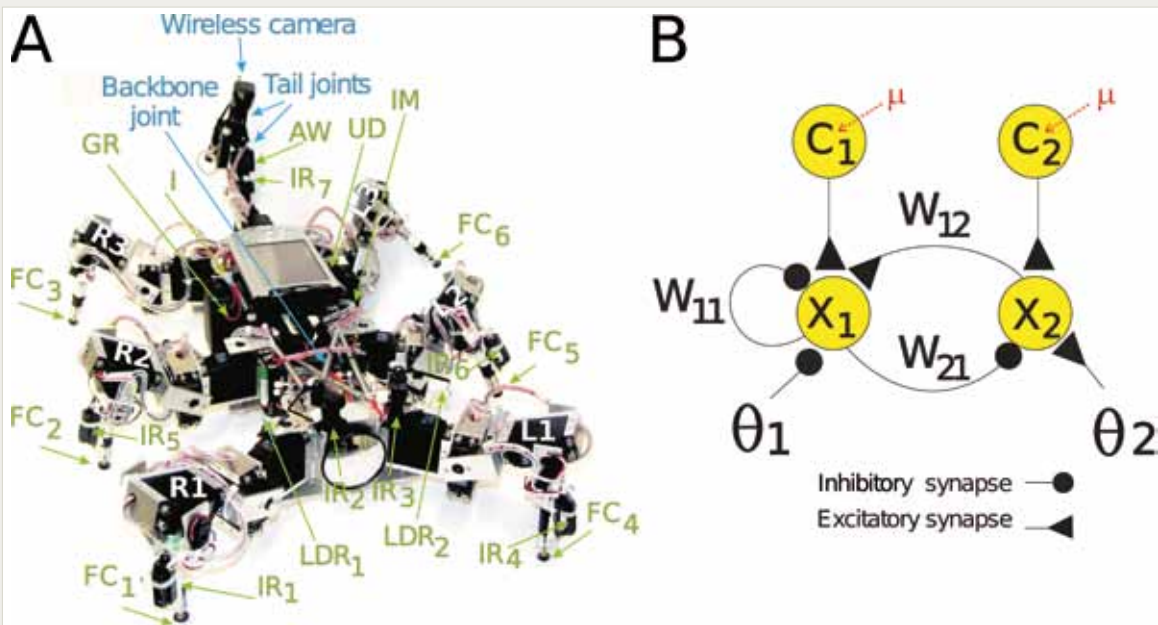


Figure 2

Adaptive neural chaos control enables versatile robotic behavior. A) The hexapod robot AMOS-WD06 with 20 sensors of various types indicated (green arrows). B) Wiring diagram of the neural control circuit (CPG).

adaptive mechanism that tunes the parameters of chaos control reliably, interactively, and in real time to regimes of fast convergence to the desired period. However, current adaptation algorithms are based on empirical studies and do not guarantee such a convergence. We are therefore currently conducting systematic theoretical studies [5, 6] to guarantee successful control, an important prerequisite for implementing such an algorithm in real world applications.

device. The synapses responsible for synchronizing these two circuits are adaptive such that their current strengths determine the influence of the memory on current actions.

Our initial work on further developing and exploiting chaos control solves a complex sensor-motor coordination problem and finally proves practical applicability for an autonomous robot. The new method of chaos control presented here brings adaptation and self-organization of a complex behaving system. A major break-

through is also the synthesis of concepts from theoretical aspects of different fields that has immediate impact on neural and robotic engineering and the physics of self-organization: It

allows the first (and very simple) solution of a complex and long-standing control problem and at the same time contributes new perspectives to insect locomotion.

- [1] C. Bick and M. Rabinovich. *Phys. Rev. Lett.* **103**, 218101 (2009)
- [2] P. Ashwin and M. Timme, *Nature* **436**, 36 (2005)
- [3] F. S. Neves and M. Timme, *J. Phys. A: Math. Theor.* **42**, 345103 (2009)
- [4] S. Steingrube, M. Timme, F. Wörgötter, and P. Manoonpong, *Nature Phys.* **6**, 224 (2010)
- [5] J. Klingmayr, C. Bettstetter, and M. Timme, Proc. IEEE Intern. Symp. Appl. Sci. in Biomedical and Communication Technologies (ISABEL), Bratislava, Slovak Republic (2009)
- [6] C. Bick, C. Kolodziejski, and M. Timme, Eur. Dyn. Days 2010, selected as talk (2010)
- [7] N. Bernstein, *The Coordination and Regulation of Movements*, Pergamon, Oxford (1967)
- [8] A. Ijspeert, A. Crespi, D. Ryczko, and J. Cabelguen, *Science* **315**, 1416 (2007)
- [9] M. Rabinovich, A. Volkovskii, P. Lecanda, R. Huerta, H. Abarbanel, and G. Laurent, *Phys. Rev. Lett.* **87**, 068102 (2001)
- [10] M. Rabinovich, R. Huerta and G. Laurent, *Science* **321**, 48 (2008)

V Patterns and Instabilities

V-1 Pattern Formation and Spatial Forcing in Thermal Convection

E. Bodenschatz, H. Nobach, M. Pennybacker, G. Seiden, S. Weiss, F. Winkel
A. Newell (Tucson), W. Pesch (Bayreuth)

FLUID MOTION driven by thermal gradients (thermal convection) is a very important phenomenon in nature. Thermal convection occurs when a sufficiently steep temperature gradient is applied across a fluid layer. For this system, over the past 30 years, many fundamental aspects of patterns and their instabilities have been studied [1]. Pattern formation is common also to many other non-equilibrium systems as found in physics, chemistry or biology. Even though the underlying processes are different, the observed patterns are often of striking similarity and indeed their understanding in terms of general, unifying concepts continues to be a main direction of research. In a traditional Rayleigh-Bénard Convection (RBC) experiment a horizontal fluid layer of height d is confined between two parallel plates that have a high thermal conductivity. When the temperature difference between the bottom and the top plate exceeds a certain critical value, the conductive motionless state

is unstable and convection sets in. The most ideal pattern is that of straight, parallel convection rolls with a horizontal wavelength of $\sim 2d$. In the less well-known case of Inclined Layer Convection (ILC) the standard Rayleigh-Bénard cell is inclined at an angle with respect to the horizontal, resulting in a basic state that is characterized by a plane parallel shear-flow with cubic velocity profile. This shear-flow not only breaks the isotropy in the plane of the layer, but also causes at large angles a transition from a thermal into a hydrodynamic shear-flow instability. For ILC we observed an intricate phase space, consisting of nonlinear, spatio-temporally chaotic states [2]. In our experimental investigations we use a pressurized gas cell to study forcing and control of thermal convection in horizontal and inclined fluid layers. As explained in detail in [1], compressed gases have the advantage over other fluids in that they enable an experimental realization of large aspect-ratio sample cells with short vertical thermal diffusion times of a few seconds or less. In addition, the Prandtl number, which gives the relative importance of the nonlinearities in the heat conduction equation and the Navier-Stokes equation, was less than 1.5, i.e. in a regime, where non-relaxational, spatio-temporal chaos (STC) can be observed very close to the onset of convection.

Recently we began to study the influence of spatially periodic and spatio-temporal forcing schemes of various geometries on pattern formation. Two types of forcing schemes are applied. One method is to use micro-machined surfaces, as shown schematically in figure 1. The boundary modulation of the bottom plate enables us to investigate the effect of forcing on the bifurcation

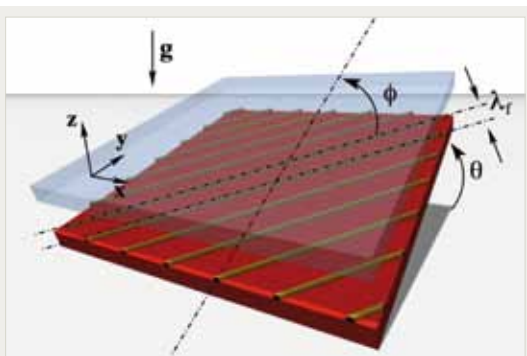


Figure 1

(a) Schematic drawing of the ILC configuration. The inclination angle θ and the relative orientation angle ϕ are tuned to explore the parameter space. The distance d between the bottom and the top plate is typically 0.5mm and the wavelength of the boundary modulation was $\lambda_r = 1\text{mm}$.

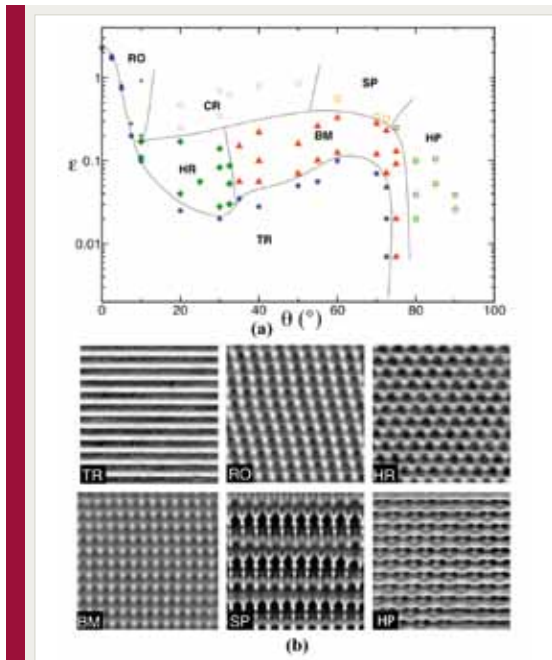


Figure 2
 (a) Phase diagram of the convection patterns observed for orthogonal forcing in ILC ($\phi = 90^\circ$). In this case the component of gravity parallel to the inclined plane is orthogonal to the orientation of the boundary modulation. In (a) ε denotes the reduced control parameter. (b) Images of the observed patterns: transverse rolls (TR), rhombic pattern (RO), hexarolls (HR), bimodals (BM), scepter-shaped patterns (SP) and heart-shaped patterns (HP).

structure and on the stabilization of spatio-temporal chaos. By changing the forcing wavelength λ_f , the inclination angle θ and the relative orientation angle ϕ with respect to the in-plane component of gravity (figure 1), we are able to study the consequences of the two competing symmetry-breaking mechanisms, namely inclination and spatial forcing. We discovered the novel state of crystal-line chaos [3]. In case of ILC the use of surface corrugated bottom plates allowed for the exploration of the phase diagram of three mode resonance patterns (see figure 2) [4, 6]. We also observed super-lattice patterns as a response to the forcing as shown in figure 3 [4, 5]. Another method of forcing is a thermal imprinting technique, in which we illuminate the experimental cell with infrared laser light from above through IR transparent pressure windows. This

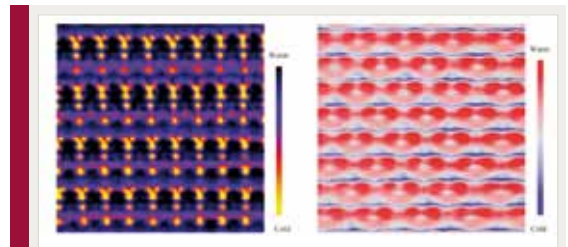


Figure 3
 False color shadowgraph image of the temperature field. (a) Scepter patterns were observed at $\phi = 90^\circ$, $\theta = 72.5^\circ$, and $\varepsilon = 0.33$. This dynamical structure consists of complex scepter-like patterns located at the sites of a rectangular lattice. (b) Heart patterns were observed at $\phi = 90^\circ$, $\theta = 90^\circ$, and $\varepsilon = 0.04$. Here the structure consists of heart-shaped patterns located at the sites of an oblique square lattice.

way the pattern can be forced and simultaneously observed with the shadowgraph technique. The main trick is to also use an IR and visible light transparent liquid coolant for the top plate temperature regulation. Such a fluid is CS_2 that is liquid at the pressures used in the experiment. The convection cell is illuminated with a 10.6 micron infrared beam emitted by a CO_2 laser, which is absorbed by the main spectral band of the convecting fluid SF_6 . This allows the study of not only spatio-temporal forcing, but also convection with internal heating.

- [1] E. Bodenschatz, W. Pesch, and G. Ahlers, *Annu. Rev. Fluid Mech.* **32**, 709 (2000)
- [2] K. E. Daniels, and E. Bodenschatz, *Phys. Rev. Lett.* **88**, 4501 (2002)
- [3] J.H. McCoy, W. Brunner, W. Pesch, and E. Bodenschatz, *Phys. Rev. Lett.* **101**, 254102 (2008)
- [4] G. Seiden, S. Weiss, J. H. McCoy, W. Pesch and E. Bodenschatz, *Phys. Rev. Lett.* **101**, 214503 (2008)
- [5] G. Seiden, S. Weiss, and E. Bodenschatz, *Chaos*. **19**, 041102 (2009)
- [6] S. Weiss, G. Seiden, and E. Bodenschatz, *New J. Phys.*, submitted.

V-2 Spiral Waves, Cell-Cell Signaling and Cell Aggregation

N. Oikawa, V. S. Zykov, E. Bodenschatz

STARVING *DICTYOSTELIUM discoideum* cell populations are a well-established paradigm for the study of cell-cell signaling, cell-cell interaction, cell differentiation and tissue formation [1]. They also provide a generic example for self-organization and pattern-formation in excitable media [2-4]. It is well known, that the signaling of starving Dictyostelium cells is controlled by the chemo-attractant, cyclic AMP (cAMP), and the extracellular enzyme phosphodiesterase. On the cellular level cAMP is secreted to the extracellular space when a cell encounters stimulation by cAMP. Simultaneously extracellular cAMP is degraded by extracellular phosphodiesterase that is continuously secreted by the cells. Waves of cAMP can form by cell-cell induced rise and diffusion of cAMP and permanent decay by phosphodiesterase. Thus the dynamics can be described by the reaction diffusion mechanism. When Dictyostelium cells are plated on a surface, *i.e.*, in two dimensions, spontaneous emission of a few starving cells gives rise to a macroscopic dynamics exhibiting typical excitable media attractor states, namely target waves and spiral waves [5, 6]. We are investigating both experimentally and theoretically the pattern-formation processes during the early stages of the Dictyostelium aggregation with particular interest on the impact of the magnitude of the diffusion coefficient D of cAMP and

also of the spatial inhomogeneity of excitability due to signal induced cellular development. In the experiment a monolayer of cells was plated on the surface of the agar layer and the cAMP induced contraction waves were monitored using a dark field optical setup [7]. By increasing the agar concentration of the substrate the cAMP diffusion coefficient was decreased. From the experimentally observed dark field images the local phase of the temporal oscillations of the cAMP induced contraction was reconstructed. We found that initially disordered oscillations synchronized over time. We characterized the synchronization with the spectral entropy $S(t)$ derived from the averaged spatial power spectra. Figure 1 shows the phase maps corresponding to the minimum of $S(t)$, *i.e.*, best synchronization, for two different agar concentrations. As shown in figure 1, for fast cAMP diffusion D we obtained spirals, and for lower D target patterns. For intermediate agar concentrations spirals and targets coexisted. We observed the wavelength of the pattern to gradually decrease with decreasing D . For even slower diffusion, the number of wave-centers increased and the pattern was disordered. We also found that the onset of the synchronization shifted to later times as D decreased.

In order to understand the observed behavior we have investigated theoretically models for Dictyostelium signaling. In particular, we are interested in the relationship between the medium properties and parameters of the spiral wave dynamics, such as the rotation frequency, the core radius, and the spiral's wavelength. We analyzed the Kessler-Levine model for cAMP dynamics [8] numerically and semi-analytically by exploiting a free-boundary approach [9]. The common assumption of the free-boundary analysis is that the boundary of an excited region is sharp and consists of two trigger waves representing the front and the back of the wave, so-called TT-waves

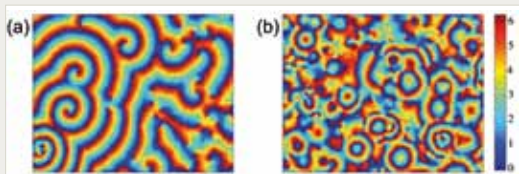


Figure 1

Phase maps for the temporal oscillations of the signaling patterns observed for agar concentration of (a) 0.2 wt% and (b) 2.3 wt%. The size of the images is 16.24x12.18 mm. The phase measured in the range from 0 to 2π is shown by color code.

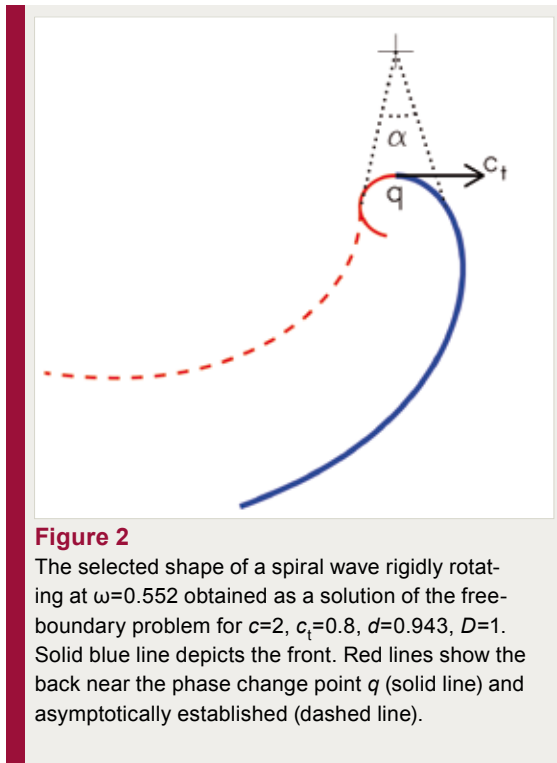


Figure 2
 The selected shape of a spiral wave rigidly rotating at $\omega=0.552$ obtained as a solution of the free-boundary problem for $c=2$, $c_t=0.8$, $d=0.943$, $D=1$. Solid blue line depicts the front. Red lines show the back near the phase change point q (solid line) and asymptotically established (dashed line).

[10-12]. The normal velocity of the front and of the back depends on the local value of inhibitor and on the curvature. Since the Kessler-Levine model does not include any inhibitor, the normal front velocity, c_n , depends only on its curvature k , namely, $c_n = c - Dk$, where c is the plane wave velocity and D is the cAMP diffusion coefficient. Very importantly in the Kessler-Levine model the trigger wave is followed by a phase wave, not a trigger wave. For these TP-waves, the normal velocity of the wave back is not determined by the back curvature and the existing free-boundary approaches for TT-waves described, for instance, in [10-12] are not applicable. Therefore we developed a free-boundary theory for TP-waves. In the case of rigidly-rotating spirals it consists of two ordinary differential equations, which are describing the normal and tangential velocities of the wave boundary as functions of the arc-length s [12]. It is convenient to measure the arc-length from the point q , where the front coincides with the back of the spiral wave. If the plane front velocity is given, the front curvature at the point q is well determined, since the normal velocity here should

be zero. Then, for an arbitrary chosen tangential velocity c_t at the point q there exists only one single value of the angular velocity ω , which satisfies the boundary conditions for $s \rightarrow \infty$. Thus the shape of the wave front is selected. Far away from the point q the wave back should simply follow the wave front with a time delay equal to the pulse duration d . Thus, the shape of the wave back should be identical to the front shape, but has to be turned by the angle $\alpha = \omega d$. However, in a vicinity of the point q a front-back time delay is small and this phase wave is not created yet. The back shape here still obeys the equations, which are valid for the front, and can be easily computed for the ω selected before. As shown in figure 2, then the angle α should be chosen in such a way, that the part of the wave front computed near the point q is smoothly connected to the asymptotically established phase wave. Namely this smoothness condition determines the single possible value of the angle α and, hence, the pulse duration d . Thus, for given value of the tangential velocity of the point q two values ω and d have been selected by application of the free-boundary approach. This gives us an opportunity to present ω as a function of d . By simple rescaling procedure we have generalized this relationship. The main result of this consideration is the dimensionless angular velocity Ω represented as a function of a single dimensionless parameter B , as can be seen in figure 3. This parameter characterizes the medium excitability and is specified as $B = 2D/(d c^2)$. The angular velocity W is determined as $\Omega = \omega D/c^2$. A very important and unexpected result is that the dimensionless angular velocity Ω can be represented as a function of the same dimensionless parameter B , as it was the case for TT-waves [12]. It can be seen in figure 3 that the rigidly rotating spiral wave exists only within a restricted region of the parameter B . In the high excitability limit, $B = B_{min}$ the spiral wave core vanishes and the angular velocity approaches the value $\Omega = 0.331$. This limit practically coincides with a similar one found for the case of TT-waves [12]. In the low excitability

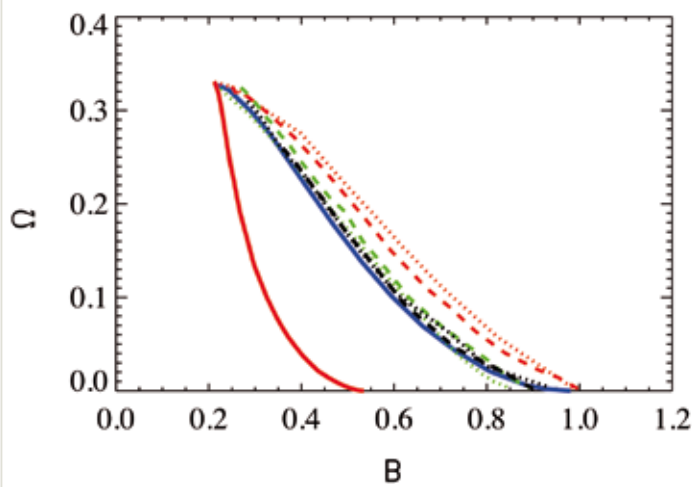


Figure 3

The selected values of the dimensionless angular velocity Ω vs. the dimensionless parameter B obtained from numerical solutions of the free-boundary problem (blue solid line). Dashed and dotted lines depict results of direct numerical integrations of the reaction-diffusion Kessler-Levine model for several different excitation thresholds. Thick red line represents the relationship $\Omega(B)$ obtained for TT-waves in [12].

ty limit, $B = B_{cp}$, the angular velocity vanishes, and the core radius diverges. A similar transition was also found earlier for media with a TT-wave [10, 12], but for considerably smaller $B = B_c$. The core radius and the wavelength of the spiral waves can be also determined. The relationships found in the framework of the free-boundary approach are in good quantitative agreement with results from numerical reaction-diffusion simulations of the Kessler-Levine model, as can be seen in figure 3.

In summary, the experimental study of the influence of the cAMP diffusion constant on the spatio-temporal dynamics during the signaling stage of *Dictyostelium discoideum* aggregation clearly demonstrated that spiral waves can exist only in the case of a sufficiently large diffusion of cAMP.

The proposed modified free-boundary approach supplies a novel effective tool to study dynamics of these wave patterns. Moreover, the universal relationships obtained in the framework of this approach can be easily applied to analyze the spiral wave dynamics under temporal variations of the medium parameters, for instance, for the cells following a developmental path [6], or subjected to a genetic feedback [13]. The proposed approach also allows us to extrapolate a selection principle for rigidly rotating spiral in the Kessler-Levine model to a broad class of excitable media with TP-waves, e.g., including cardiac tissue. That is also a challenge for a future work.

- [1] S.J. Annesley and P.R. Fisher, *Mol. Cell Biochem.* **329**, 73 (2009)
- [2] A.T. Winfree, *The Geometry of Biological Time* (Springer, Berlin Heidelberg, 2000)
- [3] A.S. Mikhailov, *Foundations of Synergetics* (Springer, Berlin Heidelberg, 1994)
- [4] J.D. Murray, *Mathematical Biology* (Springer, 2003)
- [5] S. Sawai, P.A. Thomason, and R.E. A. Cox, *Nature*, **433**, 323 (2005)
- [6] D. Geberth and M.-T. Huett, *PLoS Comp. Biol.* **5**, 1 (2009)
- [7] J.G. Gross, M.J. Peacey, and D.J. Trevan, *J. Cell Sci.* **22**, 645 (1976)
- [8] D. Kessler and H. Levine, *Phys. Rev. E* **48**, 4801 (1993)
- [9] V.S. Zykov, N. Oikawa, and E. Bodenschatz submitted.
- [10] A. Karma, *Phys. Rev. Lett.* **66**, 2274 (1991)
- [11] D. Margerit and D. Barkley, *Phys. Rev. Lett.* **86**, 175 (2001)
- [12] V.S. Zykov, *Physica D* **238**, 931 (2009)
- [13] H. Levine, I. Aranson, L. Tsimring, and T.V. Truong, *Proc. Nat. Acad. Sci. USA*, **93**, 6382 (1996)

V-3 Pattern Formation and instabilities in the Actin Cortex of Motile Cells

C. Westendorf, A. Gholami, M. Tarantola, A. Bae, C. Beta, E. Bodenschatz

J. Negrete Jr., J. Enderlein (University of Goettingen), M. Falcke (MDC Berlin), R. Firtel (UCSD), G. Gerisch (MPI for Biochemistry, Martinsried), A. Janshoff (University of Goettingen), H. Levine (UCSD), W. Loomis (UCSD), W. Rappel (UCSD), T. Salditt (University of Goettingen)

THE ACTIN cytoskeletal dynamics provides the fundamental basis of eukaryotic cell motility [1]. The cross-linked actin network at the front of a cell pushes the leading edge of the membrane towards the source of attractant. It is our aim to provide a quantitative understanding of the spatio-temporal dynamics of the actin cytoskeleton within the leading edge. To achieve this goal, we have developed experimental methods to address single cells with well-controlled chemical stimuli in space and time. We use the social amoeba *Dictyostelium discoideum* (Dictyostelium) as a model.

Methods

A. Flow photolysis for well-defined spatio-temporal stimulation of cells

We apply stimuli in microfluidic devices in combination with photochemical component release termed “flow photolysis” [2]. A signaling molecule is photochemically cleaved from a biological inert caged precursor. A sketch of this method is given in figure 1. We have carefully analyzed the effects of cell-shape and microfluidic flow on the chemical signals reaching the cell membrane [3,4]. We have shown that the flow photolysis method provides well-controlled stimuli and the fastest switching of concentrations in a microfluidic flow. This gives us the opportunity to approach the limit

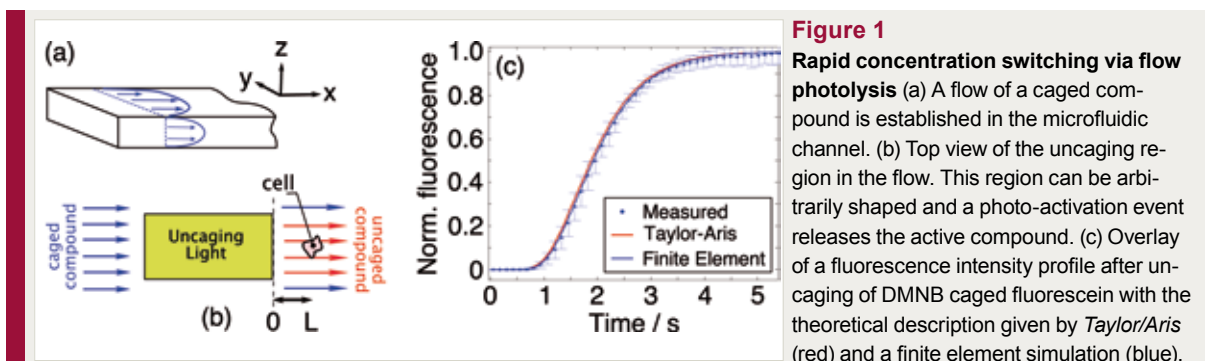
of delta peak or step input in addition to well-controlled gradients.

B. Cell flattening

To investigate the leading edge dynamics of Dictyostelium cells in detail with optical microscopy, we have developed microfluidic flattening devices [5]. Figure 2 a to c show a sketch, the mode of operation, and an image of a double layered flattening device. The top layer expands under pressure, decreasing the height of the channel below (figure 2 b). In figure 2 d-e the cell flattening is visualized with a Dictyostelium mutant tagged with the membrane receptor label cAR1-GFP. The left confocal micrographs display the unflattened cell, while the right show the effect of flattening. This way we enlarge the region observable with total internal reflection fluorescence (TIRF) microscopy (see figure 2 f) and with single molecule spectroscopy at the cell membrane. This gives the interesting possibility to investigate simultaneously the actin cytoskeleton and the dynamics at the leading edge, including processes like tip splitting.

C. Non-optical biosensors

As a further approach to investigate Dictyostelium, we recently adopted non-optical biosensors to exclude influence of the imaging technique on the observed oscillatory instabilities. In collaboration with the Janshoff group (Universi-



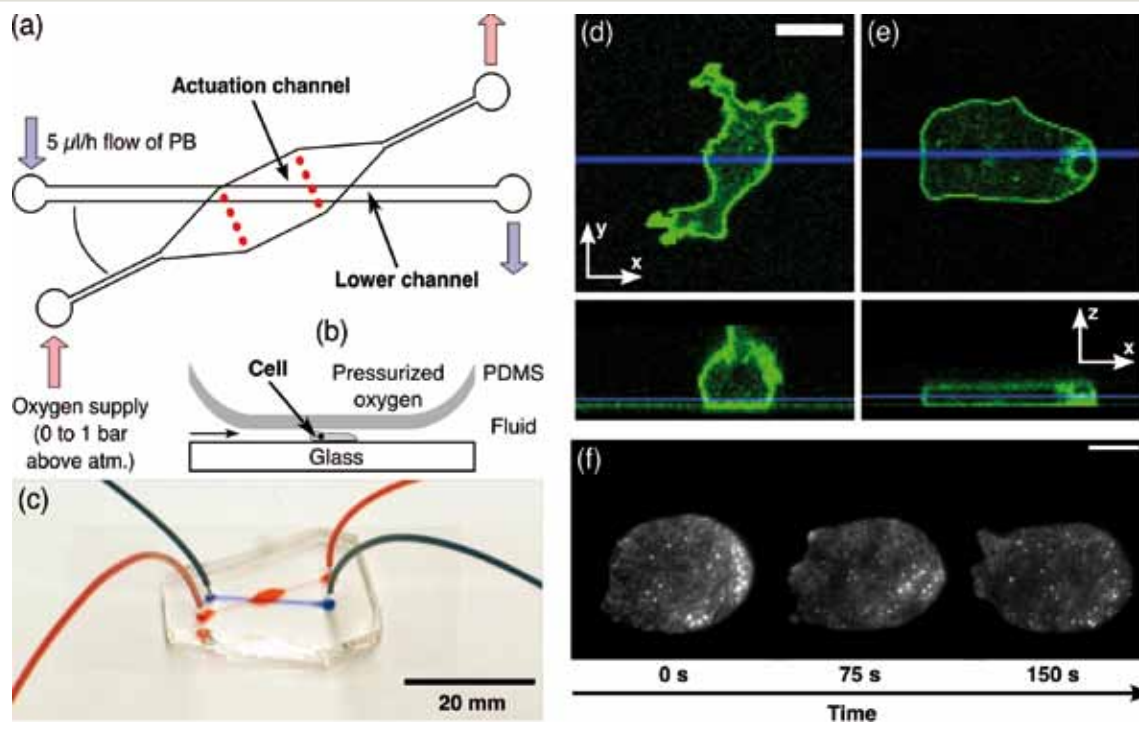


Figure 2

Microfluidic actuator (a) Cells are contained in the bottom channel. The actuation channel is open – allowing oxygen to flow through. The oxygen is supplied to the cells via the permeable PDMS membrane, which separates the two layers. (b) By adjusting the pressure of the oxygen supply at the inlet, the PDMS membrane is deformed and flattens the cells below. (c) Assembled double layer microfluidic channel with connected tubing. The actuation channel is filled with red and the lower channel with blue dye. (d, e) Flattening of *Dictyostelium* cells: confocal xy (top) and xz (bottom) sections are shown for a cAR1-GFP cell before flattening (d) and during flattening (e). The blue lines show the y and the z cuts. Scale bar: 10 μm . (f) Tip – splitting process of a flattened *Dictyostelium* cell migrating in buffer and imaged with TIRF microscopy. Actin filaments are labeled with LimE-GFP. Scale bar is 10 μm .

ty of Goettingen) we applied Electrical Cell substrate Impedance Sensing (ECIS) successfully to detect synchronous oscillations of *Dictyostelium* cells [6]. We are currently developing a system for single cell studies. Furthermore, we recently began to analyze *Dictyostelium* cells via single cell force spectroscopy.

D. Wide-field optical imaging of single molecules

Together with the Enderlein group (University of Goettingen) we started to investigate the molecular and cytoskeletal structure and dynamics at the leading edge. We will apply image correlation microscopy and fluorescence image moment analysis. We will analyze fluorescently labeled proteins involved in the development of the leading edge at the single molecule scale

and correlate it to the membrane curvature. The cell lines will be developed in our laboratory in collaboration with our partners at UCSD.

E. X-ray imaging and diffraction

In collaboration with the Salditt group (University of Goettingen) we are applying lens-less X-ray imaging and diffraction to improve our understanding of the cytoskeletal structure at the leading edge of *Dictyostelium*. Specifically targeted towards the present project, first nano-beam X-ray experiments on *Dictyostelium* cells have been carried out [7], which allowed the mapping of several ionic components specific to the cell body. A sample environment for X-ray based imaging of freeze-dried and frozen hydrated *Dictyostelium* cells has been devised.

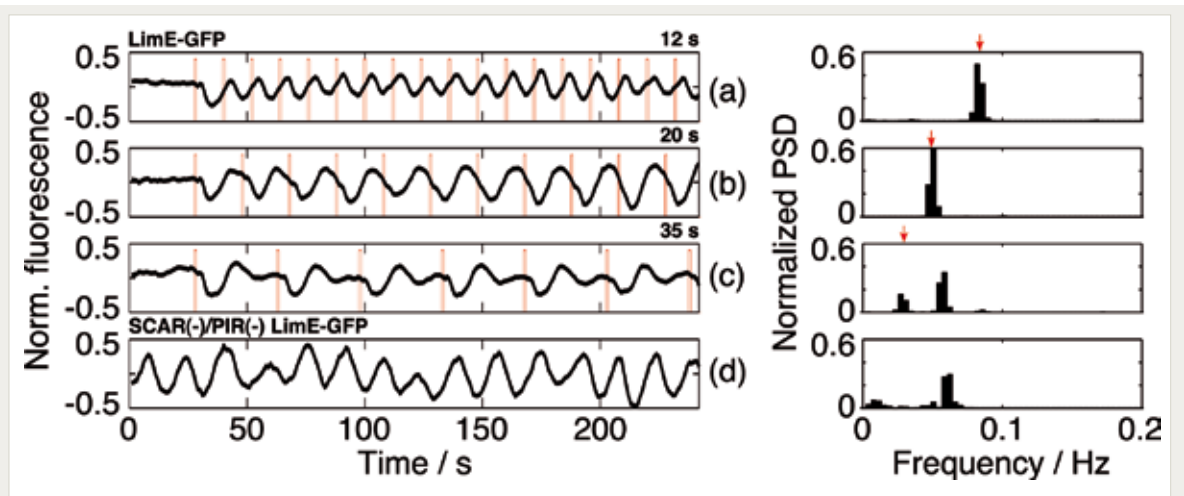


Figure 3

Forced and autonomous oscillations in the *Dictyostelium discoideum* cytoskeleton Impulse trains with various periods have been applied to *Dictyostelium* LimE-GFP. Shown are $T = 12$ s (a), $T = 20$ s (b) and $T = 35$ s (c). The stimulus is displayed in red and the corresponding power spectral density of the cytosolic response function on the right. Arrows highlight the dominant input frequency. (a-c) are averaged signals over at least 10 cells. (d) Self sustained oscillations on a single cell level found in the cytoskeletal defective double knock-out mutant SCAR⁻/PIR⁻ with an additional LimE-GFP tag.

Results

A. Temporal response of the actin cytoskeleton to rapid stimulations

We applied periodic chemical pulses with a rise time of less than a second and a total duration of less than two seconds and recorded cytoskeletal actin response via confocal laser scanning microscopy of the filamentous actin label LimE-GFP. The observed response was periodic for input periods above 6 s and it showed a π phase shift between input periods of 8 s to 15 s. This shows that the intrinsic time scale of the *Dictyostelium* signal processing system is within this range. Stimulated with longer periods the response power spectral densities show a second dominant frequency approximately twice the input frequency (figure 3 a-c).

We also found self-sustained oscillations in the cortex of *Dictyostelium* SCAR⁻/PIR⁻ mutant cells also tagged with LimE-GFP. These mutants are deficient in cytoskeletal regulator proteins for actin. In our experiments, these mutants exhibit self-sustained, cell-autonomous oscillations of cortical actin polymerization with periods of about 10 s to 15 s, while a steady state

of polymerization with only slight fluctuations is observed in wild-type cells (see figure 3 d). Hence, these self-sustained oscillations are on the same time scale as the “resonance” condition. Further investigations are on the way.

B. Spatiotemporal dynamics of the leading edge

We have carried out exploratory observations of the tip splitting of flattened *Dictyostelium* LimE-GFP cells chemotaxing in the presence of a cAMP gradient. The gradient of cAMP was induced by flow photolysis. A reconstruction of cell shape and membrane contour during a tip-splitting process is presented in figure 4 a and 4 b. Contours of a typical flattened *Dictyostelium* cell (figure 5 a) and the corresponding contour curvature plot (figure 5 b) show that, while a cell is crawling, the leading edge bifurcates, and protrusions move from the cell front to the back [8]. Recently, Barry and Bretscher [9] showed that *Dictyostelium* amoebae are also capable of swimming towards chemoattractants. They hypothesized that the mechanism for swimming is intimately related to crawling. We were able to show that the measured cell membrane dy-

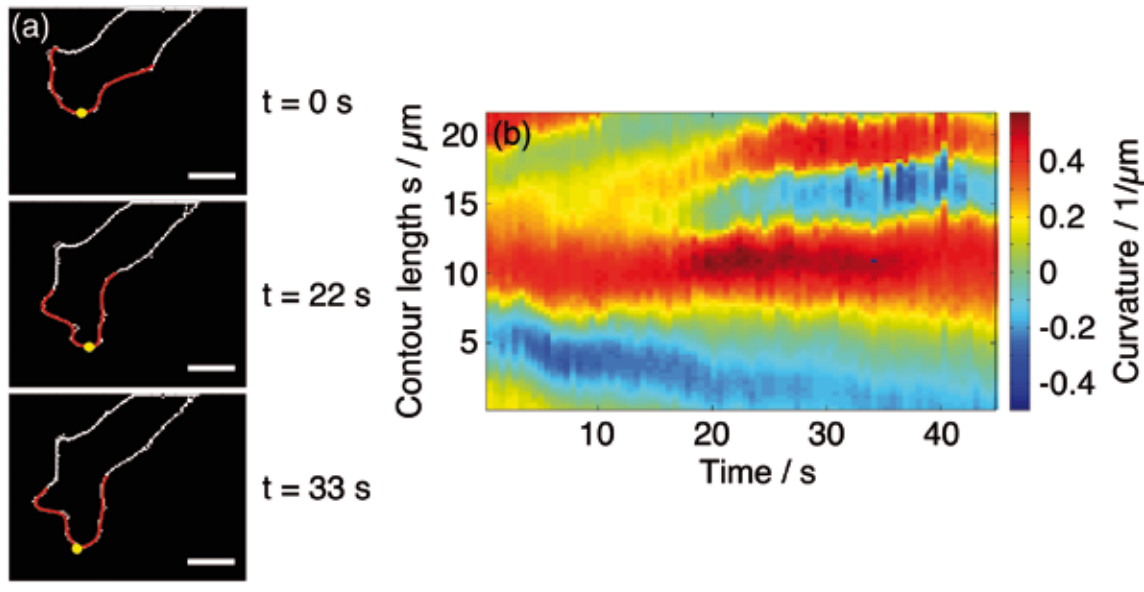


Figure 4

Leading edge dynamics Reconstructed cell shape and membrane contour marked by bright red (a). The yellow spots mark the middle of the contour length plotted in the bottom (b): up to 18 s, the size of the almost constant curvature increases, at 18 s a flat region develops, and for > 18 s a furrow develops splitting two tips. Then the region of almost constant curvature increases again.

namics are sufficient to explain their observations [8] and that the alternative mechanism of membrane streaming is not required.

C. Numerical simulations of the actin/membrane dynamics

In collaboration with M. Falcke (MDC-Berlin) we model actin driven membrane dynamics. Building on the mathematical model introduced in [10] we added a shape mediated spatial global coupling by assuming that the surface tension of the membrane changes as a function of the cell's projected area [11]. The filament network close to the membrane is formed by two parts: i) a highly dense cross-linked actin gel and ii) a brush formed of free fluctuating actin filaments which polymerize and undergo cycles of attachment and detachment to the membrane (figure 6 a). Free fluctuating filaments in the brush transfer mechanical forces to the membrane only if they are anchored in a scaffold. We assume that the actin gel itself, cross-linked and adherent to the substrate, provides this support. Then actin filaments, which are flexed by Brownian motion are able to exert force on the

membrane. Numerical simulations of this model show that in a cell with initially symmetric shape and a symmetric polymerizing actin network, weak noise is sufficient to break the symmetry and the cell starts to move (figure 6 b).

Conclusion and Outlook

In summary, intrinsic time scales, resonant behavior, and intracellular synchronization have been systematically investigated to unravel a detailed picture of the dynamical properties of the actin system. By exploiting mechanisms and instabilities of the actin cortex of motile cells, we have begun to study the spatio-temporal dynamics with a special focus on the leading edge dynamics. Further study of pattern formation and oscillatory instabilities of *Dictyostelium* cells with labels for and genetic knock-outs of several key players in the chemotactic response will be necessary: these are the motor protein myosin-II, coronin (an Arp 2/3 inhibitor), Aip 1 (a cofilin activator) and the actin-regulating Ras-GTPases.

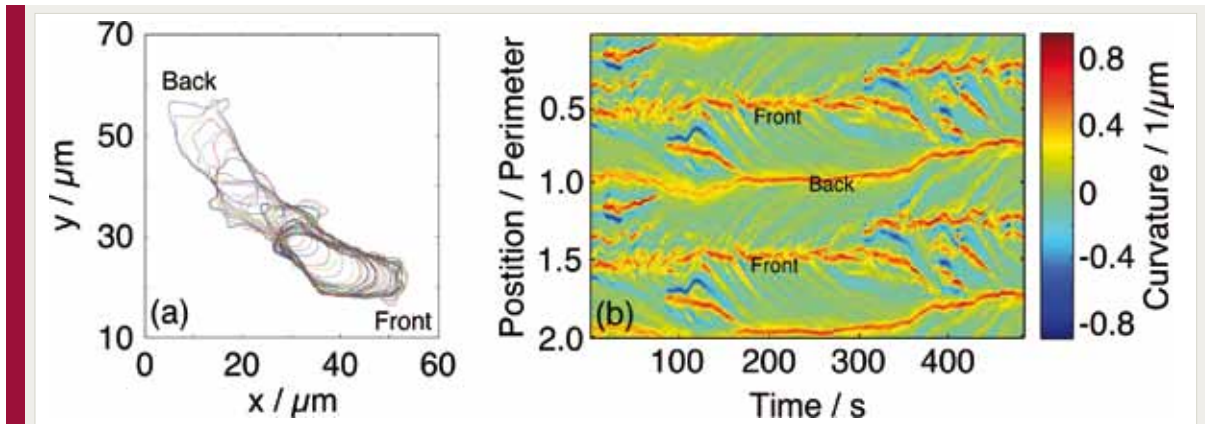


Figure 5
Curvature space-time plot Typical cell contour of a crawling cell (a) and the corresponding curvature space-time plot (b) show the herringbone structure with regions of high curvature, which bifurcate at the front and travel to the back. To prevent a loss of detail at the edges, the curvature has been plotted over two contour lengths.

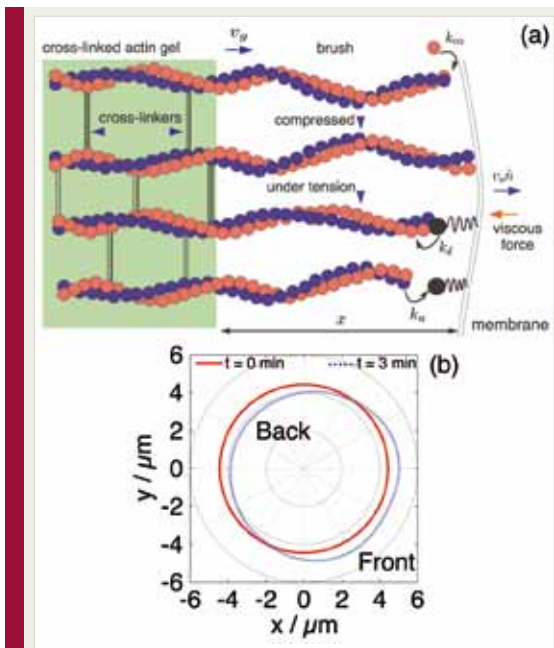


Figure 6
Symmetry breaking in a simulated circular cell
 (a) Schematic representation of actin filaments oriented normal to the membrane. While attached filaments are under tension and pull back the membrane, detached filaments are compressed, polymerize and deform the membrane locally. This generates a global coupling between the dynamics of all the points on the membrane. (b) A small noise in actin polymerization rate grows nonlinearly to break the symmetry in a circular cell ($t = 0$). The cell with a polar shape ($t = 3$ min) moves with the velocity of $0.2 \mu\text{m}/\text{min}$.

[1] K.F. Swaney, C.H. Huang, and P.N. Devreotes, *Annu. Rev. Biophys.* **39**, 265 (2010)
 [2] C. Beta, D. Wyatt, W.J. Rappel, and E. Bodenschatz, *Anal. Chem.* **79**, 3940 (2007)
 [3] C. Beta, T. Frohlich, H.U. Bodeker, and E. Bodenschatz, *Lab Chip* **8**, 1087 (2008)
 [4] A.J. Bae, C. Beta, and E. Bodenschatz, *Lab Chip* **9**, 3059 (2009)
 [5] C. Westendorf, A.J. Bae, C. Erlenkamper, E. Galland, C. Franck, E. Bodenschatz, and C. Beta, *PMC Biophys.* **3**, 9 (2010)
 [6] E. Schaefer, C. Westendorf, E. Bodenschatz, C. Beta, B. Geil, and A. Janshoff, *Small* **7**, 723 (2011)
 [7] K. Giewekemeyer, S.P. Krüger, S. Kalbfleisch, M. Bartels, C. Beta, T. Salditt, *Phys. Rev. A* **83**, 023804 (2011)
 [8] A.J. Bae and E. Bodenschatz, *PNAS* **107**, E165 (2010)
 [9] N.P. Barry and M.S. Bretscher, *PNAS* **107**, 11376 (2010)
 [10] A. Gholami, M. Falcke, and E. Frey, *New J. Phys.* **10**, 033022 (2008)
 [11] E. Evans and W. Rawicz, *Phys. Rev. Lett.* **64**, 2094 (1990)

V-4 Coupling Chemical Oscillators through Bilayer Membranes

S. Thutupalli, S. Herminghaus, R. Seemann

WE HAVE DEMONSTRATED before that mono-disperse gel emulsions can be produced and manipulated in micro-fluidic environments with high accuracy and reproducibility [1, 2]. It is possible to create large rafts of droplets arranging in a 'crystalline' manner due to their mutual repulsion and their interaction with the geometry of the channel system they are produced in (figure 1). They can be filled with different contents, moved with respect to each other, or their contents merged by rupturing the oil lamellae separating them in a controlled manner [3-5]. It turns out that if the surfactant stabilizing the emulsion is properly chosen and the dispersed (aqueous) phase volume fraction is sufficiently high, the residual oil between adjacent droplets may be squeezed out, along with the formation of a surfactant double layer between the droplets (figure 2).

The formation of the double layer takes place on a millisecond time scale, with details depending on the properties of the surfactant and the oil. In our experiments we used mono-olein as the surfactant in most cases, and squalane as the oil. In this case, the formation of the double

layer proceeds in a zipper-like process (figure 2), where the velocity of the contact line was observed to be about 2 mm/sec. The resulting mono-olein double layers had a specific capacitance of 0.72 μF per square centimeter, which is very close to the literature value for oil-free mono-olein membranes.

It turned out that these membranes have particularly interesting properties concerning the coupling of chemical oscillations in adjacent droplets. We have produced emulsions whose droplets carried the reactands of the Belouzhov-Zhabotinski (BZ) reaction. This produces chemical oscillations with a period of a few seconds, which can be made visible by using Ferroin as a redox agent and optical indicator. In our experiments, the oil phase was laden with mono-olein at concentrations well above the critical micelle concentration (CMC) in order to securely stabilize the emulsion.

The BZ reaction relies on bromine compounds for both the promoter and the inhibitor molecules. Since the mono-olein has a chemical C-C double bond in its backbone, it acts as an efficient bromine scavenger: bromine spontaneously reacts with such double bonds saturating the backbone alkane chain. Consequently, no bromine can traverse the oil phase, and the oscillations of individual droplets remain uncoupled. This is in strong contrast to earlier work by others, which used a different formulation [6] with a double-bond-free oil phase. As soon as two droplets are only separated by a mono-olein double layer, their chemical oscillations become coupled.

This is demonstrated in figure 3 where three droplets are shown in the inset. The main panel displays the optical transmission traces for the three droplets. Clearly, the traces of the two droplets in intimate contact (green and red trace) are phase-coupled, while the oscillation of the somewhat remote droplet runs free (blue

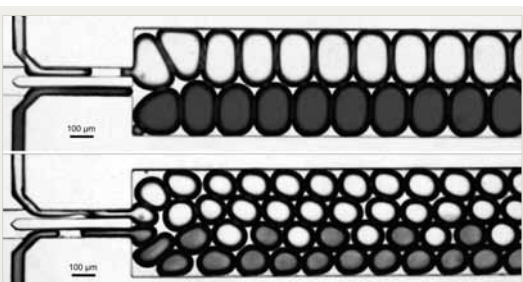


Figure 1

Gel emulsions of water in oil generated by step emulsification, forming rafts in a wider channel. The channel width is 500 microns, the volume fraction of the aqueous phase is 0.75. The elementary cells of such rafts can be quite complex, as the lower example shows. Controlled rearrangement of these configurations are possible by appropriately chosen channel geometries

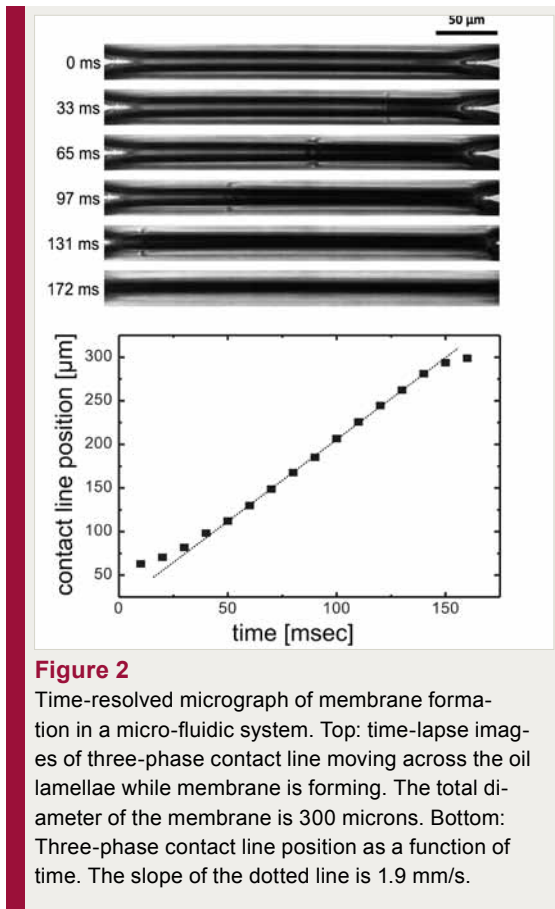


Figure 2 Time-resolved micrograph of membrane formation in a micro-fluidic system. Top: time-lapse images of three-phase contact line moving across the oil lamellae while membrane is forming. The total diameter of the membrane is 300 microns. Bottom: Three-phase contact line position as a function of time. The slope of the dotted line is 1.9 mm/s.

trace). The black curve indicates the distance of the centers of the droplets corresponding to the red and blue traces. By some drift in the setup, they approach each other, until around 100 seconds their mutual motion comes to a halt. This indicates that their surfaces are virtually in intimate contact, which results in a diverging viscous resistance. However, their chemical oscillations are still out of phase. For phase coupling to occur, the formation of a double layer is obviously necessary. This happens at about 120 seconds, as is visible from the abrupt drop in the distance of the droplet centers (black curve). After this has happened, the blue and red traces are phase coupled. We have also observed anti-phase coupling of adjacent droplets separated by a double layer (figure 4), which shows that the significance of the double layer is more complex than just providing a free passage for the bromine molecules

(after the few molecules constituting the membrane have been brominated). In a raft of droplets of the kind discussed above, fronts of excitation can propagate in the same way as in a raft of heart muscle cells, or in a colony of Dictyostelium Discoideum. Figure 5 shows a detail of such an excitation front, which would occur periodically, with a period corresponding roughly to the free oscillation period of the chemical reaction. It is instructive to observe that the gap marked with the red arrow is already very narrow, but has not yet formed a double layer. As it may be anticipated from the discussion above, the excitation front is not able to traverse this gap, but will rather propagate around it. The figure shows three snapshots at equidistant times. The front chooses the longer path along the left rim of the image, before it reaches the droplet above the red arrow, just behind the narrow gap [7].

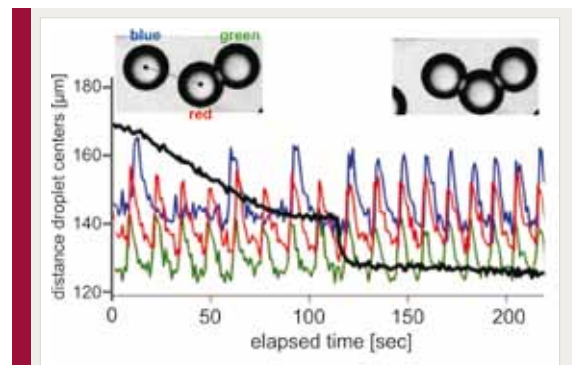


Figure 3 Effect of membrane formation upon the phase coupling of chemical oscillators. The blue, red, and green traces represent the transmittance of the three droplets shown in the insets as a function of time. The black curve shows, on the same time axis, the distance of the 'blue' from the 'red' droplet (measured center-to-center). The oscillations couple in phase as soon as the membrane is formed (jump in the black curve), but not before.

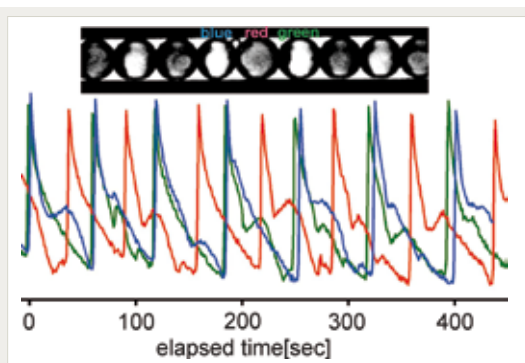


Figure 4

Traces showing antiphase coupling of droplets separated by bilayer membranes between them. This shows that the membranes play a more complex role in the coupling process than just providing free exchange of the promotor and inhibitor molecules.

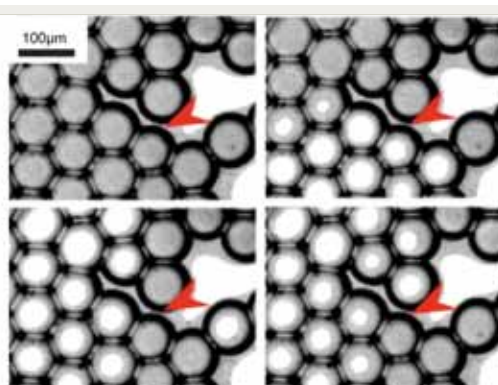


Figure 5

Demonstration of the influence of membrane coupling on an excitation wave in a larger raft of droplets. The oil phase consists of squalane with 50 mM/l mono-olein. The aqueous phase is 0.5 M sulphuric acid, 280 mM sodium bromate, 0.5 M malonic acid, and 3 mM ferroin. The droplet surfaces indicated by the red arrow are very close, but there has yet no membrane been formed. The excitation wave (coming from below) passes around the arrow, the excitation does not directly cross the gap between the two droplets

- [1] E. Surenjav, S. Herminghaus, C. Priest, R. Seemann, „Discrete Micro-Fluidics: Reorganizing Droplets at a Bend“, *Appl. Phys. Lett.* **95**, 154104 (2009)
- [2] E. Surenjav, C. Priest, S. Herminghaus, S. Seemann, „Manipulation of Gel Emulsions by Variable Microchannel Geometry“, *Lab on a Chip* **9**, 325 (2009)
- [3] V. Chokkalingam, S. Herminghaus, R. Seemann, „Self-Synchronizing Pairwise Production of Monodisperse Droplets by Micro-Fluidic Step Emulsification“, *Appl. Phys. Lett.* **93**, 254101 (2008)
- [4] V. Chokkalingam, B. Weidenhof, M. Krämer, S. Herminghaus, R. Seemann, W. F. Maier, „Template-Free Preparation of Mesoporous Silica Spheres through Optimized Microfluidics“, *Chem. Phys. Chem.* **11**, 2091 (2010)
- [5] V. Chokkalingam, B. Weidenhof, M. Krämer, W. F. Maier, S. Herminghaus, R. Seemann, „Optimized Droplet-Based Microfluidics Scheme for Sol-Gel Reactions“, *Chem. Phys. Chem.* **11**, 2091 (2010)
- [6] M. Toiya, V. K. Vanag, I. Epstein, *Angew. Chem. Int. Ed.* **47**, 7753 (2008)
- [7] S. Thutupalli, S. Herminghaus, R. Seemann, „Bilayer membranes in micro-fluidics: from gel emulsions to soft functional devices“, *Soft Matter* **7**, 1312 (2011).

V-5 Patterns, Structures, and Surface Ordering in Complex Fluids

C. Bahr, S. Herminghaus, R. Seemann

X. Feng, W. Guo, Y. Iwashita, K. Peddireddy, B. Schulz

UNDERSTANDING the behavior of soft matter at interfaces is essential for numerous topics in fields such as nanotechnology, biophysics, colloidal systems, etc. We study experimentally various complex fluid systems in which the presence of one or two interfaces induces structures which are not present in the corresponding volume phase. Our systems comprise micrometer-thick and ultra-thin (one to four molecular layers) smectic films on silicon substrates, smectic membranes in aqueous environment, microfluidics with surface-ordering systems, and surfactant-laden interfaces separating a liquid-crystal and an aqueous volume phase.

Micrometer-thick smectic films with antagonistic anchoring conditions

These films, prepared on silicon wafers, possess a smectic/substrate and a smectic/air interface. The molecular smectic layers prefer to be parallel to the air interface but are forced to stand perpendicular on the substrate surface. The antagonistic anchoring conditions result in the formation of focal conic domains (FCDs): Defect structures, in which the smectic layers are bend around two singular lines, namely a circle on the substrate surface and a straight line running from the circle center to the air interface. FCDs, which can arrange themselves in regular arrays, might be used as templates or matrices for self-organizing soft matter systems and the goal of our project is to explore the targeted generation and the controlled arrangement of these structures [1-3] (figure 1).

Ultra-thin smectic films

Smectic films consisting of only one or few molecular layers are prepared by spin-coating from solution. By controlling the concentration of the smectic material in the spin-coating solution, films with a defined small number of smectic

layers can be prepared. Unless the concentration is precisely tuned to certain values, the top-most smectic layer of the films is formed only partially, i.e., it is either fragmented into isolated islands or it shows a porous structure (figure 2). There is a well-defined relation between the 8CB concentration in the spin-coating solution

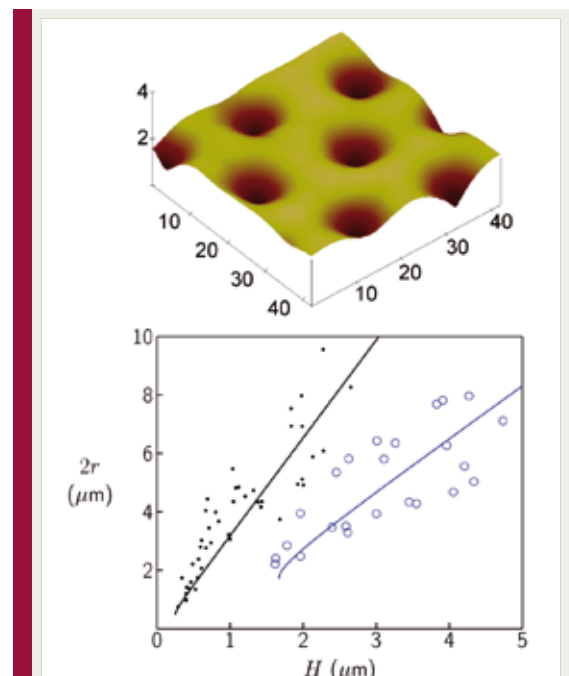


Figure 1

Top: AFM image (the numbers give the dimensions in micrometers) of the surface of a 6 micrometer thick smectic film on a silicon wafer. The antagonistic anchoring conditions (random planar at the substrate surface, homeotropic at the air interface) generate an array of circular focal conic domains (FCDs) in the film. The bending of the molecular smectic layers in each domain result in a depression in the air interface above each FCD the depth of which can be measured by AFM. Bottom: Relation between the diameter $2r$ of the FCDs and the thickness H of the smectic film. The two data sets are obtained for two substrates possessing different strengths of the random planar anchoring. The anchoring strength was tuned by coating the silicon wafers with differently composed silane mixtures. Solid lines are fits to a theoretical model (see [2]).

and the resulting surface structure, thereby enabling the targeted generation of island or pore structures [4]. These films might be of interest for the preparation of structured two-dimensional soft matter systems.

Smectic membranes in aqueous environment and microfluidics with surface-ordering systems:

Smectic films which are freely suspended on a solid frame in air are well established experimental model systems for the study of the structure of smectic phases, phase transitions in two dimensions, and surface and dimensionality effects in fluid systems. We could prepare freely suspended smectic films in water with a size of 1 cm² using surfactants ensuring a strong homeotropic anchoring at the smectic/water interfaces [5]. Since the ordering surface field at the smectic/water interface can be tuned via the surfactant coverage, smectic films in aque-

ous environment may expand the general range of possible studies of freely suspended smectic films. We studied the stability and the thinning transitions which occurred at temperatures above the volume smectic-A – isotropic transition temperature. We investigated further the formation and rupture kinetics of thin smectic membranes separating water droplets in microfluidic devices. Smectic membranes and alkane membranes separating gas bubbles in microfluidic devices were also studied, especially with respect to the development of dynamic compound refractive lenses for the focussing of x-rays [6]: The smectic surface order at isotropic liquid-crystal/air interfaces and the surface freezing at liquid alkane/air interfaces stabilize the gas bubbles against coalescence and are thus essential prerequisites for this purpose.

Surfactant-laden liquid-crystal/aqueous interfaces:

In most of the above mentioned systems, surfactants, accumulated at liquid-crystal/water interfaces, play an essential role. We have continued our systematic studies of the influence of surfactants on the surface ordering behavior of liquid crystals above the liquid-crystal – isotropic transition. A number of experimental results indicate that the magnitude of the surfactant coverage of a liquid-crystal/water interface controls the strength of the ordering surface field. We could recently show that the precise tuning of the surfactant concentration enables the experimental realization of a first-order prewetting transition at which the thickness of a nematic wetting film jumps between two finite values [7]. Increasing the surfactant concentration drives the prewetting transition towards a critical point, again demonstrating the experimental control of the surface field (figure 3). Future work will focus on the influence of the molecular structure of the surfactant and on the role of the aqueous phase, e.g., by replacing the pure water phase by water/glycerol mixtures.

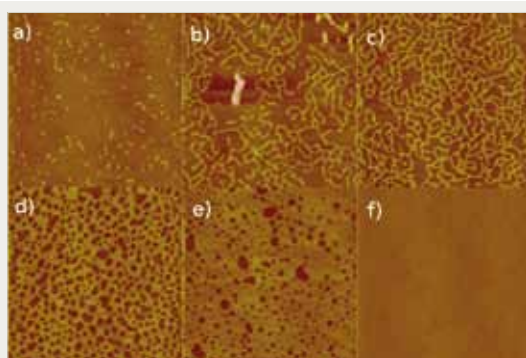
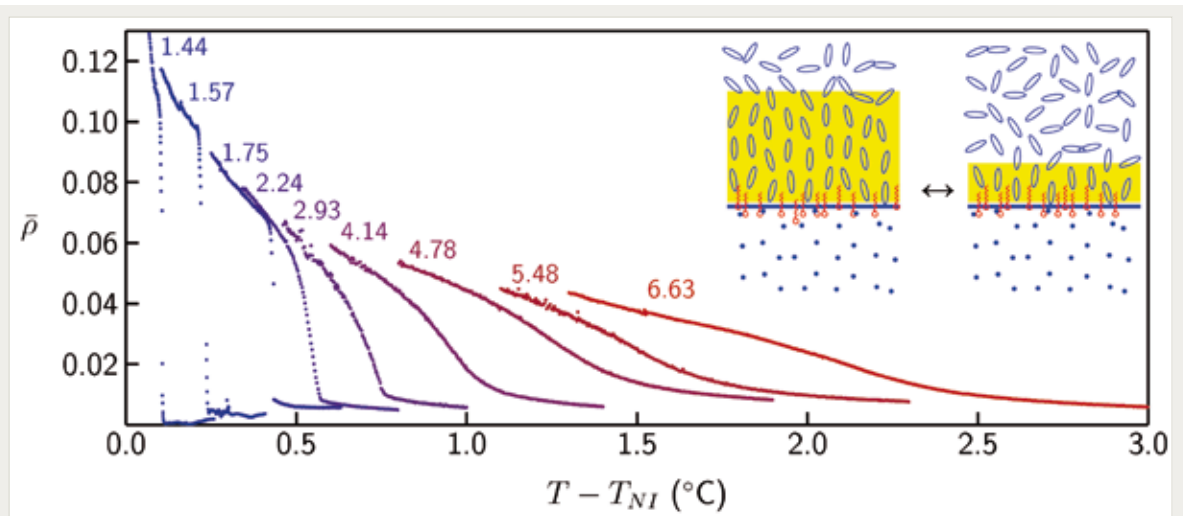


Figure 2

AFM height images (area 20 x 20 micrometers) of ultra-thin (two to three molecular layers) smectic films spin coated from solution onto silicon wafers. The concentration of the smectic compound (8CB) in the spin-coating solution was 2.8 mg/ml (a), 3.0 mg/ml (b), 3.2 mg/ml (c), 3.4 mg/ml (d), 3.6 mg/ml (e), and 3.8 mg/ml (f). The images demonstrate the partial formation of the smectic top layer: with increasing concentration, a structural sequence is observed which starts with isolated islands which grow to a porous structure and finally form a complete layer. The height difference between the thicker and the thinner parts of the film is about 3.2 nm, corresponding to the thickness of one molecular smectic layer.


Figure 3

Temperature dependence of the ellipticity coefficient $\bar{\rho}$ of a surfactant-laden liquid-crystal/water interface in the temperature range above the nematic – isotropic transition temperature T_{NI} ; $\bar{\rho}$ is a linear measure of the thickness of the nematic layer at the interface. The curves are obtained with different surfactant concentrations (the number at each curve give the molar fraction in 10^{-3} in the liquid crystal volume phase). The discontinuous jump observed for low concentrations indicates a first-order prewetting transition at which the thickness of the nematic wetting layer changes abruptly (see schematic drawings in which the nematic layer is marked in yellow). With increasing surfactant concentration, the prewetting transition is driven towards a critical point beyond which the wetting layer thickness varies continuously.

- [1] W. Guo, S. Herminghaus, Ch. Bahr, *Langmuir* **24**, 8174 (2008)
- [2] W. Guo, Ch. Bahr, *Phys. Rev. E* **79**, 011707 (2009)
- [3] W. Guo, Ch. Bahr, *Phys. Rev. E* **79**, 061701 (2009)
- [4] B. Schulz, Ch. Bahr, *Phys. Rev. E* **83**, 041 710 (2011)
- [5] Y. Iwashita, S. Herminghaus, R. Seemann, Ch. Bahr, *Phys. Rev. E* **81**, 051709 (2010)
- [6] Y. Iwashita, Ch. Bahr, C. Priest, S. Herminghaus, R. Seemann, *La Houille Blanche* **6**, 129 (2009)
- [7] Ch. Bahr, *EPL* **88**, 46001 (2009)

V-6 Dynamics of Droplets in Microchannels

M. Brinkmann, J.-C. Baret, R. Seemann

B. Semin, X. Qu, Q. Brosseau, E. Kadivar, J.-B. Fleury (Saarland University)

MOST MICROFLUIDIC applications rely on a thorough understanding of the dynamics and interaction of droplets flowing in microchannels [1]. But even the simple problem to predict the terminal velocity of an isolated droplet flowing in a straight channel is not fully solved [2]. The literature provides many examples for measurements of the droplet velocity as function of water and oil flow rates but these data are scattered and depend significantly on the channel geometry and specific details such as the material of the channel walls or the surfactant used to stabilize the dispersed droplets. Additional complexity of the droplet behavior arises in dense packings of flowing droplets leading to unexpected instabilities and droplet rearrangements [3].

One of the central aims in this project is to analyze and model quantitatively the dynamics of single droplets and droplet packings, and to link it to the external control parameter pressure drop or flow rates of the liquid phases. Preliminary experiments show that surfactants play a key role in the dynamics of isolated droplets [4]. Part of the scattering in the velocity measurements reported in literature may be due to prolonged time scales of surfactant adsorption relative to the time lag between droplet production and velocity measurement. This raises the question whether the instantaneous velocity of droplet in a straight channel of suitable geometry can be employed to determine the surfactant concentration at the interface. This part of the project will rely on a combination of accurate measurement of the droplet velocity in combination with numerical simulations of fluid flow for different boundary conditions at the water oil interface. It will provide additional insights in the stabilization of interfaces beneficial for the project described in section II-9.

Besides velocity measurements we will investi-

gate numerically the visco-capillary relaxation of droplets in microchannels upon hydrodynamic forcing. A number of microfluidic applications require a large volume fraction of the dispersed phase which leads to a spontaneous arrangement of the droplets in the confinement of a microchannel. At sufficiently low flow rates the observed droplet packings will be still close to a local minimum of the interfacial free energy. Viscous dissipation inside the liquid phases and effects of surfactant dynamics comes into play at higher flow rates.

So far, we considered packings of effectively two-dimensional droplets in flat straight microchannels. Figure 1 shows two examples of numerical simulations of droplets flowing in flat (Hele-Shaw) microchannels. This Hele-Shaw geometry has the advantage that the dynamics of the two fluid phases can be well approxi-

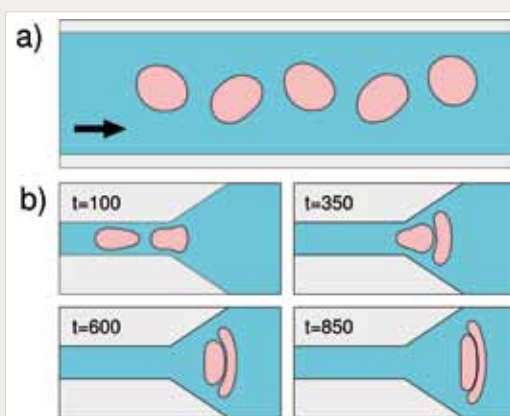


Figure 1

Shapes of monodisperse droplets in flat (Hele-Shaw) microchannels computed using boundary element methods for a fixed flow rate of the continuous phase. a) Train of five droplets at moderate capillary number. The arrow indicates the direction of flow. b) Two droplets entering an elongational flow in a funnel at a higher capillary number. A short ranged disjoining pressure has been added to account for the repulsive interaction between the menisci.

mated by two dimensional Darcy flow. Given appropriate boundary conditions at the interfaces and channel walls, the Darcy equation is solved numerically using boundary elements methods and the droplets are propagated according to the normal velocity at the interface.

Droplet packings in the quasi-static limit of slow flows are obtained from analytical construction and numerical minimization of the interfacial free energy. The mechanical stability of several fundamental single and two-row packings shown in figure 2a) can be represented in terms of a packing diagram, cf. figure 2b). Surprisingly, certain types of packings turn out to be unstable under longitudinal compression and decay into domains of different packings of high and low density. This instability is generically observed not only for trains of droplets in flat microchannels for channels but for various other geometries. This spontaneous separation occurs once the volume of fraction of the dispersed phase falls into the range where the longitudinal compressibility is negative.

One further aim of the project will be to quantify the role of viscous dissipation and compressibility of the dispersed phase on the appearance and stability of different packings under flowing conditions [5]. In addition we will extend our studies to the stability analysis of droplet packings in arbitrary channel geometries.

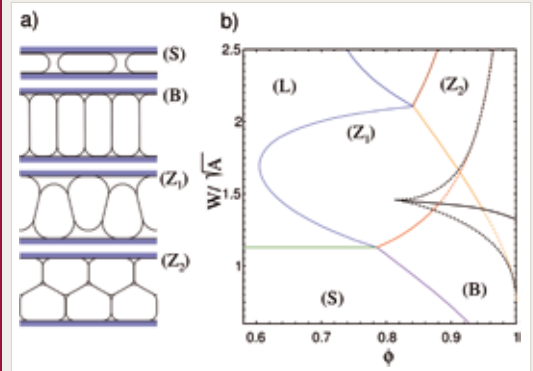


Figure 2

a) Packing of congruent droplets in a flat microchannels: (S) slugs, (L) loose packing, (Z_1) zig-zag packing, (Z_2) staircase packing, and (B) bamboo packing. b) Packing diagram for congruent droplet shapes in terms of the control parameter volume fraction ϕ and rescaled channel width W/\sqrt{A} , where W is the width of a channel and A_d is the area covered by one droplet. The full lines delimit the regions where certain droplet packings are global minima among all possible congruent packings. Crossing a dashed line leads to a decay of a certain packing. More than one stable shape exists in the region bounded by the black dashed lines.

- [1] T.M. Squires, S.R. Quake, Microfluidics: Fluid physics at the nanoliter scale, *Reviews of Modern Physics* **77**, 977-1025 (2005)
- [2] F. Sarrazin, et al., Experimental and numerical study of droplets hydrodynamics in microchannels, *AIChE Journal* **52**, 4061-4070 (2006)
- [3] J.-B. Fleury, et al., Topological transitions in a stack of water droplets, Proceedings of the 2nd European Conference on Microfluidics, Toulouse, December 8-10 (2010)
- [4] J.-C. Baret, et al., *Langmuir* **25** (11), 6088-6093 (2009)
- [5] P. Marmottant, J.P. Raven, *Microfluidics with foams*, *Soft Matter* **5**: 3385-3388 (2009)

V-7 Magneto-microfluidics and Phyllotaxis

J.-C. Baret, E. Bodenschatz

Q. Brosseau, S. H. Tan, M. Pennybacker (University of Arizona in Tucson, AZ, USA), A. Newell (University of Arizona in Tucson, AZ, USA)

FERROFLUIDS ARE colloidal suspensions of magnetic nanoparticles in water or oil stabilized by surfactants. They exhibit fascinating structures in magnetic fields resulting from the balance of magnetic forces that tend to align the dipole moments of the nanoparticles along the field lines and surface tension which tends to guarantee the cohesion of the liquid structure [1].

The control of ferrofluid droplet-droplet interaction by a magnetic field has a rather – a priori – unexpected application in phyllotaxis. Indeed, about 20 years ago, it has been demonstrated that phyllotactic patterns can be obtained using a very simple experimental setup by dripping droplets in the middle of a coil [2]. The insertion of droplets in the middle of the system, the radial advection of the droplets at constant speed (due to the gradient of the magnetic field) and the droplet-droplet short-range repulsive interactions (dipole-dipole interaction) are the sole ingredients required to reproduce the phyllotactic pattern of sunflower (figure 1). In sunflower, primordia are generated in the center of the flower, grow to the edge and their initial position depend on the available space provided by the previous primordia. The ferrofluid experiment reproduces these constraint and leads to similar pattern formation. Only a limited number of experiments have been performed on this topic, with only a few droplets, most of the data available on the patterns being obtained by numerical simulations. Our aim is to perform experiments in order to study the pattern formation in more details. We are indeed interested in the dynamics of the transitions between patterns that can be observed for example by a change in dripping frequency. Such transitions can be observed in plants for example when the growth rate of the plan changes in time. To reliably study the transitions, the patterns should

be clearly obtained which requires a large number of droplets. Microfluidic systems are then a perfect tool to study such a system. Using droplet based microfluidics, we have started to produce droplets of ferrofluid stable against coalescence. We will have access to a large number of droplets (potentially more than 10^4 over a square centimeter as depicted on figure 2). By controlling the frequency of droplet production we hope to see patterns emerging in microfluidics as they appear in the corresponding bulk experiments (figure 1). Here we expect to have a large number of droplets, which will give us access to the pattern rearrangement dynamics that is not accessible in the bulk experiments. This work is in collaboration with Prof. Alan Newell and Matt Pennymaker from the University of Arizona in Tucson.

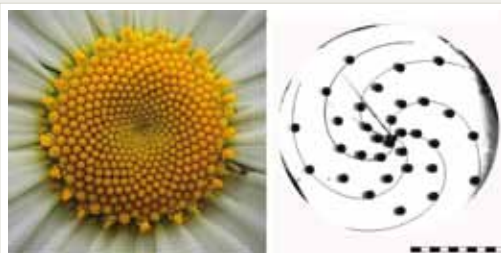


Figure 1

Pattern formation in plants (left) can be explained by a simple model including radial advection of the primordia generated in the center of the flower. The initial position of the primordia depends on the previous primordia by steric repulsion. Analogous model experiments are using ferrofluid droplets (see [5] for a description of the original experiments). Here, in our experiments the droplets are about 1 mm in diameter and are generated in the center of a coil. The magnetic field pushes the droplets to the edge of the device and induces dipole-dipole repulsive interactions between the droplets. Spiral patterns similar to those observed in plants are obtained depending on the dripping frequency.

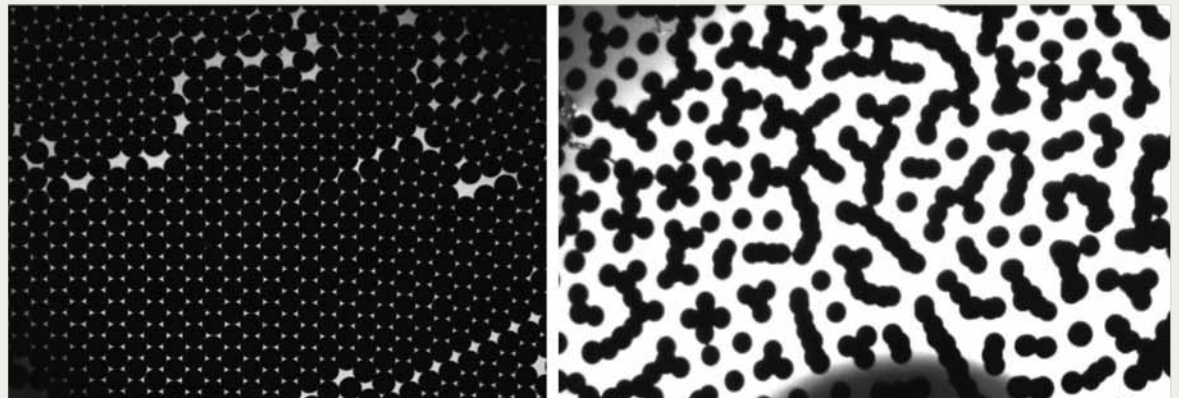


Figure 2

(left) Ferrofluid emulsion produced in a microfluidic device. The droplet size is about 100 microns. The droplets of aqueous ferrofluid are produced by flow focussing (see figure 3) in fluorinated oil and stabilized by a fluorinated surfactant. The droplets are here about 10 times smaller in diameter compared to the droplets of figure 1. In the absence of field, the droplets organize as hexagonal array. In the magnetic field (right), droplets align in the field lines by dipole-dipole attractive interaction leading to other patterns (the orientation of the field has here components both in plane and out of plane).

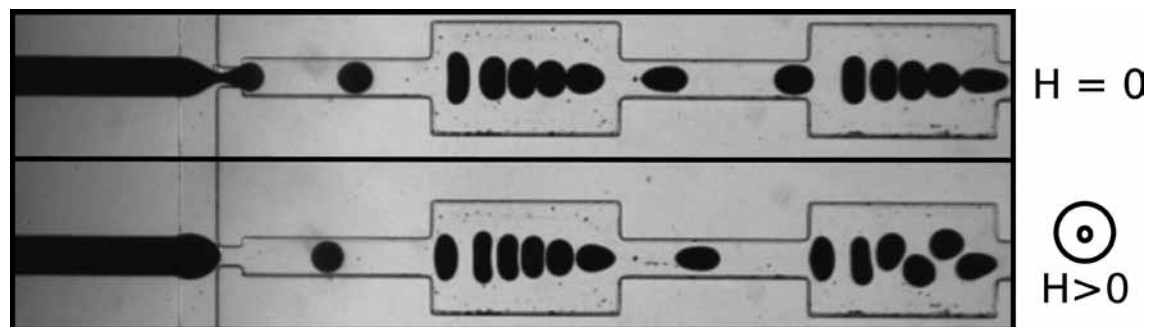


Figure 3

Microfluidic production of ferrofluid droplets without (top) and with (bottom) magnetic field. The magnetic field is oriented outside of the plane of the device leading to repulsive interactions between droplets that can be seen on the separation between droplets in the first expansion and by the change in the droplet arrangement in the second expansion (droplets are 100 microns in diameter).

Ferrofluid droplets are also a versatile model system to probe the behavior of liquid structures in external fields, namely here in a magnetic field. We have started to integrate microfluidic modules to manipulate ferrofluid droplets in microchannels. Electromagnets can be implemented on chip using for example the so-called microsolidics techniques [3] that we already use to manufacture electrodes for electric fields. We plan to pattern electromagnets on the chip to control the orientation of the ap-

plied field or simply use Helmholtz coils to generate uniform fields. Magnetic field is an input to control the interaction between droplets (figure 1 and figure 3). The interaction can be attractive when the magnetic field is applied in the direction of the droplet-droplet axes or repulsive when the field is perpendicular to the droplet-droplet axis. Therefore by choosing the orientation of the field we can tune on-demand the interactions between droplets (figure 3). We want to use this system to study the packing of

emulsions in magnetic field or to probe the hydrodynamic interactions between droplets [4]. We also want to use magnetic field as a micro-manipulator to control droplet-droplet interfaces in order to separate them at different speed to

study droplet coalescence. It has been demonstrated recently that separation of droplet induces coalescence [5] and we will use our magneto-microfluidic system to quantitatively analyze this phenomenon.

- [1] P. Bourgine and A. Lesne, *Morphogénèse, l'origine des formes*. Belin, ISSN 1635-8414 (2006)
- [2] S. Douady and Y. Couder, *Phys. Rev. Lett.* **68** (13), 2098-2101 (1992)
- [3] A.C. Siegel, et al., *Advances Materials* **19** (5), 727 (2007)
- [4] T. Beatus, T. Tlusty and R. Bar-Ziv, *Nature Physics* **2**, 743-748 (2006)
- [5] N.Bremond, A.R. Thiam and J.Bibette, *Phys. Rev. Lett.* **1** (2), 024501 (2008)

V-8 Biophysical Aspects of Biofilm Formation

O. Hallatschek, B. Hof, S. Herminghaus, A.C. Rowat (University of California, Los Angeles), H. Porada (University Göttingen)
N. Podewitz, F. Stiewe, M. Korsten

MOST MICROBIAL species have the ability to attach to surfaces and to form dense multispecies communities that are extremely robust to antibiotics or mechanical perturbations. Gaining control over the formation of such biofilms is of tremendous socioeconomic interest because they are implicated in many diseases and cause significant industrial costs (e.g. through clogging) [1]. The distinctiveness of the biofilm phase was fully appreciated when gene expression data became available, and came as a big surprise to classical microbiology, which had focused on the planktonic or free-swimming microbial phase. While this paradigm shift spurred intensive research efforts to uncover the unique biology of biofilms, still little is known about physical constraints on the formation of biofilms. Yet, we believe that controlling biofilm growth will eventually involve an interdisciplinary effort due an intricate coupling of hydrodynamics, elasticity, fluctuations and population growth. In the following, we present experimental research projects that highlight potential interplays between physics and biology in the formation of dense microbial colonies grown in the lab and of naturally occurring biofilms.

Forces of growth and division

When cells grow and divide to form clusters, colonies or dense tissues, they have to exert forces onto their surroundings. Mechanical stresses are required to create the void necessary to accommodate new cell material. They act upon the extracellular matrix, adhesive and cohesive bonds, and against steric constraints due to confinement. Familiar examples are growing tumors, expanding wings in *Drosophila* or the formation of bacterial colonies and biofilms. These forces of growth and division are an important aspect of both multi-cellular and sin-

gle-celled organisms. They can feedback onto growth either by triggering signaling cascades in mechano-sensing cells or, more directly, by mechanically stalling out cellular proliferation. However, the feedback loop between force and growth remains poorly characterized even in the simplest microbial systems. In part, this is due to the fact that the classical way of cultivating microbes in flasks of liquid media, the batch culture, allows cells to divide in the absence of any mechanical stress. Hence, batch culture studies are “blind” to the effects of mechanical stress.

We have designed an experimental project to measure the (time-dependent) pressures that are generated by microbial cells proliferating in confined geometries under well-defined chemical conditions. This project is funded since 2011 by the German Research Foundation within the framework of a newly established collaborative research center SFB 937. Here, we report on our preliminary experiments.

A key challenge for measuring the microbial population pressure is to constrain the volume available to the population while maintaining a constant biochemical environment. Both challenges could be met by the use of microfluidics. Previous studies have shown [2], that in micro-meter sized bioreactors, diffusion is strong enough to ensure a homogenous supply of nutrients (and removal of waste products) throughout the growth chamber. Hence, microbial growth is limited by the availability of space instead of chemicals. This can be seen in figure 1 where budding yeast cells (*S. cerevisiae*) were trapped and grown in long channels with narrow constrictions on one end. As cells grew and filled the channel, they got jammed and deformed the side walls of the chambers. This effect could be amplified by the addition of small amounts of colloidal particles. The walls of the

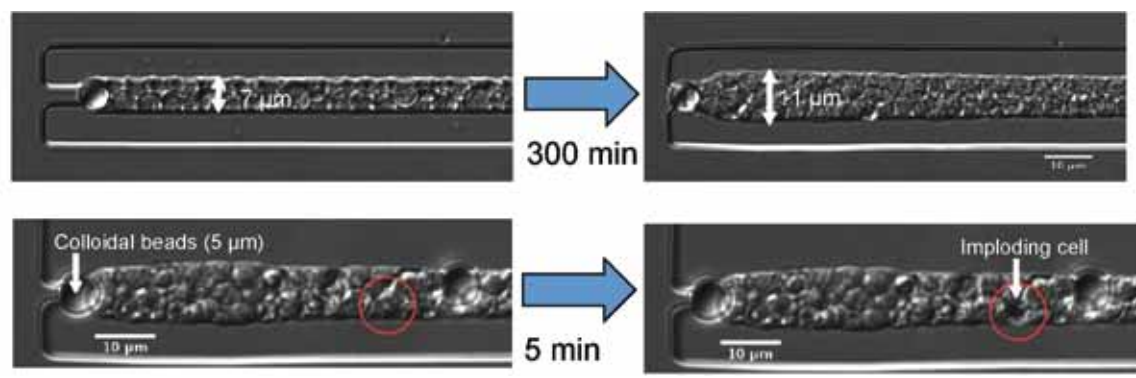


Figure 1

The image documents that growing yeast cells (*S. cerevisiae*) can produce pressures large enough to significantly widen silicone walls of microfluidic channels. The channels (width 10 μm) were seeded by a mixture of yeast cells (*S. cerevisiae*) and colloidal particles (5 μm diameter). As the yeast population expanded, colloidal particles blocked the channel inlets, thereby effectively caging the yeast population. During such blockades, population pressure built up and widened the channels. By comparing the top images, it can be seen that the channel walls are pushed apart by about 10%-20%. Given a Young's modulus of 1 MPa for the wall material (PDMS), this corresponds to a population pressure of 0.1-0.2 MPa. Bottom: The red circle indicates a cell that suddenly deflated in the 5 min time lag between both the times at which both images were taken. This observation demonstrates that the population pressure has a strong feedback onto cellular growth, and might indicate pressure induced apoptosis.

channels in figure 1 were made of Polydimethylsiloxane (PDMS) with a Young's modulus of about 1.2 MPa. From the deformation of the walls of the chamber, we estimate a lower bound on the maximal population pressure of 0.4-0.6 MPa [3]. Note that this population pressure is different from the hydrostatic pressure, as the channels are open on both sides to allow for the exchange of fluids. Our preliminary results demonstrate that the pressures are indeed in the range of the osmotic pressure inside the cells. Furthermore, we found that the cellular growth dynamics is quite markedly influenced by the presence of these (self-generated) pressures. A quite striking manifestation of the feedback mechanism between force and growth is shown at the bottom image of figure 1, which documents the sudden shrinkage of a yeast cell under pressure. At this point, it is not clear, whether these shrinkages follow from a simple balance of forces or whether they are regulated cell death (pressure driven apoptosis [4]).

In the future, we plan to complement our experimental investigations by a theoretical analysis of the non-equilibrium elasticity of growing microbial populations. The goal is to rationalize the measured mechano-chemical character-

istics, and their variation among species. We hope that this combination of theory and experiments will eventually elucidate the role of mechanosensing in the formation of biofilms.

Effect of turbulent and non-turbulent shear on biofilm growth

Biofilms commonly form on the walls of vessels and conduits, such as industrial pipelines and can lead to increased drag as well accelerated corrosion or contamination of the transported liquid. Consequently many studies have been concerned with the formation of biofilms on surfaces under hydrodynamic shear (e.g. [7]). Typically at high shear rates biofilms are found to be more compact and more strongly attached. It has also been observed that under turbulent flow conditions biofilms form filamentous streamers. Typically in these studies flows were laminar at low flow rates and transition to turbulence occurred with increasing velocity. In contrast we here want to carry out experiments at constant Reynolds number (Re) (or alternatively constant wall shear) by making use of the sub critical nature of the transition in pipe and Taylor Couette flows. In either configuration

flows are laminar when unperturbed even at relatively high Reynolds numbers (e.g. in the present pipe set up flows remain laminar for Re in excess of 10000) if on the other hand the flow is disturbed the motion will be turbulent. Hence we can realize flows which are laminar or turbulent both with identical wall stress (on average). We hope that this study will clarify if the structural differences reported for biofilm formation are caused by the action of turbulence or simply by the increased shear. It is possible that turbulent fluctuations are more efficient in detaching microbial colonies than a steady shear. On the other hand turbulence strongly enhances mixing which in turn may improve the nutrient supply.

In pipes wall stresses can be directly determined from pressure drop measurements. Pressure drops are proportional to the inverse of the diameter to the fourth power. This makes pressure measurements also a highly accurate way to determine the effective pipe diameter, i.e. the diameter minus the biofilm thickness. This method can therefore be used to determine the thickness of the grown biofilms and we have tested this in a water flow through a 4 mm pipes where after two days a 10 micron bio-

film had formed. Furthermore we observed the formation of streamers (a streamer formed in a microfluidic device at low Re is shown on the left hand side of figure 2) at non smooth pipe junctions which at large enough Re ($Re > 2800$) was found to trigger transition to turbulence.

Fossile biofilms: *Kinneyia* and the emergence of cellular mechano-sensing

Biofilms may as well be found in fossile forms. A widespread facies is the so-called *Kinneyia*, which is characterized by a well developed undulation of its surface. It occurs in formerly littoral or limnic settings, from the Ediacaran (about 600 Ma b.p.) to the Jurassic [5]. A glance at the details of this pattern suggests to interpret it as the result of a dynamic instability in the film. The wavelength is of the same order as a typical thickness of a modern littoral biomat (few millimeters). It decreases significantly towards the rim of the fossile, suggesting a monotone relation between the wavelength and the local thickness of the mat. It has been reported that biofilms behave physically like viscoelastic materials, with an astonishingly universal relaxation time of about 18 minutes [6]. It is clear that a viscoelastic film on a substrate which is subject to a flowing liquid above will undergo a Kelvin-Helmholtz-instability, resulting in a surface undulation with a wavelength of about 3 times the film thickness. Since microbial mats easily reach thicknesses of a few millimeters, this model is at least in principle capable of explaining the observed structures.

However, there is an interesting problem with this interpretation: if it is true that modern microbial mats are just viscoelastic media, *Kinneyia*-like undulations would have to be encountered on modern microbial mats as well, wherever they are subject to, e.g., occasional tidal or seasonal currents. Such undulations, however, are not observed. One must thus conclude that while modern microbial mats may appear as viscoelastic media for some standard measurement devices, they actually respond in a more complex fashion to external stress. An



Figure 2

Left: A “streamer” biofilm formed at a corner in a micro channel. These experiments were carried out in a 50 micron wide channel at low Reynolds numbers and we observed streamer formation for *E. coli* bacteria as well as *Bacillus subtilis*. Right: A fossile biofilm, about 545 Ma old (Ediacara; Nama group, Schwarzrand Subgroup, Vingerbreek member, Namibia). The characteristic undulation pattern of these fossiles called ‘*Kinneyia*’ is so far unexplained, but might be the result of a Kelvin-Helmholtz instability caused by the onset of flow in the aqueous (limnic or littoral) environment of the live biofilm.

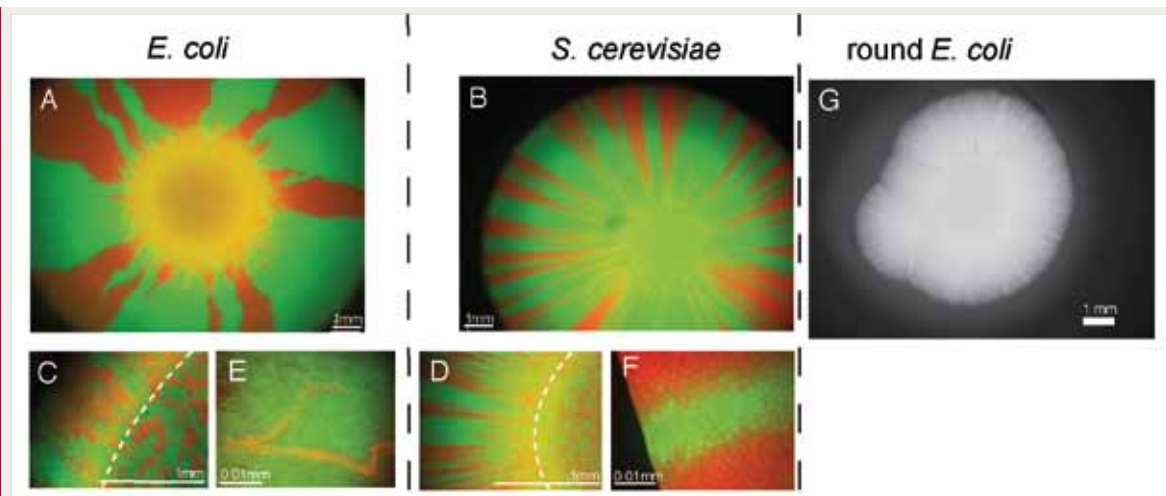


Figure 3

Segregation patterns of two different microbial species are qualitatively similar but different in detail. (A and B) Both bacteria (*E. coli*) and yeast (*S. cerevisiae*) colonies exhibit spatial gene segregation when they grow colonies on agar plates. However, the number of (surviving) sectors is much larger in yeast colonies. (C and D) Continuous patches of boundary regions and homeland (bounded by dashed line) at a magnification of 51x for *E. coli* (C) and yeast (D). (E and F) Images at single-cell resolution (100x). (E) Tip of a sector dies out (*E. coli*). (F) Section boundary at the frontier (yeast). (adapted from Hallatschek et al. (2007)). (G) Round *E. coli* mutants (*mreB* deletion) give rise to striped patterns very similar to the yeast case, suggesting that cell shape is controlling the roughness of domain boundaries.

active mechanical response to stress is abundantly known from living cells, which as well appear as purely viscoelastic at first glance. The evolutionary benefit of such active response in the case of biomats is obvious: the Kelvin-Helmholtz undulation destroys the mutual relation of cellular neighborhood as well as the material internal transport system of the mat, which it will hardly survive. A mechanical response which is capable of sidestepping the Kelvin-Helmholtz instability would thus open up the whole range of flowing waters as possible new habitats. In fact, modern biomats are found in strong flow, such as rivers and mountain creeks, as well as tidal currents.

A direct interpretation of the above reasoning is that *Kinneyia* is a witness of the emergence of mechanosensing in early cellular organisms. According to this idea, biofilms in the ediacara were in fact physically completely equivalent to passive viscoelastic films, such that every seasonal change or tectonic event leading to a change in current patterns would lead to the dy-

namical surface instability, thus to the destruction of the mat and to the formation of the fossile. We are now conducting experiments and simulations on Kelvin-Helmholtz instabilities of viscoelastic films under flow. One goal is to generate the fossile facies by providing an appropriate sedimental load to the flowing aqueous phase. Furthermore, we will repeat these experiments with live biomats the mechano-sensing of which has been knocked out, in order to see whether this leads to the (expected) formation of the undulations under flow. In parallel, we perform simulations of flow on active pseudo-viscoelastic media in order to learn how the instability can be circumvented in a real setting.

Sectoring within biofilms: differences between species

Fluorescence imaging techniques are ideal to study basic aspects of the microbial colony formation, as they allow tracking lineages in a growing population. In this way, we could show that the appearance of organization in biofilms

can emerge without active coordination [8]. That is, familiar biofilm properties such as phenotypic differentiation or species stratification [1] do not necessarily require that cells communicate with one another using specialized signaling molecules. Instead stochastic number fluctuations decompose the biofilm into compartments called sectors. A phenomenological theory was formulated to predict the mesoscopic consequences of this effect [9, 10].

A biophysical explanation of the surprising strength of these stochastic fluctuations, and their variation among species, is still lacking. In an ongoing project, we are testing whether the difference between patterns observed in bacteria and yeasts is due to the difference in shape. Whereas *S. cerevisiae* is spherical and grows by budding, *E. coli* is rodlike and grows by elongation and subsequent equatorial division. As a consequence *E. coli* has the tendency to form “streets” of aligned bacteria on a plate. From an initially isotropic mixture of cells, these

streets will bump into one another until the frustration is released by buckling events. Our hypothesis is that the kink-like structures in figure 3 are actually a microscopic footprint of these buckling events, and cause the vigorous random wandering of domain boundaries in *E. coli* colonies. To investigate this hypothesis directly, we are repeating the competition experiments using spherical *E. coli* (*mreB* mutants and A22-induced) and rodlike yeasts (*S. pombe*). Figure 3 G displays preliminary results for a competition experiment with round *E. coli* mutants. Notice that, consistent with our cell shape hypothesis, the genetic patterns is very similar to the striped pattern of *S. cerevisiae*. Our goal for the future is to understand the roughness as a function of cell shape quantitatively. In particular, we expect to find the domain boundary roughness is set by a characteristic microbial “street” length, which results from the competition of adhesion forces (favoring alignment) and excluded volume interactions (favoring buckling).

- [1] P. Watnick and R. Kolter. *Biofilm, city of microbes*. *J. Bact.* **182** (10), 2675-2679 (2000)
- [2] Alex Groisman, Caroline Lobo, Hojung Cho, J Kyle Campbell, Yann S Dufour, Ann M Stevens, and Andre Levchenko, *Nat. Meth.* **2** (9), 685–689, (2005)
- [3] Nils Podewitz. Diploma thesis in Physics, Göttingen University, (2011)
- [4] J. Ranft, M. Basan, J. Elgeti, J.F. Joanny, J. Prost, and F. Jülicher, *Proceedings of the National Academy of Sciences* **107** (49), 20863 (2010)
- [5] H. Porada, J. Ghergut, and E.H. Bouougri, *Palaïos* **23** (2), 65 (2008)
- [6] T. Shaw, M. Winston, C. J. Rupp, I. Klapper, and P. Stoodley, *Physical Review Letters* **93** (9), 98102 (2004)
- [7] P. Stoodley, R. Cargo, C.J Rupp, S. Wilson, and I. Klapper. Biofilm material properties as related to shearinduced deformation and detachment phenomena. *J. Ind. Microbiol. Biot.*, **29** (6), 361–367 (2002)
- [8] Oskar Hallatschek, Pascal Hersen, Sharad Ramanathan, and David R Nelson, *P. Natl. Acad. Sci. USA*, **104** (50), 19926–19930 (2007)
- [9] Oskar Hallatschek and David R Nelson, *Theor. Popul. Biol.* **73** (1):158–170 (2008)
- [10] O. Hallatschek and D.R. Nelson, *Evolution*, **64** (1), 193–206 (2010)

V-9 Evolutionary Dynamics: The Speed of Adaptation

E. A. Martens, F. Stiewe, O. Hallatschek

EVOLUTIONARY THEORY tries to explain how the organized complexity of today's biosphere may have arisen over time. This puzzle was resolved in principle by Charles Darwin who showed that continual adaptation (inevitably) arises due to heritable variation and natural selection. But is Darwinian evolution by small adaptive steps fast enough to explain, for instance, the evolution of a wing, an eye, a brain or Human social behavior in 3 billion years of evolution after the first cell emerged? Not even our largest computers implementing the most complex evolutionary scenarios are getting close to a realistic simulation of Darwinian evolution over such long time scales.

Biological evolution shares its long term unpredictability with other complex nonlinear stochastic systems, such as human economies, social structures, the nervous system or the climate. For instance, it is impossible to predict the weather in one year's time, even though we know, and have tested, the governing laws (e.g. the Navier-Stokes equation) to an excellent degree. However, computer models can predict the weather on short times extremely accurately. Similarly, evolutionary theorists are in search of models of "microevolution", that allow predicting the course of evolution on short times in simple systems.

Microevolution is usually studied under fairly restrictive assumptions that are rarely realized in nature. The following project, which combines a model with a concrete evolution experiment, tries to break with one of the most crucial restrictions in order to achieve a more accurate description of natural populations.

Adaptation by the continual accumulation of beneficial mutations

Suppose a population well-adapted to one environment suddenly has to face a harsher, or unseen, environment. How fast will the popu-

lation adapt to the new environment? From the genetics point of view, two phases must be distinguished: First, there will be a rather quick adaptive response due to pre-existing genetic variation in the population. If prior to the change in environment the population exhibits some variation in a trait that is strongly selected in the old environment, then the better adapted among the pre-existing phenotypes will leave more offspring in the next generation, and thus increase in abundance. This mode of adaptation will slow down, however, after the initially existing variation (also called standing variation) has dissipated. On long time scales, then, adaptation must proceed by the accumulation of new beneficial mutations that spontaneously arise after the environmental change. This second much slower phase of adaptation has been studied extensively in controlled microbiological evolution experiments [1]. Amongst others, these experiments have revealed two very different dynamical scenarios for the accumulation of new beneficial mutations [2]. In the simplest case, adaptation is mutation limited: the population "waits" most of the time for a new beneficial mutation to arise. Once a beneficial mutation has arisen and become sufficiently frequent, it will expand deterministically until it is present in all individuals of the population. After the completion of such a sweep, the population is stationary again until the next beneficial mutation arises. The accumulation rate of beneficial mutation is, hence, controlled by the rate of appearance of new beneficial mutations, which is proportional to the population size and the mutation rate. Notice however that this regime of "periodic selection" requires sufficiently small population sizes. For large populations, beneficial mutations do not appear strictly sequentially. Instead, multiple beneficial mutations will be present on different genetic backgrounds simultaneously and compete with one another for

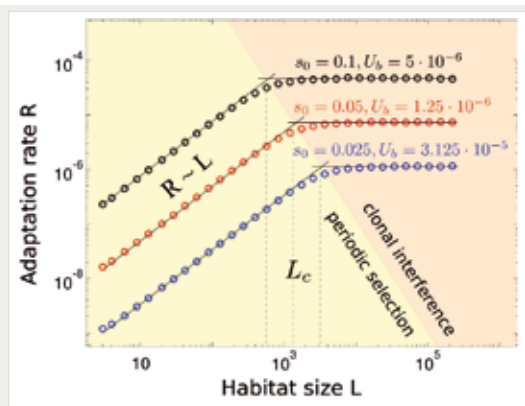


Figure 1

Speed limit of evolution for large habitats. The adaptation rate R (fixation rate of beneficial mutations) grows linearly with the habitat size L in the periodic selection regime. When the habitat size exceeds a crossover length L_c the adaptation rate saturates completely due to clonal interference. The characteristic length L_c measures the typical size of clones when they first “collide”. Simulations are run for a linear habitat, with exponentially distributed selective advantages s and wave speeds equal to the deterministic Fisher wave speed.

sweeping through the population. In population genetics terms: multiple “clones” are present in the population and “interfere”. Clonal interference generally leads to a reduction in adaptation rate because beneficial mutations are often lost if they appear on an unfavorable genetic background. Nature has found an elegant way around clonal interference by the invention of sex and recombination, which allows beneficial mutations to be combined on a single genetic background even if they appeared on different ones. Hill and Robertson proposed this argument as the primary reason for why sexual reproduction is so wide-spread in multi-cellular organisms.

In recent years, extensive efforts have been spent to replace a purely verbal description of clonal interference by a quantitative theory of the speed of adaptation [3–6] that could be compared with experiments [2]. A major limitation of the resulting models is, however, that they apply only to well-mixed populations. The key difference between spatially extended and well-mixed populations is that beneficial muta-

tions spread through spatially structured systems in the form of waves, first described by R. A. Fisher [7]. Adaptation by Fisher waves leads to important qualitative and quantitative differences for the speed of adaptation in a spatially extended population, as we find in an on-going theoretical study: First, viewed as a function of system size, we find a strict speed limit of adaptation, when clonal interference becomes important, see figure 1. This contrasts strongly with the well-mixed case, where the adaptation rate never reaches a plateau due to a logarithmic dependence on system size. On the other hand, we find that in the clonal interference regime, beneficial mutations accumulate at a rate that scales as $(\mu p)^{1/(d+1)}$ in d dimensions, where μ and p are mutation rates and population densities, respectively. This dependence on mutation rates is much stronger than predicted logarithmic dependence for the well-mixed case, and should be testable in the experiments described below. Finally, we could show that spatial mixing can strongly suppress clonal interference: Small amounts of long-range migration lead to a significant speed up of adaptation. The underlying reason is that reduction in spatial structure shortens fixation times in a population and hence reduces amounts of clonal interference. In fact, mixing will lower fixation times in the presence of any kind of structure be it due to spatial extend, age difference, environmental heterogeneities or other differentiating forces. This general mechanism has lead us to hypothesize that whatever improves mixing in structured populations is selectively favored in the clonal interference regime. The evolutionary biology of structured populations, in particular biofilms but also tumors, should be revisited in light of this “extended Hill-Robertson” hypothesis.

Preliminary Experiments

Microbes, like bacteria and yeast cells are the ideal testing ground for microevolutionary theories, as they allow evolution to be observed as it is happening in the lab. Since microbes are small and have

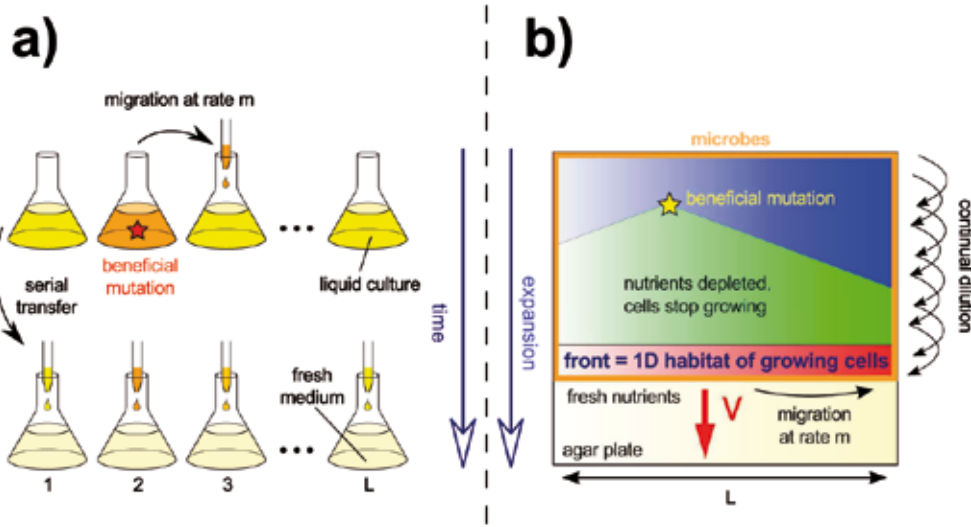


Figure 2

Two ways of realizing a continual evolution experiment in one spatial dimension. a) A classical serial dilution experiment. Microbes are grown in separate flasks (demes) in liquid culture. Each day, a certain amount of cells from an overnight culture is transferred to fresh medium. Migration between demes is achieved by cross-transfer. In flask 2 a beneficial mutation has just occurred and partially swept through the deme. By migration and differential growth (natural selection), this mutation can spread through the whole population. b) Our setup for a spatial evolution experiment is based on microbial colony growth. Microbes are inoculated along a line at the top of the agar plate, and the population is allowed to expand downwards. The expansion velocity v depends, amongst others, on the growth rate of the active cells (red). In the upper part a beneficial mutation occurred and spread linearly through the habitat.

short division times on the order of 20 minutes to hours, it is possible to evolve billions of microbes over thousands of generations in small flasks of liquid media. The most famous of these experiments, due to Richard Lenski, now runs for over 20 years and has recently completed 50,000 microbial generations [1]. In Lenski's experiment, bacteria normally grown in rich media adapted to grow in minimal media, in which only one carbon source is provided (10% glucose). Over the course of the 23 years since the beginning of the evolution experiment, the bacteria have accumulated a growth rate increase by about more than 70%.

The continual evolution of well-mixed microbial populations such as in the Lenski experiment has produced a large number of valuable insights into the dynamics of adaptation, but these experiments are blind to the effects of spatial structure. Testing evolutionary models that include spatial degrees of freedom requires a novel experimental setup. The simplest way of maintaining spatial structure in a population of microbes is grow-

ing them on a surface. Agar plates are an ideal system for this purpose, since growing microbial colonies on agar plates is a cheap standard lab technique. Moreover, wherever the nutrients in the agar plate are depleted, cells stop dividing. For this reason only the outer boundary – the “front” – of the colony consists of actively growing cells. So the front is the actual habitat, which can be considered effectively one-dimensional, since it is typically very thin (80 μm in the case of *E. coli* [8]). The inner region of the colony does not change over time and therefore represents a “fossil” frozen time record of the colonization process. The speed at which the front moves forward into new territory provides a measure for the mean fitness of the cells within the active layer.

The idea of our experiment is illustrated in figure 2. A population of microbes is inoculated on one side of a long rectangular agar plate of width L . As the population of microbes grows over the surface, we monitor the velocity of the expanding edge. An increase in expansion velocity reflects adapta-

tion of the front population: Mutations accumulate at the expanding edge if they confer an increase in the expansion velocity. This experimental setup can be viewed as the continual evolution of the thin band of “pioneers” at the expanding frontier (of the growing microbial population). As the population expands, its front population is subject to continual dilution and growth. In effect, the band of pioneers evolves as in a quasi-one-dimensional chemostat.

We have recently analyzed the dynamics of single selective sweeps in expanding microbial colonies [9]. We have shown that sweeping beneficial mutations give rise to sectors in the wake of the expanding population, whose opening angle is reflective of the selective advantage they confer, see figure 3 (left). Using these techniques, we plan to sensitively measure the difference in expansion velocity between the derived and

ancestral strains and to visualize the effects of clonal interference, c.f. figure 3 (right).

Our experimental system has several parameters that can be manipulated without difficulty: By comparing strains with strongly increased mutation rate (mutators) with wild type strains, as well as varying the width of the agar plate (i.e., the size of the one-dimensional habitat), we will test whether the speed of adaptation in our setup indeed follows the predicted square root scaling. Our experimental setup opens the door to a number of further tests of evolutionary theory. For instance, we will investigate adaptation to heterogeneous environments by imposing gradients of antibiotics in the agar substrate. By increasing mutation rates (genetically, chemically, or by radiation), we plan to measure critical mutation rates, at which adaptation stops altogether due to genetic melt-down (also called error threshold).

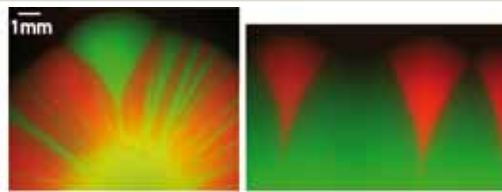


Figure 3

Beneficial mutations give rise to sectors with unusually large opening angles. left: This colony of yeast (*S. cerevisiae*) was grown from a 5:1 mixture of CFP (red) and RFP (green) labeled cells. The large funnel-like green sector, which arose spontaneously, outgrows both wild type strains. right: A linear inoculation of a mixture of a CFP (red) strain that has a beneficial mutation compared to an otherwise neutral RFP (green) strain. The resulting sectors of CFP mutants have similar shape and are well separated, due to the small ratio (1:40) of mutant to wild type

- [1] J. E. Barrick, D. S. Yu, S. H. Yoon, H. Jeong, T. K. Oh, D. Schneider, R. E. Lenski, and J. F. Kim. *Nature*, **461** (7268), 1243–7 (2009)
- [2] P.J. Gerrish and R.E. Lenski, *Genetica* **102**, 127–144 (1998)
- [3] I.M. Rouzine, J. Wakeley, and J. M Coffin, *Proc. Natl. Acad. Sci. USA* **100** (2), 587–92 (2003)
- [4] S.C. Park and J. Krug, *Proceedings of the National Academy of Sciences* **104** (46), 18135 (2007)
- [5] M. M. Desai and D. S. Fisher, Beneficial mutation selection balance and the effect of linkage on positive selection, *Genetics* **176** (3), 1759 (2007)
- [6] O. Hallatschek. *Proc Natl Acad Sci.*, **108** (5), 1783 (2011)
- [7] R. A. Fisher, *Annals of Eugenics* **7**, 355–369 (1937)
- [8] O. Hallatschek, P. Hersen, S. Ramanathan, and D. R Nelson, Genetic drift at expanding frontiers promotes gene segregation, *P. Natl. Acad. Sci. Usa* **104** (50), 19926–19930 (2007)
- [9] O. Hallatschek and D.R. Nelson, *Evolution* **64** (1), 193–206 (2010)

V-10 Transition to Turbulence in Shear Flows

B. Hof

K. Avila, A. deLozar, Liang Shi, M. Avila, D. Barklye (University of Warwick)

SOME OF the fundamentally most important shear flows, such as pipe, channel, Couette and boundary layer flows become turbulent although the laminar state is linearly stable. The transition process occurring in these flows has turned out to be much more complicated than in linearly unstable situations like Rayleigh Bénard convection or Taylor Couette flow. Because of its fundamental and practical importance pipe flow is the probably most prominent example amongst those linearly stable shear flows. Even for this simple geometry it has not been possible to clarify some central and seemingly simple questions regarding how turbulence first arises. It has already been noted in the pioneering study of Reynolds [1] that turbulence does not arise through a linear instability and that the perceived transition point strongly depends on disturbances present in a given set up. Following these observations Reynolds postulated that a ‘real critical point’ exists below which flows will always return to laminar even if subject to a strong perturbation initially. The existence of such a critical point was the basis of the Reynolds number concept introduced in his 1883 paper [1]. In a subsequent attempt to determine the exact value of this transition point Reynolds introduced the so called ‘Reynolds decomposition’ [2] which is widely regarded as the starting point of modern turbulence research, however the method was unsuccessful in determining the critical point. Even in the following 125 years it has not been possible to resolve its value or the nature of the transition process.

We here apply a combined experimental and numerical approach to obtain a general understanding of the transition in these shear flows. While in direct numerical simulations we can study quantities not accessible in experiments, experiments allow long observation times that cannot be re-

alized in simulations. An important aspect of our work is to compare the transition processes in different flows in order to identify universal aspects. In particular experiments and direct numerical simulations are carried out for pipe, Couette, Taylor Couette, duct and channel flow.

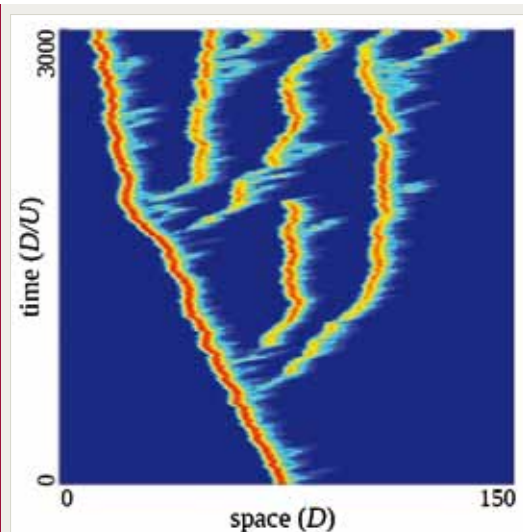


Figure 1

Space time plot showing the streamwise vorticity squared in a numerical simulation of pipe flow in a 150D long domain starting with a single puff which over time splits into multiple one leading to an overall increase in the turbulent fraction.

In order to establish if turbulence becomes sustained at a critical point as postulated we separated decay from growth processes. Starting from a localized spot (or ‘puff’) of turbulence, which is the typical flow structure at transitional Reynolds numbers, we investigated if the turbulent fraction increases or decreases over time. Although such a study may appear simple at first sight it is greatly complicated by the fact that turbulent spots are transient and decay after extremely long times with decay times increasing faster than exponential with Re . In de-

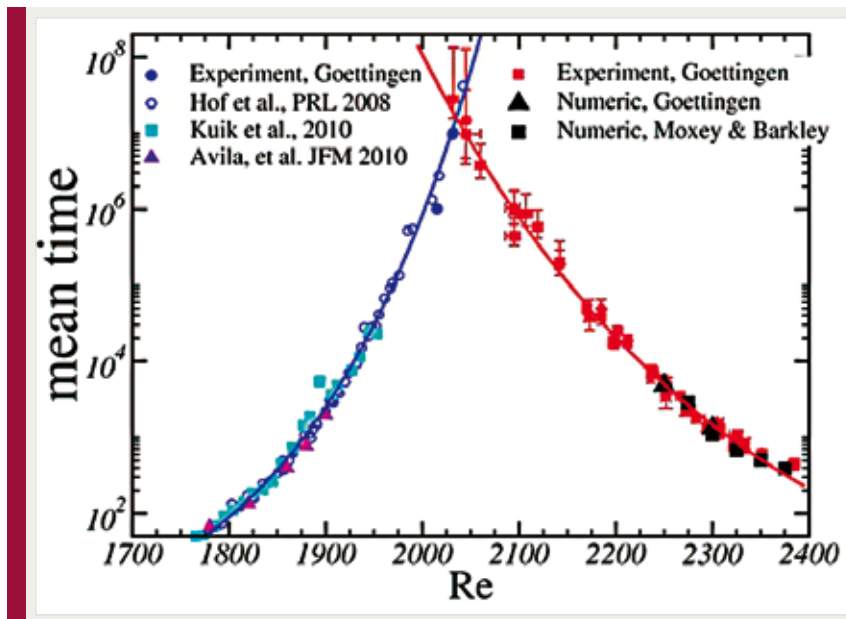


Figure 2

Decay vs. growth. The left branch shows the median times for the memoryless decay of turbulent puffs/spots in pipe flow. The right branch gives the median times for the memoryless growth. The crossing at $Re \approx 2040$ marks where structures grow faster than they decay and turbulence eventually becomes sustained.

tailed studies we have been able to show that this transient nature is intrinsic to turbulence and that despite the very fast increase of lifetimes there does not appear to be a critical point where this lifetime becomes infinite [3-6]. The circumstance that individual spots are transient does not necessarily mean that the entire flow will return to laminar. Other mechanisms have to be taken into account and it turns out that turbulent spots also have tendency to nucleate new ones (see figure 1) and that the rate at which new spots occur increases with Re . Indeed as for lifetimes also the spreading of turbulence follows a Poisson process. This circumstance allows us to resolve the extremely small probabilities for decay as well as spreading in the transitional regime. The balance point between the two competing processes (see figure 2) marks the critical Reynolds number [7] where turbulence first becomes sustained in accord with Reynolds proposition. The sustainment of turbulence here is a consequence of the increasing spatial complexity and in contrast with the classical view that turbulence arises purely from an increase in temporal complexity (as proposed by Landau and Ruelle-Takens). In order to clarify if the same transition process observed in pipe flow also holds in other linearly stable shear flows we carry out experiments

and simulations for Couette, duct and channel flows. Here equally critical points can be measured as a competition between decay and spreading processes. In a first study we have already shown that turbulent spots in channels and ducts also exhibit a memoryless decay (figure 3). However differences may arise in channel and Couette flow due to the additional spanwise dimension which as such is not present in pipes and square ducts. Some propositions have been made that due to the spanwise width the transition may change from a second order to a first order non-equilibrium phase transition. Investigations are underway in our group and a first study of plane Couette flow suggests that here the critical point can be determined in the same manner as in pipe flow.

The stochastic nature of the transition process in these flows is akin to critical phenomena in model systems such as coupled map lattices and directed percolation. These systems display scale invariance at the critical point and are characterized by universal critical exponents. Having developed a method to determine critical points for the onset of turbulence in shear flows offers a unique opportunity to elucidate the very nature of the transition process and to probe if it is equally characterized by universal exponents.

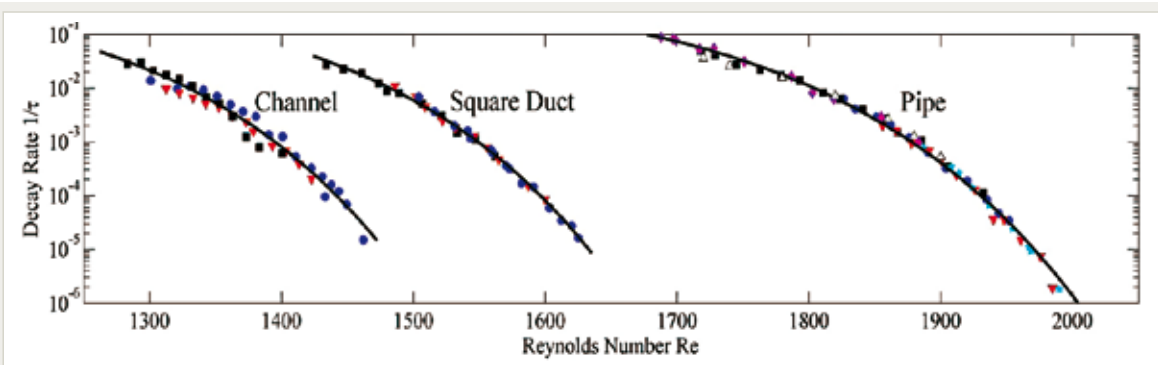


Figure 3

Decay rates of turbulent spots in channel (aspect ratio of 25), square duct and pipe flow. In all three cases lifetimes increase super-exponentially.

- [1] O. Reynolds, *Phil. Trans. R. Soc. London A* **174**, 935-982 (1883)
- [2] O. Reynolds, *Phil. Trans. R. Soc. London A* **186**, 123-164, (1895)
- [3] B. Hof, et al. *Nature*, **443**, 05089, pp 59-62. (2006)
- [4] B. Hof et al. *Phys. Rev. Lett.* **101**, 214501 (2008)
- [5] A. de Lozar, B. Hof, *Phil. Trans. R. Soc. London. A* **367**, 589 (2009)
- [6] M. Avila, A. Willis, B. Hof, *J. Fluid Mech.* **646**, 127 (2010)
- [7] K. Avila, D. Moxey, A. de Lozar, M. Avila, D. Barkley, B. Hof, *Science* (accepted)

V-11 Data Driven Modeling of Cardiac Dynamics and Model Evaluation

S. Luther

U. Parlitz, A. Squires, P. Bittihn, D. Hornung, J. Schroeder-Schetelig, T. Baiq, S. Berg, J. Schumann-Bischoff, N. Raad, S.E. Lehnart (University Medicine Göttingen), F.H. Fenton (Cornell), E.M. Cherry (Cornell/RIT)

THE DEVELOPMENT of detailed physiological models of the heart, the availability of large quantities of high-quality structural and functional experimental data, and ever-increasing computational power have significantly enhanced the understanding of cardiac dynamics and hold the promise of new clinical applications for diagnosis and treatment of heart disease [1]. However, the systematic integration of experimental data into high-dimensional, multi-scale models and their subsequent evaluation, validation and analysis remains a major challenge. Therefore, we are developing a data driven, integrative strategy that combines high-resolution imaging techniques with state of the art numerical modeling through innovative state estimation methods. Within this approach, model evaluation plays an important role for the validation and the selection of model complexity on all relevant scales from subcellular, cell, tissue to organ and organism level. The models will be used to study genetic and environmental factors contributing to initiation, perpetuation and termination of cardiac arrhythmias. In the following, we will briefly describe the experimental techniques used to characterize detailed anatomical structure and high-resolution spatial-temporal dynamics of the heart, the available mathematical models, and provide examples of state and parameter estimation.

High-resolution Cardiac Imaging

Physiological cardiac modeling requires detailed structural, functional, and dynamical characterization of the heart. The MPRG Biomedical Physics develops high-resolution fluorescence imaging techniques (optical mapping) for intact, Langendorff-perfused hearts (see figure 1). Techniques from computer vision research are applied to reconstruct the three-dimen-

sional shape of the heart from multiple silhouettes. We combine optical mapping with motion tracking, which permits, for the first time, fluorescence imaging of contractile, moving cardiac tissue. This unique experimental technique enables the simultaneous measurement of membrane voltage, intracellular calcium, and surface strain. The dynamical characterization of cardiac tissue is based on the restitution relations of action potential duration and conduction velocity, obtained from optical mapping. This functional data is complemented by structural information, including coronary vasculature and fiber orientation obtained from micro-computed tomography, diffusion-tensor magnetic resonance imaging, and histological data. Measurements on cellular and subcellular level, including patch clamp, sharp electrode patch, and STED microscopy, are available through our research partners and complement the experimental techniques developed by the MPRG Biomedical Physics.

Mathematical Modeling of the Heart

We are using mathematical models of cardiac tissue with various levels of complexity, ranging from generic to detailed physiological descriptions. The choice of the model depends on the specific problem at hand. Generic models play an important role for the understanding of fundamental principles of excitable media. For example, we have used generic models to explore the nonlinear dynamics underlying the interaction of rotating waves with heterogeneities. However, generic models do not permit to elucidate the molecular basis of cardiac function. The Fenton-Karma model has the minimal ionic complexity necessary to reproduce essential qualitatively characteristic dynamical properties of the system [2], while being computationally

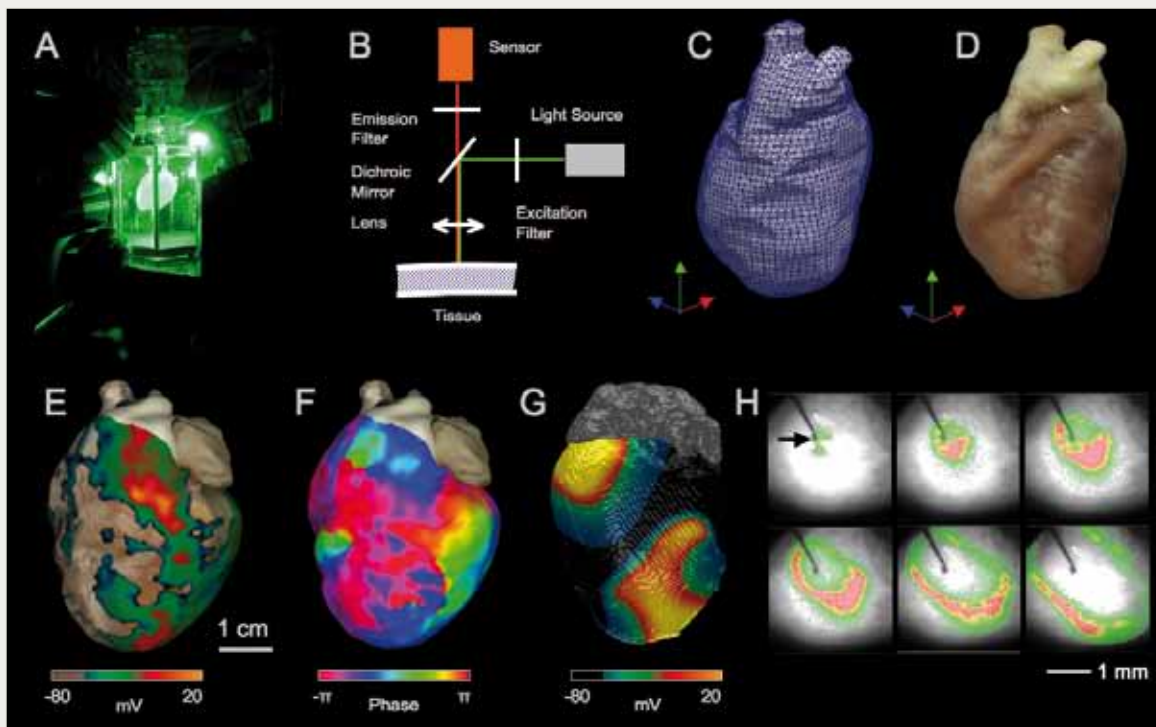


Figure 1

(A) High-resolution optical mapping of intact, Langendorff-perfused rabbit heart. (B) Schematic of the imaging setup. (C,D) Reconstructed 3D surface of a rabbit heart (C) with photorealistic texture mapping (D). (E) Complex spatio-temporal wave dynamics during ventricular fibrillation (VF). (F) Phase map during VF indicating phase singularities. (G) Numerical simulation of VF using the Fenton-Karma model [2] adapted for rabbit ventricle. (H) Pacing experiment on mouse ventricle is used to obtain action potential and conduction velocity restitutions under physiological and pathological conditions [3].

efficient. In contrast, physiological models aim at a detailed quantitative description of cellular physiology. However, model selection and the reliable estimation of model parameters from experimental data is utmost difficult. We focus on *in silico* modeling of different Na^+ and Ca^{2+} transport dysfunction and their role in arrhythmia onset and perpetuation. The numerical models are implemented using finite differences and parallelized using the message-passing interface (MPI). Irregular tissue boundaries are implemented using the phase field method, an elegant approach to satisfy no-flux boundary conditions on arbitrary geometries [4].

State and Parameter Estimation

While physical models often can be derived from first principles, they may contain parameters whose values are not or only partially known and may depend on the physical con-

text. To identify these parameters, the model may be adapted to experimental data. Here both (unknown) parameters and model variables have to be adjusted, including hidden (i.e. not observed) state variables determining the temporal evolution of the model. For some applications this adaption has to be continuously updated to “track” some process by continuously incorporating measured data into the model (a procedure called *data assimilation* in geosciences and meteorology). To accomplish the task of parameter estimation we employ synchronization and nonlinear optimization methods. With the synchronization approach [5] the available time series is used to drive a simulation model in order to achieve (generalized) synchronization. The synchronization error depends on the model parameters and attains a global minimum if they coincide with the “true” values holding for the experimental system. As

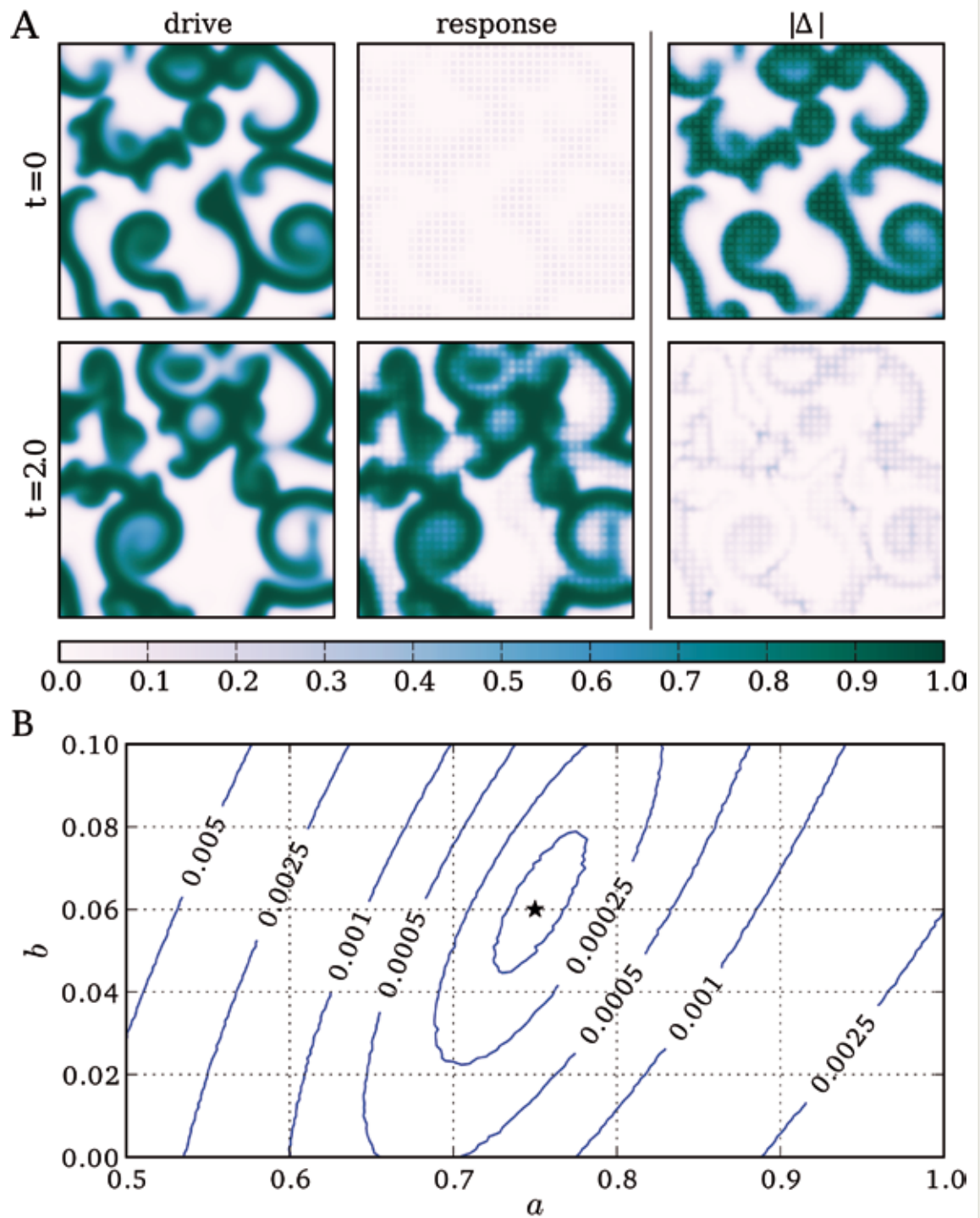


Figure 2

Synchronization-based state and parameter estimation of a chaotic 2D Barkley model ($a=-0.75$, $b=0.06$, $\varepsilon=1/12$). (A) Snapshots of the solution of the driving and response systems as well as their differences are plotted in columns 1-3, respectively. The first row shows conditions at $t=0$, i.e. when coupling is applied. The second row shows solution at $t=20$, when synchronization has almost been reached (from [7]). (B) Contours showing the Eukclidean norm of the synchronization error if the parameters a and b of the Barkley model of the response system do not match those of the driving system. The star indicates the minimum of the synchronization error.

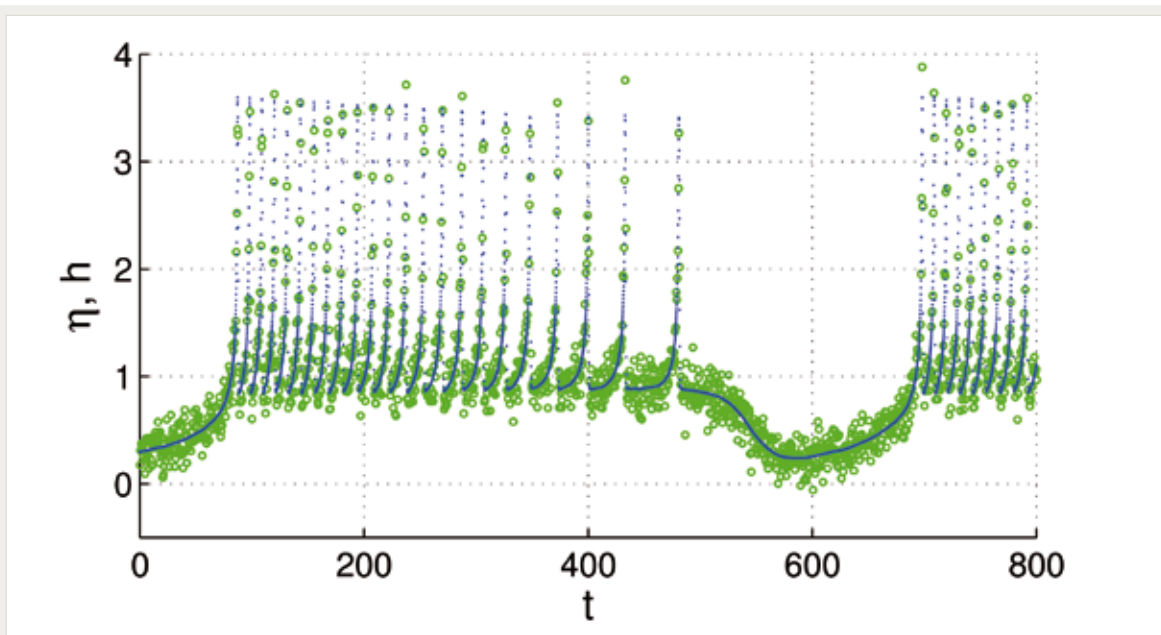


Figure 3

Optimization-based state and parameter estimation of a chaotic Hindmarsh-Rose neuron model. The time series generated by the model (blue dots) was adapted to the observed time series (green circles) (from [9]).

an advantage of this approach all (unobserved) state variables approach their true values due to synchronization and have not to be explicitly estimated.

As an example for synchronization based data assimilation we developed a scheme for synchronizing extended excitable media [6]. Similar to possible experimental situations we assume that time series are sampled at sensors providing local (spatial) averages of the measured variable. Multivariate time series from different sensors are then fed into the model to synchronize it with the observed dynamics. Relevant parameters of this synchronization scheme are the sensors' size and (mutual) distance and the coupling strength. This is demonstrated using a generic model of excitable media exhibiting spiral wave dynamics and chaotic spiral break-up. The system generating the data and the adapted "model" are both implemented on a graphics processing unit (GPU) providing a speedup factor of 50 – 100 compared to a conventional CPU [6,7]. Figure 2A shows two snapshots of the synchronization process for chaotic dynamics generated by a (cubic) Barkleymod-

el. The synchronization error landscape shown in figure 2B can be used to identify the correct model parameters corresponding to the (global) minimum.

Optimization based methods aim at reproducing the observed time series by means of the corresponding model output, too. However, since no synchronization is employed, one additionally has to make sure that the underlying temporal evolution of the state variables fits to the model dynamics. This can be achieved by imposing the dynamical equations as constraints on the optimization process [8] or by including (deviations from) the dynamical equations in the cost function [9]. We use and evaluate both optimization approaches. An example for the second method is shown in figure 3, using the Hindmarsh-Rose (HR) neuron model [9], where the adapted model output (solid blue line) has been fitted to the data. Despite the two time scales in the observed signal and the superimposed measurement noise the implemented parameter estimation algorithm is able to recover the correct values of four system parameters and the dynamics of the (slow) "hidden" variables.

We also succeeded in identifying hyperchaotic dynamics (dimension > 8) and system parameters of a generalized Rössler system [9] from a scalar time series and parameters of cardiac cell models [10], which indicates the enormous potential of the estimation method.

In general, an important topic and task is the detection of parameter redundancies that (may) occur if many model parameters are unknown (as is the case, for example, in cardiac cell models). In such a case the true parameter values may be not observable, *i.e.* different combinations of model parameters provide the same output (compared with the observed time series) [9].

Outlook

Future activities in data assimilation and parameter estimation will focus on two major goals: (i) development of efficient, robust and reliable methods for parameter estimation, (including error bounds and indications of observability by employing probabilistic methods, for example); and (ii) application of advanced identification methods for model evaluation and comparison (“How well can a simple model reproduce the dynamics of a more complex model?”) and for data assimilation of extended systems (fed by experimental data).

- [1] S. Luther et al. *Nature* (accepted for publication)
- [3] F.H. Fenton and A. Karma, *Chaos* **8**, 20-47 (1998).
- [2] S. Petitprez et al., *Circ. Research* **108**, 294-304 (2011)
- [4] F.H. Fenton, E.M. Cherry, A. Karma, W.-J. Rappel, *Chaos* **15**, 013502 (2005)
- [5] U. Parlitz, L. Junge and L. Kocarev, *Phys. Rev. E* **54**, 6253-6529 (1996).
- [6] S. Berg, P. Bittihn, S. Luther, U. Parlitz, *Proceedings of the 6th ESGCO 2010*, April 12-14, 2010, Berlin, Germany.
- [7] S. Berg, S. Luther, and U. Parlitz, (submitted for publication).
- [8] H.D.I. Abarbanel, D. R. Creveling, R. Farsian, and M. Kostuk, *SIAM J. Appl. Dyn. Syst.* **8**, 1341-1381 (2009).
- [9] J. Schumann-Bischoff and U. Parlitz (submitted for publication)
- [10] J. Schumann-Bischoff, J. Schröder-Schetelig, S. Luther, and U. Parlitz, *Proceedings of the International Biosignal Processing Conference*. Berlin, Germany, 2010: 097: 1-4

V-12 Time Series Analysis of Cardiovascular Biodata

S. Luther

U. Parlitz, S. Berg, A. Schlemmer, N. Otani (Cornell), N. Wessel (Humboldt U.), J. Kurths (Humboldt U.), M. Zabel (Univ. Medicine Göttingen), S.E. Lehnart (Univ. Medicine Göttingen)

CHARACTERIZATION AND CLASSIFICATION

of cardiac dynamics on the basis of measured time series (e.g. electrocardiogram, ECG) is crucial for distinguishing physiological from pathological states with potential applications for diagnosis and risk assessment. Since the heart is an extended system, its spatiotemporal electro-mechanical activities in combination with additional control loops of the cardiovascular system form the basis of most observed signals and any (nonlinear) response to perturbations. In particular, complex spatiotemporal dynamics in terms of rotating action potential waves called spiral waves and their subsequent breakup into additional spiral waves has a strong impact on heart rate variability and may cause many cardiac disorders. Much progress has been made on the microscopic dynamics underlying cardiac rhythm (i.e., ion channel dynamics) and intermediate-scale dynamics (i.e., individual spiral waves). However, characterization of the macroscopic dynamics, including the global behavior of multiple spiral waves, underlying molecular or genetic mechanisms, and its implications for clinically relevant signals including the ECG remain largely elusive. Therefore, we determine characteristic features of measured signals that are suitable for classification using state of the art machine learning methods, and we investigate the corresponding underlying spatiotemporal dynamics. The development and application of novel analysis and classification methods require an interdisciplinary and collaborative research environment, integrating data acquisition, analysis and interpretation within the biomedical context.

Characterization of multiple spiral waves

This project aims at characterizing a multiple spiral wave system from a large-scale perspec-

tive. Our goal was to develop improved intuition into the complex behavior of these systems for possible applications to the study and diagnosis of cardiac tissue during fibrillation [1]. Accordingly, we focused our study on two quantities that are defined from the state of the entire system. The quantities correspond to the classical predator and prey quantities. In our model, the collection of all excited cells play the role of a predator, while excitable cells play the role of the prey (figure 1A). The use of “predator” and “prey” dynamical variables has provided diagnostic tools that we can use to characterize the behavior of systems containing many interacting spiral waves. Study of these quantities has allowed us to identify two characteristic types of behavior we call type 1 and type 2. The behavior of all the simulations and optical mapping experiments we studied fell into one of these categories, or in transitions between these two categories. Both types of behavior possessed a number of different distinguishing characteristics, including the degree of repetitiveness of wave propagation patterns in time, the distribution of spectral power, and inferred dynamical organization. Type-2 behavior also exhibited a strong correlation between the time intervals between consecutive extrema in the predator time history and the change in the value of the predator quantity that occurs within these time intervals. These characterizations led to the development of a theory based on the summation of behavior of the dynamics within the “domains of influence” of the individual waves present in the system as shown in figure 1B. We find that this theory yields behavior consistent with all the characteristics observed, and thus is a starting point towards additional understanding of this complex spatio-temporal dynamics in the heart [1].

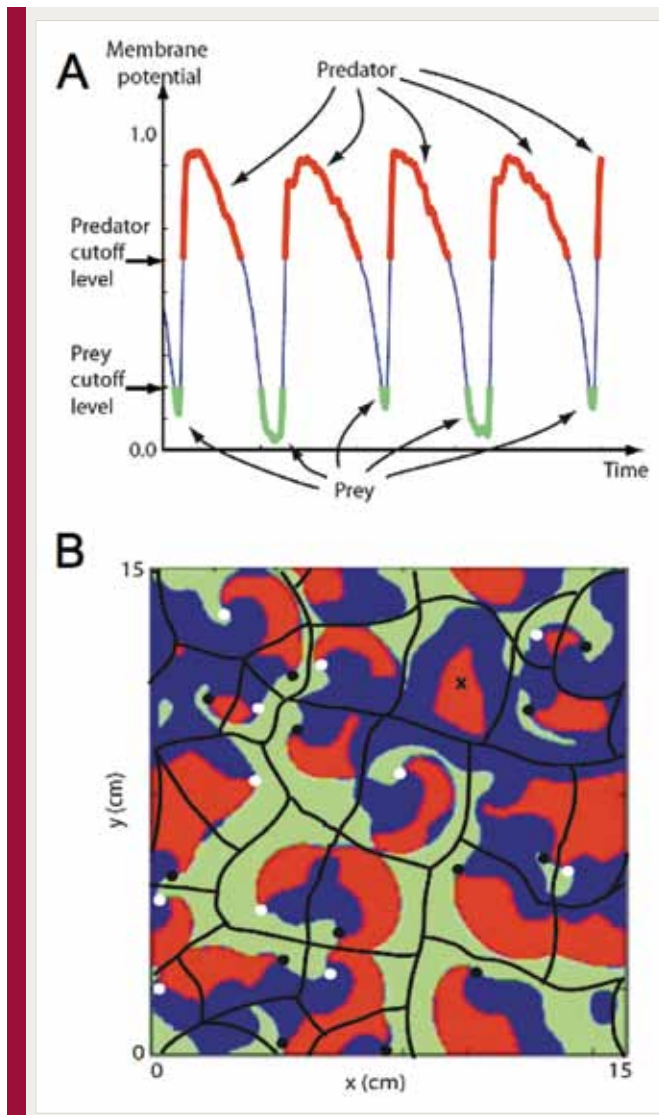


Figure 1

(A) Definitions of the predator and prey states as applied to the time record of a single pixel taken from typical filtered optical mapping data. (B) An example of how the domains of influence might be drawn for a particular pattern of action potential propagation in numerical simulation. Red=predator (action potential) regions; green=prey regions; blue=neither predator nor prey. Black and white dots mark spiral wave tips rotating in the clockwise and counterclockwise directions, respectively. The black lines mark the boundaries of the domains of influence (from [1]; see also “Phys. Rev. E Kaleidoscope Images 2008”).

Synchronization patterns in transient spiral wave dynamics

An important approach for analyzing spatially extended systems is “network analysis” (also called graphical methods) where time series are observed (or measured) at different spatial locations and then investigated with respect to potential interrelations between different parts or regions of the system. If strong relations are found this is often interpreted as being the result of structural inhomogeneities, hidden connections or other causalities. In view of applications to experimental heart data we have applied this approach to spatiotemporal dynamics of a homogeneous excitable medium exhibiting periodic dynamics in

terms of (multiple) spiral waves (figure 2A; [2]). Time series were sampled on a (fine) grid of measurement points and mutually (cross) predicted using a nearest neighbor approach. Since the system is homogeneous with (global) periodic dynamics one would expect that all pairwise predictions provide similar errors. However, this is not the case. Instead we found regions of low mutual prediction errors separated by borders across which relatively high prediction errors are obtained (figure 2B). The origin of these patterns is a transient process during which regions of the excitable medium adjust their dynamics by fine-tuning their oscillation periods. Once this synchronization transient is over all patterns disappear and

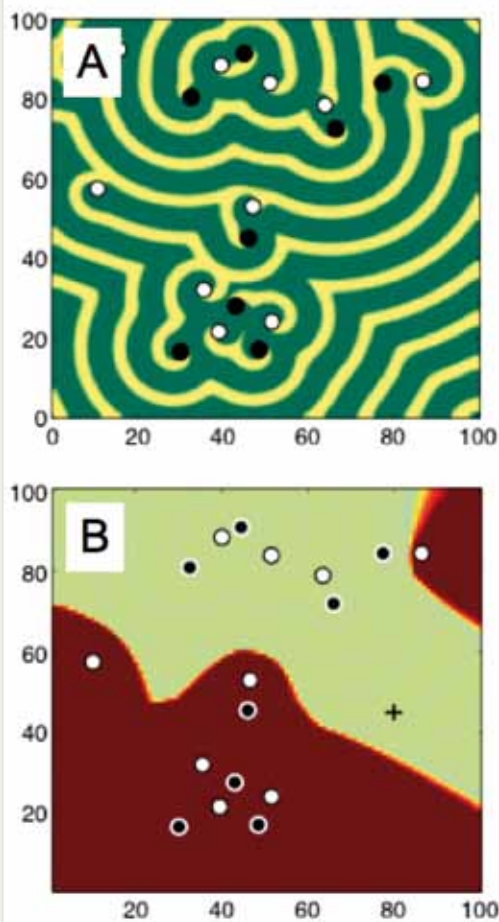


Figure 2

(A) Snapshot of the periodic spatiotemporal dynamics generated by the Barkley model. The black and white circles indicate phase singularities with clockwise and counter-clockwise rotation, respectively. (B) Predictability chart of the Barkley model showing (color coded) averaged prediction errors at different spatial locations when using forecasts based on a time series from a given site indicated by +. Bright and dark colors correspond to low errors (<0.002) and high (>0.024) prediction errors, respectively (from [2]).

the network time series analysis provides the expected result (homogeneous cross prediction errors). However, convergence to this asymptotic state is very slow. Therefore, in particular in experiments, it is very likely that measurements are taken during the transient and may lead to wrong interpretations, for example concerning “inhomogeneity” of the underlying system or concerning additional connections between remote regions.

Analyzing and Classifying Cardiac Biosignals

The electrocardiogram (ECG) provides a non-invasive transthoracic interpretation of the electrical activity of the heart. Cardiovascular dysfunction often manifests itself in characteristic alterations of the ECG, in the heart rate variability and in the corresponding patterns of so-called beat-to-beat intervals (BBI), *i.e.* periods of time between consecutive heart beats (or QRS-complexes; see figure 3A). The ability to classify physiological and pathological BBI patterns is critically important for the development of new diagnostic tools. Successful classification of BBI time series, however, strongly depends on the availability of significant features. There exist a large number of so-called heart rate variability parameters that we have implemented for application and evaluation, including time and frequency domain parameters, or methods based on nonlinear or symbolic dynamics [3,4]. Time domain parameters are based on statistical methods derived from the RR-intervals as well as the differences between them. The mean heart rate (meanNN) is the simplest parameter, while the standard deviation for the whole time series (sdNN) is the most prominent HRV measure for estimating overall HRV. Frequency domain HRV parameters focus on periodic components in the heart rate time series. High frequency power reflects modulation of vagal activity by respiration, whereas low frequency power represents vagal and sympathetic activity via the baroreflex loop. The low-to-high frequency ratio is used as an index of sympathovagal balance. Symbolic dynamics provides a class of features by transforming the time series into a sequence of symbols from a finite alphabet, which is then characterized by entropies or related statistical concepts. In this context we introduced a new family of features based on ordinal pattern statistics that turned out to be very competitive with respect to conventional heart rate variability measures [4-6]. Ordinal patterns describe the relations within short segments of length W of a given time

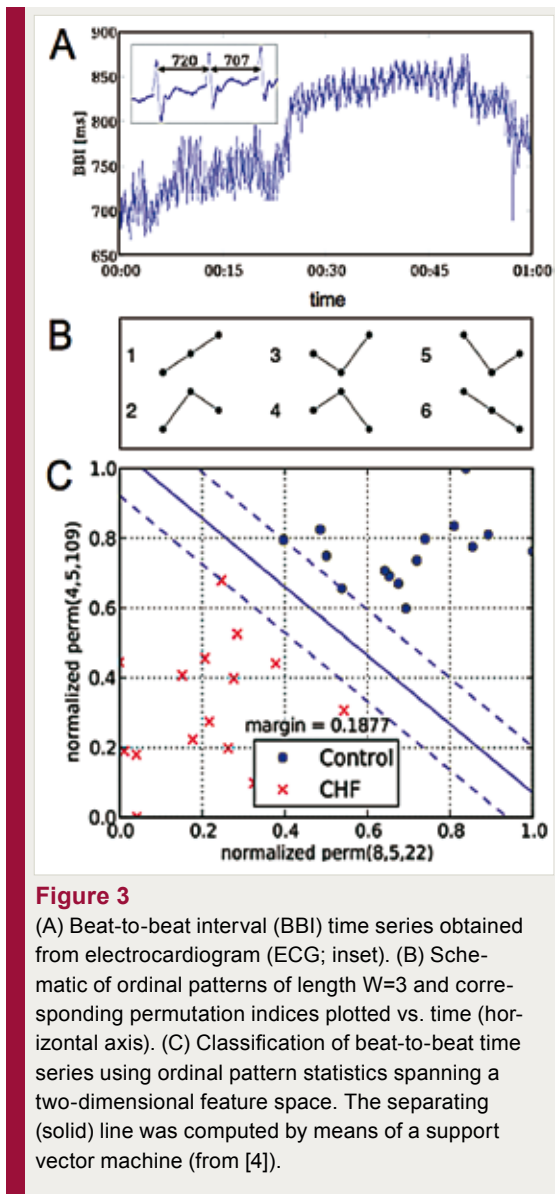


Figure 3
 (A) Beat-to-beat interval (BBI) time series obtained from electrocardiogram (ECG; inset). (B) Schematic of ordinal patterns of length $W=3$ and corresponding permutation indices plotted vs. time (horizontal axis). (C) Classification of beat-to-beat time series using ordinal pattern statistics spanning a two-dimensional feature space. The separating (solid) line was computed by means of a support vector machine (from [4]).

series as illustrated in figure 3B. A unique index can be assigned to each ordinal pattern by interpreting the subsequence as a permutation that is characterized by a permutation index as shown in figure 3B for subsequences of length $W=3$. Ordinal patterns and permutation indices are easy to compute and robust against noise. Each time series can be transformed into a sequence of permutation indices providing a sequence of symbols from a finite alphabet of size $W!$. The concept of ordinal pattern can be extended by considering not only consecutive samples but also subsequences with samples

$x(n)$, $x(n+L)$, $x(n+2L)$, ..., $x(n+(W-1)L)$ that are separated in time by a lag of L sampling times T_s which corresponds to a delay of $T = L \cdot T_s$ in (absolute) time units. The probabilities of occurrence of specific patterns with permutation index I for a given delay T and length W are used as features for characterizing the underlying time series and will be denoted in the following by “perm(T,W,I)”.

As an example we distinguished 15 patients suffering from Congestive Heart Failure (CHF) from a control group of 15 healthy subjects using beat-to-beat time series [4-6].

Figure 3C shows a plot where for each (filtered) beat-to-beat time series (i.e. for each test person) the values of perm($3,4,3$) are plotted vs. the probability perm($4,4,3$). Both probabilities of ordinal patterns are normalized with respect to the smallest and the largest value occurring in the full data set. Points representing patients suffering from CHF are marked as a (red) cross while data associated with persons from the control group are plotted as filled (blue) circles. As can be seen, both sets of points are clearly separated. To quantify the amount of separation, a linear support vector machine has been used to compute a separating line with a maximal margin [4].

Comparison of features based on ordinal pattern statistics with conventional heart rate variability parameters using p-values as well as Leave-One-Out Cross Validation errors shows that they provide valuable, non-redundant information about the underlying time series, increasing the discriminative power of signal classification methods [4].

The availability of different parameters (or “biomarkers”) efficiently describing a (ECG-) time series is an important prerequisite for employing multidimensional classification schemes to separate signal classes (see figure 3C).

Outlook

Optical mapping techniques provide spatio-temporal data of complex wave dynamics observed with different modes of operation of the

heart (including external pacing). These data contain valuable information about the underlying system including inhomogeneities or additional conductance of impulses along fiber connections. Therefore, we plan to continue, improve and apply network analysis to multivariate excitation data. Ordinal pattern analysis will be extended, evaluated and applied to different kinds of time series. A representative and (as far as possible) complete set of features describing ECG time series will be compiled and tested

with different data sets from laboratory experiments with animals as well as clinical measurements. These features will also serve as input for multidimensional classification methods developed in the field of statistical learning. In collaboration with colleagues from University Medicine Göttingen, data analysis will also play a crucial role in investigating the impact of genetic modifications (e.g. ion channel mutations) in mice or other animal models.

- [1] N.F. Otani et al., *Phys. Rev. E* **78**, 021913 (2008).
- [2] U. Parlitz, A. Schlemmer and S. Luther, *Phys. Rev. E* **83**, 057201 (2011).
- [3] A. Schlemmer et al., *Proc. Int. Biosignal Processing*. Berlin, Germany, 2010: 094: 1-4.
- [4] U. Parlitz, S. Berg, S. Luther, A. Schirdewan, J. Kurths, N. Wessel, *Computers in Biology and Medicine* (in press). <http://dx.doi.org/10.1016/j.combiomed.2011.03.017>
- [5] U. Parlitz et al., Proceedings of the 6th Conference of the European Study Group on Cardiovascular Oscillations (ESGCO 2010), April 12-14, 2010, Berlin, Germany, P030:1-4
- [6] S. Berg et al., *Proc. Int. Biosignal Processing*. Berlin, Germany, 2010: 049: 1-4.

V-13 Electro-mechanical Waves and Instabilities in Cardiac Tissue

S. Luther

P. Bittihn, T. Baig, J. Christoph, D. Hornung, C. Richter, A. Squires, U. Parlitz, N. Otani (Cornell), F.H. Fenton (Cornell), R. Gilmour (Cornell), W.-H. Zimmermann (Univ. Medicine Göttingen)

DURING CARDIAC fibrillation, the coherent mechanical contraction of the heart is disrupted by vortex-like rotating waves or scroll waves of electrical activity, which share topological analogies to point vortices and vortex filaments in hydrodynamic turbulence [1]. The dynamics of these filaments and their electro-mechanical instabilities due to the nonlinear interaction with the anisotropic, heterogeneous substrate and the complex boundaries of the heart result in self-organized disordered dynamics. Furthermore, it has been shown that tissue deformation itself may affect electrical wave propagation and its stability, where both pro-arrhythmic and anti-arrhythmic effects have been observed [2]. While cardiac electrophysiology has been studied in great detail both experimentally and theoretically, the nonlinear dynamics and interplay of electrical and mechanical phenomena in the heart remain largely elusive. Our research focuses on three specific aims: (i) development of advanced experimental methods to study electro-mechanical wave phenomena; (ii) modeling of electrical and mechanical motion of cardiac tissue by means of simplified (generic) reaction-diffusion-mechanics; and (iii) development of methods to study the system's stability.

Imaging Electro-mechanical Waves

The measurement of electro-mechanical waves in cardiac tissue remains a major experimental challenge. Conventional fluorescence imaging of the heart (optical mapping) is significantly compromised by tissue deformation resulting in substantial motion artifacts in the optical signal. This limitation is usually addressed by preventing contractile motion using pharmacological motion uncouplers, which are known to alter the dynamical properties of the tissue. To overcome these limitations, we have developed an ad-

vanced optical mapping system that is capable of imaging contracting tissue. Using innovative camera calibration and image registration techniques, we not only recover the undisturbed fluorescence signal (i.e. membrane potential and/or intracellular calcium), but also obtain surface displacement and strain. However, with excitation and emission wavelengths in the visible or near infrared, optical mapping does not permit to measure waves inside the heart wall. Therefore, we have proposed a new imaging modality based on ultrasound elastography [3,4], which shows promise to visualize patterns of propagation of excitation waves inside the cardiac tissue through the mechanical deformations they induce, as shown in figure 1. We have provided a numerical proof-of-concept of this novel imaging modality, indicating the potential for non-invasive structural and functional diagnosis of the heart. In order to advance this new diagnostic modality, we study the propagation of electrical and mechanical waves in engineered heart tissue (EHT). EHT is available in the form of ring-like artificial tissue constructs with quasi-physiological action potential propagation and force development [5]. EHT are made in the Department of Pharmacology (University Medicine Göttingen, UMG). Due to their simple, accessible geometry, they are an ideal "test bed" for the development and evaluation of novel imaging modalities as well as quantitative, data driven modeling of cardiac electro-mechanics. Mechanical motion and electrical activation in EHT is observed simultaneously using high-resolution ultrasound (Vevo 2100, VisualSonics Inc.) and fluorescence imaging using calcium and voltage sensitive dyes (figure 2A). Mechanical motion obtained from the local displacement of the ultrasound speckle pattern using a cross-correlation technique. To advance the devel-

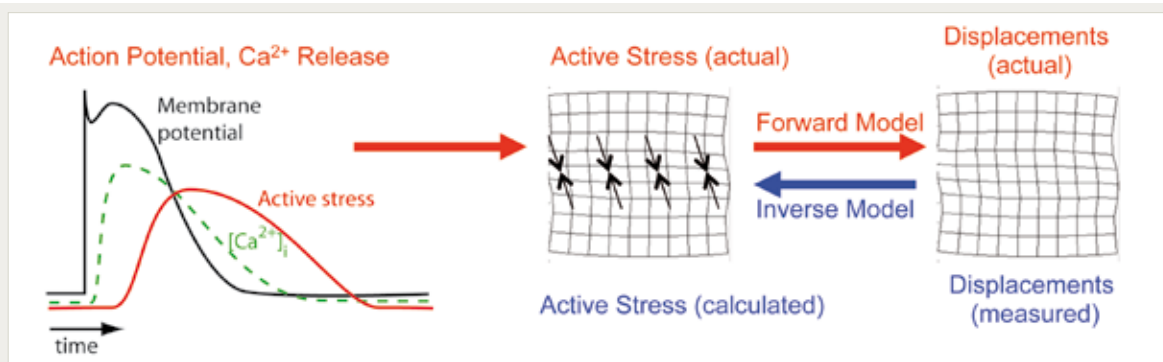


Figure 1

As indicated by the red arrows, the passage of action potentials through individual cells causes time-dependent processes in these cells (left panel), which lead to local contraction of the tissue primarily in the fiber direction (black arrows in the center panel); with the large-scale tissue represented schematically as an imaginary rectangular grid drawn on an arbitrary cross section of the tissue), causing deformation and therefore displacement of the entire tissue (right panel). Computer models of both of the forward problem (the creation of displacements from known active stresses; red arrow on right) and the inverse problem (the determination of the stresses that had to be present to create a given displacement field; blue arrow) are used in this study (from [1]).

opment of a three-dimensional ultrasound imaging modality, we studied the propagation of periodic wave propagation by stroboscopic ultrasound imaging in transversally shifted image planes (figure 2B). The resulting three-dimensional, spatio-temporal data set reveals three-dimensional wave propagation and characteristic filament-like strain patterns (figure 2C). These strain patterns are observed in the vicinity of muscle fibers, as evidenced by confocal microscopy. Further experiments are underway to characterize the structural and functional development of EHT during maturation. Our experimental findings suggest that the available spatial and temporal resolution should permit the observation of transient phenomena.

Modeling Reaction-diffusion-mechanics

In the heart, electrical excitation propagates through diffusively coupled cardiac cells and subsequently results in contraction and force generation (excitation-contraction or electro-mechanic coupling). Mechanical forces on cardiac cells may in turn change electrophysiological properties of the tissue, e.g. action potential duration, or induce after-depolarizations resulting in premature beats. This so-called mechano-electric feedback is therefore considered an important mechanism facilitating cardiac arrhythmias, however many of its details remain elusive. The objective of this project is to de-

velop and analyze a generic model of cardiac electro-mechanics and to study mechanisms underlying the onset and perpetuation of cardiac arrhythmias. In order to answer this question, we are following Panfilov et al. and model cardiac tissue as a reaction-diffusion-mechanics system. This model consists of reaction-diffusion equations describing (simplified) cardiac electrophysiology, equations describing soft tissue mechanics, and the coupling between them. Finite deformation elasticity theory is required to describe the tissue dynamics, due to the significant change in cell length during contraction (typically 10-20%). Numerical simulations indicate that mechanical deformation may result in spiral wave drift and subsequent breakup [2]. Moreover, deformation may also result in spiral wave stabilization as shown in figure 3.

Stability Analysis

Two important questions in the investigation of cardiac arrhythmias are how these activation patterns develop and how their complexity can be characterized. What properties of the tissue determine its susceptibility to arrhythmias? Where and when are certain activation patterns most sensitive to perturbations? What makes irregular activity easy or difficult to terminate? We expect that the answers will yield valuable information for the prevention of arrhythmias and about strategies to terminate them. One of our

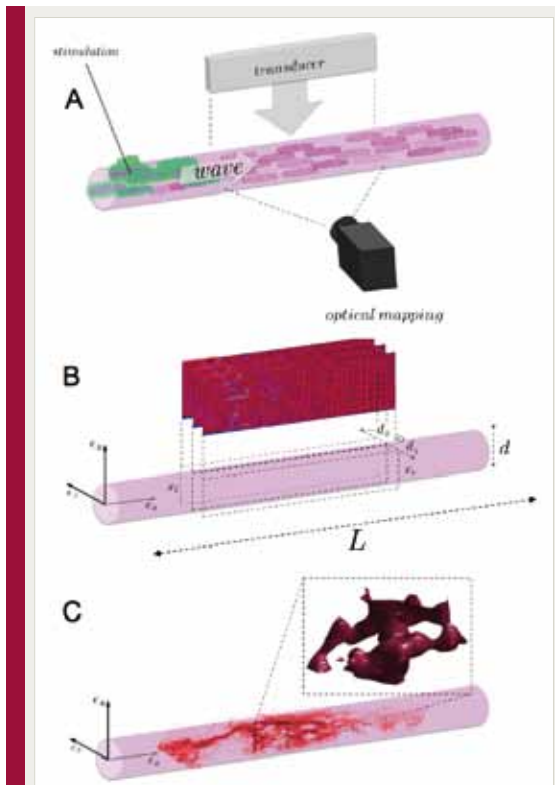


Figure 2
 (A) Experimental setup for studying electromechanical waves in EHT constructs showing high-resolution ultrasound transducer and its imaging plane (Vevo 2100, VisualSonics Inc.), fluorescence imaging camera (MiCAM Ultima L, SciMedia Inc.), and stimulation electrode. (B) Three-dimensional elastography using parallel imaging planes with periodic stimuli. (C) Qualitative comparison of strain pattern (red iso-surface) with muscular fiber structure obtained using macroconfocal microscopy. Red points within the EHT indicates actin and muscle tissue. The 3D strain pattern shows a magnification of a small, representative volume within the EHT (dashed lines).

approaches to tackle these questions is to view cardiac tissue as a high-dimensional non-linear dynamical system. Using a number of different numerical models of cardiac tissue, we carry out stability analysis of different activation patterns to assess their (ir)regularity. As a very general method that can be applied to arbitrary attractors of the system, this procedure yields growth rates (so-called Lyapunov exponents) of perturbations localized at specific sensitive spots (given by Lyapunov vectors) and allows us to estimate the attractor dimension – a quantitative measure for the complexity of the dynamics. Abrupt changes of excitation patterns (figure 4) and symmetries in the system can be

detected as well as the onset of chaotic activity. In extended media instabilities often occur first locally and then grow and spread out. Such scenarios can be investigated and characterized by means of Lyapunov vectors. For spatio-temporal systems Lyapunov vectors are given as patterns evolving in time and may thus be interpreted as generalizations of the concept of (active) modes [6]. In state space (more precisely, in the tangent space of the state space) Lyapunov vectors point in the directions of characteristic growth of perturbations (on average quantified by Lyapunov exponents). Usually two types of “Lyapunov vectors” have to be distinguished: (i) the orthogonal set of vectors occurring with the standard algorithm for computing Lyapunov exponents (based on QR-decomposition or Gram-

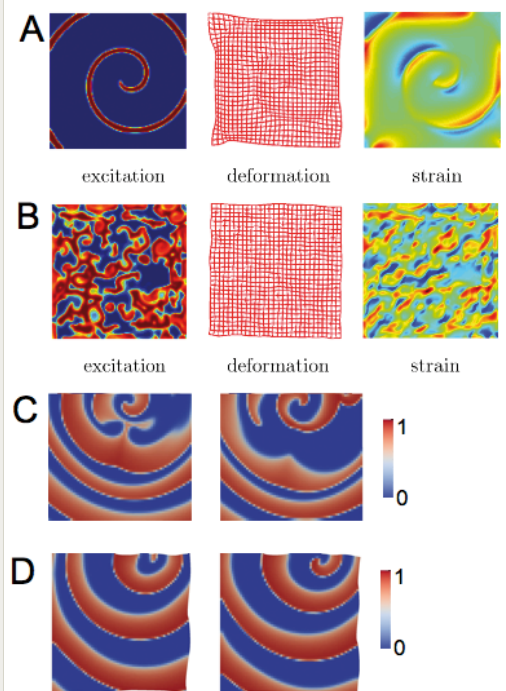


Figure 3
 Reaction-Diffusion-Mechanics. (A) Excitation, deformation and strain in a homogeneous, generic excitable and deformable two-dimensional medium. The image shows a stable spiral wave. (B) Spiral wave breakup results in spatio-temporal chaos. (C) Spiral wave in non-deforming medium shows wave breakup. (D) Stable spiral wave in the deforming medium (same initial conditions and parameters as in panel (C)).

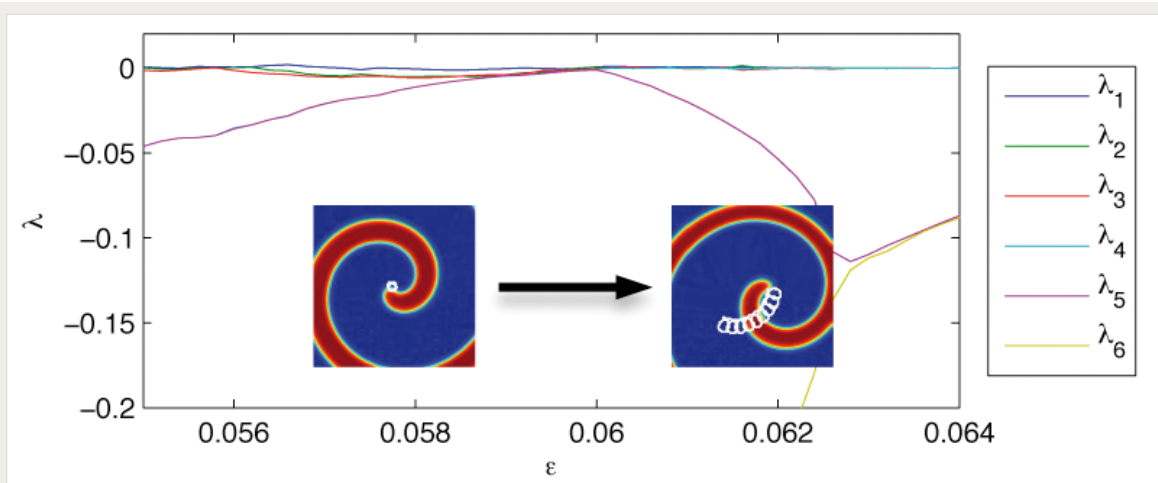


Figure 4

Detection of bifurcations via Lyapunov exponents. The bifurcation parameter ϵ is a model parameter, which turns a rigidly rotating spiral wave (left) into a meandering spiral (right). Transitions between qualitatively different activation patterns (bifurcations) are indicated by one or more Lyapunov exponents becoming zero, which is the case at $\epsilon \approx 0.06$ here. Lyapunov exponents (*i.e.* growth rates of perturbation modes) are ordered by size, with λ_1 being the largest. All Lyapunov exponents are less or equal to zero, since both the rigidly rotating spiral wave and the meandering spiral wave are stable activation patterns.

Schmidt reorthogonalisation) and (ii) so-called covariant Lyapunov vectors, that are not orthogonal but possess several desirable (invariant) features. Covariant Lyapunov vectors became practically available only recently due to novel numerical algorithms proposed by Ginelli et al. [7] and Wolfe and Samuelson [8]. With a view to applications to excitable media we prepared a detailed study of the theory and computation of covariant Lyapunov vectors including new alternatives for their efficient computation [9].

In order to transfer the knowledge we gain about the nature of certain instabilities to experiments, the next step will be to connect these rather abstract measures to quantities that can be measured in real cardiac tissue, e.g., the number of phase singularities or the propagation velocity. Preliminary results show that there is a close connection between the complexity of spatio-temporal chaos and the number of rotating waves. Another focus is on the relationship between the stability of wave patterns and the degree of cellular heterogeneity (e.g., fibrotic tissue).

Outlook

While our current studies are limited to the development, analysis and validation of gener-

ic models of reaction-diffusion-mechanics, our long-term aim is the development of a (realistic) physiological model of the heart. Combining detailed electrophysiological models (see Sec. V-11) with a quantitative model of soft tissue continuum mechanics. To this end, data driven modeling, parameter estimation and model evaluation techniques currently under development in our group will be essential. Numerical models will be used to further enhance the diagnostic potential of the proposed advanced ultrasound imaging technique (patent pending). The physiological heart model will be used to study the arrhythmogenesis and loss of function associated with the transition from silent to overt heart failure within the Heart Research Center Göttingen (HRCG).

- [1] F.H. Fenton and A. Karma, *Chaos* **8**, 20-47 (1998).
- [2] R.H. Keldermann and M.P. Nash and A.V. Panfilov, *Physica D* **238**, 1000-1007 (2009).
- [3] N.F. Otani, S. Luther, R. Singh and R.F. Gilmour, *Ann. of Biomed. Eng.* **38**, 3112-3123 (2010).
- [4] N.F. Otani et al., *Computers in Cardiology* **36**, 617-620 (2009).
- [5] W.-H. Zimmermann et al., *Circ.* **106**, I151-7 (2002).
- [6] P.V. Kuptsov and U. Parlitz, *Phys. Rev. E* **81**, 036214 (2010).
- [7] F. Ginelli et al., *Phys. Rev. Lett.* **99**, 130601 (2007).
- [8] C.L. Wolfe and R.M. Samuelson, *Tellus* **59A**, 355-366 (2007).
- [9] P.V. Kuptsov and U. Parlitz, (submitted for publication).

V-14 Non-additive Dendritic Coupling in Neural Circuits

S. Jahnke, D. Breuer, M. Timme

R.-M. Memmesheimer (Radboud University, Nijmegen, The Netherlands and Harvard University, USA)

SPATIO-TEMPORALLY coordinated spiking activity has been experimentally observed in different neuronal systems. Pronounced inter-neuronal locking, significant synchrony (unitary events), and more complex spike patterns seem to be particularly prevalent. They are established not only in various central pattern generators [3] but also, e.g., in circuits of the sensory/motor areas of birds [4] and in different cortical areas of awake behaving monkeys [5]. Such coordinated spiking activity correlates with sensory stimuli as well as internal states and is thus considered a key feature of neural computation. Its dynamical origin, however, is still not well understood [1].

The propagation of synchrony through recurrent neural circuits offers a possible mechanism for coordinated spiking activity. One current theory supporting synchrony propagation is that of synfire chains [6, 7], simultaneously active groups of neurons that are densely connected in a feed-

forward way. Synchronous spiking activity may stably propagate from group to group along such chains. The dense feed-forward coupling, however, has not been observed and is anatomically questionable. It can also bring several functional problems such as “epileptic” activity where synchrony spreads across extensive parts or even the whole of local neural circuits [8]. Recently, a nonlinear enhancement of simultaneously incoming presynaptic signals has been found experimentally in neuronal dendrites in the hippocampus and other neo-cortical areas [9, 10]. This nonlinearity serves as a promising candidate for generating emergent synchrony propagation. However, theoretical studies on spiking neural networks so far have focused on linear, additive dendritic coupling. Systematic investigations on the impact of nonlinear dendritic enhancement on collective circuit dynamics were still missing. We have now shown that already purely random networks, with dendritic nonlinearities but with-

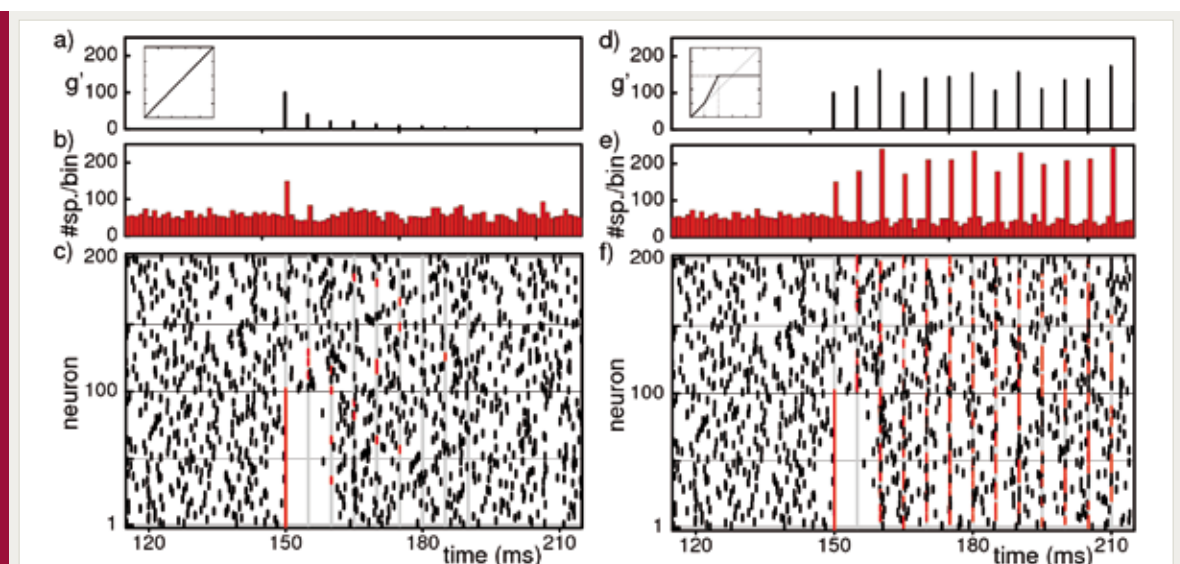


Figure 1

Dendritic nonlinearities may induce synchrony propagation in purely random networks without any super-imposed feed-forward anatomy. (a) Propagation of synchrony is hard to achieve in random networks of linearly coupled neurons where synchronous groups often die out; (b) non-additive dendritic coupling in an otherwise identical network actively supports the propagation of synchrony. Top panels: synchronous group size extracted from total network activity; lower panels: raster plot of a subset (200 out of 1000) of model neurons.

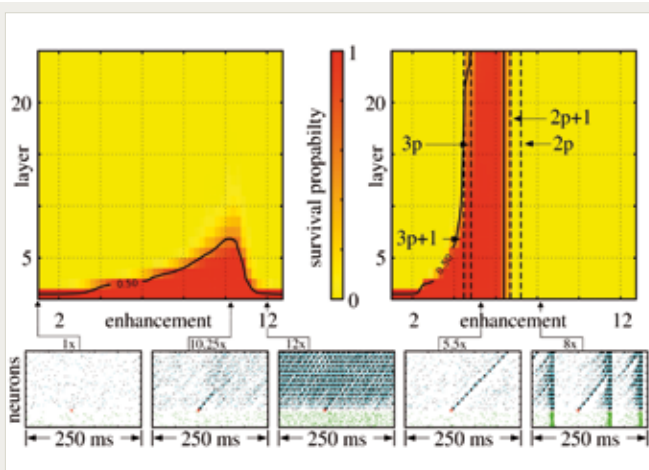


Figure 2

Organized propagation of synchrony in randomly connected networks with embedded feed-forward structure. (a) The top panels show the probability of detecting that a synchronous pulse, initiated in the first layer of the feed-forward structure, occurs in the n th layer. The horizontal axis shows the relative strength of the synapses in the feed-forward structure compared to the synapses of the remaining recurrent network. For linearly coupled neurons (left) only a moderate propagation for high enhancements is achieved, whereas in networks of neurons with dendritic spikes (right) stable propagation results for moderate enhancements already. The lower panels show examples of network activities for given enhancements.

out any superimposed feed-forward anatomy, may exhibit robust propagation of synchrony and thus precisely timed spike patterns [2]. This even holds if an identical random network with linear (instead of nonlinear) addition of stimuli at the dendrite is incapable of showing such forms of synchrony propagation (cf. figure 1).

These results indicate that nonlinear dendritic coupling may induce emergent coordinated spiking activity in neural circuits and may dynamically compensate for the absence of densely coupled feed-forward topologies.

A bifurcation analysis of an exactly solvable limiting model identifies a mechanism for the generation of synchrony propagation that is markedly different from the one found for embedded synfire chain models; in particular it contains local and non-local contributions: dendritic processing and co-action of two or more synapses; further, it relies in part on the saturation nonlinearity at high input strengths and on the interplay between inhibition and excitation. Our analysis also shows that the mechanism is insensitive to changes in the onset and the precise form of the dendritic nonlinearity such that synchrony propagation robustly occurs in spiking neural networks with nonlinear dendritic coupling.

Currently, we are systematically studying how efficiently dendritic (i.e. neuron-specific) nonlinearities may compensate for inter-neuronal connectivity. We have shown that even in very sparsely connected random networks naturally occurring feed-forward structures can be employed to transfer synchronous activity. If the synaptic strength

of synapses between neurons, which belong to groups which are connected more dense than the average (but still far away from fully connected regime) is amplified, dendritic spikes provide the possibility of propagating a synchronous signal with only weakly interfering with the background activity (cf. figure 2). Further we investigate how such synaptic connectivity structures may self-organize in the presence of nonlinear enhancement and simultaneous synaptic plasticity.

The final aim is a consistent theory of how complex neural circuits may robustly generate spatio-temporal patterns of spikes, even though the networks are connected sparsely, the intrinsic neurons' dynamics are nonlinear and the coupling is non-additive, and the synapses are often unreliable and typically changing in response to the network activity.

Part of the material presented here has been taken, sometimes in modified form, from the Research Report 2011 of the Network Dynamics Group (c) Marc Timme, et al., MPIDS.

- [1] R.-M. Memmesheimer and M. Timme, In: Handbook of Biological Networks, eds.: S. Boccaletti, V. Latora, Y. Moreno, World Scientific (2010)
- [2] R.-M. Memmesheimer and M. Timme, Front. Comput. Neurosci. Conference Abstract: Bernstein Symposium (2008)
- [3] A. Büschges, *J. Neurophysiol.* **93**, 1127 (2005)
- [4] R. Hahnloser, A. Kozhevnikov, and M. Fee, *Nature* **419**, 65-70 (2002)
- [5] S. Grillner, *Neuron* **52**, 751-766 (2006)
- [6] M. Abeles, *Corticonics: Neural Circuits of the Cerebral Cortex*, Cambridge University Press, Cambridge (1991)
- [7] M. Diesmann, M. Gewaltig, and A. Aertsen, *Nature* **402**, 529 (1999)
- [8] A. Kumar, S. Rotter, and A. Aertsen, *J. Neurosci.* **28**, 5268 (2008)
- [9] G. Ariav, A. Polsky, and J. Schiller, *J. Neurosci.* **23**, 7750 (2003)
- [10] A. Polsky, B. Mel, and J. Schiller, *Nature Neurosci.* **7**, 621 (2004)

V-15 Timing-Based Information Processing in Biological Systems

W.-C. Chou, C. Kirst, T. Geisel, M. Timme

D. Fliegner, H. Vester (Ocean Sounds, Henningsvaer, Norway), M. Denker and S. Grün (RIKEN Brain Science Institute, Japan), K. Hammerschmidt, J. Fischer, A. Fiala (Faculty of Biology, University of Göttingen)

PRECISE TIMING and distributed coordination of a biological system's activity is crucial for many of its functions, including the detection and representation of external stimuli as well as the planning of behavioral tasks and the communication with other individuals. As mean field theories do not typically account for spatio-temporal structure, but rather average over space or time, methods of analysis of such patterns are rare, and even simple modeling approaches come with fundamental challenges.

Locking between Spikes and Local Field Potentials in Neural Circuits

Coding in the brain is hypothesized to rely on information represented and transmitted in the simultaneous activation of groups of neurons, commonly termed assemblies. Such assembly activity would be expressed through coherent spatio-temporal patterns of neuronal firing, rather than by the simple rate response of populations of neurons. However, it is often difficult to analyze neuronal recordings with respect to the occurrence of such temporal patterns. In current typical experimental setups the number of neurons recorded simultaneously rarely exceeds the order of 100, providing only a very limited sample of the neuronal population activity of hundreds of thousands of neurons.

We thus aimed at examining the coarse-scale local field potential (LFP) in parallel with the local spike patterns (cf. figure 1). The LFP is a spatially slowly changing, extracellularly recorded signal, composed of low frequencies up to about 300 Hz. It is thought to reflect primarily synaptic currents in a large area containing hundreds or thousands of neurons around the recording site. Increased oscillation strength of this signal, as observed in numerous experimental paradigms, is hypothesized to be relat-

ed to synchronized network activity rather than an overall increase in activity. Up to now, however, the intricate details of the relationship between neuronal spiking activity, network dynamics and LFP signals in the cortex are not fully clarified. A deeper understanding of how activity at the neuron level is connected to LFP oscillations might aid in combining simultaneous LFP and single neuron recordings to characterize the network dynamics.

In collaboration with the Bernstein Center for Computational Neuroscience (BCCN) Berlin and the RIKEN Brain Science Institute, Japan, we recently developed a novel method for detecting precise timing dependencies between spiking activity and the coarser signal of local field potentials [1, 2]. It uses circular statistics and specifically adapted tools from phase synchronization. Applying the method to activity recorded from the motor cortex of awake behaving monkeys revealed that during a movement preparation task spikes tend to keep a fixed phase relationship to the LFP, largely independent of the LFP amplitude [2]. Related methods assessing phase locking and related quantities are used in other fields of neuroscience to understand neural coding.

Distributed Representation and Processing in *Drosophila* Antennal Lobe

In a related study, we recently started to investigate distributed odor representation and processing in the antennal lobe of *Drosophila*, in collaboration with André Fiala (Faculty of Biology, University of Göttingen).

Sensory processing in *Drosophila* is spatially and temporally complex, highly multidimensional, and transient. Via sensory neurons, external odor stimuli activate or inhibit a diverse array of olfactory neurons, thereby inducing dynamical

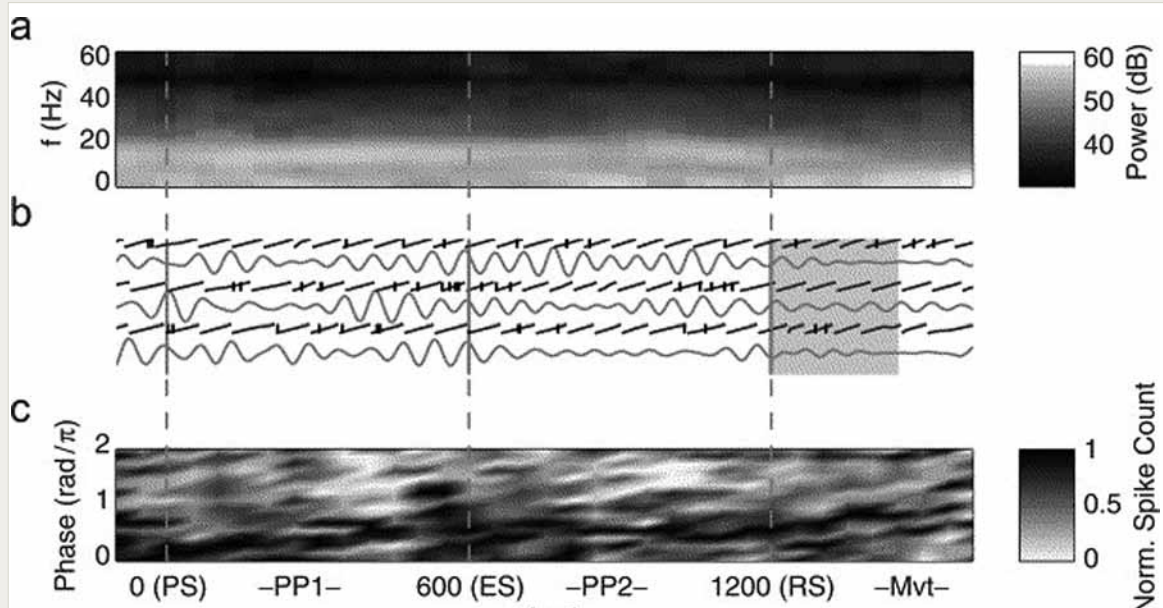


Figure 1

Detecting instantaneous phase relationships between LFP and spikes. (a) Trial-averaged power spectrum of one LFP recording in one possible experimental condition. During the preparatory periods (PP1 and PP2) a prominent oscillatory component around 16 Hz is visible. (b) Filtered LFP signal (gray) of three example trials. The extracted phase signal (black step function) from 0 to 2π is sketched above each LFP. Ticks indicate the location of spikes of a neuron recorded from the same electrode. The shaded region marks the time interval where movement started. (c) Time-resolved histogram of the phase distribution for the LFP-neuron pair shown in (b), but across all trials. The neuron shows a sustained preference for spiking during the falling flank of the LFP.

processes in downstream circuits. In particular, such sensory signals affect a neuronal network within the antennal lobe, where odors are represented by dynamically interacting neurons of three main types: sensory neurons (SNs), excitatory and inhibitory local interneurons (eLIs, iLIs), and projection neurons (PNs). So far, it is unclear how SNs, LIs, and PNs cooperatively interact to support odor distinction and odour classification. *Drosophila* provides an ideal model system for studying spatio-temporal olfactory processing, because subpopulations of neurons can be genetically targeted.

In our collaborative study, we aim at describing, quantifying and modeling how the primary olfactory circuitry contribute to spatio-temporal odor representation and how their dynamics directly relate to computations and resulting behaviors. To achieve this goal we are bridging experimental imaging, with advanced data analysis and mathematical modeling. So far, the antennal lobe is thought to manage two main tasks,

(i) increasing the signal-to-noise ratio of sensory signals, thereby emphasizing important parts of the signal and (ii) clarifying the separation of stimulus responses to different odors, thereby solving a distinction task. Very recent evidence indicates that the olfactory bulb in vertebrates (the analog to the antennal lobe in insects) performs active pattern classification, suggesting that a separate activation pattern may be associated with each given odor.

Our imaging analysis now shows that in fact, for some sets of odors, representations are joined together rather than separated (figure 2), an astounding finding given the common belief that the purpose of the antennal lobe system is to separate sensory inputs more clearly.

We now plan studies to systematically quantify differences between odor representations and classify pairs yielding joint and pairs yielding separate representations. Mathematical, activity-based models of neural circuitry will be based on known dynamical and anatomical data, to in-

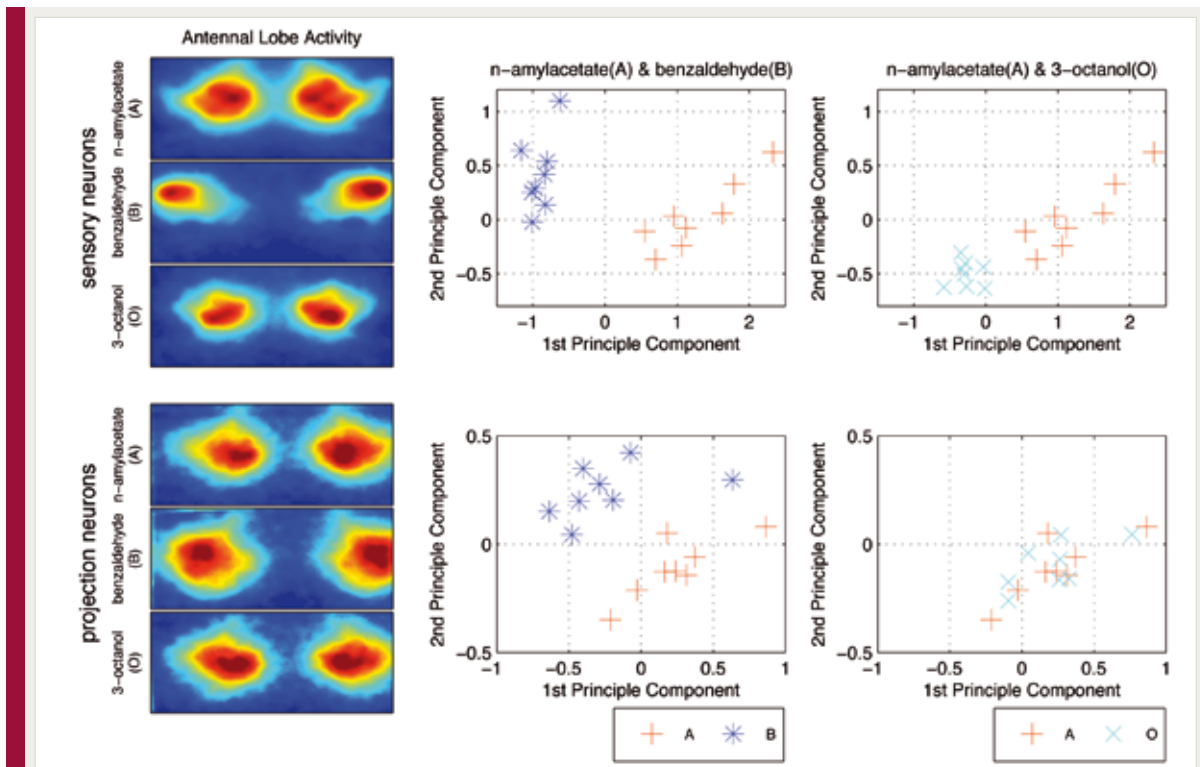


Figure 2

Drosophila's antennal lobe is capable of joining representations of different odors. Left column: The neuronal activity of sensory neurons and projection neurons measured by two photon imaging. Warmer colors indicate regions of higher activity. The animals were tested using three different odors including n-amylacetate (A), benzaldehyde (B), and 3-octanol (O). Middle and right column: Image projection to the first two principle component analysis (PCA), that account for nearly 90% of the original signal variability. The odors n-amylacetate and benzaldehyde are well separated on both the level of sensory neurons and the level of projection neurons (middle column), as expected for the system. Contrary to this commonly accepted view, the representations of n-amylacetate and 3-octanol test (right column) are separated on the level of sensory neurons, but clearly joined on the level of projection neurons. (Imaging data courtesy of the laboratory of André Fiala, University of Göttingen).

investigate how spatio-temporal coding in the antennal lobe comes about mechanistically and whether it may indeed rely on transient switching dynamics [3-5].

In summary, current [6] and future studies of olfactory processing in *Drosophila* will help to dissect the contributions of various neuronal subpopulations for odor coding and thus provide important functional information for both odor coding and olfactory conditioning in flies.

Complex Structure of Vocal Communication in Social Whales

Communication in social whales

Highly social animals generally develop complex communication systems due to the need to socialize with more than a few individuals. One

of the main functions of communication signals in these societies is to foster cohesion among members. Other functions may include, e.g., signaling social and breeding status, as well as group distinction and relatedness.

Vocal communication is highly evolved in social marine mammals. They are long-lived, and often stay in stable groups; in particular mother-offspring bonds can last for a lifetime. In such communities, group-specific calls are used to recognize individuals and groups, either to maintain cohesion or to avoid contact, to coordinate social behavior, and to recognize the relatedness of potential mates in order to avoid close inbreeding.

Matrilineal whales, in particular killer whales (*Orcinus Orca*) and long finned pilot whales

(*Glophicephala Melas*), developed an advanced communication system resulting from intra- and inter-group social interactions and environmental factors. Their vocal repertoire consists of a variety of sounds such as pulsed calls, whistles, clicks and buzzes. For killer whales, the vocal repertoire is well-known. The structure of individual calls, and whistles, and their duration as well as frequency of call usage varies, and it is known that social and foraging behavior strongly influences breadth and detailed content of the vocal repertoire.

Complex phrases

Our preliminary studies now suggest an even more complex temporal organization of the multiple sounds in both species. A systematic study of such higher level communication phrases in matrilineal whales, however, is still missing.

Systematic studies on birds and other highly cognitive mammals such as dolphins indicate the use of complex communication structures, for instance specific sequences of vocal sounds obeying a “pre-grammar”. We thus expect a similar mechanism of high-level communication in social whales, which will be investigated in detail in the future.

In the proposed project, we aim at analyzing the vocal repertoire of killer whales and pilot whales with special emphasis on complex communication phrases. We focus on their dependence on social behavior within and between groups, as well as their bio-geographic and inter-species differences. Besides gaining insights into the complexity of whale communication, our study thus aims to provide the first systematic bio-

geographic comparison, in particular with respect to geographic occurrences in Norway and Chile regions. In parallel to preliminary studies about geographic marine mammal distribution, we also recently also reported severe threats on marine ecosystems in one area in Chile [7] that caused broad and immediate international reactions.

New automated methods of analysis

As the many sounds and sound elements can be combined in a vast number of ways, standard methods of observer-based analysis used so far cannot reveal the full complexity already suggested by our preliminary data. We will thus set up a consistent data base management system and develop computer based tools of non-linear time series for automated analysis and classification of sound patterns. Here methods of clustering, pattern association and unsupervised learning will assist a classification of phrases that is fast, systematic, and transferable across killer whales and pilot whales, their different acoustic clans and individual groups. Simultaneously we will collect further acoustic data from killer whales and pilot whales in the Northeast Atlantic and Southeast Pacific, thus enabling us to compare their different usage of sounds and phrases depending on bio-geographic, group and species specific characters. A successful study will not only contribute to a systematic overview of the compounds used in social whale communication, but also reveal basics about their complex composition and give key hints about their specific evolutionary adaptation.

- [1] C. Kirst and M. Timme, *Front. Neurosci.* 3, 2 (2009)
- [2] M. Denker, S. Roux, M. Timme, A. Riehle, and S. Grün, *Neurocomputing* 70, 2096 (2007)
- [3] M. Timme, F. Wolf, and T. Geisel, *Phys. Rev. Lett.* 89, 154105 (2002)
- [4] P. Ashwin and M. Timme, *Nature* 436, 36 (2005)
- [5] C. Kirst and M. Timme, *Phys. Rev. E (Rapid Comm.)* 78, 065201 (2008)
- [6] T. Niewalda *et al.*, submitted (2011)
- [7] H. Vester and M. Timme, *Nature* 465, 869 (2010)

V-16 Self-Organization in the Evolution of Neural Circuits

F. Wolf

W. Keil, L. Reichl, J. D. Flórez-Weidinger, E. Bodenschatz, D. Tsigankov, M. Kaschube (Princeton, USA), M. Schnabel (Northwestern U, USA), D. M. Coppola (Randolph-Macon College, USA), J. Crowley (Carnegie Mellon U, USA), S. Löwel (U Göttingen), L. E. White (Duke U, USA)

THE OCCURRENCE of universal quantitative laws in a strongly interacting multi-component system indicates that its behavior can be elucidated through the identification of general mathematical principles rather than by the detailed characterization of its individual components. We recently discovered that apparently universal quantitative laws govern the spatial layout of orientation selective neurons in the visual cortex in three mammalian species [1] separated in evolution for more than 65 million years [2-5]. Most suggestive of a mathematical structure underlying this phenomenon, the average number of pinwheel centers per orientation hyper-column in all three species was found to be statistically indistinguishable from the constant π [1, 6]. We showed that mathematical models of neural pattern formation can reproduce all observed quantitative laws of cortical column design if non-local interactions are dominant, indicating that non-local interactions are constitutive in visual cortical development. These and other results demonstrate that mathematical principles can shape the organization of the brain as powerfully as an organism's genetic makeup. The laws governing strongly interacting multi-component systems frequently detach from the detailed nature of microscopic interactions resulting in the robustness of collective properties and in their insensitivity to external and internal perturbations. Quantitative laws exhibiting such insensitivity are called universal because they characterize an entire class of systems rather than an individual system in all its specific detail. In biological systems, measurements precise enough to uncover universal quantitative laws are rarely performed and might appear misguided, when qualitatively new types of cellular and molecular components and interac-

tions are continuously being discovered. Nevertheless, universality may play important roles in living systems. Neuronal, immune and genetic networks are strongly interacting multi-component systems and universal behavior, particularly the robustness associated with it, may often be beneficial for the functioning of an organism. To clarify the role and impact of quantitative universality in the formation, operation, and potential optimization of visual cortical architecture, we are performing a coordinated program of modeling studies (e.g. [7-12]) complemented by data analysis projects in collaboration with neurobiological laboratories (e.g. [1, 13, 14]). Our studies are designed to screen for signatures of functional optimization of visual cortical architecture, to determine the mathematical structure of candidate optimization principles explaining the common statistical laws found in experiments and to test the theoretically predicted critical role of long-range interactions in visual cortical self-organization. Our theoretical work utilizes a model independent symmetry-based approach to the analysis of neuronal self-organization in the visual cortex developed in our group [15, 7].

To examine the functional architecture of the visual cortex for signatures of quantitative universality we developed image analysis methods for the automated detection, localization and counting of so called pinwheel defects [1, 16, 17], point-like orientation singularities of orientation preference maps around which stimulus orientations are represented in a radial fashion. Using these tools we were able to compare fundamental statistical properties of orientation preference maps with an unprecedented precision in the range of a few percent [1, 6]. We found that virtually all characteristics but the ab-

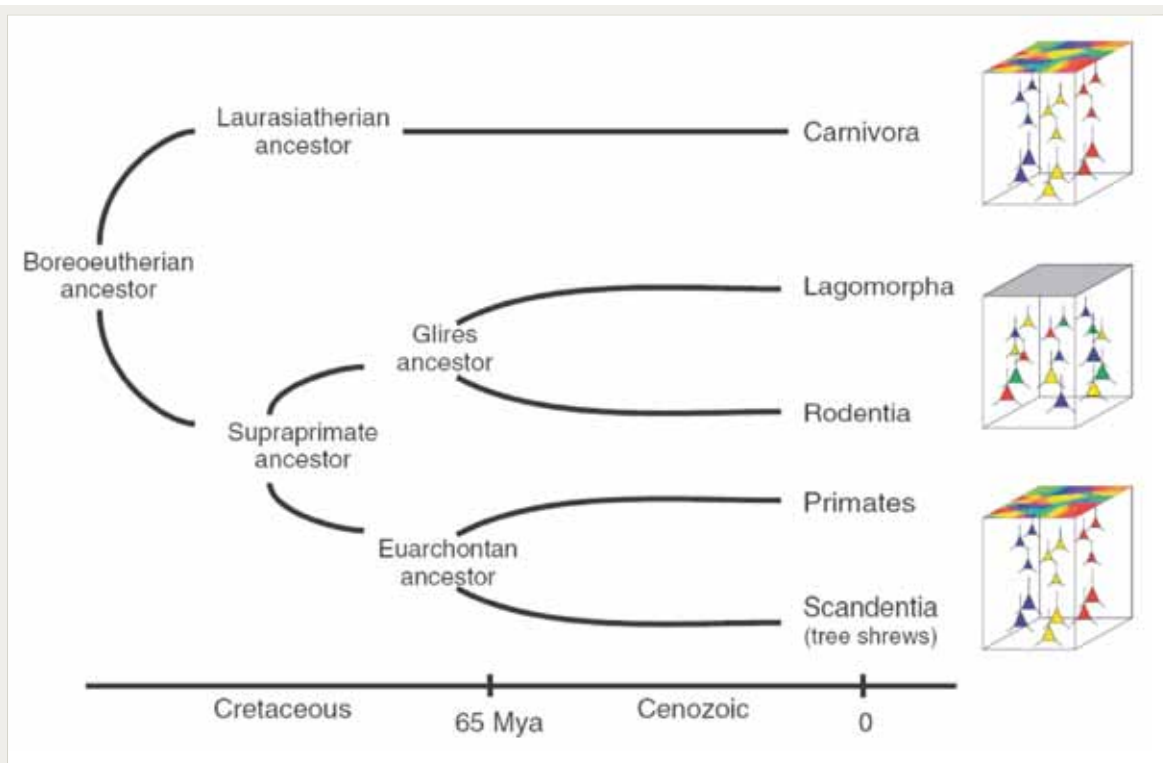


Figure 1

Phylogenetic relationships between mammalian ancestors and present day mammals exhibiting and lacking orientation column. Arrangements of orientation-selective neurons in these species are indicated. Preferred orientations of representative subsets of neurons are color coded in the schemes to the right. Rodents and lagomorphs show salt-and-pepper arrangement of preferred orientations (ORs). Carnivores, primates, and tree shrews show columnar arrangement of preferred ORs (modified from Kaschube et al. Science 2010).

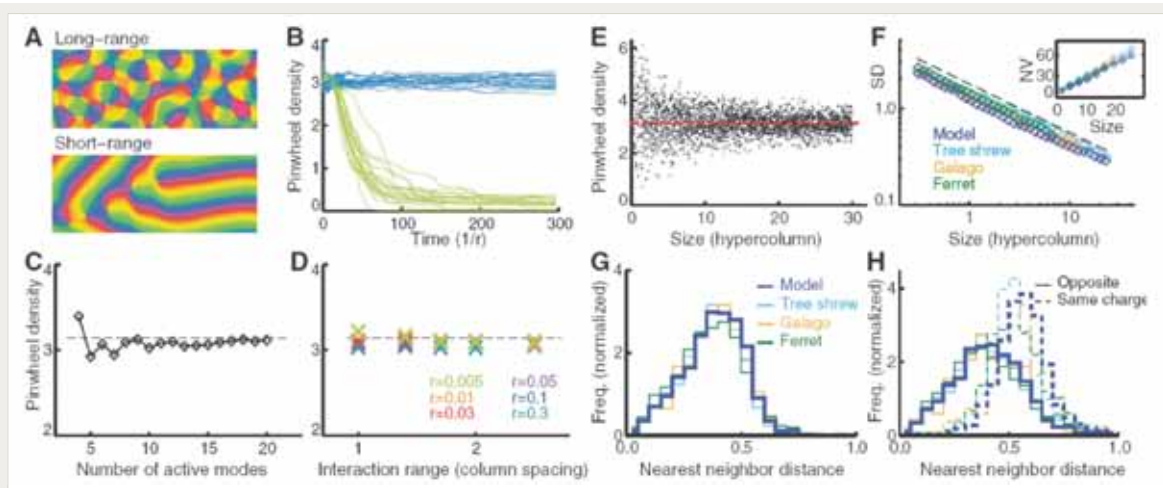


Figure 2

Self-organization of orientation columns dominated by long-range interactions explains the common design of orientation maps in primates and carnivours. (A) Nearly stationary solutions of the long-range interaction model are pinwheel-rich when long-range interactions dominate and pinwheel-sparse when they are absent. (B) Pinwheel densities as a function of time without long-range interactions (green, $n = 30$ different random initial conditions) and when long-range interactions dominate (blue, $n = 30$ different random initial conditions). (C) Average pinwheel densities of closed-form solutions near threshold (solutions contain n active modes) (D) Average pinwheel densities in numerical solutions of the long-range interaction model for different r at $t = 300$. (E to H) Spatial statistics of pinwheels for $n = 26$ randomly chosen closed-form solutions superimposed on these statistics in the three species. (E) Density fluctuations as a function of subregion size, (F, G) Unsigned and signed next-neighbour distance distributions (modified from Kaschube et al. Science 2010).

solute scale of structures were statistically indistinguishable in the three species examined. In particular the frequency of occurrence of orientation pinwheel defects per mm^2 was proportional to the inverse hypercolumn size. Whereas the average column spacing and thus the average hypercolumn size varied by more than a factor of 2 across species, the average pinwheel density was virtually identical. Furthermore, we compared numerous additional statistics characterizing the spatial arrangement of pinwheels within the primary visual cortex, such as the count variance as a function of sampling area, or the charged and uncharged next neighbor distance distributions. None of these quantities indicated a systematic interspecies difference in pattern layout ([1] e.g. figure 2). These observations justified obtaining a more precise estimate of the apparently universal mean pinwheel density by pooling the data from the three species. The grand average of the pinwheel density obtained from a total set of about 10000 defects was 3.14 ± 0.03 .

The finding of this seemingly universal statistics tempts one to conjecture that visual cortex development is essentially guided by an abstract mathematical structure. As the formation and maintenance of orientation preference maps is activity-dependent, we thus examined orientation maps generated by mathematical models involving activity-dependent self-organization. In many models, maps reminiscent of the common design transiently appeared but – in agreement with previous reports – subsequently broke down either by pinwheel annihilation producing pinwheel-sparse maps or by crystallization of pinwheels into a regular lattice (see [1, 7, 15] and references therein). However, in a model of Swift-Hohenberg type, in which pinwheels are stabilized through long-range neuronal interactions [7, 9, 1], we found that theoretically predicted maps exhibited all essential features of the common design in a dynamically stable and robust fashion (figure 2). In this model and many related models from a symmetry defined universality-class (1) pinwheel statistics

can be studied analytically using known closed form expressions for approximate solutions; (2) the parameter dependence of the emerging patterns can be comprehensively characterized and (3) numerical simulations of systems approaching the size of the entire primary visual cortex can be performed efficiently and accurately [7-12].

The emergence of average pinwheel densities close to π appears to be a very robust feature of the formation of orientation maps in the long-range interaction dominated regime. It is relatively insensitive to the absolute range of long-ranging interactions and to the distance from the bifurcation point. In the long-range regime, the model also reproduced all other observed universal statistical properties of visual cortical orientation maps (figure 2e – h). Our results reveal a striking quantitative invariance of pin-

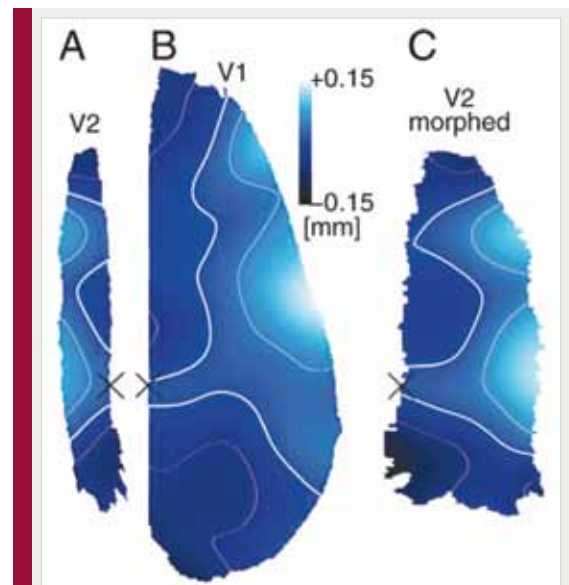


Figure 3

Statistical features of orientation preference maps are matched in directly connected subregions of visual cortical areas V1 and V2. The maps show the population averaged spacing of orientation columns in areas V1 and V2. Column spacings are matched in subregions in regions of areas V1 and V2 that are mutually connected. (A and B) maps for V2 (A) and V1 (B) (color scale codes systematic deviation from the mean value). (C) The morphed map from V2 in A. Scale bar, 10 mm. (correlation between B and C, $r = 0.69$, modified from Kaschube et al., PNAS 2009)

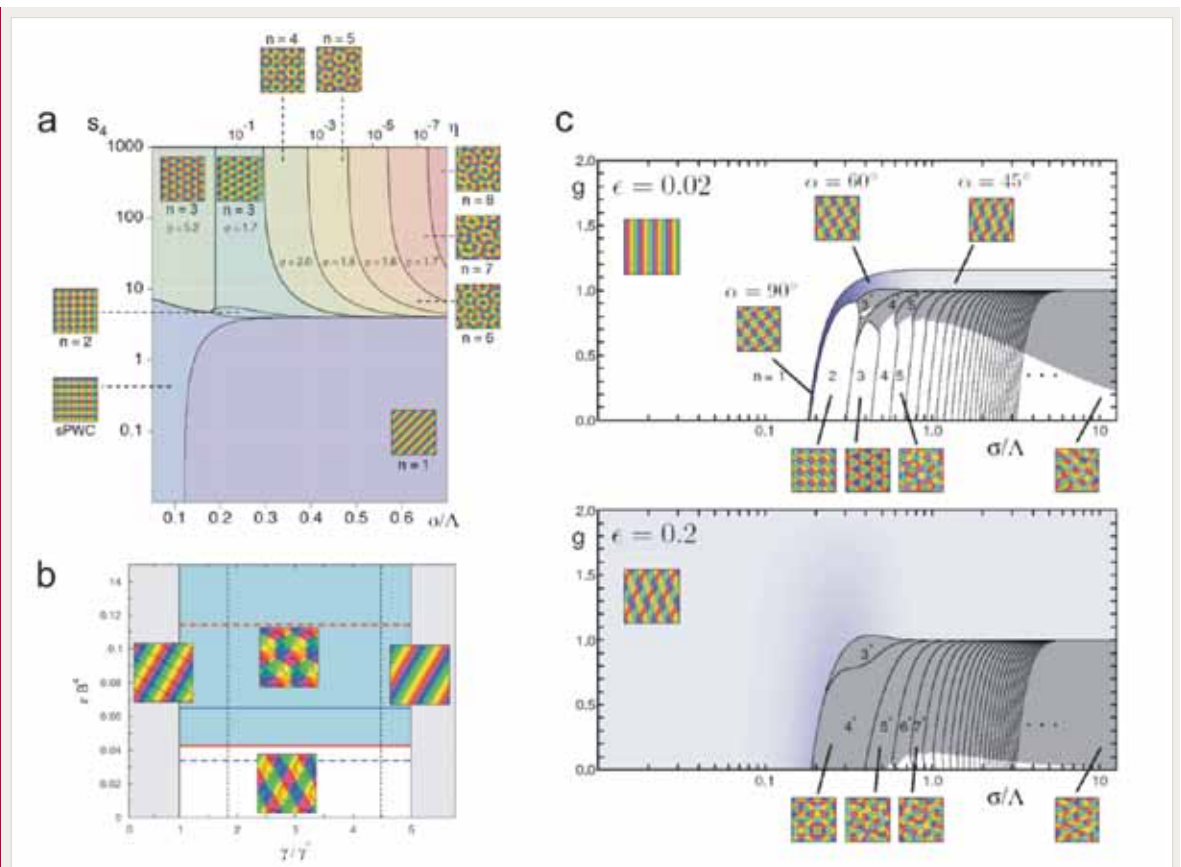
wheel organization across animals and species that strongly contrasts the huge interindividual and interspecies variability exhibited by other aspects of visual cortical architecture [3, 4]. The theoretically predicted critical role of long-ranging interaction for the exact layout of columns in the visual cortex, was independently confirmed by a recent study that examined the relationships of orientation preference maps in different area of visual cortex [13]. This study pointed out that long-ranging interareal connections are present already at the earliest stages of cortical circuit development, such that processes specifying the local functional architecture of one area might be strongly influenced or even guided by large-scale cortical networks extending across many areas.

Utilizing the previously described pronounced intra-areal variability of orientation column layouts in the visual cortex [16, 17] we analyzed whether the columnar architectures in different cortical areas are laid out independently or in a coordinated manner. We analyzed orientation columns processing contours in different parts of the visual field in visual cortical areas V1 and V2 in the left and right hemispheres of kittens aged between 6 and 15 weeks. The spacing of these columns was quantified locally by using a previously developed wavelet method [16]. Because this method provides highly precise estimates of local column spacing (LCS) with an error much smaller than the large intrinsic variability column spacings (SEM, 15 – 50 μm), differences and similarities of column spacings in the sample could be identified reliably. Our data clearly showed that columns at topographically corresponding locations in the two areas that are representing similar visual field positions and are selectively and mutually connected by cortico–cortical connections were matched in their layout parameters. Furthermore these became more similar over the course of postnatal development (e.g. figure 3) [13]. This study thus experimentally confirms the overall concept of dynamical self-organization of neuronal circuits on the scale of entire areas and provides the

first direct evidence that this process is shaped by long-ranging interactions.

According to our self-organization scenario, the common design of orientation maps in the visual cortex is predicted to result from developmental constraints imposed by adopting a general kind of self-organization mechanism for structuring visual cortical circuitry. Even if this scenario is correct, one fundamental question still remains: What drove the different animal lineages to adopt similar self-organization mechanisms in evolution? It is, in fact, not easy to conceive that this adoption was favored by the specific demands of the particular visual habitats of the different species. It is, however, conceivable that general requirements for a versatile and representationally powerful cortical circuit architecture are realized by the common design. It would then be plausible that the evolutionary benefit of meeting these requirements has driven the adoption of large-scale self-organization and the emergence of the common design over evolutionary times.

To test this hypothesis theoretically we are currently extending our symmetry based methods to examine different candidate optimization model for visual cortical architecture. The most prominent example for a general optimization principle is the hypothesis of a coverage-continuity-compromise [18]. It states that the columnar organization should optimally trade off the coverage of the space of visual stimulus features and the continuity of their cortical representation. On the one hand, each combination of stimulus features should be well-represented in a cortical map to avoid “blindness” to certain stimuli. On the other hand, the wiring cost to establish connections within the map of orientation preference should be kept low which can be achieved if neurons that are physically close in the cortex tend to have similar stimulus preferences. These two design goals generally compete with each other. The better a cortical representation covers the stimulus space, the less smooth it has to be. The trade-off between the two has been modeled in the so-called di-


Figure 4

Phase diagrams of different optimization models for the layout of orientation preference columns indicate that suppressive long-range interactions are essential for the selection of aperiodic orientation maps reproducing the common column design observed in Kaschube et al. *Science* 2010. (a) Phase diagram of the elastic network as a function of effective interaction range (abscissa) and kurtosis of the stimulus ensemble (ordinate) (Keil & Wolf 2011). (b) Phase diagram of a coordinated optimization model for ocular dominance and orientation preference maps as a function of contralateral eye dominance (abscissa) and coupling strength (ordinate) and (Reichl, Löwel, *Wolf Phys. Rev. Lett.* 2008, Reichl et al. 2011). (c) Phase diagram of a shift-twist symmetric variant of the long-range interaction model as a function of interaction range (abscissa) and relative strength of local and long range interactions (ordinate). The purely local coordinated optimization model although exhibiting pinwheel rich phases, completely lacks aperiodic ground states of realistic pinwheel statistics. Optimization models including long-range interactions such as the EN for high kurtosis stimulus ensembles or the long-range interaction model can reproduce aperiodic map layouts and the common design of orientation maps in the visual cortex when the effective interaction range is sufficiently large.

mension reduction framework in which cortical maps are represented by two-dimensional sheets which fold and twist in a higher-dimensional stimulus space to cover it as uniformly as possible while minimizing continuity [18].

To test whether this kind of functional optimization can drive the evolutionary emergence of the design of orientation columns we have examined whether the elastic net (EN) model [18] can reproduce the apparently universal pin-

wheel statistics [12]. While this model has been used in numerous numerical studies, no analytical results about its optimal solutions have been obtained so far. We thus generalized our mathematical approach to analytically calculate the optimal cortical representations predicted by the EN model for the joint mapping of stimulus position and orientation [12]. We found that in all previously studied regimes, optimal OPM layouts are perfectly periodic strongly de-

viating from experimental observations. An unbiased search through the complete EN parameter space however identified a novel regime of aperiodic solutions (figure 4). In an extreme limit, aperiodic solutions quantitatively resembling experimental observations were found to become optimal [12]. Our mathematical analysis reveals that stabilization of these layouts results from strong nonlocal interactions rather than from a coverage-continuity-compromise. This re-analysis of the EN model thus independently confirms a critical role of long-ranging intra-cortical interactions for the emergence of orientation maps exhibiting the common design. Extending our approach we also are currently re-examining or de novo characterizing a whole range of other candidate optimization principles for visual cortical architecture (see [10-12] and figure 4) in order to obtain a comprehensive picture of the critical ingredients of realistic optimization principles.

Our empirical results and theoretical analyses suggest that the precise spatial organization of pinwheels in the visual cortex reflects cortical

network self-organization rather than genetic prespecification or environmental instruction of neuronal circuit development. Our theory reveals that dynamical network self-organization can robustly constrain the spatial organization of cortical circuitry to a specific design. Currently, only one alternative arrangement has been observed in nature: the columnless, apparently random, salt-and pepper organization of rodent visual cortex (figure 1) [3, 4, 19]. Because a complete lack of local order appears to be its key feature, we expect that fundamental properties of local rather than long-range circuit formation are essential for its self-organization. It is possible that this fundamentally different organization can also be derived from a dynamical theory of network self-organization. If so, the principles of network self-organization operating on a local order would account for the presence or absence of orientation columns, whereas long-ranging interactions would explain the organization of orientation columns into pinwheels, with a spatial layout conforming to the common design.

- [1] M. Kaschube, M. Schnabel, S. Löwel, D.M. Coppola, L.E. White, F. Wolf, *Science* **330**, 1113 (2010)
- [2] J. H. Kaas, *Brain Res. Bull.* **75**, 384 (2008)
- [3] K. Ohki, S. Chung, Y. H. Ch'ng, P. Kara, R. C. Reid, *Nature* **433**, 597 (2005)
- [4] S. D. Van Hooser, *Neuroscientist* **13**, 639 (2007)
- [5] F. Wolf, F. Kirchhoff, *Science* **320**, 1597 (2008)
- [6] K.D. Miller, *Science* **330**, 1059 (2008)
- [7] F. Wolf, *Phys. Rev. Lett.* **95**, 208701 (2005)
- [8] M. Schnabel, M. Kaschube, S. Löwel, F. Wolf, *Eur. Phys. J* **145**, 137 (2007)
- [9] M. Kaschube, M. Schnabel, F. Wolf, *New J Phys.* **10**, 015009 (2008)
- [10] L. Reichl, S. Löwel, F. Wolf, *Phys. Rev. Lett.* **102**, 208101 (2009)
- [11] L. Reichl, D. Heide, S. Löwel, J. C. Crowley, M. Kaschube, F. Wolf, *arXiv*, **1102.3353** (2011)
- [12] W. Keil, F. Wolf, *arXiv* **1104.1946** (2011)
- [13] M. Kaschube, M. Schnabel, F. Wolf, S. Löwel, *Proc. Nat. Acad. Sci. USA* **106**, 117205 (2009)
- [14] W. Keil, K. Schmidt, S. Löwel, M. Kaschube *Proc. Nat. Acad. Sci. USA* **107**, 12293 (2010)
- [15] F. Wolf, T. Geisel, *Nature* **395**, 73 (1998)
- [16] M. Kaschube, F. Wolf, T. Geisel, S. Löwel, *J. Neurosci.* **22**, 7206 (2002)
- [17] M. Kaschube, F. Wolf, M. Puhlmann, S. Rathjen, K.F. Schmidt, T. Geisel, S. Löwel, *Eur. J. Neurosci.* **22**, 7206 (2003)
- [18] R. Durbin, G. Mitchison *Nature* **343**, 644 (1990)
- [19] D.M. Coppola, M. Kaschube, S. Löwel, M. Schnabel, L.E. White, F. Wolf, *Science* (in press)

VI Networks

VI-1 Self-organized Criticality and Avalanches in Neural Networks

M. Herrmann, A. Levina, D. Battaglia, T. Geisel

S. Dasgupta, H. Schrobsdorff, O. Stetter, E. Moses (Weizmann Institute), J. Soriano (Universitat de Barcelona)

THE CONCEPT of self-organized criticality (SOC) [1] describes a variety of phenomena ranging from plate tectonics, the dynamics of granular media and stick-slip motion. These examples have in common that a marginally stable dynamics is maintained by self-tuning of parameters towards critical values and that the event sizes obey a characteristic power-law distribution. Neuronal systems tend also to operate near a critical state [2], characterized by avalanches of neuronal activity with a power-law distribution of avalanche sizes. It is known that critical states possess properties of computational optimality [3] and maximal sensitivity [4] both of which are beneficial prop-

erties in living beings. In a previous study [5], we have demonstrated analytically and numerically that by assuming biologically realistic depressing synapses in a spiking neural network, the neuronal avalanches turn from an exceptional phenomenon into a typical and robust self-organized critical behaviour, if the total resources of neurotransmitter are sufficiently large. We have now generalized our finding to the case of pulse-coupled neurons interacting via dynamical synapses, which exhibit both depression and facilitation as found in neurophysiological experiments. We have analytically described a transition scenario to SOC that is new for physics as well as neuro-

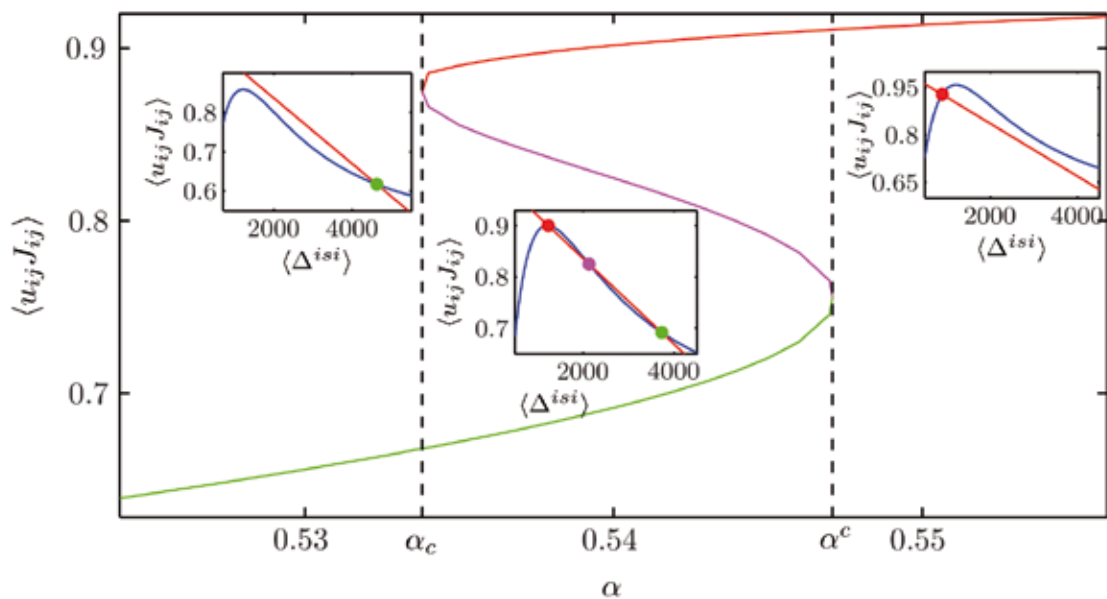


Figure 1

Bistability between a subcritical and a critical state in a network of pulse-coupled neurons with depressing and facilitating synapses. The horizontal axis gives the scale of synaptic strength scale. The vertical axis gives the effective strength of synaptic interactions [6]. Note the bistability region for intermediate scales of synaptic strength.

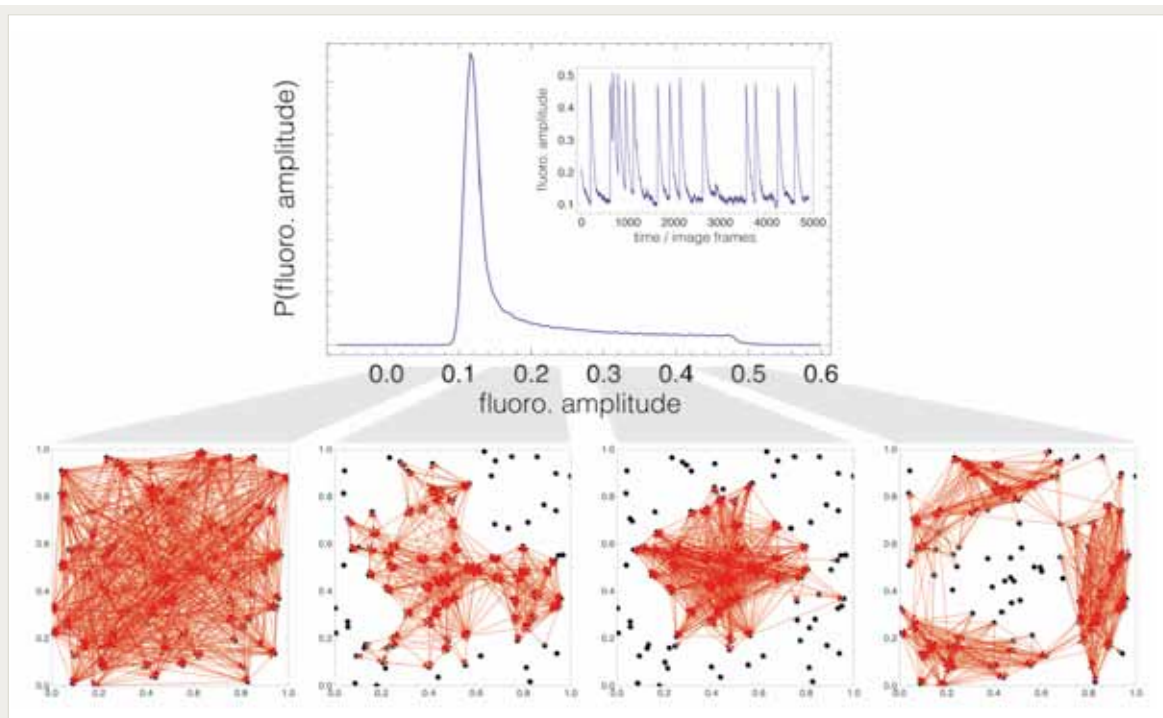


Figure 2

State-dependent network reconstruction from synthetic calcium imaging signals. Synthetic calcium fluorescence signals are generated by simulating the dynamics of a network exhibiting avalanches of neuronal activity. Effective connectivity is assessed from the time-series of simulated calcium fluorescence using Transfer Entropy and compared with the structural network. Conditioning on different ranges of the fluorescence signal provides different effective connectivities. High fluorescence values associated to avalanching lead to effective connectivity with densely connected components. Effective connectivity provides a good approximation to structural connectivity in dynamical states between avalanches.

science. It combines the criticality of first and second-order phase transitions with a SOC phase. We have analytically shown the coexistence of a SOC phase and a subcritical phase connected by a cusp bifurcation. Switching between the two phases can be triggered by varying the intensity of noisy inputs [6]. The model has implications for the study of cognitive effects of aging [7, 8], a ramification which is currently studied in an ongoing project at the Bernstein Center for Computational Neuroscience in Göttingen.

Avalanches of neuronal activity akin to the one observed in SOC states are observed in neuronal cultures. Their occurrence can be detected through calcium imaging techniques that allow visualizing the activity of hundredths of cells simultaneously [9]. A small minority of neurons in the cultures may be called “Leaders”, as they

form an interconnected subnetwork that consistently fires much before the rest of the culture. Once initiated, the activity spreads from the Leaders to the less connected majority of the culture. We have shown that the distribution of the in-degrees of Leader neurons determine the growth-rate of the number of neurons active in a burst [10]. We have then explored the possibility of reconstructing the underlying structural topology of the network formed by neurons cultured in vitro from the measurement of their spontaneous neuronal activity through calcium imaging. A successful reconstruction algorithm would allow for the characterization of bulk properties of these networks, such as the dependence of connection probability of two nodes on the distance between them, distributions of degrees or clustering co-

efficients, which are currently inaccessible with single-cell or even typical multi-electrode techniques. We estimate an approximation to the structural connectivity of the network evaluating effective connectivity by means of Transfer Entropy [11]. It is important to remark that the effective connectivity depends on the dynamical state. For instance, during the ignition of a critical burst it is almost all-to-all, reflecting a situation of high susceptibility in which the addition of a single spike can cause the entire network to fire. Effective connectivity provides a good approximation to structural connectivity in phases of activity where the dynamics in the network are dominated by direct monosynaptic interactions [12]. We have demonstrated post-process-

ing improvements of the reconstruction using the Data Processing Inequality. These methods, already applied with success in the reconstruction of gene regulatory networks [13], help to discriminate indirect from direct interactions. Finally, we have applied our algorithm to real data from large cultures of hippocampal neurons in vitro. Data have been provided by the Labs of Elisha Moses (Weizmann Institute) and Jordi Soriano (Universitat de Barcelona). Preliminary investigations have allowed us to probe and quantify the distance-dependent probability of connection and to identify other topological properties of the reconstructed network deviating from pure randomness, like an elevated average mean clustering coefficient [12].

- [1] P. Bak, C. Tang, K. Wiesenfeld, Self-organized criticality: An explanation of the $1/f$ noise, *Phys. Rev. Lett.* **59**, 381 (1987)
- [2] J.M. Beggs, D. Plenz, Neuronal avalanches in neocortical circuits. *J. Neurosci.* **23**, 11167-77 (2003)
- [3] R. Legenstein, W. Maass, Edge of chaos and prediction of computational performance for neural circuit models, *Neural Networks* **20**, 323-334 (2007)
- [4] O. Kinouchi, M. Copelli, Optimal dynamical range of excitable networks at criticality, *Nature Physics* **2**, 348-351 (2006)
- [5] A. Levina, J.M. Herrmann, T. Geisel, Dynamical synapses causing self-organized criticality in neural networks. *Nature Physics* **3**, 857-860 (2007)
- [6] A. Levina, J.M. Herrmann, T. Geisel, Phase Transitions towards Criticality in a Neural System with Adaptive Interactions. *Phys. Rev. Lett.* **102**, 118110 (2009)
- [7] H. Schrobsdorff, M. Ihrke, J. Behrendt, J.M. Herrmann, T. Geisel, A. Levina, Are aging effects caused by optimization?, abstract for the CNS 2009 meeting (Berlin, 18-23 July 2009)
- [8] S. Dasgupta, J.M. Hermann, Critical dynamics in homeostatic memory networks, abstract for the COSYNE 2010 meeting (Salt Lake City, 25-28 February 2010)
- [9] I. Breskin, J. Soriano, E. Moses, T. Tlusty, Percolation in living neural networks. *Phys. Rev. Lett.* **97**, 188102 (2006)
- [10] J.P. Eckmann, E. Moses, O. Stetter, T. Tlusty, C. Zbinden, Leaders of neuronal cultures in a quorum percolation model, *Front. Comp. Neurosci.* **4**, 132 (2010)
- [11] T. Schreiber, Measuring information transfer. *Phys. Rev. Lett.* **85**, 461-464 (2000)
- [12] O. Stetter, D. Battaglia, T. Geisel, Network reconstruction from calcium imaging signals, abstract for the 7th FENS Forum of European Neuroscience (Amsterdam, 3-7 July 2010)
- [13] A. Margolin et al., ARACNE: An algorithm for the reconstruction of gene regulatory networks in a mammalian cellular context. *BMC Bioinformatics* **7**(Suppl 1), S7 (2006)

VI-2 Interplay of Self-Organization and Molecular Guidance Clues in the Formation of Neural Circuits

D. Tsigankov,

A. Koulakov (Cold Spring Harbor Lab., USA)

IN DEVELOPING brain, connectivity is established under the influence of several factors. Neurons initially find appropriate targets based on sets of chemical labels [1, 2]. This *chemospecificity hypothesis*, originally postulated by Rodger Sperry [3], motivated the search for molecules that could be used as such cues and suggested the principles which direct growing axons to their targets. The precision of axonal projections is further affected through mechanisms based on correlated neural activity. These activity-dependent mechanisms are thought to implement the rules for modification of neuronal connections that were proposed by Donald Hebb [4]. Hebbian rules provide a paradigm through which sensory experience may influence the formation of the neuronal connectivity. This is in contrast to molecular labels that are controlled primarily by genes. One of the central questions in the studies of the developing nervous system is how the influences of molecular labels are combined with Hebbian learning rules to yield connectivity that is both precise and adaptive [5].

Here we study a computational model for the formation of connectivity between neurons in visual cortex that combines the effects of molecular labels and correlated neural activity. We show that these factors may cooperate or carry conflicting requirements under different conditions. During the development of topographic maps for the projections of neurons from the retina to the brain the gradients of chemical labels establish a crude map that is further refined by the effects of correlated electrical activity. In contrast during the formation of ocular dominance patterns these two mechanisms have the opposite tendencies to merge and segregate the inputs from different eyes.

In our model we formulate an energy function that depends on the neuronal connectivity matrix W . When accounting for molecular labels, we sug-

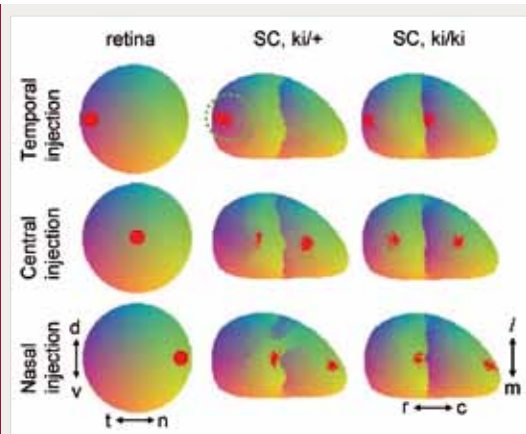


Figure 1

The mapping in knock-ins as obtained in the computational model. The complete map structure is color-coded according to the axonal origin in retina as shown by the left column. In addition the termination zones for a small subset of axons indicated by the red points are shown for temporal (upper row), central (center row) and nasal (lower row) labeling. The heterozygous knock-ins (central column) has less amount of the additional EphA receptor than homozygotes (right column).

gest that the final connectivity minimizes the total number of receptors bound/activated by the ligands in case of chemorepulsion and maximizes this quantity for chemoattraction. Likewise the effects of correlated activity are included by maximizing the Hebbian interactions with neighbouring neurons for the excitatory connections and minimizing it for the inhibitory connections. Thus the energy function in the model is given by

$$E = E_{chem} + E_{act} = \sum_{\alpha\beta} M_{\alpha\beta} \sum_{ij} W_{ij} R_i^\alpha L_j^\beta + \frac{1}{2} \sum_{ijml} C_{ij} W_{mi} W_{jl} U_{ml}$$

Here M is the matrix describing the affinities between the receptor concentrations R and the ligand concentrations L , U is the activity-dependent interaction function and C is the cross-correlation matrix of the neuronal activities. Because both E_{chem} and E_{act} are functions of neuronal connectivity, the minimum of their sum yields a set

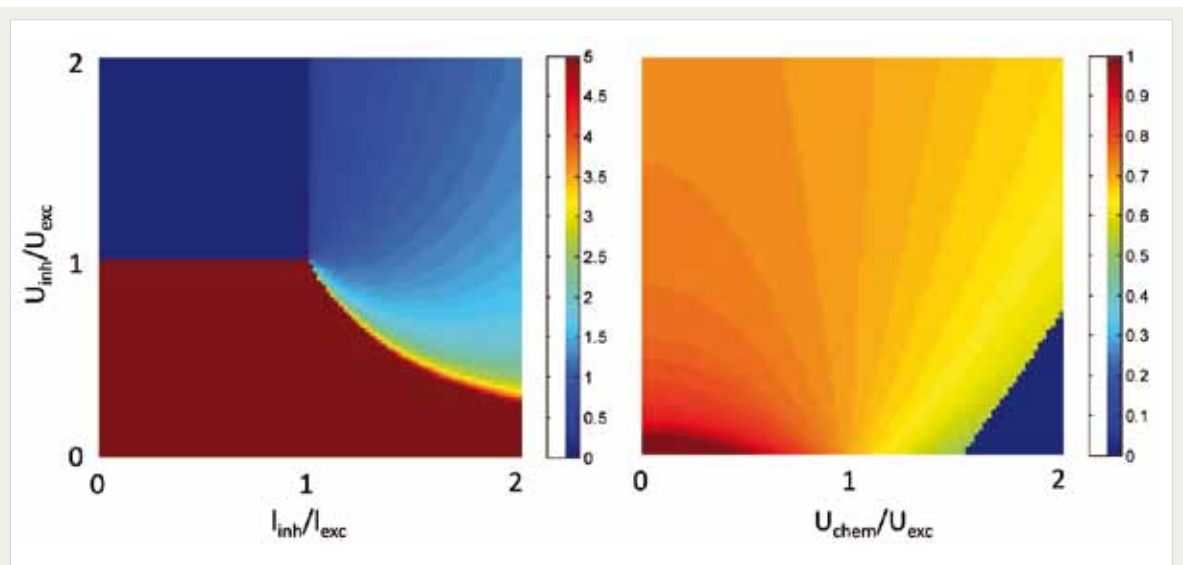


Figure 2

Phase diagrams for ocular dominance structures in the 1D model. The colorbar shows the width of the ocular dominance stripes in the periodic structure. Different phases can be obtained even in the absence of the gradients of chemical labels (left panel) where the interplay between the excitation and inhibition determines the period of ocular dominance for Mexican-hat type of interactions. The blue region corresponds to salt and pepper configuration, while brown represents the maximum separation of the inputs from left and right eye. In the presence of the gradients the dependence of the period on the inhibitory interactions reverses its sign for strong interactions between chemical labels (right panel).

of projections that forms a compromise between the molecular labels and the effects of correlated activity.

We minimize this function both numerically and analytically to obtain the connectivity layouts in the visual system. In figure 1 we show the retinocollicular topographic maps in the *Isl2/EphA3* mutant mice where the expression levels of the molecular labels are changed. As a result the topographic projection is rewired so that the neighborhood relationships between the retinal ganglion cell axons are disrupted. According to our model, the experiments in *Isl2/EphA3* knock-in mice test the interactions between the effects of molecular labels and correlated activity during the development of neural connectivity. Correlated activity can restore topographic order even when molecular labels carry conflicting information. In contrast, during the formation of ocular dominance pattern, the interactions between chemical labels and activity-dependent interactions counteract each other even in wild-type animals. We show that the emerging periodicity, i.e. the width of the ocular

dominance stripes is determined by the relative strength of these two mechanisms. We show the phase diagram for ocular dominance patterns in the 1D case on figure 2. Overall, we suggest that various structures in the visual system emerge as a result of an interplay between interactions of chemical labels and activity-dependent contributions.

- [1] Tessier-Lavigne M, Goodman CS *Science* **274** (5290), 1123-1133 (1996)
- [2] O'Leary DD, Wilkinson DG *Curr Opin Neurobiol* **9** (1), 65-73 (1999)
- [3] Sperry RW *Proc Nat Acad Sci USA* **50**, 703-710 (1963)
- [4] Hebb DO: *The organization of behavior; a neuropsychological theory*. New York, : Wiley; (1949)
- [5] Cline H *Trends Neurosci* **26** (12), 655-661 (2003)

VI-3 Dynamic Interactions between Neuronal Circuits

D. Battaglia, A. Witt

X.-J. Chen, T. Geisel, C. Kirst, W. Wei, F. Wolf, A. Gail (DPZ, Göttingen),
D. Hansel (University Paris Descartes – CNRS)

NEURONS IN THE BRAIN are wired into a synaptic network that spans multiple scales, from very local circuits within cortical columns (< 1 mm) to fiber tracts interconnecting distant brain areas (1–10 cm). Anatomic connections affect the information flow within and between neuronal circuits, as well as the synchronization of neuronal activity. However, brain functions, from vision or motor preparation up to consciousness require the dynamic control of inter-areal interactions on time-scales faster than synaptic changes. In particular, strength and direction of causal influences between areas – described by the so-called effective connectivity [1] – must be reconfigurable even when the underlying structural (i.e. anatomic) connectivity is fixed. Such effective connectivity can be quantified resorting to causal analysis of time-series based on tools like Granger Causality [2] or Transfer Entropy [3]. The ability to quickly reshape effective connectivity is a chief requirement for performance in a changing and competitive natural environment. Yet it is an open problem to understand which mechanisms allow to achieve this ability. How can manifold effective connectivities result from a single fixed structural connectivity? How can effective connectivity be controlled dynamically without resorting to structural changes? In the framework of this project we have explored the hypothesis that the self-organization of collective neuronal oscillations underlies the fast reorganization of brain effective connectivity. Synchronous oscillations across different frequency ranges, and in particular in the so-called *gamma* range (40–100 Hz), are involved in a steadily growing repertoire of cognitive processes [4]. Based on the analytic and numerical analysis of mean-field and of spiking network models of interacting brain areas, we have found that “causality follows dynamics” [5]. Different dynamic states of a same

structural network – e.g. different phase-locking patterns of local coherent oscillations – are associated to different effective connectivities. Switching between these effective connectivities is reliably induced in our models through pulse perturbations suitably phased with respect to the ongoing rhythm. This mechanism is neurally plausible and metabolically efficient.

Furthermore, we have found that “information follows causality” (and, therefore, dynamics) [5]. We have directly verified that different effective networks associated to a same structural network have different information routing properties. Oscillations in the rate of neuronal activity act as the “carrier” of rich information encoded in precise patterns of neuronal firing. The self-organization of interacting brain rhythms allows then the transmission and the processing of this complex information in a way akin to a “clocked” digital combinatorial circuit. Note that selective information routing based on carrier coher-

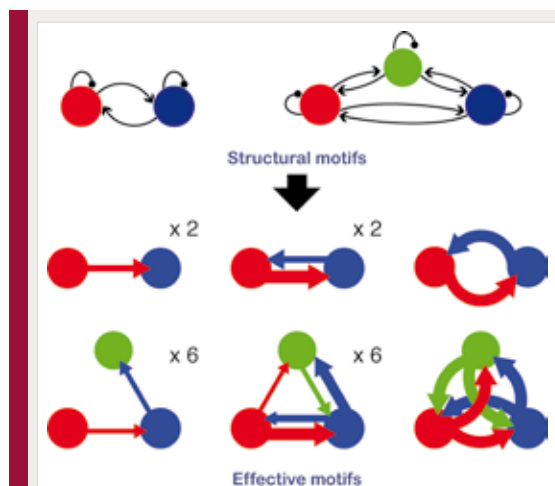


Figure 1

One structural connectivity leads to many effective connectivities. Even very simple structural motifs involving a small number of reciprocally connected local circuits can give rise to a large number of effective motifs with different topologies.

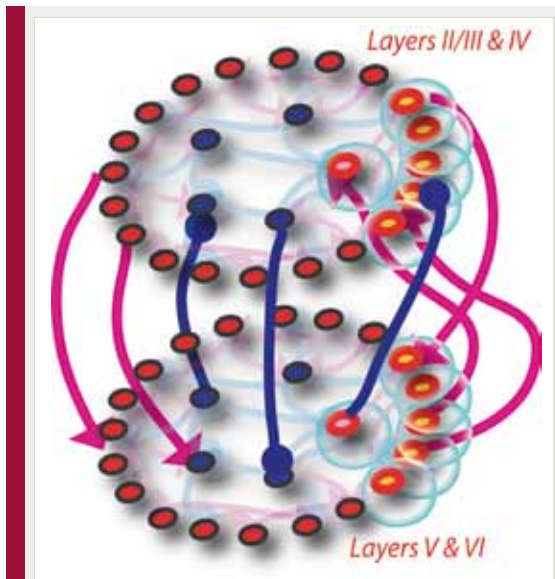


Figure 2

Minimal multi-layer model of a functional hypercolumn. A single hypercolumn of primary visual cortex is modeled as a network with two modules with ring-topology, representing deep and more superficial cortical layers. In such a multi-layer network qualitatively novel dynamical responses can emerge. In particular, the neuronal activity evoked by stimuli with high contrast is chaotically synchronous, giving rise to realistic broad-band spectra.

ent oscillations can occur also within local circuits. In an inhomogeneous network, dynamic phase-locking takes place among clusters of more densely connected neurons [6]. We have derived analytic expressions for the time-delayed mutual information between different groups of neurons modeled as phase oscillators. Furthermore we have shown that local changes in the strength of few synaptic couplings can remotely control information flow between distant neuronal clusters [6].

The dynamics of neuronal circuits with interacting sub-modules can be very different from the dynamics of the isolated sub-modules themselves. In particular, qualitatively different dynamical states can emerge, characterized by very different functional properties. As canonical examples of circuits with interacting components, we have investigated multi-layer models of small portions of cerebral cortex. Very often the cortex is modeled as a two-dimensional system, neglecting the existence of a six-layered structure, with a largely stereotyped architecture of inter-layer connections [7]. We have considered a minimal multi-layer model of a functional hypercolumn of striate

cortex [8]. In our architecture, two networks with ring topology, representing respectively deep and more superficial cortical neuronal layers, interact through excitatory and inhibitory inter-layer synapses. Thanks to the interaction between neuronal populations at different depths in the cortical tissue, the oscillatory responses evoked by visual stimulation are synchronous, but, at the same time, chaotic. The chaotic nature of this evoked dynamics makes possible to reconcile the experimentally observed broad-band power spectra together with synchrony, unlike previous models without interacting layers, giving rise instead to exceedingly harmonic evoked spectra [8]. We have also developed a mean-field model of a single cortical column [9] that embeds a realistic six-layers architecture based on anatomical observations [7]. We have found that inter-layer interactions endow the cortical column with the capacity to adapt dynamically its own response to stimuli depending on the context. Thanks to the vertical competition between neuronal populations in different layers, small changes in the currents describing classical and extra-classical surround stimulation are non-linearly amplified, leading to strong contextual modulations of the column response [9].

Finally, in parallel to modeling and theoretical analyses, we have also analyzed inter-areal interactions in real brain, through the causal analysis of multi-channel recordings in behaving macaque monkeys. We have focused on experiments performed at the German Primate Center in Göttingen, in the lab of Alexander Gail. In these experiments, a monkey performs reach movements, instructed by visually presented cues. Different rules can be used to map a sensory cue into a reach direction. In the “PRO” case, the monkey has to reach in the same direction of the stimulus, when a go signal is presented after a delay period. In the “ANTI” case, the monkey has to reach in the opposite direction [10]. Even simple hand movements activate a complex fronto-parietal network involving many brain areas. In the case of reach movements, two areas participate to the decision of a motor goal, the Parietal Reach Region (PRR) and the Premotor dorsal area (PMd). PRR receives directly sensory-related inputs, whereas

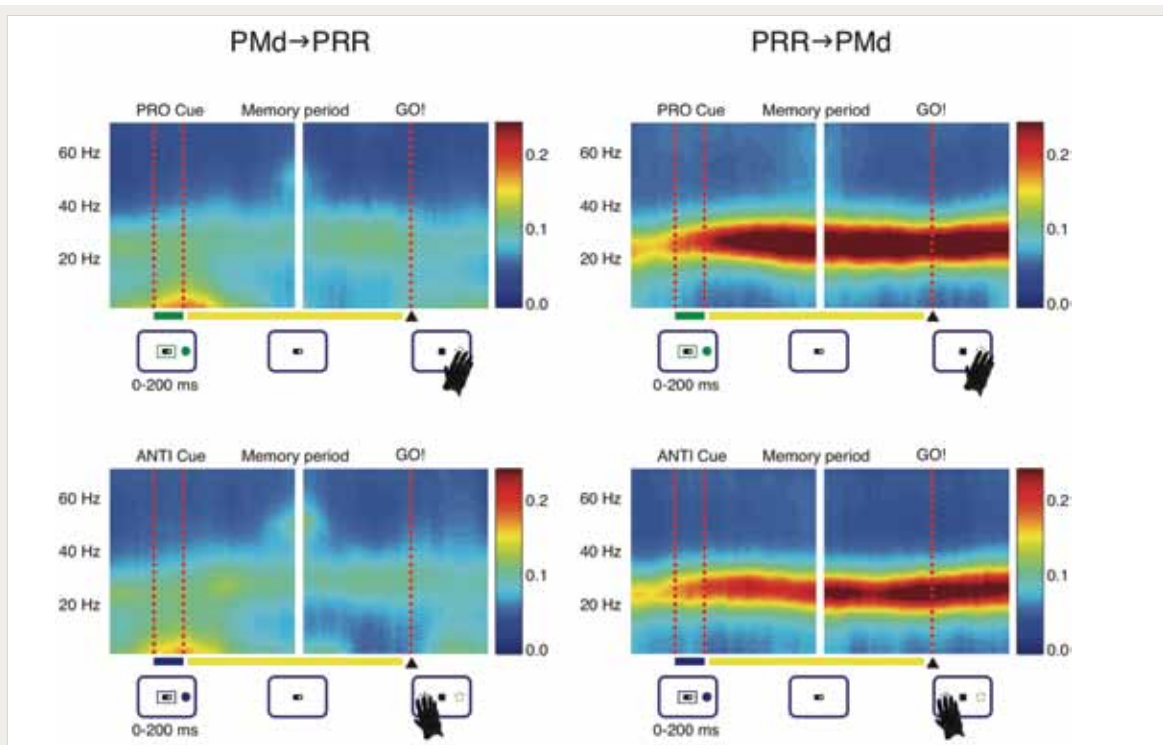


Figure 3

Inter-areal interactions in goal-directed reaching. Dynamic effective connectivity between brain areas PRR and PMd is represented here in causogram form. Effective connectivity from PMd to PRR is shown in the left column and from PRR to PMd in the right column. The top row refers to a sensorimotor mapping task with a “PRO” rule (reach movement in direction of the sensory cue) and the bottom row to a task with a “ANTI” rule (reach movement in direction opposite to the sensory cue). The time-line of the experiment is reported below each causogram. The color encodes the strength of effective connectivity, frequency-band by frequency-band, as measured by spectral Granger Causality. Causal interactions occur in different frequency bands and are modulated by changes in task phases and remapping rules.

PMd integrates also inputs coming from higher order areas involved in the representation of abstract rules. The causal analysis of time-series of Local Field Potentials simultaneously recorded in PRR and PMd have unveiled that the effective connectivity between areas PRR and PMd is highly dynamic and is modulated across task phases and by changes in the rule for sensorimotor mapping [11]. Furthermore, causal interactions from PRR to PMd

and from PMd to PRR occur into different coherent frequency bands. Cue-related causality from PMd to PRR (in the 5-15 Hz frequency range) can be interpreted as a “top-down” kick informing PRR about the rule to be used for motor goal decision. Causality from PRR to PMd (in the 20-30 Hz frequency range) is particularly strong during the delay period and is enhanced for a PRO rule, reflecting the larger weight assigned to sensory inputs in this case.

- [1] K.J. Friston, Functional and effective connectivity: a synthesis. *Human Brain Mapping* **2**, 56-78 (1994)
- [2] M. Ding, Y. Chen, S.L. Bressler, Granger causality: Basic theory and application to neuroscience. In Schelter S, Winterhalder N, and Timmer J, *Handbook of Time Series Analysis*. Wiley, Wienheim (2006)
- [3] T. Schreiber, Measuring information transfer. *Phys Rev Lett* **85**:461-464 (2000).
- [4] X.J. Wang, Neurophysiological and computational principles of cortical rhythms in cognition. *Physiol Rev.* **90**, 1195-1268 (2010)
- [5] D. Battaglia, A. Witt, F. Wolf, T. Geisel, Dynamic control of effective connectivity between interacting brain areas, abstract for the Society for Neuroscience meeting - SFN 2010 (San Diego, USA, 13-17 November 2010); manuscript submitted
- [6] C. Kirst, M. Timme, D. Battaglia, Changes in a single synaptic link control global network effective connectivity and information routing, abstract for the Society for Neuroscience meeting - SFN 2010 (San Diego, USA, 13-17 November 2010)
- [7] T. Binzegger, R.J. Douglas, K.A.C. Martin, A quantitative map of the circuit of cat primary visual cortex. *J Neurosci.* **24**, 8441-8453 (2004)
- [8] D. Battaglia, D. Hansel, Synchronous chaos and broad band gamma rhythm in a minimal multi-layer model of primary visual cortex, manuscript in revision for PLOS Comp Biol. (2011)
- [9] X.J. Chen, W. Wei, F. Wolf, D. Battaglia, Interacting sub-circuits in a primary visual cortex column: Insights from a multi-layer rate model, abstract for the Society for Neuroscience meeting - SFN 2010 (San Diego, USA, 13-17 November 2010)
- [10] S. Westendorff, C. Klaes, A. Gail, The cortical timeline for deciding on reach motor goals. *J Neurosci* **30**, 5426-5436 (2010)
- [11] A. Witt, D. Battaglia, T. Geisel, A. Gail, Dynamic effective connectivity analysis of goal-directed reaching, abstract for the Bernstein Conference on Computational Neuroscience (Berlin, 27 September - 1 October 2010)

VI-4 Flux Cycles as Fundamental Building Blocks of Non-Equilibrium Steady States

J. Vollmer, S. Herminghaus, M. Timme

B. Altaner, L. Katthäs (Univ. Marburg), S. Grosskinsky (Univ. Warwick), L. Rondoni (Politecnico di Torino, Italy)

A MAJOR challenge of statistical physics is to identify principles organizing the structure of steady states. In equilibrium systems such a mechanism is provided by a free energy functional from which one can derive all thermodynamic properties of the system [1]. The origin of this feature is Liouville's theorem which provides a symmetry condition between different states of the system known as detailed balance. In non-equilibrium systems detailed balance is broken in the steady state. Consequently, there is no reason to expect that there is a potential function for these systems that allows one to calculate the steady-state properties of the system. Remarkably, this expectation is premature [2]: the dynamics of every non-equilibrium steady state (NESS) can be mapped onto a dual space, where detailed balance is restored. In this representation the fundamental building blocks are flux cycles, and a thermodynamic potential can be defined.

In our argument [2] we idealize observable processes as irreducible, positively recurrent Markov processes on a finite state space. The enterprise [1] to formulate a "stochastic thermodynamics" in such a setting has recently been flourishing again [3, 4] since it is the appropriate setting to describe the thermodynamics of molecular machines like motor proteins [5].

We make use of a simple analogy: The system is thought of as a passenger on a mass transit system described by a graph like the one in figure 1. The mesoscopic states are the vertices of the graph and therefore the stations i of the transit system. Non-vanishing transition rates between two states i and j are marked by a directed edge (i, j) . They correspond to one or more lanes running from station i to station j . The numbers on the edges in figure 1 are the fluxes. They are a measure for the number of passengers traveling

from one station to another per unit time. The representation of the steady state in terms of fluxes is equivalent to specifying the steady state occupation probabilities p_i of the states i , and the transition rates w_{ij}^i to proceed from state i to j . Consequently, we suggest [2] to promote the fluxes rather than currents to the fundamental objects to build NESS.

Our approach is based on a decomposition of NESS in terms of flux cycles, which are labeled by greek letters ($\alpha, \beta, \gamma, \delta$ in the example shown in the figures). They correspond to different lanes of the transit systems running one way in closed cycles. Each passenger is proceeding along a lane selected by a ticket he is carrying. A passenger can switch lanes at any station and proceed on another lane by changing his ticket at random with other passengers. Ticket switching between any two lanes defines a "meta flux" Ψ_{β}^{α} of passengers between lanes α and β rather than between stations. The resulting dynamics in cycle space is again a Markov process on a new graph where the vertices represent the cycles of the original problem, cf. figure 2.

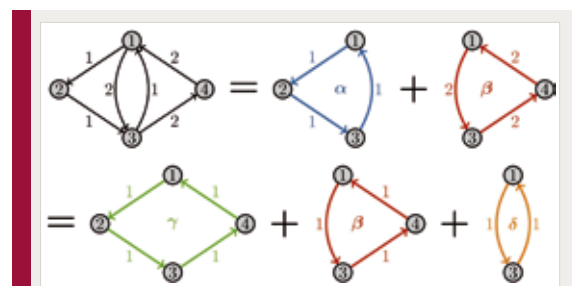


Figure 1

Markov graph representing a NESS with states ①, ②, ③ and ④. The numbers at the edges connecting the states correspond to the steady state fluxes $\phi_{ij}^i = p_i m_j^i$. The steady state can be decomposed into the cycle fluxes with positive weights. In the example, two different decompositions, in terms of α, β and in γ, β, δ are possible.

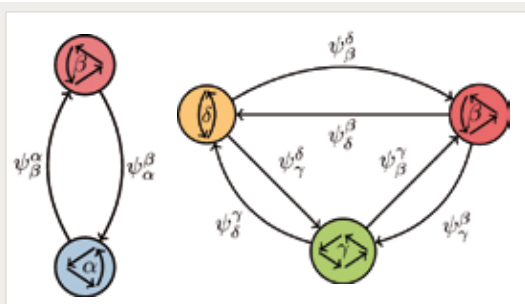


Figure 2

Representation of the equilibrium dynamics on the cycle spaces obtained from the two decomposition introduced in figure 1.

For each pair of lanes α and β sharing a common station, the “meta flux” Ψ_{β}^{α} indicates the rate of passengers transferred between the respective lines.

A crucial observation of our work is that the meta-fluxes Ψ_{β}^{α} between lanes fulfill detailed balance. Hence one can proceed along the lines of equilibrium thermodynamics to assign Boltzmann weights to the cycles and define averages on cycle space which exactly represent

the steady-state averages of the steady state of the original system. This formalism can also be used to assign an entropy production to individual cycles. Proceeding along this line, an extended electric and thermodynamic analogy was established which provides an easy measure quantifying how strongly a system is deviating from an equilibrium steady state.

Future work will basically proceed in two directions. (i) From the point of view of (molecular) thermodynamic machines a cycle corresponds to an operation mode of the machine. For small systems noise plays a huge role for the dynamics. We will characterize these fluctuations by fluctuation theorems which can easily be formulated for the cycle dynamics (cf [3]). (ii) The fluxes and forces along cycles together with their mutual connection (as shown in figure 2) are considered the fundamental entities in our approach. Consequently, two steady states agreeing in those properties are equivalent. We explore presently how this leads to a new way of model reduction for Markov processes.

- [1] O. Penrose: “Foundations of statistical mechanics: a deductive treatment”, *Pergamon Press*, Oxford, (1970)
- [2] B. Altaner, J. Vollmer, L. Katthän, S. Grossinsky, M. Timme S. Herminghaus.: “Flux Cycles as Fundamental Building Blocks of Non-Equilibrium Steady States” *arXiv*: 1105.2178 (2011); S. Herminghaus, “Tackling master equations with a flux loop transform”, *arXiv*: 0710.4913 (2007)
- [3] U. Seifert, *Eur. Phys. J.* **64**, 423 (2008)
- [4] M. Esposito, C. van den Broeck, *Phys. Rev. E* **82**, 011143 (2010)
- [5] S. Liepelt, R. Lipowski, *Phys. Rev. E* **79**, 011917 (2008)

VI-5 Network Dynamics as an Inverse Problem

M. Timme, F. v. Bussel, J. L. Casadiego

L. Anand, C. Henrich, F. Faraci, S. G. Shandilya (Yale, USA), B. Kriener (As, Norway), R.-M. Memmesheimer (Harvard, USA and Nijmegen, The Netherlands)

HOW DOES a network's interaction topology relate to its collective dynamics? Biological neural networks, for instance, are characterized by highly intricate anatomical structures and often complex dynamics. Yet, little is still known about how structural features shape the ongoing activity dynamics and which of these features are pivotal to network function.

Technological advances in electrophysiology allow us to record extracellular activity from large sets of neurons simultaneously. To help analyze and interpret these data is an important goal of neuronal network theory. Most theoretical approaches take a forward perspective: they make assumptions about neuron properties and network structure and analyze the resulting dynamics. The inverse problem, i.e. deriving network topology from network activity has received much less attention and has mainly focused on *functional* or *effective connectivity* between neurons, neuronal assemblies or brain areas derived on the grounds of implicit correlation-based methods [8-11]. Explicit approaches that reconstruct actual structural connections between individual elements are more difficult in general, but where feasible, they offer exact fine-grained results [12], for instance by establishing the presence or absence of individual synapses which may make a functional difference.

We are currently addressing a set of inverse problems of collective network dynamics focusing on three key questions:

- Can we identify the topology of a network from measuring (some of) its dynamical features?
- How do networks have to be wired to generate a given spatio-temporal dynamics?
- Which of the networks that produce a specific dynamics and function are then favored by principles of optimal stability and robustness?

The answers to these questions may eventually provide valuable insights into the evolutionary design principles that form the basis of the anatomy of brain circuits, as well as the interaction topology of other networks.

Inferring Network Topology from Dynamics

What does the collective network dynamics tell us about the interaction topology? To address this question, we first asked how the coarse network structure, as represented by a network's *strongly connected components* (SCC) controls the collective dynamics of coupled units. SCCs are subsets of the nodes of a network such that every given pair of nodes within this subgroup is connected via a directed path of interactions, thus enabling indirect communication from each node to each other within that subset. We have demonstrated that the number of SCCs alone does not qualitatively influence the stationary dynamics of networks. Nevertheless, the mutual interconnectivity between SCCs does qualitatively impact the collective dynamics: the hierarchy of SCCs in terms of the resulting input flow between them determines if networks synchronize or exhibit more irregular, partially clustered activity [1]. Hence, information about topology is directly reflected in the collective network activity.

These insights provide a conceptual step towards reconstructing the interaction topology of a network from its resulting spatio-temporal dynamics. When driving a generic network by a constant external input, every steady state moves in state space in a way that depends on both the driving signal and the interaction topology. Using this general feature we have analyzed the response dynamics to external driving inputs and thereby revealed the underlying interaction topology. For simple systems, such as coupled phase oscillators,

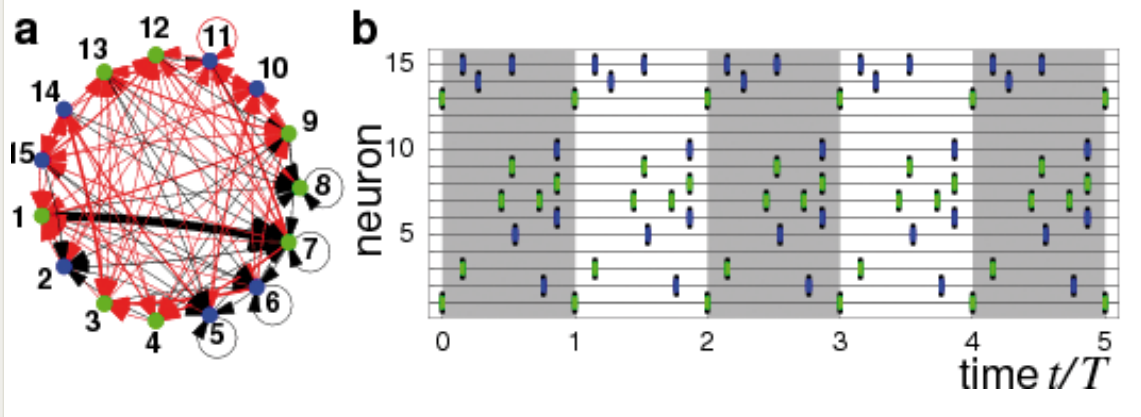


Figure 1

One selected heterogeneous network that generates a predefined complex spike pattern. (a) Network of two types of neurons (marked as blue and green, respectively). Connections are either excitatory (black) or inhibitory (red) (thicknesses proportional to coupling strengths). (b) The spiking dynamics actually generated (green and blue bars according to neuron type) by the network shown in (a) perfectly agrees with the desired predefined pattern of precisely timed spikes (black bars underlying the colored ones). The pattern includes several coincident spikes, neurons with different spike rate and three neurons {4, 11, 12} that are switched off (nonspiking).

tors [2], a first order theory analytically yields the network topology even if system details, e.g. the interaction functions, are not known exactly. We have recently generalized these results to systems where the local unit dynamics and the interaction functions are known and found that network reconstruction reduces to finding an optimal solution to an overdetermined large linear system of equations, also allowing a closed form solution [3]. Our results moreover indicate that for a given average number of connections per node the number of driving experiments necessary to reconstruct networks scales sublinearly with system size. Hence, highly accurate reconstructions can be obtained from a comparably small number of experiments. Recent progress suggests that closely related methods can successfully reconstruct networks of higher-dimensional or even chaotic units [3, 4] and that these approaches are not confined to fixed point or periodic dynamical states, but work for complex dynamics of very heterogeneous systems, including neural systems with non-trivial spatio-temporal spiking activity [3, 5]. We continue working towards a general theory to reconstruct the topology of real-world networks from measured observables.

Designing Complex Networks

Which networks are capable of generating a given dynamics? Analyzing a general model class of spiking neural networks, we have recently

worked out explicit constraints that exactly define the set of all admissible network topologies that generate a predefined spatio-temporal spike pattern [6, 7]. It turns out that two types of constraints restrict the space of network topologies consistent with a given dynamics, i.e. the space of *admissible* networks. First, individually fixed spike times reduce the dimensionality of admissible network space (equational constraints). Second, the ordering among collective neural circuit events (sending and receiving of spikes) restricts network space to certain areas (e.g. inhibitory coupling of a minimum strength for a specific synapse) by posing inequality constraints.

Our work provides complete analytical access to these constraints, even for strongly heterogeneous networks consisting of various types of neurons, both excitatory and inhibitory, and with very different local neuron parameters (cf. figure 1). Solving this set of constraints yields the set of all admissible coupling strengths of networks that enable a predefined spike pattern. The generality of this approach and the high dimensionality of solution space imply that additional restrictions may be imposed. For instance, the statistics of network topology, such as the degree distribution, as well as functional features like the distribution of delays may be pre-specified, enabling us to check whether and for which precise topologies a given network is capable of generating desired collective dynamics.

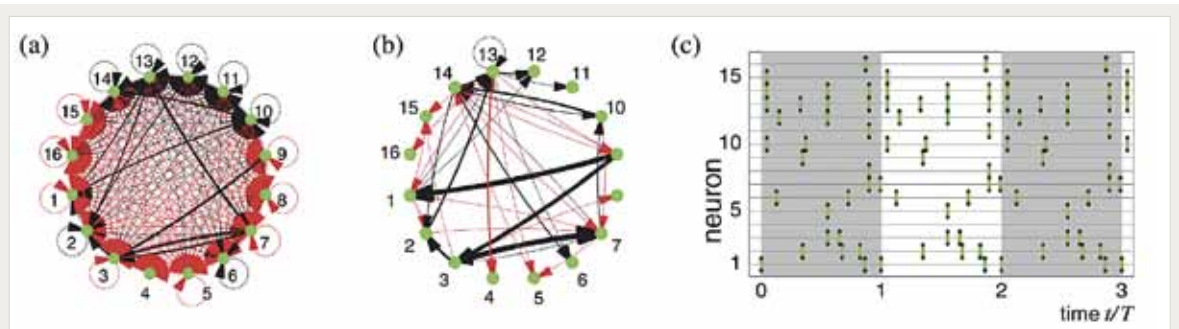


Figure 2

Distinct optimal networks generate the same predefined spike pattern. The two networks minimize wiring costs in (a) the Euclidean (L2) norm and (b) in the absolute value (L1) norm. Both networks collectively generate the same complex spike pattern (c).

Structurally Optimized Networks

If a multitude of different network topologies may generate the same collective dynamics, which of these topologies are realized in biological systems and which may be particularly suitable? To start to address this question, we have investigated how minimizing wiring costs affects the topology of networks that generate a predefined spike pattern [7]. Standard L2 (Euclidean norm) minimization of total wiring costs yielded particular homogeneous networks whereas L1 (absolute value norm) minimization showed that even very sparse, very heterogeneous networks are capable of generating a complex spatio-temporal pattern (cf. figure 2).

The spatial constraints of connectivity in real neuronal tissue as well as considerations of metabolic energy consumption suggest minimal wiring cost as an evolutionary principle. The combination of such cost principles and dynamical requirements such as stability is expected to yield further valuable insights into the design of neuronal networks for specific functions. Currently, we are working towards extending the theoretical understanding to optimal network topologies in analytically tractable classes of models and at the same time strive to understand how biologically more detailed systems may be constrained and selected to achieve a desired dynamics and thus function.

Along these lines, a very recent conceptual analysis (unpublished) indicates that an important finding about neural circuits is in fact inevitable rather than surprising: In 2004, Prinz and coworkers [15] found that similar network activity can arise from very disparate neural circuits. Our current research on bursting, multi-param-

eter models of stomatogastric ganglion circuits [3] now indicates that measuring only a few dynamical observables in such complex, high-dimensional systems necessarily yields a many-to-one mapping. As a consequence, there are necessarily many disparate neural circuits that generate essentially the same dynamics.

These conceptual, analytical as well as complementary numerical results on interrelations between network topologies and collective dynamics open up a new branch of theoretical research about topology identification in complex networks – mathematically a high-dimensional inverse problem. Together with other theoretical studies [12–14, 16] our works complement very well the experimental progress of data acquisition in the neurosciences and other areas of science, e.g. on gene and protein interaction networks.

- [1] M. Timme, *Europhys. Lett.* **76**, 367 (2006)
- [2] M. Timme, *Phys. Rev. Lett.* **98**, 224101 (2007)
- [3] S. Gorur Shandilya, *Relating Topology and Dynamics in Neuronal Networks*, MSc Thesis in Neuroscience, University of Göttingen (2010)
- [4] S. Gorur Shandilya and M. Timme, *New J. Phys.* **13**, 013004 (2011)
- [5] F. van Bussel, B. Kriener, and M. Timme *Front. Comput. Neurosci.* **5**, 3 (2011)
- [6] R.-M. Memmesheimer and M. Timme, *Phys. Rev. Lett.* **97**, 188101 (2006)
- [7] R.-M. Memmesheimer and M. Timme, *Physica D* **224**, 182 (2006)
- [8] G. L. Gerstein and A. M. H. J. Aersten, *J. Neurophys.* **54**, 1513 (1985)
- [9] A. M. H. J. Aersten, G. L. Gerstein, M. K. Habib, and G. Palm, *J. Neurophys.* **61**, 900 (1989)
- [10] B. Horwitz, *NeuroImage* **19**, 466 (2003)
- [11] A. A. Fingelkurts, A. A. Fingelkurts, and S. Kähkönen, *Neurosci. Biobehav. R.* **28**, 827 (2005)
- [12] M. K. S. Yeung, J. Tegner, and J. J. Collins, *Proc. Natl. Acad. Sci. USA* **99**, 6163 (2002)
- [13] D. Yu, M. Righero, and L. Kocarev, *Phys. Rev. Lett.* **97**, 188701 (2006)
- [14] D. Yu and U. Parlitz, *Europhys. Lett.* **81**, 48007 (2008)
- [15] A. Prinz, D. Bucher, and E. Marder, *Nature Neurosci.* **7**, 1345 (2004)
- [16] D. Napoletani and T. Sauer, *Phys. Rev. E* **77**, 026103 (2008)

VI-6 Renewable Energy Sources in Future Power Grids

M. Rohden, A. Sorge, M. Timme, D. Witthaut

D. Heide (University of Aarhus, Denmark), R. Sollacher (Siemens Corporate Research and Technologies)

Renewable energy sources will dominate future power grids

The ongoing change of our energy supply from large, centralized power plants based on nuclear or fossil fuels to smaller, decentralized sources based on renewable energies poses an enormous challenge for the development of the power grid. Many billions of Euros are currently invested to upgrade the grid (figure 1) [3]: not only is it necessary to connect all the new power generators and to enable large-scale energy storage and transport, e.g. from off-shore wind parks to the consumers in the inland. At the same time the structure of the power grid has to be optimized to increase its stability against fluctuations and robustness against device errors. Already the current power grid with its relatively few, reliable sources, is sometimes too fragile to cascading failures causing major power outages, despite the fact that all elements of the grid are carefully designed and tested. A

partial future solution will be provided by transmitting consumer information over the so-called *smart grid* [4, 5] and adapt energy production and distribution, thus aiming to control the entire grid. However, large-scale failures, for instance, are consequences of the *collective* dynamics of the power grid. We thus urgently need to understand the intrinsic network dynamics on the *large scale* to complement partial solutions of control engineering and to be able to develop efficient strategies for operating the future grid [3, 4].

To date, most research on the collective dynamics of power grids follows one of two distinct approaches: Electrical engineers model the behavior of single units of the power grid, such as generators and motors, in great detail and try to approximate the entire grid using a rough proxy structure of only a few units [6]. At the other extreme, physicists and mathematicians mostly studied abstract transportation or flow networks, disregarding all the details of the generators and transmission lines [7, 8].

Modeling the emergent dynamics of large power grids

Bridging the gap between these two approaches, we are now aiming to understand power grid dynamics at an intermediate level. We model each generator or motor as a simple rotor, whose current state is characterized by its phase angle and phase velocity [9]. This approach captures the essential features of every element, but is still simple enough to study the emergent behavior of the entire power grid and to perform simulations of realistic network structures. One of our main objectives is to find out how synchrony and stability depend on the structure of the power grid, in particular the network topology and the composition of the power

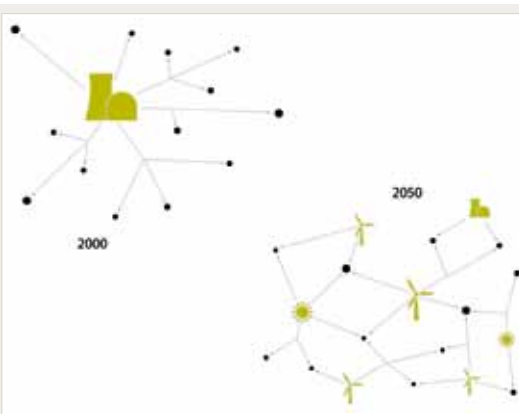


Figure 1

Change of the electric power grid. Today, power is mostly generated in large centralized power stations based on fossil fuel or nuclear energy. In 2050, power supply will rely on renewable energy sources, which are typically small, strongly fluctuating and heterogeneously distributed. This change in energy supply is only possible if the structure of the power grid is adapted and extended.

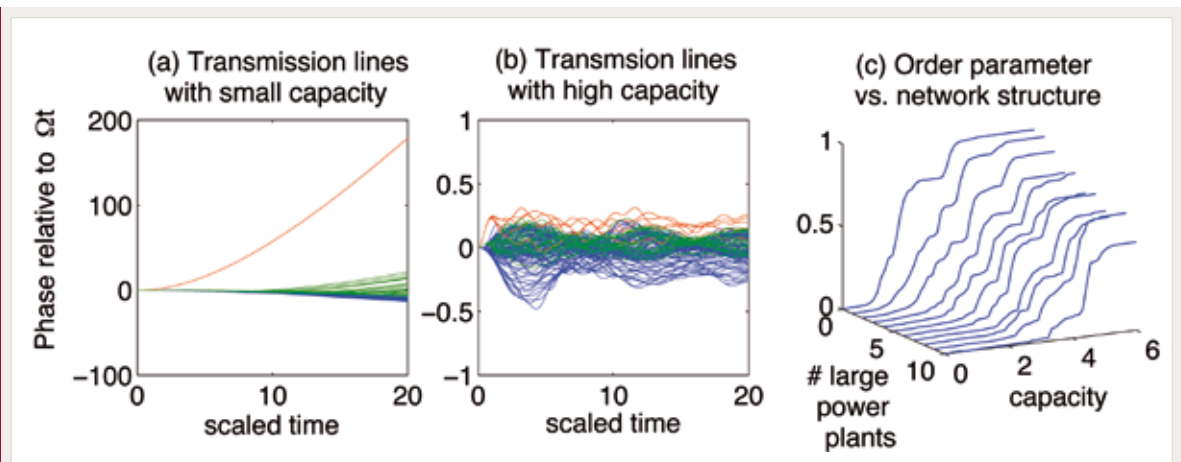


Figure 2

Dynamics of an intermediate-scale network model of electric power grids. (a) Phases of large power plants (red), small power generators (green) and the consumers (blue) relative to the reference $\Omega \times t$. The elements of the grid desynchronize if the capacity of the transmission lines is too small. (b) The phases remain synchronized if the capacity is increased sufficiently. (c) The order parameter measuring the degree of synchronization as a function of the capacity of the transmission lines and the number of large power grids, where the remaining power is provided by small sources of renewable energy [2].

generators (large conventional, mostly centralized power plants vs. small regional power stations mostly based on renewables).

Self-organized synchronization

In a first project we have analyzed the synchronization of different power grids consisting of a few hundred consumer units linked to few large power plants and a varying fraction of small sources of renewable energy. Figure 2 shows numerical results for the dynamics of the phases of the generators and consumers relative to the reference $\Omega \times t$, Ω being the grid frequency of 50 Hz. If the capacity of the transmission lines is too small, the generators accelerate while the consumers decelerate (cf. figure 2 (a)), requiring an emergency shutdown of the power grid. However, if the capacity is increased, spontaneous synchronization sets in without the need for an active phase control of the generators as shown in figure 2 (b) on a chosen scale. Figure 2 (c) shows the order parameter, measuring the degree of phase synchronization, as a function of the capacity of the transmission lines, varying the number of large conventional power plants. If this number is reduced and large power plants are replaced by many small sources of renewable energy, the degree of phase synchroniza-

tion is larger – the entire power grid becomes more stable and reliable, at least under stationary conditions [1, 2].

Preventing failures and optimizing the grid

Future research will be devoted to the dynamics of cascading failures, optimal transportation networks and applications to real-world power grids. Major power outages result from a cascade of failures: Commonly, a single element breaks down which would not be crucial as such. But due to the redistribution of the power load, other elements become overloaded such that finally large parts of the network break down. In order to prevent these major breakdowns, a profound understanding of the dynamics of cascading failures and the relation to the network structure is essential. Furthermore, power grids should be efficient in the sense that they transport electrical energy with a minimum of transmission lines and thus with a minimum of costs for construction and maintenance. For a wide class of problems it has been shown that an optimal efficiency is achieved with a tree-like network structure [10, 11]. However, such a network is certainly no longer secure against failures as the breakdown of a single link disconnects the network in two parts. We will thus

develop a theory for optimal dynamical transportation networks under certain stability constraints and apply this approach to power grids. With the knowledge gained from these model systems, we will then model and simulate the real-world power grid in Central Europe. We will apply our results on optimal transportation and fault-tolerant operation to develop strategies for the future development of the grid with special emphasis on efficiency and stability.

- [1] M. Rohden, *Eur. Dyn. Days* 2009, talk
- [2] M. Rohden, A. Sorge, D. Witthaut, and M. Timme, Synchronisation and stability of modern power grids, in preparation
- [3] E. Marris, *Nature* **454**, 570 (2008)
- [4] Editorial Smart thinking, *Nature* **458**, 125 (2009)
- [5] D. Butler, *Nature* **445**, 586 (2007)
- [6] P. Kundur, *Power system stability and control*, McGraw-Hill, New York (1993)
- [7] D. Heide, M. Schäfer, and M. Greiner, *Phys. Rev. E* **77**, 056103 (2008)
- [8] D. Heide, L. von Bremen, M. Greiner, C. Hoffmann, M. Speckmann, and S. Bofinger, *Renew. Energ.* **35**, 2483 (2010)
- [9] G. Filatrella, A. H. Nielsen, and N. F. Pedersen, *Eur. Phys. J. B* **61**, 485 (2008)
- [10] F. Corson, *Phys. Rev. Lett.* **104**, 048703 (2010)
- [11] E. Katifori, G. J. Szöllösi, and M. O. Magnasco, *Phys. Rev. Lett.* **104**, 048704 (2010)

VI-7 Impact of Single Links in Growing Networks

J. Nagler, A. Levina, M. Timme

Explosive Phase Transitions in Competitive Percolation

New links in complex networks often compete for addition.

How a complex network is connected crucially impacts its dynamics and function. Percolation, the transition to large-scale connectedness of networks upon gradual addition of links, occurs during growth and evolutionary processes in a large variety of natural, technological, and social systems [1-4]. Percolation arises in atomic and molecular solids in physics as well as in social, biological and artificial networks. In many of these systems, links often compete for addition. For instance, a human host carrying a virus may travel at any given time to one but not to another geographic location. He therefore links the people of his origin by transporting the infection to other people only at one of the places [3]. Across all percolating systems, once the number of added links exceeds a certain critical value, extensively large connected components (clusters) emerge that dominate the system.

Continuous or discontinuous percolation?

Given the breadth of experimental and numerical studies, as well as several theoretical results and analytic arguments [4] percolation was commonly believed to exhibit a continuous transition where the relative size of the largest cluster increases continuously from zero in the thermodynamic limit once the number of links crosses a certain threshold. So recent work by Achlioptas, D'Souza and Spencer [5] came as a surprise because it suggested a new class of random percolating systems that exhibit "explosive percolation". Close to some threshold value, the system they considered displays a steep increase of the largest cluster size with an increasing number of links; moreover, numerical scaling analysis of finite size systems suggests a discontinuous percolation transition. This study initiated several follow-up works (e.g. [6-9]), confirming the original results for a number of system modifications. In particular, these studies support that competition in the addition of links is crucial; the key mechanisms underlying

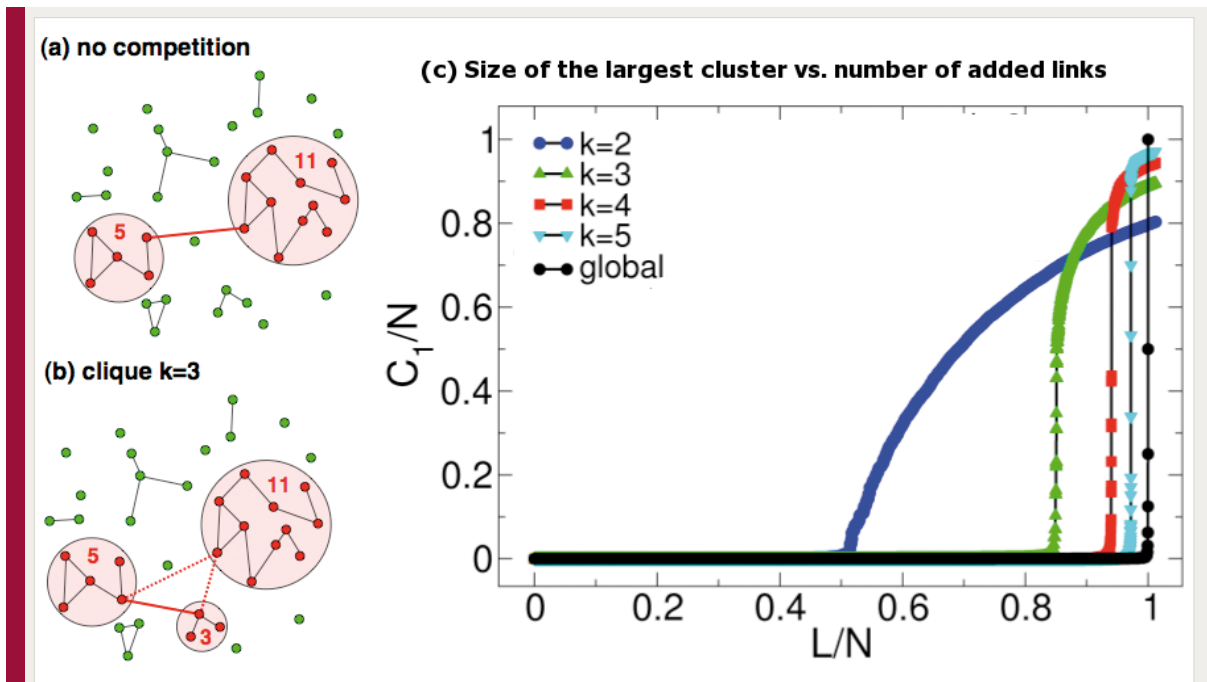


Figure 1

Impact of single link additions in percolation processes with competition. (a) No competition – a link is added at random. (b) Clique competition ($k=3$) – Three different clusters are selected at random and compete for the new link. The two smallest clusters win and get connected. (c) Growth of the largest cluster C_1 as a function of the number of links L added so far. The percolation transition appears to show jumps as soon as competition $K \geq 3$ occurs. See Ref. [1] for details.

ing discontinuous percolation, however, are still not well understood, and the impact of individual link additions has been unknown so far.

How do single links impact the transition?

The first hint was provided by the numerical results presented in the 2009 Science article [5]. To explain the key microscopic mechanisms underlying this transition, we have now combined stochastic numerical simulations with a new, link-based form of analysis [1]. The analysis reveals a particularly strong impact of single link additions. In generic competitive percolation processes, including those displaying explosive percolation, single links do not induce a discontinuous gap in the largest cluster size in the thermodynamic limit as shown in figure 1 (c), in contrast to what one might expect from the original study [5]. Nevertheless, our results highlight that for large finite systems single links may still induce substantial gaps because gap sizes scale weakly algebraically with system size. Two or more essentially macroscopic clusters

coexist immediately before the transition, thus announcing percolation. These results explain how single links may drastically change macroscopic connectivity in networks where links add competitively. The findings may be particularly relevant for many real systems where competitive features are strong enough.

- [1] J. Nagler, A. Levina, and M. Timme, Impact of Single Links in Competitive Percolation, *Nature Phys.* **7**, 265 (2011)
- [2] S. H. Strogatz, *Nature* **410**, 268–276 (2001)
- [3] R. D'Souza, *Nature Phys.* **5**, 627 (2009)
- [4] D. Stauffer and A. Aharony, *Introduction to Percolation Theory*, Taylor and Francis, London (1993)
- [5] D. Achlioptas, R. D'Souza and J. Spencer, *Science* **323**, 1453 (2009)
- [6] Y. S. Cho, J. S. Kim, J. Park, B. Kahng, and D. Kim, *Phys. Rev. Lett.* **103**, 135702 (2009)
- [7] F. Radicchi and S. Fortunato, *Phys. Rev. Lett.* **103**, 168701 (2009)
- [8] R. M. Zipf, *Phys. Rev. Lett.* **103**, 045701 (2009)
- [9] E. J. Friedman and A. S. Landsberg, *Phys. Rev. Lett.* **103**, 255701 (2009)

VI-8 Chaotic Dynamics and Information Decay in Spiking Neural Networks

F. Wolf

M. Monteforte, W. Wei, P. Hiemayer, D. Festa, M. Puelma-Touzel, E. Bodenschatz, D. Battaglia, T. Geisel, M. Timme, T. Tchumatchenko, J. Kerr (MPIbK Tübingen), S. Shoham (Technion, IL), S. Löwel (U Göttingen)

NEURONS IN the cerebral cortex fire action potentials (spikes) in highly irregular, seemingly random sequences [1]. Since neurons in isolation reproducibly respond to the repeated injection of identical temporally varying inputs [2], the irregular activity in the cortex is not believed to result from a randomness in the spike generating mechanism, but rather from strongly fluctuating synaptic inputs [3]. The prevailing explanation for this phenomenon is a dynamic balance between excitatory and inhibitory inputs, also known as the balanced state of cortical networks. Such a balance in neuronal circuits

has been demonstrated experimentally *in vitro* and *in vivo* [4]. The statistical characteristics of self-balancing networks have been studied theoretically in networks of excitatory and inhibitory neurons [5, 6] and in networks of only inhibitory neurons, where the recurrent inhibition balances external excitatory currents [7]. These studies established that in sparsely connected networks with relatively strong synapses the balanced state emerges robustly from the collective dynamics of the network, without any external source of randomness (for an illustration see figure 1).

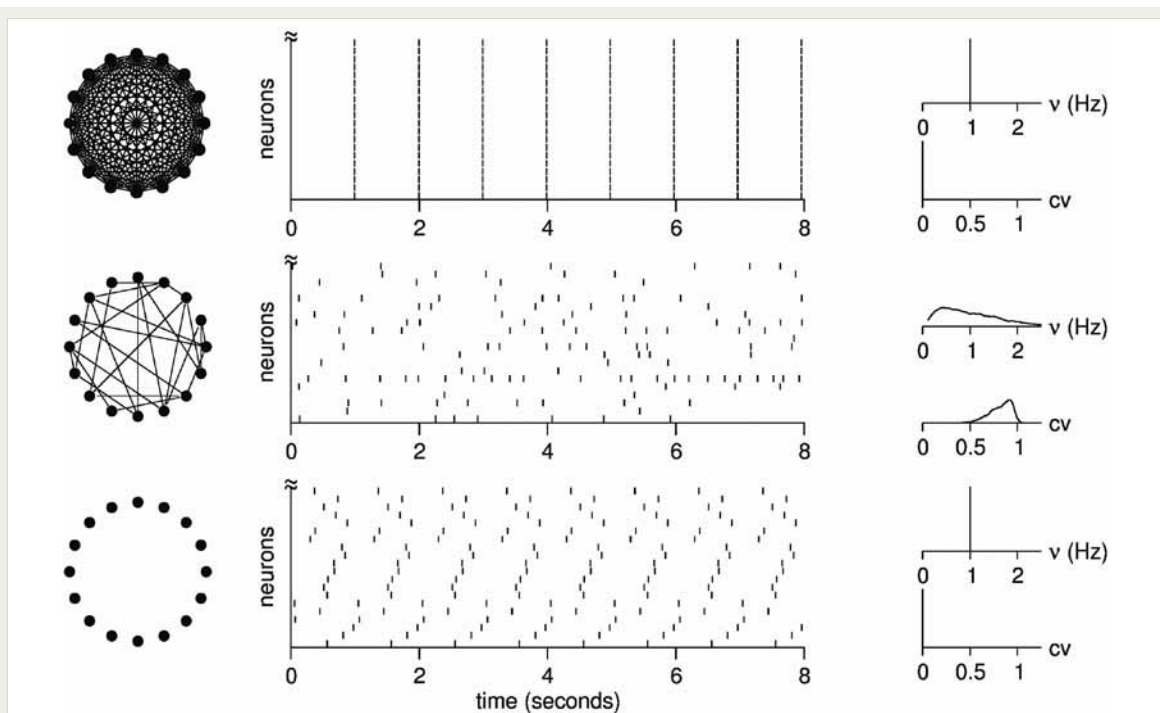


Figure 1

Complex network topology induces irregular asynchronous dynamics in large networks of identical model neurons. Left column schematic representation of different network structures ranging from fully connected over sparse random to completely disconnected networks. The graphs to the right of each network show representative spike patterns and spiking statistics of identical deterministic integrate and fire neuron models interacting in such networks. Middle column: spike raster of a random subset of neurons in a network of 2000 neurons. Right column: histograms of single neuron firing rates and CV values, indicating the asynchronous and irregular firing pattern induced by recurrent interactions in the sparse random network.

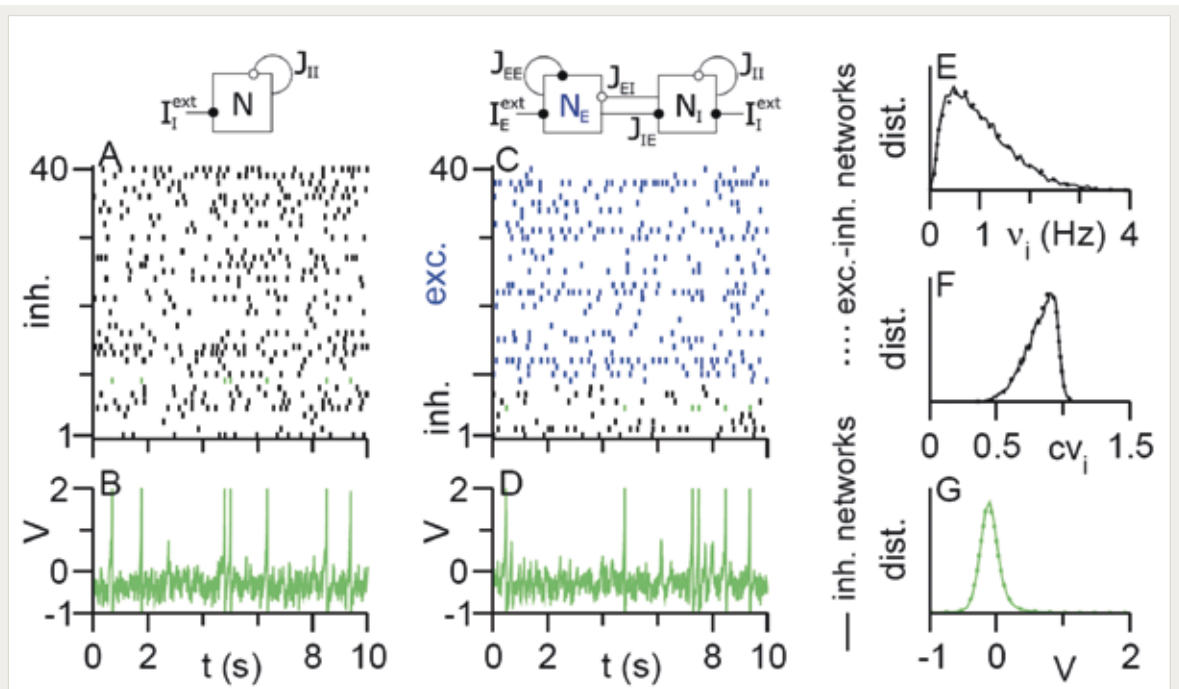


Figure 2

Invariant statistics of spike activity in spiking neuron networks with and without recurrent excitatory connections. Characteristics of the balanced state in inhibitory and excitatory-inhibitory networks of theta neurons: (a,c) Spike patterns of 40 random neurons, (b,d) Voltage traces of one random neuron, (e) Firing rate distributions, (f) Coefficient of variation distributions and (g) Stationary voltage distributions (modified from Monteforte & Wolf, PRL 2010).

The dynamical nature of the balanced state, however, has remained largely controversial and poorly understood. In a seminal paper, van Vreeswijk and Sompolinsky developed a powerful mean field theory of the balanced state for excitatory-inhibitory networks of binary neurons [5]. In their model, nearby trajectories diverged faster than exponentially, demonstrating an extremely intense chaos with an infinite largest Lyapunov exponent. More recently, studies of inhibitory networks of leaky integrate and fire neurons instead reported stable chaos, a kind of dynamics in which all Lyapunov exponents are negative definite such that the dynamics is stable but temporally irregular [7], a behavior apparently completely inconsistent with the original findings of van Vreeswijk and Sompolinsky. Answering the question of whether the balanced state is predicted to be chaotic or not in real biological networks, however, is obviously of fundamental importance for understanding information representation and processing

in the cortex. If cortical networks were to generate stable complex firing patterns as in networks exhibiting stable chaos, these might serve as a coding space for the storage and processing of, e.g., sensory information. This possibility is particularly important in view of our recent results that spike latency codes generated by the predominantly inhibitory networks of the olfactory bulb are powerful encoders of olfactory sensory information [8]. If, however alternatively, cortical networks operate in a chaotic regime, information processing would be intrinsically limited by the dynamical entropy production of a chaotic system that turns microscopic perturbations such as ion channel noise into global firing patterns.

To resolve the controversy about the dynamical nature of the balanced state and to comprehensively assess the conditions and determinants for the occurrence of extreme, conventional, or “stable” chaos in cortical networks we recently developed methods for the semi-analytical

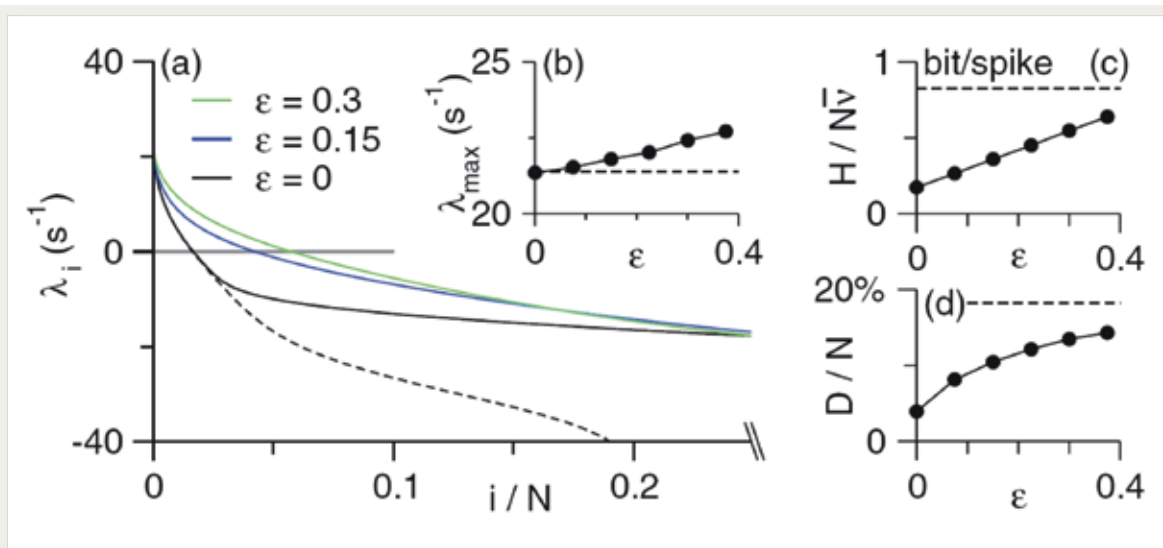


Figure 3

Extensive and high dynamical entropy production and fat attractor structure in large networks of spiking neuron models. Chaotic dynamics in balanced excitatory-inhibitory networks at different excitatory feedback loop activations ε : (a) Lyapunov spectra, (b) Maximal Lyapunov exponent, (c) Entropy production per spike per neuron, (d) Attractor dimension density, dashed lines: isolated inhibitory networks (modified from Monteforte & Wolf, PRL 2010)

spike based calculation of the complete spectrum of all Lyapunov exponents, the Kolmogorov Sinai entropy production rate and the attractor dimension in large networks of spiking neurons. In a first series of studies we have used these methods to quantitatively examine the nature of balanced state chaos in networks of neuron models covering the most extreme choices of a biologically plausible single neuron dynamics [9, 10]. Our results demonstrate an extreme sensitivity of the collective dynamics to fine details of the single neuron dynamics and quantify the consequences of the different types of collective dynamics on the preservation and decay of information encoded in neuronal spiking patterns.

We first performed a comprehensive characterization of the balanced state in networks of N canonical type I neuronal oscillators, called theta neurons (figure 2). The theta neuron model explicitly describes dynamic action potential generation and is equivalent to the normal form of a saddle node bifurcation on an invariant circle. In contrast to previously considered network models that exhibit phase spaces of varying dimensionality, the phase space of our network mod-

el is a fixed N -torus. Obviously a phase space of fixed dimensionality is an important prerequisite for the definition and calculation of characteristic exponents. For these networks, we performed numerically exact calculations of the full spectrum of Lyapunov exponents, the rate of dynamical entropy production and the attractor dimension, and analyzed the statistics of the first Lyapunov vector [9]. We found that both inhibitory networks and excitatory-inhibitory networks exhibit deterministic extensive chaos (figure 3). In all considered networks, the chaotic attractors had a large dimensionality on the order of the phase space dimension N . Most surprisingly, the average entropy production (information loss) was found to be very high, on the order of one bit per spike per neuron. This rate of dynamical entropy production in these networks appears large, in particular, compared to experimental estimates that estimated the information content of spike patterns in sensory cortices. Such studies found maximal information rates on the order of 1 bit per spike [11], i.e. on the same order as the network dynamics is capable of “destroying” information encoded in its state. Thus, if the rate of dynamical entropy

production in cortical networks is as high as in our models, all information inserted into a pattern of neuronal spike times would be essentially erased by the time a typical neuron fires its the next spike.

From a theoretical perspective, already the observation of extensive chaos in these networks is not a trivial property. Extensive chaos can be expected on general grounds in spatially extended systems, that can be decomposed into weakly interacting subsystems, whose number grows linearly with system size. This condition however is not fulfilled for network dynamical systems on random graphs. The extensivity found for balanced chaos presumably reflects the lack of correlations between neurons in the balanced state: In the completely uncorrelated limit the invariant measure of the network dynamics is expected to factorize and the attractor becomes $O(N)$ dimensional and the dynamics extensive in the large system limit. An exact understanding of the conditions for extensive dynamics in spiking neuron models thus rep-

resents an important theoretical challenge for further studies.

Considered biologically, our results highlight that the collective dynamics of balanced networks strongly depends on the single neuron dynamics. While networks of theta neurons in the balanced state exhibit conventional extensive chaos, previous studies of topologically identical networks of leaky integrate and fire neurons demonstrated stable chaos [7]. We showed that the origin of this qualitative difference apparently results from differences in single neuron spike initiation dynamics [9]. Opposed to the leaky integrate and fire model, the theta neuron model incorporates the dynamic instability underlying spike initiation. The membrane potential distribution of the neurons when most sensitive to perturbations indeed is shifted towards this instability [9]. Our results thus suggest, that this feature of single neuron dynamics renders the collective dynamics of balanced networks robustly chaotic. Since the theta neuron model is the canonical form of type I

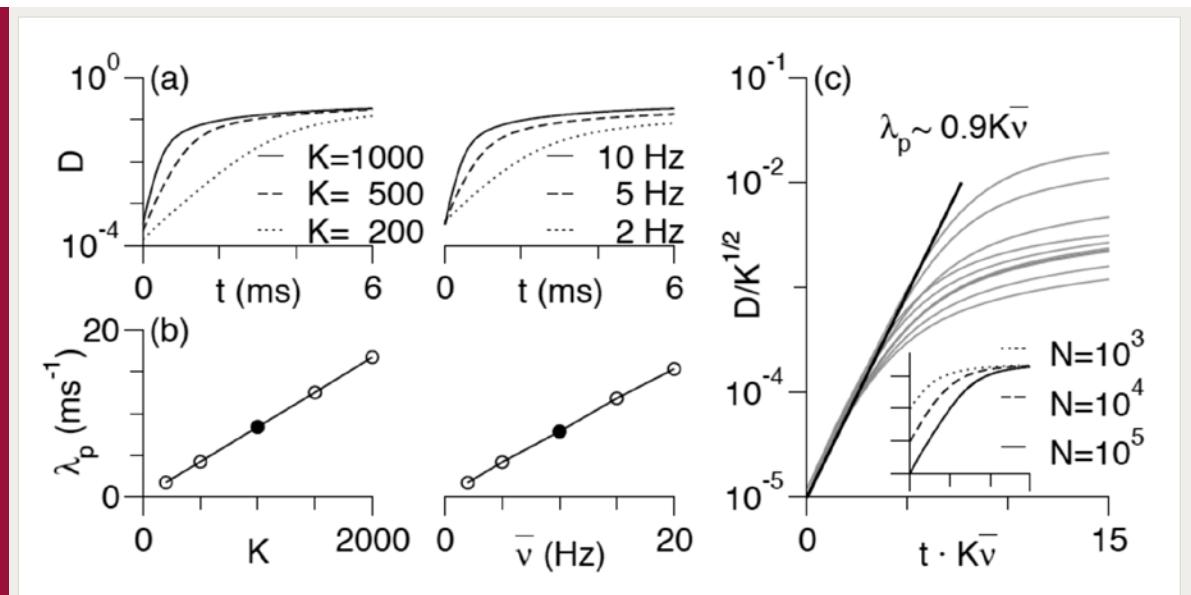


Figure 4

Sensitivity to single spike failures in networks of integrate-and-fire neurons: (a) Distance D between trajectory after spike failure and a reference trajectory versus time in log-linear plots for different connectivities K and average firing rates, (b) pseudo Lyapunov exponent from exponential fits to $D(t)$ before reaching saturation versus connectivity K and average firing rate (c) distance- evolution of all parameter sets (rescaled with approximate perturbation strength versus time (rescaled with average input rate) collapse to one characteristic exponential state separation (inset: different network sizes N for $K = 100$), (modified from Monteforte & Wolf, 2011).

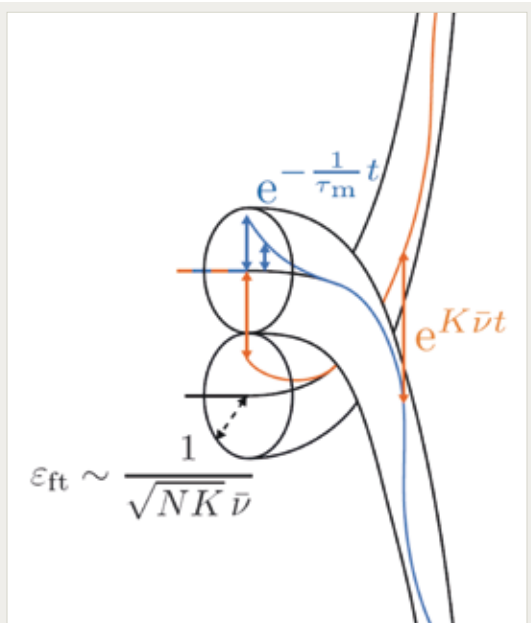


Figure 5

Flux tubes in the phase space of spiking neuron models. Phase space structure underlying simultaneous stability to infinitesimal state perturbations and strong instability to single spike perturbations. Indicated are the scaling of the flux tube diameter and pseudo Lyapunov exponent with system size, N , mean in-degree, K , and firing rate, as well as the typical timescale for the decay of infinitesimal perturbations, set by the membrane time constant (modified from Monteforte & Wolf, 2011).

excitability, our finding of extensive and strong conventional chaos are expected to be representative of a wide range of single neuron dynamics.

The strikingly large entropy production we found raises fundamental questions about the neural code in cortical networks. If the entropy production is in fact of the same order of magnitude as sensory information carried by spikes, sensory information would be hard to maintain in spike patterns beyond the immediate stimulus response. This would be in line with experimental observations indicating that spike timing information in barrel cortex about whisker deflections is encoded to 83% in the first spike after the stimulus and reduced in each successive spike by roughly two thirds [11]. The reliable generation of long and precisely timed spike sequences by cortical networks would seem un-

likely under such conditions. In line with our theoretical results London and coworkers recently reported experimental evidence for a highly unstable dynamics of cortical networks *in vivo* [12]. In these experiments single additional spikes were triggered artificially in single neurons of the rat barrel cortex. London et al. showed that these additional spikes caused a cascade of extra spikes in the network and argued that this cascade is likely to rapidly decorrelate the network's microstate.

To uncover the mechanisms involved in this extreme sensitivity of cortical networks we thus examined the response of balanced model networks to single spike perturbations. Surprisingly we found that even in models with a formally stable dynamics, single spike perturbations induced an exponential state separation reminiscent of a chaotic dynamics [10]. The simplest example for the occurrence of this phenomenon is provided by the dynamics of networks of instantaneously pulse-coupled, inhibitory integrate-and-fire neurons. To clarify the phase-space structure underlying this sensitive dependence on single spike perturbations in stable networks we thus performed a comprehensive study of the responses to infinitesimal, single spike and general finite state perturbations in such networks [10].

First we demonstrated that random networks of inhibitory LIF neurons in fact exhibit negative definite Lyapunov spectra, confirming the existence of stable chaos [10]. The Lyapunov spectra were invariant to the network size, demonstrating for the first time that the stable dynamics in response to infinitesimal perturbations is representative for large networks, is extensive and is thus predicted to be preserved in the thermodynamic (large system) limit. We analytically calculated the mean (negative) Lyapunov exponent showing remarkably, that in the limit of large connectivity, perturbations decay as fast as in a collection of uncoupled neurons.

In these networks, single spike failures, the most elementary type of single spike perturbations, induced extremely weak firing rate responses

that became negligible for large networks. Nevertheless, such single spike perturbations typically put the network state on a very different dynamical path that diverges exponentially from the original one. The rate of exponential state separation was quantified with a so called pseudo Lyapunov exponent (figure 4). We found that the pseudo Lyapunov exponent increases linearly with the average input rate. For networks of large connectivity K this scaling implies extremely rapid, practically instantaneous, decorrelation of network microstates. In fact even in networks of moderate connectivity, single spike perturbations caused complete decoherence of the networks' microstates within milliseconds. Examining the transition from unstable dynamics to stable dynamics for arbitrary perturbation sizes, we derived a picture of tangled flux tubes composing the networks' phase space (figure 5). These flux tubes form reservoirs of stability enclosing unique stable trajectories. Whereas adjacent trajectories separate exponentially fast. In the large system limit the flux tubes become vanishingly small, implying that eventually even in the limit of infinitesimal perturbations the dynamics would be unstable. This contradicts the prediction from the Lyapunov spectrum analysis and reveals that characterizing the dynamics of such networks qualitatively depends on the order in which the weak perturbation limit and the thermodynamic limit are taken.

Our results show that the seemingly paradoxical coexistence of local stability and exponential state separation reflects the partitioning of the networks' phase space into a tangle of flux tubes. States within a flux tube are attracted to a unique, dynamically stable trajectory. Different flux tubes, however, separate exponentially fast. The decreasing flux tube radius in the large system limit suggests that an unstable dynamics dominates the thermodynamic limit. The resulting sensitivity to initial conditions is then described by the rate of flux tube separation, the pseudo Lyapunov exponent, that showed no sign of saturation.

Our results [9, 10] suggest that apparently unconditionally stable networks may develop an infinite largest Lyapunov exponent in the thermodynamic limit. We have shown that the previously reported infinite Lyapunov exponent on the one hand [5] and local stability on the other hand [7] can occur in the same system. We propose that they were obtained in different studies only because of the different order in which the weak perturbation limit and the thermodynamic limit were taken. In particular in view of the increasing recognition of the power of spike timing codes (e.g. [8]) exact analysis of information preservation, transformation and decay by spiking network dynamics using the methods introduced in our recent work represents an important new topic in the theory of spiking neuronal networks.

- [1] B. D. Burns and A. C. Webb, *Proc. R. Soc. B* **194**, 211 (1976); W. R. Softky and C. Koch, *J. Neurosci.* **13**, 334 (1993)
- [2] Z. F. Mainen and T. J. Sejnowski, *Science* **268**, 1503 (1995)
- [3] G. R. Holt et al., *J. Neurophysiol.* **75**, 1806 (1996)
- [4] Y. Shu, A. Hasenstaub and D. A. McCormick, *Nature* **423**, 288 (2003); B. Haider et al., *J. Neurosci.* **26**, 4535 (2006); R. W. Berg, A. Alaburda and J. Hounsgaard, *Science* **315**, 390 (2007)
- [5] C. van Vreeswijk and H. Sompolinsky, *Science* **274**, 1724 (1996); C. van Vreeswijk and H. Sompolinsky, *Neural Comput.* **10**, 1321 (1998)
- [6] M. Tsodyks and T. Sejnowski, *Network* **6**, 111 (1995); D. J. Amit and N. Brunel, *Cereb. Cortex* **7**, 237 (1997); D. J. Amit and N. Brunel, *Network* **8**, 373 (1997); T. W. Troyer and K. D. Miller, *Neural Comput.* **9**, 971 (1997); N. Brunel, *J. Comput. Neurosci.* **8** 183 (2000); A. Lechner et al., *Neural Comput.* **18**, 634 (2006)
- [7] S. Jahnke, R. M. Memmesheimer and M. Timme, *Phys. Rev. Lett.* **100**, 048102 (2008); R. Zillmer, N. Brunel and D. Hansel, *Phys. Rev. E* **79**, 031909 (2009)
- [8] S. Junek, E. Kludt, F. Wolf, D. Schild, *Neuron* **67**:872 (2010)
- [9] M. Monteforte, F. Wolf, *Phys. Rev. Lett.* **105**:268104 (2010)
- [10] M. Monteforte, F. Wolf *arXiv*:**1102.5428** (2011)
- [11] S. Panzeri et al., *Neuron* **29**, 769 (2001)
- [12] M. London et al., *Nature* **466**, 123 (2010)

VI-9 Freely Switchable Networks of Biological Neurons

F. Wolf

A. El Hady, A. Neef, K. Bröking, R. Fleischmann, G. Afshar, D. Fliegner, T. Geisel, S. Herminghaus, H. Schrobsdorf, A. Witt, E. Bamberg (MPI BP Frankfurt), E. Moses (Weizmann Institute, Israel), W. Stühmer (MPI EM Göttingen)

THE PROCESSING capabilities and collective dynamics of biological neural networks are determined to a large degree by the topology and nature of synaptic interactions between the interconnected nerve cells. Driven by the recognition of this fact, substantial attention in theoretical neuroscience is currently devoted to the problem of neural circuit reconstruction [1-3]. In addition to reconstructions of network structure it would be highly desirable to have means to assemble biological neurons into circuits is experimentally controlled topology. Ideally the topology of such artificial circuits should be freely switchable such that the circuit structure can be changed by the researcher “on the fly”. Such systems would then enable to test how the information processing properties of a fixed set of neurons change when the same neurons are embedded in different circuits, directly demon-

strating how collective neural computation can be programmed by circuit topology and structure. While the ability to impose circuit structures by cell culture patterning have seen substantial progress in recent years (e.g. [4, 5]) it appears inconceivable to achieve reversible switching between different circuits by this approach.

In principle, optogenetic control of neurons [6] combined with high bandwidth multi-side optical stimulation, could be used to establish freely switch-able artificial circuits of biological neurons. In such an approach individual neurons expressing light gated ion channels would be optically targeted and stimulated with emulated synaptic inputs from other cells. A functional network of such neurons could then be established by making the photo stimulation of each neuron dependent on the recorded past activity

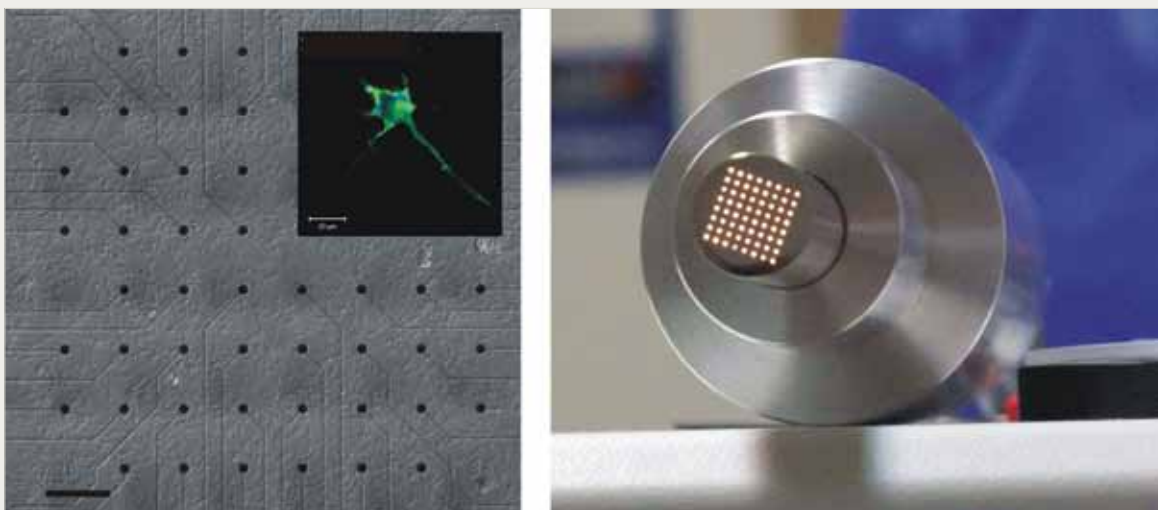


Figure 1

Elements for the synthesis of freely switch-able networks of biological neurons. Left: Network of primary hippocampal neurons cultured on a 8x8 multi electrode array (MEA). Neurons are transfected to express channel rhodopsin 2 (ChopII). Scale bar 0.2 mm. Inset: Fluorescence image of a single neuron expressing Chop 2. Right: Light guide array for delivering emulated synaptic input by selectively photo-activating neurons in the vicinity of each MEA electrode.

of other neurons in the synthetic network. Realising such systems requires the development of high bandwidth multi-site stimulation technology and its integration into a parallel multi-channel closed-loop architecture.

To test the feasibility and to explore the power of such a “synthetic biology” approach to the dynamics of neural circuits, we are developing and testing different prototype systems and archi-

tectures of high-bandwidth multi-site stimulation systems. Elements of a first generation optical fiber-based LED driven closed-loop multi-site stimulation system are shown in figure 1. This instrument development project is jointly pursued in collaboration with the Group of Walter Stühmer at the Max Planck Institute for experimental Medicine and the optical instrumentation provider Rapp OptoElectronic GmbH.

- [1] H.S. Seung, *Neuron* **62**, 17 (2009)
- [2] K.L. Briggman, M. Helmstaedter, W. Denk, *Nature* **471**, 183 (2011)
- [3] D.D. Bock et al., *Nature* **471**, 177 (2011)
- [4] O Feinerman, A. Rotem, E. Moses, *Nature Phys.* **4**, 967 (2008).
- [5] F. Wolf, T. Geisel, *Nature Phys.* **4**, 905 (2008)
- [6] E.S. Boyden, F. Zhang, E. Bamberg, G. Nagel, K. Deisseroth, *Nat Neurosci.* **8**, 1263 (2005)

Publications

Department of Nonlinear Dynamics

2011

M. Ihrke, H. Schrobsdorff (Degering), and J.M. Herrmann, "Recurrence-Based Estimation of Time-Distortion Functions for ERP Waveform Reconstruction", *International Journal of Neural Systems* **21** (2011) 65-78.

M. Ihrke, J. Behrendt, H. Schrobsdorff (Degering), J.M. Herrmann, and M. Hasselhorn, "Response-Retrieval and Negative Priming: Encoding- and Retrieval-Specific Effects", *Experimental Psychology* **58** (2011) 154-161.

J. Nagler, A. Levina, and M. Timme, "Impact of single links in competitive percolation", *Nature Physics* **7** (2011) 265.

F. Trimborn, D. Witthaut, H. Hennig, G. Kordas, T. Geisel, and S. Wimberger, "Decay of a Bose-Einstein condensate in a dissipative lattice - the mean-field approximation and beyond", *Eur. Phys. J. D* (accepted).

D. Witthaut, F. Trimborn, H. Hennig, G. Kordas, T. Geisel, and S. Wimberger, "Beyond mean-field dynamics in open Bose-Hubbard chains", *Phys. Rev. A* (in press).

W. Wei, and F. Wolf, "Spike Onset Dynamics and Response Speed in Neuronal Populations", *Phys. Rev. Lett.* **106** (2011) 088102.

M. Kaschube, D.M. Coppola, M. Schnabel, S. Löwel, L.E. White, and F. Wolf, "An Alternative Hypothesis for Orientation Columns in the Visual Cortex (Reply)", *Science* DOI:[10.1126/science.1194869](https://doi.org/10.1126/science.1194869) (2011)

T. Tchumatchenko, T. Geisel, M. Volgushev, and F. Wolf, "Spike correlations – what can they tell about synchrony", *Front. Neurosci.* (2011) doi: [10.3389/fnins.2011.00068](https://doi.org/10.3389/fnins.2011.00068)

2010

G. Baranauskas, A. Mukovskiy, F. Wolf, and M. Volgushev, "The Determinants of the Onset Dynamics of Action Potentials in a Computational Model", *Neuroscience* **167**(4) (2010) 1070-90.

J. Behrendt, H. Gibbons, H. Schrobsdorff (Degering), M. Ihrke, J.M. Herrmann, and M. Hasselhorn, "Event-related brain potential correlates of identity negative priming from overlapping pictures", *Psychophysiology* **47** (2010) 921-930.

O. Bendix, R. Fleischmann, T. Kottos, and B. Shapiro, "Optical structures with local PT-symmetry", *J. Phys. A* **43** (2010) 265305.

J.D. Bodyfelt, T. Kottos, and B. Shapiro, "One Parameter Scaling Theory for Stationary States of Disordered Nonlinear Systems", *Phys. Rev. Lett.* **104** (2010) 164102.

M. Chuchem, K. Smith-Mannschott, M. Hiller, T. Kottos, A. Vardi, and D. Cohen, "Semiclassical analysis of quantum dynamics in the bosonic Josephson junction", *Phys. Rev. A* **82** (2010) 053617.

J. Eckmann, E. Moses, O. Stetter, T. Tlusty, and C. Zbinden, "Leaders of neuronal cultures in a quorum percolation model", *Front. Comput. Neurosci.* doi: [10.3389/fncom.2010.00132](https://doi.org/10.3389/fncom.2010.00132) (2010).

H. Gutch, P. Gruber, and F. Theis, "ICA over Finite Fields", in *Latent Variable Analysis and Signal Separation*, edited by Vincent Vigneron and Vicente Zarzoso and Eric Moreau and Rémi Gribonval and Emmanuel Vincent, Springer (2010) 645-652.

H. Gutch, T. Maehara, and F. Theis, "Second Order Subspace Analysis and Simple Decompositions", in *Latent Variable Analysis and Signal Separation*, edited by Vincent Vigneron and Vicente Zarzoso and Eric Moreau and Rémi Gribonval and Emmanuel Vincent, Springer (2010) 370-377.

H. Hennig, J. Dornigac, and D.K. Campbell, "Transfer of Bose-Einstein condensates through discrete breathers in an optical lattice", *Phys. Rev. A* **82** (2010) 053604.

F. Hesse, and J.M. Herrmann, "Homeokinetic Prosthetic Control : Collaborative Selection of Myosignal Features", in *19th IEEE International Symposium on Robot and Human Interactive Communication*, Principe di Piemonte - Viareggio, Italy. IEEE, (2010) 437-442.

F. Hesse, and J.M. Herrmann, "Homeokinetic Proportional Control of Myoelectric Prostheses", in *IEEE/RSJ International Conference on Intelligent Robots and Systems*, Taipei, Taiwan. IEEE, (2010) 1786-1791.

- S. Juneak, E. Kludt, F. Wolf, and D. Schild, "Olfactory Coding with Patterns of Response Latencies", *Neuron* **67** (2010) 872-884.
- M. Kaschube, M. Schnabel, S. Loewel, D.M. Coppola, L.E. White, and F. Wolf, "Universality in the Evolution of Orientation Columns in the Visual Cortex", *Science* **330** (2010) 1113-1116.
- W. Keil, K. Schmidt, S. Löwel, and M. Kaschube, "Reorganization of columnar architecture in the growing visual cortex", *Proc Nat Acad Sci* **107** (2010) 12293-12298.
- T. Kottos, "Optical Physics: Broken symmetry makes light work", *Nature Physics* **6** (2010) 166.
- G. Martius, and J.M. Herrmann, "Taming the Beast: Guided Self-organization of Behavior in Autonomous Robots", in *From Animals to Animats 11*, edited by Doncieux, Stéphane and Girard, Benoît and Guillot, Agnès and Hallam, John and Meyer, Jean-Arcady and Mouret, Jean-Baptiste. Springer, (2010) 50-61.
- R.M. Memmesheimer, and M. Timme, "Synchrony and Precise Timing in Complex Neural Networks", in *Handbook on Biocircuit Networks*, edited by Stefano Boccaletti, Vito Latora and Yamir Moreno. World Scientific, Singapore, chapter 13, (2010) 279-304.
- J.J. Metzger, R. Fleischmann, and T. Geisel, "Universal Statistics of Branched Flows", (2010) in *EDP Sciences*, pages 01018.
- J.J. Metzger, R. Fleischmann, and T. Geisel, "Universal Statistics of Branched Flows", *Phys. Rev. Lett.* **105** (2010) 020601.
- M. Monteforte, and F. Wolf, "Dynamical Entropy Production in Spiking Neuron Networks in the Balanced State", *Physical Review Letters* **105** (2010) 268104.
- J. Nagler, and P.H. Richter, "Simple model for dice loading", *New J. Phys.* **12**. doi: 10.1088/1367-2630/12/3/033016 (2010).
- J. Nagler, and P.H. Richter, "How does God play dice?", in *Reviews of Nonlinear Dynamics and Complexity*, edited by H. G. Schuster. Wiley (2010) 37-58.
- H. Ramezani, T. Kottos, R. El-Ganainy, and D.N. Christodoulides, "Unidirectional nonlinear PT-symmetric optical structures", *Phys. Rev. A* **82** (2010) 043803.
- T. Tchumatchenko, A. Malyshev, T. Geisel, M. Volgushev, and F. Wolf, "Correlations and synchrony in threshold neuron models", *Phys. Rev. Lett.* **104** (2010) 5.
- T. Tchumatchenko, T. Geisel, M. Volgushev, and F. Wolf, "Signatures of synchrony in pairwise count correlations", *Front. Comput. Neurosci.* doi:10.3389/neuro.10.001.2010 (2010).
- D. Tsigankov, and A. Koulakov, "Sperry versus Hebb: Topographic mapping in Isl2/EphA3 mutant mice", *BMC Neuroscience* **11** (2010) 155.
- C.T. West, T. Kottos, and T. Prosen, "PT-symmetric Wave Chaos", *Phys. Rev. Lett.* **104** (2010) 054102.
- M.C. Zheng, D.N. Christodoulides, R. Fleischmann, and T. Kottos, "PT optical lattices and universality in beam dynamics", *Phys. Rev. A* **82** (2010) 010103(R).
- 2009**
- A. Karagiannis, T. Gallopin, D. Csaba, D. Battaglia, H. Geoffroy, J. Rossier, E. Hillman, J. Staiger, and B. Cauli, "Classification of NPY-expressing neocortical interneurons", *J Neurosci* **29** (2009) 3642-3659.
- A. Levina, J.M. Herrmann, and T. Geisel, "Phase transitions towards criticality in a neural system with adaptive interactions", *Phys. Rev. Lett.* **102** (2009) 118110.
- A.Y. Shahverdian, "A Decomposition of Quasi-Oscillators", *Asian-European Journal of Mathematics* **2**(4) (2009) 681-705.
- C. Kolodziejcki, C. Tetzlaff, and F. Wörgötter, "Investigation of the dynamics of small networks' connections under Hebbian plasticity", in *Frontiers in Computational Neuroscience. Conference Abstract: Bernstein Conference on Computational Neuroscience*. Frontiers. (2009).
- C.T. West, T. Prosen, and T. Kottos, "Short-time Loschmidt gap in dynamical systems with critical chaos", *Phys. Rev. E* **79** (2009) 050107.
- D. Battaglia, "Neuron-less Neural-like Networks with Exponential Association Capacity at Tabula Rasa", in *Methods and Models in Artificial and Natural Computation*, vol. 1 (WINAC 2009), edited by J. Mira, J.M Ferrandez, J. R. Alvarez et al. Springer-Verlag, Berlin-Heidelberg, (2009) 184-194.
- D. Battaglia, and A. Witt, "Dynamic transitions in the effective connectivity of interacting cortical areas", in *Frontiers in Computational Neuroscience. Conference Abstract: Bernstein Conference on Computational Neuroscience*. (2009).
- D. Battaglia, and D. Hansel, "Spatiotemporal structure of evoked gamma rhythms in a minimal multi-layer model of primary visual cortex", *BMC Neuroscience* **10**(Suppl. 1) (2009) 279.
- D. Bibitchkov, H. Taschenberger, and E. Neher, "Model of synaptic transmission in the calyx of Held", *BMC Neuroscience* **10**(Suppl 1) (2009) 219.
- D. Brockmann, V. David, and A. Morales Gallardo, "Human Mobility and Spatial Disease Dynamics", in *Diffusion Fundamentals III*, edited by C. Chmelik, N. Kanellopoulos, J. Kärgler, D. Theodorou. Leipziger Universitätsverlag, Leipzig, (2009) 1-27.
- D. Tsigankov, and A. Koulakov, "Optimal axonal and dendritic branching strategies during the development of neural circuitry", *Frontiers in Neural Circuits* **3** (2009) 18.
- D. Witthaut, K. Rapeldius, and H.J. Korsch, "The nonlinear Schrödinger equation for the delta-comb potential: quasi-classical chaos and bifurcations of periodic stationary solutions", *J. Nonlin. Math. Phys.* **16**(2) (2009) 207.

- D.M. Wittmann, F. Blöchl, D. Trümbach, W. Wurst, N. Prakash, and F.J. Theis, „Spatial Analysis of Expression Patterns Predicts Genetic Interactions at the Mid-Hindbrain Boundary“, *PLoS Comput. Biol.* **5**(11) (2009) e1000569.
- F. Hesse, G. Martius, R. Der, and J.M. Herrmann, “A Sensor-Based Learning Algorithm for the Self-Organization of Robot Behavior”, *Algorithms* **2**(1) (2009) 398-409.
- F. Hesse, R. Der, and J.M. Herrmann, „Modulated Exploratory Dynamics can shape Self-Organized Behavior“, *Advances in Complex Systems (ACS)* **12**(3) (2009) 273 - 291.
- F. Trimborn, D. Witthaut, and H.J. Korsch, „Beyond mean-field dynamics of small Bose-Hubbard systems based on the number-conserving phase-space approach“, *Phys. Rev. A* **79** (2009) 013608.
- G.S. Ng, H. Hennig, R. Fleischmann, T. Kottos, and T. Geisel, „Avalanches of Bose-Einstein Condensates in Leaking Optical Lattices“, *New J. Phys.* **11** (2009) 073045.
- H. Affan, R. Friedrich, and S. Eule, „Anomalous diffusion in a field of randomly distributed scatterers“, *Phys. Rev. E* **80** (2009) 011137.
- J. Haß, S. Blaschke, T. Rammsayer, and J.M. Herrmann, „Detection of irregularities in auditory sequences: A neural-network approach to temporal processing“, in *Proceedings of the 11th Neural Computation and Psychology Workshop: Connectionist Models of Behaviour and Cognition*, edited by J. Mayor, N. Ruh and K. Plunkett. World Scientific. (2009).
- J.D. Bodyfelt, M.C. Zheng, T. Kottos, U. Kuhl, and H. Stöckmann, „Fidelity in Quasi-1D Systems as a Probe for Anderson Localization“, *Acta Physica Polonica A* **116** (2009) 756-764.
- K. Smith-Mannschott, M. Chuchem, M. Hiller, T. Kottos, and D. Cohen, „Occupation Statistics of a Bose-Einstein Condensate for a Driven Landau-Zener Crossing“, *Phys. Rev. Lett.* **102** (2009) 230401.
- L. Reichl, S. Loewel, and F. Wolf, „Pinwheel Stabilization by Ocular Dominance Segregation“, *Phys. Rev. Lett.* **102** (2009) 208101.
- M. Hiller, T. Kottos, and T. Geisel, „Wave-packet dynamics in energy space of a chaotic trimeric Bose-Hubbard system“, *Phys. Rev. A* **79** (2009) 023621.
- M. Kaschube, M. Schnabel, F. Wolf, and S. Löwel, „Inter-areal coordination of columnar architectures during visual cortical development“, *Proceedings of the National Academy of Sciences*, 10.1073/pnas.0901615106, (2009).
- M. Schnabel, M. Kaschube, L.E. White, and F. Wolf, „Pattern selection, pinwheel stability and the geometry of visual space“ in *Eighteenth Annual Computational Neuroscience Meeting: CNS*2009 Berlin, Germany*. 18–23 July 2009.
- M. Schnabel, M. Kaschube, L.E. White, and F. Wolf, „Quantifying signatures of collinearity and cocircularity in natural images and in orientation maps“ in *Society for Neuroscience, Annual Meeting*, Vol. **34** (2009).
- O. Bendix, R. Fleischmann, T. Kottos, and B. Shapiro, „Exponentially Fragile PT-Symmetry in Lattices with Localized Eigenmodes“, *Phys. Rev. Lett.* **103** (2009) 030402.
- P. Gruber, H. Gutch, and F. Theis, „Hierarchical Extraction of Independent Subspaces of Unknown Dimensions“, in *Independent Component Analysis and Signal Separation*, edited by Tülay Adalı and Christian Jutten and João Marcos Travassos Romano and Allan Kardec Barros. Springer, (2009) 259–266.
- S. Eule, and R. Friedrich, „Subordinated Langevin equations for anomalous diffusion in external potentials —Biasing and decoupled external forces“, *EPL* **86**(3) (2009) 30008.
- T. Frank, D. Khimich, A. Neef, and T. Moser, „Mechanisms contributing to synaptic Ca²⁺ signals and their heterogeneity in hair cells“, *PNAS* **106**(11) (2009) 4483-4488.
- T. Geisel, „Dem Geld auf der Spur: Lévy Walks, Lévy Flights und ihre Verwendung in neuen epidemiologischen Modellen“, *Physik Journal* **8**(8/9) (2009) 51.
- T. Ingalls, G. Martius, M. Hellmuth, M. Marz, and S.J. Prohaska, „Converting DNA to Music: ComposAlign“, in *German Conference on Bioinformatics 2009*, (2009) 93-103.
- V. Belik, T. Geisel, and D. Brockmann, „The impact of human mobility on spatial disease dynamics“. In: *Proceedings of 2009 International Conference on Computational Science and Engineering*. IEEE Computer Society (2009) 932-935.
- C. Kirst, T. Geisel, and M. Timme “Sequential Desynchronization in Networks of Spiking Neurons with Partial Reset“, *Phys. Rev. Lett.* **102** (2009) 068101.
- N. Strenzke, S. Chanda, C. Kopp-Scheinflug, D. Khimich, K. Reim, A.V. Bulankina, A. Neef, F. Wolf, N. Brose, M.A. Xu-Friedman, T. Moser Complexin-I is required for high-fidelity transmission at the endbulb of held auditory synapse. *J Neurosci.* **29** (2009) 7991

2008

- C. Kolodziejcki, and F. Wörgötter, “On the plasticity of many synapse systems“, in *Frontiers in Computational Neuroscience*. Conference Abstract: Bernstein Symposium. Frontiers. (2008).
- C. Kolodziejcki, B. Porr, and F. Wörgötter, “Mathematical properties of neuronal TD-rules and differential Hebbian learning: A comparison“, *Biological Cybernetics* **98** (2008) 259-272.
- C. Kolodziejcki, B. Porr, and F. Wörgötter, “On the equivalence between differential Hebbian and temporal difference learning“, in *Proceedings of the Computational and Systems Neuroscience meeting COSYNE*2008, Salt Lake City* (2008).

- C. Kolodziejcki, B. Porr, M. Tamosiunaite, and F. Wörgötter, "On the equivalence between TD-learning and differential Hebbian learning using a local third factor", in *Advances in Neural Information Processing Systems* 21. MIT Press (2008).
- D. Battaglia, N. Brunel, and D. Hansel, "Stimulus-dependent temporal decorrelation of evoked oscillatory responses in primary visual cortex", in *COSYNE 2008*. Book of abstracts, pages II-4 (2008).
- D. Brockmann, "A physicist enthuses about criticality in biological development", *Nature* **451** (2008) 11.
- F. Wolf, L. Reichl, and S. Loewel, "Contralateral eye dominance induces pinwheel crystallization in models of visual cortical development", in *Society for Neuroscience Abstracts* Vol **34**, (2008) 326.18.
- G. Martius, K. Fiedler, and J.M. Herrmann, "Structure from Behavior in Autonomous Agents", in *IEEE International Conference on Intelligent Robots and Systems (IROS)*. IEEE Press, (2008) 858—862.
- G. Martius, S. Nolfi, and J.M. Herrmann, "Emergence of Interaction Among Adaptive Agents", in *From Animals to Animats 10*, 10th International Conference on Simulation of Adaptive Behavior, SAB, Japan, Proceedings. Springer, (2008) 457-466.
- J. Haß, S. Blaschke, T. Rammsayer, and J.M. Herrmann, "A neurocomputational model for optimal temporal processing", *J Comput Neurosci* **25** (2008) 449--464.
- J. Nagler, and P.H. Richter, "How random is dice tossing?" (featured in Nature 455, p.434, 2008) *Phys. Rev. E* **78** (2008) 036207.
- K. Doubrovinski, and J.M. Herrmann, "Stability of localized patterns in neural fields", *Neural Computation*, **21** (2008) 1125-44.
- M. Hiller, T. Kottos, and D. Cohen, "Control of atomic currents using a quantum stirring device", *Europhys. Lett.* **82** (2008) 40006.
- M. Ihrke, H. Schrobsdorff (Degering), and J.M. Herrmann, "Compensation for Speed-of-Processing Effects in EEG-Data Analysis", in *Intelligent Data Engineering and Automated Learning – IDEAL 2008*. Springer Verlag, (2008) 354-361.
- M. Kaschube, M. Schnabel, and F. Wolf, "Self-Organization and the Selection of Pinwheel Density in Visual Cortical Development", *New Journal of Physics* **10** (2008) 015009 (20pp).
- M. Kreissl, and W. Nolting, "Two-band ferromagnetic Kondo-lattice model for local-moment half-metals", *Journal of Physics: Condensed Matter* **20** (2008) 035222.
- S. Eule, R. Friedrich, F. Jenko, and I. Sokolov, "Continuous-time random walks with internal dynamics and subdiffusive reaction-diffusion equations", *Phys. Rev. E (R)*(**78**) (2008) 060102.
- T. Geisel, and D. Brockmann, "Seuchen und Reisen - Neue Modelle zur Vorhersage von Epidemien in einer globalisierten Welt". in *Natur und Migration*, edited by Harald zur Hausen. *Nova Acta Leopoldina* **97**, Nr. 358, pages 31—40 (2008).
- T. Kulvicius, C. Kolodziejcki, P.d. Prodi, M. Tamosiunaite, B. Porr, and F. Wörgötter, "On the analysis and evaluation of closed loop learning systems", in *Frontiers in Computational Neuroscience*. Conference Abstract: Bernstein Symposium (2008).
- F. Wolf, F. Kirchhoff. Imaging astrocyte activity, *Science* **320** (2008) 5883
- F. Wolf, T. Geisel. Logic gates come to life, *Nature Phys.* **4** (2008) 905
- M. Timme, F. Wolf. The simplest problem in the collective dynamics of neural networks: is synchrony stable? *NONLINEARITY* **21** (2008) 1579
- E. Bodenschatz, F. Wolf. Focus on Heart and Mind *New J. of Physics* **10** (2008) 015002
- B. Adamcio, D. Sargin, A. Stradomska, L. Medrihan, C. Gertler, F. Theis, M. Zhang, M. Müller, I. Hassouna, K. Hannke, S. Sperling, K. Radyushkin, A. El-Kordi, L. Schulze, A. Ronnenberg, F. Wolf, N. Brose, J.S. Rhee, W. Zhang, H. Ehrenreich. Erythropoietin enhances hippocampal long-term potentiation and memory. *BMC Biol.* **6** (2008) 37.
- M. Volgushev, A. Malyshev, P. Balaban, M. Chistiaikova, S. Volgushev, F. Wolf. Onset dynamics of action potentials in rat neocortical neurons and identified snail neurons: quantification of the difference. *PLoS One.* **3** (2008):e1962.

Research Group Theoretical Neurophysics

2011

M. Kaschube, D.M. Coppola, M. Schnabel, S. Löwel, L.E. White, and F. Wolf. An Alternative Hypothesis for Orientation Columns in the Visual Cortex (Reply), *Science* DOI:10.1126/science.1194869 (2011)

T. Tchumatchenko, T. Geisel, M. Volgushev, and F. Wolf. Spike correlations – what can they tell about synchrony *Front. Neurosci.* (2011) doi: **10.3389/fnins.2011.00068**

W. Wei, and F. Wolf. Spike Onset Dynamics and Response Speed in Neuronal Populations. *Phys. Rev. Lett.* **106** (2011) 088102

2010

M. Kaschube, M. Schnabel, S. Löwel, D.M. Coppola, L.E. White, and F. Wolf. Universality in the Evolution of Orientation Columns in the Visual Cortex. *Science* **330** (2010) 1113.

M. Monteforte, and F. Wolf. Dynamical Entropy Production in Spiking Neuron Networks in the Balanced State. *Phys. Rev. Lett.* **105** (2010) 268104

S. Junek, E. Kludt, F. Wolf, and D. Schild. Olfactory Coding with Patterns of Response Latencies *Neuron* **67** (2010) 872

D. Tsigankov & A.A. Koulakov, Sperry versus Hebb: topographic mapping in Isl2/EphA3 mutant mice, *BMC Neurosci.* **11** (2010) 155.

W. Keil, K. Schmidt, S. Löwel, and M. Kaschube (2010). Reorganization of columnar architecture in the growing visual cortex *Proc. Natl. Acad. Sci. USA* **107** (2010) 12293

G. Baranauskas, A. Mukovskiy, F. Wolf, and M. Volgushev. The Determinants of the Onset Dynamics of Action Potentials in a Computational Model. *Neuroscience* **167** (2010) 1070

T. Tchumatchenko, T. Geisel, M. Volgushev, and F. Wolf. Signatures of synchrony in pairwise count correlations. *Front. Comput. Neurosci.* (2010) doi:10.3389/neuro.10.001.

T. Tchumatchenko, A. Malyshev, T. Geisel, M. Volgushev, and F. Wolf. Correlations and Synchrony in Threshold Neuron Models. *Phys. Rev. Lett.* **104** (2010) 058102

2009

L. Reichl, S. Lowel, F. Wolf. Pinwheel Stabilization by Ocular Dominance Segregation, *Phys. Rev. Lett.* **102** (2009) 208101

M. Kaschube, M. Schnabel, F. Wolf*, S. Löwel. Interareal coordination of columnar architectures during visual cortical development. *Proc. Natl. Acad. Sci. USA* **106** (2009) 17205.

D. Tsigankov & A.A. Koulakov AA., Optimal axonal and dendritic branching strategies during the development of neural circuitry, *Front Neural Circuits.* **3** (2009) 18

N. Strenzke, S. Chanda, C. Kopp-Scheinflug, D. Khimich, K. Reim, A.V. Bulankina, A. Neef, F. Wolf, N. Brose, M.A. Xu-Friedman, T. Moser Complexin-I is required for high-fidelity transmission at the endbulb of held auditory synapse. *J Neurosci.* **29** (2009) 7991

2008

M. Kaschube, M. Schnabel, F. Wolf. Self-organization and the selection of pinwheel density in visual cortical development *New J. of Physics* **10** (2008) 015009

F. Wolf, F. Kirchhoff. Imaging astrocyte activity, *Science* **320** (2008) 5883

F. Wolf, T. Geisel. Logic gates come to life, *Nature Phys.* **4** (2008) 905

M. Timme, F. Wolf. The simplest problem in the collective dynamics of neural networks: is synchrony stable? *NONLINEARITY* **21** (2008) 1579

E. Bodenschatz, F. Wolf. Focus on Heart and Mind *New J. of Physics* **10** (2008) 015002

B. Adamcio, D. Sargin, A. Stradomska, L. Medrihan, C. Gertler, F. Theis, M. Zhang, M. Müller, I. Hassouna, K. Hanneke, S. Sperling, K. Radyushkin, A. El-Kordi, L. Schulze, A. Ronnenberg, F. Wolf, N. Brose, J.S. Rhee, W. Zhang, H. Ehrenreich. Erythropoietin enhances hippocampal long-term potentiation and memory. *BMC Biol.* **6** (2008) 37.

M. Volgushev, A. Malyshev, P. Balaban, M. Chistiaikova, S. Volgushev, F. Wolf. Onset dynamics of action potentials in rat neocortical neurons and identified snail neurons: quantification of the difference. *PLoS One.* **3** (2008):e1962.

Department of Dynamics of Complex Fluids

2011

Theodore F. Argo IV, Matthew D. Guild, Preston S. Wilson, Matthias Schröter, Charles Radin, and Harry L. Swinney: Sound speed in water-saturated glass beads as a function of frequency and porosity. *J. Acoust. Soc. Am.* **129** (2011) EL101.

A. Dimakis and F. Müller-Hoissen, "KP line solitons and Tamari lattices", *J. Phys. A: Math. Theor.* **44** (2011) 025203.

A. Dimakis, N. Kanning and F. Müller-Hoissen, "Bidifferential calculus, matrix SIT and sine-Gordon equations", *Acta Polytechnica* **51** (2011) 33-37.

Hüseyin Burak Eral, Jolet de Ruiter, Riëlle de Ruiter, Jung Min Oh, Ciro Semperebon, Martin Brinkmann, and Frieder Mugele: "Drops on functional fibers: from barrels to clamshells and back" *Soft Matter Advance Article* (2011).

Jean-François Métayer, Donald J. Suntrup III, Charles Radin, Harry L. Swinney, and Matthias Schröter: Shearing of frictional sphere packings. *Eur. Phys. Lett.* **93** (2011) 64003.

Diego F. M. Oliveira, Jürgen Vollmer, and Edson D. Leonel: "Fermi acceleration and its suppression in a time-dependent Lorentz gas" *Physica D* **240** (2011) 389.

Shashi Thutupalli, Stephan Herminghaus, and Ralf Seemann: "Bilayer membranes in micro-fluidics: from gel emulsions to functional devices" *Soft Matter* **7** (2011) 1312.

2010

Izabella Benczik, and Jürgen Vollmer: "A reactive-flow model of phase separation in fluid binary mixtures with continuously ramped temperature" *EPL* **91** (2010) 36003.

Venkatachalam Chokkalingam, Boris Weidenhof, Michael Krämer, Wilhelm F. Maier, Stephan Herminghaus, and Ralf Seemann: "Optimized droplet-based microfluidics scheme for sol-gel reactions" *Lab Chip* **10** (2010) 1700.

Venkatachalam Chokkalingam, Boris Weidenhof, Michael Krämer, Stephan Herminghaus, Ralf Seemann, and Wilhelm F. Maier: "Template-free Preparation of Mesoporous Silica Spheres through Optimized Microfluidics" *ChemPhysChem* **11** (2010) 2091.

A. Dimakis and F. Müller-Hoissen, "Quasi-symmetric functions and the KP hierarchy", *J. Pure and Applied Algebra* **214** (2010) 449-460.

A. Dimakis and F. Müller-Hoissen, "Solutions of matrix NLS systems and their discretizations: A unified treatment", *Inverse Problems* **26** (2010) 095007.

A. Dimakis and F. Müller-Hoissen, "Bidifferential calculus approach to AKNS hierarchies and their solutions", *SIGMA* **6** (2010) 055.

Pontus S. H. Forsberg, Craig Priest, Martin Brinkmann, Rossen Sedev, and John Ralston: "Contact Line Pinning on Microstructured Surfaces for Liquids in the Wenzel State" *Langmuir* **26** (2010) 860.

Christoph Gögelein, Martin Brinkmann, Matthias Schröter, and Stephan Herminghaus: "Controlling the Formation of Capillary Bridges in Binary Liquid Mixtures" *Langmuir* **26** (2010) 17184.

Yasutaka Iwashita, Stephan Herminghaus, Ralf Seemann, and Christian Bahr: "Smectic membranes in aqueous environment" *Phys. Rev. E* **81** (2010) 051709.

Konstantina Kostourou, Dirk Peschka, Andreas Münch, Barbara Wagner, Stephan Herminghaus and Ralf Seemann: "Interface morphologies in Liquid/liquid dewetting" *Chemical Engineering and Processing Journal (CEP)* (Article in Press) (2010)

Seyed Habibolla Ebrahimpour Rahbari, Jürgen Vollmer, Stephan Herminghaus, and Martin Brinkmann "Fluidization of wet granulates under shear" *Phys. Rev. E* **82** (2010) 061305.

Claudia Schäfle, Martin Brinkmann, Clemens Bechinger, Paul Leiderer and Reinhard Lipowsky: "Morphological Wetting Transitions at Ring-Shaped Surface Domains" *Langmuir* **26** (2010) 11878–11885.

Gerd E. Schröder-Turk, Walter Mickel, Matthias Schröter, Gary W. Delaney, Mohammad Saadatfar, Tim J. Senden, Klaus Mecke, and Tomaso Aste: "Disordered spherical bead packs are anisotropic" *EPL* **90** (2010) 3001.

2009

Christian Bahr: "Experimental study of prewetting transitions by systematic variation of the surface

- field at nematic liquid crystal/water interfaces" *EPL* **88** (2009) 46001.
- Pedro Bleuca, Martin Brinkmann, Reinhard Lipowsky, and Jan Kierfeld: „Morphological Transitions of Liquid Droplets on Circular Surface Domains" *Langmuir* **25** (2009) 13493.
- Matthew A. Brown, Bernd Winter, Manfred Faubel, and John C. Hemminger: "Spatial Distribution of Nitrate and Nitrite Anions at the Liquid/Vapor Interface of Aqueous Solutions" *J. Am. Chem. Soc.* **131** (2009) 8354.
- Matthew A. Brown, Manfred Faubel, and Bernd Winter: "X-Ray photo- and resonant Auger-electron spectroscopy studies of liquid water and aqueous solutions" *Annu. Rep. Prog. Chem. C* **105** (2009) 174.
- A. Dimakis and F. Müller-Hoissen, "Weakly non-associative algebras and the Kadomtsev-Petviashvili hierarchy", *Glasgow Math. J.* **51A** (2009) 49-57.
- A. Dimakis and F. Müller-Hoissen, "Bidifferential graded algebras and integrable systems", *Discrete and Continuous Dynamical Systems (DCDS) Supplements* 2009, 208-219.
- A. Dimakis and F. Müller-Hoissen, "BKP and CKP revisited: The odd KP system", *Inverse Problems* **25** (2009) 045001.
- A. Dimakis and F. Müller-Hoissen, "Multicomponent Burgers and KP hierarchies, and solutions from a matrix linear system", *SIGMA* **5** (2009) 002.
- Heather M. Evans, Enkhtuul Surenjav, Craig Priest, Stephan Herminghaus, Ralf Seemann, and Thomas Pfohl: „In situ formation, manipulation, and imaging of droplet-encapsulated fibrin networks" *Lab Chip* **9** (2009) 1933.
- Christian Finke, Jürgen Vollmer, Svetlana Postnova, and Hans Albert Braun: "Propagation effects of current and conductance noise in a model neuron with sub-threshold oscillations" *Math. Biosci.* **214** (2009) 109.
- Wei Guo, and Christian Bahr: "Influence of phase sequence on focal conic domains in smectic films" *Phys. Rev. E* **79** (2009) 061701.
- Kai Huang, Masoud Sohaili, Matthias Schröter, and Stephan Herminghaus: „Fluidization of granular media wetted by liquid Superscript He" *Phys. Rev. E* **79** (2009) 010301.
- Kai Huang, Klaus Röller, and Stephan Herminghaus: "Universal and non-universal aspects of wet granular matter under vertical vibrations" *Eur. Phys. J. Special Topics* **179** (2009) 25.
- Yasutaka Iwashita, Christian Bahr, Craig Priest, Stephan Herminghaus, and Ralf Seemann: „Dynamic x-ray optics with microfluidics: stabilization of gas bubbles by surface ordering and freezing" *La Houille Blanche* **6** (2009) 129.
- Krishnasharya Khare, Martin Brinkmann, Bruce M. Law, Stephan Herminghaus, and Ralf Seemann: "Switching wetting morphologies in triangular grooves" *Eur. Phys. J. Special Topics* **166** (2009) 151.
- Oliver Link, Eugen Lugovoy, Katrin Siefertmann, Yaxing Liu, Manfred Faubel, and Bernd Abel: "Ultrafast electronic spectroscopy for chemical analysis near liquid water interfaces: concepts and applications" *Applied Physics A* **96** (2009) 117.
- Oliver Link, Esteban Vöhringer-Martinez, Eugen Lugovoy, Yaxing Liu, Katrin Siefertmann, Manfred Faubel, Helmut Grubmüller, R. Benny Gerber, Yifat Miller, and Bernd Abel: "Ultrafast phase transitions in metastable water near liquid interfaces" *Faraday Discuss* **141** (2009) 67.
- Niklas Ottosson, Manfred Faubel, Stephen E. Bradforth, Pavel Jungwirth, and Bernd Winter: "Photoelectron spectroscopy of liquid water and aqueous solution: Electron effective attenuation lengths and emission-angle anisotropy" *Journal of Electron Spectroscopy and Related Phenomena* (2009).
- Seyed Habibolla Ebrahimnashad Rahbari, Jürgen Vollmer, Stephan Herminghaus, and Martin Brinkmann: "A response function perspective on yielding of wet granular matter" *EPL* **87** (2009) 14002.
- Klaus Röller, Jürgen Vollmer, and Stephan Herminghaus: "Unstable Kolmogorov flow in granular matter" *CHAOS* **19** (2009) 041106.
- Ralf Seemann, Martin Brinkmann, and Stephan Herminghaus: "Auf Sand gebaut" *Physik Journal* **8** (2009) 31.
- Robert Seidel, Manfred Faubel, Bernd Winter, and Jochen Blumberger: "Single-Ion Reorganization Free Energy of Aqueous Ru(bpy)₃²⁺/3⁺ and Ru(H₂O)₆²⁺/3⁺ from Photoemission Spectroscopy and Density Functional Molecular Dynamics Simulation" *J. Am. Chem. Soc.* **131** (2009) 16127.
- Petr Slavicek, Bernd Winter, Manfred Faubel, Stephen E. Bradforth, and Pavel Jungwirth: "Ionization Energies of Aqueous Nucleic Acids: Photoelectron Spectroscopy of Pyrimidine Nucleosides and ab Initio Calculations" *J. Am. Chem. Soc.* **131** (2009) 6460.
- Erik J. Stalcup, Ralf Seemann, Stephan Herminghaus, and Bruce M. Law: „Dissipation mechanism in ionic liquids" *Journal of Colloid and Interface Science* **338** (2009) 523.
- Enkhtuul Surenjav, Stephan Herminghaus, Craig Priest, and Ralf Seemann: "Discrete microfluidics: Reorganizing droplet arrays at a bend" *Appl. Phys. Lett.* **95** (2009) 154104.
- Enkhtuul Surenjav, Craig Priest, Stephan Herminghaus, and Ralf Seemann: "Manipulation of gel emulsions by variable microchannel geometry" *Lab on a Chip* **9** (2009) 325.
- Stephan Ulrich, Timo Aspelmeier, Anette Zippelius, Klaus Röller, Axel Fingerle, and Stephan Herminghaus: "Dilute wet granular particles: Nonequilibrium dynamics and structure formation" *Phys. Rev. E* **80** (2009) 031306.

Stephan Ulrich, Timo Aspelmeier, Klaus Röller, Axel Fingerle, Stephan Herminghaus, and Anette Zippe: "Cooling and Aggregation in Wet Granulates" *Phys. Rev. Lett.* **102** (2009) 148002.

Jürgen Vollmer, Tobias M. Schneider, and Bruno Eckhardt: "Basin boundary, edge of chaos and edge state in a two-dimensional model" *New J. Phys.* **11** (2009) 013040.

Bernd Winter, Manfred Faubel, Robert Vácha, and Pavel Jungwirth: "Behavior of hydroxide at the water/vapor interface" *Chemical Physics Letters* **474** (2009) 241.

2008

Emad F. Aziz, Niklas Ottosson, Manfred Faubel, In-golf V. Hertel, and Bernd Winter: "Interaction between liquid water and hydroxide revealed by core-hole de-excitation" *Nature* **455** (2008) 89.

Venkatachalam Chokkalingam, Boris Weidenhof, Wilhelm F. Maier, Stephan Herminghaus, and Ralf Seemann: "Step-emulsification microfluidics for production of monodispersed high surface area silica microparticles" *Proceedings of the 1st European Conference on Microfluidics – Microfluidics 2008 Conference, 10-12 December 2008, Bologna* (2008)

Venkatachalam Chokkalingam, Stephan Herminghaus, and Ralf Seemann: "Self-synchronizing pairwise production of monodisperse droplets by microfluidic step emulsification" *Appl. Phys. Lett.* **93** (2008) 254101.

Venkatachalam Chokkalingam, Boris Weidenhof, Wilhelm F. Maier, Stephan Herminghaus, and Ralf Seemann: "Controlled Production of Monodispersed Silica Microspheres using a Double Step-Emulsification Device" *Proceedings of the Sixth ICNMM (Darmstadt)* ISBN 0-7918-4834-5 (2008) 1527-1535.

Venkatachalam Chokkalingam, Stephan Herminghaus, and Ralf Seemann: "Self-Synchronizing Droplets with double Step-Emulsification Devices" In: *The Proceedings of the μ TAS 2008* „J.L. E. Locascio, M. Gaitan, B. M. Paegel, D. J. Ross, W. N. Vreeland" ISBN: 978-0-9798064-1-4 (2008) 1438-1440.

Venkatachalam Chokkalingam, Boris Weidenhof, Wilhelm F. Maier, Stephan Herminghaus, and Ralf Seemann: "Synthesis of Silica Microparticles with Step-Emulsification Microfluidics" In: *The Proceedings of the μ TAS 2008* „L. E. Locascio, M. Gaitan, B. M. Paegel, D. J. Ross, W. N. Vreeland" ISBN: 978-0-9798064-1-4 (2008) 444-446

Lukasz Cwiklik, Udo Buck, Waldemar Kulig, Piotr Kubisiak, and Pavel Jungwirth: "A sodium atom in a large water cluster: Electron delocalization and infrared spectra" *J. Chem. Phys.* **128** (2008) 154306.

Ingo Dauster, Martin A. Suhm, Udo Buck, and Thomas Zeuch: "Experimental and theoretical study of the microsolvation of sodium atoms in methanol clusters: differences and similarities to sodium–water and sodium–ammonia" *Phys. Chem. Chem. Phys.* **10** (2008) 83.

A. Dimakis and F. Müller-Hoissen, "From the Kadomtsev-Petviashvili equation halfway to Ward's chiral model", *J. Gen. Lie Theory Appl.* **2** (2008) 141-146.

A. Dimakis and F. Müller-Hoissen, "Weakly nonassociative algebras, Riccati and KP hierarchies", in *Generalized Lie Theory in Mathematics, Physics and Beyond*, S. Silvestrov, E. Paal, V. Abramov and A. Stolin (eds.), Springer (2008) 9-27.

A. Dimakis and F. Müller-Hoissen, "Dispersionless limit of the noncommutative potential KP hierarchy and solutions of the pseudodual chiral model in 2+1 dimensions", *J. Phys. A: Math. Theor.* **41** (2008) 265205.

Axel Fingerle, Klaus Röller, Kai Huang, and Stephan Herminghaus: "Phase transitions far from equilibrium in wet granular matter" *New Journal of Physics* **10** (2008) 053020.

Axel Fingerle, and Stephan Herminghaus: "Equation of state of wet granular matter" *Phys. Rev. E* **77** (2008) 011306.

Christian Finke, Jürgen Vollmer, Svetlana Postnova, and Hans Albert Braun: "Propagation effects of current and conductance noise in a model neuron with subthreshold oscillations" *Mathematical Biosciences* **109** (2008) 531.

Wei Guo, Stephan Herminghaus, and Christian Bahr: "Controlling Smectic Focal Conic Domains by Substrate Patterning" *Langmuir* **24** (2008) 8174.

Markus Hauck, Sascha-Rene Jürgens, Martin Brinkmann, and Stephan Herminghaus: "Surface Hydrophobicity Causes SO₂ Tolerance in Lichens" *Annals of Botany* **101** (2008) 531.

Stephan Herminghaus, Martin Brinkmann, and Ralf Seemann: "Wetting and Dewetting of Complex Surface Geometries" *Annu. Rev. Mater. Res.* **38** (2008) 10.1-10.21.

Karin Jacobs, Ralf Seemann, and Stephan Herminghaus: "Stability and Dewetting of Thin Liquid Films" in: *Polymer Thin Films* O. Tsui, T. Russell eds., Series in Soft Condensed Matter - Vol. 1, World Scientific ISBN 978-981-281-881-2 (2008).

Melissa Jerkins, Matthias Schröter, Harry L. Swinney, Tim J. Senden, Mohammad Saadatfar, and Tomaso Aste: "Onset of mechanical stability in random packings of frictional spheres, *Phys. Rev. Lett.* **101** (2008) 018301.

Sarah Köster, Heather M. Evans, Joyce Y. Wong, and Thomas Pfohl: "An In Situ Study of Collagen Self-Assembly Processes" *Biomacromolecules* **9** (2008) 199.

Sarah Köster, Jan Kierfeld, and Thomas Pfohl: "Characterization of single semiflexible filaments under geometric constraints" *Eur. Phys. J. E* **25** (2008) 439.

F. Müller-Hoissen, "Noncommutative Geometries and Gravity", *AIP Conference Proceedings* **977** (2008) 12-29.

Dirk Nolting, Niklas Ottosson, Manfred Faubel, Ingolf V. Hertel, and Bernd Winter: "Pseudoequivalent Nitrogen Atoms in Aqueous Imidazole Distinguished by Chemical Shifts in Photoelectron Spectroscopy" *J. Am. Chem. Soc.* **130** (2008) 1850.

Milan Oncak, Petr Slavicek, Viktoria Poterya, Michal Farnik, and Udo Buck: "Emergence of Charge-Transfer-to-Solvent Band in the Absorption Spectra of Hydrogen Halides on Ice Nanoparticles: Spectroscopic Evidence for Acidic Dissociation" *J. Phys. Chem. A* **112** (2008) 5344.

Viktoriya Poterya, Ondrej Votava, Michal Fárník, Milan Ončák, Petr Slavíček, Udo Buck, and Bretislav Friedrich: "Generation and orientation of organoxenon molecule H–Xe–CCH in the gas phase" *J. Chem. Phys.* **128** (2008) 104313.

Mario Scheel, Ralf Seemann, Martin Brinkmann, Marco Di Michiel, Adrian Sheppard, and Stephan Herminghaus: "Liquid distribution and cohesion in wet granular assemblies beyond the capillary bridge regime" *J. Phys.: Condens. Matter* **20** (2008) 494236.

Mario Scheel, Ralf Seemann, Martin Brinkmann, Stephan Herminghaus, Marco Di Michiel, Boris Breidenbach, and Adrian Sheppard: "Morphological clues to wet granular pile stability" *Nature Materials* **7** (2008) 189.

Enkhtuul Surenjav, Craig Priest, Stephan Herminghaus, and Ralf Seemann: "Manipulation of gel emulsions by variable microchannel geometry" *Lab Chip* **9** (2008) 325.

Emmerson J. De Souza, Martin Brinkmann, Camilla Mohrdieck, and Eduard Arzt: "Enhancement of Capillary Forces by Multiple Liquid Bridges" *Langmuir* **24** (2008) 8813.

Emerson J. De Souza, Martin Brinkmann, Camilla Mohrdieck, Alfred Crosby, and Eduard Arzt: "Capillary Forces between Chemically Different Substrates" *Langmuir* **24** (2008) 10161.

Jürgen Vollmer: "Phase separation under ultraslow cooling: Onset of nucleation" *J. Chem. Phys.* **129** (2008) 164502.

Jürgen Vollmer, Jozsef Hegedüs, Frank Grosse, and Joachim Krug: "Impurity-induced step interactions: a kinetic Monte Carlo study" *New J. Phys.* **10** (2008) 053017.

Bernd Winter, Emad F. Aziz, Niklas Ottosson, Manfred Faubel, Nobuhiro Kosugi, and Ingolf V. Hertel: "Electron Dynamics in Charge-Transfer-to-Solvent States of Aqueous Chloride Revealed by Cl- 2p Resonant Auger-Electron Spectroscopy" *J. Am. Chem. Soc.* **130** (2008) 7130.

Department of Fluid Dynamics, Pattern Formation and Nanobiocomplexity

2011

S. Luther, F. H. Fenton, B. G. Kornreich, A. Squires, P. Bittihn, D. Hornung, M. Zabel, J. Flanders, A. Gladuli, L. Campoy, E. M. Cherry, G. Luther, G. Hasenfuss, V. I. Krinsky, A. Pumir, R. F. Gilmour, E. Bodenschatz, "Low-energy control of electrical turbulence in the heart", *Nature* (accepted, 2011)

C. Beta and E. Bodenschatz, "Microfluidic tools for quantitative studies of eukaryotic chemotaxis", *European Journal of Cell Biology*, to appear.

A. Töbrens, R. Mettin, U. Parlitz, "Dynamics of a driven oscillator carrying a freely sliding mass", *Int. J. of Bifurcation and Chaos*, to appear

E. Bodenschatz und M. Eckert, "Prandtl and The Goettingen School", to appear in "A Voyage Through Turbulence", edited by P. A. Davidson, Y. Kaneda, K. Moffatt and K. R. Sreenivasan, Cambridge Univ. Press, Cambridge 2011.

Guenter Ahlers, Denis Funfschilling and Eberhard Bodenschatz, "Transitions in heat transport by turbulent convection at Rayleigh numbers up to 10^{15} ", *New J. Phys.* **13**, 049401 (2011)

Haitao Xu, Alain Pumir and Eberhard Bodenschatz, "The Pirouette Effect in Turbulent Flows", *Nature Physics* (to appear)

D. Tordella, M. Belan, S. Massaglia, S. De Ponte, A. Mignone, E. Bodenschatz, A. Ferrari, "Astrophysical jets: insight into long term hydrodynamics", *New Journal of Physics* **13** (2011) 043011.

U. Parlitz, A. Schlemmer, S. Luther, "Synchronization patterns in transient spiral wave dynamics", *Phys. Rev. E* **83**, 057201 (2011).

U. Parlitz, S. Berg, S. Luther, A. Schirdewan, J. Kurths, N. Wessel, "Classifying Cardiac Biosignals using Ordinal Pattern Statistics and Symbolic Dynamics", *Comput. Biol. Med.* 2011 Apr 19. [Epub ahead of print].

T. H. van den Berg, W. D. Wormgoor, S. Luther, D. Lohse, "Phase-sensitive constant temperature anemometry", *Macromol. Mater. Eng.* **296** (2011) 230-237.

S. Petitprez, A. F. Zmoos, J. Ogrodnik, E. Balse, N. Raad, S. El-Haou, M. Albesa, P. Bittihn, S. Luther, S. E.

Lehnart, S. N. Hatem, A. Coulombe, H. Abriel, "SAP97 and dystrophin macromolecular complexes determine two pools of cardiac sodium channels Nav1.5 in cardiomyocytes", *Circulation Research* **108** (2011) 294-304.
E. Schäfer, C. Westendorf, E. Bodenschatz, C. Beta, B. Geil, A. Janshoff, "Shape oscillations of Dictyostelium discoideum cells on ultramicroelectrodes monitored by impedance analysis", *Small* (2011) DOI:10.1002/sml.201001955.

2010

A. J. Bae, E. Bodenschatz, "On the swimming of Dictyostelium amoebae", *PNAS* **107** (2010) E165-E166.

G. C. McBane, L. T. Nguyen, R. Schinke, "Photodissociation of ozone in the Hartley band: Product state and angular distributions", *Journal of Chemical Physics* **133** (2010) 144312.

C. Beta, "Bistability in the actin cortex", *PMC Biophysics* **3** (2010) 12.

P. Bittihn, A. Squires, G. Luther, E. Bodenschatz, V. Krinsky, U. Parlitz, S. Luther, "Phase-resolved analysis of the susceptibility of pinned spiral waves to far-field pacing in a two-dimensional model of excitable media", *Philosophical Transactions of the Royal Society A* **368** (2010) 2221-2236.

H. U. Bodeker, C. Beta, T. D. Frank, E. Bodenschatz, "Quantitative analysis of random ameboid motion", *EPL* **90** (2010) 28005.

E. Bodenschatz, S. P. Malinowski, R. A. Shaw, F. Stratmann, "Can we understand clouds without turbulence?", *Science* **327** (2010) 970-971.

M. Gibert, H. Xu, E. Bodenschatz, "Inertial effects on two-particle relative dispersion in turbulent flows", *EPL* **90** (2010) 64005.

M. V. Ivanov, R. Schinke, "Vibrational energy transfer in Ar-O₃ collisions: comparison of rotational sudden, breathing sphere, and classical calculations", *Molecular Physics* **108** (2010) 259-268.

S. A. Ndengué, F. Gatti, R. Schinke, H. D. Meyer, R. Jost, "Absorption cross section of ozone isotopologues calculated with the multiconfiguration time-dependent Hartree (MCTDH) method. I. The Hartley and Huggins bands", *Journal of Physical Chemistry A* **114** (2010) 9855-9863.

- H. Nobach, "Influence of individual variations of particle image intensities on high-resolution PIV", *Experiments in Fluids* (2010) Online First.
- N. F. Otani, S. Luther, S. Singh, R. F. Gilmour, "Trans-mural ultrasound-based visualization of patterns of action potential wave propagation in cardiac tissue", *Annals of Biomedical Engineering* **38** (2010) 3112-3123.
- A. Pumir, S. Sinha, S. Sridhar, M. Argentina, M. Hörning, S. Filippi, C. Cherubini, S. Luther, V. Krinsky, "Wave-train-induced termination of weakly anchored vortices in excitable media", *Physical Review E* **81** (2010) 010901 (R).
- R. Schinke, J. Suarez, S. C. Faranos, "Communication: Photodissociation of N₂O – Frustrated NN bond breaking causes diffuse vibrational structures", *Journal of Chemical Physics* **133** (2010) 091103.
- R. Schinke, G. C. McBane, "Photodissociation of ozone in the Hartley band: Potential energy surfaces, nonadiabatic couplings, and singlet/triplet branching ratio", *Journal of Chemical Physics* **132** (2010) 044305.
- Z. Sun, L. Liu, S. Y. Lin, R. Schinke, H. Guo, D. H. Zhang, "State-to-state quantum dynamics of O + O₂ isotope exchange reactions reveals nonstatistical behavior at atmospheric conditions", *PNAS* **107** (2010) 555-558.
- C. Westendorf, A. Bae, C. Erlenkamper, E. Galland, C. Franck, E. Bodenschatz, C. Beta, "Live cell flattening – traditional and novel approaches", *PMC Biophysics* **3** (2010) 9.
- R. Zimmermann, H. Xu, Y. Gasteuil, M. Bourgoïn, R. Volk, J. F. Pinton, E. Bodenschatz, "The Lagrangian exploration module: An apparatus for the study of statistically homogeneous and isotropic turbulence", *Review of Scientific Instruments* **81** (2010) 055112.
- 2009**
- G. Ahlers, E. Bodenschatz, D. Funfschilling, J. Hogg, "Turbulent Rayleigh-Bénard convection for a Prandtl number of 0.67", *Journal of Fluid Mechanics* **641** (2009) 157-167.
- G. Ahlers, D. Funfschilling, E. Bodenschatz, "Transitions in heat transport by turbulent convection at Rayleigh numbers up to 10¹⁵", *New Journal of Physics* **11** (2009) 123001.
- A. J. Bae, C. Beta, E. Bodenschatz, "Rapid switching of chemical signals in microfluidic devices", *LAB ON A CHIP* **9** (2009) 3059-3065.
- G. P. Bewley, "The generation of particles to observe quantized vortex dynamics in superfluid helium", *Cryogenics* **49** (2009) 549-553.
- C. Bardos, U. Frisch, W. Pauls, S. S. Ray, E. S. Titi, "Entire solutions of hydrodynamical equations with exponential dissipation", *Communications in Mathematical Physics* **293** (2009) 519-543.
- G. P. Bewley, K. R. Sreenivasan, "The decay of a quantized vortex ring and the influence of tracer particles", *Journal of Low Temperature Physics* **156** (2009) 84-94.
- D. Funfschilling, E. Bodenschatz, G. Ahlers, "Search for the „ultimate state“ in turbulent Rayleigh-Bénard convection", *Physical Review Letters* **103** (2009) 014503.
- N. T. Ouellette, H. Xu, E. Bodenschatz, "Bulk turbulence in dilute polymer solutions", *Journal of Fluid Mechanics* **629** (2009) 375-385.
- H. Nobach, E. Bodenschatz, "Limitations of accuracy in PIV due to individual variations of particle image intensities", *Experiments in Fluids* **47** (2009) 27-38.
- F. Toschi, E. Bodenschatz, "Lagrangian properties of particles in turbulence", *Annual Review of Fluid Mechanics* **41** (2009) 375-404.
- F. H. Fenton, S. Luther, E. M. Cherry, N. F. Otani, V. Krinsky, A. Pumir, E. Bodenschatz, R. F. Gilmour, "Termination of atrial fibrillation using pulsed low-energy far-field stimulation", *Circulation* **120** (2009) 467-476.
- S. Y. Grebenshchikov, R. Schinke, "Towards quantum mechanical description of the unconventional mass-dependent isotope effect in ozone: Resonance recombination in the strong collision approximation", *Journal of Chemical Physics* **131** (2009) 181103.
- S. Y. Grebenshchikov, "A quantum mechanical study of ozone isotope effect", *Few-Body Systems* **45** (2009) 241-243.
- R. Schinke, G. C. McBane, L. Shen, P. C. Singh, A. G. Suits, "Production of O₂ Herzberg states in the deep UV photodissociation of ozone", *Journal of Chemical Physics* **131** (2009) 011101.
- S. C. Farantos, R. Schinke, H. Guo, M. Joyeux, "Energy localization in molecules, bifurcation phenomena, and their spectroscopic signatures: The global view", *Chemical Reviews* **109** (2009) 4248-4271.
- P. Defazio, C. Petrongolo, G. C. McBane, L. Adam, W. Hack, S. Akpınar, R. Schinke, "Relaxation of NH(a¹Δ, v = 1) in collisions with H⁽²S): An experimental and theoretical study", *Journal of Physical Chemistry A* **113** (2009) 14458-14464.
- M. V. Ivanov, S. Y. Grebenshchikov, R. Schinke, "Quantum mechanical study of vibrational energy transfer in Ar-O₃ collisions: Influence of symmetry", *Journal of Chemical Physics* **130** (2009) 174311.
- Z. W. Qu, H. Zhu, V. May, R. Schinke, "Time-dependent density functional theory study of the electronic excitation spectra of chlorophyllide a and pheophorbide a in solvents", *Journal of Physical Chemistry B* **113** (2009) 4817-4825.
- 2008**
- J. H. McCoy, W. Brunner, W. Pesch, E. Bodenschatz, "Self-organization of topological defects due to applied constraints", *Physical Review Letters* **101** (2008) 254102.
- A. M. Crawford, N. Mordant, H. Xu, E. Bodenschatz, "Fluid acceleration in the bulk of turbulent dilute polymer solutions", *New Journal of Physics* **10** (2008) 123015.

- G. Seiden, S. Weiss, J. H. McCoy, W. Pesch, E. Bodenschatz, "Pattern forming system in the presence of different symmetry-breaking mechanisms", *Physical Review Letters* **101** (2008) 214503.
- C. Beta, G. Amselem, E. Bodenschatz, "A bistable mechanism for directional sensing", *New Journal of Physics* **10** (2008) 083015.
- U. Frisch, S. Kurien R. Pandit, W. Pauls, S. S. Ray, A. Wirth, J. Z. Zhu, "Hyperviscosity, Galerkin truncation, and bottlenecks in turbulence", *Physical Review Letters* **101** (2008) 144501.
- H. Xu, E. Bodenschatz, "Motion of inertial particles with size larger than Kolmogorov scale in turbulent flows", *Physica D* **237** (2008) 2095-2100.
- L. Biferale, E. Bodenschatz, M. Cencini, A. S. Lanotte, N. T. Ouellette, F. Toschi, H. Xu, "Lagrangian structure functions in turbulence: A quantitative comparison between experiment and direct numerical simulation", *Physics of Fluids* **20** (2008) 065103.
- A. Arneodo, R. Benzi, J. Berg, L. Biferale, E. Bodenschatz, A. Busse, E. Calzavarini, B. Castaing, M. Cencini, L. Chevillard, R. T. Fisher, R. Grauer, H. Homann, D. Lamb, A. S. Lanotte, E. Leveque, B. Luthi, J. Mann, N. Mordant, W. C. Müller, S. Ott, N. T. Ouellette, J. F. Pinton, S. B. Pope, S. G. Roux, F. Toschi, H. Xu, H; P. K. Yeung, "Universal intermittent properties of particle trajectories in highly turbulent flows", *Physical Review Letters* **100** (2008) 254504.
- C. Beta, T. Frohlich, H. U. Bodeker, E. Bodenschatz, "Chemotaxis in microfluidic devices - a study of flow effects", *Lab on a Chip* **8** (2008) 1087-1096.
- K. E. Daniels, O. Brausch, W. Pesch, E. Bodenschatz, "Competition and bistability of ordered undulations and undulation chaos in inclined layer convection", *Journal of Fluid Mechanics* **597** (2008) 261-282.
- H. Xu, N. T. Ouellette, E. Bodenschatz, "Evolution of geometric structures in intense turbulence", *New Journal of Physics* **10** (2008) 013012.
- H. Xu, "Tracking Lagrangian trajectories in position-velocity space", *Measurement Science and Technology* **19** (2008) 075105.
- E. M. Cherry, F. H. Fenton, "Visualization of spiral waves in simulated and experimental cardiac tissue", *New Journal of Physics* **10** (2008) 125016.
- P. Bittihn, G. Luther, E. Bodenschatz, V. Krinsky, U. Parlitz, S. Luther, "Far field pacing supersedes anti-tachycardia pacing in a generic model of excitable media", *New Journal of Physics* **10** (2008) 103012.
- N. F. Otani, A. Mo, S. Mannava, F. H. Fenton, E. M. Cherry, S. Luther, R. F. Gilmour, "Characterization of multiple spiral wave dynamics as a stochastic predator-prey system", *Physical Review E* **78** (2008) 021913.
- R. Schinke, "Theoretical study of the $D \rightarrow C$ emission spectrum of NO_2 ", *Chemical Physics* **129** (2008) 124303.
- R. Schinke, S. Y. Grebenshchikov, "On the photodissociation of ozone in the range of 5–9 eV", *Chemical Physics* **347** (2008) 279-287.
- R. Schinke, S. Y. Grebenshchikov, H. Zhu, "The photodissociation of NO_2 in the second absorption band: Ab initio and quantum dynamics calculations", *Chemical Physics* **346** (2008) 99-114.

Max Planck Research Group Droplets, Membranes and Interfaces

2010

J.J. Agresti, et al. "Ultra-high-throughput screening in drop-based microfluidics for directed evolution of peroxidases", PNAS, USA, **107** (2010) 4004 - 4009.

J.-C. Baret, et al. "Quantitative cell-based reporter gene assays using droplet-based microfluidics", Chemistry and Biology **17** (2010) 528-536.

L. Granieri, et al. "High-throughput screening of enzymes by retroviral display using droplet-based microfluidics", Chemistry and Biology **17** (2010) 229-235.

2009

J.-C. Baret, et al., "Kinetic aspects of emulsion stabilization by surfactants: a microfluidic analysis", Langmuir **25** (2009) 6088-6093.

J.-C. Baret, "A remote syringe for cells, beads and particles injection in microfluidic channels", Lab on a Chip – Chips and Tips (2009) http://www.rsc.org/Publishing/Journals/lc/Chips_and_Tips/remote_syringe.asp)

J.-C. Baret, et al., "Droplet and Emulsions: Very High Throughput in biology", Medecine Sciences **25** (2009) 627-632.

J.-C. Baret, et al., "Fluorescent-activated droplet sorting (FADS): Efficient microfluidic cell sorting based on enzymatic activities", Lab on a Chip **9** (2009)1850-1858.

L. Mazutis, et al., "Multi-step microfluidic droplet processing: kinetic analysis of an in vitro translated enzyme", Lab on a Chip **9** (2009) 2902 – 2908.

L. Mazutis, J.-C. Baret, and A.D. Griffiths, "A fast and efficient microfluidic system for highly selective one-to-one droplet fusion", Lab on a Chip **9** (2009) 2665-2672.

L. Mazutis, et al., "Droplet-based microfluidic systems for high-throughput single DNA molecule isothermal amplification and analysis", Analytical Chemistry **81** (2009) 4213-4221.

2008

J. Clausell-Tormos, et al., "Droplet-based microfluidic platforms for the encapsulation and screening

of mammalian cells and multicellular organisms", Chemistry and Biology **15** (2008) 427-437.

L. Frenz, et al., "Microfluidic production of droplet pairs", Langmuir **24**(2008) 12073-12076.

L. Frenz, et al., "Droplet-based microreactors for the synthesis of iron-oxide nanoparticles", Angewandte Chemie Int. Ed., **47** (2008) 6817-6820.

Max Planck Research Group Network Dynamics

2011

F. van Bussel, B. Kriener, and M. Timme "Inferring synaptic connectivity from spatio-temporal spike patterns *Frontiers*", *Comput. Neurosci.* **5** (2011) 3.

J. Nagler, A. Levina, and M. Timme (2011). Impact of single links in competitive percolation. *Nature Physics* **7** (2011) 265

S. Gorur Shandilya, and M. Timme "Inferring network topology from complex dynamics", *New J. Phys.* **13** (2011) 013004.

D. Witthaut, F. Trimborn, H. Hennig, G. Kordas, T. Geisel, and S. Wimberger "Beyond mean-field dynamics in open Bose-Hubbard chains", *Phys. Rev. A* (2011) (in press).

D. Witthaut, F. Trimborn, V. Kegel, and H. Korsch "Quantum dynamics of Bose-Einstein condensates in tilted and driven bichromatic optical lattices", *Phys. Rev. A* **83** (2011) 013609.

2010

F. van Bussel, C. Ehrlich, D. Fliegner, S. Stolzenberg, and M. Timme "Chromatic polynomials of random graphs", *J. Phys. A: Math. Theor.* **43** (2010) 175002

C. Grabow, S. Hill, S. Grosskinsky, and M. Timme "Do small worlds synchronize fastest?" *Europhys. Lett.* **90** (2010) 48002.

C. Kirst, and M. Timme "Partial Reset in Pulse-coupled Oscillators", *SIAM J. Appl. Math.* **70** (2010) 2119-2149.

C. Kolodziejcki, C. Tetzlaff, and F. Woergoetter "Closed-form treatment of the interactions between neuronal activity and spike-timing-dependent plasticity in networks of linear neurons", *Frontiers in Computational Neuroscience* **4** (2010) 134.

T. Kulvicius, C. Kolodziejcki, M. Tamosiunaite, B. Porr, and F. Woergoetter "Behavioral analysis of differential Hebbian learning in closed-loop systems", *Biological Cybernetics* **103** (2010) 255-271.

R.M. Memmesheimer, and M. Timme "Stable and unstable periodic orbits in complex networks of spiking neurons with delays", *Discr. Cont. Dyn. Syst.* **28** (2010) 1555 - 1588.

R.M. Memmesheimer M. Timme "Synchrony and Precise Timing in Complex Neural Networks", *Handbook on Biological Networks* **279** (2010)

C. Olavarria, J. Acevedo, and H. Vester "Southernmost Distribution of Common Bottlenose Dolphins (*Tursiops truncatus*) in the Eastern South Pacific", *Aquatic Mammals* **36** (2010) 288.

S. Steingrube, M. Timme, F. Woergoetter, and P. Manoonpong "Self-organized adaptation of a simple neural circuit enables complex robot behaviour", *Nature Physics* **6** (2010) 224-230.

K. Rapadius, C. Elsen, D. Witthaut, S. Wimberger, and H. Korsch "Nonlinear resonant tunneling of Bose-Einstein condensates in tilted optical lattices", *Phys. Rev. A* **82** (2010) 063601 .

F. Trimborn, D. Witthaut, V. Kegel, and H.J. Korsch "Nonlinear Landau-Zener tunneling in quantum phase space", *New J. Phys.* **12** (2010) 053010.

H. Vester, and M. Timme "Call for cooperation to contain damage by Chile's salmon farms", *Nature* **465** (2010) 869.

D. Witthaut, M. D. Lukin, and A.S. Sørensen, "Photon sorters and QND Detectors using single photon emitters", *Phys. Rev. A* (under review), arXiv:1007.3273

D. Witthaut "Quantum walks and quantum simulations with Bloch-oscillating spinor atoms", *Phys. Rev. A* **82** (2010) 033602.

D. Witthaut, and A.S. Sørensen "Photon scattering by a three-level emitter in a one-dimensional waveguide", *New J. Phys.* **12** (2010) 043052.

2009

C. Bick, and M. Rabinovich "Dynamical Origin of the Effective Storage Capacity in the Brain's Working Memory", *Phys. Rev. Lett.* **103** (2009) 218101.

S. Jahnke, R.M. Memmesheimer, and M. Timme "How chaotic is the balanced State?" *Frontiers Comput. Neurosci.* **3** (2009) 13.

C. Kirst, and M. Timme "How precise is the timing of action potentials?" *Frontiers in Neurosci.* **3** (2009) 2.

C. Kirst, T. Geisel, and M. Timme "Sequential Desynchronization in Networks of Spiking Neurons with Partial Reset", *Phys. Rev. Lett.* **102** (2009) 068101.

J. Klingmayr, C. Bettstetter, and M. Timme "Globaly Stable Synchronization by Inhibitory Pulse Coupling". *Proc. IEEE Intern. Symp. Appl. Sci. in Biomedical and Communication Technologies (ISABEL)*, Bratislava, Slovak Republic (2009).

F.S. Neves, and M. Timme "Controlled perturbation-induced switching in pulse-coupled oscillator networks", *J. Phys. A: Math. Theor.* **42** (2009) 345103.

M. Timme, F. van Bussel, D. Fliegner, and S. Stolzenberg "Counting Complex Disordered States by Efficient Pattern Matching: Chromatic Polynomials and Potts Partition Functions", *New J. Phys.* **11** (2009) 023001.

B. Kriener, M. Helias, A. Aertsen, and S. Rotter "Correlations in spiking neuronal networks with distance dependent connections", *Journal of Computational Neuroscience* **27** (2009) 177-200.

C. Kolodziejcki, B. Porr, and F. Woergoetter "On the asymptotic equivalence between differential Hebbian and temporal difference learning", *Neural Computation* **21** (2009) 1173-1202.

T. Kulvicius, C. Kolodziejcki, M.T. Porr, and F. Woergoetter (2009) On the analysis of differential hebbian learning in closed-loop behavioral systems. In: *Frontiers in Computational Neuroscience. Conference Abstract: Bernstein Conference on Computational Neuroscience. Frontiers.*

D. Witthaut, K. Rapedius, and H.J. Korsch "The nonlinear Schrödinger equation for the delta-comb potential: quasi-classical chaos and bifurcations of periodic stationary solutions", *J. Nonlin. Math. Phys.* **16** (2009) 207.

D. Witthaut, F. Trimborn, and S. Wimberger "Dissipation-induced coherence and stochastic resonance of an open two-mode Bose-Einstein condensate. *Phys. Rev. A* **79** (2009) 033621.

2008

S. Jahnke, R.M. Memmesheimer, and M. Timme "Stable Irregular Dynamics in Complex Neural Networks", *Phys. Rev. Lett.* **100** (2008) 048102.

C. Kirst, and M. Timme "From networks of unstable attractors to heteroclinic switching", *Phys. Rev. E (Rapid Communication)* **78** (2008) 065201.

D. Kozen, and M. Timme (2008). *Indefinite Summation and the Kronecker Delta. Technical Report, Cornell University.*

B. Kriener, T. Tetzlaff, A. Aertsen, M. Diesmann, and S. Rotter "Correlations and Population Dynamics in Cortical Networks. *Neural Computation* **20** (2008) 2185-2226.

A.M. Thompson, B. Porr, C. Kolodziejcki, and F. Woergoetter (2008) *Second Order Conditioning in the*

Sub-cortical Nuclei of the Limbic System. In: *SAB ,08: Proceedings of the 10th international conference on Simulation of Adaptive Behavior.* Springer-Verlag, Berlin, Heidelberg, pages 189–198.

M. Timme, and F. Wolf "The simplest problem in the collective dynamics of neural networks: is synchrony stable?" *Nonlinearity* **21** (2008) 1579-1599.



Max Planck Research Group Biological Physics and Evolutionary Dynamics

2011

O. Hallatschek. Noise driven evolutionary waves. *PLoS Comput Biol* **7** (2011) e1002005, 2011.

O. Hallatschek. The noisy edge of traveling waves. *Proc. Natl. Acad. Sci.*, **108** (2011) 1783-1787. see also commentary article D.S. Fisher. Leading the dog of selection by its mutational nose. *Proc. Nat. Acad. Sci.*, **108** (2011) 2633.

2010

O. Hallatschek and D. R. Nelson. Life at the front of an expanding population. *Evolution* **64** (2010) 193–206.

K.S. Korolev, M. Avlund, O. Hallatschek, and D. R. Nelson. Genetic demixing and evolution in linear stepping stone models. *Rev. Mod. Phys.* **82** (2010) 1691–1718. featured in Mark Buchanan. *Nature Physics* **6** (2010) 555.

2009

O. Hallatschek and K. S. Korolev. Fisher waves in the strong noise limit. *Phys. Rev. Lett* **103** (2009) 108103.

O. Hallatschek and D. R. Nelson. Population Genetics and Range Expansions. *Physics Today* **62** (2009) 42-47.

B. Obermayer, W. Möbius, O. Hallatschek, E. Frey and K. Kroy. A freely relaxing polymer remembers how it was straightened. *Phys. Rev. E.*, **79** (2009) 021804-021817.

2008

J. Glaser, O. Hallatschek and K. Kroy. Dynamic structure factor of a stiff polymer in a glassy solution. *Eur. Phys. J. E.*, **26** (2008) 123-136.

O. Hallatschek and D. R. Nelson. Gene surfing in expanding populations. *Theor. Pop. Biol.*, **37** (2008) 158-170.

Max Planck Research Group Onset of Turbulence and Complexity

2011

K. Avila, D. Moxey, A. de Lozar, M. Avila, D. Berkley and B. Hof. the onset of turbulence in pipe flow. *Science* accepted

D. Samanta, A. de Lozar and B. Hof. Experimental investigation of laminar turbulent intermittency in pipe flow. *J. Fluid Mech.*, accepted.

2010

M. Avila, A. P. Willis and B. Hof. On the transient nature of localized pipe flow turbulence. *J. Fluid Mech.*, **646** (2010) 127–136.

B. Hof, A. de Lozar, M. Avila, X. Tu and T. M. Schneider. Eliminating turbulence in spatially intermittent flows. *Science*, **327** (2010) 1491–1494.

M. Kinzel, M. Wolf, M. Holzner, B. Lüthi, C. Tropea and W. Kinzelbach, Simultaneous two-scale 3D-PTV measurements in turbulence under the influence of system rotation, *Exp. Fluids*, published online: DOI 10.1007/s00348-010-1026-6, (2010).

X.Z. Kong, M. Holzner, Stauffer F. and W. Kinzelbach, Time-resolved 3D visualization of air injection in a liquid-saturated refractive-index-matched porous medium, *Exp. Fluids*, published online: DOI 10.1007/s00348-010-1018-6, (2010)

2009

J. M. Lopez, F. Marques, A. Rubio and M. Avila. Crossflow instability of finite Bödewadt flows: transients and spiral waves. *Phys. Fluids*, **21** (2009) 114107.

A. de Lozar and B. Hof, An experimental study of the decay of turbulent puffs in pipe flow *Phil. Trans. Roy. Soc. Lond. A* **367**, 589, (2009)

A. de Lozar, A. Heap, F. Box, A.L. Hazel, A. Juel, Tube geometry can force switchlike transitions in the behavior of propagating bubbles, *Phys. Fluids*, **21**, 102702, (2009).

A. Meseguer, F. Mellibovsky, M. Avila and F. Marques. Instability mechanisms and transition scenarios of spiral turbulence in Taylor–Couette flow. *Phys. Rev. E*, **80**:046315, (2009).

A. Meseguer, F. Mellibovsky, M. Avila and F. Marques. New families of subcritical spirals in highly counter-rotating Taylor–Couette flow. *Phys. Rev. E*, **79**:036309, (2009).

2008

B. Hof, A. de Lozar, DJ Kuik and J. Westerweel, Repeller or Attractor? Selecting the Dynamical Model for the Onset of Turbulence in Pipe Flow, *Phys. Rev. Lett.* **101** (2008) 214501.

A. de Lozar, A. Juel. A.L. Hazel, The steady propagation of an air finger in a rectangular tube, *J. Fluid Mech.*, **614** (2008) 173-195.

Max Planck Research Group Biomedical Physics

2011

S. Luther, F. H. Fenton, B. G. Kornreich, A. Squires, P. Bittihn, D. Hornung, M. Zabel, J. Flanders, A. Gladuli, L. Campoy, E. M. Cherry, G. Luther, G. Hasenfuss, V. I. Krinsky, A. Pumir, R. F. Gilmour, E. Bodenschatz, "Low-energy control of electrical turbulence in the heart", *Nature* (accepted, 2011)

A. Többens, R. Mettin, U. Parlitz, "Dynamics of a driven oscillator carrying a freely sliding mass", in: *International Journal of Bifurcation and Chaos* (to appear).

U. Parlitz, A. Schlemmer, S. Luther, "Synchronization patterns in transient spiral wave dynamics", *Phys. Rev. E* **83**, 057201 (2011).

U. Parlitz, S. Berg, S. Luther, A. Schirdewan, J. Kurths, N. Wessel, "Classifying cardiac biosignals using ordinal pattern statistics and symbolic dynamics", *Comput. Biol. Med.* 2011 Apr 19. [Epub ahead of print]

T. H. van den Berg, W. D. Wormgoor, S. Luther, D. Lohse, "Phase-sensitive constant temperature anemometry", *Macromol. Mater. Eng.* **296** (2011) 230-237.

S. Petitprez, A. F. Zmoos, J. Ogrodnik, E. Balse, N. Raad, S. El-Haou, M. Albesa, P. Bittihn, S. Luther, S. E. Lehnart, S. N. Hatem, A. Coulombe, H. Abriel, "SAP97 and dystrophin macromolecular complexes determine two pools of cardiac sodium channels Nav1.5 in cardiomyocytes", *Circulation Research* **108** (2011) 294-304.

2010

N. F. Otani, S. Luther, R. Singh, R. F. Gilmour, "Trans-mural ultrasound-based visualization of patterns of action potential wave propagation in cardiac tissue", *Ann. Biomed. Eng.* **38** (2010) 3112-23. Epub 2010 May 25.

P. Bittihn, A. Squires, G. Luther, E. Bodenschatz, V. Krinsky, U. Parlitz, S. Luther, "Phase-resolved analysis of the susceptibility of pinned spiral waves to far-field pacing in a two-dimensional model of excitable media", *Philosophical transactions of the Royal Society A* **368** (2010) 2221-2236.

A. Pumir, A. Sinha, S. Sridhar, M. Argentina, M. Hörning, S. Filippi, C. Cherubini, S. Luther, V. Krinsky, "Wave-train-induced termination of weakly anchored vortices in excitable media", *Phys. Rev. E* **81** (2010) 010901(R).

2009

F. H. Fenton¹), S. Luther²), E. M. Cherry, N. F. Otani, V. Krinsky, A. Pumir, E. Bodenschatz, R. F. Gilmour, "Termination of atrial fibrillation using pulsed low-energy far-field stimulation", *Circulation* **120** (2009) 467-476. ¹) Authors contributed equally.

2008

P. Bittihn, G. Luther, E. Bodenschatz, V. Krinsky, U. Parlitz, S. Luther, "Far field pacing supersedes anti-tachycardia pacing in a generic model of excitable media", *New Journal of Physics* **10** (2008) 103012.

N. F. Otani, A. Mo, S. Mannava, F. H. Fenton, E. M. Cherry, S. Luther, R. F. Gilmour, "Characterization of multiple spiral wave dynamics as a stochastic predator-prey system", *Physical Review E* **78** (2008) 021913.

Max Planck Fellow Group Polymers, Complex Fluids and Disordered System

2010

T. Kranz, M. Sperl, and A. Zippelius "Glass transition for driven granular fluids", *Phys. Rev. Lett.* **104** (2010) 225701.

A. von der Heydt, M. Müller, and A. Zippelius "Sequence fractionation in symmetric random block copolymers", *Macromolecules* **43** (2010) 3161.

S. Ulrich, A. Zippelius, and P. Benetatos "Random networks of cross-linked directed polymers", *Phys. Rev. E* **81** (2010) 021802.

2009

M. K. Jaiswal, W. D. Zech, M. Goos, C. Leutbecher, A. Ferri, A. Zippelius, M. T. Carri, R. Nau, and B. U. Keller "Impairment of mitochondrial calcium handling in a mtSOD1 cell culture model of notoneuron disease", *BMC Neuroscience* **10** (2009) 1-16.

W. T. Kranz, N. V. Brilliantov, T. Pöschel, and A. Zippelius "Correlation of spin and velocity in the homogeneous cooling state of a granular gas of rough particles", *Eur. Phys. J. Special Topics* **179** (2009) 91 – 111.

H. Ücker, W. T. Kranz, T. Aspelmer, and A. Zippelius "Partitioning of energy in highly polydisperse granular gases", *Phys. Rev. E* **80** (2009) 041303.

S. Ulrich, T. Aspelmeier, K. Röller, A. Fingerle, S. Herminghaus, and A. Zippelius "Dilute wet granulates: Nonequilibrium dynamics and structure formation", *Phys. Rev. E* **80** (2009) 031306.

X. Mao, X. Xing, P. M. Goldbart, and A. Zippelius "Soft random solid and their heterogeneous elasticity", *Phys. Rev. E* **80** (2009) 031140.

A. Fiege, T. Aspelmeier, and A. Zippelius "Long-time tails and cage effect in driven granular fluids", *Phys. Rev. Lett.* **102** (2009).

S. Ulrich, T. Aspelmeier, K. Roeller, A. Fingerle, S. Herminghaus, and A. Zippelius "Cooling and aggregation in wet granulates", *Phys. Rev. Lett.* **102** (2009).

2008

S. Ulrich, A. Glisovic, T. Salditt and A. Zippelius "Diffraction from the β -sheet crystallites in spider silk", *Eur. Phys. J. E* **27** (2008).

X. Xing, S. Pfahl, S. Mukhopadhyay, P. M. Goldbart and A. Zippelius "Nematic elastomers: From a microscopic model to macroscopic elasticity theory", *Phys. Rev. E* **77** (2008) 051802.

Emeritus Group Molecular Interactions

2010

G. Benedek, M. Bernasconi, V. Chis, E. Chulkov, P. M. Echenique, B. Hellsing and J. P. Toennies: Theory of Surface Phonons at Metal Surfaces: Recent Advances, *J. Phys. Cond. Mat.*, **22** (2010) 084020-1 -20-17.

G. Benedek, P. M. Echenique, J. P. Toennies and F. Traeger: Atoms Riding Rayleigh Waves, *J. Phys. Cond. Mat.*, **22** (2010) 304016-1 -16-11. Corrigendum: *J. Phys. Cond. Mat.*, **22** (2010) 359801-1 -01-1.

G. Benedek, P. Nieto and J. P. Toennies: The Geysier Effect in the Expansion of Solid Helium into Vacuum, *EPJ B*, **76** (2010) 237-249.

S. Grebenev, B. G. Sartakov, J. P. Toennies and A. F. Vilesov: Spectroscopic Investigation of OCS ($p\text{-H}_2$)_n ($n=1-16$) Complexes Inside Helium Droplets: Evidence for Superfluid Behavior, *J. Chem. Phys.*, **132** (2010) 064501-1 -01-19.

V. Lebedev, P. Moroshkin, J. P. Toennies and A. Weis: Spectroscopy of the Copper Dimer in Normal Fluid, Superfluid, and Solid ^4He , *J. Chem. Phys.*, **133** (2010) 154508-1 -08-8.

M. B. Sevryuk, J. P. Toennies and D. M. Ceperley: Why Are Para-Hydrogen Clusters Superfluid? A Quantum Theorem of Corresponding States Study, *J. Chem. Phys.*, **133** (2010) 064505-1 -05-13.

K. T. Tang and J. P. Toennies: Johannes Diderik van der Waals: A Pioneer in the Molecular Sciences and Nobel Prize Winner in 1910, *Angew. Chem. Int. Ed.*, **49** (2010) 9574-79.

K. T. Tang and J. P. Toennies: Johannes Diderik van der Waals: Pionier der Moleklwissenschaften und Nobelpreistrger von 1910, *Angew. Chem.*, **122** (2010) 9768-74.

S. Warnecke, M. B. Sevryuk, D. M. Ceperley, J. P. Toennies, R. Guardiola and J. Navarro: The Structure of Para-Hydrogen Clusters, *EPJ D*, **56** (2010) 353-58.

2009

V. M. Akimov, L. I. Kolesnikova, L. Y. Rusin, M. B. Sevryuk and J. P. Toennies: Structure of Small Hydrogen Nanoclusters Containing Ortho-Molecules, *Russ. J. Phys. Chem. B*, **3** (2009) 743-52.

V. M. Akimov, G. Witte, L. I. Kolesnikova, L. Y. Rusin and J. P. Toennies: An Apparatus for Obtaining Microwave Discharge under Pressures up to Several Atmospheres, *Pribory I Tekhnika Experimenta (Russ. J. Exp. Instr. and Techn.)*, **3** (2009) 91-97 (in Russian).

V. M. Akimov, G. Witte, L. I. Kolesnikova, L. Y. Rusin and J. P. Toennies: A Microwave Discharge Source Operating at Pressures of Several Atmospheres, *Instrum. Exp. Tech.*, **52**, (2009) 394-99.

V. M. Azriel, V. M. Akimov, L. I. Kolesnikova, L. Y. Rusin, M. B. Sevryuk and J. P. Toennies: On the Maximum in the Differential Cross Sections of the $F + H_2$ Reaction in the Region of Small Scattering Angles, *Russ. J. Phys. Chem. B*, **3** (2009) 857-63.

V. M. Azriel, V. M. Akimov, L. I. Kolesnikova, L. Y. Rusin, M. B. Sevryuk and J. P. Toennies: Structure of the Maximum of the Differential Cross Sections of the $F + H_2$ Reaction in the Region of Small Scattering Angles, *Khimicheskaya Fizika (Russ. J. 'Chem. Phys.')*, **28**, (2009) 3-9 (in Russian).

J. Braun, P. Ruggerone, G. Zhang, J. P. Toennies and G. Benedek: Surface Phonon Dispersion Curves of Thin Pb Films on Cu(111), *Phys. Rev. B*, **79**, (2009) 205423-1 -23-13.

V. Chis, B. Hellsing, G. Benedek, M. Bernasconi, E. V. Chulkov and J. P. Toennies: Large Surface Charge Density Oscillations Induced by Subsurface Phonon Resonances (Correction of Vol 101, 206102, 2008), *Phys. Rev. Lett.*, **103** (2009) 069902-1 -02-4.

E. L. Knuth and J. P. Toennies: Condensed Phase Mass Fraction in a Supersonic Molecular Beam Containing Clusters, Conference Proceedings of 26th International Symposium on Rarefied Gas Dynamics, Kyoto, Japan, AIP Conf. Proc. **1084**, ed. T. Abe, p. 583-87; AIP, Melville, NY, USA (2009).

O. Kornilov and J. R. Toennies: The Determination of the Mean Sizes of Large He Droplets by Electron Impact Induced Attenuation, **280** (2009) 209-12.

N. Poertner, J. P. Toennies, A. F. Vilesov, G. Benedek and V. Hizhnyakov: Anomalous Sharp Phonon Excitations in ^3He Droplets, *EPL*, **88** (2009) 26007-1 -07-6.

2008

G. Benedek and J. P. Toennies: Probing the Dispersion of Surface Phonons by Light Scattering, in *Epi-optics (9)* (World Scientific Press, Singapore, 2008); ed. A. Cricienti; p. 162-80.

V. Chis, B. Hellsing, G. Benedek, M. Bernasconi, E. V. Chulkov and J. P. Toennies: Large Surface Charge Density Oscillations Induced by Subsurface Phonon Resonances, *Phys. Rev. Lett.*, **101** (2008) 206102-1-02-4.

S. Grebenev, B. G. Sartakov, J. P. Toennies and A. F. Vilesov: Infrared Q-branch Anomalies on Cooling Small OCS (pH_2)_N Clusters from 0.38K to 0.15K, *EPL*, **83** (2008) 66008-1-08-6.

O. Kornilov and J. P. Toennies: Electron Impact Ionization of Size Selected Hydrogen Clusters (H_2)_N: Ion Fragment and Neutral Size Distributions, *J. Chem. Phys.*, **128** (2008) 194306-1-06-12.

A. Slenczka and J. P. Toennies: Chemical Dynamics inside Superfluid Helium Droplets at 0.37 K, in *Low Temperatures and Cold Molecules* (World Scientific Press, Singapore, 2008); ed. I. W. M. Smith; p. 345-92.

K. T. Tang and J. P. Toennies: The Dynamical Polarizability and van der Waals Dimer Potential of Mercury, *Mol. Phys.*, **10** (2008) 1645-53.

Services

THE SERVICE GROUPS of the institute are headed by the delegate manager, relieving the board of directors and the managing director from a range of tasks. The delegate manager (Mr. A. Bock) and his team support the scientific departments and research groups, ensuring that all staff and guests enjoy an excellent research environment. In addition to financial affairs, human resources, grant administration, and coordination with the central administration of the MPG, the institute management is in charge of the information technology services, facility management including the machine shop, and all outreach activities. Further tasks have been arising for all services due to the construction activities for the new site at the 'Fassberg' (completed early 2011), as well as general continual support for the two sites of the institute ('Bunsenstrasse' and 'Fassberg').

Workshops – Design and Engineering

Based on the requests from the scientific departments, the mechanical design group develops and engineers solutions for scientific apparatuses. The group uses the most advanced software tools that allow the design of complex parts in three dimensions. This includes the simulation of the components as well as their three-dimensional assembly. Once the technical design has been finished, technical drawings are generated or the design is directly entered into the CAD engines that generate instruction sets understood by the CNC-machines. The workshop is equipped with conventional as well as



Precision Mechanics Interns

computer controlled lathes, milling and EDM (electrical discharge) machines. The associated metal shop manufactures frames and other large metal parts, and has state-of-the-art welding equipment for handling steel and aluminum. The research workshop not only trains apprentices to become precision mechanics, but every scientist can acquire practical know-how here. In collaboration with the mechanical workshop the design group also certifies the conformity of the apparatuses with the European and German laws. New parts are manufactured in the respective workshop. The machine shop also assembles components and apparatuses. It is also indispensable for the maintenance and repair of existing machines and apparatuses.

Central IT Services

All departments and research groups of the institute make use of HPC clusters for demanding computations, simulations and data analysis. In order to provide flexible configurations and a high level of availability a considerable part of the corresponding cluster and storage hardware is actually located at the institute in several server rooms. It is administrated and maintained by the institute's HPC group, which is also responsible for the HPC cooling facilities, networks, provisioning and monitoring systems. While each department and research group has direct access to its own clusters tailored to their specific applications there is a common concept with a homogenous hard- and software setup. Consequently similar resources can easily be shared among the groups.

The institute's compute clusters are still growing rapidly. At the moment they consist of almost 600 servers and provide a total of more than 5000 CPU cores, 20TB RAM and 900TB disk space. Because of a power consumption of more than 300kW efficient cooling systems are essential. The institute was among the first to construct water-cooled server racks and use turbine-based condensers in the cooling units



Water-cooled server racks with an highly available file server and two compute clusters

Outreach, media relations, and internal communication

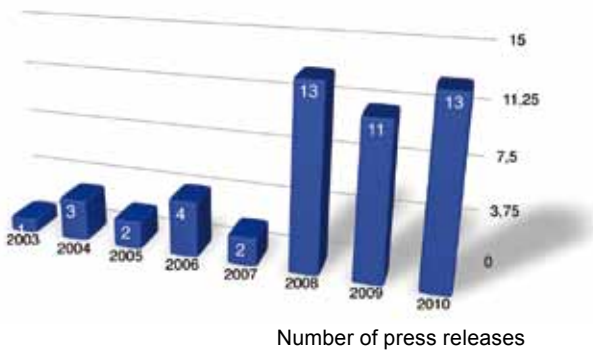
At the Max Planck Institute for Dynamics and Self-Organization public outreach and media relations are recognized as an important part of the institute's work. Since April 2008 a press office has been established at the institute that coordinates all activities related to outreach and media relations. Different target groups (from specialized journalists to students) are addressed by different means: participation in special events and exhibitions, press releases, a regular series in a local newspaper, and public lectures.

In addition, the internal communication at MPIDS has been promoted by a series of scientific lectures for the non-scientific employees and a newsletter.

Press releases

The number of press releases informing the local, national and international media about scientific results and events has been increased considerably since 2008.

In 2009 and 2010 press releases dealing with scientific topics from all departments and all Max Planck Research Groups have been issued. In most cases, these press releases were issued in both German and English.



DATE	GERMAN TITLE	ENGLISH TITLE
Feb. 6th, 2009	Kurzichtig durch ein Netz von Farben	A new kind of counting
May 18th, 2009	Startschuss für den Windkanal	
May 22nd, 2009	Drehbuch für die Gehirnentwicklung	A screenplay for brain development
June 5th, 2009	Die Zukunft im Zug	The future in a train
June 25th, 2009	Wasser im Innern eines Saturnmondes	Water within a Saturn moon
June 30th, 2009	Von Gehirnzellen und Geldscheinen	
Aug. 6th, 2009	Lawinen im Gehirn	Avalanches in the brain
Aug. 28th, 2009	Weiche Materie in hartem Gestein	Soft matter in hard rock
Aug. 31st, 2009	Warum die linke Gehirnhälfte zur rechten passt	Why the left brain hemisphere matches the right
Sept. 14th, 2009	Den evolutionären Zufall im Griff	Getting a handle on evolutionary coincidence
Dec. 1st, 2009	Wirbel um den Wärmetausch	Turbulence around heat transport
Jan. 17th, 2010	Organisiertes Chaos macht Robotern Beine	Organized chaos gets robots going
Feb. 5th, 2010	Nervenzellen achten auf ihre Nachbarn	Nerve cells pay attention to their neighbors
Mar. 7th, 2010	Strahlentherapie: Gelöste Elektronen gefährlicher als freie Radikale?	
Mar. 19th, 2010	Turbulenzen im Griff	Turbulences under control
May 3rd, 2010	Neues „Herzforschungszentrum Göttingen“ gegründet	New „Heart Research Center Göttingen“ founded
May 19th, 2010	Mit voller Fahrt voraus	With full speed ahead
June 17th, 2010	Umweltskandal in Chile	Environmental scandal in Chile
June 21st, 2010	Wachsendes Gehirn ist besonders flexible	Growing brain is particularly flexible
Jul. 12th, 2010	Katastrophen zählen	Counting catastrophes
Aug. 6th, 2010	Bernstein Zentrum Göttingen wird erneut gefördert	
Nov. 4th, 2010	Selbstorganisation statt Umwelt und Genen	Self-Organization instead of environment and genes
Dec. 9th, 2010	Göttinger Research Campus: Forschungseinrichtungen rücken näher zusammen	
Dec. 29th, 2010	Wie schnell ist Evolution?	How fast is evolution?

Many of these press releases led to articles in notable national and international newspapers and internet journals. Highlights include:

NEWSPAPER/DATE	TITLE OF THE ARTICLE	BASED ON PRESS RELEASE
Spiegel Online/Feb. 26th, 2009	Rätsel der 3D-Sudokus gelöst	Kurzichtig durch ein Netz von Farben
Frankfurter Allgemeine Zeitung/March 4th, 2009	Die Kunst des komplexen Zählens	Kurzichtig durch ein Netz von Farben
Bild Online/June 24th, 2009	Forscher: Saturnmond hat unterirdischen Ozean	Wasser im Innern eines Saturnmondes
Die Zeit/Jan. 21st, 2010	Die Kraft der zwei Zellen	Organisiertes Chaos macht Robotern Beine
The New York Times/March 22nd, 2010	Taming Turbulences inside Pipelines	Turbulences under control
Leipziger Volkszeitung/Jul. 9th, 2010	Bedrohliche Lachsfarmen	Umweltskandal in Chile
Dag Ugvaerhandelen/Aug. 13th, 2010	Forårsaker en miljøkatastrofe	Umweltskandal in Chile

In addition, several TV and radio stations reported about the activities at MPIDS. Examples are:

DATE	TITLE	PROGRAM/STATION
July 15 th, 2008	Aus Sand gebaut	Nano/3Sat
Jan. 5th, 2009	Sieg der Ordnung	Forschung Aktuell/Deutschland Radio
Aug. 13th, 2009	Wesen im All	Wissen Xakt/RTL regional
Aug. 27th, 2009	Der Turbulenz-Windkanal	DAS! forscht/NDR Fernsehen
April 18th, 2010	Von Kakerlaken lernen – die kleinen Insekten als Helfer der Wissenschaft	Planetopia/Sat1
June 20th, 2010	Skulpturen aus Sand – Was hält die Bauwerke zusammen?	Planetopia/Sat1
June 26th, 2010	Thema: Umweltskandal in Chile	Deutsche Welle Radio
Aug 6th, 2010	Statik und Dynamik von Sandburgen	Drehscheibe Deutschland/ZDF
Nov. 5th, 2010	Thema: Selbstorganisation statt Umwelt und Genen	Radio ffn

„Frag' den Wissenschaftler“**(engl.: „Ask the Scientist“)**

The series „Frag' den Wissenschaftler“ (engl.: „Ask the Scientist“) was continued successfully. In this series, that appears every other Sunday in the Göttingen newspaper ExtraTip, a scientist from Göttingen answers questions asked by readers. These questions cover all scientific areas (biology, physics, history, economics, medicine, etc.), but often deal with topics related to the institute's current research. The series therefore offers an excellent opportunity to communicate MPIDS research topics to a wide audience and foster an interest in science. All in all, in 2009 and 2010 51 questions were answered.

They included:

How do large-scale electrical power outages occur? Can computers be creative? How does a touch-screen work? How do patterns in the desert sand originate? Is it true, that humans only use ten percent of their brain? How do left- and right-handedness develop?

Special events**Inauguration of the Göttingen High Turbulence Windtunnel**

On May 8th, 2009 the institute's new Turbulence Windtunnel was inaugurated. The inauguration was accompanied by an international scientific conference and an official ceremony for the participants of the conference and invited guests. The inauguration was covered by the local and national media.

Science Festival: Stadt der jungen Forscher

On June 12th, 2009 the city of Göttingen organized a science festival in the downtown area called „Stadt der jungen Forscher“ (engl.: City of young researchers). The MPIDS presented itself with an information stand dealing with sand and granular matter. This stand featured posters describing the research at MPIDS, a short movie on granular matter, an exhibit providing insights into the extraction of crude oil from

the porous layers of rock in oil reservoirs and a sand box, where the young researchers were able to try out what they had just learned.

Science Train 2009

In 2009 the Max Planck Society organized a science exhibition within a train. Throughout the year, this train travelled to 62 cities in Germany and reached approximately 260 000 people. Apart from many other exhibits the train featured the movie „Around the world in 80 days“ describing the research performed at MPIDS on the spreading of infectious diseases.

MS Wissenschaft 2010

In 2010 the MPIDS contributed to the MS Wissenschaft, a science exhibition within a boat that was devoted to the topic “energy”. Throughout the year the boat traveled to 34 cities within Germany. The exhibit provided by MPIDS was a model of an oil reservoir that explained the role of porous layers of rock in the extraction of crude oil.

Future Day

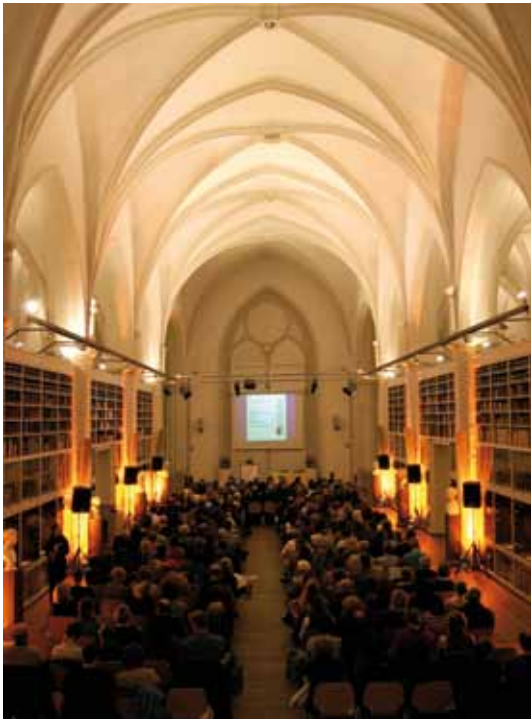
On April 23rd 2009 and April 22nd 2010 the MPIDS hosted the „Future Day“. On this day young girls and boys throughout Germany explore different career options in a hands-on manner.

In 2009 – as in the years before – the day was organized by the head of the institute management and was open to approximately 30 girls and boys. The children were given the opportunity to try out different techniques in the institute’s workshops and perform a few simple experiments.

In 2010 the concept of the Future Day at MPIDS was changed: Only girls were invited to join, the activities were organized by the institute’s female scientists and featured mainly scientific experiments. This new concept was developed in order to create an environment that encourages girls to show an interest in natural sciences and to bring them face to face with role models.



Future Day



Göttinger Literaturherbst

Göttinger Literaturherbst

As in the years before, the MPIDS took part in the annual literary festival in Göttingen the „Literaturherbst“. This festival features a scientific lecture series, where internationally renowned scientists present their latest books in the unique atmosphere of the historic Paulinerkirche in Göttingen. These lectures are introduced and chaired by scientists from the Max Planck Institutes thus allowing for a vivid and entertaining exchange of ideas. In 2009 the scientific lecture series was visited by 1275 guests, in 2010 by 1262. The series therefore offers an unique opportunity of communicating scientific topics to a wide audience.

How to get to the Max Planck Institute for Dynamics and Self-Organization

Fassberg site (new building)



Am Fassberg 17
D-37077 Göttingen

Departments:	Nonlinear Dynamics (Prof. Geisel) Dynamics of Complex Fluids (Prof. Herminghaus) Fluid Dynamics, Pattern Formation and Nanobiocomplexity (Prof. Bodenschatz)
Research Groups:	Droplets, Membranes and Interfaces (Dr. Baret) Nonlinear Dynamics and Cardiac Arrhythmias (Dr. Luther)
Services:	Institute Management, Administration, Facility Management, Electronic and Mechanic Workshop, IT-Services, Library, Outreach Office, Stock Rooms, Lecture Hall, Experimental Hall, Clean Room and Cell Biology Laboratories

By plane

From Frankfurt am Main Airport (FRA): Use one of the railway stations at the airport. Trains to Göttingen (direct or via Frankfurt main station) leave twice an hour during daytime (travel time: 2 hours).

From Hannover Airport (HAJ): Take the suburban railway (S-Bahn) to the Central Station (»Hannover Hauptbahnhof«). From here direct ICE trains to Göttingen depart every 1/2 hour.

By train

Göttingen Station is served by the following ICE routes: Hamburg-Göttingen-Munich, Hamburg-Göttingen-Frankfurt am Main, and Berlin-Göttingen-Frankfurt.

From Göttingen railway station:

On arrival at Göttingen station take a taxi (15 minutes) or the bus (35 minutes). At platform A take the bus No. 8 (direction: »Geismar-Süd«) or No 13 (direction: »Weende-Ost/Papenberg«). At the second stop »Groner Straße« change to bus No. 5 (direction »Nikolausberg« and get off at the »Faßberg« stop, which is directly in front of the entrance of the Max Planck Campus (MPI SDS and MPI for Biophysical Chemistry). Ask at the gate to get directions.

By car

Leave the freeway A7 (Hanover-Kassel) at the exit »Göttingen-Nord«, which is the northern of two exits. Follow the direction for Braunlage (B 27). Leave town – after about 1.5 km at the traffic light (Chinese restaurant on your right) turn left and follow the sign »Nikolausberg«. The third junction on the left is the entrance to the Max Planck Campus (MPI SDS and MPI for Biophysical Chemistry). Ask at the gate to get directions.

Bunsenstraße site (old building)



Bunsenstraße 10
D-37073 Göttingen

Departments:	Dynamics of Complex Fluids (Prof. Herminghaus) Fluid Dynamics, Pattern Formation and Nanobiocomplexity (Prof. Bodenschatz)
Research Groups:	Biophysics and Evolutionary Dynamics (Dr. Hallatschek) Network Dynamics (Dr. Timme) Onset of Turbulence and Complexity (Dr. Hof)
Max Planck Fellow Group:	Polymers, Complex Fluids and Disordered Systems (Prof. Zippelius)
Emeritus Group:	Molecular Interactions (Prof. Toennies)
Services:	Guest Houses

By plane

From Frankfurt am Main Airport (FRA): Use one of the railway stations at the airport. Trains to Göttingen (direct or via Frankfurt main station) leave twice an hour during daytime (travel time: 2 hours).
From Hannover Airport (HAJ): Take the suburban railway (S-Bahn) to the Central Station (»Hannover Hauptbahnhof«). From here direct ICE trains to Göttingen depart every 1/2 hour.

By train

Göttingen Station is served by the following ICE routes: Hamburg-Göttingen-Munich, Hamburg-Göttingen-Frankfurt, and Berlin-Göttingen-Frankfurt.
From Göttingen railway station:
From the Göttingen station you can take a taxi (5 minutes) or walk (20 minutes). If you walk, you need to leave the main exit of the station and walk to the right. Follow the main street, which after the traffic lights turns into Bürgerstraße. Keep walking until you come to the Bunsenstraße. Turn right – you will reach the entrance gate of the MPIDS after about 300m.

By car

Leave the freeway A7 (Hanover–Kassel) at the exit »Göttingen«, which is the southern exit. Follow the direction »Göttingen Zentrum« (B3). After about 4 km you will pass through a tunnel. At the next traffic light, turn right (direction »Eschwege« B27) and follow the »Bürgerstraße« for about 600 m. The fourth junction to the right is the »Bunsenstraße«. You will reach the institute's gate after about 300m.



MAX-PLANCK-GESELLSCHAFT